APPENDIX A

A. Seismicity along the boundary between the Modoc Plateau, southern Cascade Mountains and northern Sierra Nevada.

Humphrey, J., McLaren, M.

APPENDIX B

A. Late Cenozoic tectonics of great Walker Lane belt and implications for active deformation in the Almanor region, northeastern California.

Unruh, J.R.

APPENDIX 1-1

A. A Magmatic Model of Medicine Lake Volcano, California. Donnelly-Nolan, J.M.

B. Medicine Lake Volcano, Northern California: Cascade or Basin and Range Volcano? Donnelly-Nolan, J.M.

C. Post-11,000-Year Vocanism at Medicine Lake Volcano, Cascade Range, Northern California.

Donnelly-Nolan, J.M., Champion, D.E., Miller, C.D., Grove, T.L., Trimble, D.E.

D. Crustal Subsidence, Seismicity, and Structure Near Medicine Lake Volcano, California.

Dzurisin, D., Donnelly-Nolan, J.M., Evans, J.R., Walter, S.R.

APPENDIX 1 - 2

A. The Giant Crater Lava Field: Geology and Geochemistry of a Compositionally Zoned, High-Alumina Basalt to Basaltic Andesite Eruption at Medivine Lake Volcano, California.

Donnelly-Nolan, J.M., Champion, D.E., Grove, T.L., Baker, M.B., Taggart, J.E., Bruggman, P.E.

B. Duration of Eruption at the Giant Crater Lava Filed, Medicine Lake Volcano, California, Based on Paleomagnetic Secular Variation.

Champion, D.E., Donnelly-Nolan, J.M.

APPENDIX 1 - 3A

$^{40}Ar/^{39}Ar$ Dating of Young Low-K Tholeiites: Examples from Northeast California, U.S.A.

Becker, T.A., Sharp, W.D., Renne, P.R., Turrin, B.D. Page, W.D., Wakabayashi, J.

$^{40}Ar/^{39}Ar$ Dating of Quaternary Basalt, Western Modoc Plateau, Northeastern California: Implications to Tectonics.

Page, W.D., Renne, P.R.

APPENDIX 1 - 3B

Table 1- Evaluation of faults in the Mayfield, Soldier Mountain, Soldier Creek, and Rodney Ledger fault zones along the PGT pipeline trench, Modoc Plateau, California.
Page, W.D.

Table 2- Dated basalt flows in the Modoc Plateau near Burney, California.
Page, W.D.

APPENDIX 1 - 4A

A. Origin and features of Mayfield Ice Cave, Siskiyou County, California.
Sowers, J.M., Simpson G.D.

APPENDIX 1 - 5

A. Evaluation of Risk From Surface Fault Rupture to a Penstock Using the $^{40}Ar/^{39}Ar$ Dating Technique.
Bachhuber, J., Page, W.D., Renne, P.R.

APPENDIX 2 - 1

A. Late Quaternary faulting of the Hat Creek Basalt, Northern California.
Muffler, L., Clynne, M., and Champion, D.

B. Vesicle Cylinders in the Warner and Hat Creek Basalts, Northeastern California.
Goff, F.

APPENDIX 2 - 3

A. Volcanic and Glacial Stratigraphy in the Hat and Lost Creek Drainages and the Age of Lassen Park.
Gerstel, W.J., and Clynne, M.A.

B. Stratigraphic, Lithologic, and Major Element Geochemical Constraints on Magmatic Evolution at Lassen Volcanic Center, California.
Clynne, M.A.

C. Late Cenozoic Volcanism, Subduction, and Extension in the Lassen Region of California, Southern Cascade Range.
Guffanti, M., Clynne, M.A., Smith, J.G., Muffler, L.J.P., Bullen, T.D.

APPENDIX 2 - 6

A. Displacement of Late Pleistocene Glacial Moraines by the Almanor fault, Plumas County, California.
Kelson, K.I., Hitchcock, C.S., Zeeb, R.B., Lettis, W.R., Page, W.D.

APPENDIX 3 - 1A

A. The Mulshoe Mine Fault at Prattville Trench Site.
Sawyer, T.L., Hitchcock, C.H., Crampton, T., Sowers, J.M., Caskey, J.S. and Sawyer, J.E.

APPENDIX 3-1B

A. Voluminous, theoleiitic basalt fields of the Lake Almanor basin, and their deformations due to post-emplacement faulting.
Champion, D., Clynne, M., Muffler, P.

APPENDIX 3 - 2

A. Quaternary Faulting, Incision of the North Fork Feather River, and Neotectonics of the Northeastern Sierra Nevada, California.
Wakabayashi, J., Page, W.D., Renne, P.R., Sharp, W.D., Becker, T.

APPENDIX 3 - 2A

A. Trenching study of the Skinner Flat fault at the Rush Hill Motorway site.
Simpson, G.D., Knudson, K.L., and Drouin, P.E.

APPENDIX 3 - 3

A. Tectonic deformation of the Lovejoy basalt, a late Cenozoic strain gage across the northern Sierra Nevada and Diamond Mountains, California.
Page, W.D., Sawyer, T.L., and Renne, P.R.

APPENDIX 3-6

Southern Mohawk Valley Fault Zone at the Calpire trench Site.
Sawyer, T.L., Page, W.D., Hemphill-Haley, M.A.

APPENDIX A

A. Seismicity along the boundary between the Modoc Plateau, southern Cascade Mountains and northern Sierra Nevada.
Humphrey, J., McLaren, M.

SEISMICITY ALONG THE BOUNDARY BETWEEN THE MODOC PLATEAU, SOUTHERN CASCADE MOUNTAINS, AND NORTHERN SIERRA NEVADA

James R. Humphrey, Lahontan Geoscience, Inc., 21380 Castle Peak Road, Reno, NV

Marcia K. McLaren, Pacific Gas and Electric Company, POB 770000, F22A, San Francisco, CA

Introduction

The 1995 FOP field trip traverses through four major tectonic provinces: the Southern Cascades, Modoc Plateau, the Sierra Nevada block, and the Great Basin (Figure 0-2 in logbook). Seismicity in the northern section of this region (from Klamath Falls to Lassen Peak) occurs mostly in tight clusters associated with activity in specific fault zones or with volcanoes. Seismicity in the southern section (from Lake Almanor to Lake Tahoe) is dominated by activity along the Sierra Nevada-Great Basin boundary zone (SNGBZ; VanWormer and Ryall, 1980), a subprovince within the Walker Lane belt. The SNGBZ is a seismic belt formed by a nearly continuous north-northwest trending zone of earthquakes extending from the Garlock fault in southern California to the Lake Almanor region. Earthquakes in the zone tend to concentrate along the east flank of the Sierra Nevada.

The level of seismic activity in the field area (relative to other areas in the western United States) ranges from very low in the northeastern corner of the Modoc Plateau to moderate in the region north of Lake Tahoe. Seismicity in the northern section along the southern Cascades-Great Basin boundary north of Lake Almanor generally occurs in clusters associated with volcanoes (Lassen Peak, Mt. Shasta, Medicine Lake) or north-northwest trending faults (Hat Creek fault, Klamath Falls area). Significant recent earthquakes in this area are the 1993 Klamath Falls sequence (two M6 events), the surface rupturing 1978 M4.6 Stephens Pass earthquake, and the 1950 Lassen Peak earthquake (M5.5). No significant historical earthquakes have been reported in the northern region, although the minimum detectable earthquake has been estimated to be a magnitude 6 during the 1870's (Toppozada and others, 1981). Seismicity in the southern section along the SNGBZ from Lake Almanor to Lake Tahoe occurs in diffuse bands associated with northwest trending faults in the boundary zone. The most significant recent event is the 1966 M6 Dog Valley earthquake north of Truckee. Five earthquakes of magnitude 6 or greater may have occurred in the southern region between 1850 and 1920 (Toppozada and others, 1981; Toppozada and Parke, 1982).

Earthquake focal depths in the region show a distinct trend across the boundary between the Great Basin and adjacent provinces. Earthquakes in the Sierra Nevada block generally extend down to 40 km depth whereas earthquakes in the Walker Lane belt are located at depths less than 20 km reflecting a difference in rheological properties between the two provinces (Hill and others, 1991; Rogers and others, 1991). In the immediate vicinity of Lake Almanor 90 percent of the earthquakes are located above 10 to 15 km.

Focal mechanisms derived from recordings of well-located earthquakes in the study area suggest a relatively consistent orientation of least principal stress axes. In the Modoc Plateau and

southern Cascades the dominant mechanism is normal faulting with approximate east-west extension (Klein, 1979; Simila, 1981; Braunmiller and others, 1995). Within the Sierra Nevada block, deformation occurs in a mix of strike-slip, normal, and reverse mechanisms (Wong and Savage, 1983). The maximum principal stress orientation is approximately north-south and the least principal direction is east-west, consistent with north-south crustal shortening and east-west extension (Hill and others, 1991). Along the SNGBZ and in the Walker Lane belt to the east earthquakes exhibit both normal and strike-slip faulting consistent with a tectonic regime influenced by both east-west extension of the Great Basin and right-lateral shear of the North American plate boundary (VanWormer and Ryall, 1980; Vetter and Ryall, 1983; Zoback, 1989).

Historical Seismicity from 1850 through 1969

Moderate to strong earthquakes have been reported in western Nevada and northeastern California since the mid 1800's. Since 1852, there have been five earthquakes of magnitude 6 or larger in this region. In addition there have been several smaller earthquakes which, despite their size, have resulted in surface rupture.

The record of historical earthquakes in northern California began with the settlement of gold mining camps in the foothills of the Sierra Nevada in 1849-50. Similar settlements in western Nevada, mostly related to gold and silver mining in the Virginia Range, were founded starting in the 1850's. It was not until the 1870's, when the population had increased along the east side of the Sierra from the Owens Valley in the south to the Modoc Plateau in the north, that newspaper coverage was complete along most of the study area (Toppozada and others, 1981). Figure 1 shows the approximate location of the pre-1900 events.

The completeness of the historical catalog varies in direct proportion to the felt intensity and the population density. Before the gold rush in central California in 1849, information on earthquakes was obtained from the written records of the Franciscan missions located on the California coast from San Diego in the south to Sonoma in the north (Toppozada and others, 1981). Events were rarely recorded unless they caused significant damage which means that only pre-1850 earthquakes of magnitude 7 or greater within 100 km of the coast appear in the catalogs. Following the gold rush, newspapers were established throughout California and the Comstock mining district in western Nevada. This lowered the magnitude threshold to 6.0 for the gold country (from Quincy south to Mariposa and as far east as Virginia City) and 6.5 for the rest of the region in the 1850's (Toppozada and others, 1981). Earthquakes of magnitude 7 or less could have gone unrecorded in Mono and Inyo counties (Toppozada and others, 1981). By the 1870's, newspaper coverage had extended into the Modoc Plateau and the detection threshold decreased to magnitude 6 for the majority of the study area (Toppozada and others, 1981; Slemmons and others, 1965). By 1950, the threshold was magnitude 3 for most of the study area except for the portion in southern Oregon where adequate coverage was not obtained until the Klamath Falls sequence in 1993 (Engdahl and Rinehart, 1991). Figure 2 is a map of epicenters in the region from 1900 through 1969.

Significant Regional Historical Earthquakes

Selected earthquakes in the study area are discussed in the following paragraphs. These earthquakes are significant because they highlight the active nature of the southern section of the

study area in the late 19th and early 20th centuries. The descriptions are taken from Toppozada and others (1981), Slemmons and others (1965), and dePolo (1992).

January 25, 1855

No reports of damage were found for this magnitude 5.5 located near the Nevada-California border (Toppozada and others, 1981). Rockfall was reported at Sierra Buttes and miners ran from the 400 foot level at the Blue Banks Mine in Sierra or Nevada county (Toppozada and others, 1981).

September 3, 1857

Due to sparse settlement of the region at this time this earthquake is imprecisely located. It was strongly felt at California mining camps in the Downieville, Nevada City, and Placerville areas (intensity V-VI) and as far away as San Francisco (Toppozada and others, 1981). Toppozada and others (1981) have placed the location as the California-Nevada border region and assigned the event a magnitude 6.0.

January 24, 1875

This earthquake has been placed both in the Mohawk Valley (Slemmons and others, 1965) and near Honey Lake (Toppozada and others, 1981). The Mohawk Valley location was based on reports by Turner (1896) of ground rupture in Pleistocene lakebeds. Toppozada and others (1981) base their location on observed intensities. Damage was reported in Janesville (VII) and Susanville (VI) and intensity V effects were reported in Truckee. Toppozada and others (1981) has assigned this event a magnitude 5.8. Figure 1 shows the two different locations mentioned in the literature. Hawkins and others (1986) review the geologic evidence for ground rupture and suggest that Turner's 1896 interpretation is incorrect.

January 31, 1885

A magnitude 5.7 earthquake damaged buildings throughout Honey Lake Valley, causing intensity VII damage in Susanville (Toppozada and others, 1981).

April 29, 1888

A magnitude 5.9 event occurred in the northern section of the Mohawk Valley causing intensity VII damage in Cromberg. Rockslides were reported north of Downieville and in Rattlesnake Canyon it was reported that the earth vibrated continuously all night (Toppozada and others, 1981).

June 20, 1889

This event caused intensity VII damage in Susanville and numerous aftershocks followed the magnitude 5.9 mainshock (Toppozada and others, (1981). People near Eagle Lake reported hearing loud booms during the aftershock sequences.

1914 Reno Earthquakes

In 1914, two magnitude 6 earthquakes occurred in the Truckee Meadows. The first occurred on February 18, a magnitude 6 event which caused minor damage to buildings in Reno (Slemmons and others, 1965). Intensity data suggest that this event was located in the Verdi area, west of Reno (dePolo, 1992). The second event, a magnitude 6.4, occurred just northeast of Reno (Bolt and Miller, 1975). Strong ground shaking from this event lasted about ten seconds, toppling chimneys in the Truckee Meadows (Slemmons and others, 1965). This was the largest earthquake to be felt in this region since 1868. The largest aftershock to the April 24 event was a magnitude 5 on April 27. The Truckee Meadows continued to experience aftershocks for the remainder of the year (Slemmons and others, 1965).

December 29, 1948

Intensity VII damage in Verdi was caused by a magnitude 6.0 earthquake on this date. This event was preceded by six widely-felt foreshocks on December 27 and in Verdi during the following day there were almost continuous vibrations. The activity lessened during the next 36 hours followed by the mainshock on the morning of the 29th. Damage occurred to nearly every building in Verdi. Some damage also occurred in Reno to the east. Rockslides were reported in the Truckee River canyon west of Verdi. dePolo (1992) suggests that the earthquake was centered in Dog Valley, along the north-trending Verdi fault or the northeast-trending Dog Valley lineament.

1946 - 1950 Lassen Earthquakes

Three moderate earthquakes occurred in the Lassen region; a M_L 5.0 event on 7 July 1946 and two events in 1950, a M_L 5.5 on March 20 and a M_L 4.6 on November 14. The 1946 event is located north of Lassen Peak, between Chaos Crags and Badger Mtn., and the 1950 events were located along the south flank of Reading Peak and the south flank of Lassen Peak, respectively. No other activity is reported with the 1946 event, however, the two 1950 events were accompanied by earthquake swarms, including foreshocks and numerous aftershocks.

The March 20, 1950 earthquake was the largest in a prolific swarm. Twenty-nine small foreshocks and over 7000 aftershocks were recorded. (Bolt and Miller, 1975). The November 14 earthquake was the largest of a swarm that included one hundred and sixty-five foreshocks in the 18 hours before the main shock and approximately 1700 earthquakes during the next 7 days (Bolt and Miller, 1975). Seismic activity from these swarms continued through the 1950s.

December 14, 1950

A surface-rupturing magnitude 5.6 earthquake occurred near the Fort Sage Mountains at the southeastern end of Honey Lake Valley, approximately 70 km east of Lake Almanor. A 9.5 km long down-to-the-west scarp formed at the western base of the Fort Sage Mountains (Gianella, 1951, 1957). Estimates of dip-slip offset range from 20 cm to 60 cm if folding of alluvium is considered (Gianella, 1957). Gianella (1957) found no evidence of lateral offset.

September 12, 1966

This magnitude 6.0 event occurred northeast of Truckee causing minor damage to the Prosser Creek and Boca dams, highways, railways, water flumes, and local buildings (Kachadoorian and others, 1967). Rockfall in the Truckee River canyon damaged the Southern Pacific Railroad line, a powerhouse at Farad, and US highway 40. Aftershocks of this event formed a linear zone about 10 km long trending northeast along the Dog Valley lineament (Ryall and others, 1968; Greensfelder, 1968).

The focal depth for this event was estimated by Ryall and others (1968) and Tsai and Aki (1970) to be 10 km, with aftershocks distributed between 0 and 12 km depth. Tsai and Aki (1970) used surface waves as well as short-period body waves in constraining the focal depth. The focal mechanism calculated by Tsai and Aki (1970) shows strike-slip motion with a minor component of dip slip along either a northeast-trending (left-lateral slip) or northwest-trending (right-lateral slip) fault plane. The distribution of aftershocks, mainshock and aftershock focal mechanisms, and geomorphic evidence suggest left-lateral slip on a northeast trending structure (Hawkins and others, 1986).

Recent Regional Seismicity, 1970 - 1994

Recent seismicity in the region from latitude 39°N to 43°N is shown in Figure 3. Earthquake locations are from the U. S. Geological Survey Northern California Seismic Network (NCSN) and inlcude merged data from the University of Nevada Reno. The distribution of epicenters for this time period is similar to that of the historical earthquakes. Seismicity in the northern section of the study area is at a low to moderate level. The Klamath Falls region has experienced relatively few historic earthquakes. The concentrated cluster of events in this region is related to the 1993 Klamath Falls sequence (next section). To the south seismicity is diffusely distributed between several clusters of events related to volcanic activity (Medicine Lake, Mt. Shasta, Lassen Peak) or associated with active structures (Stephens Pass, Tennant and Hat Creek graben). The Lake Almanor region has experienced a number of moderate earthquakes from 1850 to 1969 (next section). Recent seismicity continues at a moderate level. Along the SNGBZ from Lake Almanor south to the north Lake Tahoe region the rate of historical seismicity is higher than in the northern section. Recent seismicity is at a low to moderate level. West of the SNGBZ, seismicity in the Great Valley-Sierra Nevada block is at a low level, with the exception of the 1975 Lake Oroville sequence which includes a magnitude 5.7 mainshock. To the east of the SNGBZ seismic activity is at a very low level with the epicenters diffusely distributed throughout the region. The north Lake Tahoe region has moderate activity with earthquakes associated with north-, northwest-, and northeast-trending structures. This region was very active from 1850 to 1900 (see preceding section). The period from 1900 to 1970 was less active with five magnitude 6 events occurring. The recent period of seismicity remains as active in term of numbers of small to moderate earthquakes with the largest being a magnitude 5.2 earthquake in Soda Springs, California, 20 km southwest of the 1966 Dog Valley earthquake.

Seismicity from Klamath Falls to Lassen Peak

The 1993 Klamath Falls Sequence

Figure 3 shows the location of the 1993 Klamath Falls sequence north of the California-Oregon border. Klamath Falls is located at the northwestern edge of the Great Basin province in a region dominated by north to northwest trending normal faults, some of which are Holocene in age (Hawkins and others, 1989). Historical seismicity in this area has been very low. Only ten earthquakes greater than magnitude three have been recorded since 1920 (Sherrod, 1993). The largest of these events was a magnitude 4.3 in 1948 northeast of Klamath Falls.

The 1993 sequence started on September 20, with a magnitude 4.2 foreshock followed 12 minutes later by the first magnitude 6.0 event. Two hours later a second mainshock, also magnitude 6.0, occurred several kilometers northwest of the first. Numerous aftershocks followed during the next three months. On December 4, a magnitude 5.1 aftershock occurred several kilometers to the southeast of the first mainshock. The two largest events in the sequence and many of the aftershocks had focal mechanisms exhibiting almost pure dip-slip motion on north and northwest trending nodal planes (Braunmiller and others, 1995). The orientation of T-axes suggest east-west extension is occurring on faults in the area, possibly on the northwest-trending Lake of the Woods fault zone (Braunmiller and others, 1995). This style of deformation is consistent with that observed elsewhere in the Great Basin (Zoback, 1989).

Seismicity of the Medicine Lake Region

Seismic activity in the Medicine Lake region from Medicine Lake volcano west to Stephens Pass has been low to very low. No earthquakes were reported between 1909 and 1950 (Bolt and Miller, 1975), although the detection threshold was probably about magnitude 4. More stations were added in the 1950s in the Mt. Shasta area, lowering the detection threshold to less than magnitude 3. Still, no earthquakes were reported in the area between 1950 and 1975 (Dzurisin and others, 1991). In 1980 the U. S. Geological Survey (USGS) added nine short period seismographic stations. Between 1978 and 1988, seismic activity increased with the occurrence of three earthquake swarms; the Stephens Pass area in 1978, near the town of Tennant, midway between Medicine lake and Mt. Shasta, in 1981, and within the Medicine Lake caldera in 1988 (Figure 3). All three swarms are shallow, less than 5 km deep. The Tennant and Stephens Pass earthquake sequences occurred within the dominant regional structural grain of north-south trending extension faults of the western edge of the Basin and Range. The Medicine Lake earthquakes are related to subsidence of the Medicine Lake caldera.

1978 Stephens Pass

The Stephens Pass swarm began on August 1, 1978 with a magnitude 4.6 earthquake. The event was followed by 5 earthquakes of magnitude 3.5-4.5 in the next 90 minutes (U. C. Berkeley catalog), and 100 to 200 magnitude 2 and greater events in the next 24 hrs. (Bennett and others, 1979). The epicentral area is 15 km south of the town of Tennant. A second swarm began on August 12 with a magnitude 4.3 event that was followed by several events of magnitude 3-4.

CDMG and the USGS installed a temporary seismographic network that monitored seismicity until the end of November 1978 (Bennett and others, 1979). On August 14 U. S. Forestry personnel reported north-south trending fractures that crossed the road about 5 km south of Stephens Pass (Dzurisin and others, 1991). The fractures follow an east facing scarp. Later observations documented a 2-km long 75-m-wide zone of tensional fractures, grabens, and circular depressions within the grabens (Bennett and others, 1979). Well located aftershocks show an 8-km-long aftershock zone dipping to east, away from the ground breakage to 4 km depth (Cramer, 1978).

1981 Tennant Sequence

The second shallow swarm occurred from January through February 1981, beneath the town of Tennant, about 10 km north of Stephens Pass. The following information is from Dzurisin and others (1991). The sequence began with a locally felt earthquake on January 1, followed by several dozen events of magnitude less than 3.0 from January 5-8. Activity increased on January 9 peaking with a magnitude 4.1 earthquake. Seismicity declined considerably during the next few weeks with sporadic activity on January 12 and early February. A temporary seismic network was installed by January 15. Well determined focal depths from the network were shallow, <2 km. The 10-km long aftershock zone trends north-south, consistent with the region structural grain. No ground breakage was reported.

1988 Medicine Lake Swarm

The following is summarized from Dzurisin and others (1991). The Medicine Lake swarm began on 29 September 29, 1988 with 20 events. The largest was a magnitude 3.3. Activity peaked in afternoon with 80 events in one hour including a magnitude 4.1, the largest event in the sequence. Activity declined rapidly with a few events per hour, to several events per day in October, and several per week through end of the year. Sporadic activity of small events (less than magnitude 3) continued into 1989. All of the earthquakes occurred within the caldera in the upper 2 km and most of them occurred in the center of the caldera. Dzurisin and others' (1991) model sees the Medicine Lake sequence as a reaction to subsidence induced by bending of a weak brittle surface layer containing lava flows and related sediments.

Hat Creek Seismicity

The Hat Creek area contains several north to north-northwest trending faults, including the Hat Creek, Rocky Ledge, McArthur, and Pratville Holocene faults. The Hat Creek graben is bounded on the east by the west-side-down Hat Creek fault and on th west by the east-side-down Rock Ledge fault and the unnamed Quaternary faults to the southeast. Recent microearthquakes are of magnitude 3 and under (Figure 4). Seismicity patterns show activity in the southwest that steps northeastward in a right-step fashion into the Hat Creek graben, continues to the northwest, within the Rocky Ledge fault zone, and then steps to the northeast again before dying out. Very few earthquakes have occurred along the Pittville and McArthur faults.

Most of the seismicity within the Hat Creek graben has occurred in the southern part, between the Hat Creek fault and the unnamed Quaternary faults. There are two and possibly three diffuse north-northeast trends that are bounded by the graben, a distinct northeast-trending cluster of earthquakes within the unnamed faults on the west side of the graben, and a smaller denser cluster with a possibly east-west trend, located about 7 km south of the northeast trending cluster and west of the unammed faults. The diffuse north-northeast trends across the graben are events that have occurred fairly steadily over time. These trends may reflect a reaction of the graben to regional shear stresses. The distinct and larger cluster to the north predominantly consists of earthquakes from a swarm than began in October 1991 and continued through the end of that year. Over 60 events were recorded. The largest was a magnitude 3.1 on 5 October. Cross section A-A' in Figure 4 shows activity to about 20 km depth along vertical to steeply west-dipping fault planes, consistent with the nearby mapped west-dipping faults that may dip into the west boundary of the graben. The nearly vertical pattern between 10 and 20 km supports a nearly vertical west boundary of the graben. Finally, the small dense cluster to the south consists of a swarm in 1982. The largest event was a magnitude 3.0 on August 17, 1982.

Lassen Seismicity

The majority of the seismicity in the Lassen region is associated with the volcanic activity beneath Lassen Peak and adjacent peaks. Moderate earthquakes and accompanying swarms are documented in the historical record. The recent seismicity shows continued cluster activity. The U. C. Berkeley catalog reports seismic activity in the Lassen region dating back to the 1914 to 1915 eruptions. Earthquakes were reported felt in the Lassen region for 20 minutes preceding the 1915 eruption. Significant historical earthquakes in this area were discussed in the preceding historical earthquake section.

Lassen seismicity recorded from 1977 through 1994 predominantly consists of 3 distinct and fairly evenly spaced earthquake clusters that span about 8 km east-west across the southern flank of Lassen Peak, between Mt. Diller and Reading Peak (Figure 5). Non of the clusters are particularly tight, rather, they are somewhat diffuse and elongate, northwest to southeast. The density of the clusters increases from east to west. Projecting the clusters on an east-west cross section (Figure 5) shows that they generally occur at the same depth, between about 3 and 7 kilometers. The west and middle clusters are more concentrated at 4-5 km depth, while the eastern cluster has a more diffuse distribution and possibly dips to the east.

To study the spatial and temporal relationship of the three clusters we have plotted them as time-slice map views in Figure 6. The approximate cluster boundaries are drawn around the clusters for comparison of one time-slice to another. Seismicity patterns from 1977-through 1981 show that the west and middle clusters were the most active at that time. The 1982 map shows a shift of activity to the middle and east clusters. The 1988 map shows that activity has again shifted back to the middle and west clusters. In 1992 activity was fairly evenly distributed. Finally, in 1994 we see that most of the activity has shifted back to the middle and west clusters. Except for the higher rate of activity in the west cluster in 1988 and the low rate in 1994, the activity rates of these clusters is fairly constant. It is interesting to note that the 1994 data show no activity in the east cluster.

The close proximity of these clusters, both horizontally and at depth and the shifting back and forth of activity over time suggest that their sources may be related, or linked, by a common conduit. The northwest trending elongate shape of the clusters suggests that they may be a reaction to magma movement along similar striking dikes. The east- west alternating of activity may be related to a reaction to fairly constantly changing loading pressures, stresses, or temperatures within and surrounding the magma bodies beneath Lassen Peak.

Seismicity from Lake Almanor to Lake Tahoe

Recent Seismicity in the Lake Almanor Region, 1970-1994

Figure 7 shows the distribution of seismicity in the Lake Almanor region from the Pit River south to the north Lake Tahoe area. The most prominent regional trend of seismicity is along the SNGBZ which extends southeast from Lassen Peak to Truckee parallel to the Tahoe-Medicine Lake trough. This structure includes the Lake Almanor basin. Seismicity along this trend (roughly parallel to line B-B' on Figure 7) occurs in three separate clusters, highlighted by red ellipses in Figure 7. The northern-most Almanor cluster lies in the Lake Almanor basin extending northwest from the Indian Valley graben through Lake Almanor to south of Lassen Peak. To the southeast is the Quincy cluster, a more diffuse clustering of events along the Tahoe-Medicine Lake trough from Gold Lake in the south to Quincy in the north. This region was the locus of the recent magnitude 4.4 earthquake 20 km east-southeast of Quincy. This event (on June 18, 1995) was located 8 km deep and the focal mechanism showed nearly pure strike-slip motion on either a northwest-trending or northeast-trending fault plane. The southern-most zone is near the intersection of the north-trending Mohawk Valley fault zone and the Dog Valley lineament in the north Tahoe region (point B' in Figure 7). This area was the locus of the 1966 magnitude 6.0 Dog Valley earthquake.

A second trend (the west Almanor cluster) is a subparallel and more diffuse trend west of Lake Almanor that extends 25 km northwest from the Butt Valley Reservoir to just south of Lassen Peak. This trend is, in part, spatially associated with the tectonic transition zone between the Sierra Nevada and the southern Cascades. West of here seismicity is reduced to a very low level, increasing again at the western margin of the study area.

Focal Depths in the Lake Almanor Region

Figure 7 shows the location of five seismicity cross-sections which show the spatial distribution of earthquake focal depths in the Lake Almanor region. Data from the catalog were filtered to remove those events having vertical and/or horizontal errors greater than 5 km. Section A-A' (Figure 8) is oriented perpendicular to the trend of the Tahoe-Medicine Lake trough and intersects the southern end of Lake Almanor. The western end of the section lies outside the seismicity study area, therefore, no earthquakes have been plotted. This section exhibits a trend which is repeated in sections C, D, and E, namely, a deepening of seismicity from east (or northeast) to the west. This is consistent with the view point that the Great Basin province, represented by the Walker Lane belt in this region, is a region of high average heat flow relative to the interior of the Sierra Nevada block resulting in a relatively shallow brittle-ductile transition zone. Earthquakes within the western Great Basin rarely occur deeper than 20 km, with 95

percent of the events occurring in the upper 15 km (Ryall and Savage, 1969, Rogers and others, 1991). Detailed source parameters studies of large Great Basin earthquakes indicate that mainshocks initiate between 8 and 16 km (Doser and Smith, 1985). These data support the suggestion of Smith and Bruhn (1984) that the base of the seismogenic crust is coincident with the brittle-ductile transition zone at about 15 km depth.

Section B-B' (Figure 8) is oriented approximately parallel to the trend of the Tahoe-Medicine Lake trough. Because events from both the Sierra Nevada block and the Walker Lane belt are projected on to this plane information about the depth to the base of the seismogenic zone in these provinces is not efficiently presented. What this section does show is the relative increase in seismic activity at the intersection of the southern Cascades, Sierra Nevada, and Great Basin provinces (northwest of the intersection with A-A' in the Almanor region; Figure 8).

Section C-C' (Figure 9) extends from Lake Oroville to Honey Lake passing through the Quincy cluster along the Tahoe-Medicine Lake trough. The concentration events near point C are primarily aftershocks from the 1975 Oroville earthquake. In the northeast end of the section, seismic activity is very low, despite the presence of the Honey Lake fault zone, a major right-lateral fault in the northern Walker Lane belt which has an estimated Holocene slip rate of 2 mm/yr (Wills and Borchardt, 1993), and several moderate historic earthquakes (Figure 1).

Section D-D' (Figure 9) is oriented east-west across the intersection of the southern Cascades, Great Basin, and Sierra Nevada tectonic provinces. In the western end of the section the increasing depth of Great Valley earthquakes can be clearly seen. There is a diminution of activity as the line progresses east until the Lassen area is reached where the three provinces intersect. The seismicity at the intersection is clearly more shallow than the Great Valley province in the west, yet deeper than the very sparse seismic activity indicates to the east.

Section E-E' (Figure 9) extends from the Klamath Mountains province in the west to the Modoc Plateau in the east. This section shows a west dipping seismogenic zone with focal depths in the west averaging 20 km and those in the east about 60 km away averaging 8 km. About 60 km from point D the line intersects the Hat Creek graben where earthquakes extend down to a depth of 25 km.

Association of Seismicity with Structure in the Lake Almanor Region

Figure 10 is a map of the Lake Almanor vicinity showing earthquake epicenters in relation to the faults mapped during PG&E's field program. The map shows some of the seismicity clusters described in the previous section (see Figure 7 for a better view of the clusters). In the lower right hand corner of the map the northern part of the Quincy cluster can be seen along with the location of several historic events. As with all the earthquakes observed in this region a definitive spatial association of hypocenters with a specific mapped fault is difficult, in part because the dataset lacks sufficient spatial resolution but also because the diffuse distribution is a common characteristic of seismicity in the western Great Basin and Sierra Nevada block (Rogers and others, 1991; Hill and others, 1991; Wong and Savage, 1983). Northwest of the Quincy cluster there is a gap in seismicity followed by the Almanor cluster which extends from the Round Valley Reservoir northwest to Juniper Lake. The location of this cluster is consistent with activity on faults comprising the Lake Almanor-Indian Valley graben, bounded on the

northeast side by the Keddie Ridge and Almanor faults and on the west by the Muleshoe Mine, Rock Lake, and Stover Mountain faults. Focal depths in the graben range from near surface to 20 km with a distinct clustering between 5 and 12 km (Figure 8, cross section A-A' beneath B-B' intersection). There is a clear break in seismicity to the west of the Lake Almanor-Indian Valley graben followed by the west Almanor cluster. This cluster is another diffuse grouping of epicenters with a general northwest trend located west of the Stover Mountain, Rock Lake, Butt Creek faults. This seismicity may be associated with activity on a system of late Cenozoic faults west of the Stover Mountain fault. Focal depths in the west Almanor cluster range from near surface to 20 km, with a slight deepening of events to the southwest (**Figure 8, cross section A-A'**). Focal mechanisms from this cluster show mostly reverse slip on nodal planes ranging in orientation from northeast to northwest to west.

The average depth to the base of the seismogenic crust at Lake Almanor was determined by constructing a histogram of focal depths in the area. Events from the Almanor and west Almanor clusters were used in the compilation. The depth above which 90 percent of the earthquakes occur is 12.3 km. After considering the average vertical error of 2.5 km a reasonable range for the depth to the base of the seismogenic zone for this area is 10-15 km, consistent with other estimates in the Great Basin province (Smith and Bruhn, 1984; Rogers and others, 1991).

Seismicity in the Lake Tahoe region

Figure 11 shows the distribution of epicenters from the catalog in the north Lake Tahoe region from 1970 through 1994. Also shown in Figure 11 are Holocene (red), late Pleistocene (blue) and undifferentiated Quaternary and late Cenozoic (black) faults. The cross-sections are oriented to highlight characteristics of seismicity along the SNGBZ as was done for the Almanor area. Section I-I' (Figure 12) is oriented approximately perpendicular to the SNGBZ. The intersection of line J-J' with I-I' marks the location of the Sierra Nevada frontal fault zone in this region. West of the intersection with J-J' (about 45 km northeast of point I) is the Sierra Nevada block, with its typically lower levels of seismic activity and significantly deeper focal depths. About 15 km northeast from point I, along section I-I', is a cluster of events containing a magnitude 5.2 earthquake on November 11, 1980, near Soda Springs, California. This event is located within the Sierran block and focal depths of the aftershocks extend down to 25 km. The focal mechanism for the mainshock indicate oblique-slip on northeast- or northwest-trending nodal planes. To the northeast of this cluster, about 45 km from point I, the cross-section extends through the epicenter of the 1966 magnitude 6.0 Dog Valley earthquake (located in the cluster near the intersection of the cross-sections). This cluster contains events from a swarm of earthquakes in 1983 which are associated with the 1966 aftershock zone (Hawkins and others, 1986). Relocation of these events by Hawkins and others (1986) show that they have focal depths ranging from 10 to 20 km. This is below the focal depth of the 1966 earthquake which was located at 10 km (Tsai and Aki, 1970). The study by Hawkins and others (1986) concludes that the majority of seismic energy released in the Dog Valley aftershock zone since 1973 has occurred directly below the rupture area of the 1966 event. Focal mechanisms for the larger events in the 1983 swarm indicate strike-slip faulting on either northeast- or northwest-trending fault planes (Hawkins and others, 1986) which is consistent with the 1966 mainshock focal mechanism. Northeast of the intersection with J-J' the section traverses the Walker Lane belt in the Reno area. Seismicity in this area exhibits the same characteristics as seen in Section A-A',

C-C', and D-D' in the Almanor region, namely, diffuse clustering of events with focal depths primarily above 15 km. This distribution of seismicity is typical of the Walker Lane belt in this region.

Section J-J' (Figure 12) is oriented parallel to the general trend of the transition between the Sierra Nevada block and the Walker Lane belt. As seen in cross-section B-B' in Figure 8 seismicity occurs in clusters along the trend of the transition zone. The near vertical alignment of hypocenters at the intersection with I-I' is consistent with the interpretation of the Dog Valley fault as a vertically dipping structure (Hawkins and others, 1986). Seismicity between the intersection with I-I' and point J' is generally clustered between 5 and 15 km depth. This seismicity is probably related to the Mohawk Valley fault zone, although uncertainties in hypocentral location preclude assigning these events definitively to this structure (Hawkins and others, 1986).

The denser configuration of seismographic stations in the Reno-Tahoe region gives more confidence in the location of earthquake hypocenters. The pattern of seismicity across the SNGBZ show an abrupt deepening of average focal depths across the transition going from east to west, a pattern repeated in the Lake Almanor region. Therefore, we conclude that the pattern of seismicity in the Lake Almanor region south of Lassen Peak, despite the unfavorable station coverage, is representative of the transition from the Great Basin province to the Sierra Nevada block.

Focal Mechanisms and Style of Deformation from Lake Almanor to Lake Tahoe

Focal mechanisms from selected events in the region from Lake Almanor to north Lake Tahoe were calculated using event phase data from Northern California Earthquake Data Center. In Figure 13, the P- and T-axes from these data are plotted on a base map showing the location of faults compiled by Sawyer (1995). In order to highlight any systematic change in orientation of stress axes across the SNGBZ only axes with plunges within 20 degrees of horizontal are used. In Figure 13 the P-axes (the maximum principal stress axes) are shown in green and the T-axes (least principal stress axes) in red. The orientation of T-axes indicate west to northwest directed least principal stress as is found along most of the Walker Lane belt and SNGBZ (Zoback, 1989). This stress orientation is consistent with a tectonic regime influenced by both east-west extension of the Great Basin and right-lateral shear of the North American plate boundary (VanWormer and Ryall, 1980; Vetter and Ryall, 1983; Zoback, 1989). The P-axes are oriented north to northeast south of Quincy and northwest in the Almanor region and to the north. The orientation of stress axes do not, by themselves, provide a means to delineate province boundaries. But, as will be seen in Appendix B, an inversion of these data to obtain the orientation of the principal strain axes provides a framework in which to determine the potential for slip on faults of various orientations in the Lake Almanor region.

REFERENCES

Bennett, J. H., R. W. Sherburne, C. H. Cramer, C. W. Chesterman, and R. H. Chapman, Stephens Pass earthquakes, Mount Shasta-August 1978, Calif. Geol., 32(2), 27-34, 1979.

Bolt, B. A. and Miller, R. D., 1975. Catalogue of earthquakes in northern California and adjoining areas 1 January 1910 - 31 December, 1972,: Berkeley, University of California Seismographic Station, 576p.

Braunmiller, J., Nabelek, J., and Leitner, B., 1995. The 1993 Klamath Falls, Oregon, earthquake sequence: Source mechanisms from regional data, Geophysical Research Letters, v.22, p.105-108.

Cramer, C. H., The Stephens Pass earthquake swarm of August 1978, east of Moutn Shasta, California (abstract), Eos Trans. AGU, 59(12), 1130, 1978.

dePolo, C. M., 1992. Seismic hazards in the Reno-Carson City urban corridor, Nevada Geology, v. 14, 3p.

dePolo, C. M., Johnson, G. L., Jacobson, S. L., Rigby, J. G., Anderson, J. G., and Wythes, T. J., 1995. Planning scenario for a major earthquake, Reno-Carson City urban corridor, western Nevada, Nevada Bureau of Mines and Geology, Open File Report 95-2, 32p.

Doser, D. I. and Smith, R. B., 1989. An assessment of source parameters of earthquakes in the Cordillera of the western United States, Seismological Society of America Bulletin, v.79, 1383-1409..

Dzurisin, D., Donnelly-Nolan, J. M., Evans, J. R., and Stephen R. Walter, 1991, Crustal subsidence, seismicity, and structure near Medicine Lake volcano, California, Journal of Geophysical Reasearch, Vol 96, No., B10, p 16,319-16,333.

Engdahl, E. R. and Rinehart, W. A., 1991. Seismicity map of North America project, in Slemmons, D. B., Engdahl, E. R., Zoback, M. D., and Blackwell, D. D., eds. Neotectonics of North America, p.21-27.

Gianella, V. P., 1951. The Fort Sage Mountain, California, earthquake of December 14, 1950 (abs), Bulletin of the Geological Society of America, v. 62, p. 1502.

Gianella, V. P., 1957. Earthquake and faulting, Fort Sage Mountains, California, December, 1950, Seismological Society of America Bulletin, v.47, p. 173-177.

Greensfelder, R., 1968. Afertshocks of the Truckee, California, earthquake of September 12, 1966, Seismological Society of America Bulletin, v.58, p. 1607-1620.

Hawkins, F. F., LaForge, R., and Hansen, R. A., 1986. Seismotectonic study of the Truckee/Lake Tahoe area, northeastern Sierra Nevada, California for Stampede, Prosser Creek, and Lake Tahoe dams, U.S. Bureau of Reclamation Seismotectonic Report 85-4, 210p.

Hawkins, F. F., Foley, L. L., and LaForge, R. C., 1989. Seismotectonic study for Fish Lake and Fourmile Lake dams, Rogue River project, Oregon, U.S. Bureau of Reclamation, Seismoteconic Report 89-3, 26p.

Hill, D. P., Eaton, J. P., Ellsworth, W. L., Cockerham, R. S., and Lester, F. W., 1991. The seismotectonic fabric of central California, in Slemmons, D. B., Engdahl, E. R., Zoback, M. D., and Blackwell, D. D., eds. Neotectonics of North America, p.107-132.

Kachadoorian, R., Yerkes, R. F., and Waananen, A. O., 1967. Effects of the Truckee, California, earthquake of September 12, 1966, U.S. Geological Survey Circular 537, 14p.

Klein, F. W., 1979. Earthquakes in Lassen Volcanic National Park, Seismological Society of America Bulletin, v.69, 867-875.

Rogers, A. M., Harmsen, S. C., Corbett, E. J., Priestley, K., and dePolo, D., 1991. The seismicity of Nevada and some adjacent parts of the Great Basin, in Slemmons, D. B., Engdahl, E. R., Zoback, M. D., and Blackwell, D. D., eds. Neotectonics of North America, p.153-184.

Ryall, A. S., VanWormer, J. D., and Jones, A. E., 1968. Triggering of microearthquakes by earth tides and other featrues of the Truckee, California, earthquake sequence of September, 1966, Seismological Society of America Bulletin, v.58, 215-248.

Ryall, A, S. and Savage, W. U., 1969. A comparison of seismological effects for the Nevada underground test Boxcar with natural earthquakes in the Nevada region, Journal of Geophysical Research, v. 74, p. 4281-4289.

Sherrod, D. R., 1993. Historic and prehistoric earthquakes near Klamath Falls, Oregon, Earthquakes and Volcanoes, v. 24, p. 106-120.

Simila, G. E., 1981. Seismic velocity structure and associated tecnoics of northern California [Ph.D. thesis]: Berkeley, University of California, 108p.

Slemmons, D. B., Jones, A. E., and Gimlett, J. I., 1965. Catalog of Nevada earthquakes 1852-1960, Seismological Society of America Bulletin, v.55, 537-583.

Smith, R. B., and Bruhn, R. L., 1984, Intraplate extensional tectonics of the eastern Basin and Range; Inferences on structural style from seismic reflection data, regional tectonics, and

15

thermal-mechanical models of brittle-ductile deformation: Journal of Geophysical Research, v. 89, p. 5733-5762.

Toppozada, T. R., Real, C. R., and Parke, D. L., 1981. Preparation of isoseismal maps and summaries of reported effects for pre-1900 California earthquakes: California Division of Mines and Geology Open File Report 81-11SAC, 182p.

Tsai, Y.-B. and Aki, K., 1970. Source mechanism of the Truckee, California, earthquake of Spetember 12, 1966, Seismological Society of America Bulletin, v.60, 1199-1208.

Turner, H. W., 1986. Further contributions to the geology of the Sierra Nevada, U.S. Geological Survey 17th Annual Report, Part 1, p. 521-762.

VanWormer, J. D. and Ryall, A. S., 1980. Sierra Nevada - Great Basin boundary zone: Earthquake hazard related to structure, active tectonic processes, and anomalous patterns of earthquake occurrence, Seismological Society of America Bulletin, v. 70, p. 1557-1572.

Vetter, U. R. and Ryall, A. S., 1983. Systematic change of focal mechanism with depth in the western Great Basin, Journal of Geophysical Research, v. 88, p. 8273-8250.

Wills, C. J. and Borchardt, G., 1993. Holocene slip rate and earthquake recurrence on the Honey Lake fault zone, northeastern California, Geology, v. 21, p. 853-856.

Wong, I. G. and Savage, W. U., 1983. Deep intraplate seismicity in the western Sierra Nevada, California, Seismological Society of America Bulletin, v. 73, p. 797-812.

Zoback, M. L., 1989, State of stress and modern deformation of the northern Basin and Range province: Journal of Geophysical Research, v. 94, p. 7105-7128.

Figure 1.

Earthquake epicenters from 1850 through 1899 in the northern half of the study area. California locations from Toppozada and others (1981) and Townley and Allen (1939). Nevada locations from the UNR catalog. The two locations for the 1875 discussed in the text are shown with an arrow.

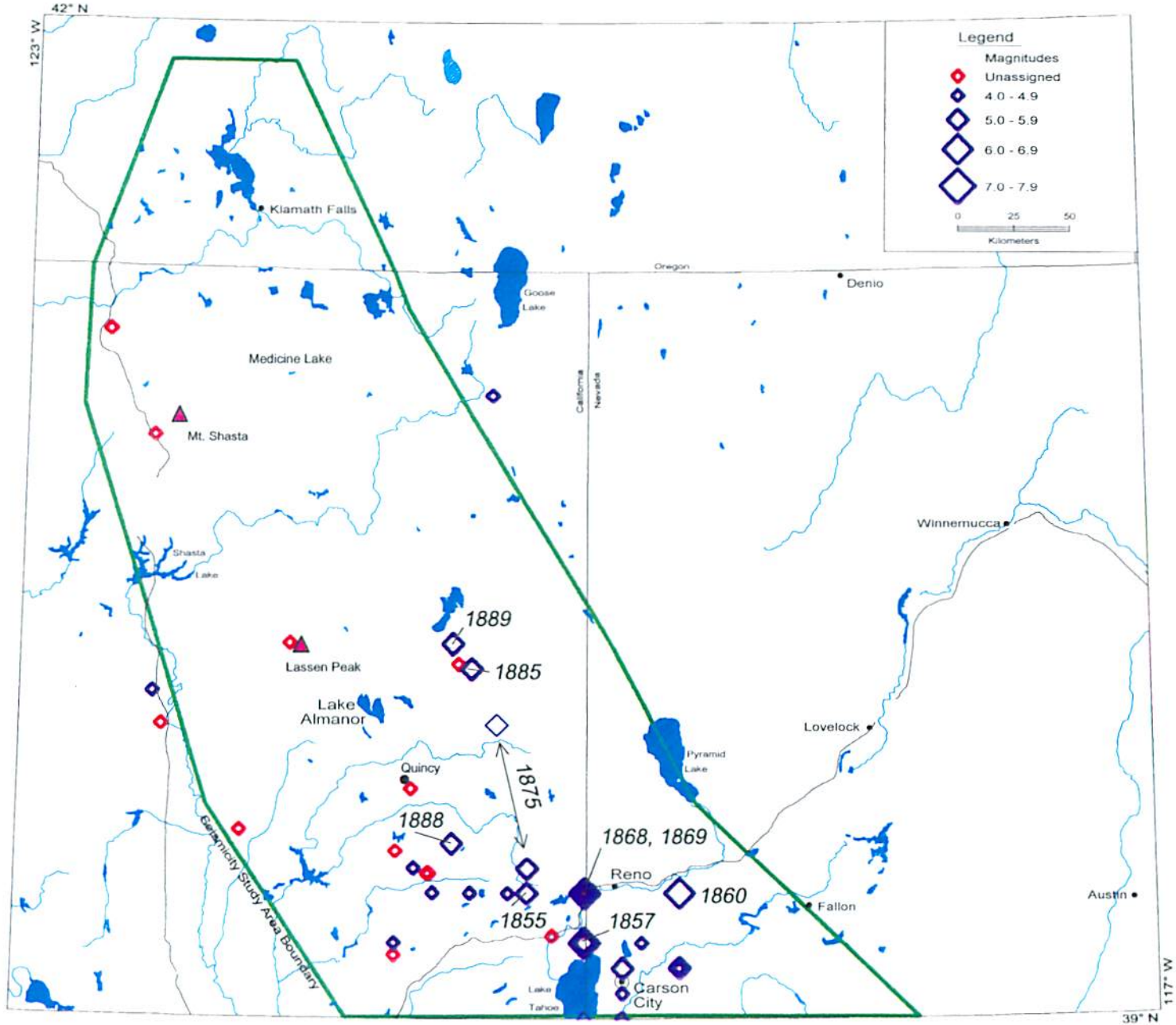

Figure 2.

Earthquake epicenters from 1900 through 1969 located in the northern half of the study area. Data from UCB and UNR catalogs. The red squares represent events for which no magnitude has been assigned in the catalogs. The dates refer to earthquakes discussed in the text.

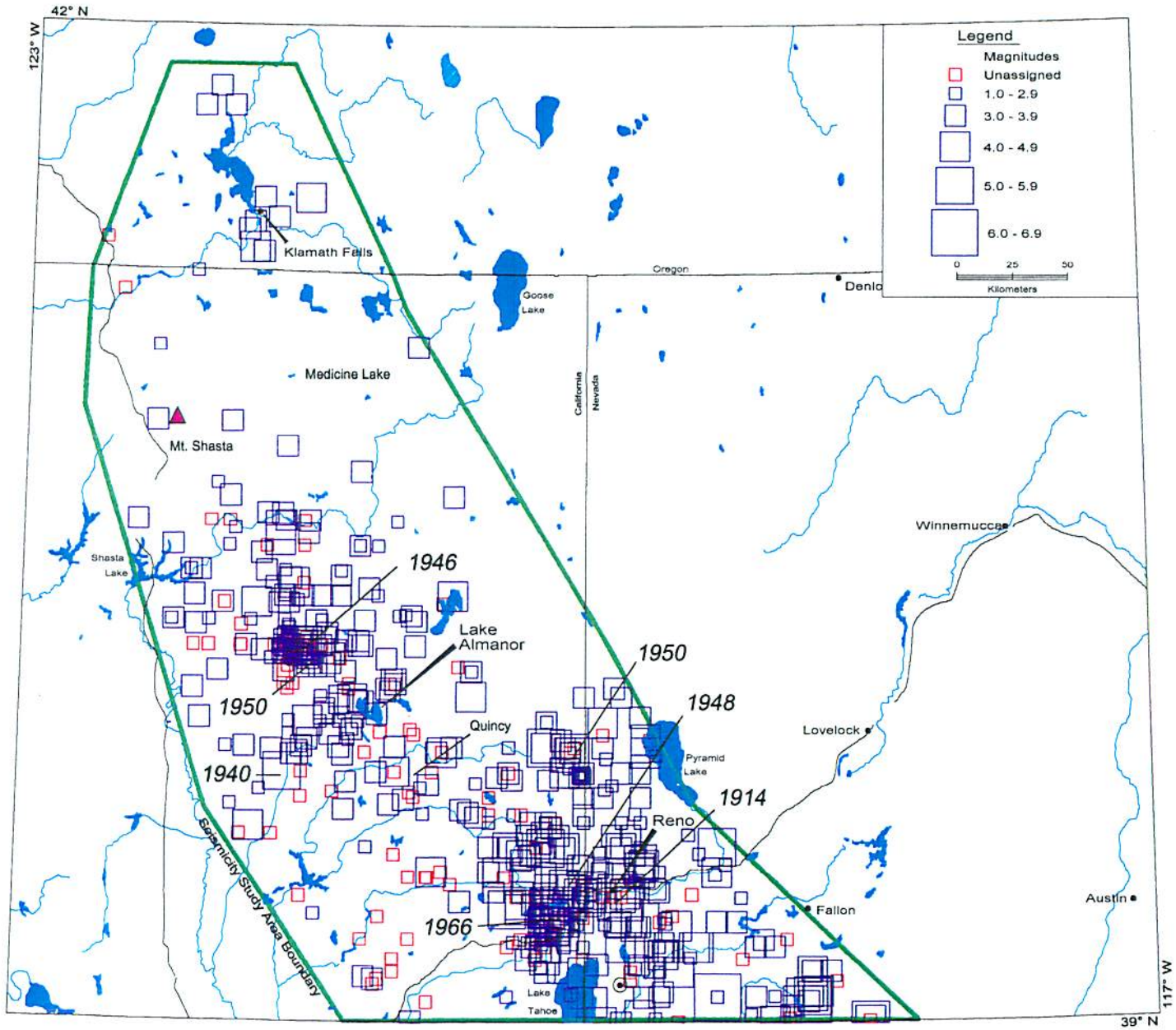

Figure 3.

Instrumentally located seismicity in northern California, Nevada, and southern Oregon from 1971 through 1994. Data from the Northern California Seismic Netwwork.

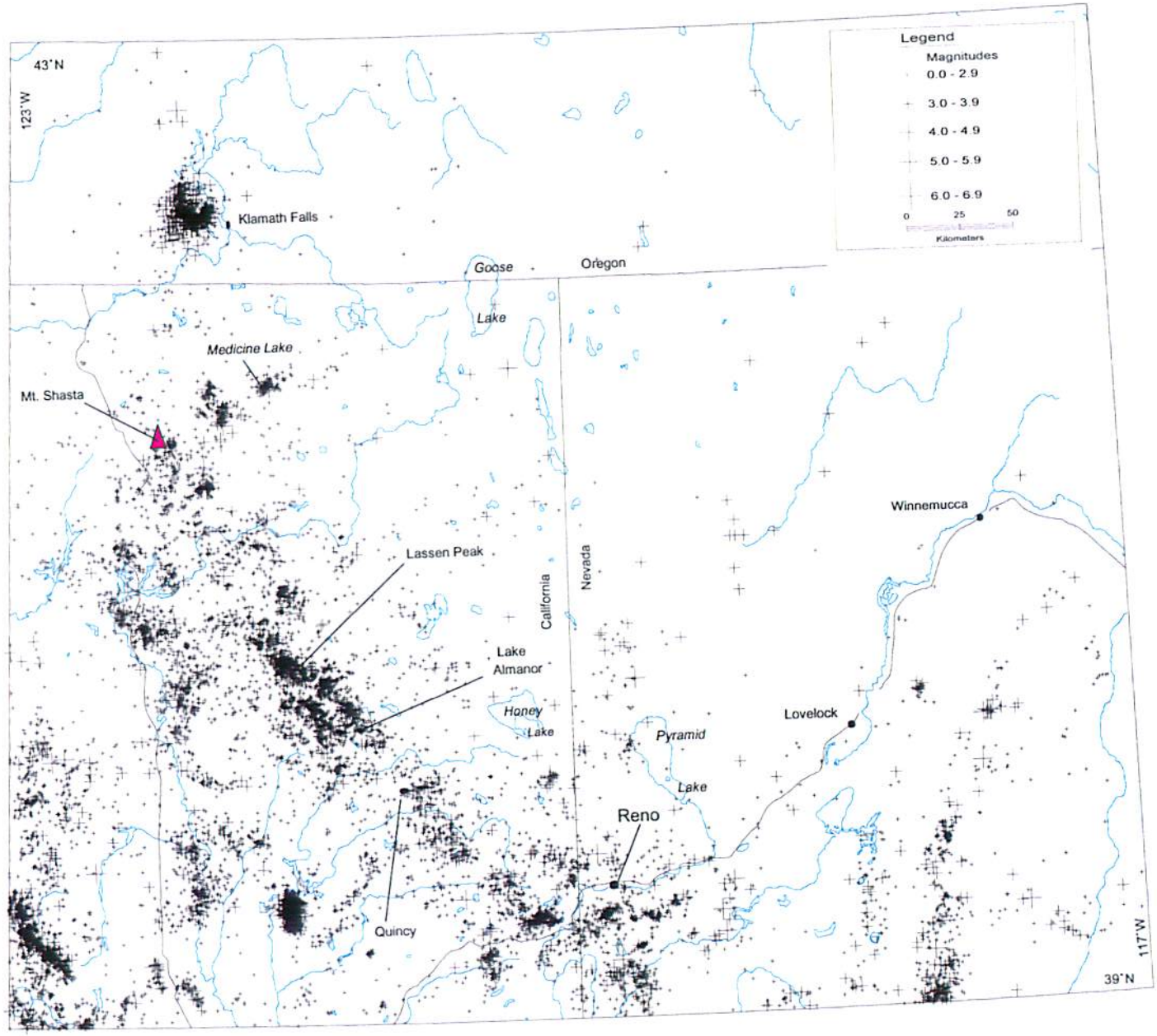

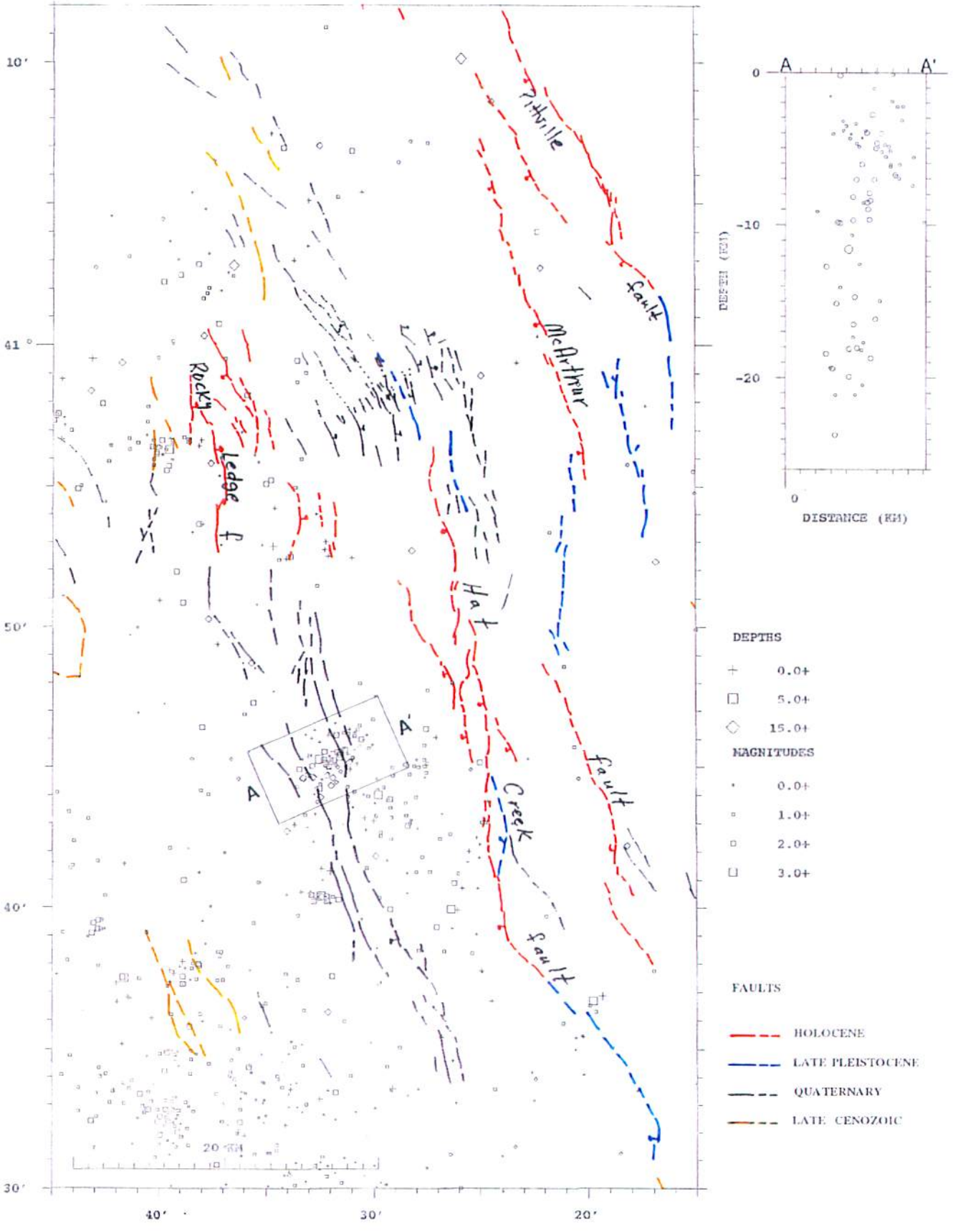

Figure 4. Map of the Hat Creek fault zone showing faults mapped by Sawyer (1995) and earthquakes 1977 through 1994 (NCSN). Cross section A-A' predominantly consists of events from the October-December 1991 sequence.

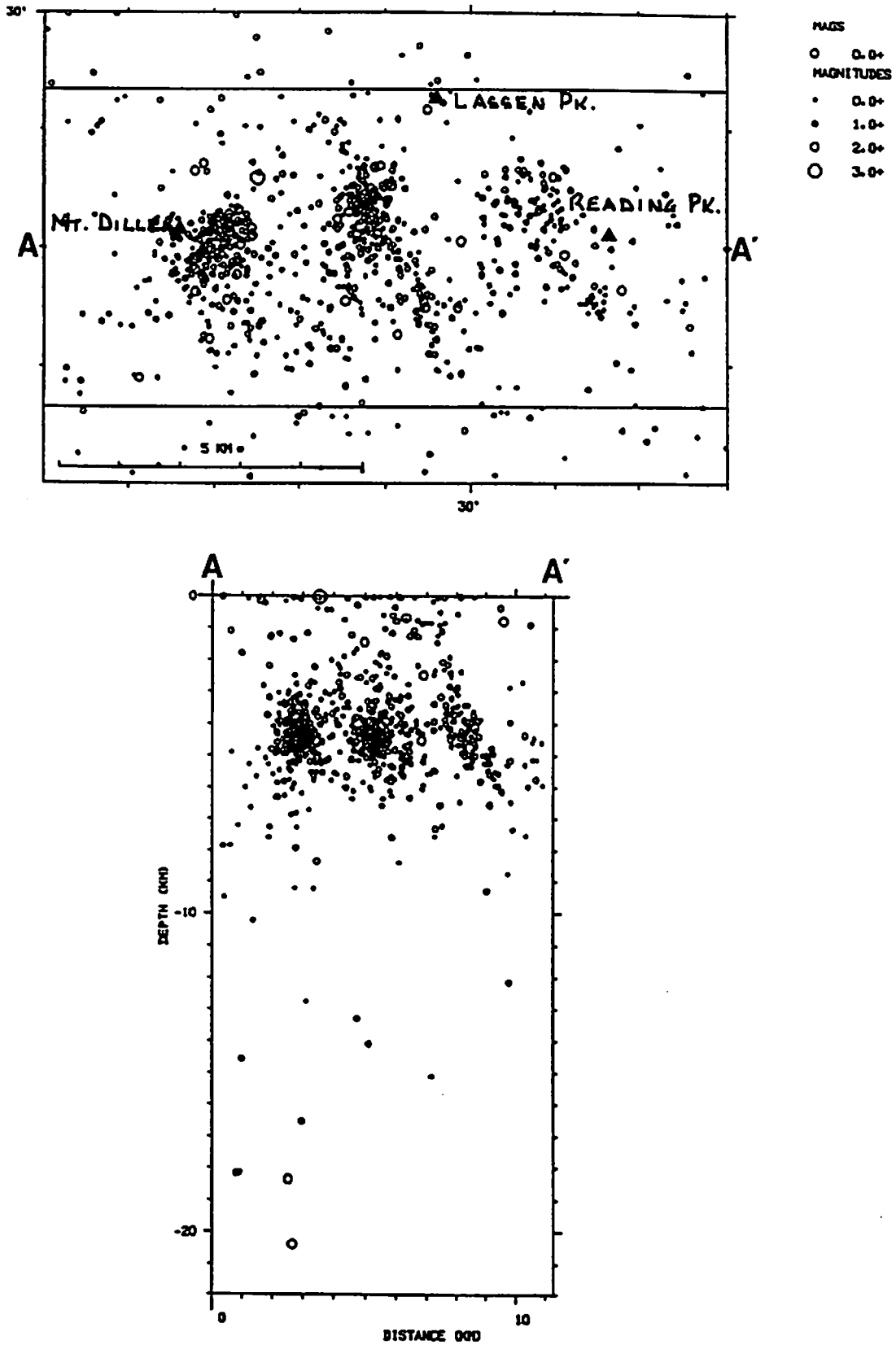

Figure 5. Map and cross section of Lassen seismicity, 1977 through 1994 (NCSN).

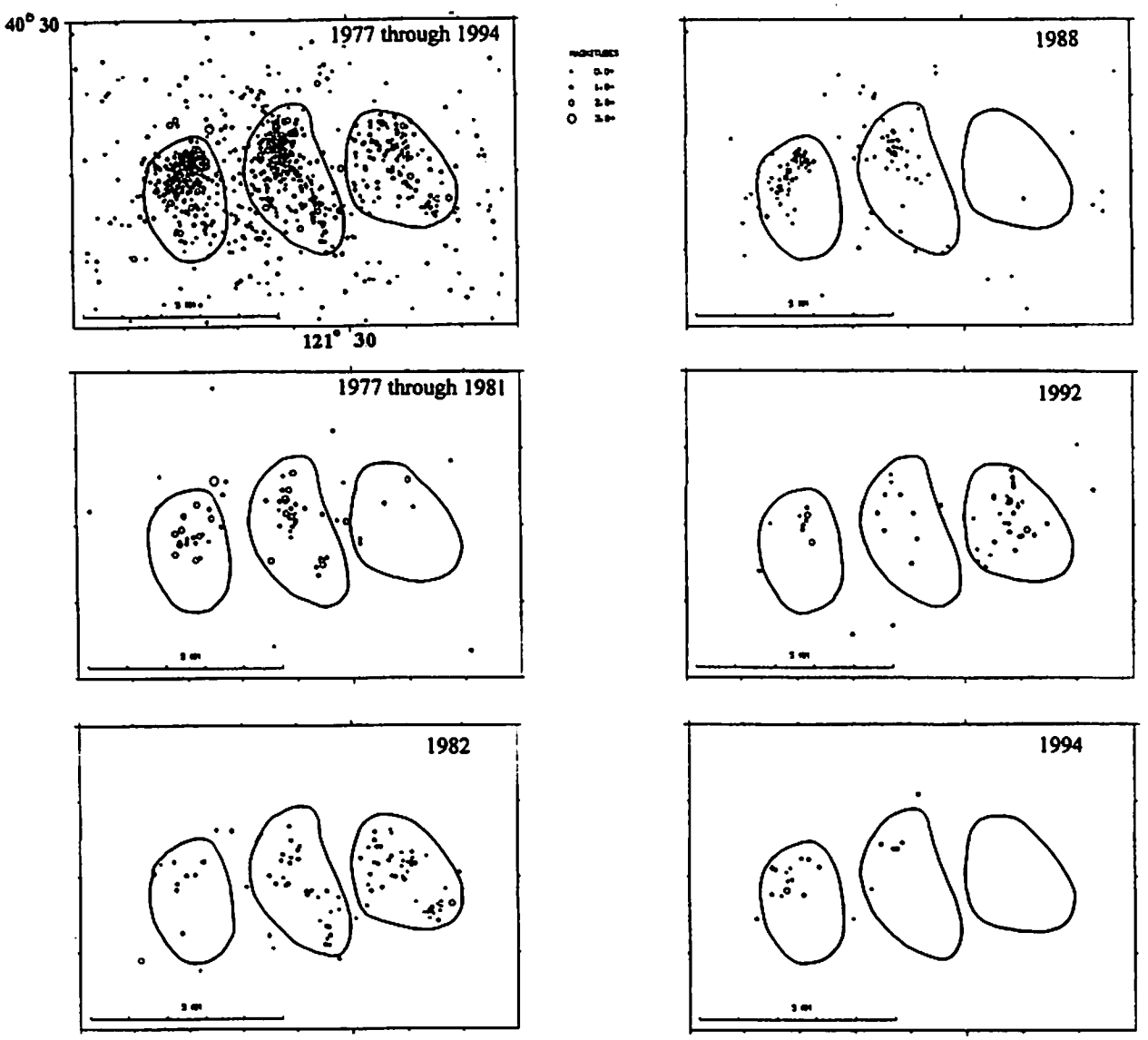

Figure 6. Selected time-slice maps of the Lassen area. The approximate boundaries of the three prominant clusters are circled. Data are from the NCSN.

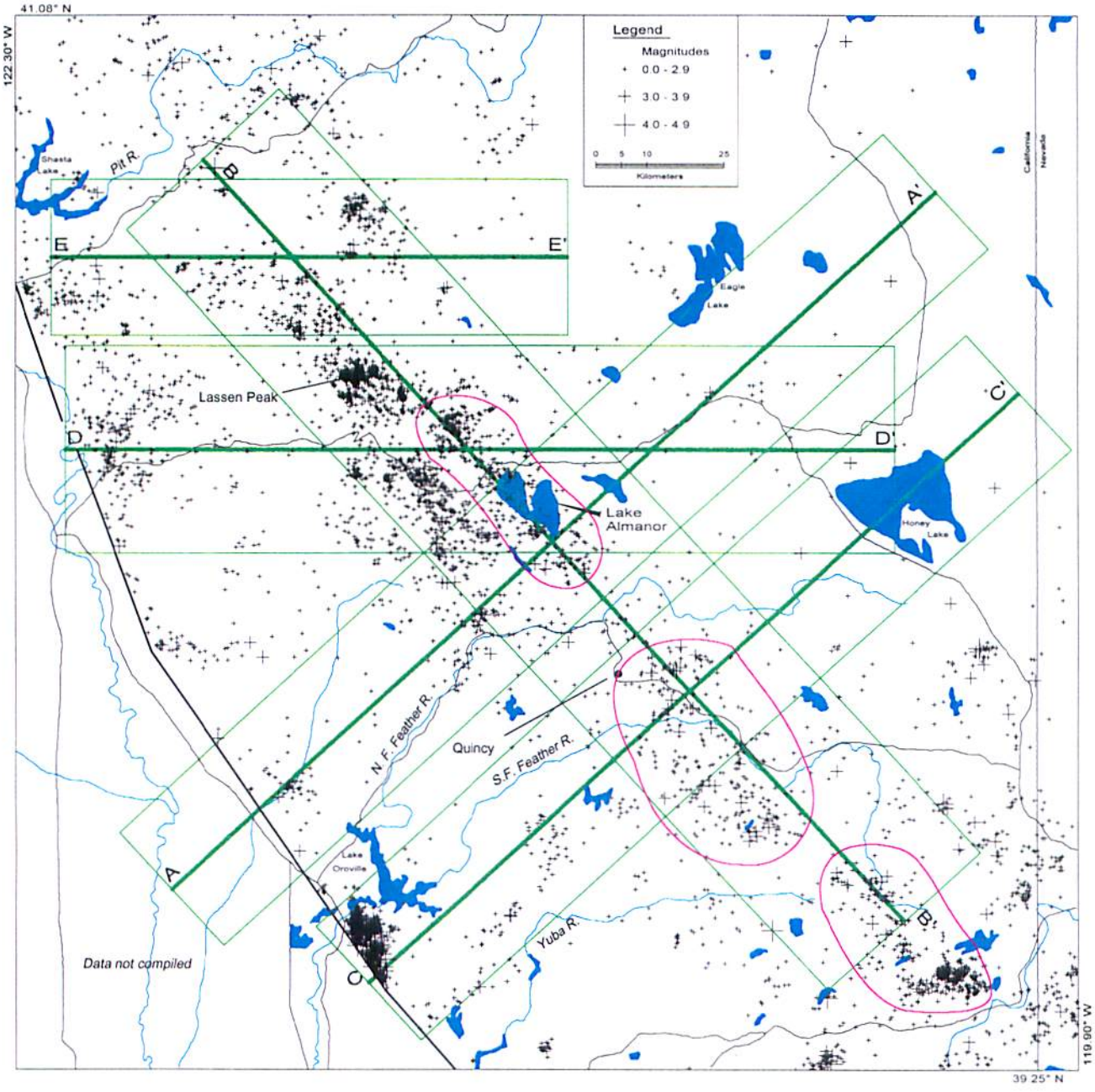

Figure 7. Earthquake epicenters in the Lake Almanor region during the period 1970 through 1994. Data from the NCSN. The bold green lines represent the plane of seismicity cross-sections drawn through the region. The lighter weight lines represent the area from which data are projected onto the cross-section. The red elipses refer to earthquake clusters along the Sierra Nevada -Great Basin boundary zone discussed in the text.

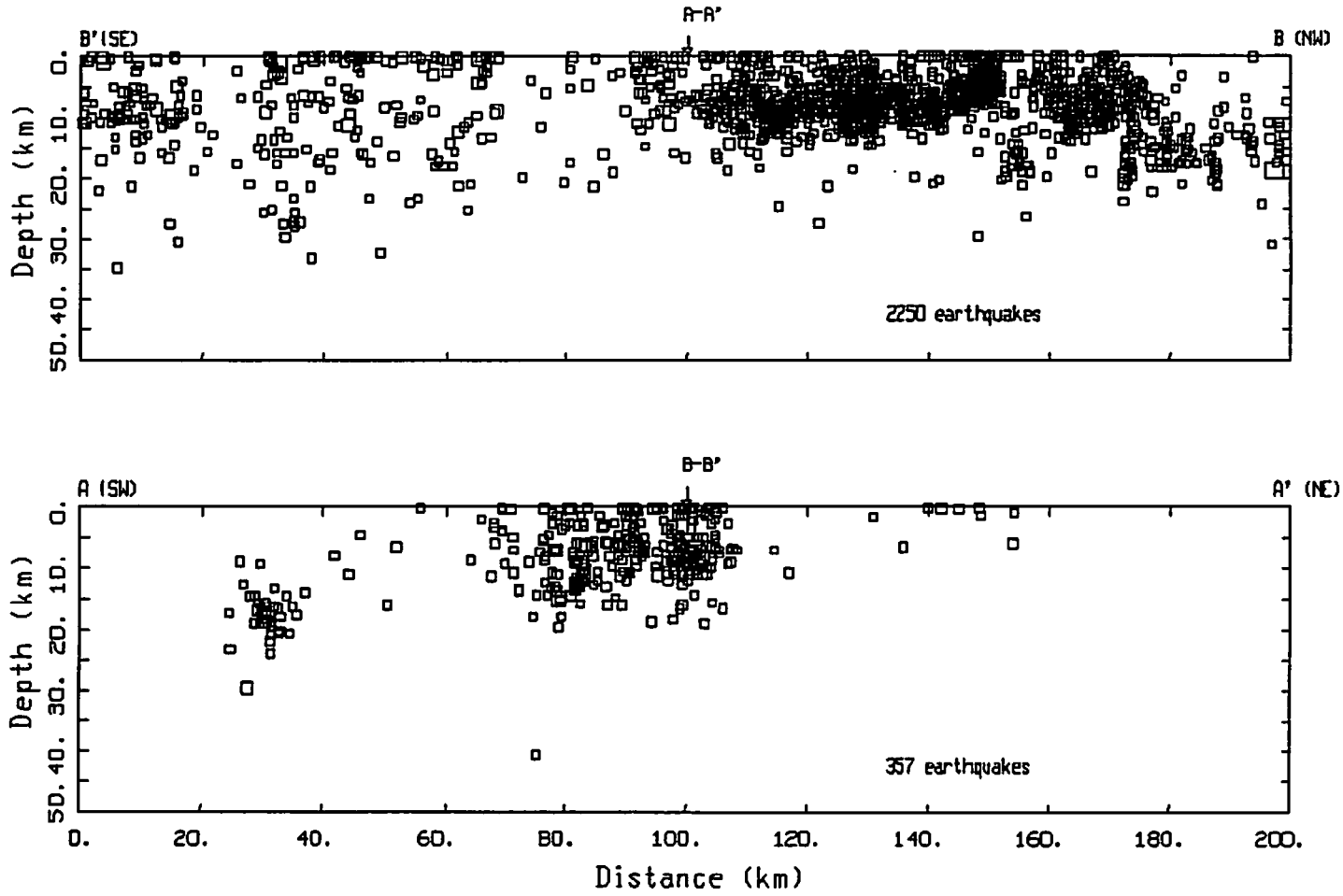

Lake Almanor Region

Figure 8. Seismicity cross-sections in the Lake Almanor region, see Figure 7 for location. No vertical exaggeration.

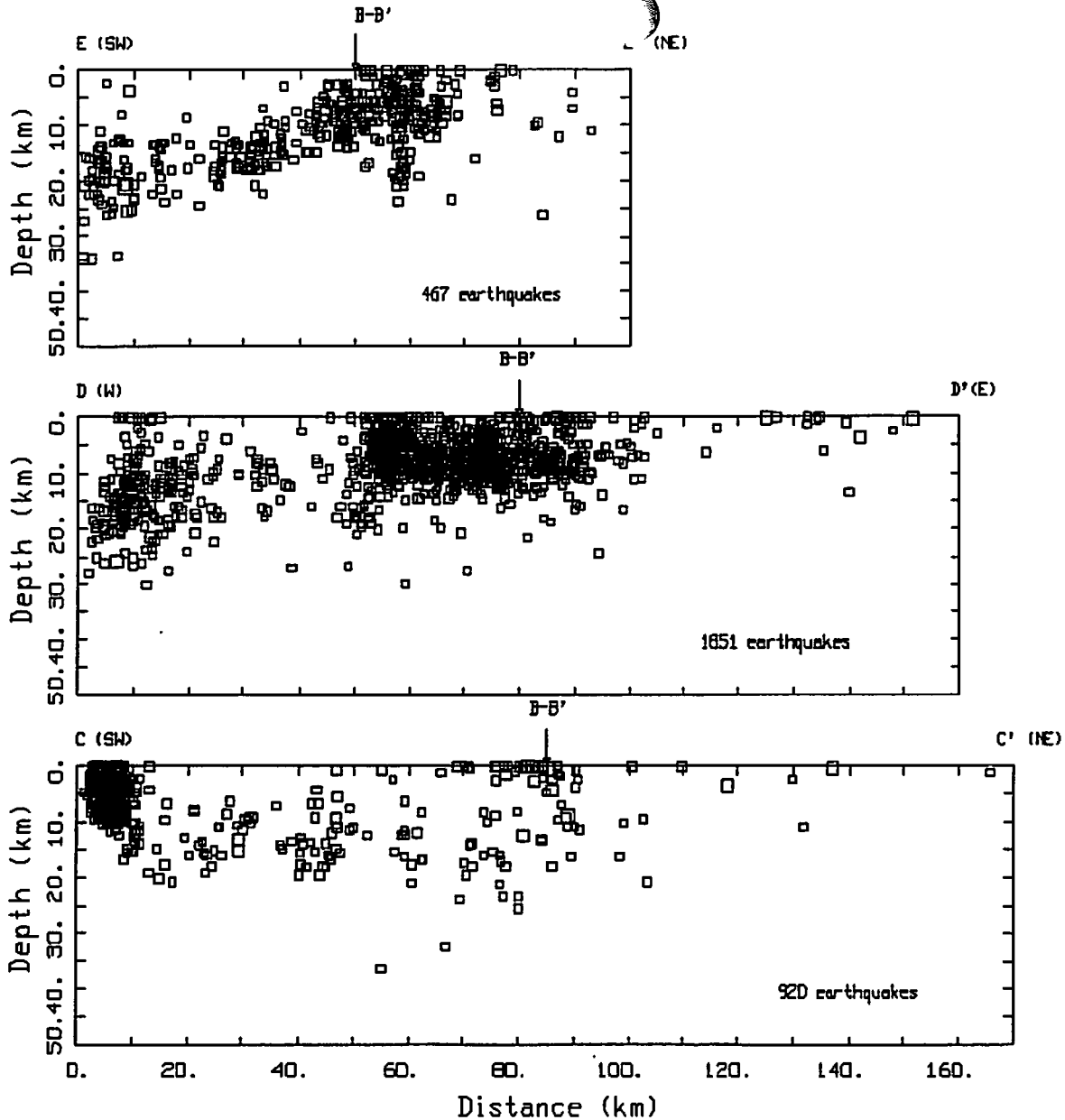

Lake Almanor Region

Figure 9. Seismicity cross-sections in the Lake Almanor region, see Figure 7 for location. No vertical exaggeration.

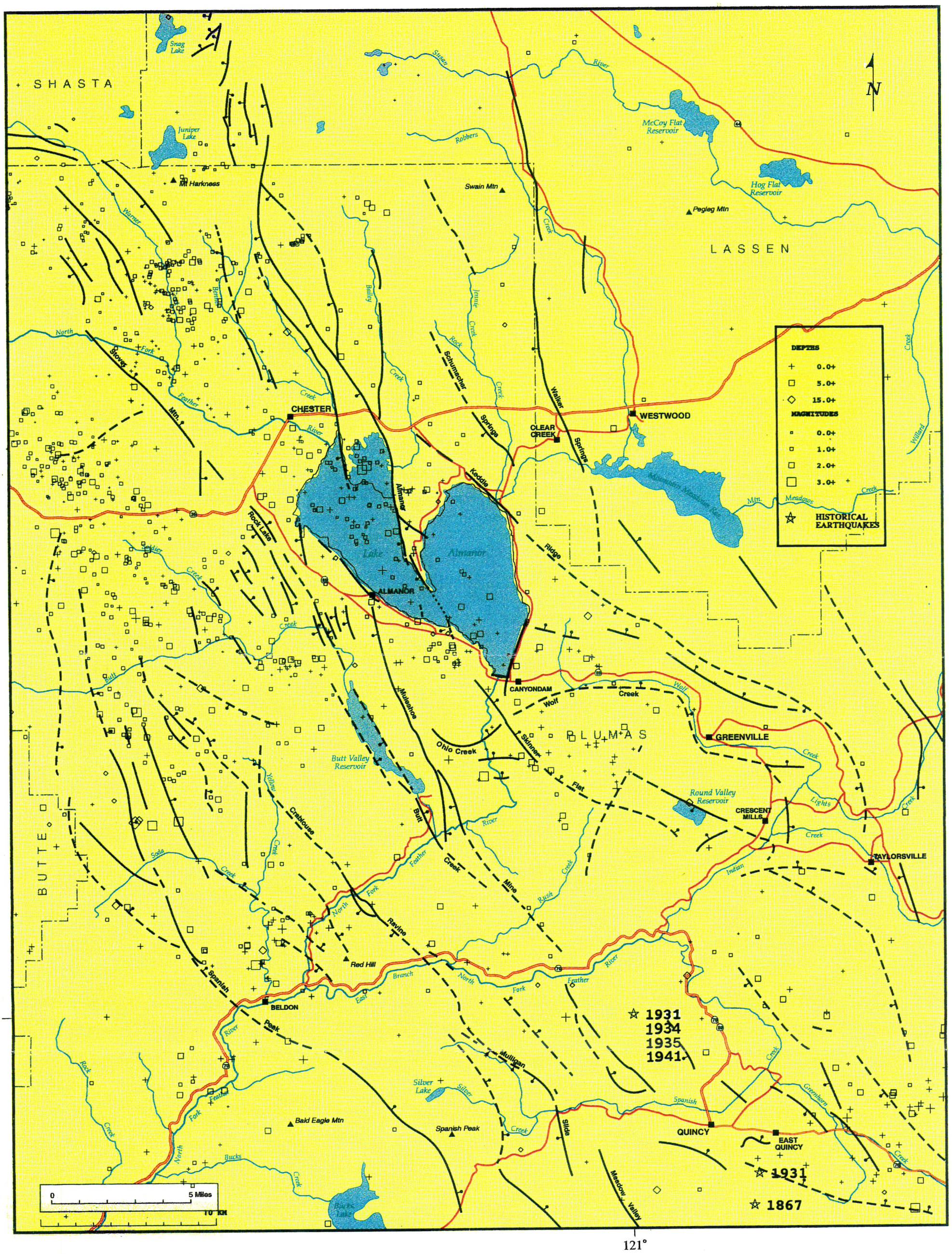

Figure 10. Pre-1970 historical earthquakes and instrumental seismicity from 1977 through 1994 (NCSN). Quaternary faults by Sawyer (1995).

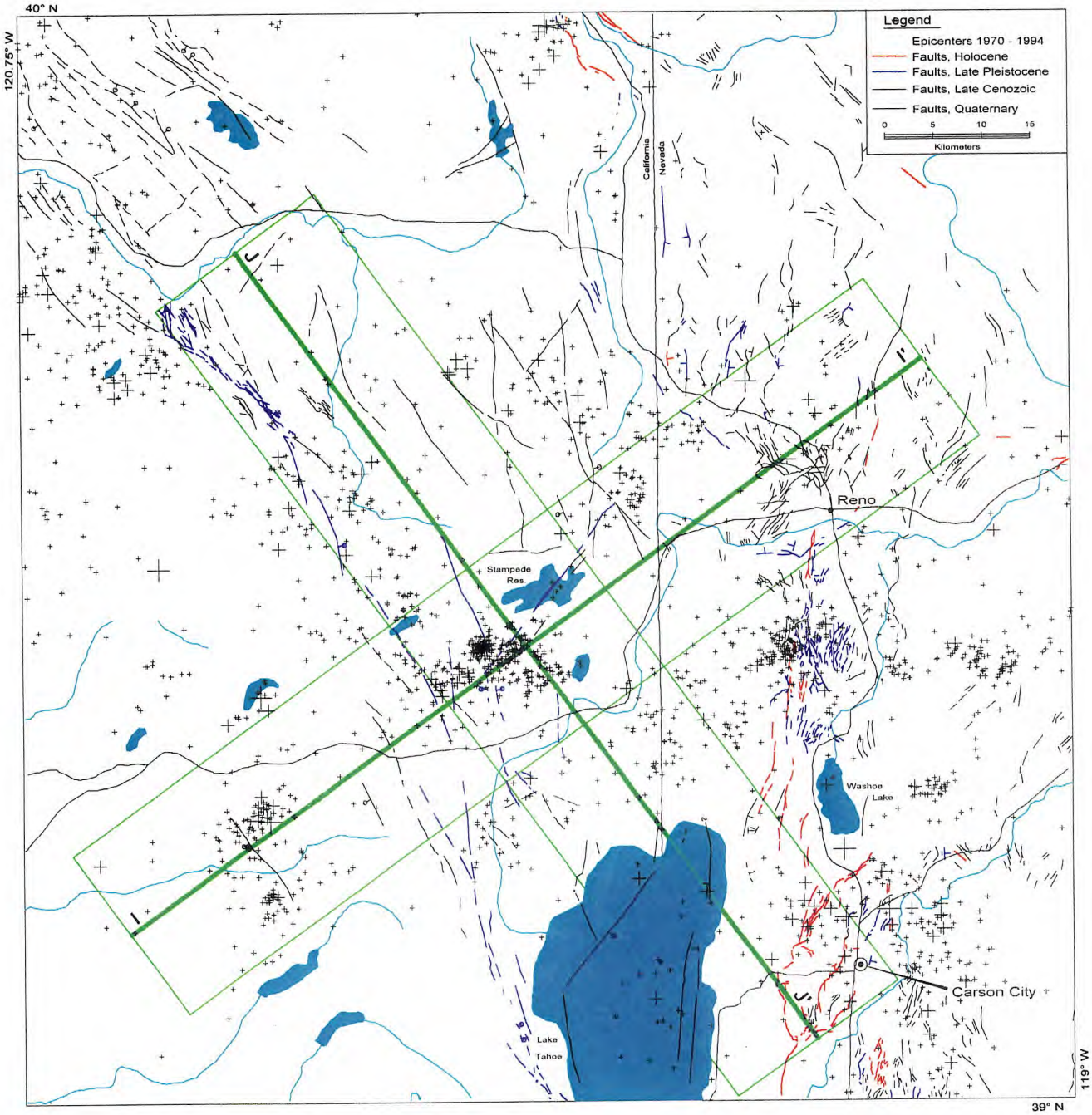

Figure 11. Earthquakes located in the north Lake Tahoe region from 1970 through 1994. Data from NCSN. Green lines show location of seismicity cross-sections.

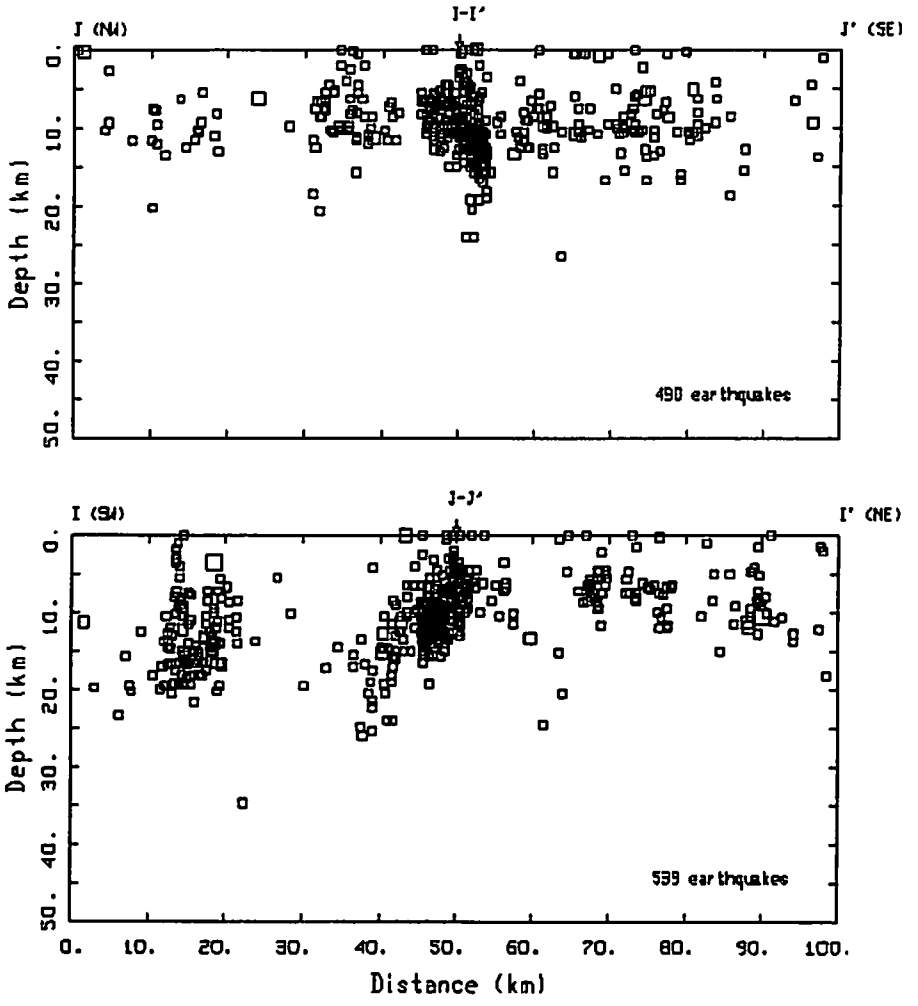

North Lake Tahoe Region

Figure 12. Seismicity cross-sections in the north Lake Tahoe region, see Figure 11 for location. No vertical exaggeration.

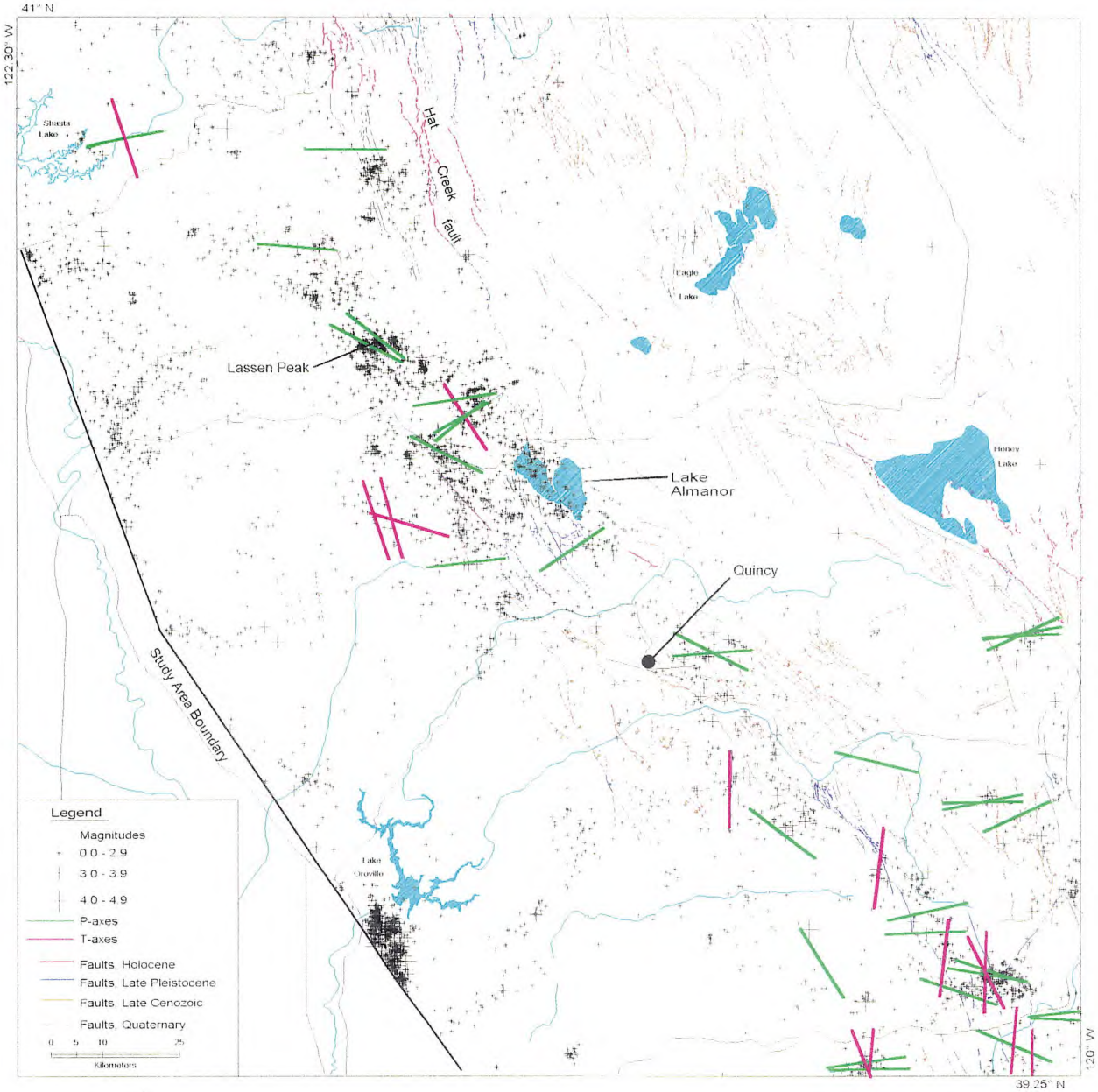

Figure 13. Map of Lake Almanor region showing earthquake epicenters from 1970 through 1994, Cenozoic faults.(Sawyer, 1995), and P- and T-axes from selected focal mechanisms. The P-axes (magenta lines) are the maximum principal stress axes. The T-axes (green lines) are the minimum principal stress axes. Only those axes with plunges within 20 degrees of horizontal are shown.

APPENDIX B

A. Late Cenozoic tectonics of great Walker Lane belt and implications for active deformation in the Almanor region, northeastern California

Unruh, J.R.

Late Cenozoic Tectonics of the Greater Walker Lane Belt and Implications for Active Deformation in the Lake Almanor Region, Northeastern California

Jeffrey R. Unruh
William Lettis & Associates
1777 Botelho Drive, Suite 262
Walnut Creek, CA 94596

Abstract

Regional patterns of late Cenozoic faulting and modern seismicity show that deformation in a 100-300 km wide region in eastern California and western Nevada primarily accommodates northward translation and counterclockwise rotation of the Sierran block, rather than distributed motion of the Pacific plate with respect to stable North America as defined by the NUVEL-1 model. Space-based geodetic studies define the independent motion of the Sierran block microplate as counterclockwise rotation about an Euler pole located off the coast of southern California (lat 32°N, long 128°W). Faults in the eastern California shear zone, Walker Lane belt and Tahoe-Medicine Lake trough lie within an approxmately 100 km wide region bounded by two small circles drawn about the Sierran block Euler pole, and collectively comprise what is referred to in this paper as the greater Walker Lane belt. Strike-slip faults in the greater Walker Lane belt typically are subparallel to small circles drawn about the Sierran block Euler pole, and major normal faults exhibit a left-stepping en echelon geometery with respect to the small circles that is consistent with accommodation of dextral shear parallel to motion of the microplate. The Lake Almanor region lies within a broad releasing stepover along the eastern margin of the Sierran block microplate whereby dextral strike-slip faulting in the Mohawk Valley region is transferred to primarily extensional deformation in the Hat Creek graben. Kinematic analysis of earthquake focal mechanisms shows that the direction of macroscopic NW dextral shearing progressively rotates counterclockwise to more westerly orientations from south to north in the greater Walker Lane belt, subparallel to the trajectories of small circles about the Sierran block Euler pole. Macroscopic dextral shearing defined by the seismicity is only locally parallel to NUVEL-1 Pacific/North American plate motion. If this interpretation is correct, regional patterns of faulting and seismicity suggest that much of northern California west of the Tahoe-Medicine Lake trough is moving in the same direction, although perhaps at not the same rate, as the Sierran block microplate.

Introduction

The Lake Almanor study region is located within a 100-300 km wide zone of distributed late Cenozoic deformation that lies between the Sierra Nevada to the west and the Basin and Range to the east, and extends from the southern Mojave desert in southern California to at least as far north as the Oregon-California border (Figure 1). Although active seismicity and evidence for Quaternary faulting have been observed along most of the 1300 km length of this zone, workers have assigned different names to the southern, central and northern reaches. The southern reach, which extends across the central Mojave desert from the San Andreas fault to the Garlock fault, was named the "Eastern California shear zone" by Dokka and Travis (1990). The central reach, which extends from the Garlock fault northward to the south end of the Tahoe basin, is referred to in the literature as the "Walker Lane belt" (Stewart, 1988). The northern reach, which includes the Lake Almanor basin, extends from Lake Tahoe basin on the south to at least as far north as Klamath Lakes in southern Oregon, and was named the "Tahoe-Medicine Lake Trough" by Page et al. (1993). Most of the workers cited above have recognized or speculated that the individual reaches probably are part of a much longer, and probably continuous, zone of late Cenozoic deformation. For simplicity, the entire 1300 km zone is referred to in this paper

as the greater Walker Lane belt because this name has precedence in the literature (see Stewart, 1988, for a summary of previous work on the Walker Lane).

The predominant style of active deformation within the greater Walker Lane belt is distributed northwest dextral shear accommodated by strike-slip and normal faulting (Dokka and Travis, 1990; Wright, 1976; Stewart, 1988; VanWormer and Ryall, 1980; Page et al., 1993). Based on analysis of geodetic data, Sauber et al. (1994) determined that up to 12 mm/yr of northwest dextral shear strain is accommodated by distributed deformation in the central Mojave block (e.g. the Eastern California shear zone) at the southern end of the greater Walker Lane belt. Based on analysis of space geodetic data, Dixon et al. (1995) estimated that distributed deformation at the latitude of Owens Valley between the Sierra Nevada and a site at Ely, Nevada, accommodates approximately 9 mm/yr of northwest dextral shear strain, with the bulk of active deformation occurring within the greater Walker Lane belt. Northwest dextral shear strain probably extends into the northern reach of the greater Walker Lane belt (e.g. the Tahoe-Medicine Lake trough), because space-based geodetic studies show that an observation site at Quincy along or near the northeastern margin of the Sierra Nevada presently is moving approximately 8.9 mm/yr toward N64W (Dixon et al., 1995). Although space-based geodetic data are not available north of the Tahoe-Medicine Lake trough, characteristic northwest-directed motion of the greater Walker Lane belt may extend north of the California border. Based on a kinematic analysis of late Cenozoic faulting, Pezzopane and Weldon (1993) concluded that distributed faulting in a broad, northwest-trending zone between eastern Oregon and central Washington probably accommodates a minimum of 3 mm/yr of northwest-directed motion.

The rate and direction of the northwestward displacement of the Sierra Nevada indicated by Very Long Baseline Interferometry (VLBI) geodesy suggests that up to 22-25% of the total motion between the Pacific and North American plates is taken up by distributed deformation in the greater Walker Lane belt and the Basin and Range province (Argus and Gordon, 1991). The VLBI data also indicate, however, that distributed shearing in the Walker Lane belt does not exclusively accommodate Pacific/North American plate motion. This clearly is shown by the N64W motion of the VLBI station at Quincy, which lies along the eastern margin of the Sierra Nevada and is moving approximately 28° more westerly than the N36W azimuth of Pacific/North American plate motion given by the NUVEL-1 plate motion model. Argus and Gordon (1991) found that the motion of the Sierra Nevada with respect to stable North America is defined by counterclockwise rotation about an Euler pole located at lat 32° N, long 128°W, which lies approximately 10° southwest of the Sierran block off the coast of western California. The motion predicted by the Sierran Euler pole includes a component of counterclockwise rotation of the Sierra block in addition to northwest translation, which accounts for the more westerly motion of the VLBI site at Quincy than predicted by the NUVEL-1 Pacific/North American plate model. Argus and Gordon (1991) concluded that the Sierra Nevada and Central Valley of California together comprise a microplate that moves independently of distributed Pacific/North American plate motion.

This interpretation of the behavior of the Sierran block, or microplate, has important implications for assessing the style of faulting in the greater Walker Lane belt, especially if distributed deformation primarily accommodates displacement of the Sierran block with respect to North America rather than Pacific/North American plate motion. If the motion of the Sierra Nevada with respect to North America is best defined by rotation about its independent Euler pole, then the trajectories of strike-slip faults in the greater Walker Lane belt that are most effectively oriented to accommodate this motion will be parallel to small circles drawn about the Euler pole, rather than parallel to the N36W azimuth of Pacific/North American plate motion given by the NUVEL-1 model. In addition, the direction of maximum northwest dextral shear in the greater Walker Lane belt will not be

constant, but rather will vary systematically from south to north in order to follow curving trajectories described by small circles about the Sierran block Euler pole.

This paper presents an analysis of regional patterns of faulting and seismogenic deformation in order to assess the relationships between deformation in the greater Walker Lane belt, motion of the Sierran block microplate, and distributed Pacific-North American plate motion. The implications for late Cenozoic faulting in the Lake Almanor region also are discussed.

Late Cenozoic Faulting in the Greater Walker Lane Belt

Most late Cenozoic and active faults in the greater Walker Lane belt lie within a 100 km wide region bounded by two small circles drawn about the Sierra Nevada Euler pole (Figure 1). At the southern end of the greater Walker Lane belt, the 100 km wide region encompassed by the two small circles passes through the central Mojave block and includes most of the distributed shearing in what is formally defined as the Eastern California shear zone (Dokka and Travis, 1990; Sauber et al., 1994). At the latitude of Owens Valley north of the Garlock fault, the 100-km-wide region spanned by the small circles borders the eastern margin of the Sierra Nevada and encompasses the major active strike-slip faults within the formally defined Walker Lane belt of Stewart (1988), including the Owens Valley fault, Panamint Valley-Hunter Mountain fault zone, and Death Valley-Furnace Creek fault zone. These strike-slip faults generally are subparallel to the trajectories of the small circles. Extensional step-overs between the strike-slip faults are bounded by north-northeast-striking normal faults in Eureka Valley and Deep Springs Valley (Figure 1) that are oblique to the trajectories of the small circles.

At approximately lat 38°N, and continuing at least as far north as the Lake Tahoe basin, the major late Cenozoic faults that comprise the Sierra Nevada frontal fault system assume a more northerly orientation with respect to the small circles about the Euler pole, and exhibit a left-stepping, en echelon geometry (Figure 1). The map-scale pattern of the Sierran frontal fault system in this reach of the greater Walker Lane belt is consistent with accommodation of distributed dextral shear parallel to the trajectories of the small circles by extension within a series of left-stepping normal faults. The only major dextral strike-slip fault within this reach of the greater Walker Lane belt is the Walker Lake fault in west-central Nevada (Figure 1), which appears to be approximately parallel to the trajectories of the small circles at this latitude.

A significant change in the pattern and locus of faulting occurs at the latitude of Lake Tahoe. Normal faults bounding the Lake Tahoe basin form a right-stepping pattern with respect to the trajectories of the small circles, indicating that slip along the eastern margin of the Sierra Nevada is being transferred to a more easterly locus of deformation that includes the primarily dextral Mohawk Valley and Honey Lake faults (Figure 1). Examination of the fault patterns with respect to the small circle trajectories shows that the Owens Valley fault and the series of normal faults bordering the Sierra Nevada between Lake Tahoe and Owens Valley lie along a more westerly small circle than either of the Mohawk Valley or Honey Lake faults. The change in the geometry of the Sierran frontal fault system at the latitude of Lake Tahoe is thus interpreted as a releasing step-over within the greater Walker Lane belt, where the locus of dextral shearing is transferred in a right-stepping pattern with respect to the trajectories of the small circles about the Sierran Euler pole. This interpretation is consistent with the conclusion of Page et al. (1993) that normal faults bordering the Lake Tahoe basin represent the northern continuation of the Sierran frontal fault system.

Both the Mohawk Valley and Honey Lake strike-slip faults appear to be subparallel to the trajectories of the small circles (Figure 1), consistent with motion about the Sierran block Euler pole. Note that the strike-slip faults in the region between the Lake Tahoe and Lake Almanor basins trend approximately 25°-30° more westerly than strike-slip faults at the latitude of Owens Valley. In the Lake Almanor basin, structural and tectonic trends turn abruptly to the north, diverging from the trajectories of the small circles and assuming the geometry of a releasing stepover similar to the eastward transfer of slip at the latitude of Lake Tahoe. This geometry is consistent with development of the Almanor structural depression and the north-northwest-trending Hat Creek graben north of the Lake Almanor basin. If correct, this interpretation suggests that much of northern California west of the Hat Creek graben is moving in the same direction as the Sierran microplate.

Kinematic Analysis of Seismogenic Deformation

In addition to regional patterns of late Cenozoic faulting, seismicity in the greater Walker Lane belt was analyzed to evaluate the kinematics of active, seismogenic deformation. The analysis consisted of inverting seismic P and T axes from earthquake focal mechanisms to obtain a reduced strain rate tensor for selected domains. The theoretical basis for the inversion is discussed in Twiss et al. (1993), and the analytical approach is presented in detail in Unruh et al. (in review). The best-fit model obtained from the inversion provides the orientation of the principal strain rate axes, a scalar parameter D that characterizes the shape of the strain rate ellipsoid, and a scalar parameter W that describes the contribution of independent block rotations to the direction of coseismic slip. This analysis focuses on the orientation of the principal strain rate axes obtained from the inversion. The orientations of the principal strain rate axes for domains in the greater Walker Lane belt are shown graphically in Figure 2.

Results of the inversion analysis show that seismogenic deformation in the greater Walker Lane belt primarily accommodates horizontal plane strain deformation. With only a few exceptions, seismogenic deformation in the greater Walker Lane belt is characterized by subhorizontal shortening directed approximately north-south, and subhorizontal extension directed approximately east-west (Figure 2). Both of the principal strain rates are approximately equal and opposite in magnitude. This deformation geometry is consistent with dextral faulting on northwest-southeast-striking faults, sinistral faulting on northeast-southwest-striking faults, normal faulting on north-striking faults, and is consistent with previous analyses of seismogenic deformation in the central reach of the greater Walker Lane belt (VanWormer and Ryall, 1980). Because the general trend of the greater Walker Lane belt is northwest-southeast, distributed shearing in this zone indicated by analysis of seismicity is interpreted to primarily accommodate northwest-directed dextral simple shear.

Because the inversion approach used in this analysis is kinematically-based (e.g. designed to obtain a strain rate or deformation rate tensor, rather than a stress tensor; see discussion in Twiss et al., 1993), the orientation of the principal strain rates axes can be used to determine the direction of the maximum rate of dextral shearing, which should bisect the principal axes in the northwest and southeast quadrants. Figure 3 shows that the predicted direction of maximum dextral shear from the inversion analysis progressively rotates counterclockwise from south to north along the greater Walker Lane belt, subparallel to the trajectories of small circles drawn about the Sierra Nevada/North American Euler pole. The counterclockwise rotation of the principal strain rate axes and direction of NW dextral shearing is especially pronounced in the Lake Almanor region. The results of the inversion analysis (Figure 3) clearly show that the direction of seismogenic dextral shearing in the greater Walker Lane belt only locally is parallel to the N36W direction of shearing predicted by the NUVEL-1 model for Pacific/North American plate motion.

Formation of Quaternary Tectonic Basins in the Lake Almanor Region
The Lake Almanor basin lies within a reach of the greater Walker Lane belt where motion of the Sierran block microplate shifts from being accommodated by strike-slip faulting in the Mohawk Valley region, to extension and normal faulting in the Hat Creek graben. In a general sense, therefore, the development of numerous Quaternary tectonic basins in the study area is consistent with the presence of a broad, releasing stepover in the greater Walker Lane belt. The geometry of late Cenozoic faults, the motion of the Quincy VLBI site, and the inversion of local earthquake focal mechanisms suggest that the direction of maximum dextral shearing in the lake Almanor region ranges between N50W and N75W. For the following discussion of late Cenozoic faulting in the Almanor region, the N64W motion of the VLBI site at Quincy (Dixon et al., 1995) is adopted as as the most likely direction of maximum dextral shearing.

The transition from primarily strike-slip faulting in Mohawk Valley to extension in the north-northwest-trending Hat Creek graben occurs within a 30-50 km-wide zone that extends approximately from Quincy southeast of Lake Almanor, to the vicinity of Humbug Valley southwest of Lake Almanor. From southeast to northwest, late Cenozoic faults within this transitional region assume progressively more northerly orientations. For example, faults bounding the southwestern and northeastern margin of American Valley near Quincy strike approximately N70W and N40W, respectively, whereas the strike of faults in the vicinity of Butt Valley reservior to the northwest ranges from approximately N40W to almost due north-south. If the deformation in this 30-50 km wide region primarily accommodates distributed N64W dextral shear, then late Cenozoic faults should exhibit significant components of normal dip-slip separation as the general structural strike rotates to a more northerly orientation. Thus the appearance of numerous small tectonic basins such as Butterfly Valley, Meadow Valley, Humbug Valley, Round Valley and Indian Valley, many of which are bounded on one or more margins by faults that strike nearly due north-south, is consistent with distributed transtensional deformation in the region between Quincy and Lake Almanor.

In addition to the transitional nature of slip transfer from the Mohawk Valley region to the Hat Creek graben, the development of late Quaternary tectonic basins may be influenced by pre-existing structures in the Paleozoic and Mesozoic basement rocks. For example, bedding, cleavage, and the axial planes of folds in the vicinity of Butt Valley reservoir strike between N22W and N50W (data taken from compilation by J. Hannah and E. Moores, unpublished bedrock mapping), with an average orientation of approximately N30W. This range of orientations for pre-existing bedrock structures is similar to the general N25W to N45W strike of faults in the combined Butt Creek-Stover Mountain fault system, but oriented 20° to 30° more northerly of the assumed N64W direction of macroscopic dextral shear. This comparison suggests that the general strike of the Butt Creek-Stover Mountain fault system may be more strongly influenced by pre-exisiting basement structures than the regional direction of shearing. If so, the more northerly trend of the basement fabric favors formation of right-normal oblique faults instead of dextral strike-slip faults.

Structural and neotectonic relations in the vicinity of Round Valley provide additional support for the hypothesis that basement structures may have influenced the development of late Cenozoic faults. The southwest-side down normal or oblique-slip fault that forms the northeastern margin of the late Cenozoic Round Valley basin lies along the mapped trace of the southwest-dipping Mesozoic Grizzly Mountain thrust fault (J. Hannah and E. Moores, unpublished bedrock mapping). The coincidence of the two structures strongly suggests that the Grizzly Mountain thrust has been locally reactivated as a normal or oblique-slip fault to form the modern Round Valley basin. A possibly analogous example

of reactivation of Mesozoic thrust faults as late Cenozoic normal faults in the Idaho-Wyoming thrust belt was documented by West (1993).

Based on these observations, the local transtensional nature of distributed deformation in the Lake Almanor region can be explained by (1) the progressive transition from strike-slip deformation in the Mohawk Valley area to extension in the Hat Creek graben across a 30-50 km wide region, and (2) the possible influence of pre-existing Mesozoic basement structure on the development and geometry of late Cenozoic faults. Speculatively, the apparent control exerted by pre-existing structures in Lake Almanor region may reflect an immature stage of development of late Cenozoic faults such as the Butt Creek-Stover Mountain fault system. These structures may be so youthful and/or have such a low slip rate that they have not yet formed an integrated through-going rupture plane that extends laterally and vertically through the seismogenic crust, and thus the pattern of faulting in the shallow crust is strongly influenced by the anisotropy associated with the Mesozoic structural fabric. If this interpretation is correct, the influence of the pre-existing basement structures will diminish as the faults become more integrated and mature, as suggested by West (1992) for reactivation of Mesozoic thrust faults in the Intermountain seismic belt as late Cenozoic normal faults.

Summary

Based on this analyses, distributed deformation in the greater Walker Lane belt, which includes the Eastern California shear zone, Walker Lane and Tahoe-Medicine Lake trough, is interpreted to primarily accommodate motion of the Sierran block microplate with respect to stable North America, rather than distributed Pacific/North American plate motion. Major late Cenozoic faults within the greater Walker Lane belt that are parallel to small circles drawn about the independent Sierra Nevada/North America Euler pole (Argus and Gordon, 1991), such as the Owens Valley, Walker Lake, Honey Lake and Mohawk Valley faults, are predominantly dextral strike-slip faults. Major late Cenozoic faults that are oriented oblique to and strike somewhat easterly of small circle trajectories, such as the Sierra Nevada frontal fault system north of Owens Valley and faults bounding the Lake Tahoe basin, primarily accommodate extension and exhibit left-stepping, en echelon geometries consistent with right-releasing transfers of deformation to more easterly small circles.

The Lake Almanor study area is located within a large releasing stepover between the dextral Mohawk Valley fault system and the extensional Hat Creek graben. The orientation of major right-lateral strike-slip faults in the Lake Almanor region predicted by this model is approximately N50W to N75W, which is consistent with the N64W motion of the VLBI site at Quincy (Dixon et al., 1995) but directed approximately 15° to 35° more westerly of the N36W azimuth of Pacific/North American plate motion predicted by the NUVEL-1 model. The more northerly strike of late Cenozoic faults in the Lake Almanor region relative to the approximately N64W direction of maximum dextral shear suggests that the structures should accommodate components of normal dip-slip separation, consistent with the development of numerous small tectonic basins. Pre-existing structural fabric in the basement may have exerted some control on the development of late Cenozoic faults in the Lake Almanor region.

Acknowledgements

I wish to thank Pacific Gas & Electric Company for the opportunity to study the tectonics of the Lake Almanor region and the greater Walker Lane belt. The ideas and interpretations in this paper were developed through conversations with Jim Humphrey, Rob Twiss, Tom Sawyer, John Wakabayashi, Bill Page, Keith Kelson, Bill Lettis, Marsha McLaren,

Kathryn Hanson and Eldridge Moores. Comments by Bill Lettis and Bill Page on an early draft of the manuscript greatly improved the paper.

References

Argus, D.F., and Gordon, R.G., 1991, Current Sierra Nevada-North American motion from very long baseline interferometry: implications for the kinematics of the western United States: Geology, v. 19, p. 1085-1088.

Dixon, T.H., Robaudo, S., Lee, J., and Reheis, M.C., 1995, Constraints on present-day Basin and Range deformation from space geodesy: Tectonics, v. 14, p. 755-772.

Dokka, R.K., and Travis, C.J., 1990, Late Cenozoic strike-slip faulting in the Mojave desert: Tectonics, v. 9, p. 311-340.

Page, W.D., Sawyer, T.L., McLaren, M.K., Savage, W.U., and Wakabayashi, J., 1993, The Quaternary Tahoe-Medicine Lake trough: the western margin of the Basin and Range transition, NE California: Geological Society of America Abstracts with Programs, Cordilleran and Rocky Mountain sections, v. 25, no. 5, p. 131.

Pezzopane, S.K., and Weldon, R.J. II, 1993, Tectonic role of active faulting in central Oregon: Tectonics, v. 12, p. 1140-1169.

Sauber, J., Thatcher, W., Solomon, S.C., and Lisowski, M., 1994, Geodetic slip rate for the eastern California shear zone and recurrence time of Mojave desert earthquakes: Nature, v. 367, p. 264-266.

Savage, J.C., Lisowski, M., and Prescott, W.H., 1990, An apparent shear zone trending north-northwest across the Mojave desert into Owens Valley, eastern California: Geophysical Research Letters, v. 17, p. 2113-2116.

Stewart, J.H., 1988, Tectonics of the Walker Lane belt, western Great Basin: Mesozoic and Cenozoic deformation in a zone of shear, in Ernst, W.G., ed., Metamorphism and cause of evolution of the western United States, Rubey Volume 7: Prentice-Hall, Englewood Cliffs, New Jersey, p. 683-713.

Twiss, R.J., Souter, B.J. and Unruh, J.R., 1993, The effect of block rotations on the global seismic moment tensor and patterns of seismic **P** and **T** axes: Journal of Geophysical Research, v. 98, p. 645-674.

Unruh, J.R., Twiss, R.J., and Hauksson, E., in review, Seismogenic deformation field in the Mojave Block and implications for the tectonics of the Eastern California shear zone: manuscript submitted to the Journal of Geophysical Research.

VanWormer, J., and Ryall, A., 1980, Sierra Nevada-Great Basin boundary zone: earthquake hazard related to structure, active tectonic processes and anomalous patterns of earthquake occurreence: Bulletin of the Seismological Society of America, v. 70, p. 1557-1572.

West, M.W., 1992, An integrated model for seismogenesis in the Intermontane Seismic Belt: Bulletin of the Seismological Society of America, v. 82, p. 1350-1372.

West, M.W., 1993, Extensional reactivation of thrust faults accompanied by coseismic surface rupture, southwestern Wyoming and north-central Utah: Geological Society of America Bulletin, v. 105, p. 1137-1150.

Wright, L., 1976, Late Cenozoic fault patterns and stress fields in the Great Basin and westward displacement of the Sierra Nevada block: Geology, v. 4, p. 489-494.

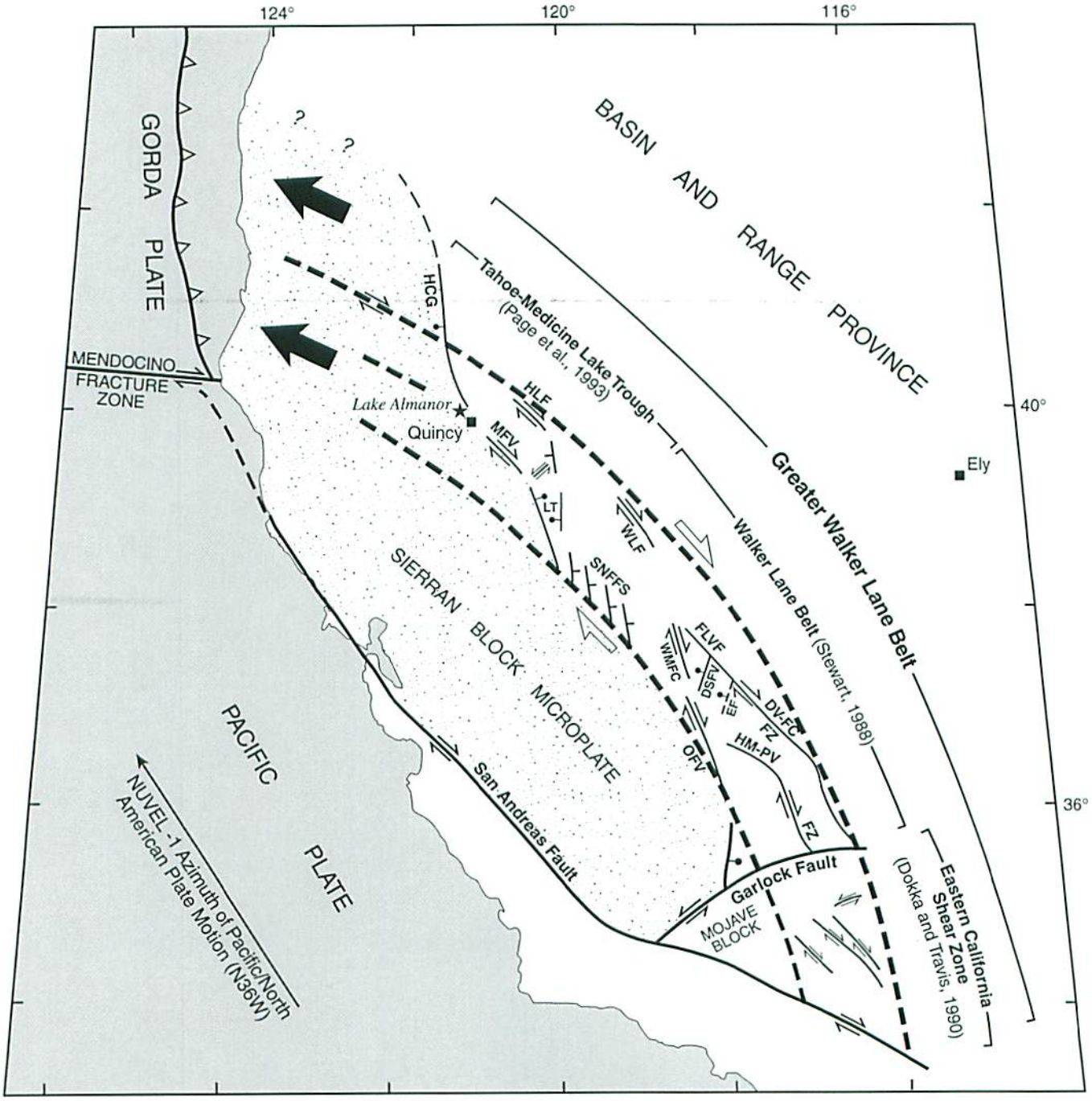

EXPLANATION

- Right-lateral strike-slip fault
- Normal fault; barb points toward hanging wall
- Trajectories of small circles drawn about Sierran Block Euler pole of rotation
- VLBI Observation Site

LT – Lake Tahoe Basin
HCG – Hat Creek Graben
HM-PV FZ – Hunter Mountain–Panamint Valley Fault Zone
DV-FC FZ – Death Valley–Furnace Creek Fault Zone
FLVF – Fish Lake Valley Fault Zone
OVF – Owens Valley Fault
EF – Eureka Valley Fault
DSFV – Deep Spring Valley Fault
WMFZ – White Mountain Fault Zone
SNFFS – Sierra Nevada Frontal Fault System
WLF – Walker Lake Fault
MVF – Mohawk Valley Fault
HLF – Honey Lake Fault

Figure 1. Major tectonic elements of the Greater Walker Lane Belt.

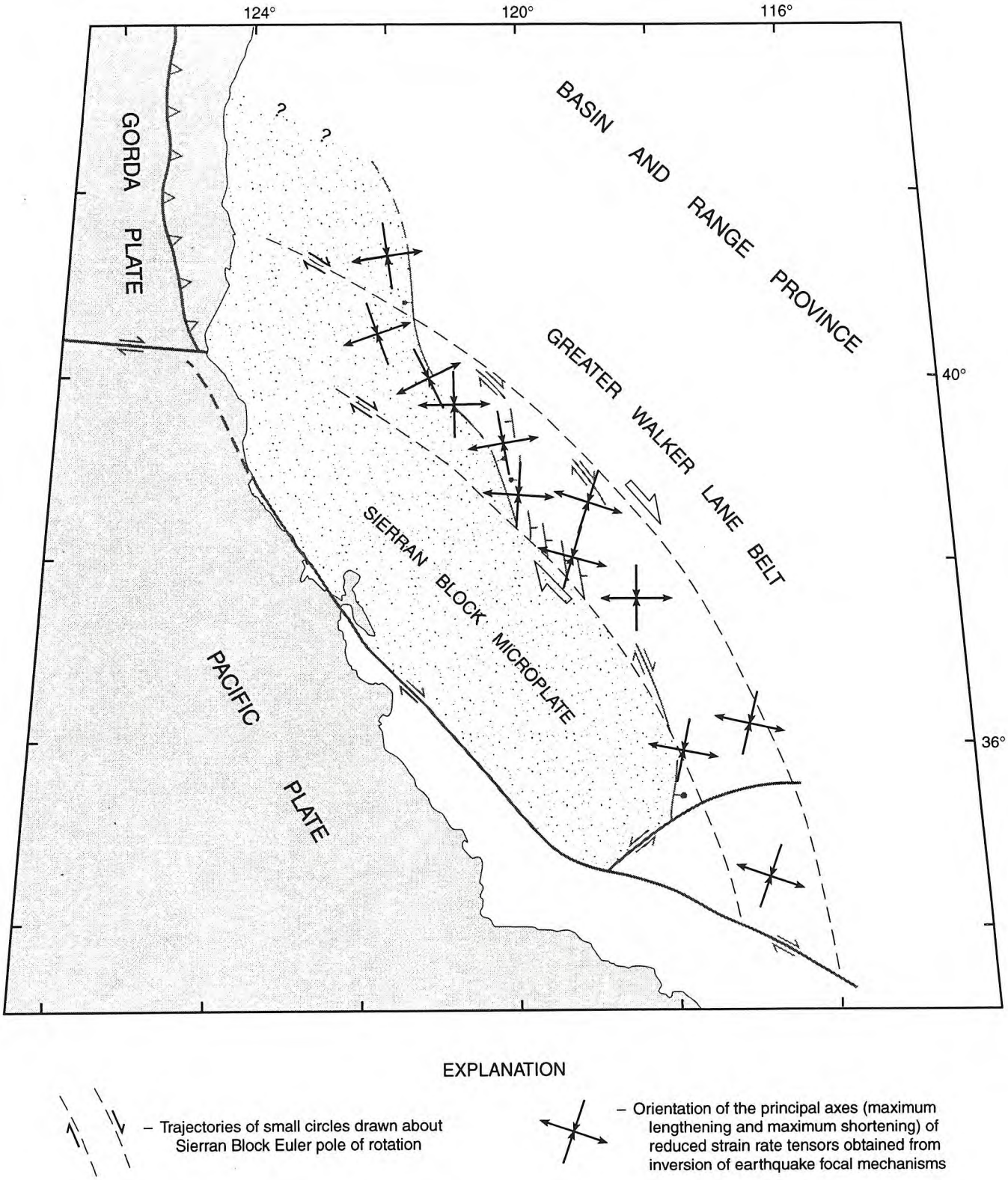

Figure 2. Results of kinematic analysis of seismogenic deformation in the Greater Walker Lane Belt.

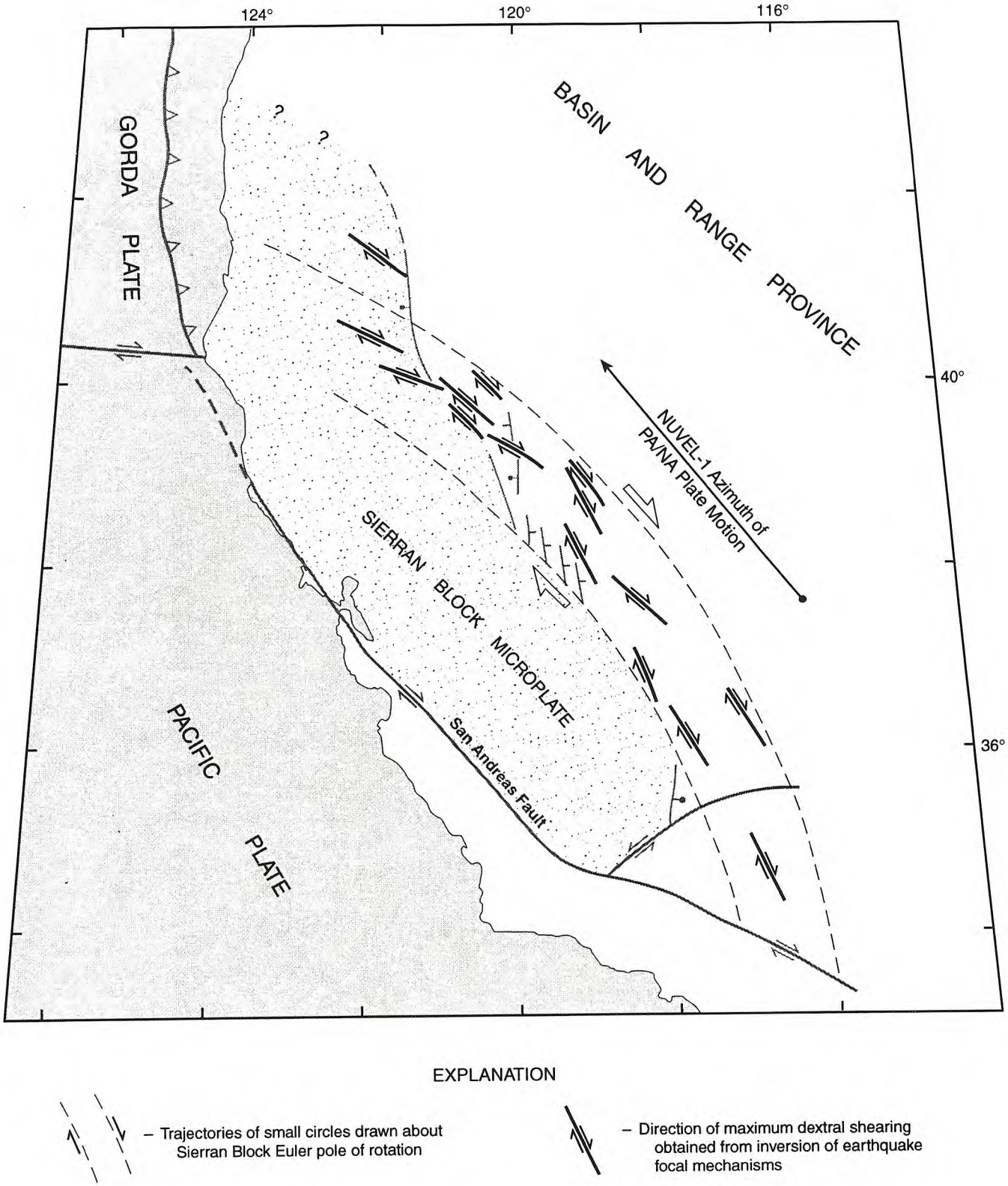

Figure 3. Predicted directions of maximum dextral shearing in the Greater Walker Lane Belt from analysis of seismogenic deformation.

APPENDIX 1-1

A. A Magmatic Model of Medicine Lake Volcano, California. Donnelly-Nolan, J.M.

B. Medicine Lake Volcano, Northern California: Cascade or Basin and Range Volcano?

Donnelly-Nolan, J.M.

C. Post-11,000-Year Vocanism at Medicine Lake Volcano, Cascade Range, Northern California.

Donnelly-Nolan, J.M., Champion, D.E., Miller, C.D., Grove, T.L., Trimble, D.E.

D. Crustal Subsidence, Seismicity, and Structure Near Medicine Lake Volcano, California.

Dzurisin, D., Donnelly-Nolan, J.M., Evans, J.R., Walter, S.R.

JOURNAL OF GEOPHYSICAL RESEARCH, VOL. 93, NO. B5, PAGES 4412–4420, MAY 10, 1988

A Magmatic Model of Medicine Lake Volcano, California

JULIE M. DONNELLY-NOLAN

U.S. Geological Survey, Menlo Park, California

Medecine Lake volcano is a Pleistocene and Holocene shield volcano of the southern Cascade Range. It is located behind the main Cascade arc in an extensional tectonic setting where high-alumina basalt is the most commonly erupted lava. This basalt is parental to the higher-silica calc-alkaline and tholeiitic lavas that make up the bulk of the shield. The presence of late Holocene, chemically identical rhyolites on opposite sides of the volcano led to hypotheses of a large shallow silicic magma chamber and of a small, deep chamber that fed rhyolites to the suface via cone sheets. Subsequent geophysical work has been unable to identify a large silicic magma body, and instead a small one has apparently been recognized. Some geologic data support the geophysical results. Tectonic control of vent alignments and the dominance of mafic eruptions both in number of events and volume throughout the history of the volcano indicate that no large silicic magma reservoir exists. Instead, a model is proposed that includes numerous dikes, sills, and small magma bodies, most of which are too small to be recognized by present geophysical methods.

INTRODUCTION

Medicine Lake volcano is a Quaternary shield volcano that lies about 50 km east-northeast of Mount Shasta, the largest of the Cascade stratovolcanoes (Figure 1). It is located east of the axis of the Cascade volcanic arc. Its low shield shape, similar to Newberry volcano of central Oregon which is also behind the arc, contrasts with the stratovolcanoes that dot the length of the Cascade chain. Medicine Lake volcano could be considered a Basin and Range volcano unrelated to the Cascades, but chemical and temporal similarities as well as close spatial association indicate that Medicine Lake and Newberry volcanoes are indeed Cascadian. The setting of these two volcanoes behind the arc in a more extensional environment has contributed to their physical differences from the more impressive stratocones. The Medicine Lake shield was built mostly by numerous very fluid lavas that flowed relatively long distances from their sources. More viscous lavas constitute a smaller volume.

The presence of several late Holocene, high-silica lava flows on the upper parts of Medicine Lake volcano (Figure 2) has been used to argue for the existence of a moderately large silicic magma chamber [*Eichelberger*, 1981; *Christiansen*, 1982]. Eichelberger proposed a silicic reservoir about 10 km across, with a flat bottom underplated by mafic magma (Figure 3). However, geophysical evidence discussed below indicates that no large silicic magma body exists. Large magma bodies have apparently been found by geophysical methods at Yellowstone, at Long Valley, and at Clear Lake, California, but in many cases the geophysical search for magma bodies has been fruitless, notably in the Cascade Range [*Iyer*, 1984]. In some instances the magmatic system may be temporarily depleted, but in most the magma bodies are probably small. Geophysical data (J. R. Evans, written communication, 1986) indicate the presence of a small low-velocity zone under the center of Medicine Lake volcano. Taken together with geologic evidence, the data are consistent with an underlying complex of dikes, sills, and small magma bodies.

Paper number 7B7064.

PREVIOUS STUDIES

Numerous geologic and petrologic studies of the volcano have been published. Early studies by *Peacock* [1931] and *Powers* [1932] described its main features and were followed by the classic study of *Anderson* [1941]. Anderson's geologic map remains the primary source of published geologic mapping for much of the volcano. Some K-Ar dates have been published by *Luedke and Lanphere* [1980], *Mertzman* [1982, 1983], and *Hart et al.* [1984]. Other geologic studies include *Anderson* [1933], *Eichelberger* [1975], *Heiken* [1978], and *Ciancanelli* [1983]. Petrologic studies include *Barsky* [1975], *Condie and Hayslip* [1975], *Mertzman*, [1977*a*, *b*], *Mertzman and Williams* [1981], and recently a series of papers by Grove and coworkers: *Gerlach and Grove* [1982], *Grove et al.* [1982], *Grove and Baker* [1984], and *Grove and Donnelly-Nolan* [1986]. This recent petrologic work together with remapping of the volcano [*Donnelly-Nolan and Champion*, 1987; J. M. Donnelly-Nolan, unpublished mapping, 1979–1987] has led to new interpretations, some of which are published here.

GEOLOGIC SETTING

Lavas from the volcano cover nearly 2000 km^2, and their volume is estimated at 600 km^3. Tholeiitic and calc-alkaline lavas are represented, including the silica range from 47 to 77%, although dacites are rare. Temporal patterns of eruption are poorly understood because of limited K-Ar data, lack of incision and stratigraphic exposure, and near absence of significant marker beds for stratigraphic control. However, some patterns can be discerned. Growth of the volcano began about a million years ago (J. M. Donnelly-Nolan and L. B. Pickthorn, unpublished data, 1980–1987), following eruption of a large volume of tholeiitic high-alumina basalt that is the principal rock type of the Modoc Plateau. High-alumina basalt has continued to erupt around the flanks of Medicine Lake volcano throughout its history. The main edifice consists mostly of calc-alkaline lavas, dominantly basaltic andesite and andesite. Rhyolite and dacite are typically found on the higher parts of the volcano. Few eruptions have been explosive. Most eruptive events have produced lavas and their associated spatter vents and cinder cones. Ashfall tephra deposits are uncommon and only one ash flow tuff is known.

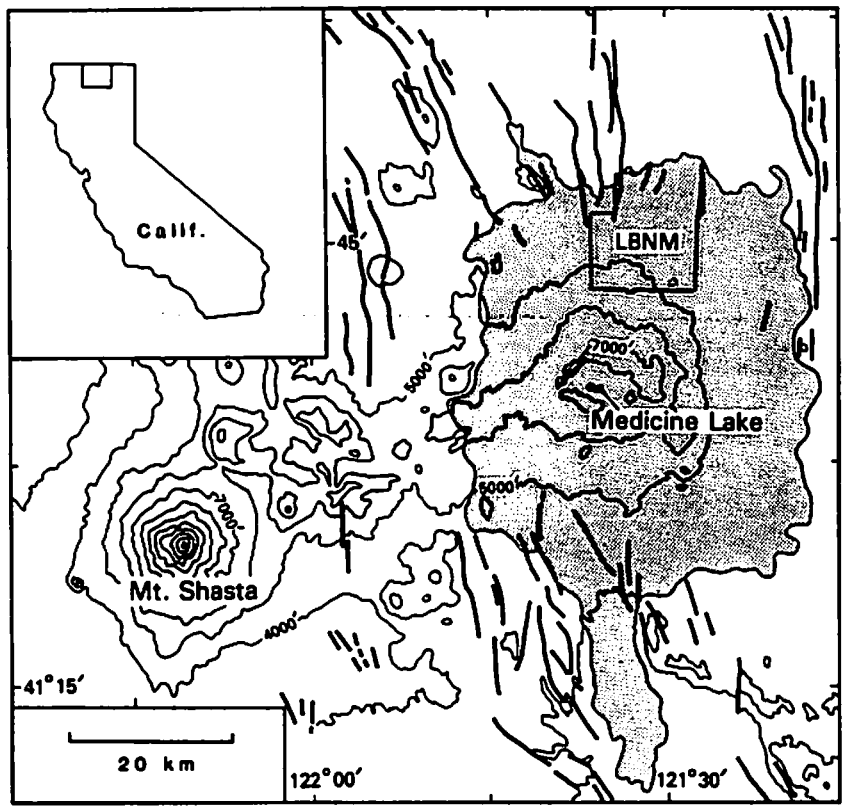

Fig. 1. Location map showing extent of lavas of Medicine Lake volcano in lined pattern. LBNM is Lava Beds National Monument. Contour interval is 1000 feet. Medicine Lake volcano is entirely below 8000 feet and mostly above 4000 feet. Heavy lines are faults [*Gay and Aune*, 1958].

GEOLOGIC EVIDENCE FAVORING A LARGE SILICIC MAGMA BODY

The presence across the top of the volcano of several young silicic lava flows erupted in late Pleistocene and Holocene time strongly suggests the presence of additional silicic magma at depth. Two of the late Holocene silicic eruptions, at Glass Mountain and Little Glass Mountain, occurred on opposite sides of the caldera, 16 km apart, and yet the rhyolitic products of these eruptions are essentially identical in composition for the 10 major elements and about 30 minor and trace elements that have been determined. No primitive basalts are known to have have erupted since late Pleistocene time within the area where young silicic flows occur, although they have erupted to the south and north. Two late Pleistocene vents within the caldera have produced basaltic flows with silica contents of 50.2 and 52.3%. However, most of the lava in the area of the caldera is late Pleistocene andesite.

GEOPHYSICAL DATA AND INTERPRETATIONS

Gravity

Medicine Lake volcano lies at the edge of a regional, roughly circular gravity low that also includes Mount Shasta [*LaFehr*, 1965]. A gravity high characterizes Medicine Lake volcano and is modeled by *Finn and Williams* [1982] as a high-density intrusive body, located 2 to 4 km below the surface approximately centered under and extending beyond the 7 × 12 km central caldera. They state that the body may extend below 4-km depth but cannot confirm this structure using gravity data.

Magnetotelluric Data

Magnetotelluric soundings by *Stanley* [1982] show that a resistive body lies 1.5 km below the caldera, not the conductive body expected if magma is present.

Seismic Refraction

Modeling of a seismic refraction survey across the volcano [*Zucca et al.*, 1986] indicates a shallow high-velocity body under Medicine Lake volcano. A horstlike or pluglike structure of high-velocity material explains the travel time advance seen there. The authors propose a shallow pluton consisting of dikes and sills of basalt and small bodies of rhyolite.

Teleseismic P Wave Residuals

Preliminary analysis of teleseismic *P* wave travel time residuals from an array across the volcano indicates high-velocity anomalies in the crust and possibly the upper mantle to 100 km beneath the volcano [*Evans*, 1982]. One small low-velocity feature was identified near a young lava flow on the southeast side of the volcano, but the absence of any other significant low-velocity region suggested to Evans that melt or partial-melt pockets forming before an eruption must be either very small, very short lived, or both. The 3-km station spacing employed along the center of the array is sufficient to resolve features larger than 3 to 5 km across at any depth in the crust.

Active Seismic Imaging Experiment

In September 1985, 140 seismometers were deployed over a 17 × 12 km area centered over the caldera and the youngest eruptive center at Medicine Lake volcano, the thousand-year-

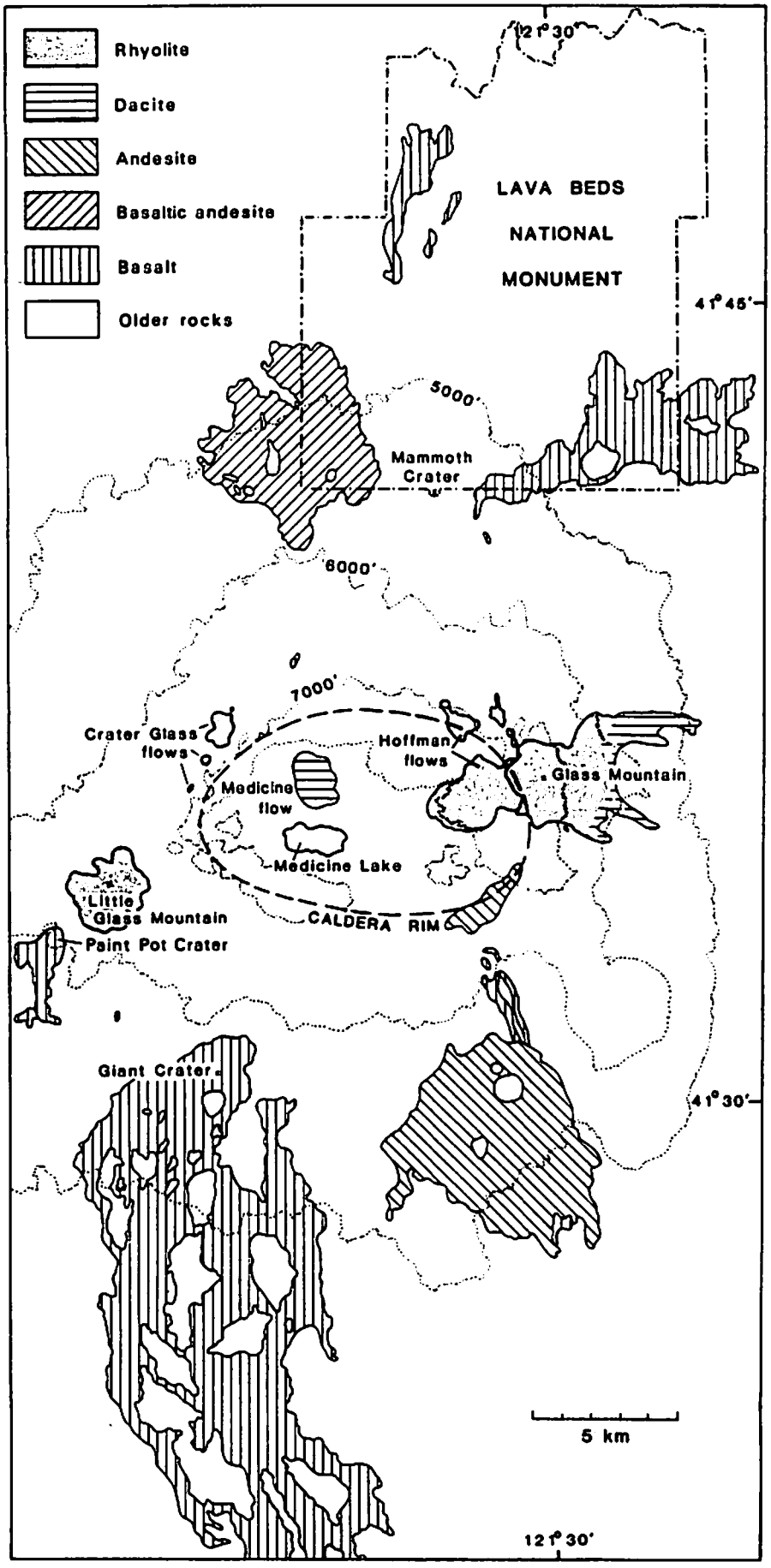

Fig. 2. Map of Medicine Lake volcano showing Holocene lavas, approximate location of caldera rim, and named locations referred to in text.

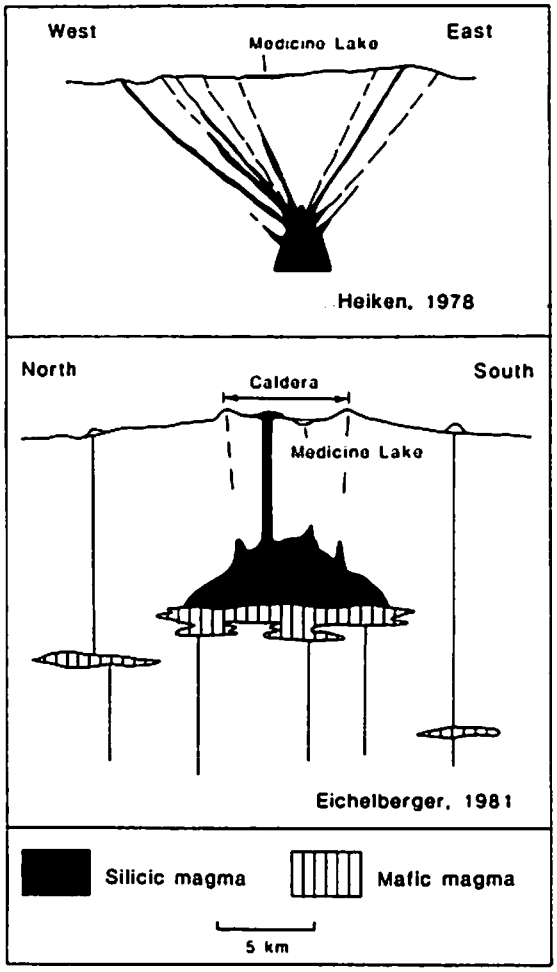

Fig. 3. Previously published models of Medicine lake magma system. Volume of *Heiken* [1978] magma reservoir as shown is approximately 10 km^3. Volume of *Eichelberger* [1981] silicic reservoir is approximately 140 km^3.

old Glass Mountain, which is located near the poorly defined eastern caldera rim (Figure 2). About 1 km^3 of rhyolite and subordinate dacite erupted from at least 13 vents along a N25°W trend extending 5 km. These areas were considered the most likely on the volcano for a detectable shallow silicic magma chamber [*Berge et al.*, 1985].

A series of explosions were set off in a circular array about 50 km away from the study area to provide a high-frequency *Pg* phase at the array. *Pg* travel time anomalies were inverted to obtain a velocity structure (J. R. Evans, written communication, 1986). The method is capable of resolving, in three dimensions, velocity anomalies as small as 1 km^3 in the upper 4–6 km of the crust even when they are part of complex structures that make reflection seismology impractical. The experiment was designed to test the hypothesis that Cascades magma chambers are smaller than other magma bodies studied and simply cannot be seen by the previously applied methods of seismic refraction and teleseismic *P* wave tomography. A similar study at Newberry volcano in Oregon identified a small low-velocity anomaly that may be a silicic magma chamber containing about 1 km^3 to a few cubic kilometers, located about 3 km below the surface [*Evans et al.*, 1986]. Data from the Medicine Lake experiment are more equivocal but suggest a small, shallow low-velocity body under the east central caldera. This feature is located beneath a high-velocity caldera feature, suggesting that it is not simply caldera fill but probably is a magma chamber with a volume of a few to a few tens of cubic kilometers.

Discussion of Geophysical Findings

Several conclusions can be drawn from the results of these geophysical studies: (1) no large magma body of any kind is present; (2) very small magma bodies are probably present, and one has apparently been identified; and (3) a high-velocity, relatively high-density body is present at shallow depth under the volcano, perhaps as close to the surface as 1.5 km.

If we accept that the geophysical techniques that have been applied at Medicine Lake volcano should have been able to detect a large magma body such as the 10-km-diameter chamber suggested by *Eichelberger* [1981] (Figure 3), then we must conclude that no such body exists in spite of the apparent shadow zone. The model of *Heiken* [1978] (Figure 3) is similar in general to the seismic imaging findings of J. R. Evans (written communication, 1986), although the magma body as shown by Heiken is deeper than that modeled by Evans.

GEOLOGIC CONSTRAINTS ON SILICIC MAGMA BODIES

Young Silicic Lavas

Young rhyolite and dacite lavas dot the upper surface of Medicine Lake volcano (Figure 2). The largest and youngest flow is at Glass Mountain to the east of the caldera. The Glass Mountain (GM) event occurred about a thousand years ago and began with the eruption of a Plinian rhyolitic air fall tephra [*Heiken*, 1978] followed by 67% SiO_2 mixed dacite containing abundant mafic magmatic inclusions of basaltic andesite [*Eichelberger*, 1975, 1980, 1981]. As the eruption proceeded, rhyolite containing similar mafic magmatic inclusions formed part of the main flow as well as other domes to the south and north. Some of the domes to the north and south contain a broader range of inclusion compositions, sometimes in a rhyodacite host rather than rhyolite. Ten domes are present to the north and one to the south along a N25°W trend about 5 km long. Inclusion-free rhyolite containing 73.5–74% SiO_2 was the last lava to erupt at GM and at adjacent small domes to the north. Granitic inclusions have been found in the dome to the south and in the sixth and tenth domes to the north. The volume of the GM event including the initial tephra blanket is about 1.0 km^3.

Just prior to the GM event, Little Glass Mountain, located 16 km west of GM, erupted rhyolitic magma of identical chemical composition at about 10 sites including the Crater Glass flows along a 7.5 km N30°E trend. No noticeable chemical variation is known to occur within these 73.5–74% SiO_2 lavas, but in contrast to the GM rhyolite, Little Glass and Crater Glass rhyolites are porphyritic, containing about 1% of phenocrysts, mostly plagioclase together with a scattering of orthopyroxene and oxide minerals. The suite of inclusions also differs somewhat from the suite at GM, having a slightly higher average silica content and an apparently random spatial distribution. Granitic inclusions have been found in both of the flows at Little Glass Mountain and in several of the domes of the Crater Glass flows. The identical chemical composition of Little Glass Mountain (LGM) and Crater Glass flows together with identical inclusion suites and the same petrographic character indicates that these rhyolites

erupted during a single event, referred to here as the LGM event. Volume of the LGM event, including the initial tephra deposit, is estimated at 0.3 km^3.

Hundreds of years before the GM event at an unknown time in the late Holocene, a dike-fed silicic eruption occurred parallel to the trend of the GM dike. The dike that emplaced the Hoffman dacite of *Anderson* [1941] trends N25°-30°W and lies less than 2 km west of the GM dike. Two flows are included in this event based on morphologic, petrographic, and chemical criteria: the Hoffman dacite flow of Anderson and a flow to the north, shown as the Hoffman flows in Figure 2. Both flows have silica contents of 71-72% SiO_2, a value that would be higher if all of the mafic inclusions could be removed from the analyzed samples and thus are classified here as rhyolite rather than dacite. The inclusion suites are not so variable as those of the GM and LGM events, but the inclusions are more mafic. The Hoffman flows together with a probable preceding tephra deposit (C. D. Miller, written communication, 1986) are here referred to as the Hoffman event. Volume of this event is estimated at 0.2 km^3.

The Medicine dacite flow is the only young silicic flow to erupt through the floor of the caldera. It contains 68-69% SiO_2 and possesses granitic and gabbroic fragments together with andesitic magmatic inclusions. The dacite erupted from two closely spaced vents on the northern floor of the caldera in late Holocene time prior to the GM and LGM events. Its age relation to the Hoffman event is unknown. The Medicine dacite apparently erupted nonexplosively, as it appears to lack an associated tephra deposit. Volume of the flow is about 0.1 km^3.

The total volume of Holocene silicic magma erupted to the surface at Medicine Lake volcano is about 1.5 km^3. Even if 10 times this amount still resides in a single silicic magma body under the volcano, the volume of the body would be only 15 km^3. Such a body could be represented by a cylinder 2.5 km in diameter and 3 km high. A magma body of this size is near the limit of detection of geophysical techniques used to search for magma.

Eruptive Patterns

Medicine Lake volcano is dominantly mafic. The volume ratio of mafic to silicic eruptive products during Holocene time is about 10 to 1, and it is about 20 to 1 in late Pleistocene time. The largest known eruptions at Medicine Lake volcano are basaltic, with volumes of about 5 km^3. The largest known silicic eruption probably has a volume of about 1 km^3. A rhyodacitic ash flow tuff initially interpreted to be an early eruptive product of the volcano [*Donnelly-Nolan*, 1983] may be much older based on tephrostratigraphy (A. M. Sarna-Wojcicki, oral communication, 1986). This tuff may be the unit dated by *Mertzman* [1982] as 1.25 ± 0.24 m.y. old.

This pattern contrasts sharply with the eruptive products of volcanoes inferred to have large silicic magma chambers, e.g., Yellowstone, Wyoming, and Long Valley, California, and even the much smaller Crater Lake, Oregon, whose magma body emptied about 50 km^3 to the surface about 6850 years ago [*Bacon*, 1983]. Since the eruption of the andesite tuff from Medicine Lake caldera in late Pleistocene time [*Donnelly-Nolan and Nolan*, 1986], additional andesite has erupted from the caldera rim and at least two basaltic lavas have erupted through the caldera floor. Since then, the only caldera eruptions have been silicic: the late Pleistocene rhyolite of Mount Hoffman from the north rim of the caldera, the late Holocene Medicine dacite flow through the floor of the caldera, and the late Holocene Hoffman event near the eastern edge.

The Caldera

The caldera clearly exists as a 7 × 12 km topographic depression in the top of the volcano, but the location of the rim is poorly constrained except by alignments of vents. No faulting associated with caldera collapse has been identified. *Anderson* [1941] suggested that the caldera formed by collapse following extrusion of large volumes of andesite erupted from vents at the caldera rim. However, the distribution of late Pleistocene vents, mostly concentrated along the caldera rim, suggests that ring faults already existed along which the andesite traveled to the surface. No single large eruption can be related to formation of the caldera; the only eruption known to have resulted in ash-flow tuff occurred in late Pleistocene time and was not accompanied by caldera faulting [*Donnelly-Nolan and Nolan*, 1986]. Much of the volcano, however, is covered by relatively young lavas, and an early caldera-forming event cannot be discounted. The most likely explanation for the existence of the caldera is a variation on Anderson's 1941 idea. In this revised model the caldera formed early in the history of the volcano after collapse of the top. Collapse followed extrusion of fluid lava that moved downslope away from the center in a manner similar to the formation of Kilauea caldera, Hawaii. The caldera has persisted through time by the same mechanism and is not related to any one or more large explosive events. The volcano consists mostly of fluid lavas, and once the ring faults were established, they may have served to localize vents and allow net movement of lava away from the central focus of the volcano, thus maintaining a depression at the top by repeated downsagging of the caldera floor.

Primitive basalt has not erupted in the caldera in late Pleistocene or Holocene time despite numerous eruptions outside it. Eruptions outside the caldera are strongly controlled by the regional tectonic stress field as indicated by alignments of vents typically within 30 degrees of north. More easterly directions are present southwest of the caldera at Giant Crater where one set of vents is oriented N55°E and in the Paint Pot Crater area where two different basalt flows erupted from vents oriented N40°E. These vent orientations may reflect the strong ENE locus of volcanic activity that forms a highland extending from Mount Shasta. This ENE trend may reflect some aspect of the regional stress pattern.

Dikes and Tectonic Control

According to *Bacon* [1985], large magma bodies affect the stress regime in roof rocks so that precaldera leaks occur in nontectonic patterns. He further suggests that silicic vents that form linear arrays in areas of focused silicic volcanism may lead to small calderas; linear arrays of coeval silicic vents whose orientation is a consequence of the regional tectonic stress regime of the upper crust may be fed from small or deep reservoirs incapable of catastrophic eruption. Linear arrays of silicic vents at Medicine Lake volcano indicate that one of the latter possibilities is most likely. The 7.5-km-long dike eruption of LGM shows no evidence of curvature and is interpreted by *Fink and Pollard* [1983] to be vertical. Similarly, the 5-km-long dike that fed GM appears to consist of shorter, straight, en echelon segments with no evidence of curvature toward the caldera.

Small Silicic Chamber

Heiken [1978] suggested that a small deep magma chamber exists under Medicine Lake volcano and that this body fed the Glass Mountain, Little Glass Mountain, and Crater Glass flows via cone sheets. The body (Figure 3) is inferred to lie 7 km below the caldera and to be 3 km across at its widest point; no bottom is shown. This hypothesized body is similar to that modeled by J. R. Evans (written communication, 1986), although the latter model suggests a much shallower body. In the Heiken model the cone sheets dip 45°–60° and the required distance of travel to the surface is 8–12 km. The shallower depth of the body as modeled by Evans would require shallower dips of about 25°–35° and shorter distances of travel of 7.5–8.5 km or more complicated indirect pathways to the surface. If a single body such as that envisioned by Heiken or Evans fed eruptions of the GM and LGM dikes, then the rhyolite magma must have traveled a minimum of 7.5 km from the magma body to the surface and erupted over lengths of 5 km in the case of GM and 7.5 km for the LGM event. In both cases the magma must bypass the ring faults of the caldera and the more direct path straight up to the caldera floor and erupt at the surface along straight alignments rather than the curved ones that might be expected from cone sheets erupting at the surface.

Granitic Inclusions

The GM and LGM events and Medicine dacite brought rare partially melted granitic inclusions to the surface. Such inclusions, although usually more melted, are also present in several basalts and basaltic andesites. They may represent both slowly cooled rhyolitic equivalents and bedrock fragments derived from the arc-type bedrock inferred by seismic refraction work [*Zucca et al.*, 1986; *Fuis et al.*, 1987]. Short residence times are indicated for the granitic fragments in the host melts, particularly for mafic host magmas which would quickly melt such inclusions. Fast travel times to the surface or shallow depth of origin or both are indicated.

CONTROLS ON THE MEDICINE LAKE MAGMA SYSTEM

Tectonic Setting

Medicine Lake volcano is located at the western edge of the Modoc Plateau where north-south trending normal faults with up to a few hundred meters of displacement project toward the volcano and are buried beneath it. These faults decrease in number to the west and are not present at Mount Shasta. The faulted region around Medicine Lake volcano is evidently a transition zone between the Cascade volcanic arc and the Basin and Range province to the east. Intersecting with the N-S structural trend is a strong ENE trending lineament that crosses the Cascades from Mount Shasta to Medicine Lake. A concentration of volcanic vents forms a highland that connects the two volcanoes. An older structural trend of NW trending normal faults also projects under Medicine Lake volcano. Thus the location of the volcano is likely to be a result of the intersection of structural trends forming a locus of weakness within the crust. *Heiken* [1978] pointed out that Medicine Lake volcano lies at the intersection of several fault systems, an additional similarity with Newberry volcano.

Open ground cracks are common on and around Medicine Lake volcano. Cracks that are associated with the late Holocene LGM event have been described by *Fink and Pollard* [1983], who use the geometry of the cracks to argue for a dike eruption of the rhyolite. Sawtooth edges of the cracks can be shown to fit back together in an east-west direction, consistent with the extension direction indicated by the regional normal faults (Figure 1). The structural evidence indicates that Medicine Lake volcano lies in a region of east-west extension. This back-arc, strongly extensional environment [*McKee et al.*, 1983; *Hart et al.*, 1984] provides the necessary tectonic setting for some primitive basalt to reach the surface after traversing 35–40 km [*Hill*, 1978; *Zucca et al.*, 1986] of crust without evidence of contamination. Many basalt magmas may travel upward from the mantle along pathways previously traveled by similar basalt, thus decreasing the possibility of crustal contamination.

High-Alumina Basalt

Primitive high-alumina basalt has erupted around the flanks of Medicine Lake volcano throughout its history. Lavas erupted at Giant Crater on the south flank of the volcano in early Holocene time are as primitive as any erupted early in the volcano's history (Figure 4). Basaltic lavas with K_2O contents of 0.1% and less are relatively common; their major and trace element signatures, hand specimens, and thin sections are nearly indistinguishable. Based on the long span of time during which it has erupted, its consistent chemistry and areal distribution, and petrological experiments and modeling, high-alumina basalt magma is here and elsewhere [*Grove et al.*, 1982; *Grove and Baker*, 1984; *Grove and Kinzler*, 1986] interpreted to be parental to the higher silica lavas of the volcano, in part by fractional crystallization and in part by other processes including contamination and mixing of magmas.

The total volume of high-alumina basalt erupted to the surface at Medicine Lake volcano during its history is unknown. During Holocene time an estimated 5 km^3 erupted, nearly all of that at vents for the basalt of Giant Crater (Figure 2) over a time span estimated from paleomagnetic

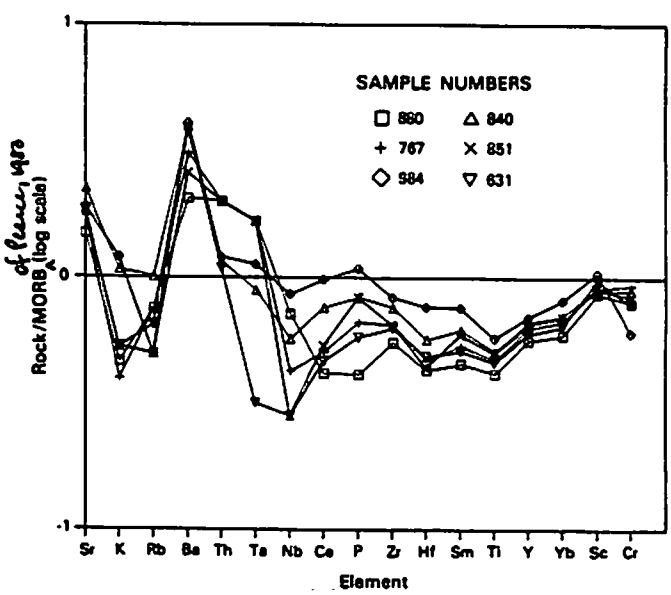

Fig. 4. Spider diagram of Medicine Lake high-alumina basalts. Sample number 880 is early Holocene basalt of Giant Crater. Samples 767 and 840 are latest Pleistocene in age. Samples 984, 851, and 631 represent early basalts of the volcano, mid-Pleistocene in age. Note that there is no difference between young and old basalts. Note also the unusual K and Rb depletions and the Sr and Ba enrichments, the latter typical of island arc basalts.

data (D. E. Champion, oral communication, 1986) to be less than 100 yr. The initial part of the Giant Crater material has a higher silica content and contains granitic inclusions, but this contaminated lava represents only a relatively small part of the total volume. High-alumina basalt accounts for about 60% of the volume of all material erupted at Medicine Lake volcano in Holocene time. Because most of the Holocene high-alumina basalt erupted in a single episode, the volume erupted in Holocene time may not be an accurate predictor of total volume. Other large-volume high-alumina basalt eruptions occurred in late Pleistocene time, e.g., the Mammoth Crater event on the north flank of the volcano during which about 5 km^3 of basaltic lava erupted. Lack of stratigraphic exposure limits the accuracy of volume estimates for lavas in pre-late Pleistocene time. The volcano is surrounded by a broad apron of high-alumina basalt, mostly of unknown age and from unknown vents. The very fluid nature of this basalt may account for its relative scarcity in outcrop on the main edifice of the volcano when compared with the abundant derivative lavas of higher viscosity.

An estimate can be made of the magma supply rate. Assuming that two times as much magma is intruded as extruded, as is the case in Hawaii [*Dzurisin et al.*, 1984], then the calculated rate of supply to Medicine Lake volcano in Holocene time is 0.002 km^3/yr. Assuming that the volume of all products of Medicine Lake volcano is 600 km^3 and that the oldest lavas are 1 m.y. old, the calculated long-term rate is the same, 0.002 km^3/yr. The ratio of intruded to extruded magma at Medicine Lake is probably higher than that in Hawaii in order to account for the much larger volume of high-silica derivative magmas, but even assuming 10 times as much intruded as extruded, the calculated magma supply rate of 0.01 km^3/yr is still only a tenth of the rate of Hawaii. During a particular episode of basaltic volcanism at Medicine Lake such as that of Giant Crater, the rate is about the same as at Kilauea.

The high-alumina basalt at Medicine Lake volcano has been compared to mid-ocean ridge basalt by *Hart* [1971], *Philpotts et al.* [1971], *McKee et al.* [1983], and *Hart et al.* [1984]. Its primitive nature can be seen in Figure 4, which shows it to be depleted in many elements including K_2O compared to the mid-ocean ridge basalt (MORB) of *Pearce* [1983]. However, enrichments in Ba and Sr are typical of primitive island-arc basalts [*Arculus and Johnson*, 1981]. Behind the Cascade arc, high-alumina basalt is a common rock type, particularly in Oregon, northern California, southwestern Idaho, and northwestern Nevada [*Waters*, 1962; *McKee et al.*, 1983; *Hart et al.*, 1984].

Origin of Derivative Magmas

Grove and his students [*Grove et al.*, 1982; *Gerlach and Grove*, 1982; *Grove and Baker*, 1984] have convincingly demonstrated that the calc-alkaline andesite of Medicine Lake volcano can be derived from high-alumina basalt by a combination of processes including fractional crystallization, assimilation of crustal material, and magma mixing. *Grove and Donnelly-Nolan* [1986] showed that rhyolitic magmas can be produced by fractional crystallization of andesite. Inclusion suites in Holocene silicic lavas include granite and other plutonic fragments, chilled mafic melts, and cumulate gabbros. The granitic fragments provide physical evidence of contamination, and the cumulates represent material removed from the andesite parent during fractional crystallization.

The chilled mafic melt inclusions are of variable composition even within a single host rhyolite or dacite, varying from 49.5 to 57.5% SiO_2 in Glass Mountain and its associated domes and from 52.2 to 61.8% SiO_2 in the Little Glass Mountain–Crater Glass rhyolite. *Grove and Donnelly-Nolan* [1986] successfully modeled the production of a similar rhyolite using two of the andesitic inclusions as starting points. The range of inclusion compositions suggests that the eruption process may have tapped underlying compositionally zoned mafic magma.

GM and LGM rhyolitic lavas have essentially identical major and trace element compositions and were erupted within a very short time span [*Heiken*, 1978] on opposite sides of the volcano in late Holocene time. This fact led Heiken to suggest that both lavas were fed by cone sheets from a single small magma body. There are some differences between the GM and LGM magmas, e.g., the slightly different inclusion suites, the porphyritic nature of LGM rhyolite versus the aphyric GM rhyolite, and the initial eruption of mixed lava at GM. Such differences may be accounted for by variations in the process of transport of the magma to the surface, or perhaps by tapping of different parts of the magma reservoir. Alternatively, the magmas may have developed simultaneously on opposite sides of the caldera by fractionation of andesites of very similar composition. Very similar late Pleistocene andesite lavas are present in both areas.

POSSIBLE MAGMATIC MODELS

The lack of geophysical evidence for a large silicic magma body together with tectonic control of vent alignments and the dominance of mafic eruptions throughout the history of the volcano suggests that no such body exists. A large silicic magma body may have existed in the past based on the presence of older high-silica rhyolites, although no other evidence such as ash flow tuffs or large Plinian ashfall deposits has been found.

A single small silicic reservoir such as that envisioned by *Heiken* [1978] is a viable model, particularly in light of the discovery by J. R. Evans (written communication, 1986) of an apparent small low-velocity body under the caldera. Such a body also explains the essentially identical compositions of GM and LGM rhyolites on opposite sides of the caldera if tapped by dipping cone sheets. The model does not explain why the 5- and 7.5-km dikes that fed GM and LGM erupted outside the caldera, the magma bypassing both the direct vertical path to the surface and the ring faults of the caldera as conduits.

One possible explanation for the lack of basaltic vents in the caldera is that there is not enough pressure in the system for primitive basalt to erupt at the top of the volcano and instead it erupts on the flanks. This situation occurs frequently in Hawaii where magma intrudes into the rift zones of Kilauea rather than erupting in its caldera. Or the caldera may contain unconsolidated sedimentary fill or hydrothermally altered material that does not sustain fracturing. Such material could inhibit propagation of cracks to the caldera floor and thus promote subjacent intrusion and ponding. If something is interfering with the passage of the basalt to the surface, another possibility is that numerous small pockets of derivative magma too small to be seen by geophysical techniques have formed and are forming under the central part of the volcano. Numerous small magma bodies and liquid-filled cracks may inhibit the flow of basalt to the surface and promote ponding

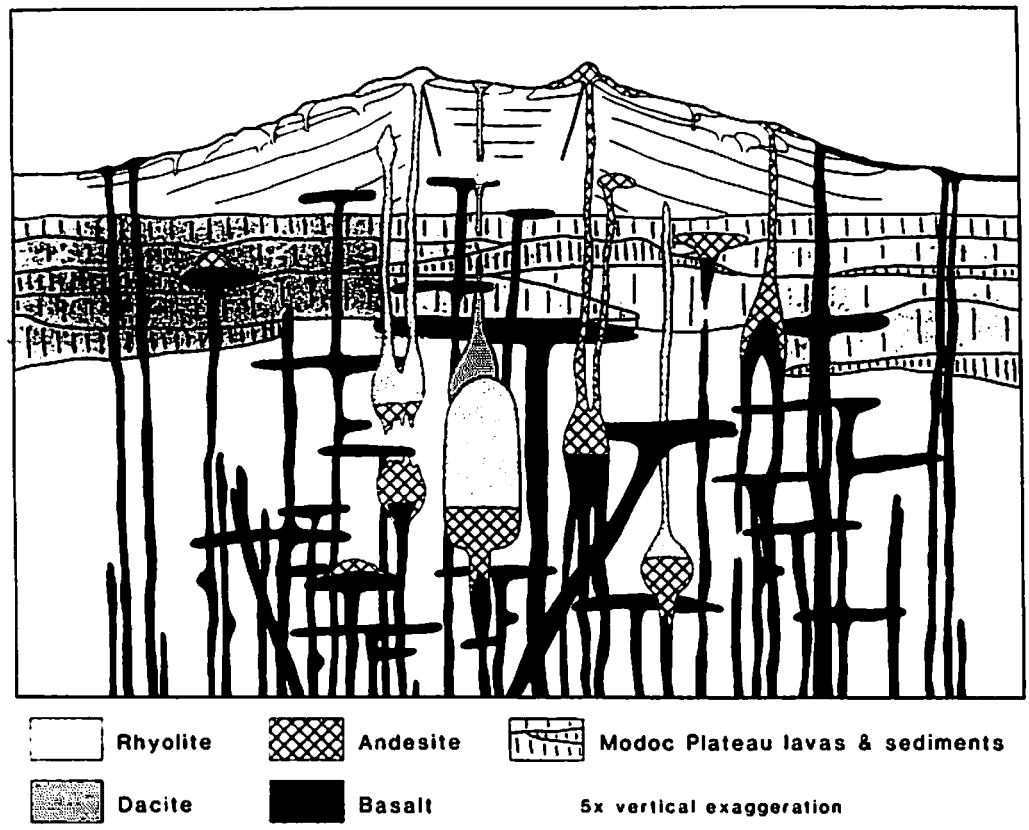

Fig. 5. Cartoon of Medicine Lake magma system. The field of view is approximately 40 km wide by 5 km high, with 5 × vertical exaggeration. The width of conduits is greatly exaggerated. Underlying the Modoc Plateau lavas and sediments is an arc terrane similar to the Sierra Nevada [*Zucca et al.*, 1986; *Fuis et al.*, 1987].

as sills and dikes. The presence of lower-density magma beneath the caldera could prevent the ascent of higher-density primitive basalt to the surface by ponding or mixing with the more silicic magma. Thus ultimately more heat and raw material are provided for still more derivative magmas to form, most commonly andesite and basaltic andesite, but also occasionally dacite and rhyolite. More time is probably required to form dacite and rhyolite, and the process may be interrupted by extensional episodes with consequent eruption before high-silica magma has been formed.

The numerous small lava flows and their vents, the dominance of mafic over silicic eruptions in both number and volume, and the alignments of both mafic and silicic vents indicating tectonic control on the system all combine to suggest a system with one or perhaps more small differentiated magma bodies. The models of *Heiken* [1978] and J. R. Evans (written communication, 1986) of a single small silicic magma body may be too simplified. Figure 5 is a more complicated possible model showing a silicic reservoir corresponding to Evans' model plus several smaller bodies of varying compositions together with numerous dikes and sills mostly of basalt.

CONCLUSIONS

Medicine Lake volcano is fundamentally basaltic and lacks a large silicic magma chamber. High-alumina basalt is probably the single most abundant rock type erupted from the volcano and is almost certainly the most abundant intruded rock type. Primitive basalt is parental to the other lavas by fractional crystallization, contamination, and mixing. If silicic lavas are produced by partial melting of crustal rocks, intruded basalt provides the heat. The common occurrence of open ground cracks on and around the volcano, typically oriented NNW to NNE, attests to the E-W extension that allows large volumes of low-K_2O, high-Al basalt to reach the surface. The dominant N-S fabric of vent alignments and fault orientations intersects the strong ENE trending lineament along which volcanism is focused between Medicine Lake and Mount Shasta. These two structural trends intersect at Medicine Lake volcano. Thus the tectonic setting influences both the location and style of volcanism.

The inability of geophysical techniques to identify a large magma body is most likely due to the absence of such a body. Geologic evidence exists to support this idea. Located in an extensional environment behind the Cascade volcanic arc, Medicine Lake volcano experiences episodes of extension at frequent intervals and lavas erupt to the surface along tectonically controlled alignments. As a consequence, large magma bodies are unlikely to form. In this tectonic environment, the most likely magma system is one of numerous dikes, sills, and small bodies of magma.

Acknowledgments. I thank J. R. Evans, T. L. Grove, D. E. Champion, C. R. Bacon, and J. H. Fink for stimulating discussions on this and related topics. M. A. Clynne, N. S. MacLeod, Grant Heiken, and S. A. Mertzman provided helpful reviews.

REFERENCES

Anderson, C. A., Volcanic history of Glass Mountain, northern California, *Am. J. Sci.*, *26*, 485-506, 1933.

Anderson, C. A., Volcanoes of the Medicine Lake Highland, California, *Univ. Calif. Publ. Bull. Dep. Geol. Sci.*, *25*, 347–422, 1941.

Arculus, R. J., and R. W. Johnson, Island-arc magma sources: A geochemical assessment of the roles of slab-derived components and crustal contamination, *Geochem. J.*, *15*, 109–133, 1981.

Bacon, C. R., Eruptive history of Mount Mazama and Crater Lake caldera, Cascade Range, U.S.A., *J. Volcanol. Geotherm. Res.*, *18*, 57–115, 1983.

Bacon, C. R., Implications of silicic vent patterns for the presence of large crustal magma chambers, *J. Geophys. Res.*, *90*, 11,243–11,272, 1985.

Barsky, C. K., Geochemistry of basalts and andesites from the Medicine Lake Highland, California, Ph.D. Dissertation, 373 pp., Washington Univ., St. Louis, Mo., 1975.

Berge, P. A., P. B. Dawson, and J. R. Evans, Active seismic imaging experiment (abstract), *Eos Trans. AGU*, *66*, 603–604, 1985.

Christiansen, R. L. Volcanic hazard potential in the California Cascades, *Calif. Div. Mines Geol. Spec. Publ.*, *63*, 41–59, 1982.

Ciancanelli, E. V., Geology of Medicine Lake volcano, *Trans. Geotherm. Resour. Counc.*, *7*, 135–140, 1983.

Condie, K. C., and D. L. Hayslip, Young bimodal volcanism at Medicine Lake volcanic center, northern California, *Geochim. Cosmochim. Acta*, *39*, 1165–1178, 1975.

Donnelly-Nolan, J. M., Two ash-flow tuffs and the stratigraphy of Medicine Lake volcano, northern California Cascades, *Geol. Soc. Am. Abstr. Programs*, *15*, 330, 1983.

Donnelly-Nolan, J. M., and D. E. Champion, Geologic map of Lava Beds National Monument, northern California, *Map I-1804*, scale 1:24,000, U.S. Geol. Surv., Reston, Va., 1987.

Donnelly-Nolan, J. M., and K. M. Nolan, Catastrophic flooding and eruption of ash-flow tuff at Medicine Lake volcano, California, *Geology*, *14*, 875–878, 1986.

Dzurisin, D., R. Y. Koyanagi, and T. T. English, Magma supply and storage at Kilauea volcano, Hawaii, 1956–1983, *J. Volcanol. Geotherm. Res.*, *21*, 177–206, 1984.

Eichelberger, J. C., Origin of andesite and dacite: Evidence of mixing at Glass Mountain in California and at other circum-Pacific volcanoes, *Geol. Soc. Am. Bull.*, *86*, 1381–1391, 1975.

Eichelberger, J. C., Vesiculation of mafic magma during replenishment of silicic magma reservoirs, *Nature*, *288*, 446–450, 1980.

Eichelberger, J. C., Mechanism of magma mixing at Glass Mountain, Medicine Lake Highland volcano, California, Guides to Some Volcanic Terranes in Washington, Idaho, Oregon, and Northern California, edited by D. A. Johnston and J. M. Donnelly-Nolan, *U.S. Geol. Surv. Circ.*, *838*, 183–189, 1981.

Evans, J. R., Compressional-wave velocity structure of the Medicine Lake volcano and vicinity from teleseismic relative travel-time residuals, paper presented at the 52nd Annual International Meeting, Soc. of Explor. Geophys., Dallas, Tex., 1982.

Evans, J. R., D. A. Stauber, and P. B. Dawson, Prospecting for shallow magma chambers in the Cascade Range using seismic topography, *U.S. Geol. Surv. Circ.*, *974*, 15–16, 1986.

Fink, J. H., and D. D. Pollard, Structural evidence for dikes beneath silicic domes, Medicine Lake Highland volcano, California, *Geology*, *11*, 458–461, 1983.

Finn, C., and D. L. Williams, Gravity evidence for a shallow intrusion under Medicine Lake volcano, California, *Geology*, *10*, 503–507, 1982.

Fuis, G. S., J. J. Zucca, W. D. Mooney, and B. Milkereit, A geologic interpretation of seismic-refraction results in northeastern California, *Geol. Soc. Am. Bull.*, *98*, 53–65, 1987.

Gay, T. E., Jr., and Q. A. Aune, Alturas sheet, Geologic map of California, scale 1:250,000, Calif. Div. of Mines and Geol., Sacramento, 1958.

Gerlach, D. C., and T. L. Grove, Petrology of Medicine Lake Highland volcanics, characterization of endmembers of magma mixing, *Contrib. Mineral. Petrol.*, *80*, 147–159, 1982.

Grove, T. L., and M. B. Baker, Phase equilibrium controls on the tholeiitic versus calc-alkaline differentiation trends, *J. Geophys. Res.*, *89*, 3253–3274, 1984.

Grove, T. L., and J. M. Donnelly-Nolan, The evolution of young silicic lavas at Medicine Lake volcano, California, implications for the origin of compositional gaps in calc-alkaline series lavas, *Contrib. Mineral. Petrol.*, *92*, 281–302, 1986.

Grove, T. L., and R. J. Kinzler, Petrogenesis of andesites, *Annu. Rev. Earth Planet. Sci.*, *14*, 417–454, 1986.

Grove, T. L., D. C. Gerlach, and T. W. Sando, Origin of calc-alkaline series lavas at Medicine Lake volcano by fractionation, assimilation and mixing, *Contrib. Mineral. Petrol.*, *80*, 160–182, 1982.

Hart, S. R., K. Rb, Cs, Sr and Ba contents and Sr isotope ratios of ocean floor basalts, *Philos. Trans. R. Soc. London, Ser. A*, *268*, 573–587, 1971.

Hart, W. K., J. L. Aronson, and S. A. Mertzman, Areal distribution and age of low-K, high-alumina olivine tholeiite magmatism in the northwestern Great Basin, *Geol. Soc. Am. Bull.*, *95*, 186–195, *Suppl. Data*, *84-3*, 1984.

Heiken, G., Plinian-type eruptions in the Medicine Lake Highland, California, and the nature of the underlying magma, *J. Volcanol. Geotherm. Res.*, *4*, 375–402, 1978.

Hill, D. P., Seismic evidence for the structure and Cenozoic tectonics of the Pacific Coast states, Cenozoic Tectonics and Regional Geophysics of the Western Cordillera, edited by R. B. Smith and G. P. Eaton, *Mem. Geol. Soc. Am.*, *152*, 145–174, 1978.

Iyer, H. M., Geophysical evidence for the locations, shapes and sizes, and internal structures of magma chambers beneath regions of Quaternary volcanism, *Philos. Trans. R. Soc. London, Ser. A.*, *310*, 473–510, 1984.

LaFehr, T. R., Gravity, isostasy and crustal structure in the southern Cascade Range, *J. Geophys. Res.*, *70*, 5581–5597, 1965.

Luedke, R. G., and M. A. Lanphere, K-Ar ages of upper Cenozoic volcanic rocks, northern California, *Isochron/West*, *28*, 7–8, 1980.

McKee, E. H., W. A. Duffield, and R. J. Stern, Late Miocene and early Pliocene basaltic rocks and their implications for crustal structure, northeastern California and south-central Oregon, *Geol. Soc. Am. Bull.*, *94*, 292–304, 1983.

Mertzman, S. A., Jr., The petrology and geochemistry of the Medicine Lake volcano, California, *Contrib. Mineral. Petrol.*, *62*, 221–247, 1977*a*.

Mertzman, S. A., Jr., Recent volcanism at Schonchin and Cinder buttes, northern California, *Contrib. Mineral. Petrol.*, *61*, 231–243, 1977*b*.

Mertzman, S. A., K-Ar results for silicic volcanics from the Medicine Lake Highland, northeastern California—A summary, *Isochron/West*, *34*, 3–7, 1982.

Mertzman, S. A., An addendum to "K-Ar results for silicic volcanics from the Medicine Lake Highland, northeastern California—A summary," *Isochron/West*, *38*, 3–5, 1983.

Mertzman, S. A., and R. J. Williams, Genesis of Recent silicic magmatism in the Medicine Lake Highland, California, evidence from cognate inclusions found at Little Glass Mountain, *Geochim. Cosmochim. Acta*, *45*, 1463–1478, 1981.

Peacock, M. A., The Modoc lava field, northern California, *Geogr. Rev.*, *21*, 259–275, 1931.

Pearce, J. A., Role of the sub-continental lithosphere in magma genesis at active continental margins, in *Continental Basalts and Mantle Xenoliths* edited by C. M. Hawkesworth and M. J. Norry, pp. 230–249, Shiva Publishing, Nantwich, Cheshire, United Kingdom, 1983.

Philpotts, J. A., W. Martin, and C. C. Schnetzler, Geochemical aspects of some Japanese lavas, *Earth Planet. Sci. Lett.*, *12*, 89–96, 1971.

Powers, H. A., The lavas of the Modoc Lava-Bed quadrangle, California, *Am. Mineral.*, *17*, 253–295, 1932.

Stanley, W. D., A regional magnetotelluric survey of the Cascade Mountains region, *U.S Geol. Surv. Open File Rep.*, *82-126*, 1982.

Waters, A. C., Basalt magma types and their tectonic associations: Pacific Northwest of the United States, in *The Crust of the Pacific Basin, Geophys. Monogr. Ser.*, vol. 6, edited by G. A. MacDonald and H. Kuno, pp. 158–170, AGU, Washington, D. C., 1962.

Zucca, J. J., G. S. Fuis, B. Milkereit, W. D. Mooney, and R. D Catchings, Crustal structure of northeastern California, *J. Geophys. Res.*, *91*, 7359–7382, 1986.

J. M. Donnelly-Nolan, U.S. Geological Survey, M.S. 910, 345 Middlefield Road, Menlo Park, CA 94025.

(Received May 7, 1987;
revised November 24, 1987;
accepted December 22, 1987.)

10

T32B-7 1330h POSTER

Medicine Lake Volcano, Northern California: Cascade or Basin and Range Volcano?

J M Donnelly-Nolan (U.S. Geological Survey, 345 Middlefield Rd., Menlo Park CA 94025)

Medicine Lake volcano (MLV) is a large shield volcano 55 km NE of Mt. Shasta. Between these two major volcanoes lies an ENE-trending highland of volcanic vents ranging in composition from basalt to rhyolite. The main axis of the Cascades lies between MLV and Shasta where it is defined by a NNW-trending linear array of small mafic shield volcanoes and cinder cones like those that make up the bulk of the Cascade Range in California and Oregon. MLV is located behind the main arc in an extensional setting at the intersection of major tectonic features: 1. the highland of vents that joins it to Shasta, 2. the southern end of the Klamath graben, which terminates to the north at Crater Lake and is defined by N-S-trending normal faults with as much as 100 m or more of displacement, and 3. slightly older NW-trending faults. The N-S-trending normal faults apparently represent the westernmost faults generated by Basin and Range (B&R) extension. Other paired volcanoes across the arc are Three Sisters-Newberry in central Oregon, and Mt. St. Helens-Mt. Adams in southern Washington. Newberry is morphologically and chemically similar to MLV. Some authors have argued that Newberry and MLV are not Cascade volcanoes. No such suggestion has been made for Adams, a stratocone. MLV and Newberry are contemporaneous with the Cascade stratocones but the two are sometimes referred to as B&R volcanoes. The stratocone-shield pairs may result from B&R influence that provides a more extensional environment for the eastern of the paired volcanoes, in contrast with the St. Helens-Adams stratocone pair that lies N of B&R influence. The shield shape of MLV and Newberry, which distinguishes them from the stratocones but allies them with the many smaller mafic shield volcanoes of the arc, is related to the fluidity of their numerous mafic lavas including primitive and possibly some primary basalts. Silicic lavas are also present, however, in significant volume--probably 15% of the approximate total volume of 750 km^3 at MLV. MLV lavas plot within or substantially overlap the array of major and trace element data of the Cascade stratovolcanoes. If MLV and Newberry are B&R volcanoes, more such volcanoes should--but do not--lie to the east in undisputed B&R terrane. I conclude that MLV is a Cascade volcano generated by the same subduction system that created the stratocones.

11

JOURNAL OF GEOPHYSICAL RESEARCH, VOL. 95, NO. B12, PAGES 19,693–19,704, NOVEMBER 10, 1990

Post-11,000-Year Volcanism at Medicine Lake Volcano, Cascade Range, Northern California

JULIE M. DONNELLY-NOLAN,[1] DUANE E. CHAMPION,[1] C. DAN MILLER,[2]
TIMOTHY L. GROVE,[3] AND DEBORAH A. TRIMBLE[1]

Eruptive activity during the past 11,000 years at Medicine Lake volcano has been episodic. Eight eruptions produced about 5.3 km^3 of basaltic lava during an interval of a few hundred years about 10,500 years B.P. After a hiatus of about 6000 years, eruptive activity resumed with a small andesite eruption at about 4300 years B.P. Approximately 2.5 km^3 of lava with compositions ranging from basalt to rhyolite vented in nine eruptions during an interval of about 3400 years in late Holocene time. The most recent eruption occurred about 900 years B.P. A compositional gap in SiO_2 values of erupted lavas occurs between 58 and 63%. The gap is spanned by chilled magmatic inclusions in late Holocene silicic lavas. Late Holocene andesitic to rhyolitic lavas were probably derived by fractionation, assimilation, and mixing from high-alumina basalt parental magma, possibly from basalt intruded into the volcano during the early mafic episode. Many basaltic to andesitic lavas contain iron-rich crystals and have high FeO*/MgO (characteristics caused by mixing of high-alumina basalt with ferrobasalt liquid produced by fractionation of parental high-alumina basalt). When ferrobasalt and high-alumina basalt are contaminated with a granitic crustal component, a calc-alkaline trend is produced. Some eruptions have produced both tholeiitic and calc-alkaline compositions. The eruptive activity is probably driven by intrusions of basalt that occur during east-west stretching of the crust in an extensional tectonic environment. Vents are typically aligned parallel or subparallel to major structural features, most commonly within 30° of north. Intruded magma should provide adequate heat for commercial geothermal development if sufficient fluids can be found. The nature and timing of future volcanic activity cannot be predicted from the observed pattern, but eruptions high on the edifice could produce high-silica products that might be accompanied by explosive activity, whereas eruptions lower on the flanks are likely to vent more fluid mafic lavas.

INTRODUCTION

Medicine Lake volcano is a large Pleistocene and Holocene shield volcano located in the Cascade Range east of the main volcanic axis in northern California. Most products of the volcano have normal magnetic polarity, suggesting that the eruptions occurred mainly during Brunhes time. Their maximum age is probably about 1 Ma, although the older limit is not well defined by K-Ar dating [*Mertzman*, 1982, 1983; J. M. Donnelly-Nolan and L. B. G. Pickthorn, unpublished K-Ar data, 1980–1988]. Composition ranges from basalt through rhyolite; dacite is underrepresented. Mafic lavas have dominated in both volume and number of events. Post-11,000-year volcanism includes a wide range of chemical compositions distributed over a large area of the volcano. Eruptive activity began with an episode dominated by basalt. Six thousand years later, late Holocene volcanism was dominated by silicic eruptions, and only a small amount of basalt reached the surface.

Mafic magma is also represented by quenched inclusions in more than half of the Holocene lava flows. The inclusions display chilled crenulate margins, vesicular interiors, and crystal morphologies that indicate rapid growth. Large gas cavities typically occur at the ends of oblong inclusions. These features indicate that the inclusions were injected as liquids and were chilled upon incorporation into their host magma. Most of the inclusions are fine grained, but some are coarse and display cumulate textures. The host lava is always higher in SiO_2 and presumably was cooler than its magmatic inclusions.

Crustal inclusions are also present in nearly half of the Holocene lavas. All contain > 70 wt % SiO_2, and most are granitic in mineralogy and texture. All are partially melted, but a few are sufficiently melted to obscure the original mineralogy and texture; some of these could be rhyolitic. Host lava compositions range from 52.5 to 74.1 wt % SiO_2. The source of these lithic inclusions is unknown, but likely possibilities include granite from slowly cooled subjacent magmas of Medicine Lake volcano, older granites of a presumed underlying Sierra Nevada–type arc terrane [*Fuis et al.*, 1987], and older rhyolites of the volcano.

Figure 1 shows the distribution of the early mafic and late Holocene lavas; vent locations are shown on Figure 2. In this environment of east-west extension, tectonic control of vent alignments is pronounced. Vents are typically aligned parallel or subparallel to major regional structural features, such as the major normal faults that occur both north and south of the volcano and that trend within 30° of north. Some of the vents located on the southwestern side of the volcano are aligned N45° to 55°E, a much more eastward direction, which may be controlled by the linear highland of vents that projects east-northeast from Mount Shasta to the Medicine Lake caldera.

The good age control and the excellent exposures of Medicine Lake lavas less than 11,000 years old provide us with a far better understanding of this period than any previous period in the volcano's history.

PREVIOUS WORK

Previous geologic work includes the early study of Medicine Lake volcano by *Powers* [1932] followed by the classic

[1]U.S. Geological Survey, Menlo Park, California.
[2]U.S. Geological Survey Cascades Volcano Observatory, Vancouver, Washington.
[3]Department of Earth, Atmospheric, and Planetary Sciences, Massachusetts Institute of Technology, Cambridge.

Paper number 90JB01033.
0148-0227/90/90JB-01033$05.00

12

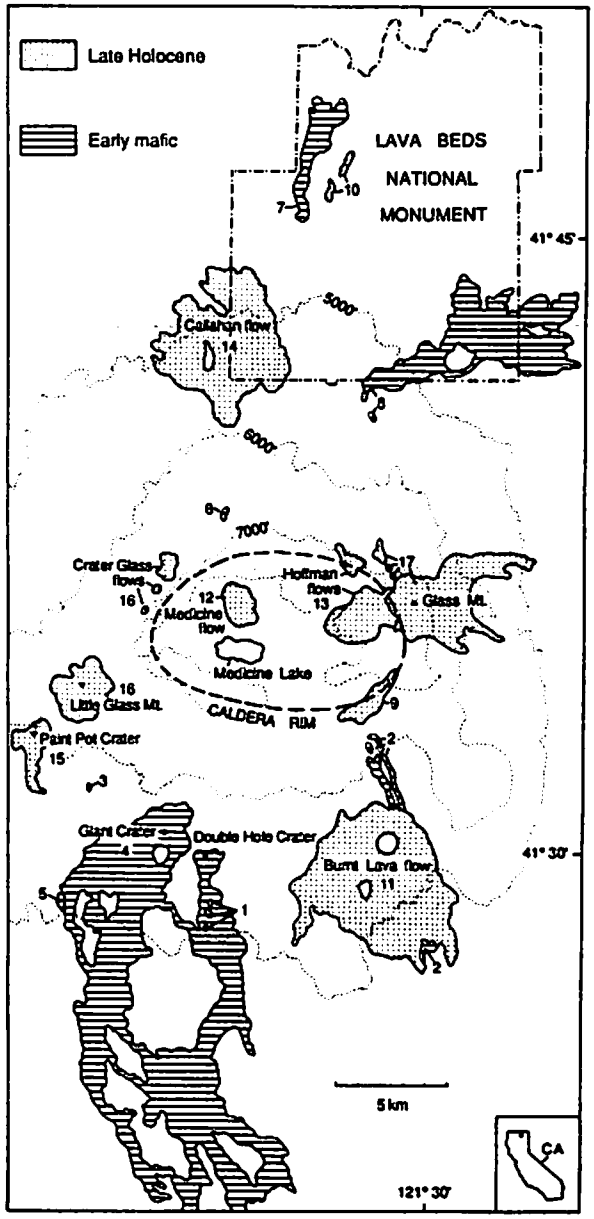

Fig. 1. Map of Medicine Lake volcano showing distribution of post-11,000-year lavas. Units are numbered 1–17 (Table 2) from oldest to youngest. Units 1–8 belong to the early mafic episode; units 9–17 are late Holocene. The basalt of Giant Crater extends more than 25 km south of the southern border of the figure (modified from *Donnelly-Nolan* [1988]). Topographic contours are in feet (1 foot ≈ 0.3 m).

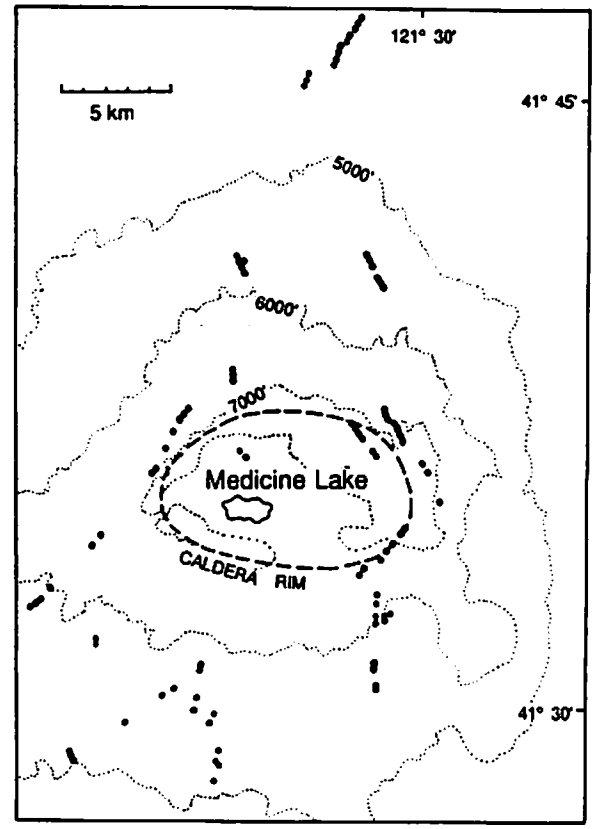

Fig. 2. Map showing vent locations of units younger than 11,000 years. Topographic contours are in feet (1 foot ≈ 0.3 m).

work of *Anderson* [1941]; the latter contains a very useful geologic map. Glass Mountain eruptive products were described by *Anderson* [1933]. Subsequently, *Condie and Hayslip* [1975], *Mertzman* [1977*a*, *b*], and *Mertzman and Williams* [1981] focused mainly on petrologic aspects of the volcano. More recent papers include detailed petrologic work by Grove and his coworkers [*Grove et al.*, 1982, 1988; *Gerlach and Grove*, 1982; *Grove and Baker*, 1984; *Grove and Donnelly-Nolan*, 1986] and a summary of the geology by *Donnelly-Nolan* [1988].

DESCRIPTION AND DATING OF POST-11,000-YEAR LAVAS

The lavas described here are all unglaciated and very young in appearance. The radiocarbon ages reported in Table 1 indicate that some of the lavas erupted in the few hundred years just prior to 10,000 years B.P. and are thus pre-Holocene in age. The 17 eruptive units included in the post-11,000-year time period are shown in Figure 1. All erupted from multiple vents. Most of the mafic lavas erupted from alignments of spatter cones, from pit craters, from cinder cones, or from a combination of vent types. The silicic lavas erupted from alignments of vents that produced flows and domes, some of which coalesced.

Table 2 lists the 17 units and their range of silica content, trend of vents, estimated area covered, and estimated volume. Figure 3 displays some of this information in graphic form, showing that the distribution of the events in time has been episodic. Each of the units is described below, beginning with the products of the early mafic episode and followed by the late Holocene units.

We use paleomagnetism, together with radiocarbon ages and stratigraphy, to constrain the lava chronology. Paleomagnetic directions for early mafic and late Holocene lavas are shown in Figures 4*a* and 4*b*, respectively. The direction of the Earth's magnetic field at a given location changes with time, a change described as secular variation. Lava flows record the direction of the magnetic field at the time when the lava cools through its Curie temperature and becomes magnetized. Each unit described below has been sampled at one or more sites to determine its paleomagnetic direction. Sites were carefully selected to avoid areas of postmagnetization rotation or deformation of the flows. Twelve cores were collected by drilling at each site, oriented by using a sun compass, and then measured in the laboratory.

Ages can be estimated for the sampled flows by compar-

13

TABLE 1. Age Data

Unit	Description	Radiocarbon Age	USGS Number or Reference	Material	Source	Estimated Age From Paleomagnetism
2	basalt of the ribbon flows	10,310 ± 60	2700	charred wood and charcoal	tree mold	≥10,600
3	spatter east of Grasshopper Flat	10,930 ± 50	2650	resinous charred root	tree mold	≥10,600
		10,690 ± 70	A-2650			
4	Giant Crater lava field	10,580 ± 80	1904A	charcoal	tree mold	10,600[a]
		10,620 ± 80	1904B	charcoal	tree mold	
5	basalt of "vent 5"	10,355 ± 50	2701	charcoal and charred wood	tree mold	10,550
6	tree molds flow	10,200 ± 110	2053	charcoal	tree mold	10,550
8	basalt of Valentine Cave	10,850 ± 60	2651	charred root	tree mold	10,450
9	andesite of the pit craters	4,430 ± 70	2649	charcoal	in road cut under tephra	
		4,280 ± 40	2709	charcoal		
10	basalt of Black Crater and Ross chimneys	3,025 ± 45	2766	charcoal	tree mold	
11	Burnt Lava flow	2,800 ± 60	2711	charcoal root	tree mold	
		2,660 ± 60	2712	charcoal root bark	tree mold	
14	Callahan flow	1,110 ± 60	858[b]	wood	tree remnants in edge of flow	1,150
		1,040 ± 100	W-5947[c]	wood		
		1,180 ± 35	2057	charcoal	in road cut under tephra	
16	Little Glass Mountain	1,065 ± 90	*Heiken* [1978]	wood, leaves, bark, cones		900–1,050
17	Glass Mountain	885 ± 40	2136	wood	tree in edge of flow	850–900

Radiocarbon ages are reported ±1 analytical standard deviation. All data are in years before present. Unit numbers comespond to Figures 1 and 2, to the text, and to Table 2.

[a]The correct radiocarbon age relative to which paleomagnetic ages were estimated was chosen arbitrarily to be 10,600 years B.P.

[b]*Donnelly-Nolan and Champion* [1987].

[c]W-5947 was analyzed by M. Rubin in Reston, Virginia.

ison with samples from areas that are both dated by radiocarbon and analyzed by paleomagnetism [*Champion*, 1980; *Sternberg*, 1982, 1989; *Kuntz et al.*, 1986]. For example, archaeological artifacts at sites of human habitation in the southwestern United States have been studied by a combination of paleomagnetic sampling and tree ring and radiocarbon dating [*Sternberg*, 1982, 1989]. Data points plotted on equal-area projections such as those of Figure 4 define curves showing the variation of magnetic direction through time. Records established in this way can be used as tools for dating paleomagnetically sampled materials. Undated material known to be of the same approximate age as an age defined by the established secular variation curve can have its direction of magnetization compared to the established curve. The shapes of such curves of secular variation change somewhat over distances of 1000 km, but the orientation and number of loops do not change significantly. Thus a secular variation curve determined elsewhere can be used to help connect directions of magnetization that are dated or stratigraphically constrained at a new locality into a continuous curve. This new curve can then be used as an age reference for undated but paleomagnetically sampled units of similar stratigraphic position at the new locality.

Time spans of a stratigraphic group of volcanic units of similar age can also be estimated by comparing their directions of magnetization and can thus provide constraints on the length of a volcanic episode. Radiocarbon data taken alone provide absolute age determinations, but, without numerous replications, they often lack the resolution required to constrain the span of time of several possibly related volcanic units. For example, a stratigraphic sequence of lava flows may have radiocarbon ages of 3000 ± 200 years B.P. for the uppermost flow and 3500 ± 200 years B.P. for the lowermost flow. Paleomagnetic sampling of this sequence may yield directions of magnetization that form a well-defined curve on an equal-area projection such as that of Figure 4. The duration of time indicated by the newly determined curve may thus be constrained by comparison with a well-dated archaeomagnetic record or an estimate of the angular rate of secular variation. The indicated time span may be 100 years, rather than the 500 years suggested by the radiocarbon ages. The approximate age indicated by comparison might be 3200 years for the upper flow and 3300 years for the lower flow, within the error limits of the radiocarbon dates. The figures indicate a possibly brief episode of volcanism, rather than the longer duration suggested by the radiocarbon ages.

Sixteen new radiocarbon ages are presented here. Radiocarbon samples were collected from three environments: (1) at the base of large tree molds, (2) under tephra layers, and (3) from tree remnants in the edges of flows. Most of the ages reported here were determined on samples of charcoal or wood collected from tree molds left behind when the lava flows engulfed trees that subsequently burned. Large trees (approximately 1 m in diameter) at Medicine Lake volcano typically have 400 or more growth rings. Large tree molds commonly yield fragments of charcoal that cannot be assigned to a particular part of the tree, and thus radiocarbon ages may be too old by hundreds of years. Charcoal from small tree molds would yield more accurate results, but small molds are difficult to sample, because they are too small to climb into. Radiocarbon ages may be too young if

TABLE 2. Post-11,000-Year Units: Area and Volume Estimates, Vent Trends, and Range of SiO_2 Content

Unit	Description	Estimated Area, km^2	Estimated Volume, km^3	Description of Vents	Vent Trends	SiO_2 Content,[a] wt %
1	spatter vents in Double Hold Crater flow	<0.01[b]	<0.0001	several spatter vents	N20°W, N15°E	50.9 (1)
2	basalt of the ribbon flows	8[c]	0.02	numerous spatter vents	scattered, N-S	49.3–50.6 (4)
3	spatter east of Grasshopper Flat	0.005	<0.0001	several spatter vents	N-S	54.3 (1)
4	Giant Crater lava field	206	4.35	spatter vents, cones, two pit craters	N5°E, N55°E N25°W	47.7–53.2 (84)
5	basalt of "vent 5"	0.01	<0.0001	several spatter vents	N20°W	52.7 (2)
6	tree molds flow	0.025	0.0001	several spatter vents	N-S	51.9 (1)
7	basalt of Devils Homestead	4.3	0.04	several spatter vents	N20°E	51.3–51.4 (2)
8	basalt of Valentine Cave	21	0.2	numerous spatter vents	N35°W	52.9–53.4 (2)
9	andesite of pit craters	2.7	0.02	several pit craters	N25°E	63.4 (2)
10	basalt of Black Crater and Ross chimneys	0.4	0.001	numerous spatter vents	N15°–25°E	48.4–50.1 (2)
11	Burnt Lava flow	37	0.5	cinder cone plus spatter vents	N-S	56.4–57.9 (5)
12	Medicine dacite flow	2.5	0.08	two vents	N45°W	68.5 (1)
13	Hoffman flows	5.5	0.12	greater than or equal to six vents	N25°W	71.3–72.6 (4)
14	Callahan flow	23	0.4	cinder cone plus spatter vents	N30°W	51.8–58.0 (20)
15	basalt of Paint Pot Crater	2.7	0.04	cinder cone plus spatter vents	N40°E	52.9 (1)
16	Little Glass Mountain	6.9	0.4	≥10 vents	N30°E	72.6–74.3 (6)
17	Glass Mountain	14.8	1.0	≥13 vents	N25°W	63.8–74.3 (36)

[a] SiO_2 contents were calculated by normalizing analyses to 100%, volatile-free, all iron as FeO. Major element analyses were performed in USGS laboratories in Lakewood, Colorado, and Menlo Park, California. The number of analyses performed is given in parentheses for each unit.

[b] Flow, if present, is buried by lava from the Double Hole Crater vent of the Giant Crater lava field.

[c] Much of flow is buried under Burnt Lava flow.

the samples are contaminated by younger charcoal or organic material, for example, by the addition of charcoal from later forest fires.

Three new ages reported here, and one previously published date, are from charcoal samples collected under tephra layers that have been correlated stratigraphically with the dated lava flows. Such charcoal may be too old, perhaps by as much as 1000 years, if it is from the inner part of large burned trees, if it is from trees already dead and then burned by the eruptive event, or if the charcoal is from trees previously burned. Two new ages, and one previously published, have been determined on wood samples taken from the edges of tree remnants found in the margins of the Glass Mountain and Callahan flows. In the former case the tree is still standing, and only a small amount of the outer part is missing. The tree remnants collected at the Callahan flow are no longer standing; they are much smaller than the Glass Mountain tree.

Stratigraphic superposition of lava flows is found in only a few cases, but tephrostratigraphy has been useful in determining age relations among late Holocene units. Air fall tephra deposits formed during several of the late Holocene mafic and silicic eruptions. Tephra sequences were identified and measured in road cuts, quarries, and numerous hand-dug holes around the volcano. Individual tephra layers were traced to their sources and correlated with specific flows and domes, thereby providing age constraints on interbedded flows.

Early Mafic Episode

The early mafic episode includes eight units; all of them erupted on the flanks of the volcano. Paleomagnetic and radiocarbon data suggest that this eruptive episode lasted about 400 years. The radiocarbon ages alone suggest a longer time span, but all of the dates were obtained from material collected in large tree molds.

A small basalt flow just south of the Paint Pot Crater flow is morphologically similar to the units of the early mafic episode. No material for radiocarbon dating has been found under this flow, and paleomagnetic data are neither precise nor apparently similar to the directions of the early mafic event. One possible correlation is with units of somewhat similar paleomagnetic direction at Mount Shasta, dated at about 9500 years B.P. (C. D. Miller et al., unpublished data, 1990). This unit is probably somewhat older, postglacial but pre–11,000 years. We base this conclusion on the degree of mantling and soil development and the morphologic degradation of the spatter vents.

Pre–Giant Crater basalts. Three units erupted immediately prior to the Giant Crater eruption.

Spatter vents surrounded by Double Hole flow (Table 2, unit 1): Small spatter vents are completely surrounded by younger lava from the Double Hole Crater vent of the Giant Crater lava field. It is not known whether a lava flow is associated with them. They have not been dated by radiocarbon, but paleomagnetic data (Figure 4*a*) suggest that they

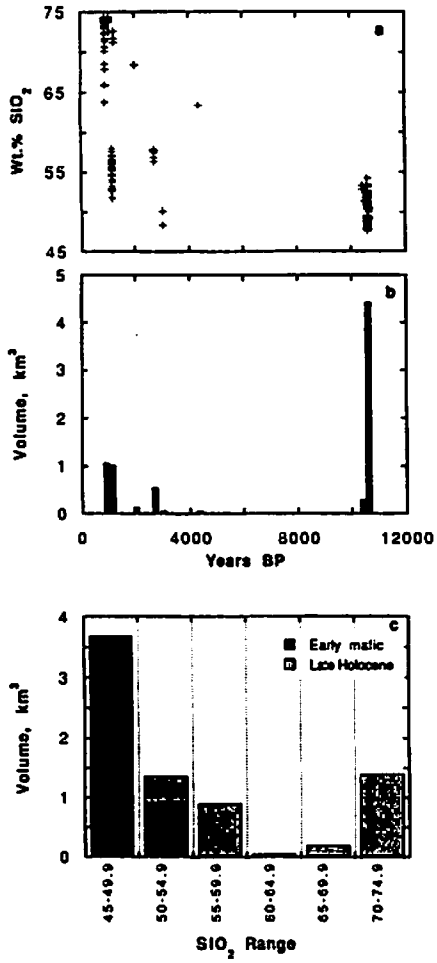

Fig. 3. Volume, time, and SiO_2 content of post-11,000-year lavas (Medicine dacite flow plotted at 2000 years): (*a*) SiO_2 content versus time, where each symbol represents one chemical analysis (note the increase in maximum silica content with time); (*b*) volume versus time plot, displaying the strongly episodic nature of this period of volcanism, as well as the major infusion of basalt represented by the Giant Crater eruption that constitutes 94% of the volume of the early mafic episode; and (*c*) volume versus SiO_2 content, where the more silicic nature and broader range of compositions of the late Holocene episode contrast with the basaltic nature of the early mafic episode. The volumes of some small units have been exaggerated in order to show their positions.

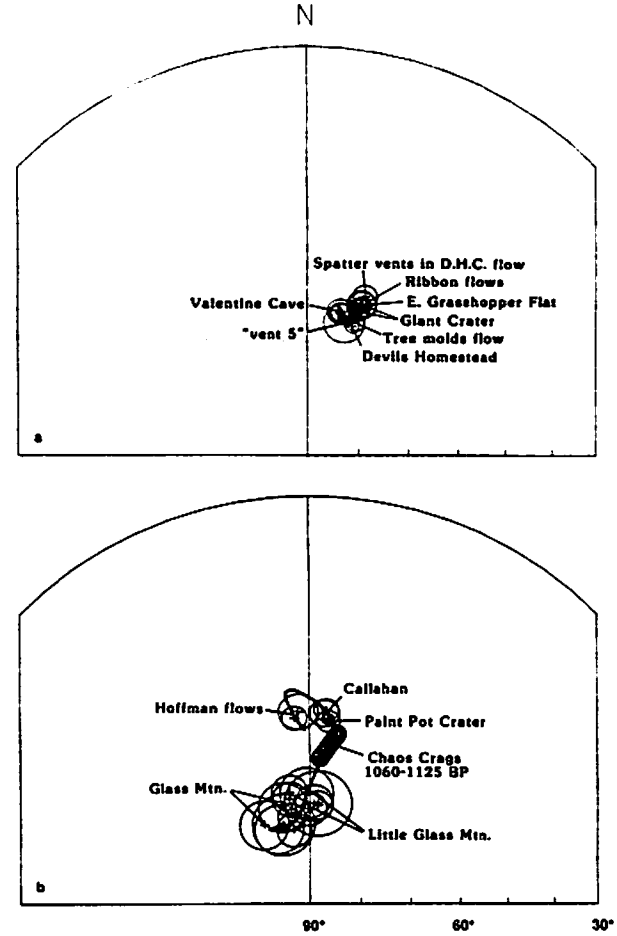

Fig. 4. Equal-area plots of paleomagnetic directions projected on lower hemisphere for (*a*) the early mafic episode (D.H.C. represents the Double Hole Crater) and (*b*) the late Holocene episode. Circles represent 95% confidence limits of the mean directions. Paths of secular variation are drawn through time with the heavy arrow. The patterned area in Figure 4*b* represents paleomagnetic directions from Chaos Crags, Lassen volcanic center (D. E. Champion and M. A. Clynne, unpublished paleomagnetic and radiocarbon data, 1990).

formed immediately before the eruption of Giant Crater lavas.

Basalt of the ribbon flows (Table 2, unit 2): Basalt erupted from numerous spatter vents located north of the Burnt Lava flow. The basalt flowed down two narrow channels (thus "ribbon flows") that had probably been cut by glacial meltwater. The southernmost extent of this unit is exposed at the south edge of the Burnt Lava flow. Most of the unit is buried by Burnt Lava, making estimates of its area highly uncertain. Charcoal from a large tree mold in the eastern ribbon flow gives a radiocarbon age of 10,310 ± 60 years B.P. (Table 1, unit 2). Paleomagnetic data indicate that the eruption occurred just before the Giant Crater eruption.

Spatter east of Grasshopper Flat (Table 2, unit 3): A small amount of basaltic andesite was erupted from a north-south alignment of spatter vents less than 4 km northwest of Giant Crater proper. Two radiocarbon ages (10,930 ± 50 years B.P. and 10,690 ± 70 years B.P., Table 1, unit 3) on a charcoal sample collected from a large tree mold place the unit in this time frame. Paleomagnetic data (Figure 4*a*) indicate that this lava erupted just before the Giant Crater eruption. The radiocarbon ages, which suggest that this unit is older than the Giant Crater lava field, may be too old for reasons discussed above.

Giant Crater lava field (Table 2, unit 4). A 45-km-long basaltic unit covers nearly 10% of the area overlain by Medicine Lake lavas. It is the largest known single eruptive event at the volcano. Its estimated 4.35 km^3 of lava represents nearly two thirds of the total estimated volume of lavas erupted during the past 11,000 years. The lavas erupted from a complex of vents located on the south flank of Medicine Lake volcano. The vents, including several spatter vents and two large pit craters, have two dominant alignments, N5°E and N55°E. The aa and pahoehoe flows were channeled to the south by the topography. Transport of much of the lava took place through lava tubes. Two radiocarbon ages on charcoal samples obtained from a single large tree mold average 10,600 years B.P. (Table 1, unit 4). We have arbitrarily chosen this age as the "real" one to which others

of this early mafic episode are compared (a simple numerical average of the eight ages for this episode gives 10,567 years B.P.).

Lava erupted during the Giant Crater eruption is compositionally zoned: the earliest lava is most silicic (53.2% SiO_2), and the latest is most mafic (47.7% SiO_2). Paleomagnetic sampling of early and late phases of the eruption yielded very slight differences in direction, suggesting a measurable but very short time duration of decades for this large-volume eruption.

Probable successors to the Giant Crater lavas. Four additional units are thought to have erupted soon after the Giant Crater eruption. Three of the four are located on the north side of the volcano (Figure 2).

Basalt of "vent 5" (Table 2, unit 5): Located at the western edge of the Giant Crater flow, a very small basalt flow overlies the Giant Crater lava flows. Charcoal from a large tree mold in the edge of one of the spatter vents yielded a radiocarbon age of 10,355 ± 50 years B.P. (Table 1, unit 5). Paleomagnetic data for this event are not as well constrained as those previously discussed, but the average direction of two sites indicates that the flow just postdates the Giant Crater eruption, although the relative age with respect to the three other successor eruptions is unknown.

Tree molds flow (Table 2, unit 6): A very small basalt flow erupted from several north-south trending spatter vents. It is located on the upper north side of the volcano and has a radiocarbon age of 10,200 ± 110 years B.P. on charcoal from a large tree mold (Table 1, unit 6). Paleomagnetic data suggest a short time interval of perhaps 50–100 years between the Giant Crater eruption and the eruption of the tree molds flow. The difference in the radiocarbon ages is 400 years, indicating that one or both of the radiocarbon ages may not be accurately dating the time of eruption.

Basalt of Devils Homestead (Table 2, unit 7): An undated flow on the far north side of the volcano in Lava Beds National Monument has a paleomagnetic direction identical to that of the tree molds flow. The Devils Homestead flow is located in a very dry area on the lower flank of the volcano. The several spatter vents for the flow are known as the Fleener Chimneys and are located on the north-south Gillem fault where this major normal fault has offset latest Pleistocene basalt. The downstream aa portion of the flow is confined on the west by the Gillem fault scarp and has a very youthful appearance. In contrast, the near-vent pahoehoe lava is relatively heavily vegetated, and its edges are covered with sediment. Overall, the morphology of the flow is similar to the basaltic andesite of Valentine Cave, which is situated in a climatically similar area.

Basaltic andesite of Valentine Cave (Table 2, unit 8): Like the basalt of Devils Homestead, the basaltic andesite of Valentine cave erupted from spatter vents on the north flank of the volcano. Near-vent lavas consist of fluid pahoehoe, whereas distal lavas to the northeast and east form a rugged aa lava field. In contrast with the Devils Homestead lava the basaltic andesite of Valentine Cave [*Donnelly-Nolan and Champion*, 1987] traveled away from its vents by lava tube. It has a radiocarbon age of 10,850 ± 60 years B.P. (Table 1, unit 8) obtained on charcoal collected from a large tree mold adjacent to one of the spatter vents. Paleomagnetic data suggest that this basalt may have erupted about 100 years after the tree molds flow and the basalt of Devils Homestead. If the Giant Crater date of 10,600 years B.P. is correct, then the Valentine Cave flow radiocarbon date is about 400 years too old, which is easily possible if the charcoal represents wood from the center of the tree.

Late Holocene Eruptions

After a hiatus of about 6000 years, nine late Holocene units were emplaced. Six of these erupted between about 1250 and 850 years B.P. Both mafic and silicic eruptions occurred. Four silicic eruptions produced 1.6 km^3 of rhyolite and dacite, representing 60% of the volume of the late Holocene lavas. The many vents for late Holocene lavas are scattered over much of the volcano, including the caldera.

Andesite of the pit craters (Table 2, unit 9). A unit of silicic andesite erupted explosively as air fall tephra and spatter from a northeast trending line of pit craters on the poorly defined southeast rim of the caldera. At the vents the hot andesitic spatter agglutinated to form thin small lava flows. Charcoal was collected from under the tephra deposit at two sites not far from one of the larger pit craters. The radiocarbon samples yielded ages of 4430 ± 70 years B.P. and 4280 ± 40 years B.P. (Table 1, unit 9). The charcoal is thought to have been formed when coarse hot blocks of air fall scoria scorched forest duff and debris, thus closely dating the actual time of eruption.

Basalt of Black Crater and Ross chimneys (Table 2, unit 10). A small amount of fluid and relatively primitive basalt erupted from en-echelon alignments of spatter cones to form small overlapping pahoehoe flows on the far north side of the volcano in Lava Beds National Monument [*Donnelly-Nolan and Champion*, 1987]. Small pockets of white air fall pumice from either the Glass Mountain or the Little Glass Mountain eruption can be found on the flow, which has a radiocarbon age of 3025 ± 45 years B.P. (Table 1, unit 10) obtained on a sample of charcoal from a tree mold.

Burnt Lava flow (Table 2, unit 11). A large andesitic lava flow, known as Burnt Lava flow, covers about 37 km^2 on the south flank of Medicine Lake volcano. It is a rugged aa and block lava flow with little tree cover and was considered by *Finch* [1933] to be as young as 300 years old, on the basis of its appearance. *Anderson* [1941] estimated it to be older, perhaps 500–1000 years. Published radiocarbon ages on charcoal from trees at the edge of the flow range from 200 ± 200 to 320 ± 200 years B.P. [*Ives et al.*, 1964]. The flow vented from a large cinder cone (High Hole Crater) and a north-south trending spatter rampart at the north edge of the flow. Rare smooth surfaces on the upper parts of Burnt Lava flow display a thin covering of white pumice (> 900 years old) from Little Glass Mountain, indicating that the young radiocarbon ages were obtained from material burned by later forest fires. Two samples of charcoal collected from a large tree mold yielded ages of 2660 ± 60 and 2800 ± 60 years B.P. (Table 1, unit 11). The discrepancy between the early estimates of the age of the flow and the > 2600-year ages published here can be explained by a combination of the scarcity of tephra and aeolian deposits on the flow and by its rugged blocky surface, both of which have inhibited the growth of vegetation. The flow is surrounded by a thick evergreen forest that has apparently limited the aeolian transport of fine-grained sediment. Burnt Lava lies at the southern edge of the tephra deposits from both Glass Mountain and Little Glass Mountain.

Medicine dacite flow (Table 2, unit 12). This viscous

pancakelike flow, located just north of Medicine Lake on the caldera floor, is undated but is morphologically very young. Its edges are 30- to 40-m-high cliffs and talus slopes at the angle of repose. Unlike the other Holocene silicic units, it apparently lacked a preceding air fall tephra deposit and so presents little opportunity for collecting radiocarbon samples. It is overlain by air fall tephra from the Callahan, Paint Pot, Little Glass Mountain, and Glass Mountain eruptions and thus is older than about 1150 years B.P. Paleomagnetic data indicate possible ages at about 2000, 3300, and 4200 years B.P. These figures are based on a comparison with directions of magnetization from radiocarbon-dated basalt flows in the Cascade Range at Mount St. Helens, Washington, central Oregon, and Medicine Lake volcano and at the Craters of the Moon, Idaho, the Jordan Crater lava field, Oregon, and Dotsero Crater, Colorado [*Champion*, 1980, also unpublished data, 1990).

Hoffman flows (Table 2, unit 13). We include in one unit the Hoffman flow proper as recognized by *Powers* [1932] as well as a rhyolite flow on the northeast shoulder of Mount Hoffman described by *Anderson* [1941]. These two flows are steep-sided viscous lavas that are identical in appearance and chemical composition. Their vents define a N25°W trend, and we think they represent a single eruptive event from the same magma reservoir. The larger of the two flows erupted at, or just within, the caldera rim and flowed both west into the caldera and east where it is overlain by the rhyolite of Glass Mountain. A tephra deposit that precedes the Hoffman flows has been recognized, but no material that dates this event has been found. The flows are overlain by air fall tephra from the Callahan, Little Glass Mountain, and Glass Mountain eruptions. The Glass Mountain tephra thins rapidly to the west, so that the western end of the larger Hoffman flow looks very youthful. Closer to the Glass Mountain vents a thick tree cover has grown in the younger pumice, obscuring the rugged topography of the flow. Comparison of the archaeomagnetic record from the American southwest [*Sternberg*, 1982] with our paleomagnetic data indicates that this unit is older than 1200 years B.P., perhaps about 1230 years B.P..

Callahan flow (Table 2, unit 14). The Callahan flow is on the north flank of the volcano. It vented from a large cinder cone (Cinder Butte) and adjacent spatter vents and consists mostly of aa lava. The Callahan flow has some similarities to the Burnt Lava flow, but it has much more compositional variability. It initially erupted andesite with 58.0 wt % SiO_2, followed by lava with a decreasing silica content. The last erupted lava contains 51.8% SiO_2. Radiocarbon ages of 1110 ± 60 years B.P. (Table 1, unit 14 [*Donnelly-Nolan and Champion*, 1987]) and 1040 ± 100 years B.P. were both obtained from wood of tree remnants. The trees were overrun by the lava at two different sites at the eastern edge of the flow. A third date of 1180 ± 35 years B.P. was determined from charcoal found immediately underneath the air fall tephra that was produced by the initial explosive part of the eruption. A weighted average of these three ages yields a date of 1130 ± 26 years B.P. for this event. Paleomagnetic data suggest an age of about 1150 years B.P., on the basis of a comparison with paleomagnetic directions of well-dated units at Lassen volcanic center (D. E. Champion and M. A. Clynne, written communication, 1989).

Basalt of Paint Pot Crater (Table 2, unit 15). A relatively small, extremely rough surfaced basalt flow erupted from the large Paint Pot Crater cinder cone and adjacent northeast trending spatter vents on the southwest flank of the volcano. Paleomagnetic data indicate that the Paint Pot Crater flow is virtually identical in age to the Callahan flow. Paint Pot air fall tephra, which preceded the flow, immediately overlies uneroded Callahan tephra and thus is younger than about 1150 years B.P. Paint Pot Crater and its flow are overlain by air fall tephra (radiocarbon dated at 1065 ± 90 years B.P.), erupted from nearby Little Glass Mountain. This white tephra blankets the red and black cone and is the reason for its name. The vent area and the upper part of the flow are thickly mantled by white pumice, obscuring the ruggedness of the flow surface. The age of the flow, based on a comparison with the Lassen paleomagnetic records as well as the radiocarbon records (D. E. Champion and M. A. Clynne, written communication, 1989), is just slightly younger than the Callahan flow, but more than 1100 years B.P.

Little Glass Mountain (Table 2, unit 16). Little Glass Mountain is a very young steep-sided obsidian flow located west of Medicine Lake caldera. A radiocarbon age of 1065 ± 90 years B.P. (Table 1, unit 16 [*Heiken*, 1978]) was obtained on a sample collected by one of us (C.D.M.) and dated at a commercial laboratory. Tephra from the Little Glass Mountain vent overlies every unit within its areal extent except the tephra from Glass Mountain and its domes. With Little Glass Mountain we include the chemically and petrographically identical, but much smaller, domes to the northeast on an approximate N30°E trend, some of which are known as the Crater Glass flows. Local tephra deposits are associated with these domes; the deposits underlie the tephra of Glass Mountain. Because paleomagnetic data are less precise on Little Glass Mountain and Glass Mountain lavas than on the more easily sampled mafic flows, the age difference between these two silicic units could be as large as the nearly 200 years suggested by the radiocarbon ages in Table 1; or alternatively, the Little Glass Mountain eruption could have immediately preceded Glass Mountain. Comparison of Medicine Lake paleomagnetic data with those on flows with multiple radiocarbon ages at the Lassen volcanic center (D. E. Champion and M. A. Clynne, written communication, 1989) suggests that the Little Glass Mountain event is probably no older than 1050 years B.P.

Glass Mountain (Table 2, unit 17). Glass Mountain consists of a spectacular, nearly treeless, steep-sided rhyolite and dacite obsidian flow that erupted just outside the eastern caldera rim and flowed down the steep eastern flank of Medicine Lake volcano. Ten additional small domes of Glass Mountain rhyolite and rhyodacite lava lie on a N25°W trend to the north and one to the south. The age of Glass Mountain and its preceding pumice deposits has been a matter of discussion for some time [*Chesterman*, 1955; *Ives et al.*, 1967; *Sullivan et al.*, 1970; *Heiken*, 1978]. A radiocarbon age of 885 ± 40 years B.P. was obtained on a dead cedar tree without limbs or bark that is preserved in the edge of one of the distal tongues of the flow. The dated material consisted of a piece of exterior wood containing about 30 annual growth rings. This age may be too old, because some of the outside of the tree is missing. The tephra deposits that precede the flow and domes may be somewhat older but are constrained to be less than about 1050 years B.P. by the Little Glass Mountain and Lassen data.

18

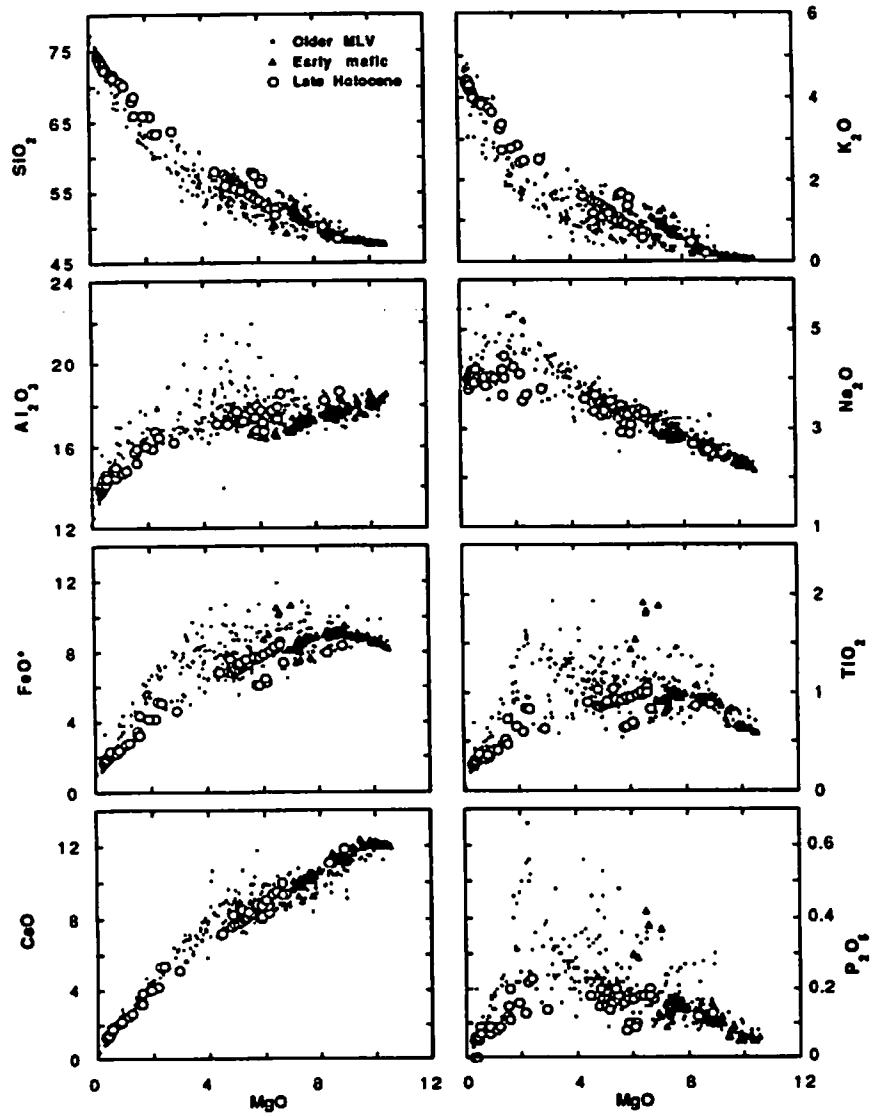

Fig. 5. MgO variation diagrams of major elements in post-11,000-year Medicine Lake lavas. Pre-11,000-year Medicine Lake lavas (n = 275) are shown with smaller symbols.

The "1910 Event"

Finch [1928] cited a report by a local rancher of earthquakes in 1910 accompanied by flames over Glass Mountain, ground breakage to the north, and "blue mud" on vegetation. No evidence of any such recent deposit nor any likely vent for an eruption has been found by the authors; accordingly, this purported eruptive event is disregarded here.

CHEMICAL COMPOSITION OF POST-11,000-YEAR UNITS

Variation diagrams of major element analyses of Medicine Lake lavas are plotted versus MgO in Figure 5. The post-11,000-year units are plotted as symbols, and the compositional variability of older Medicine Lake lavas is shown for comparison as outlined fields on each diagram. In most variation diagrams the post-11,000-year lavas show smooth coherent trends. Early mafic lavas and late Holocene lavas define a trend that is continuous over the range of 11–5 wt % MgO. A break, occupied by a few lavas, occurs in the range of 5–2 wt % MgO; the trend then continues over the range of 2–0.3 wt % MgO. All but one of the post-11,000-year lavas contain <4 vol % phenocrysts; thus the trends are defined by liquids. Magmatic inclusions show more scatter than erupted lavas in the variation diagrams (Figure 6). Some of this scatter is the result of the accumulation of crystals. Inclusions with lower FeO*, CaO, and TiO_2, higher K_2O and SiO_2, and variable Al_2O_3 at 8–12 wt % MgO contain olivine, plagioclase, and augite and have cumulate textures and interstitial silicic glass. Some inclusions and several lavas in the range of 7–2 wt % MgO also depart from the main trend defined by the post-11,000-year lavas. These inclusions and lavas show higher FeO*, TiO_2, and P_2O_5 and lower SiO_2 and K_2O as compared to the main lava trend at equal MgO values. *Grove and Donnelly-Nolan* [1986] identify these inclusions as quenched magmatic liquids.

In general, the older Medicine Lake lavas show a much broader range of composition at a given MgO value. This spread is particularly evident in the range of 6–1 wt % MgO. It is caused, in part, by the larger proportion of plagioclase phenocrysts present in some of the older lavas. The higher Al_2O_3 values are measured in lavas in which plagioclase accumulation has occurred. One of the post-11,000-year

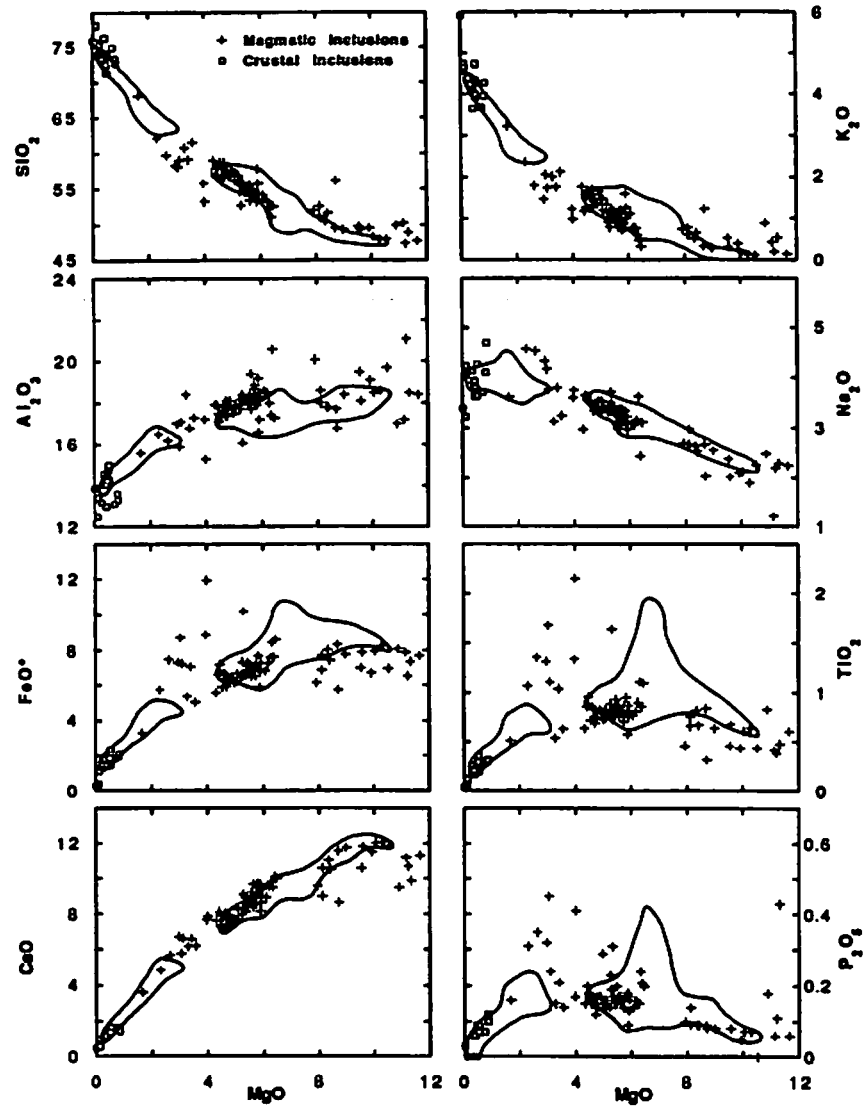

Fig. 6. MgO variation diagrams of major elements in inclusions found in post-11,000-year lavas. Post-11,000-year lava compositions are shown as fields (plotted in Figure 5). Of the 82 magmatic inclusions, 70% were collected from Glass Mountain and Little Glass Mountain. The gap between about 2.5 and 4.3 wt % MgO in lavas younger than 11,000 years does not exist in the suite of inclusions found in them.

lavas (the basalt of Black Crater and Ross chimneys) contains abundant plagioclase and exhibits a high Al_2O_3 content for its weight percent MgO, indicating plagioclase accumulation. Aphyric lavas containing higher Al_2O_3, FeO*, Na_2O, TiO_2, and P_2O_5 and lower SiO_2, CaO, and K_2O are represented in the older eruptive products, along with lavas whose characteristics are similar to those erupted during the last 11,000 years.

Grove and Donnelly-Nolan [1986] and *Grove et al.* [1988] modeled the petrogenetic processes that may have generated the Little Glass Mountain rhyolite and the Burnt Lava flow, both of which were erupted during late Holocene time. Earlier work by *Grove et al.* [1982] and *Gerlach and Grove* [1982] emphasized the role of combined fractionation, assimilation, and mixing at Medicine Lake volcano. In the case of Little Glass Mountain, mineralogical and geochemical evidence indicates that fractionation of an andesitic parent, together with assimilation, produced rhyolite. Petrologic modeling of the andesite of Burnt Lava indicates that the fractionation of basalt and the assimilation of crustal material occurred together with the mixing of magmas. The inferred parental magma at Medicine Lake volcano is high-alumina basalt [*Grove et al.*, 1982; *Grove and Baker*, 1984; *Donnelly-Nolan*, 1988], also called high-alumina olivine tholeiite (HAOT) by *Hart et al.* [1984]. Fractionation of this basalt at shallow crustal levels would produce residual liquids higher in FeO*, TiO_2, and Na_2O and lower in SiO_2 and K_2O content than the Holocene lavas at similar MgO content. *Grove et al.* [1988] recognized mineralogical evidence for such an iron-enriched magma preserved in Burnt Lava. Glomerocrysts of Fe-rich olivine, augite, and labradorite observed in the Burnt Lava flow indicate the existence of a ferrobasaltic liquid produced by a large amount of fractionation of a high-alumina basalt magma.

The same fractionation process that yielded the iron-enriched magma and the Fe-rich olivine, augite, and labradorite provided the heat to melt granitic crust at shallow crustal levels. Burnt Lava flow contains melted granitic inclusions as well as primitive high-alumina basalt inclusions similar to the basalt erupted at Giant Crater. Burnt Lava

20

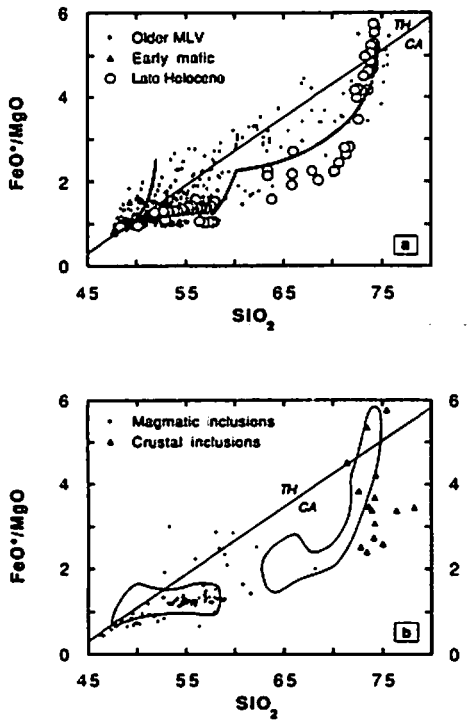

Fig. 7. FeO*/MgO versus SiO_2: (*a*) post-11,000-year lavas as larger symbols; pre-11,000-year Medicine Lake lavas (n = 275) shown with smaller symbols. The heavy curves are fractional crystallization models from *Grove et al.* [1988, Table 7, model 1] and *Grove and Donnelly-Nolan* [1986, Table 4]. (*b*) Inclusions in post-11,000-year lavas, with lavas younger than 11,000 years shown as fields. Two partially melted inclusions with FeO*/MgO values of 10.6 and 9.4 and identical SiO_2 values of 75.8 wt % are not shown so that Figures 7*a* and 7*b* may be compared directly; these two inclusions were found in the Callahan flow and match the composition of an older rhyolite of Medicine Lake volcano. The field of lavas older than 11,000 years is much broader and shows more iron enrichment than younger lavas, although the most mafic Giant Crater lavas and the Glass Mountain and Little Glass Mountain silicic lavas display iron enrichment. The line separating tholeiitic (TH) from calc-alkaline (CA) fields is from *Miyashiro* [1974].

andesite is modeled as a mixture of high-alumina basalt, 18–26% fractionated Fe-rich basalt, and 27–35% melted granitic crust [*Grove et al.*, 1988]. Mixing is thought to have been accomplished by replenishment by high-alumina basalt of a magma reservoir containing ferrobasalt and melted granitic crust. A similar process may have produced the dominant compositional trend, followed by the lavas of the early mafic episode, about 10,500 years ago. The compositionally zoned Giant Crater (47.7–53.2 wt % SiO_2) and Callahan (51.8–58.0 wt % SiO_2) flows contain partly melted granitic inclusions and ferrogabbro cumulates, indicating the incorporation of melted crust and iron-enriched magma into high-alumina basalts. The early lavas of Giant Crater are enriched in silica and have a calc-alkaline signature, which reflects the incorporation of a large component of melted crust in addition to iron-enriched magma. As the eruption progressed, the later lavas show an iron enrichment trend, caused by the mixing in of a larger proportion of the iron-enriched magma. A few post-11,000-year lavas (basalt of the ribbon flows and basaltic andesite of Valentine Cave) contain a large component of the iron-enriched liquid.

Figure 7 shows that the post-11,000-year lava trend crosses the tholeiitic-calc-alkaline dividing line twice on an FeO*/MgO versus SiO_2 diagram, once in the mafic compositional range and once at the silicic end. The mafic Giant Crater lavas show a tholeiitic trend of iron enrichment, and the basaltic lavas of Valentine Cave and the ribbon flows lie in the tholeiitic field. The most silicic lavas of Glass Mountain, Little Glass Mountain, and the Hoffman flows also follow an Fe enrichment trend. The high-SiO_2 Giant Crater lavas, Burnt Lava flow, and the Callahan flow follow calc-alkaline trends. The dacitic part of the Glass Mountain eruption, which shows clear evidence of mixing of andesite and rhyolite [*Eichelberger*, 1975, 1981], also follows a calc-alkaline trend. The fractional crystallization path of iron enrichment inferred by *Grove et al.* [1988] from Burnt Lava and the fractionation path calculated for Little Glass Mountain by *Grove and Donnelly-Nolan* [1986] are shown as solid curves in Figure 7*a*. The iron enrichment fractionation path inferred from the Burnt Lava flow passes through the iron-enriched basaltic lavas of Valentine Cave and the ribbon flows. Iron-rich lavas were more common during the pre-11,000-year eruptive history of Medicine Lake volcano (Figure 7*a*), indicating a more dominant role for fractionation in the evolution of the pre-11,000-year magmas. The calc-alkaline trend defined by the high-SiO_2 Giant Crater lavas, the Burnt Lava andesite, and the Callahan lavas in the range of 50–58 wt % SiO_2 is caused by contamination of fractionated Fe-rich basalt and parental high-alumina basalt by large amounts of melted granite.

In the case of the silicic magmas, fractionation is the dominant process that produces rhyolite from andesite. The rhyolitic lavas of Glass Mountain, Little Glass Mountain, and the Hoffman flows form a coherent trend that resembles the calculated fractional crystallization trend of *Grove and Donnelly-Nolan* [1986] shown in Figure 7*a*. The model also shows a trend of iron enrichment. Magmatic inclusions in the compositional range of 58.1–62.2 wt % SiO_2 are typically fine grained and represent liquid compositions. All inclusions with more than 70 wt % SiO_2 are partially melted crustal inclusions that are mostly granitic, although a few of the more melted ones may be rhyolitic. The granitic crustal inclusions show a widely ranging compositional variation in FeO*/MgO, different from the coherent trend that is defined by the rhyolite lavas. The compositional diversity in the crustal inclusions does not support the interpretation that Medicine Lake Holocene rhyolites are bulk melts of the underlying crust, because the majority of the granitic inclusions have lower FeO*/MgO and higher SiO_2 compared to the rhyolites.

Fine-grained andesitic magmatic inclusions with an SiO_2 content of 58.1–62.2 wt % are present in Little Glass Mountain, the Medicine dacite flow, and Glass Mountain. These three units lie atop the volcano, just west of the caldera, within the caldera, and slightly to the east. Thus andesitic magma in this compositional range was present during late Holocene time but did not erupt to the surface. Infusions of primitive basalt occurred more than once in late Holocene time, beginning with the 3000-year-old basalt of Black Crater and Ross chimneys. Basaltic magmatic inclusions are present in late Holocene lavas, notably in the Burnt Lava flow. Somewhat less primitive basaltic inclusions were erupted in the later Hoffman flows. Basaltic inclusions are also found in the rhyolite of Glass Mountain.

21

DISCUSSION

Volcanic eruptions have taken place over a broad area of Medicine Lake volcano (an area approximately 30 km north-south and 15 km east-west) during the past 11,000 years. Each of the 17 units that erupted during this period has more than one vent. Vent alignments are tectonically controlled and are parallel or subparallel to major regional structural features. In contrast to the broad spatial distribution, the eruptive activity has not occurred on a regular basis throughout the time period involved. Radiocarbon and paleomagnetic time controls indicate to us that there was a long hiatus between a brief episode early in postglacial time and subsequent late Holocene eruptions. There is also a strong contrast in composition between the early mafic and the late Holocene eruptions. The early mafic episode is characterized entirely by basaltic lava, whereas in late Holocene time, rhyolite exceeds andesitic compositions in volume, and only a very small amount of basalt was erupted. The next older rhyolitic episode occurred in late Pleistocene time, perhaps 20,000 years ago or more, when the glaciated rhyolite of Mount Hoffman erupted on the north rim of the caldera. The lack of age control and the burial by younger lavas make earlier volcanic episodes difficult to identify.

Tectonic extension and volcanism appear to be linked at Medicine Lake volcano. Episodes of basaltic intrusion result from extension that allows deep-seated magmas to reach the surface. Local ground breakage that may or may not be accompanied by eruption of lava to the surface probably occurs as a result of regional stretching of the crust related to plate movements. Some Medicine Lake basalts, including the last erupted flows of the basalt of Giant Crater, are near-primary [*Bartels et al.*, 1988] and have been compared with mid-ocean ridge basalts [*Hart*, 1971; *Philpotts et al.*, 1971; *McKee et al.*, 1983; *Hart et al.*, 1984]. Some primitive basalt travels upward rapidly enough in this extensional environment to reach the surface virtually uncontaminated. The experiments of *Bartels et al.* [1988] indicate a depth of origin by partial melting of mantle lherzolite of about 33 km for the primitive basalt of Giant Crater. Somewhat less primitive basalts may be affected by processes of fractionation, assimilation, and mixing in shallow reservoirs before erupting to the surface.

The episodes of volcanism that we have identified do not enable us to make specific predictions as to when, where, or what kind of lava might erupt next at Medicine Lake volcano. We believe, however, that any strong seismic episode should be carefully monitored; ground breakage might be followed by the eruption of lava. The pattern of silicic lavas erupting high on the volcano, and of basaltic ones on the flanks [*Donnelly-Nolan*, 1988, also unpublished mapping, 1990], suggests that future extension and ground breakage high on the volcano might result in the eruption of silicic lava. Such an eruption could be accompanied by explosive activity similar to that which produced the plinian air fall deposits that preceded the Little Glass Mountain and Glass Mountain eruptions [*Heiken*, 1978].

The amount of heat available for geothermal energy is unknown, but it is likely to be a function of the amount of heat stored in cooling magma in the upper crust below the volcano. Drilling of geothermal exploration wells in the caldera is known to have yielded temperature gradients of 88°C km^{-1}, 227°C km^{-1}, and 548°C km^{-1} in three of the drill holes [*Bureau of Land Management*, 1983]. Given the paucity of publicly available drill hole data, continued interest by industry in drilling exploratory holes suggests that sufficient heat may be available to provide a commercial resource, if an adequate fluid supply can be found. Likely sources of heat include a small silicic magma reservoir inferred from seismic tomography [*Evans and Zucca*, 1988] and basalt intruded in late Holocene time.

CONCLUSIONS

Good age control for the last 11,000 years at Medicine Lake volcano has given us an understanding of the episodic nature of volcanism during this period. The eruptive activity is probably driven by intrusions of basalt that occur as a result of crustal extension. The inferred presence of mafic dikes and small derivative magma bodies of more silicic compositions during postglacial time agrees with models proposed by *Donnelly-Nolan* [1988] and *Evans and Zucca* [1988], constrained in part by the geophysical studies of *Finn and Williams* [1982], *Zucca et al.* [1986], and *Fuis et al.* [1987]. Late Holocene lavas are derived by fractionation, assimilation, and mixing from high-alumina basalt parental magma, possibly from basalt intruded into the volcano during the early mafic episode when > 4 km^3 of basalt of Giant Crater erupted. Eruption of late Holocene lavas may be related to several basaltic intrusive episodes. These episodes, plus stored heat from the early mafic episode, should provide adequate heat for commercial geothermal development if sufficient fluids can be found. The nature and timing of volcanic activity cannot be predicted from the present data, but crustal extension and seismic swarms should be carefully monitored because they may be followed by eruptive activity.

Acknowledgments. C. R. Bacon, R. Batiza, W. Hildreth, and S. A. Mertzman, Jr., provided helpful reviews. We thank the National Park Service for permission to collect samples in Lava Beds National Monument. Plots were made using chemical analyses performed by J. Taggart, A. J. Bartel, R. V. Mendes, D. Siems, K. Stewart, and J. S. Wahlberg of the USGS, Lakewood, Colorado.

REFERENCES

Anderson, C. A., Volcanic history of Glass Mountain, northern California, *Am. J. Sci.*, *26*, 485–506, 1933.

Anderson, C. A., Volcanoes of the Medicine Lake Highland, California, *Univ. Calif. Publ. Bull. Dep. Geol. Sci.*, *25*, 347–422, 1941.

Bartels, K. S., R. J. Kinzler, and T. L. Grove, High pressure phase relations of a near-primary high alumina basalt (HAB) magma from Medicine Lake Highland, N. California (abstract), *Eos Trans. AGU*, *69*, 1494, 1988.

Bureau of Land Management, California State Office, Mineral Land Classification Board, Redefinition by addition to the Glass Mountain Known Geothermal Resources Area, Siskiyou County, California, California Known Geothermal Resources Area, *Minutes 40*, p. 4, Sacramento, 1983.

Champion, D. E., Holocene geomagnetic secular variation in the western United States: Implications for the global geomagnetic field, *U.S. Geol. Surv. Open File Rep.*, *80-824*, 314 pp., 1980.

Chesterman, C. W., Age of the obsidian flow at Glass Mountain, Siskiyou County, California, *Am. J. Sci.*, *253*, 418–424, 1955.

Condie, K. C., and D. L. Hayslip, Young bimodal volcanism at Medicine Lake volcanic center, northern California, *Geochim. Cosmochim. Acta*, *39*, 1165–1178, 1975.

Donnelly-Nolan, J. M., A magmatic model of Medicine Lake volcano, California, *J. Geophys. Res.*, *93*, 4412–4420, 1988.

22

Donnelly-Nolan, J. M., and D. E. Champion, Geologic map of Lava Beds National Monument, northern California, scale 1 : 24,000, *U.S. Geol. Surv. Map, I-1804*, 1987.

Eichelberger, J. C., Origin of andesite and dacite: Evidence of mixing at Glass Mountain in California and at other circum-Pacific volcanoes, *Geol. Soc. Am. Bull.*, *86*, 1381–1391, 1975.

Eichelberger, J. C., Mechanism of magma mixing at Glass Mountain, Medicine Lake Highland volcano, California, *U.S. Geol. Surv. Circ.*, *838*, 183–189, 1981.

Evans, J. R., and J. J. Zucca, Active high-resolution seismic tomography of compressional wave velocity and attenuation structure at Medicine Lake volcano, northern California Cascade Range, *J. Geophys. Res.*, *93*, 15,016–15,036, 1988.

Finch, R. H., Lassen report no. 14, *Volcano Lett. 161*, 1928. (Reprinted in *The Volcano Letters*, edited by R. S. Fiske, T. Simkin, and E. A. Nielsen, Smithsonian Institution, Washington, D. C., 1987.)

Finch, R. H., Burnt Lava flow in northern California, *Z. Vulkanol.*, *10*, 180–183, 1933.

Finn, C., and D. L. Williams, Gravity evidence for a shallow intrusion under Medicine Lake volcano, California, *Geology*, *10*, 503–507, 1982.

Fuis, G. S., J. J. Zucca, W. D. Mooney, and B. Milkereit, A geologic interpretation of seismic-refraction results in northeastern California, *Geol. Soc. Am. Bull.*, *98*, 53–65, 1987.

Gerlach, D. D., and T. L. Grove, Petrology of Medicine Lake Highland volcanics, characterization of endmembers of magma mixing, *Contrib. Mineral. Petrol.*, *80*, 147–159, 1982.

Grove, T. L., and M. B. Baker, Phase equilibrium controls on the tholeiitic versus calc-alkaline differentiation trends, *J. Geophys. Res.*, *89*, 3253–3274, 1984.

Grove, T. L., and J. M. Donnelly-Nolan, The evolution of young silicic lavas at Medicine Lake volcano, California: Implications for the origin of compositional gaps in calc-alkaline series lavas, *Contrib. Mineral. Petrol.*, *92*, 281–302, 1986.

Grove, T. L., D. C. Gerlach, and T. W. Sando, Origin of calc-alkaline series lavas at Medicine Lake volcano by fractionation, assimilation and mixing, *Contrib. Mineral. Petrol.*, *80*, 160–182, 1982.

Grove, T. L., R. J. Kinzler, M. B. Baker, J. M. Donnelly-Nolan, and C. E. Lesher, Assimilation of granite by basaltic magma at Burnt Lava flow, Medicine lake volcano, northern California: Decoupling of heat and mass transfer, *Contrib. Mineral. Petrol.*, *99*, 320–343, 1988.

Hart, S. R., K, Rb, Cs, Sr and Ba contents and Sr isotope ratios of ocean floor basalts, *Philos. Trans. R. Soc. London, Ser. A*, *268*, 573–587, 1971.

Hart, W. K., J. L. Aronson, and S. A. Mertzman, Areal distribution and age of low-K, high-alumina olivine tholeiite magmatism in the northwestern Great Basin, *Geol. Soc. Am. Bull*, *95*, 186–195, 1984.

Heiken, G., Plinian-type eruptions in the Medicine Lake Highland, California, and the nature of the underlying magma, *J. Volcanol. Geotherm. Res.*, *4*, 375–402, 1978.

Ives, P. C., B. Levin, R. D. Robinson, and M. Rubin, U.S. Geological Survey radiocarbon dates VII, *Radiocarbon*, *7*, 49–50, 1964.

Ives, P. C., B. Levin, C. L. Oman, and M. Rubin, U.S. Geological Survey radiocarbon dates IX, *Radiocarbon*, *9*, 513–516, 1967.

Kuntz, M. A., D. E. Champion, E. C. Spiker, and R. H. LeFebvre, Contrasting magma types and steady-state, volume-predictable, basaltic volcanism along the Great Rift, Idaho, *Geol. Soc. Am. Bull.*, *97*, 579–594, 1986.

McKee, E. H., W. A. Duffield, and R. J. Stern, Late Miocene and early Pliocene basaltic rocks and their implications for crustal structure, northeastern California and south-central Oregon, *Geol. Soc. Am. Bull.*, *94*, 292–304, 1983.

Mertzman, S. A., Jr., Recent volcanism at Schonchin and Cinder Buttes, northern California, *Contrib. Mineral. Petrol.*, *61*, 231–243, 1977*a*.

Mertzman, S. A., Jr., The petrology and geochemistry of the Medicine Lake volcano, California, *Contrib. Mineral. Petrol.*, *62*, 221–247, 1977*b*.

Mertzman, S. A., K-Ar results for silicic volcanics from the Medicine Lake Highland, northeastern California—A summary, *Isochron/West*, *34*, 3–7, 1982.

Mertzman, S. A., An addendum to "K-Ar results for silicic volcanics from the Medicine Lake Highland, northeastern California—A summary," *Isochron/West*, *38*, 3–5, 1983.

Mertzman, S. A., and R. J. Williams, Genesis of Recent silicic magmatism in the Medicine Lake Highland, California, evidence from cognate inclusions found at Little Glass Mountain, *Geochim. Cosmochim. Acta*, *45*, 1463–1478, 1981.

Miyashiro, A., Volcanic rock series in island arcs and active continental margins, *Am. J. Sci.*, *274*, 321–355, 1974.

Philpotts, J. A., W. Martin, and C. C. Schnetzler, Geochemical aspects of some Japanese lavas, *Earth Planet. Sci. Lett.*, *12*, 89–96, 1971.

Powers, H. A., The lavas of the Modoc Lava-Bed quadrangle, California, *Am. Mineral.*, *17*, 253–294, 1932.

Sternberg, R. S., Archaeomagnetic secular variation of direction and paleointensity in the American southwest, Ph.D. dissertation, 305 pp., Univ. of Ariz., Tucson, 1982.

Sternberg, R. S., Secular variation of archaeomagnetic direction in the American southwest, A.D. 750–1425, *J. Geophys. Res.*, *94*, 527–546, 1989.

Sullivan, B. M., E. Spiker, and M. Rubin, U.S. Geological Survey radiocarbon dates XI, *Radiocarbon*, *12*, 319–334, 1970.

Zucca, J. J., G. S. Fuis, B. Milkereit, W. D. Mooney, and R. D. Catchings, Crustal structure of northeastern California, *J. Geophys. Res.*, *91*, 7359–7382, 1986.

D. E. Champion, J. M. Donnelly-Nolan, and D. A. Trimble, U.S. Geological Survey, 345 Middlefield Road, Menlo Park, CA 94025.

T. L. Grove, Department of Earth, Atmosphere, and Planetary Sciences, Massachusetts Institute of Technology, Cambridge, MA 02139.

C. D. Miller, U.S. Geological Survey Cascades Volcano Observatory, 5400 MacArthur Boulevard, Vancouver, WA 98661.

(Received June 7, 1989;
revised April 20, 1990;
accepted August 14, 1989.)

23

JOURNAL OF GEOPHYSICAL RESEARCH, VOL. 96, NO. B10, PAGES 16,319–16,333, SEPTEMBER 10, 1991

Crustal Subsidence, Seismicity, and Structure Near Medicine Lake Volcano, California

DANIEL DZURISIN

David A. Johnston Cascades Volcano Observatory, U.S. Geological Survey, Vancouver, Washington

JULIE M. DONNELLY-NOLAN, JOHN R. EVANS, AND STEPHEN R. WALTER

U.S. Geological Survey, Menlo Park, California

The pattern of historical ground deformation, seismicity, and crustal structure near Medicine Lake volcano illustrates a close relation between magmatism and tectonism near the margin of the Cascade volcanic chain and the Basin and Range tectonic province. Between leveling surveys in 1954 and 1989 the summit of Medicine Lake volcano subsided 389 ± 43 mm with respect to a reference bench mark 40 km to the southwest (average rate = 11.1 ± 1.2 mm/yr). A smaller survey across the summit caldera in 1988 suggests that the subsidence rate was 15–28 mm/yr during 1988–1989. Swarms of shallow earthquakes ($M \leq 4.6$) occurred in the region during August 1978, January–February 1981, and September 1988. Except for the 1988 swarm, which occurred beneath Medicine Lake caldera, most historical earthquakes were located at least 25 km from the summit. The spatial relation between subsidence and seismicity indicates (1) radially symmetric downwarping of the volcano's summit and flanks centered near the caldera and (2) downfaulting of the entire edifice along regional faults located 25–30 km from the summit. We propose that contemporary subsidence, seismicity, and faulting are caused by (1) loading of the crust by more than 600 km^3 of erupted products plus a large volume of mafic intrusives; (2) east-west extension in the western Basin and Range province; and, to a lesser extent, (3) crystallization or withdrawal of magma beneath the volcano. Thermal weakening of the subvolcanic crust by mafic intrusions facilitates subsidence and influences the distribution of earthquakes. Subsidence occurs mainly by aseismic creep within 25 km of the summit, where the crust has been heated and weakened by intrusions, and by normal faulting during episodic earthquake swarms in surrounding, cooler terrain.

INTRODUCTION AND SCOPE

The Medicine Lake region in northeastern California, located near the margin of the Cascades volcanic chain and the Basin and Range tectonic province, provides an excellent opportunity to study the relation between tectonism and magmatism near a convergent plate margin. The region is seismically active, and earthquakes have been monitored for several decades. Extensive leveling surveys were conducted throughout the region in 1954, and they can be repeated to determine vertical strain rates. In addition, Medicine Lake volcano's recent eruptive history is well known, and the regional crustal structure has been studied using various geophysical techniques. Our study combines results from repeat leveling surveys, earthquake monitoring, and measurements of crustal structure to develop a model that explains most aspects of contemporary ground deformation and seismicity.

GEOLOGIC SETTING AND ERUPTIVE HISTORY

Medicine Lake volcano is a Pleistocene-Holocene shield volcano located about 50 km east-northeast of Mount Shasta, between the crest of the Cascade Range to the west and the Basin and Range tectonic province to the east (Figure 1). The Medicine Lake shield rises about 1200 m above the Modoc Plateau to an elevation of 2376 m. Lavas from Medicine Lake volcano cover nearly 2000 km^2, and their volume is estimated to be at least 600 km^3, making it the largest volcano by volume in the Cascade Range. Medicine Lake volcano began to grow about 1 m.y. ago, following eruption of a large volume of tholeiitic high-alumina basalt. Similar high-alumina basalt has continued to erupt around the volcano throughout its history. Although mafic lavas predominate on the volcano's flanks, all lava compositions from basalt to rhyolite have erupted during Pleistocene time. The lower flanks consist of mostly basaltic and some andesitic lavas. Basalt is mostly absent at higher elevations, where andesite dominates and rhyolite and small volumes of dacite are present [*Donnelly-Nolan*, 1988].

During the past 11,000 years, eruptive activity at Medicine Lake volcano has been episodic. Eight eruptions produced about 5.3 km^3 of basaltic lava during a time interval of a few hundred years about 10,500 years ago. That eruptive episode was followed by a hiatus that ended with a small andesitic eruption about 4300 years ago. During the most recent eruptive episode between 3000 and 900 years ago, eight eruptions produced approximately 2.5 km^3 of lava ranging in composition from basalt to rhyolite. Late Holocene lava compositions include basalt and andesite, but silicic lavas dominate [*Donnelly-Nolan et al.*, 1989].

Medicine Lake caldera is a 7 × 12 km depression in the summit area of the volcano. *Anderson* [1941] suggested that the caldera formed by collapse after a large volume of andesite was erupted from vents along the caldera rim. However, the distribution of late Pleistocene vents, mostly concentrated along the rim, suggests that ring faults already existed when most of the andesite erupted [*Donnelly-Nolan*, 1988]. No single large eruption has been related to caldera

Paper number 91JB01452.

24

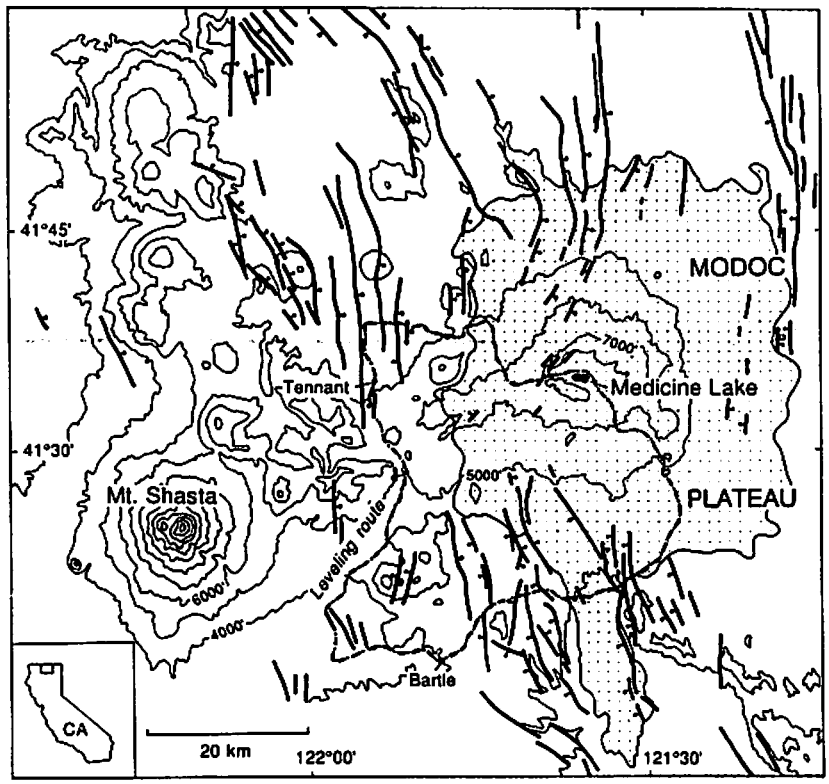

Fig. 1. Location map showing the Medicine Lake volcano–Mount Shasta area of the southern Cascade Range, northern California. Pattern indicates extent of lavas of Medicine Lake volcano. Heavy lines are faults, with bar and ball on downthrown side (*Gay and Aune* [1958] and air photograph interpretation). Heavy dotted-dashed line represents the 1954–1989 leveling route. Contour interval is 1000 feet (305 m).

formation. The only eruption recognized to have produced ash flow tuff occurred in late Pleistocene time, and this eruption was too small to account for formation of the caldera [*Donnelly-Nolan and Nolan*, 1986]. *Donnelly-Nolan* [1988] concluded that Medicine Lake caldera formed by collapse in response to repeated extrusions of mostly mafic lava beginning early in the history of the volcano (perhaps in a manner similar to the formation of Kilauea caldera, Hawaii). She hypothesized several small differentiated magma bodies fed by and interspersed among a plexus of dikes and sills. In her model, late Holocene andesitic to rhyolitic lavas were derived by fractionation, assimilation, and mixing from high-alumina basalt parental magma.

CRUSTAL STRUCTURE

The crustal structure beneath Medicine Lake volcano is dominated by a roughly columnar region, approximately 40 km thick and 50 km in diameter, consisting of mostly high-velocity material superposed on what has been interpreted as either (1) a transition zone from Klamath terrain to basement equivalent to Sierran batholith [*Fuis et al.*, 1987] or (2) an underplated Basin and Range structure in a back arc setting [*McKee et al.*, 1983; *Catchings*, 1987]. Seismic refraction measurements indicate that a high-velocity basement underlies 3–5 km of low-velocity material, which presumably consists of lava flows from Medicine Lake volcano plus interbedded lava flows and sediment of the Modoc Plateau. Schlumberger soundings in the area detected a "geoelectric basement" with a resistivity greater than 200 ohm m at a depth of 1.5 km beneath Medicine Lake caldera [*Zohdy and Bisdorf*, 1990], near the contact between the base of the volcano and the underlying Modoc Plateau.

Various lines of evidence suggest that virtually the entire crustal column beneath Medicine Lake volcano has been intruded by mafic dikes, is still hot, and may be locally molten. The low-velocity layer near the surface is underlain at the volcano by a high-velocity, high-density lens that extends from about 1 km to at least 3 km below the caldera (from about 1 km above to 1 km below sea level; Figure 9*a*). This feature has been interpreted as a complex of mafic-to-silicic material intruded into Modoc Plateau materials [*Finn and Williams*, 1982; *Zucca et al.*, 1986; *Evans and Zucca*, 1988]. An active source seismic tomography experiment indicated that seismic wave fronts are steepened by a radially symmetric, high-velocity anomaly 5–10 km beneath the volcano [*Evans and Zucca*, 1988]. This high-velocity root extends to even greater depths, as shown by inversion of teleseismic travel time data. The inversion indicates that the lower crust, upper mantle, and possibly the middle crust are 2–4% faster than surrounding material. In addition, the upper and middle crust beneath the volcano may be seismically attenuating, on the basis of interpretation of a seismic refraction study [*Catchings*, 1983].

At Newberry volcano, a shield volcano in central Oregon that is geologically similar to Medicine Lake volcano, *Stauber et al.* [1988] used teleseismic data to image a columnar high-velocity feature that extends from within 10 km of the surface to about 25 km depth. They interpreted this feature as a largely subsolidus mafic intrusive complex. On the basis of the surface geology and seismic data from

21

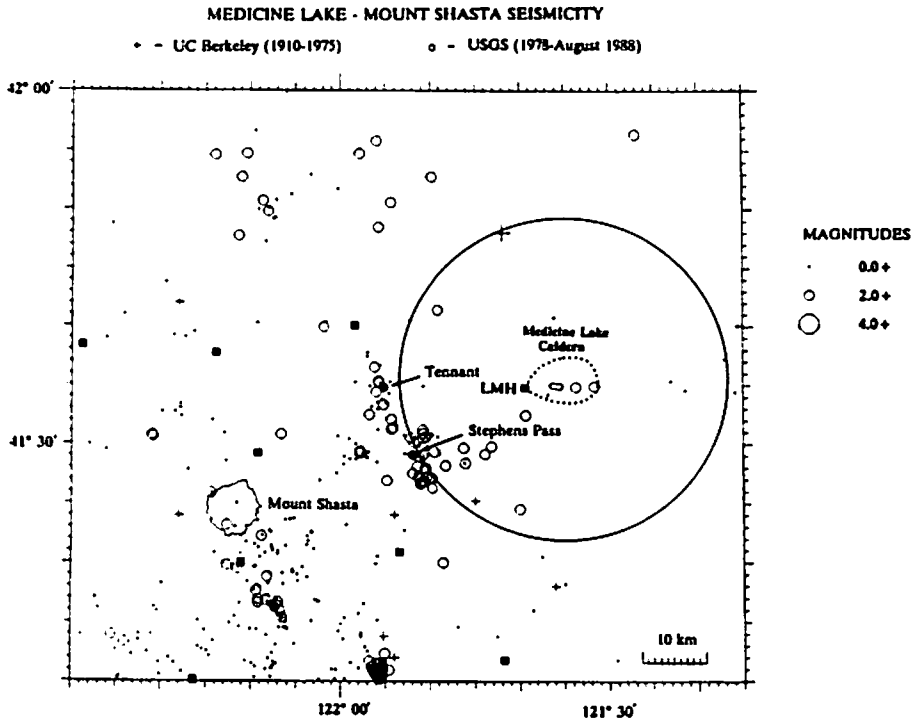

Fig. 2. Seismicity in the Medicine Lake–Mount Shasta region for the period from 1910 to August 1988. Solid squares represent seismographs of the USGS Mount Shasta network, including Little Mount Hoffman (LMH) on the west rim of Medicine Lake caldera. Large circle encloses a relatively aseismic area within 25 km of the summit of Medicine Lake volcano. Clusters of earthquakes near Tennant and Stephens Pass occurred during swarms in 1981 and 1978, respectively [from *Bolt and Miller*, 1975; USGS, unpublished data, 1991].

Medicine Lake volcano, and by analogy to Newberry volcano, we conclude that the lower and possibly middle crusts beneath Medicine Lake volcano consist of silicic rocks intruded by numerous dikes and sills that contain gabbro and diabase (slowly cooled equivalents of mafic melts), perhaps with variable amounts of basalt melt. In the upper mantle the high-velocity anomaly may represent ultramafic residuum left by removal of this basalt. This conclusion is consistent with (1) geochemical evidence suggesting that generation of intermediate and silicic melts from basaltic melts by fractionation and assimilation occurs in the upper crust [*Grove and Baker*, 1984; *Grove and Donnelly-Nolan*, 1986; *Grove et al.*, 1988] and (2) the eruption of primitive mantle-derived basalt throughout the history of Medicine Lake volcano [*Donnelly-Nolan*, 1988].

The high-resolution active seismic tomography experiment mentioned above detected a low-velocity, low-Q region in the upper crust beneath Medicine Lake caldera [*Evans and Zucca*, 1988]. The anomalous feature, which extends from about 1 to 3 km below sea level (i.e., 3–5 km beneath the caldera), has a diameter of about 3 km and a volume of the order of 10 km^3. It is interpreted as a small silicic magma body, on the basis of its distinctive seismic signature, its association with an active magmatic system, and various geologic, geochemical, and geophysical considerations [*Evans and Zucca*, 1988; *Evans and Walter*, 1989]. No other magma bodies were suggested by the experiment, which had a spatial resolution of 1–2 km in the upper 5–7 km of the crust beneath the caldera and most of the shield.

SEISMICITY

Prior to the first seismograph records in 1909, there were various reports of seismic activity in the Medicine Lake region. G. W. Courtright, a local rancher and trapper, felt numerous earthquakes and saw "flames" and ground cracks near Glass Mountain in January and February 1910 [*Finch*, 1928]. Finch also reported that "earthquakes originating in the mountain and accompanied by rattling noises have been noted by Forest Service officials for at least 15 years." He added, "Similar noises and shakes have been observed by Mr. Courtright for a much longer period."

Seismic records collected by the University of California Berkeley Seismographic Stations starting in 1909 show no earthquakes in the Medicine Lake–Mount Shasta region prior to 1950 [*Bolt and Miller*, 1975]. However, instrumental coverage during that interval was such that events smaller than M 4 probably would not have been located. As additional stations were added in the 1950s, earthquakes as small as M 3.0 began to be located in the Mount Shasta area. Still, no events were detected near Medicine Lake volcano through 1975 (Figure 2).

In 1980 the U.S. Geological Survey (USGS) extended its northern California seismic network by installing nine short-period, vertical seismometers around Mount Shasta. The new stations included one on the western edge of Medicine Lake caldera at Little Mount Hoffman (LMH, Figure 3*a*). Seismic signals are telemetered by a combination of radio and telephone lines to the USGS office in Menlo Park,

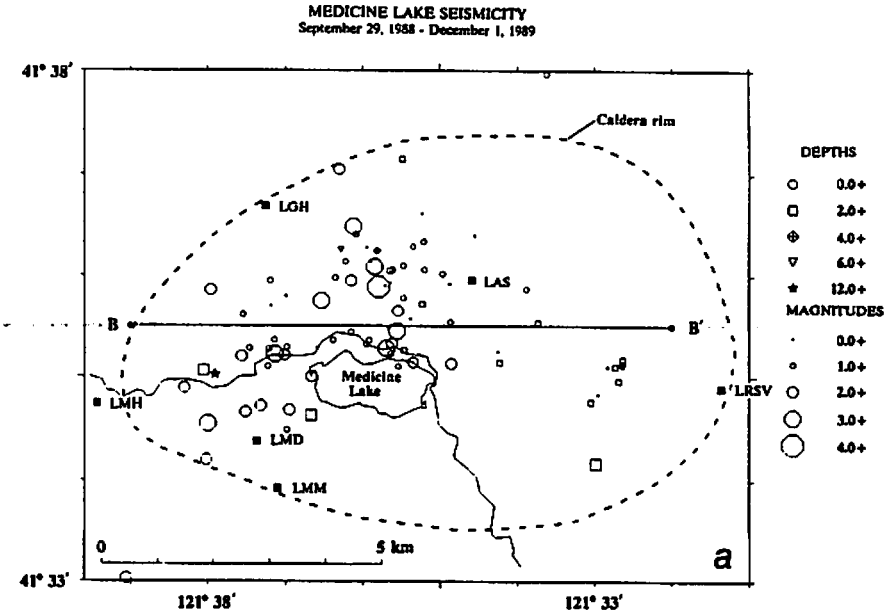

Fig. 3*a*. Located earthquakes of the 1988 Medicine Lake swarm and its aftershocks. Epicenters are shown as open symbols, and seismographs of the USGS Medicine Lake network, installed in October 1988, are shown as solid squares. Solid line at lower left represents the main road across the caldera that was leveled in 1954, 1988, and 1989; dashed line represents the caldera rim. The star about 2 km west of the west end of Medicine Lake marks the location of a long-period earthquake that occurred at 15 km depth on December 1, 1989. Line B-B′ shows the orientation of the cross section shown in Figure 3*b*.

California, where they are recorded and earthquakes are identified, timed, and located. Earthquakes are located with HYPOINVERSE [*Klein*, 1989] using a homogeneous layered crustal model determined from refraction studies [*Catchings*, 1983, 1987]. For a full discussion of instrumentation and data processing, see *Lester and Meagher* [1978] and *Stewart and O'Neill* [1980].

Between 1980 and the September 1988 swarm (see below), only three earthquakes were located in the vicinity of Medicine Lake caldera. Two of these events occurred in the eastern part of the caldera, in an area active after the 1988 swarm. The third event was a long-period earthquake that occurred on October 14, 1986. An approximate location for this event places it about 13 km beneath the western edge of the caldera, close to the hypocenter of a well-located long-period earthquake that occurred on December 1, 1989 (see the 1988 Medicine Lake swarm, Figure 3).

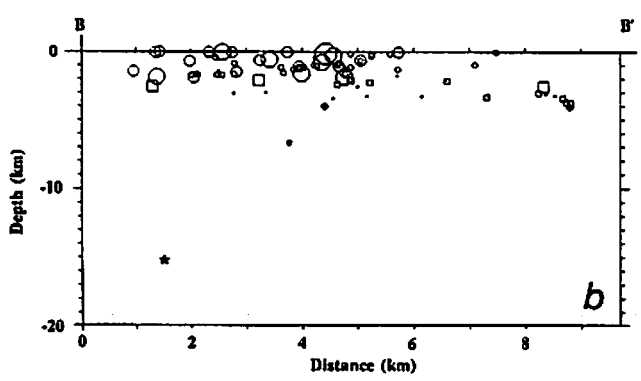

Fig. 3*b*. Cross section shows depths of the earthquakes that occurred during the 1988 swarm. All epicenters shown in Figure 3*a* were projected onto a vertical plane through B-B′. Star at about 15 km depth represents the same long-period earthquake as in Figure 3*a*.

1978 Stephens Pass Swarm

The apparent seismic quiescence near Medicine Lake volcano was broken by an intense swarm of shallow earthquakes that began with a *M* 4.6 event on August 1, 1978. The initial shock was followed within the next 90 min by six events of *M* 3.5–4.5 and within 24 hours by 100–200 events of *M* ≥ 2 [*Cramer*, 1978; *Bennett et al.*, 1979]. The epicentral area was centered 15 km south of the town of Tennant and 5 km south of Stephens Pass, approximately midway between Medicine Lake volcano and Mount Shasta (Figure 2). A second flurry of activity began with a *M* 4.3 event on August 12. On August 14, U.S. Forest Service personnel reported large fissures across Stephens Pass Road 5 km south of Stephens Pass.

Subsequent field observations documented a 2-km-long, 75-m-wide zone of tensional fractures, grabens, and circular depressions ("sink holes") within the grabens. The zone trended north-south through the epicentral area (Figure 4). Vertical displacements were as large as 1 m in the grabens and 1.5 m in the circular depressions [*Cramer*, 1978; *Bennett et al.*, 1979]. An 8-km-long aftershock zone dips eastward away from the ground breakage; focal depths increase eastward to a maximum of about 4 km. Focal mechanisms suggest east-west extension on a north striking fault dipping 35°–45° east [*Cramer*, 1978], consistent with the pattern of north striking normal faults in the region.

1981 Tennant Swarm

Another swarm of shallow earthquakes occurred during January–February 1981, in this case almost directly beneath

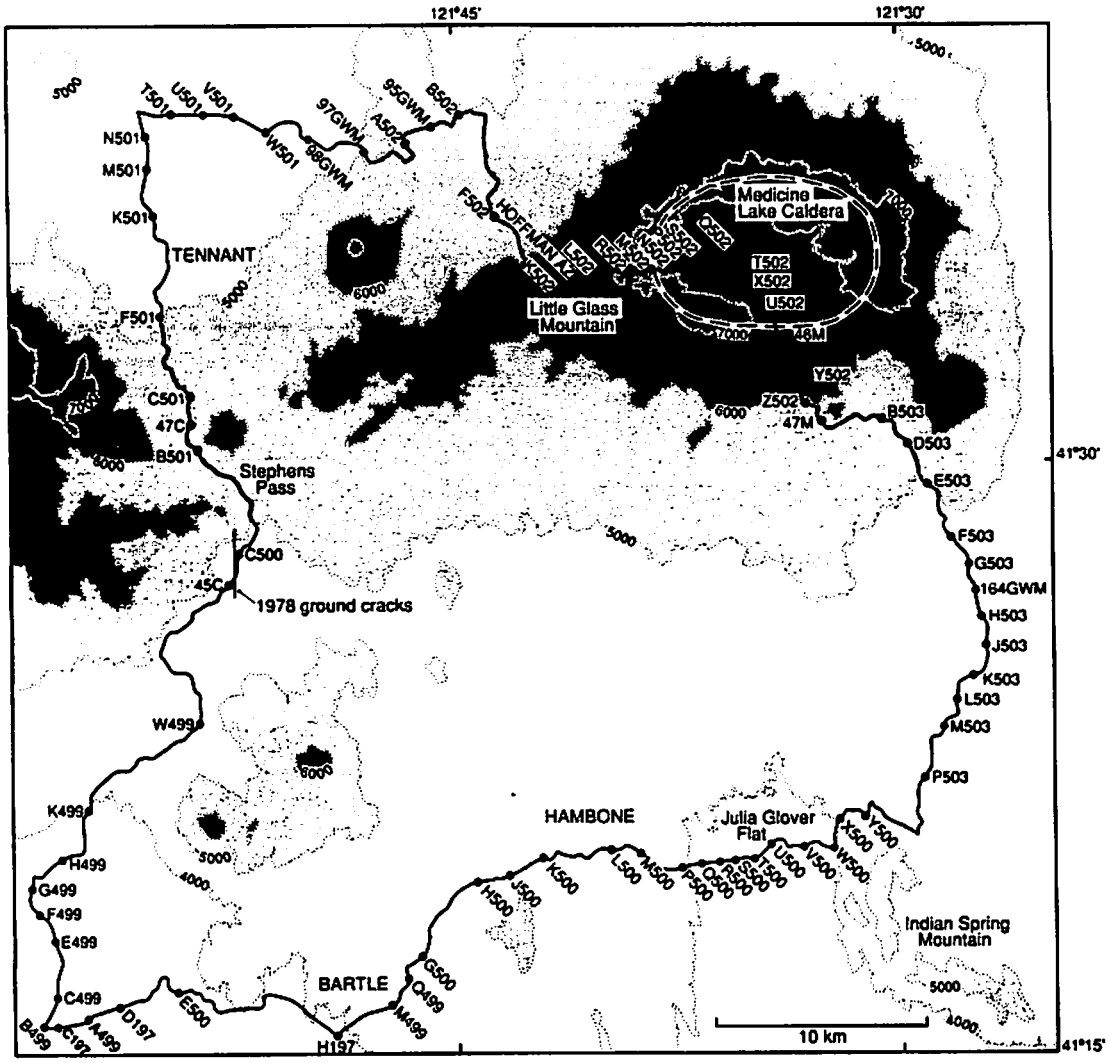

Fig. 4. Locations of bench marks along the 193-m leveling circuit across Medicine Lake volcano and Stephens Pass. Also shown are the locations of Bartle, Hambone, Tennant, and several features mentioned in the text. Stippling indicates five elevation ranges, from less than 4000 feet (1220 m) above sea level (no stippling) to more than 7000 feet above sea level (2130 m) (the heaviest stippling); contour interval is 1000 feet (305 m). Throughout the text, stadia distances are measured counterclockwise from H197, the southernmost mark in the circuit, near Bartle. Dashed line marks the boundary of Medicine Lake caldera; solid line between bench marks C500 and 45C near Stephens Pass indicates the area of ground breakage associated with the 1978 Stephens Pass earthquake swarm [from *Bennett et al.*, 1979].

the small town of Tennant, about 10 km north of Stephens Pass. The activity began on January 1, 1981, with an earthquake that was felt by residents of Tennant (A. M. Allison, personal communication, 1981). Several dozen additional events, all of $M < 3.0$, were recorded on seismographs of the Mount Shasta network from January 5 to January 8. Activity increased abruptly early on January 9 with a M 4.1 earthquake, the largest of the sequence, followed by 26 events of $M \geq 2.0$ within the next 24 hours, including 11 events of $M \geq 3.0$. Seismicity declined markedly over the next several weeks, with several flurries of small events ($2.0 \leq M \leq 3.0$) on January 12 and again in early February.

Temporary seismic stations were installed by January 15, after the main part of the sequence had ended. Well-determined focal depths for aftershocks recorded by the temporary stations all are very shallow, generally less than 2 km. The aftershock zone is about 10 km long and elongate in a north-south direction, suggesting movement on a north striking fault aligned with the regional structural pattern (Figures 1 and 2). Despite the large extent of the aftershock zone and the shallowness of the seismicity, no ground breakage was reported. However, minor ground breakage could have been obscured by a thin layer of snow covering the ground at the time (J. Coakley, personal communication, 1990).

1988 Medicine Lake Swarm

The Medicine Lake swarm began on the morning of September 29, 1988, with a flurry of some 20 small events, the largest of M 3.3. The swarm peaked in the late afternoon with more than 80 earthquakes recorded in 1 hour, including two M 3.5 events and one M 4.1 event, the largest of the

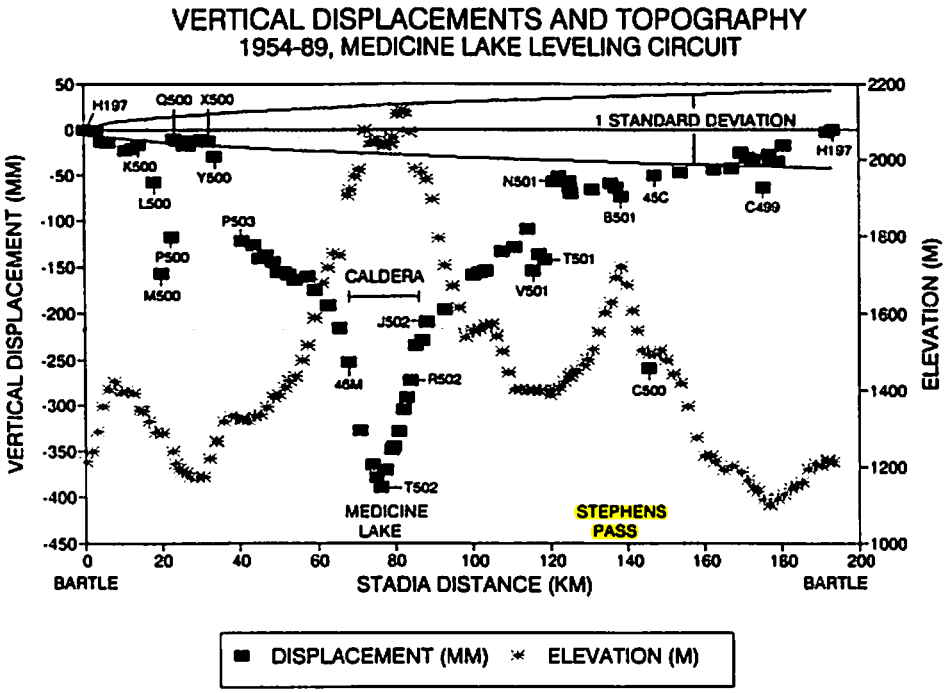

Fig. 5. Topographic profile (asterisks) and 1954–1989 vertical displacements (squares) along the Medicine Lake–Stephens Pass leveling circuit. Stadia distance is measured counterclockwise from H197 near Bartle, which is held fixed (see Figure 4). Stippled area indicates 1 standard deviation in the vertical displacements, based on published standards for second-order, class II leveling surveys (1954) and first-order, class II surveys (1989) [*Vanicek et al.*, 1980]. At any stadia distance the vertical dimension of the stippled area indicates the height of the 1-sigma error bar at that distance.

sequence. Activity declined rapidly with 90 earthquakes recorded in the next 24 hours, several events per day during October 1988, and several events per week during the remainder of 1988. Several additional seismographs were installed around Medicine Lake caldera in late October 1988 (Figure 3). Sporadic flurries of small events ($M \leq 3.1$) occurred beneath Medicine Lake caldera throughout 1989 [*Walter and Dzurisin*, 1989].

All 1988–1989 earthquakes occurred beneath Medicine Lake caldera, primarily north or west of Medicine Lake (Figure 3*a*) and within about 2 km of the surface (Figure 3*b*). A small cluster of events occurred in April 1989 at depths of 3–4 km beneath the eastern part of the caldera. With one exception, all 1988–1989 earthquakes were short-period, tectonic-type events. A long-period event of M 2.7 occurred about 15 km beneath the western part of the caldera on December 1, 1989. Similar long-period events have been recorded (1) beneath Kilauea and Mauna Loa volcanoes in Hawaii; (2) beneath Long Valley caldera, the Lassen volcanic center, and near the Geysers/Clear Lake area, all in California; and (3) at Yellowstone caldera in Wyoming. The significance of such long-period events may not be the same at every volcano, but their association with young magmatic systems suggests that they record movement of mafic magma or other fluids within the crust [e.g., *Koyanagi et al.*, 1987; *Chouet et al.*, 1987].

LEVELING RESULTS

A 193-km leveling circuit across Medicine Lake volcano and Stephens Pass via the towns of Tennant and Bartle (Figure 4) was first measured in 1954 by the National Geodetic Survey (NGS) using second-order, class II procedures. The circuit was remeasured in 1989 by the USGS Cascades Volcano Observatory (CVO), using first-order, class II procedures. CVO also measured a 20-km segment of the same circuit, from bench mark J502 near Little Glass Mountain eastward across Medicine Lake caldera via T502 to 46 M, in August 1988 and October 1988. All appropriate corrections specified by NGS [*Schomaker and Berry*, 1981; *Balazs and Young*, 1982] were applied to the measurements, including rod scale corrections based on calibrations performed at the National Bureau of Standards and refraction corrections based on measured temperatures. Misclosures for the 193-km circuit were 5.4 mm in 1954 and 19.7 mm in 1989, compared to NGS specifications of 111 mm (8 mm/km$^{1/2}$ $L^{1/2}$ for second-order, class II surveys) and 69 mm (5 mm/km$^{1/2}$ $L^{1/2}$ for first-order, class II surveys [*Vanicek et al.*, 1980]), respectively. An analysis of random and systematic errors in the surveys is given in the Appendix.

Vertical Displacements, 1954–1989

Figures 4–6 show bench mark locations, topography, and vertical displacements during 1954–1989 along the Medicine Lake leveling circuit. Displacements are relative to bench mark H197 near Bartle, which was held fixed as a reference. A broad area of subsidence centered at Medicine Lake caldera and extending across the entire volcano is evident in Figures 5 and 6. The maximum measured subsidence was 389 ± 43 mm at T502, which corresponds to an average annual rate of 11.1 ± 1.2 mm/yr during the 35-year interval spanned by the surveys. T502 is the bench mark nearest to the center of the caldera.

Between 1954 and 1989, large local displacements occurred south of Medicine Lake caldera near M500 (east of

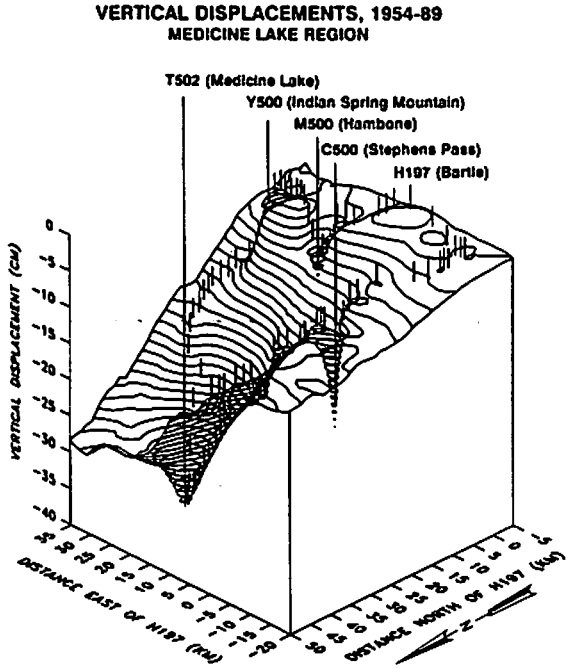

Fig. 6. Three-dimensional representation of the 1954–1989 vertical displacements in the Medicine Lake region. Curved lines represent contours of relative vertical displacement (contour interval = 10 mm). Locations of bench marks along the leveling route are indicated by small vertical lines. View is from the northwest. Displacements are known accurately only at the marks; elsewhere they were extrapolated using a gridding program with an inverse square weighting scheme. Fault displacements near M500 (Hambone), Y500 (Julia Glover Flat), and C500 (Stephens Pass) are not portrayed accurately because the leveling traverse did not sample those areas in detail.

Hambone) and Y500 (northeast end of Indian Spring Mountain), and also west of the caldera near V501 and N501 (north of Tennant) and C500 (Stephens Pass) (Figures 4–6). C500 is located within the epicentral area of the 1978 Stephens Pass earthquake swarm, near the southern end of a zone of ground cracks that formed during the swarm [*Bennett et al.*, 1979]. C500 is on the east (downthrown) side of the surface cracks, while nearby marks are on the west side. We attribute the anomalous movement of C500 to the effects of the 1978 swarm. V501 and N501 are located near the northern margin of the epicentral area associated with the 1981 Tennant earthquake swarm, near a prominent north striking regional fault (Figures 1 and 4). We suspect that the anomalous movements of V501, N501, and two intervening marks occurred during the 1981 swarm. M500 and Y500 are located near prominent, young-looking normal faults that bound Indian Spring Mountain and Julia Glover Flat in horst-and-graben terrain about 30 km south of Medicine Lake caldera (Figure 4). One fault forms the eastern boundary of Julia Glover Flat and offsets by about 10 m a basalt flow dated 10,600 years B.P. [*Donnelly-Nolan et al.*, 1989]. The large displacements of marks near M500 and Y500 indicate that some of these faults have been active since 1954. A search of regional seismic records for the period from 1911 to 1989 turned up only one earthquake larger than M 2.0 in the area; a M 3.2 event on February 16, 1959, located about 10 km east-southeast of Hambone, beneath Julia Glover Flat. However, the records are incomplete for events of $M \leq 4.5$ prior to about 1950 and of $M \leq 3.5$ during 1950–1980. Therefore a swarm of smaller earthquakes could have gone undetected, as evidenced by the absence of recorded earthquakes near Glass Mountain associated with the 1910 swarm reported by *Finch* [1928].

Inspection of Figures 4 and 5 suggests that historical faulting has downdropped Medicine Lake volcano by 5–10 cm with respect to the surrounding plateau (i.e., P503 relative to Y500 and T501 relative N501; Figure 5). Owing to the configuration of the leveling route, it is unclear whether this subsidence is bounded by a north striking graben or a basin centered at Medicine Lake caldera. The existence of a circular subsidence feature nested within a major north striking graben encompassing both Medicine Lake volcano and Mount Shasta has been proposed on the basis of regional magnetic and gravity anomalies [*Blakely et al.*, 1985; *Blakely and Jachens*, 1990], but those anomalies are considerably larger than the area of subsidence surrounding Medicine Lake caldera.

It is surprising that Julia Glover Flat, a young-looking graben that the leveling route crosses between Q500 and X500, was stable during 1954–1989 while adjacent areas to the west and northeast subsided 10–15 cm (Figure 5). This sense of movement is opposite to what has prevailed over longer time scales, as indicated by the current topography and by large Holocene movements on faults that bound the graben. Thus Julia Glover Flat seems particularly prone to faulting and subsidence in the future.

Vertical Displacements, 1988–1989

Any relation between the subsidence during 1988–1989 and the September 1988 earthquake swarm is difficult to demonstrate, because movements were barely larger than measurement error. Vertical displacements within Medicine Lake caldera from August 1988 to August 1989 are mostly less than 2 standard deviations of the measurements and therefore of marginal significance. However, the measured displacements suggest that the intracaldera subsidence rate was at least as high during 1988–1989 as during 1954–1989. The average subsidence rate at T502 with respect to J502 was 13.8 ± 3.5 mm during 1988–1989 compared to 5.2 ± 0.2 mm/yr during 1954–1989. The amount of movement at T502 during 1988–1989 seems anomalous relative to nearby bench marks (Figure 7), but even at adjacent marks the 1988–1989 subsidence rates were higher than the 1954–1989 rates (e.g., at X502, 7.6 ± 4.0 mm/yr during 1988–1989 compared to 4.8 ± 0.3 mm/yr during 1954–1989). The 1988 and 1989 surveys did not include H197, so subsidence rates with respect to H197 can only be estimated by comparison with the 1954–1989 results. From 1954 to 1989 the amount of subsidence at T502 with respect to J502 was about half the amount at T502 with respect to H197 (Figure 5). Assuming the subsidence pattern did not change, we doubled the 1988–1989 subsidence rates with respect to J502 to estimate the rates with respect to H197. Thus we estimate that the center of Medicine Lake caldera subsided 15 mm/yr (X502) to 28 mm/yr (T502) with respect to H197 during 1988–1989, compared to 11.1 ± 1.2 mm/yr at T502 during 1954–1989.

SUBSIDENCE MECHANISMS

Mechanisms that might cause subsidence of Medicine Lake volcano and sporadic earthquake swarms in the sur-

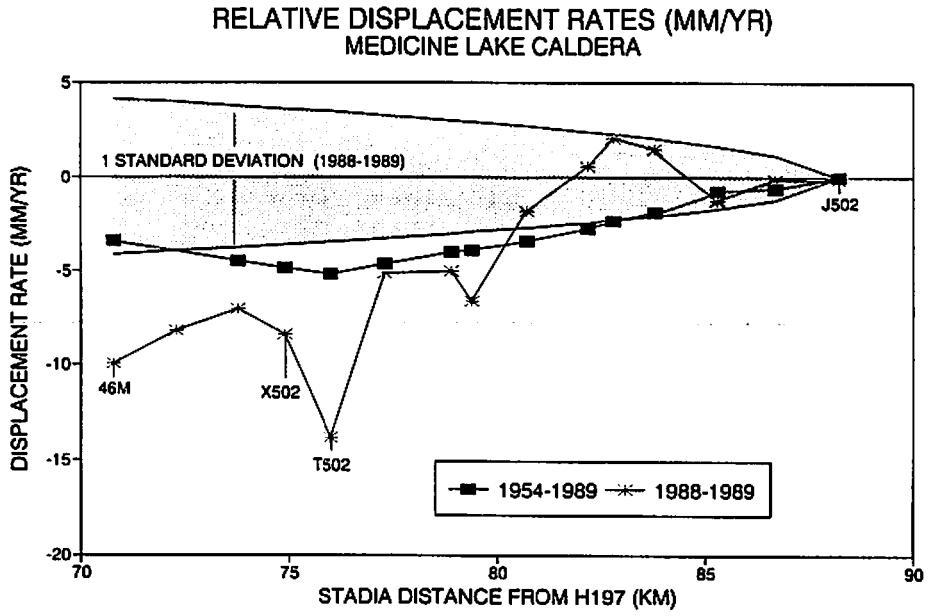

Fig. 7. Annual vertical displacement rates relative to J502 for the periods 1954–1989 (squares) and August 1988 to August 1989 (asterisks) along a 20-km leveling traverse across Medicine Lake caldera. Stippled area indicates 1 standard deviation in the 1988–1989 displacement rates. At any stadia distance the vertical dimension of the stippled area indicates the height of the 1-sigma error bar for the 1988–1989 measurements at that distance. See Figure 4 for locations of bench marks.

rounding area include (1) crustal thinning caused by extension in the western Basin and Range province, (2) loading of the crust by the weight of the volcano and its subvolcanic intrusive complex, (3) densification during cooling and crystallization of magma, and (4) deflation caused by magma withdrawal. We propose that mechanisms 1 and 2 are primarily responsible for historical subsidence and that mechanisms 3 and 4 may contribute over longer time scales.

Crustal Extension

Several lines of evidence indicate that an important mechanism for historical subsidence at Medicine Lake volcano is thinning and bending of the crust in response to regional tectonic extension. Although the contemporary extension rate has yet to be measured, structural and geologic evidence indicates that Medicine Lake volcano lies in a region of east-west extension that has been active at least through late Holocene time. Seismic and leveling data show that extension and faulting have continued to the present. The Medicine Lake area is cut by numerous north striking normal faults with up to a few hundred meters of displacement. Others may be partially or completely buried by young lava flows. Open ground cracks, common on and around Medicine Lake volcano, have N30°W to N30°E orientations and east-west opening directions consistent with the extensional direction indicated by regional faults [*Donnelly-Nolan*, 1988]. The same is true for cracks that formed during the 1978 Stephens Pass earthquakes, which had focal mechanisms indicating east-west extension on a north striking fault [*Cramer*, 1978].

If the mechanical response of the crust in the Medicine Lake region were laterally homogeneous, east-west extension would cause grabens and fissures to form along a north striking axis, creating a north trending trough. That is not the pattern observed at Medicine Lake volcano, where the known subsidence is more or less symmetric about the center of Medicine Lake caldera. However, could such a pattern result from east-west extension if the crust beneath the volcano is mechanically weaker than its surroundings? Using a finite element model of the crust and upper mantle beneath the Yellowstone region, *Meertens* [1987] demonstrated the reverse process, i.e., that regional compressive strain can cause doming of mechanically weak crust. He proposed that such weakness is a consequence of elevated temperatures and fracturing associated with the Yellowstone magmatic and hydrothermal systems. If similar conditions prevail beneath Medicine Lake volcano (as indicated by interpretation of seismic data), then subsidence of weak subvolcanic crust could be a result of Basin and Range extension.

Crustal Loading

Another mechanism that may contribute to subsidence at Medicine Lake volcano is crustal loading by the volcanic edifice and dense mafic intrusions. A similar mechanism has been proposed to account for subsidence of the Hawaiian Islands [*Moore*, 1970]. The dimension over which the crust is loaded, which determines the response depth, is an order of magnitude larger in Hawaii (400 km) than at Medicine Lake volcano (40 km). Therefore a classical isostatic response of the asthenosphere is unlikely at Medicine Lake volcano. However, a similar response might occur within the upper lithosphere, because is has been heated and weakened by numerous mafic intrusions.

Studies of samples from eight drill holes located on the upper flanks of Medicine Lake volcano indicate that five of the holes penetrated the entire volcanic pile. In drill cores from each of those holes, fresh aphyric lavas of Medicine Lake volcano abruptly give way to altered flows, sediments,

and/or porphyritic lavas, some of which are petrographically unlike Medicine Lake lavas [*Donnelly-Nolan*, 1990]. One hole on the west flank reached a highland of pre–Medicine Lake volcano vents and flows (at 4600 feet, 1402 m elevation) that connects westward to Mount Shasta. The other four holes penetrated the base of Medicine Lake volcano at elevations of 2487–3365 feet (758–1026 m), well below the level of the surrounding Modoc Plateau (1250 m). The possibility that a circular basin 0.5 km deep may have existed at the location where Medicine Lake volcano was built is thought to be unlikely. No thick sequences of sediment are present in any of the drill holes, nor do the underlying basalt flows show signs of eruption into water. We conclude that the crust under the volcano has been downwarped approximately 0.5 km relative to the surrounding plateau, at least partly as a result of crustal loading.

The downwarped part of the volcanic edifice does not contribute significantly to the isostatic load, because it displaces rocks of similar density [*Zucca et al.*, 1986]. However, the drill core observations indicate the large magnitude of subsidence that has occurred over geologic time scales, and it is likely that at least part of the historical subsidence is caused by this mechanism. More subsidence may have occurred deeper in the crustal column if magmatic intrusion caused unrecorded uplift, which seems likely on the basis of seismic evidence for dense intrusive material throughout the crustal column. One consequence of the downwarping is that the volume of the volcano may be significantly greater than the previous estimate of 600 km^3. The volume of Medicine Lake volcano that has been downwarped below 1250 m elevation is approximately 150 km^3, so the total volume of the volcanic pile is estimated to be 750 km^3.

The long-term subsidence rate calculated from the amount of downwarping can be compared to the historical subsidence rate determined from measured displacements. Geologic mapping shows that Medicine Lake volcano had attained essentially its current configuration by about 150,000 years B.P., so the current subsidence rate can be estimated as 0.5 km/1.5 × 10^5 years = 3 mm/yr (assuming that the entire load was emplaced 150,000 years ago). This estimate is of the same order as, but almost a factor of 4 less than, the subsidence rate during 1954–1989 measured by leveling (11.1 ± 1.2 mm/yr). The implication is that the effect of crustal loading has increased through time to account for the current subsidence rate or, more likely, that crustal loading is not the dominant cause of contemporary subsidence.

Cooling and Crystallization of Magma

Subsidence may also result from densification in response to fluid loss during cooling and crystallization of magma. Even for a large rhyolitic system with a vigorous hydrothermal system such as Yellowstone, the thermal contraction caused by cooling of crystalline rock is negligible. However, if heat is extracted from the crustal column by cooling and crystallization of magma, the amount of contraction is appreciable. At Yellowstone, crystallization of rhyolite initially containing 2 wt % water results in a 7% decrease in volume, assuming that all of the released aqueous fluid escapes to the shallow, hydrostatically pressured part of the hydrothermal system [*Fournier*, 1989; *Dzurisin et al.*, 1990]. The amount of contraction would be somewhat less for silicic magmas, which typically contain less water. Note that this mechanism causes both horizontal contraction and subsidence, owing to the net decrease in volume.

Although there is scant surface evidence for a significant hydrothermal system beneath Medicine lake volcano, high vertical temperature gradients in three drill holes suggest that a considerable amount of heat may be available in the shallow subsurface [*Donnelly-Nolan et al.*, 1989]. The most likely heat sources are the low-velocity, low-Q zone beneath the caldera or an underlying zone of mafic intrusions. If the heat is derived from crystallizing magma in either of these zones, resulting fluid loss may account for part of the historical subsidence. If so, the thermal and chemical signature of the magma is greatly attenuated at the surface, possibly by flushing through the shallow groundwater system.

Magma Withdrawal

Evans and Walter [1989] proposed that deflation of the shallow magma chamber identified by a seismic tomography experiment [*Evans and Zucca*, 1988] caused the floor of Medicine Lake caldera to bow downward and eventually fail under bending stresses during the September 1988 earthquake swarm (Figure 9*a*). Although deflation of this chamber might contribute to subsidence, the leveling observations and modeling results (see the section on source models) show that the chamber is too small and shallow to account for the full extent of the 1954–1989 subsidence. Two long-period earthquakes have occurred recently in the depth range 13–15 km beneath Medicine Lake caldera, but their relation to the 1954–1989 subsidence is uncertain. Perhaps intruding mafic magma accumulates temporarily at 10–15 km depth, cools, densifies, and then sinks while still fluid to cause subsidence. Withdrawal of silicic magma from shallower depth seems less likely, owing to its lower density and greater effective viscosity. In either case, magma withdrawal probably is of secondary importance except during eruptive or intrusive episodes, when large volumes of magma move rapidly to the surface or into the rift zones.

SOURCE MODELS

A realistic model of the 1954–1989 subsidence would include both viscoelastic and brittle deformation (i.e., downsagging and faulting) and would be constrained by both horizontal and vertical displacement data. Lacking horizontal data, we used a simple point source elastic model [*Mogi*, 1958] to estimate the depth of the deformation source (i.e., volume decrease) from the measured vertical displacements. Although the model assumes that the crust is homogeneous and elastic, the effects of faulting and tectonic strain can be factored in qualitatively to explore the range of likely source depths. First, we consider all of the observations except for several marks obviously affected by faulting. Then we consider only those marks within 25 km of T502, where the subsidence profile is smooth and no faulting is indicated. In each case the volume change in the source region is adjusted to match the observed subsidence at T502.

Using a single deformation source, the best fit is obtained for a source depth of 15 km and a volume decrease of 550 × 10^6 m^3 (Figure 8*a*). A slightly better fit results from including two sources: one at 15 km depth (volume decrease of 450 ×

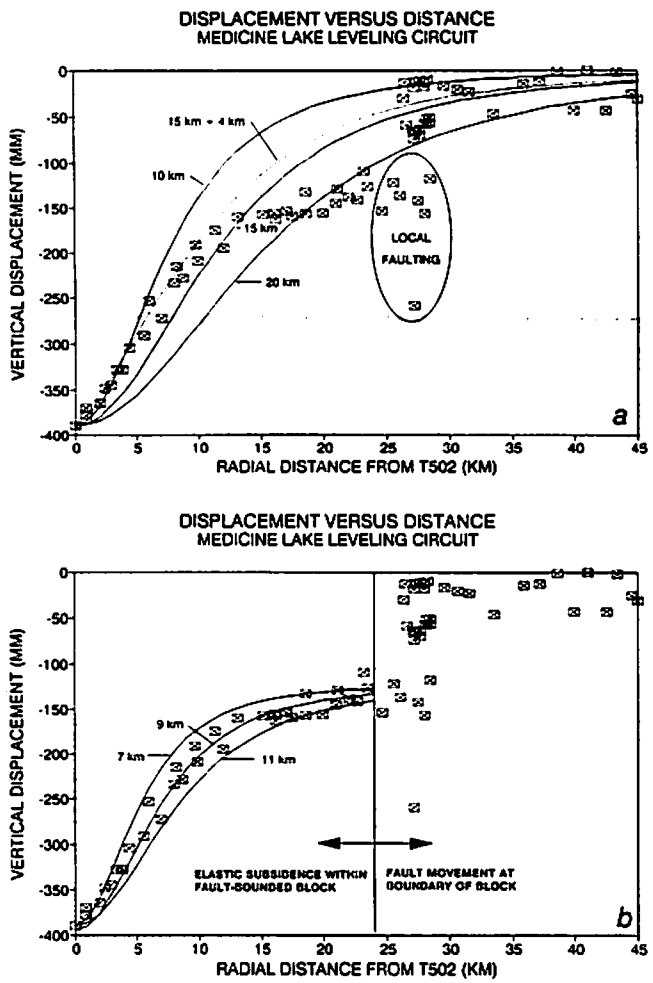

Fig. 8. Vertical displacement during 1954–1989 versus radial distance from bench mark T502 (near the center of Medicine Lake caldera) from leveling (squares) and from point source elastic models of bodies at the indicated depths (curved lines). (*a*) Attempt to fit all of the observations except those obviously affected by faulting. Solid lines represent effects of single sources centered at depths of 10, 15, and 20 km; dashed line represents the combined effect of two sources, one at 4 km depth and one at 15 km depth. The source volume decreases required to produce the indicated subsidence for sources at various depths are (in units of 10^6 m^3) 980 (depth = 20 km), 550 (15 km), 245 (10 km), and 450 + 7 (15 + 4 km). Each model was fit to the data by inspection; other combinations of depth and source volume change are possible. Ellipse encloses seven marks affected by local faulting (V501, U501, T501, C500, P503, M500, and P500) which were ignored when fitting the curves to the data. (*b*) Attempt to fit only those observations within 25 km of T502, assuming that more distant points are affected by faulting. The required source volume changes are (in units of 10^6 m^3) 205 (11 km), 140 (9 km), and 83 (7 km). Vertical line separates marks within 25 km of T502, where the subsidence profile is smooth, from those farther away and subject to faulting. Only marks to the left of the line were considered for the model.

10^6 m^3) and another at 4 km depth (volume decrease of 7 × 10^6 m^3). The deeper source corresponds to the approximate locations of two long-period earthquakes that might indicate a magma storage zone, and the upper source corresponds to the low-velocity, low-Q anomaly interpreted by *Evans and Zucca* [1988] as a silicic magma body beneath Medicine Lake caldera. The addition of a second source improves the fit slightly, but the improvement may simply reflect the increased degrees of freedom in the model.

An alternative model is illustrated in Figure 8*b*. The shape of the subsidence profile in Figure 5 and the offset near a radial distance of 25 km in Figure 8*a* suggest that the entire volcano, including the downwarped area centered at T502, has been downfaulted 5–10 cm relative to the surrounding plateau. This is illustrated in Figure 5 by the relative displacements of X500 and P503 near a stadia distance of 40 km and of N501 and T501 near a stadia distance of 120 km. To exclude the effect of faulting from the second model, we considered only those marks located within 25 km of T502. A volume decrease of 140 × 10^6 m^3 centered at 9 km depth yields the best fit. This model probably underestimates the true source depth by ignoring the far-field deformation, while the previous model may overestimate the depth slightly by ignoring the effect of faulting. A possible advantage of the second model, in view of the lack of a single large magma body beneath Medicine Lake caldera, is that smaller subsurface volume changes are needed to explain the amount of historical subsidence.

We suspect that the source is actually a vertically extended plexus of dikes with subsidiary magma storage zones at depths of 10–15 km and 3–5 km. This interpretation is based on (1) regional geophysical measurements that suggest the presence of mafic intrusions throughout the crust; (2) the occurrence of long-period earthquakes, suggesting magma movement, at 10–15 km depth; (3) seismic tomography measurements that indicate a small magma chamber at 3–5 km depth; and (4) the geodetic modeling results described above.

CONCEPTUAL MODEL

Our preferred model of the Medicine Lake magmatic system is illustrated in Figure 9. The dominant causes of subsidence are (1) crustal loading by the volcano plus dense subvolcanic intrusions and (2) crustal thinning due to Basin and Range extension. Both processes are facilitated by heat-induced crustal weakening; indeed, without such weakening, the load probably would be supported by an elastic upper lithosphere. A roughly columnar region beneath the edifice has been intruded extensively by basalt, most of which has solidified, thereby heating and weakening the crustal column (Figure 9*c*). An unknown fraction of this melt has differentiated to more silicic material that has intruded the upper crust and erupted at the surface, as has some of the parental basalt. Addition of mass and heat causes the volcano and underlying crust to subside. At the same time, Basin and Range extension thins the weakened crust, causing it to subside further. Possible subsidiary causes of surface subsidence include fluid loss during crystallization of magma and withdrawal of magma as a result of cooling or eruptions.

Earthquakes are largely absent from the heated crustal column but occur around its periphery. Historical earthquake swarms and faulting episodes mark the transition from relatively warm crust near the volcano to cooler crust 25 km or more from the summit. The inner zone deforms more steadily and mostly aseismically, while the outer zone deforms episodically by brittle failure. The pattern of subsidence is roughly symmetric about Medicine Lake caldera, except possibly for north-south elongation caused by east-west tectonic extension.

In the summit area, most tectonic strain is released by

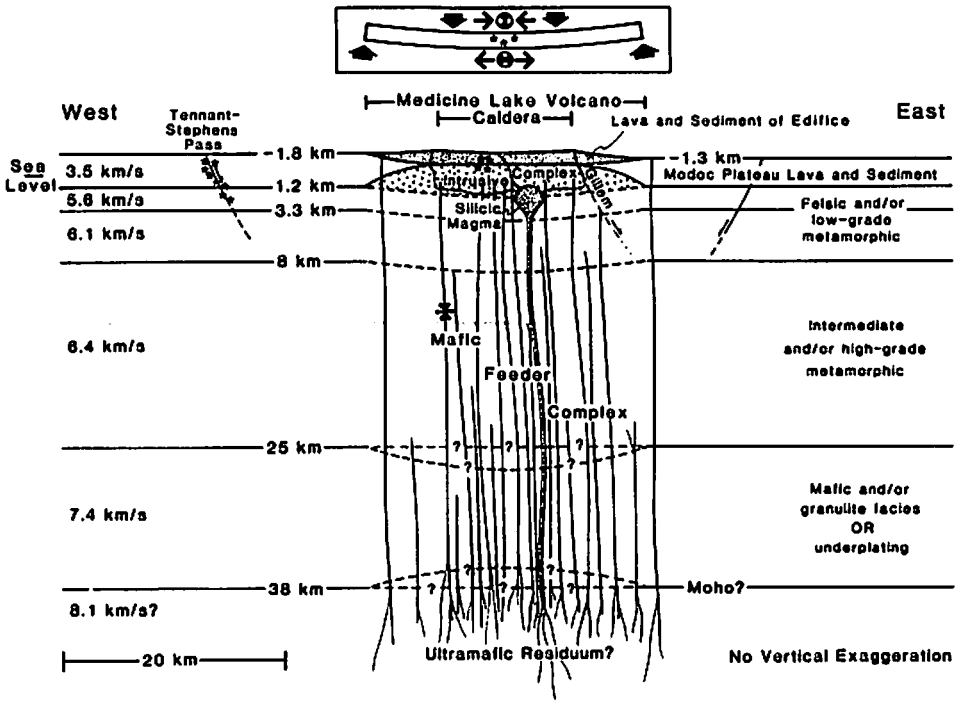

Fig. 9*a*. Conceptual model for Medicine Lake volcano. Many details are abstracted or rendered in schematic. East-west cross section through the volcano, showing major volcano-tectonic features plus the bending moment mechanism believed to be responsible for a shallow earthquake swarm in the summit region. Large arrows indicate load; small arrows, stars, and "focal spheres" indicate response. Velocity structure and rock types are abstracted from a seismic refraction study by *Zucca et al.* [1986]. Asterisk represents a relatively deep, long-period earthquake like those which occurred beneath the volcano on October 14, 1986, and December 12, 1989.

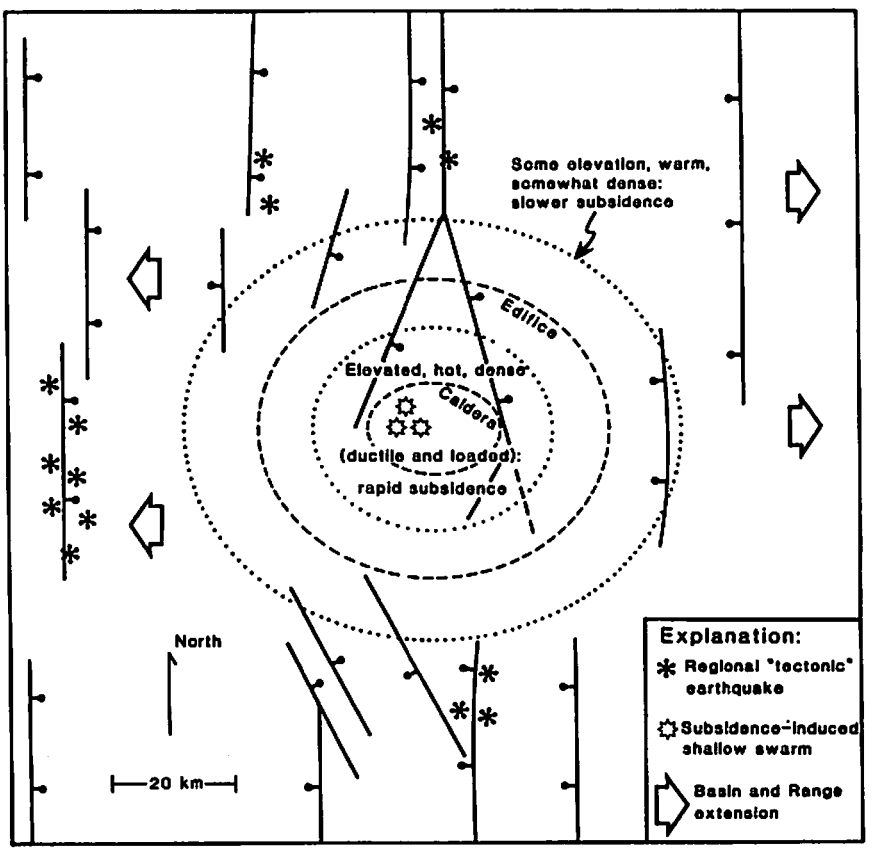

Fig. 9*b*. Plan view schematic of regional structure and loading stresses. "Tectonic" earthquakes (stars) are rare or absent in the heated crust beneath the volcano, except for shallow earthquake swarms that occur in the relatively cool, brittle lavas and sediment of the volcanic edifice.

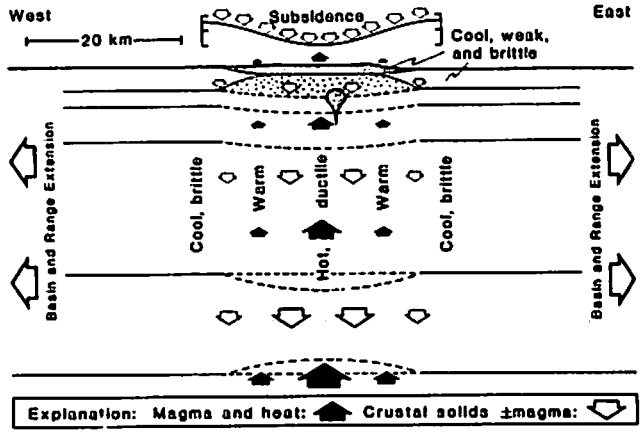

Fig. 9c. Cross section showing mass and heat transfer in the crustal column beneath the volcano. Both the edifice and a column of relatively dense, mafic intrusive material load the column. Heating by intrusions weakens the column, so it subsides in response to the load and to Basin and Range extension. It is unclear whether deeper boundaries would suffer net upward or downward deflections (dashed lines). Episodic withdrawal of magma and fluid loss during crystallization also may also contribute to subsidence.

thermally augmented creep and subsidence. Episodic swarms of shallow earthquakes are caused by subsidence-induced bending of a weak, brittle surface layer consisting of lava flows and related sediment, i.e., the volcanic edifice and possibly some underlying Modoc Plateau rocks (Figure 9a). In theory this layer fails under compression near the surface and under extension near its base. At Medicine Lake caldera, there is weak evidence from earthquake focal mechanisms for compression near the surface and extension a few kilometers deeper. Most earthquakes in the 1988–1989 swarm occurred near the center of bending, i.e., at the center of the caldera near T502.

The dominant control on the pattern of seismicity in the Medicine Lake region is the system of north striking normal faults formed by crustal extension at the western edge of the Basin and Range province. For this reason, seismic activity over geologic time scales presumably reflects the pervasive north-south structural grain in the region. The historical record is too short for this pattern to assert itself fully, but the character of earthquake swarms such as those near Stephens Pass in 1978 and Tennant in 1981 is consistent with normal faulting along north striking faults. An important secondary control on regional seismicity is the transition from warm to cool crust about 25 km from the summit of Medicine Lake caldera.

Tectonism and volcanism appear to be linked at Medicine Lake volcano to the extent that ground breakage in the context of regional crustal extension sometimes is accompanied by eruption of lava to the surface. A set of northeast striking, east-west opening ground cracks formed during the Little Glass Mountain eruption about 1000 years ago on the upper west flank of the volcano [*Fink and Pollard*, 1983]. This fracturing was accompanied by emplacement of rhyolite domes at about 10 sites along a 7.5-km-long N30°E alignment. Other vents also are located along inferred faults and fissures, and most vents form alignments oriented between N30°W and N30°E (similar to regional fault trends). Magma movement probably occurs more commonly along north striking dikes than central conduits, although the latter may occur under Medicine Lake caldera where small differentiated magma bodies may be present [*Donnelly-Nolan*, 1988; *Evans and Zucca*, 1988].

This model can be tested by repeated geodetic measurements across the inferred transition from aseismic subsidence to episodic normal faulting. The Global Positioning System (GPS) of satellite geodesy is capable of measuring vertical and horizontal displacements to an accuracy of about 1 cm over horizontal distances of at least 200 km [*Davis et al.*, 1989; *Prescott et al.*, 1989] and thus is well suited to this task. USGS established a regional network of GPS stations in the Mount Shasta–Medicine Lake region during July 1990. The network will be remeasured in 3–5 years to determine the contemporary strain rate and to characterize further the relation between tectonism and magmatism in this transitional zone between the Cascades and the Basin and Range.

APPENDIX: ANALYSIS OF LEVELING ERRORS

Random Error

The magnitude of random error in leveling surveys can be estimated by closing a circuit, double running all or part of a traverse or assuming that the error is typical of other surveys of the same order and class. On the basis of several decades of NGS experience the standard deviation σ of an observed elevation difference h measured by leveling is given by

$$\sigma(h) = \beta(L)^{1/2}$$

where β, in units of mm/km$^{1/2}$, is a constant for each order and class of leveling and L is the distance along the traverse. The standard deviation of a vertical displacement (i.e., change in an observed elevation difference between surveys) is given by

$$\sigma(\Delta h) = [\sigma_1(h)^2 + \sigma_2(h)^2]^{1/2}$$

where σ_1 and σ_2 are the standard deviations of the observed elevation differences from the first and second surveys, respectively. The contemporary value of β is 0.7 mm/km$^{1/2}$ for first-order, class II surveys and 1.3 mm/km$^{1/2}$ for second-order, class II surveys. However, NGS experience indicates that the value of β for second-order surveys during 1917–1955 (including the 1954 survey at Medicine Lake) was about 3 mm/km$^{1/2}$ [*Vanicek et al.*, 1980]. Thus the standard deviation of vertical displacements measured between the 1988 and the 1989 surveys is taken as 1 mm/km$^{1/2}$ $L^{1/2}$, and the standard deviation of vertical displacements measured between the 1954 and the 1989 surveys is taken as 3.1 mm/km$^{1/2}$ $L^{1/2}$. This corresponds to an accumulated 1-σ uncertainty of ±4.5 mm along the 1988–1989 traverse and ±43 mm around the 1954–1989 circuit.

Systematic Error

Inspection of the 1954–1989 leveling results suggests an inverse correlation between elevation and vertical displacement or, in other words, between slope and tilt (Figure 5). Such a correlation could be a consequence of (1) volcano-tectonic processes responsible for subsidence or (2) systematic leveling errors that accumulate with elevation (e.g., rod scale or refraction error) and are not completely removed by corrections. The mean slope along the leveling circuit varies

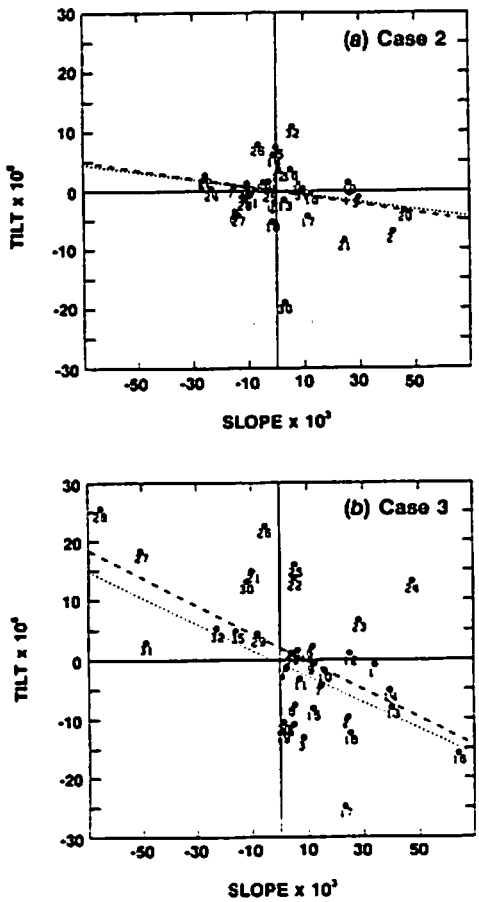

Fig. A1. Tilt versus slope plots and regression lines (*a*) for sections of the leveling circuit located off Medicine Lake volcano (case 2) and (*b*) for sections located on the volcano (case 3). Dashed regression lines are for the unweighted case; dotted lines are for the weighted case. Numbers denote bench mark pairs (i.e., sections) that differ in the two plots. See the Appendix for details.

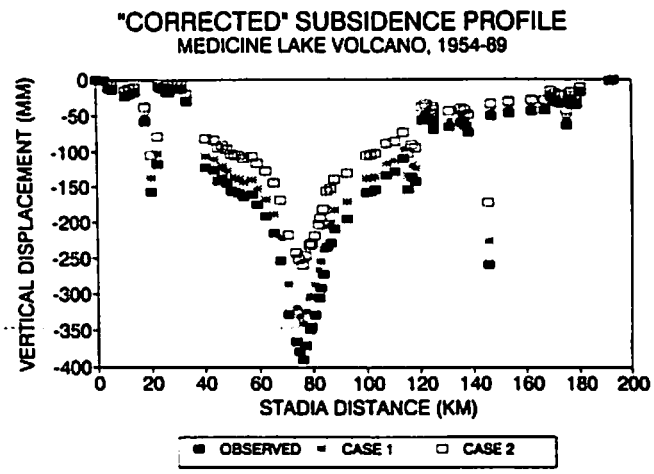

Fig. A2. Observed and "corrected" subsidence profiles showing the effect of removing the tilt-slope correlation determined in cases 1 and 2. In each case the linear regression coefficient m was used to adjust the observed values to $m = 0$.

from almost zero near Tennant to about 2% on the flanks of Medicine Lake volcano and near Stephens Pass (Figure 5). Accumulation of systematic error is possible in such terrain, but the largest cumulative correction applied to either the 1954 or the 1989 data was only 43 mm (K. Koepsell, personal communication, 1990; CVO, unpublished data, 1991). Therefore barring a serious flaw in the corrections, any residual error is likely to be much smaller than the maximum subsidence during 1954–1989 (389 ± 43 mm). We verified that conclusion in two ways. First, we applied linear regression analysis to the 1954–1989 results to determine the magnitude of any slope-dependent error [*Stein*, 1981]. Next, we analyzed a 1958 leveling survey in Virginia for evidence of slope-dependent error. The same rods were used for the 1958 Virginia survey and the 1954 Medicine Lake survey, so any rod calibration error should be common to both surveys.

To assess the significance of the apparent correlation between tilt and slope, we calculated regression coefficients m, Y intercepts b, and correlation coefficients r for the equation $\tau = m\theta + b$, where τ and θ represent tilt and slope, respectively, for each section along the leveling circuit. Two weighting functions were used: (1) equal weight for all data points (hereafter referred to as "unweighted") and (2) $1/\sigma^2$, where σ is the standard deviation from random leveling error for each section ("weighted"). The latter approach takes account of the fact that tilt is better determined for long sections than for short sections.

Three cases were evaluated in detail. Case 1 included 70 of the 81 sections measured in 1989. Twelve benchmarks were excluded for the following reasons: (1) their displacements were anomalous relative to adjacent marks, and they are judged to be unstable (Z502, C499); (2) their displacements were large and probably caused by faulting (L500, M500, P500, V501, U501, T501, C500); or (3) they formed unusually short sections ($L \leq 0.3$ km) for which tilt was poorly determined (TENNANT, TENNANT AZ). Inclusion of these marks in the regression analysis yielded ambiguous results (i.e., the unweighted and weighted fits were much different), because sections involving these marks were conspicuous outliers on plots of tilt versus slope. Such outliers strongly influence the least squares fit if data points are unweighted. Case 2 included only those sections from case 3 that are located off Medicine Lake volcano (i.e., zero to 30 km or 110–193 km from H197, measured counterclockwise along the leveling circuit; $N = 35$). Conversely, case 3 included only those sections from case 1 that are located on the volcano (30–110 km from H197; $N = 35$). Results of the regression analysis are given in Figures A1 and A2 and Table A1, along with the critical values of r for various levels of significance α (i.e., $\pm r_c(\alpha)$). Two variables are correlated at the 1-α confidence level if $r \leq -r_c(\alpha)$ (inverse correlation) or $r \geq +r_c(\alpha)$ (direct correlation).

For case 1, both unweighted and weighted values of r indicate that tilt and slope are linearly correlated at the >99% confidence level, consistent with the inference drawn earlier from inspection of Figure 5. However, when only marks located off Medicine Lake volcano are included in the regression analysis (case 2), the correlation between tilt and slope is either not significant (unweighted) or barely significant (weighted) at the 92% confidence level. Conversely, if only marks located on the volcano are included (case 3), the correlation is significant even at the 99% level (Table A1). These results can be verified by closer inspection of Figure 5: tilt and slope are inversely related on Medicine Lake volcano, but not near Stephens Pass, where steep topogra-

TABLE A1. Linear Regression Statistics

	Case 1	Case 2	Case 3
Number of sections N	70	35	35
Regression coefficient, m*	$-1.771 \pm 0.415 \times 10^{-4}$	$-0.727 \pm 0.488 \times 10^{-4}$	$-2.348 \pm 0.621 \times 10^{-4}$
	$(-1.594 \pm 0.350 \times 10^{-4})$	$(-0.640 \pm 0.369 \times 10^{-4})$	$(-2.200 \pm 0.549 \times 10^{-4})$
Y intercept b*	$+8.075 \pm 9.482 \times 10^{-4}$	$-8.645 \pm 85.284 \times 10^{-5}$	$+1.988 \pm 1.688 \times 10^{-3}$
	(0)	(0)	$(-6.311 \pm 14.895 \times 10^{-4})$
Correlation coefficient r*	−0.455	−0.247	−0.539
	(−0.478)	(−0.285)	(−0.561)
Critical values of r, $\pm r_c(\alpha = 0.10)$	±0.195	±0.279	±0.275
Critical values of r, $\pm r_c(\alpha = 0.05)$	±0.232	±0.330	±0.325
Critical values of r, $\pm r_c(\alpha = 0.02)$	±0.274	±0.387	±0.381
Critical values of r, $\pm r_c(\alpha = 0.01)$	±0.302	±0.424	±0.418

*Values that are not in parentheses are unweighted. Values that are in parentheses are weighted.

phy similar to that at the volcano is not reflected in the subsidence profile. We conclude that the strong correlation between tilt and slope is spatially associated with the volcano, presumably because the subsidence mechanism is volcanogenic. A corollary of this interpretation is that cases 1 and 3 overestimate the importance of slope-dependent error, while case 2 may be representative.

To calculate an upper bound for the magnitude of slope-dependent error in the Medicine Lake data, we "corrected" the 1954–1989 subsidence profile using the regression coefficients determined for cases 1 and 2 (Figure A2). Removal of the case 2 regression line reduces the maximum subsidence during 1954–1989 by about 13% to 340 mm. The corresponding values are 33%, to 260 mm, if the case 1 regression line is used. The possibility of nonlinear errors cannot be excluded, but lacking evidence to the contrary, we conclude that slope-dependent error accounts for less than one third of the 1954–1989 subsidence at Medicine Lake volcano.

This conclusion is supported by analysis of leveling observations in 1958 and 1985 along a 40-km traverse from Talcott, West Virginia, to Glenlyn, Virginia. First-order, class II procedures were followed for both surveys. The 1958 survey used the same pair of rods that was used for the 1954 survey at Medicine Lake; the 1985 survey used NGS rods 121176, 132181, 270711, and 277921 (K. Koepsell, personal communication, 1990). Assuming that the rods used in 1985 and 1989 were properly calibrated, any rod scale error associated with the rods used in 1954 and 1958 should be present in both the 1958–1985 (Virginia) and the 1954–1989 (Medicine Lake) data sets.

Vertical displacements and topography are apparently correlated in the Virginia data set (Figure A3), but the magnitude of the correlation is smaller than for the Medicine Lake case and is of opposite sign. In the Virginia case, approximately 20 mm of apparent uplift accumulates over 200 m of vertical relief, suggesting the possibility of a rod scale error of about 100 parts per million (ppm). At Medicine Lake, 389 mm of subsidence accumulates over 1000 m of relief, which would require a rod scale error of almost 400 ppm in the opposite sense. Clearly, both cases cannot be explained by the same rod scale error in the 1954/1958 rods; a combination of errors in at least two rod pairs would be required. Errors of such magnitude would be unprecedented for calibrated USGS or NGS rods. *Strange* [1980] showed that the largest apparent scale difference between any two sets of rods used for 64 repeat surveys over 17 profiles in southern California with topographic relief ranging from about 600 m to 2200 m was less than 160 ppm. Therefore we conclude that any rod scale error in the 1954–1989 results is small compared to the amount of real subsidence: less than 33% and probably less than 13%.

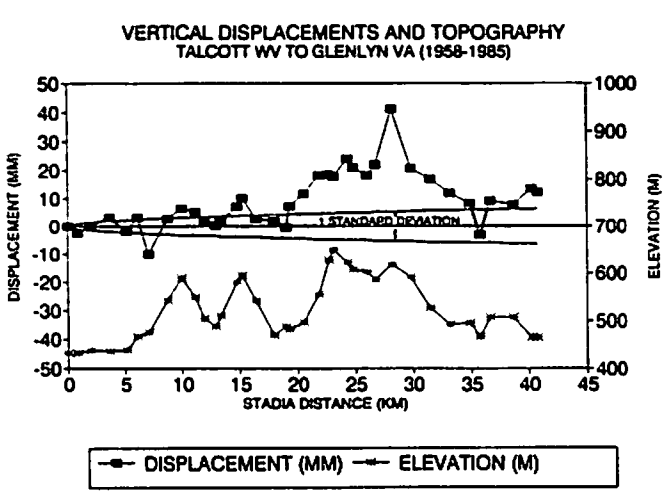

Fig. A3. Vertical displacements (1958–1985) and topography along a 40-km leveling traverse from Talcott, West Virginia, to Glenlyn, Virginia. Procedures for first-order, class II leveling were followed for both surveys. NGS data were provided by K. Koepsell (personal communication, 1990). Stippled area indicates 1 standard deviation in the leveling measurements. At any stadia distance the vertical dimension of the stippled area indicates the height of the 1-sigma error bar at that distance.

Acknowledgments. Special thanks to members of CVO's 1989 Medicine Lake leveling crews: Erika Anderson, Stuart Ashbaugh, Marvin Couchman, Steve Hoffine, Gene Iwatsubo, Gordon Keating, Jack Kleinman, Dave Schneider, Jim Sproull, Don Swanson, Mary Turner, Dave Wieprecht, Ed Wolfe, and Ken Yamashita. Kathy Koepsell of the National Geodetic Survey provided helpful information concerning the 1954 leveling survey, including additional data discussed in the Appendix. U.S. Forest Service personnel from the Klamath, Modoc, and Shasta national forests provided essential logistical support. Marianne Guffanti, Patrick Muffler, and James Smith shared their knowledge of the regional geology and contributed to the development of ideas presented in the manuscript. Ross Stein provided software and guidance for the evaluation of systematic error in the leveling surveys; John Ewert, Jeff Marso, and Arnold Okamura did the same for point source modeling of the subsidence data. Marianne Guffanti, Paul Delaney, Ross Stein, Roger Denlinger, and an anonymous colleague provided helpful reviews. Ellen Longee greatly improved one of the figures using a computer graphics software package.

REFERENCES

Anderson, C. A., Volcanoes of the Medicine Lake Highland, California, *Univ. Calif. Publ. Geol. Sci.*, *25*, 347–422, 1941.

Balazs, E. I., and G. M. Young, Corrections applied by the National Geodetic Survey to precise leveling observations, *Tech. Memo. NOS NGS 34*, 12 pp., Natl. Oceanic and Atmos. Admin., Boulder, Colo., 1982.

Bennett, J. H., R. W. Sherburne, C. H. Cramer, C. W. Chesterman, and R. H. Chapman, Stephens Pass earthquakes, Mount Shasta—August 1978, *Calif. Geol.*, *32*(2), 27–34, 1979.

Blakely, R. J., and R. C. Jachens, Volcanism, isostatic residual gravity, and regional tectonic setting of the Cascade volcanic province, *J. Geophys. Res.*, *95*, 19,439–19,451, 1990.

Blakely, R. J., R. C. Jachens, R. W. Simpson, and R. W. Couch, Tectonic setting of the southern Cascade Range as interpreted from its magnetic and gravity fields, *Geol. Soc. Am. Bull.*, *96*, 43–48, 1985.

Bolt, B. A., and R. D. Miller, Catalogue of earthquakes in northern California and adjoining areas, 1 January 1910–31 December 1972, Seismographic stations, report, Univ. of Calif., Berkeley, 1975.

Catchings, R. D., Crustal structure from seismic refraction in the Medicine Lake area of the Cascade Range and Modoc Plateau, northern California, Master's thesis, 97 pp., Univ. of Wis., Madison, 1983.

Catchings, R. D., Crustal structure of the northwestern United States, Ph.D. thesis, 182 pp., Stanford Univ., Stanford, Calif., 1987.

Chouet, B., R. Y. Koyanagi, and K. Aki, Origin of volcanic tremor in Hawaii, II, Theory and discussion, in Volcanism in Hawaii, vol. 2, edited by R. W. Decker, T. L. Wright, and P. H. Stauffer, *U.S. Geol. Surv. Prof. Pap.*, *1350*, 1259–1280, 1987.

Cramer, C. H., The Stephen's Pass earthquake swarm of August 1978, east of Mt. Shasta, California (abstract), *Eos Trans. AGU*, *59*(12), 1130, 1978.

Davis, J. L., W. H. Prescott, J. L. Svarc, and K. J. Wendt, Assessment of global positioning system measurements for studies of crustal deformation, *J. Geophys. Res.*, *94*, 13,635–13,650, 1989.

Donnelly-Nolan, J. M., A magmatic model of Medicine Lake volcano, California, *J. Geophys. Res.*, *93*, 4412–4420, 1988.

Donnelly-Nolan, J. M., Geology of Medicine Lake volcano, Northern California Cascade Range, *Trans. Geotherm. Resour. Counc.*, *Part II*, *14*, 1395–1396, 1990.

Donnelly-Nolan, J. M., and K. M. Nolan, Catastrophic flooding and eruption of ash-flow tuff at Medicine Lake volcano, California, *Geology*, *14*, 875–878, 1986.

Donnelly-Nolan, J. M., D. E. Champion, C. D. Miller, and D. A. Trimble, Implications of post-11,000-year volcanism at Medicine Lake volcano, northern California Cascade Range, in Proceedings of Workshop XLIV, Geological, Geophysical, and Tectonic Setting of the Cascade Range, *U.S. Geol. Surv. Open File Rep.*, *89-178*, 556–590, 1989.

Dzurisin, D., J. C. Savage, and R. O. Fournier, Recent crustal subsidence at Yellowstone Caldera, Wyoming, *Bull. Volcanol.*, *52*, 247–270, 1990.

Evans, J. R., and S. R. Walter, Relation of recent seismicity to tomographic structure at Medicine Lake volcano, northern California (abstract), *Seismol. Res. Lett.*, *60*, 31, 1989.

Evans, J. R., and J. J. Zucca, Active high-resolution seismic tomography of compressional wave velocity and attenuation structure at Medicine Lake volcano, northern California Cascade Range, *J. Geophys. Res.*, *93*, 15,016–15,036, 1988.

Finch, R. H., Lassen report no. 14, *Volcano Lett.*, *161*, 1928. (Reprinted in *The Volcano Letters*, edited by R. S. Fiske, T. Simkin, and E. A. Nielsen, p. 161, Smithsonsian Institution, Washington, D.C., 1987.)

Fink, J. H., and D. D. Pollard, Structural evidence for dikes beneath silicic domes, Medicine Lake Highland volcano, California, *Geology*, *11*, 458–461, 1983.

Finn, C., and D. L. Williams, Gravity evidence for a shallow intrusion under Medicine Lake volcano, California, *Geology*, *10*, 503–507, 1982.

Fournier, R. O., Geochemistry and dynamics of the Yellowstone National Park hydrothermal system, *Annu. Rev. Earth Planet. Sci.*, *17*, 13–53, 1989.

Fuis, G. S., J. J. Zucca, W. D. Mooney, and B. Milkereit, A geologic interpretation of seismic-refraction results in northeastern California, *Geol. Soc. Am. Bull.*, *98*, 53–65, 1987.

Gay, T. E., Jr., and Q. A. Aune, Alturas sheet, geologic map of California, scale 1:250,000, Calif. Div. of Mines and Geol., Sacramento, 1958.

Grove, T. L., and M. B. Baker, Phase equilibrium controls on the tholeiitic versus calc-alkaline differentiation trends, *J. Geophys. Res.*, *89*, 3253–3274, 1984.

Grove, T. L., and J. M. Donnelly-Nolan, The evolution of young silicic lavas at Medicine Lake volcano, California: Implications for the origin of compositional gaps in calc-alkaline series lavas, *Contrib. Mineral. Petrol.*, *92*, 281–302, 1986.

Grove, T. L., R. J. Kinzler, M. B. Baker, J. M. Donnelly-Nolan, and C. E. Lesher, Assimilation of granite by basaltic magma at Burnt Lava Flow, Medicine Lake volcano, northern California, *Contrib. Mineral. Petrol.*, *99*, 320–343, 1988.

Klein, F. W., User's guide to HYPOINVERSE, a program for VAX computers to solve for earthquake locations and magnitudes, *U.S. Geol. Surv. Open File Rep.*, *89-314*, 49 pp., 1989.

Koyanagi, R. Y., B. Chouet, and K. Aki, Origin of volcanic tremor in Hawaii, I, Data from the Hawaiian Volcano Observatory, 1969–1985, in Hawaiian Volcanism, edited by R. W. Decker, and T. L. Wright, *U.S. Geol. Surv. Prof. Pap.*, *1350*, 1221–1258, 1987.

Lester, R. W., and K. L. Meagher, Catalog of earthquakes along the San Andreas fault system in central California for the year 1984, *U.S. Geol. Surv. Open File Rep.*, *78-1010*, 89 pp., 1978.

McKee, E. H., W. A. Duffield, and R. J. Stern, Late Miocene and early Pliocene basaltic rocks and their implications for crustal structure, northeastern California and south-central Oregon, *Geol. Soc. Am. Bull.*, *94*, 292–304, 1983.

Meertens, C. M., Tilt tides and tectonics at Yellowstone National Park, Ph.D. thesis, 236 pp., Univ. of Colo., Boulder, 1987.

Mogi, K., Relation between the eruptions of various volcanoes and the deformation of the ground surfaces around them, *Bull. Earthquake Res. Inst. Univ. Tokyo*, *36*, 99–134, 1958.

Moore, J. G., Relationship between subsidence and volcanic load, Hawaii, *Bull. Volcanol.*, *34*, 562–576, 1970.

Prescott, W. H., J. L. Davis, and J. L. Svarc, Global positioning system measurements for crustal deformation: Precision and accuracy, *Science*, *244*, 1337–1340, 1989.

Schomaker, M. C., and R. M. Berry, Geodetic leveling, *Manual NOS NGS 3*, Natl. Geod. Surv., Natl. Oceanic and Atmos. Admin., Rockville, Md., 1981.

Stauber, D. A., S. M. Green, and H. M. Iyer, Three-dimensional *P* velocity structure of the crust below Newberry volcano, Oregon, *J. Geophys. Res.*, *93*, 10,095–10,107, 1988.

Stein, R. S., Discrimination of tectonic displacement from slope-dependent errors in geodetic leveling from southern California, 1953–1977, in *Earthquake Prediction: An International Review*, *Maurice Ewing Ser.*, vol. 4, edited by D. W. Simpson and P. G. Richards, pp. 441–456, AGU, Washington, D. C., 1981.

Stewart, S. W., and M. E. O'Neill, Calculation of the frequency response of the USGS telemetered short-period seismic system, *U.S Geol. Surv. Open File Rep.*, *80-143*, 83 pp., 1980.

Strange, W. E., The effect of systematic errors on geodynamic analysis, in *Second International Symposium on Problems Related to the Redefinition of North American Vertical Geodetic Networks*, pp. 705–729, Canadian Institute of Surveying, Surveys and Mapping Branch, Ottawa, 1980.

Vanicek, P., R. O. Castle, and E. I. Balazs, Geodetic leveling and its applications, *Rev. Geophys.*, *18*, 505–524, 1980.

Walter, S., and D. Dzurisin, The September 1988 earthquake swarm at Medicine Lake volcano, northern California (abstract), *Eos Trans. AGU*, *70*(43), 1189–1190, 1989.

Zohdy, A. A. R., and R. J. Bisdorf, Schlumberger soundings near Medicine Lake, California, *Geophysics*, *55*, 956–964, 1990.

Zucca, J. J., G. S. Fuis, B. Milkereit, W. D. Mooney, and R. D. Catchings, Crustal structure of northeastern California, *J. Geophys. Res.*, *91*, 7359–7382, 1986.

J. M. Donnelly-Nolan, J. R. Evans, and S. R. Walter, U.S. Geological Survey, 345 Middlefield Road, Menlo Park, CA 94025.

D. Dzurisin, David A. Johnston Volcano Observatory, U.S. Geological Survey, 5400 MacArthur Boulevard, Vancouver, WA 98661.

(Received October 6, 1990;
revised May 13, 1991;
accepted June 4, 1991.)

3Y

APPENDIX 1 - 2

A. The Giant Crater Lava Field: Geology and Geochemistry of a Compositionally Zoned, High-Alumina Basalt to Basaltic Andesite Eruption at Medivine Lake Volcano, California.
Donnelly-Nolan, J.M., Champion, D.E., Grove, T.L., Baker, M.B., Taggart, J.E., Bruggman, P.E.

B. Duration of Eruption at the Giant Crater Lava Filed, Medicine Lake Volcano, California, Based on Paleomagnetic Secular Variation.
Champion, D.E., Donnelly-Nolan, J.M.

JOURNAL OF GEOPHYSICAL RESEARCH, VOL. 99, NO. B8, PAGES 15,595–15,604, AUGUST 10, 1994

Duration of eruption at the Giant Crater lava field, Medicine Lake volcano, California, based on paleomagnetic secular variation

Duane E. Champion and Julie M. Donnelly-Nolan
U.S. Geological Survey, Menlo Park, California

Abstract. Nearly 500 cores were collected from the postglacial Giant Crater lava field on the south flank of Medicine Lake volcano. The basaltic lavas form a continuous set of lava flows which display strong chemical zonation from initially erupted calc-alkaline basaltic andesite to final primitive basalt of tholeiitic affinity. Six chemical-stratigraphic groups have been recognized and mapped. The eruptive sequence was sampled at numerous sites both to determine the characteristic paleomagnetic direction of each chemical group and to estimate the duration of the eruption inferred from secular variation of the geomagnetic field. Well-grouped mean directions of magnetization were obtained for 41 sites in the Giant Crater lava field. Mean directions of magnetization determined for the lava field are nearly identical. The likelihood of any extended time interval for the eruption of the different lava types is extremely small, and the data suggest an eruptive event of less than 30 years duration, analogous to historic Hawaiian eruptions. However, the average of groups 1–4, which cannot be distinguished paleomagnetically from each other, is slightly different statistically from that of the average of groups 5 and 6, which have similar directions. A time gap of 10 ± 5 years is inferred between eruption of group 4 and 5 lavas based on analysis of the probability of the observed angular difference of 1.27° ± 0.84° between their mean directions and by comparison of this angular difference to calculated field directions with similar declination and inclination determined from spherical harmonic models of the geomagnetic field for the time period 1945–1990. About 200 oriented cores were also collected from predecessor and successor basaltic lava flows on the upper flanks of the volcano. Together with remanent directions from lavas of the Snake River Plain the data define a clockwise loop of secular variation.

Introduction

The Giant Crater lavas erupted about 10,600 years ago, covering an area of about 200 km^2 on the south flank of Medicine Lake volcano in the southern Cascade Range (Figure 1). The lava field is compositionally zoned and consists of basalt and basaltic andesite, which have been subdivided into six chemical-stratigraphic groups [*Donnelly-Nolan et al.*, 1991]. The most silicic calc-alkaline lavas erupted first, followed by less silicic lavas, and finally by primitive high-alumina basalt of tholeiitic affinity. There are no exceptions to the ordered eruption sequence of the different composition groups. Additionally, there is no evidence in outcrop of soils, weathering horizons, unconformities, or intercalated stratigraphy that suggests significant passage of time within the Giant Crater flow sequence. Several other mafic eruptions took place at Medicine Lake volcano at about the same time [*Donnelly-Nolan et al.*, 1990]. These include morphologically similar lavas which are identified as predecessors and successors to the Giant Crater eruptions, based on stratigraphic relations, radiocarbon dating, and analysis of paleomagnetic secular variation. Over 200 oriented cores were collected and studied from these lavas.

Paper number 94JB00900.

The 4.4 km^3 of Giant Crater lavas erupted from numerous vents including lava ponds, spatter vents, and pit craters located within a few kilometers of each other at the north end of the 45-km-long lava field. Much of the lava was transported via lava tubes. The Giant Crater eruption mechanism is probably analogous to recent historical Hawaiian eruptions. The ongoing eruption of Kilauea volcano has similar kinds of vents and tube systems and has erupted 0.1 km^3 of basalt per year since the eruption began in 1983 [*Heliker and Wright*, 1991]. The lavas there are compositionally variable with a 3% range in MgO content, from <6 to nearly 9 wt % [*Wolfe et al.*, 1987]. The Giant Crater lavas have a 4% range in MgO content, from 6.5 to 10.5 wt % [*Donnelly-Nolan et al.*, 1991]. In contrast, the Laki eruptions of 1783–1784 in Iceland produced 14.7 km^3 of relatively homogeneous basaltic lava in only 8 months, in part via lava tubes [*Thordarson and Self*, 1993].

This paper describes the paleomagnetic data of the Giant Crater lava field as well as data for the predecessor and successor eruptions (Table 1). A geochemical model of the Giant Crater lavas suggests that their compositional zonation and eruption mechanism was produced by multiple episodes of fractionation, assimilation, replenishment, and mixing [*Baker et al.*, 1991]. Very well grouped site mean directions of magnetization give us the opportunity to evaluate the time span of this eruptive sequence, suggesting that the eruption responsible for the lavas lasted less than 30 years. Also, we

Table 1. Giant Crater Lava Field Paleomagnetic Data

Site	Latitude, °N	Longitude, °E	N/N_0	Exp	I	D	A_{95}	k	R	Plat/Plong	
				Horse Caves							
3B842	41.471	238.360	10/12	20	62.5	327.1	2.8	298	9.96984	65.9	165.1
4B543	41.474	238.364	11/12	20+	60.8	338.3	1.9	610	10.98361	73.8	156.8
B8623	41.468	238.364	12/12	20	54.1	335.6	4.2	110	11.89964	69.7	136.8
	41.5	238.3	3/3	···	59.2	333.9	8.1	234	2.99146	70.3	152.7
				Water Caves							
2B193	41.339	238.428	12/13	20	63.4	342.9	1.8	564	11.98051	77.1	170.7
2B218	41.420	238.353	10/12	10	58.7	341.5	1.1	2065	9.99564	75.8	146.4
3B782	41.461	238.366	12/12	20	59.2	346.6	2.2	378	11.97088	79.8	144.5
7A297	41.396	238.364	10/12	40	58.8	339.1	2.1	517	9.98258	74.0	148.7
B9527	41.353	238.416	9/12	10+	61.9	342.4	4.3	142	8.94357	76.9	162.2
	41.5	238.3	5/5	···	60.4	342.5	2.4	1025	4.99610	76.9	153.6
				Precursors: Spatter Vents Within Double Hole Crater Flow							
3B758	41.467	238.383	11/12	30	56.1	19.9	2.3	389	10.97431	73.9	339.2
7B943	41.479	238.386	11/12	20+	65.1	27.6	1.9	612	10.98365	69.6	302.9
B9791	41.474	238.383	12/12	20+	58.7	14.4	1.9	536	11.97948	78.9	334.1
				Precursors: Basalt of the Ribbon Flow							
5B358	41.541	238.479	11/12	20	57.8	20.0	2.6	302	10.96685	74.4	333.4
				Precursors: Spatter East of Grasshopper Flat							
5B384	41.525	238.321	10/12	30	57.9	19.7	2.8	297	9.96970	74.7	333.0
				Group 1 and 2							
2B230	41.514	238.370	10/12	20+	58.6	22.7	2.6	344	9.97387	72.6	328.1
3B794	41.519	238.373	8/12	40	57.3	18.8	4.7	141	7.95034	75.1	336.2
3B806	41.514	238.372	12/12	20	(57.5	12.8)	1.8	562	11.98042	79.6	343.2
3B818	41.502	238.370	12/12	20	56.1	19.4	0.5	6439	11.99829	74.2	339.9
7A237	41.470	238.320	12/12	30	57.1	21.5	1.8	611	11.98201	72.1	334.3
7B883	41.421	238.344	12/12	30+	58.6	16.4	2.2	387	11.97155	77.4	332.6
7B895	41.519	238.373	10/12	30	58.0	19.9	2.5	382	9.97641	74.5	332.6
7B907	41.516	238.375	11/12	20	58.9	17.1	1.2	1447	10.99309	76.9	331.1
	41.5	238.3	7/8	···	57.8	19.4	1.2	2701	6.99778	74.9	333.4
				Group 3							
7A285	41.401	238.359	12/12	20	58.1	20.5	1.2	1232	11.99107	74.2	331.0
7B871	41.422	238.342	12/12	10+	56.8	22.5	1.9	501	11.97803	72.2	333.9
7B919	41.477	238.360	12/12	10	57.6	18.7	1.7	639	11.98278	75.3	335.1
B8635	41.442	238.343	12/12	10	59.8	20.9	1.1	1513	11.99273	74.3	324.1
B8647	41.479	238.344	12/12	10	57.6	18.2	0.7	3666	11.99700	75.7	335.6
	41.5	238.3	5/5	···	58.0	20.2	1.4	3100	4.99871	74.4	332.1
				Group 4: Double Hole							
0A335	41.491	238.384	12/12	20	55.7	14.1	1.2	1426	11.99229	77.9	349.4
3B734	41.359	238.407	12/12	10	59.2	22.2	1.4	1029	11.98932	73.2	325.7
3B746	41.467	238.383	11/12	20	59.3	18.3	1.8	640	10.98438	76.1	328.0
4B555	41.499	238.381	12/12	30	59.6	22.0	2.0	465	11.97635	73.4	324.7
B8406	41.495	238.389	12/12	10+	57.7	21.3	1.4	987	11.98885	73.4	332.5
B8515	41.386	238.414	12/12	10	58.6	19.4	0.8	3256	11.99662	75.1	330.1
B8575	41.443	238.395	12/12	10+	57.3	17.9	0.8	3123	11.99648	75.8	337.0
	41.5	238.3	7/7	···	58.2	19.2	1.6	1526	6.99607	75.1	331.9
				Group 4: Giant Crater							
0A347	41.392	238.334	12/12	20	57.5	18.1	1.0	1925	11.99428	75.7	335.6
2B206	41.272	238.399	12/12	20+	58.7	24.1	1.1	1481	11.99257	71.6	326.2
2B242	41.507	238.359	11/12	20+	59.4	20.8	1.3	1187	10.99158	74.3	326.2
7A213	41.460	238.314	12/12	10	57.5	21.0	0.7	3593	11.99694	73.6	333.2
7A273	41.504	238.361	12/12	10+	56.9	17.2	3.3	179	11.93853	76.2	339.5
7B931	41.409	238.339	12/12	10	56.1	18.2	0.9	2324	11.99527	75.1	341.0
	41.5	238.3	6/6	···	57.7	19.9	1.5	1984	5.99748	74.5	333.5
				Group 5							
2B181	41.205	238.506	11/12	20+	59.8	21.6	1.1	1807	10.99447	73.7	323.3
3B722	41.154	238.430	11/12	20	58.5	16.9	1.0	2275	10.99560	77.0	331.5
B8454	41.244	238.495	12/12	20+	58.6	18.3	1.3	1068	11.98970	75.9	330.5
B8466	41.218	238.451	12/12	10	59.5	17.7	0.9	2558	11.99570	76.6	326.3
	41.5	238.3	4/4	···	59.1	18.6	1.4	4289	3.99930	75.8	328.7

3

Table 1. (continued)

Site	Latitude, °N	Longitude, °E	N/N_0	Exp	I	D	A_{95}	k	R	Plat/Plong	
					Group 6						
3B830	41.500	238.367	12/12	10	61.0	21.1	3.0	216	11.94903	74.3	319.3
7A225	41.462	238.315	12/12	10	(60.6	12.4)	1.9	519	11.97879	80.7	323.5
7A261	41.498	238.368	10/12	20+	58.7	22.8	1.3	1345	9.99331	72.6	327.6
7B955	41.492	238.321	9/12	10	59.5	18.5	2.6	392	8.97959	76.0	326.9
B8418	41.327	238.445	12/12	10	61.1	18.8	1.4	903	11.98782	76.0	319.0
B8430	41.277	238.404	10/12	10	62.1	22.8	1.2	1550	9.99419	73.1	313.5
B8442	41.330	238.386	8/12	20+	58.1	18.1	2.1	693	7.98990	76.0	332.8
B8539	41.331	238.416	12/12	10	58.1	19.5	0.9	2515	11.99563	74.9	331.6
B8563	41.342	238.381	11/12	10	56.1	21.1	0.8	3044	11.99671	73.0	337.7
B8587	41.484	238.317	12/12	10	58.4	22.1	1.1	1539	11.99285	73.0	329.2
B8599	41.462	238.314	10/12	10+	59.3	17.7	1.7	820	9.98903	76.6	328.3
	41.5	238.3	10/11	···	59.3	20.2	1.2	1586	9.99433	74.6	327.0
					Successors: Tree Molds Flow						
2B367	41.637	238.393	24/24	20+	61.7	19.7	1.8	269	23.91435	75.4	316.9
4B419	41.637	238.393	12/12	20+	61.5	19.0	2.1	415	11.97350	75.9	318.0
					Successors: Basalt of "Vent 5"						
7B967	41.482	238.305	10/11	30+	62.6	15.4	3.9	156	9.94236	78.5	310.9
B8611	41.483	238.304	12/12	20	56.5	13.4	1.7	646	11.98298	78.7	346.9

Site is alphanumeric identifier from Figures 1 and 2; N/N_0 is the number of cores used compared with the number originally taken at the site; Exp is the strength of the peak cleaning field; I and D are the remanent inclination and declination; A_{95} is the 95% confidence limit about the mean direction; k is the estimate of the Fisherian precision parameter; R is the length of the resultant vector; and Plat/Plong is the location in degrees north and east of the virtual geomagnetic pole (VGP) calculated from the site mean direction. Parentheses around site mean directions indicate they were not used in unit or group means. Unit or group means were taken at an average position of 41.5°N and 238.3°E, and average VGPs relate to that position; N/N_0 for unit or group means relate to number of site means used compared to sites originally taken.

evaluate the possibility that the eruptions were interrupted for a short time, perhaps a decade between group 4 and 5 lavas. The entire data set, Giant Crater lavas plus the predecessor and successor lavas, defines a clockwise loop of secular variation.

Procedures

A total of 696 cores were collected from 58 flow outcrops to obtain site mean directions of remanent magnetization reported in Table 1 (Figures 1 and 2). Of this total, 480 cores were taken from 41 outcrops in the Giant Crater lava field (Figure 2). Typically, 12 cores were taken at each site with a portable, water-cooled diamond coring drill and oriented in the field using a Sun compass. A pilot specimen from each core was progressively demagnetized using alternating field (AF) until it was free of secondary components. A vector component diagram for a typical sample from a group 6 lava flow shows a virtual absence of secondary components and that the characteristic magnetization is effectively removed by AF demagnetization (Figure 3). Stepwise AF cleaning with accompanying line fits was not required by this suite of samples, and instead, "blanket" AF cleaning fields could be assigned. Peak field strengths required to remove secondary components were generally of low value (10–20 mT), with some higher field strengths used for samples with large secondary components of magnetization, presumably isothermal remanence from lightning strikes.

Paleomagnetic sampling of uneroded young lava flows presents challenges not faced in older rocks. The rubbly flow surfaces that commonly mantle the structurally stable interior of a lava flow must be avoided. In many cases, roadcuts provided access to flow interiors. At natural outcrops, effort was made to sample volcanic features that represent fluid or plastically deformed lava or an inflated pahoehoe flow with a horizontal surface. These morphologic features are reliable as paleomagnetic recording media. Sampling sites were carefully selected to exclude those that might have undergone postcooling deflation or tectonic movement. The very low overall dispersion in the individual flow mean directions of the Giant Crater lavas documents the importance of careful site selection and indicates that our sampling goals were met.

Initial results from the Giant Crater lava field indicated that a noticeable amount of secular variation was represented in the data. As subsequent samples were collected over a 9-year period, directions obtained from different chemical groups showed considerable overlap. By the time one third of the paleomagnetic samples had been collected, the geologic and geochemical studies revealed a regular chemical variation within the lava field allowing it to be subdivided into six chemical-stratigraphic groups [*Donnelly-Nolan et al.*, 1991]. Following recognition of these groups, paleomagnetic sampling was focused on providing four to six spatially separate sites in each group in order to define separate and statistically robust mean directions, thus resulting in the overall large number of cores. The mean directional data are used here to estimate the duration of the Giant Crater eruptive event.

Results

Site-mean directions of remanent magnetization are well defined, and associated statistics for each of 58 sites in latest Pleistocene lavas associated with the Giant Crater lava field are reported in Table 1. Figure 4 is an equal-area plot of the mean directions. The circles of 95% confidence about these mean directions are not shown in Figure 4, for reasons of

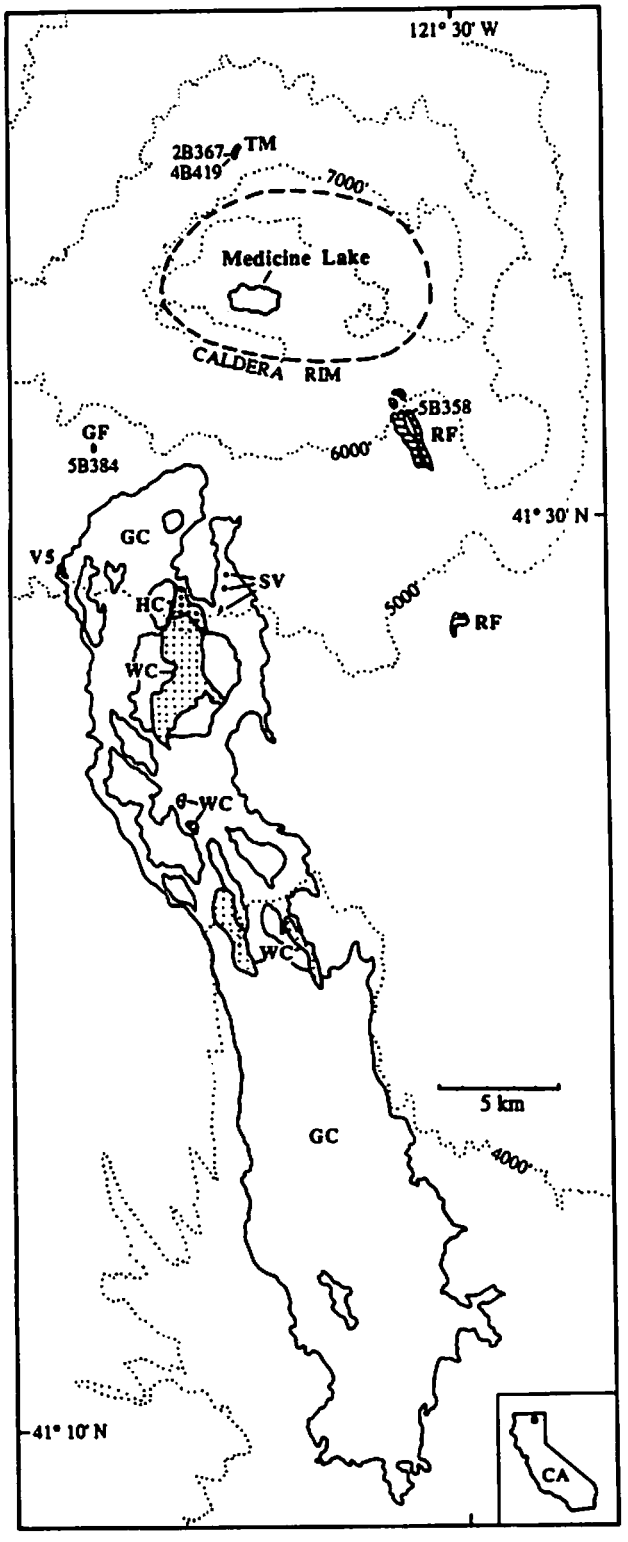

Figure 1. Location map shows Giant Crater lava field on south flank of Medicine Lake volcano. Also shown are predecessor and successor lavas and sample sites. Units are designated by symbols: HC, Horse Caves flow; WC, Water Caves flow; SV, spatter vents within Double Hole Crater flow; RF, basalt of the ribbon flows (connection between northern and southern outcrops is covered by younger lava flow); GF, spatter east of Grasshopper Flat; GC, Giant Crater lava field; TM, tree molds flow; and V5, basalt of "vent 5". Sample sites are shown for units RF, GF, and TM; all other sites are shown in Figure 2. Topographic contours are in feet (1 foot = 0.3048 m).

clarity, but they range from 0.5° to 4.7° with a median value of 1.7°.

Figure 4 shows that the site mean directions fall into two groups. Those sites with west declinations are from either the informally named Horse Caves or Water Caves flows, and those with easterly declinations are from the Giant Crater lava field or from the other predecessor and/or successor eruptions. Where overlapping outcrops exist, the flows with west declinations always underlie those with east declinations. The Horse Caves and Water Caves flows are undated but are very similar in appearance to Giant Crater lavas of similar chemical composition. Their chemical compositions, however, are distinctive, and they display petrographic differences from the Giant Crater lavas. The paleomagnetic data separate them in time from the Giant Crater lava field because the lavas do not record the same remanent direction. Horse Caves and Water Caves lavas display complex interfingering at their contact; thus their stratigraphic positions with respect to each other are undetermined.

The east declination direction recorded in lavas of the Giant Crater lava field and its associated predecessors and successors has been dated by the radiocarbon method on samples of charcoal from several tree molds, yielding an age of about 10,600 years B.P. [*Donnelly-Nolan et al.*, 1990]. The large angular distance (~20°) between the east and west declination directions suggests that the west declination group precedes the Giant Crater lava field by at least several hundred years [*Champion and Shoemaker*, 1977]. The direction for the Horse Caves and Water Caves lavas compares favorably with that obtained from the Bottleneck Lake flows of eruptive period F in the Craters of the Moon lava field in Idaho [*Kuntz et al.*, 1986a]. These flows have a minimum radiocarbon age of 11,000 ± 100 years B.P. on charred soil beneath the lava flows [*Kuntz et al.*, 1986b]. Comparisons of radiocarbon ages on this form of organic material with radiocarbon ages from burned wood or charcoal suggest that these soil ages are probably too young. We conclude that there is at least a 500-year gap in time between the eruption producing the Horse Caves and Water Caves flows and those producing the Giant Crater lava field and its immediate predecessors and successors.

The mean directions from sampling sites in the Giant Crater lava field group very well (Figure 4). It had already been established by *Donnelly-Nolan et al.* [1990] that the Giant Crater lavas are part of an approximately 200-year-long episode of basaltic volcanism, which vented from several locations on the Medicine Lake volcano. The flows from this episode constitute the bulk of the volume of lava produced in postglacial time.

In calculating the group mean directions, two of the Giant Crater sites were excluded and are shown on Figure 4 by small arrows. The mean directions for these two sites were displaced relative to other Giant Crater sites, and they differed from other sites in their chemical-stratigraphic group. These two sampling sites were examined for possible sources of directional distortion. The rejected site with the steeper inclination value is in a group 6 flow lobe draped over the near-vertical wall of a collapsed group 4 lava tube. The height of the wall (5 m) over which the flow lobe was steeply draped may have created a magnetic "edge effect," locally distorting the field. We sampled the same flow lobe again at a site about 100 m farther north and obtained results com-

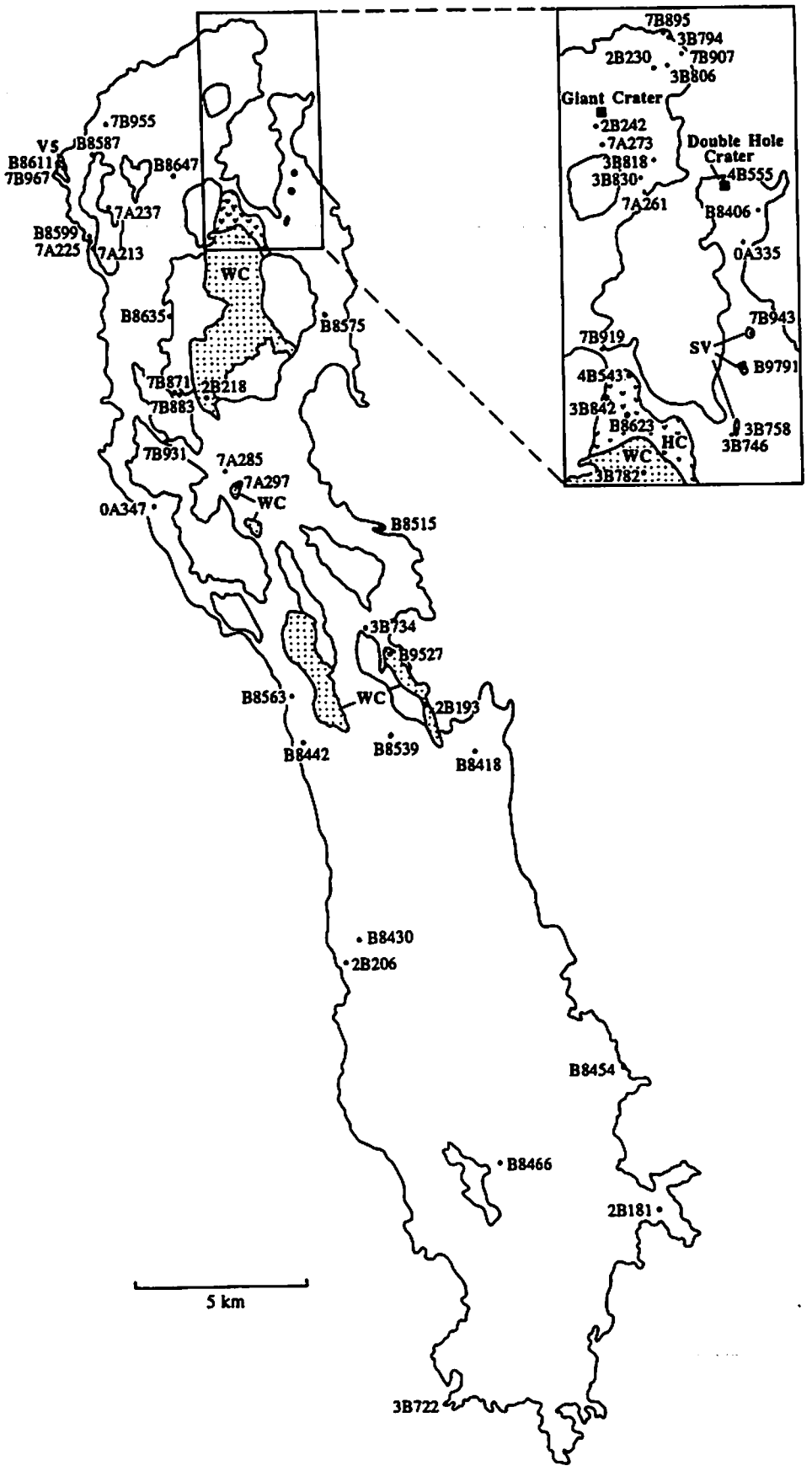

Figure 2. Map showing paleomagnetic sample site locations in Giant Crater lava field and in related lavas (letter symbols indicate units as in Figure 1).

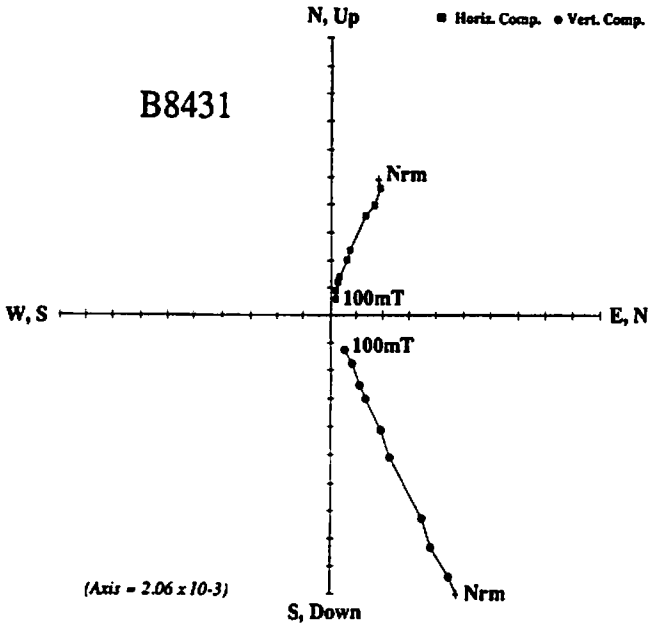

Figure 3. Vector component diagram of the alternating field demagnetization of sample B8431 from a group 6 lava, showing the minimal presence of secondary components and the smooth, linear descent to the origin. On the basis of such sample behavior, characteristic magnetizations were defined after low-peak alternating field (10–30 mT) "blanket" cleaning.

parable to the rest of the Giant Crater group 6 sites. The other rejected site is in viscous group 1 lava at the base of a steep cliff exposure within the Chimney Crater vent. We think that this viscous lava underwent postemplacement

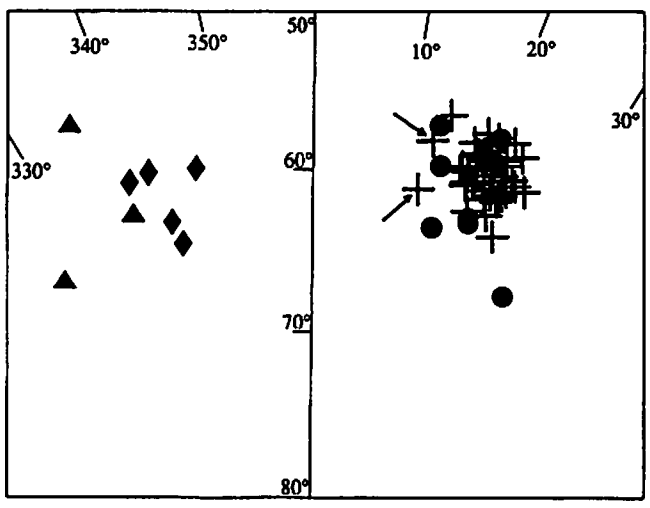

Figure 4. Enlarged part of equal-area projection showing mean directions of remanent magnetization on lower hemisphere of sites that are listed in Table 1. Circles of 95% confidence about each mean direction have been omitted for clarity; this information is listed in Table 1. Symbols are keyed to various eruptive units (triangles, Horse Caves flow; diamonds, Water Caves flow; circles, other predecessors and successors to Giant Crater lava field; crosses, Giant Crater lava field, all groups). Arrows point to site mean directions excluded from calculations.

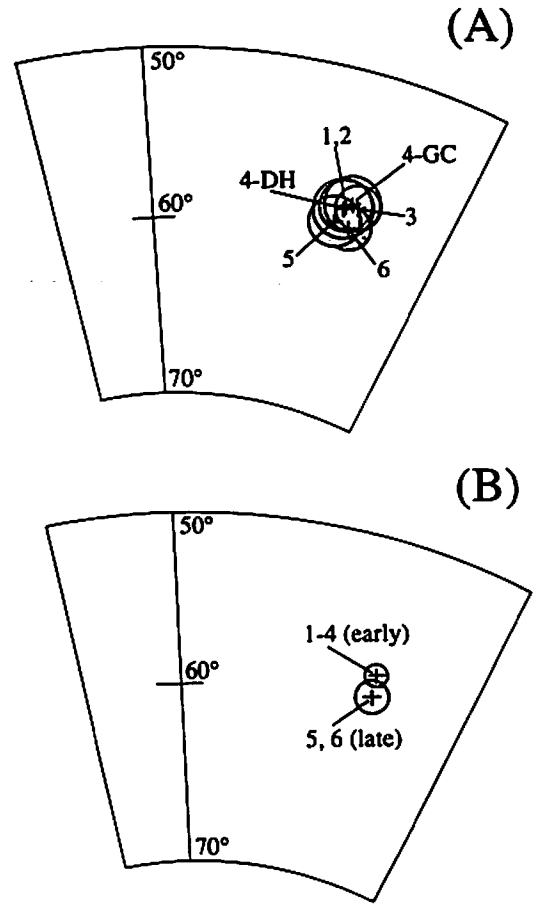

Figure 5. Greatly enlarged part of equal-area diagram showing group mean directions and circles of 95% confidence about them, for Giant Crater lava field. (a) Directions for chemical-stratigraphic groups, as labeled; (b) composite group means (1–4 and 5 and 6) showing their separation of 1.27°. Mean directions in late group are shaded.

movement. While other sites have displacements from group mean directions equivalent to the two discussed above, no mechanisms for distortion were evident upon reexamination in the field, and they were retained.

Identification of Possible Time Gaps

As the geologic and geochemical work on the Giant Crater lavas progressed, the notion of a multistage petrologic process was envisioned [*Baker et al.*, 1991] and the existence of possible time gaps was evaluated because significant time periods may have been required to generate and mix the large volumes of chemically distinct liquids. The mean directions from the different Giant Crater sites were thus grouped according to each assigned chemical group (Table 1 and *Donnelly-Nolan et al.* [1991]). Paleomagnetic sample sites in many cases are in the same outcrops that were sampled for chemical analysis. Chemical groups 1 and 2 were combined into a single paleomagnetic group because of their limited outcrop areas. Chemical group 4 was subdivided into two paleomagnetic groups because two major vents produced separate lava flows of different average chemical composition, with the lava from the Giant Crater vent always overlying that from Double Hole Crater.

Mean directions of the six paleomagnetic groups were

Table 2. Probability of Difference

	Group 1,2	Group 3	Group 4-DH	Group 4-GC	Group 5	Group 6
Group 1,2	X	0.25	0.16	0.09	0.89	0.94
Group 3	X	X	0.26	0.11	0.87	0.85
Group 4-DH	X	X	X	0.28	0.58	0.75
Group 4-GC	X	X	X	X	0.89	0.91
Group 5	X	X	X	X	X	0.58

Probabilities of difference between mean remanent magnetic directions of groups 1 to 6 of the Giant Crater lava field. Decimal probability values given such that zero (0.00) indicates impossibility and unity (1.00) represents certainty. A jump in probability values suggests a time gap between groups 4-GC and 5. Group 4-GC is group 4 lava from Giant Crater; group 4-DH is group 4 lava from Double Hole Crater. Cross is used in place of trivial or redundant comparisons.

calculated and are shown in Table 1 and Figure 5. The group dispersions are very small, with Fisherian best estimate precision parameters ranging from 1526 to 4289; 95% confidence limits on the mean directions are also small, ranging from 1.2° to 1.6°.

The mean directions for group 1–4 lavas are very similar to each other, and those for group 5 are similar to group 6. A shift to steeper inclination value seems to occur between the group means for group 4 and group 5. To statistically evaluate this small shift, a series of comparisons between group mean directions and their associated statistics was performed using the algorithm suggested by *McFadden and Lowes* [1981] (Table 2). This analysis confirms a clear step in the probability that the mean directions of group 4 lavas from Giant Crater and group 5 lavas have a 90% probability of being different. No comparable probability of direction difference between groups of ascending age was found. There is a 58% probability of difference between group 5 and group 6, and this may also represent a real time difference. No gradation exists between these two chemically distinct groups, and this fact may also support the existence of a second time gap. An alternative is that the chemical distinction between the two groups simply represents an interface that existed in the magma reservoir. The time gap, however, could not have been very lengthy because the 23-km-long lava tube that was built by group 4 lavas from Giant Crater also carried the group 5 and 6 lavas. Much of that tube system shows extensive collapse today and observation of historic Hawaiian eruptions demonstrates that breakdown of near-surface tubes can begin within days or weeks [*Hatheway*, 1971]. The Giant Crater tube system, however, does contain several levels so that the deepest level could have remained intact for years and still have been available to transport the group 5 and 6 lavas after a lull in the eruption.

On the basis of the statistical jump in Table 2 between probabilities of difference for group 4 Giant Crater and group 5 lavas, new mean directions were calculated from the original site means for groups 1 to 4 (early, N = 25) and groups 5 and 6 (late, N = 14). The early group has a mean direction of 57.9° inclination and 19.6° declination (α_{95} = 0.6°, k = 2341), and the late group has a mean direction of 59.2° inclination and 19.8° declination (α_{95} = 0.9°, k = 1943) (Figure 5). The angular distance between the early and late groups is 1.27°. Comparison of the site mean directions of the early and late groups, using the algorithm of *McFadden and Lowes* [1981], shows them to be distinct at the 98.6% confidence level.

Calculation of new mean directions for the early and late lavas using the chemical group mean directions, rather than the site mean directions, has the complementary effect of removing the dispersions associated with site selection but unfortunately leads to an interpretative impasse. The mean direction calculated from the early group mean directions has a 57.9° inclination and 19.7° declination (N = 4, α_{95} = 0.4°, k = 60,495), and from the late group mean directions has a 59.2° inclination and 19.4° declination (N = 2, α_{95} = 1.8°, k = 18,437). The angular distance between early and late mean directions is still 1.28°. Because the α_{95} of 1.8° for the late lavas is larger than 1.28°, we cannot distinguish statistically between the early and late mean directions at the 95% confidence level. However, if we apply the *McFadden and Lowes* [1981] algorithm, which uses N, R, and kappa and not α_{95}, we derive an increase in differencing confidence. Our certainty of difference was 98.6% at the site averaging level and improves to 99.0% at the group level. The contradiction lies in the small N values for averaging at the group level, particularly the N = 2 average, and the fact that α_{95} and kappa are estimates of precision that are understood to behave irregularly at values of $N \leq 3$. Because of the confidence discrepancy, we conclude that the early and late group statistics produced at the site level are more robust than those generated at the chemical group level. The statistical data suggest that a time gap in the eruptive sequence may be real, and it may correspond to a petrologic shift from the eruption of dominantly mixed magmas to dominantly fractionated magmas [*Baker et al.*, 1991].

Owing to the small shift in direction between the early and late groups, the question arises as to whether susceptibility anisotropy might explain the directional difference. For anisotropy to be an aliasing influence it has to fulfill three conditions: (1) the percentage of anisotropy should be significant (~10%), (2) the fabric for all samples from a given site must be consistent, or the anisotropy would produce more dispersion, not a biasing of the site, and (3) the K_{max} axes in the early lavas need to be subhorizontal, or the K_{min} axes in the late lavas need to be subvertical, or both. We performed susceptibility anisotropy measurements on both early and late lavas, and we conclude from our data that none of these conditions are met; susceptibility anisotropy cannot explain the 1.27° directional difference.

Having now separated the Giant Crater lavas into two groups based on chemistry, stratigraphy, and identification of a small time gap, we can analyze the statistical possibility that the early and late Giant Crater lavas arise from significantly independent eruptive episodes. *Bogue and Coe* [1981] established an algorithm to calculate the percentage possibility of random secular variation producing flows of like remanent direction, assuming only a kappa due to dispersion by secular variation. A value of 30 for kappa was taken as a general descriptor of secular variation; the Bogue and Coe statistic is not particularly sensitive to the choice in the range of 20–40 for kappa. We derive only a 5 part in 1000 chance that the Giant Crater early and late groups could be so similar in remanent direction and yet be independent in time. This agrees with the geologic, stratigraphic, and ^{14}C analysis already presented by *Donnelly-Nolan et al.* [1990] which

Table 3. Rates of Secular Variation per Decade

Site	Year	Latitude	Longitude	Angle From Axial Dipole	Degrees per Decade
1	1990	40.5°N	143.5°W	8.8°	0.23 ± 0.08
	(1945	39°N	145.5°W	9.6°	0.22 ± 0.09)
2	1990	36°S	172°W	11.2°	0.30 ± 0.07
3	1990	67°S	67°W	19.9°	0.24 ± 0.22
4	1990	46.5°S	18°W	10.8°	1.36 ± 0.15
5	1990	20.5°S	2°E	25.8°	1.83 ± 0.22
6	1990	25.5°S	44°E	19.8°	0.60 ± 0.18
7	1990	24.5°S	80.5°E	20.9°	0.33 ± 0.15
8	1990	36.5°N	50°W	10.9°	1.35 ± 0.16
A	(1945	28°N	49.5°W	16.3°	1.68 ± 0.13)
B	(1945	36.5°N	28.5°W	10.9°	1.33 ± 0.15)

Locations and data for sites having directions of magnetization, in the 1990 geomagnetic field, nearly identical to that of the late direction (mean of groups 5 and 6; ~10,600 years B.P.) from the Giant Crater field. Latitude and longitude of the site are to the nearest 0.5°; angle from axial dipole gives the angular distance between the direction of magnetization presently at each site, and the expected axially geocentric dipole direction expected for that location; and degrees per decade is the rate of geomagnetic secular variation in degrees per decade for each site during the time period 1945–1992.

argues strongly for an eruptive episode at about 10,600 years B.P.

Estimated Duration of the Giant Crater Eruptive Events

The recent history of geomagnetic secular variation has been used to estimate the time duration indicated by the difference in mean direction of the early Giant Crater lavas (groups 1–4) and the late lavas (groups 5 and 6). We assume that the present magnetic field of Earth is similar in character and behavior to that which existed 10,600 years ago. Observatory records, some longer than a century, document that the magnetic field vector at a given location changes constantly. However, the rates of motion of the field vector vary greatly at different locations [*Vestine et al.*, 1959]. Any time interval estimated from these varying motions will also increase or decrease; the faster the rate, the shorter the estimated time interval for a given angular distance. Thus the choice of location to compare present secular variation with our shift in the Giant Crater mean direction is crucial.

Records at nearly 500 magnetic observatories were checked for comparison to Giant Crater directions, but none closely matched the shift in directions. Therefore a spherical harmonic model of the geomagnetic field was used for comparison. The algorithm GEOMAG [*Peddie*, 1987] provides secular variation information for any global location. The program computes the basic geomagnetic field elements for any location on the globe for the years 1945–1992, based in large part on the records from geomagnetic observatories. When the calculated directions from the model are compared to a typical observatory record, differences that average only 0.5° are found. The secular variation rates also compare very closely.

GEOMAG was used to find locations on Earth where the 1990 geomagnetic field is closely similar to the mean direction of groups 5 and 6. Assuming north-south and east-west hemispherical geomagnetic symmetry, negative declinations and inclinations were also accepted for comparison. Eight locations were found that matched well. The search to define these locations was refined to the 0.5° level in latitude/longitude position. Residual angular differences between the group 5 and 6 direction and the declination/inclination pairs found using GEOMAG were very small (0.01–0.12°), for all except station 1. At station 1 the mean direction of group 5 and 6 does not literally exist because the 19.8° declination line approaches but does not cross the 59.2° inclination line in the 1990 geomagnetic field. Though this left a larger angular residual of 1.24°, we elected to retain station 1 for the modeling. Once the eight stations were identified, their annual declination/inclination data pairs were calculated for each year of the 48-year interval available from the program. Then the angular distance the geomagnetic field moved was calculated for the 38 running decade time intervals at each station. The mean angular decade rates of motion and their standard deviations for the eight stations are presented in Table 3. Two stations in the 1945 field were calculated forward in time, in the same manner (Table 3) and no significant difference in secular variation rate was found.

The rate of angular change for each of the eight stations ranges from a low of 0.23° ± 0.08° to a high of 1.83° ± 0.22° per decade. However, several of the stations are dissimilar to the Giant Crater site in important ways. The Giant Crater group 5 and 6 direction is 10.0° from the expected axial dipole direction (I = 60.5°, D = 0.0°) calculated for the mean Giant Crater site location. The inclination values of any of the chemical-stratigraphic groups are similar to the axial dipole value. Thus the deflection of the Giant Crater directions from the average axial dipole direction occurs in declination rather than inclination. Looking at Table 3, it is possible to eliminate stations 3, 5, 6, and 7 from comparison because they are characterized by large angular deflections from their typical site axial dipole direction and they are at latitudes for which a 60° inclination is uncommon.

The stations remaining as choices for comparison are all at temperate latitudes (36°S–46.5°N) and have similar angular distances (8.8°–11.2°) from their typical axial dipole direction. This is not surprising, as secular variation produces dispersions that vary latitudinally [*McElhinny and Merrill*, 1975], and this pattern of dispersions should also be reflected in secular variation rate. Therefore secular variation stations good for comparison with Giant Crater directions should be located at similar latitudes.

Secular variation is thought to result principally from the westward drift of the nondipole part of the geomagnetic field. The nondipole field is not uniformly distributed over Earth but is clumped into discrete foci. These foci wax and wane in intensity while they move, also contributing to secular variation. The nondipole field can be characterized as being three or four principal foci of positive or negative vertical magnetic flux (positive downward), with accompanying horizontal flux directed outward from negative vertical flux foci and inward toward positive vertical flux foci. *Cox* [1975] noted that the distribution of vertical flux in the nondipole field was nonuniform, with equatorial latitudes having an excess of negative vertical (upward) directed flux and temperate latitudes having an excess of positive vertical flux. He also conceptually combined westward drift of the nondipole field, the horizontal and vertical character of the nondipole foci, and the present bias in the latitudinal distribution of the nondipole foci to explain the common clockwise looping character of secular variation in volcanic and sedimentary rocks.

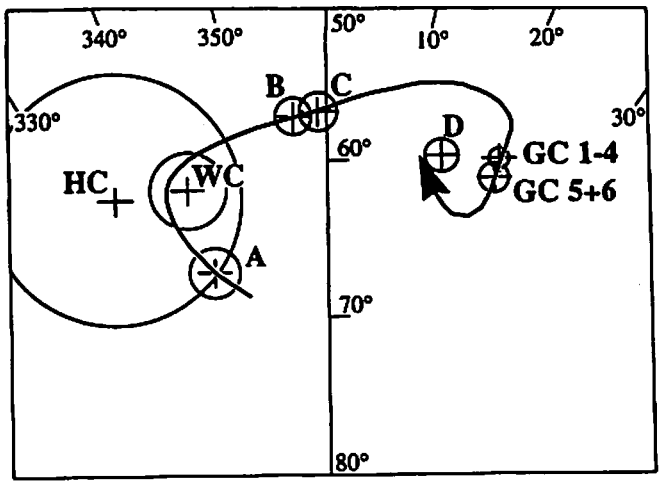

Figure 6. Enlarged part of equal-area diagram of paleomagnetic directions and circles of 95% confidence used to reconstruct the path of secular variation for the Pacific Northwest between about 11,000 and 10,000 years B.P. GC 1–4, GC 5+6, HC, and WC are directions presented in this paper for the Giant Crater, Horse Caves, and Water Caves lava flows. Directions A (Bottleneck Lake flows; minimum age of 11,000 ± 100 years B.P.), B (Heifer Reservoir flows; minimum age of 10,670 ± 150 years B.P.), C (Shoshone Ice Caves field; minimum age of 10,130 ± 350 years B.P.), and D (Pronghorn Reservoir flows; minimum age of 10,240 ± 120 years B.P.) are data from *Kuntz et al.* [1986a, b] and *Champion* [1980]. Solid arrow is forward path of secular variation through ~10,500 years B.P. episode of basaltic volcanism at the Medicine Lake Highlands [*Donnelly-Nolan et al.*, 1990].

By combining the directions of magnetization derived in this study with those presented previously [*Kuntz et al.*, 1986a, b; *Champion*, 1980], a path of secular variation defining a clockwise directional loop possibly caused by drift of the nondipole field is indicated (Figure 6). Therefore it is possible to understand the essential nature of secular variation during the Giant Crater eruptions. A clockwise loop from somewhat shallower inclinations preceded the eruptions there, although overall the loop can be viewed as one to steeper inclination values than usual. Whether the loop was to steeper or to shallower inclinations is unimportant, the sense of secular variation between the early (groups 1–4) and late (groups 5 and 6) Giant Crater lavas is of inclination steepening at constant declination. However, the records from stations 1 and 2 (Table 3) document declination variation rather than inclination variation. On this basis we eliminate stations 1 and 2 from further comparison.

Using the model described above, the 1.27° shift is in the last part of a loop initially toward shallow inclinations, caused by an equatorial focus of upward directed flux. The shift arose during the time period after the focus passed, the inclination returned to normal, and before the declination had returned to near zero values. The secular variation from GEOMAG model station 4 documents the early stages of the passage of an upward directed focus of magnetic flux, showing an inclination shift after 20° of westward declination have been obtained, and that from model station 8 shows similarly the shallowing in inclination values after 21° of westerly declination have arisen. Even though both these model stations record the beginnings rather than the end of a loop to shallow inclinations, we argue based on symmetry that their rates of secular variation are most analogous to the Giant Crater directional shift.

The rates of secular variation per decade are nearly identical for the remaining model stations 4 and 8, those that we identify as the closest analogues in behavior to the Giant Crater site. Their rates are 1.36° ± 0.15° and 1.35° ± 0.16°/decade, respectively. Using the 1.35°/decade rate and its associated standard deviation error limit, we determine a 9.4 (+1.3/−1.0) year time interval for the time interval between the group 1–4 and the group 5 and 6 directions. If we are incorrect in specifically matching the ancient and present field's secular variation by choosing stations 4 and 8, then the average rate of secular variation for all eight stations (0.78°/decade) would be a more generally applicable figure. This translates into a 16.3-year gap between early and late eruptions, and still close to our 9.4-year preferred estimate.

The 1.27° difference between the early and late directions was calculated ignoring the error limits on those directions. The root mean square error derived from the 0.6° and 0.9° α_{95} of the early and late directions is 1.08°, which is reduced by the *Demarest* [1983] factor (0.78) to 0.84°. Using this error measure, the angular difference between the early and late directions could be as little as 0.43° or as much as 2.11° at the 95% confidence level. Combining the rate of 1.35°/decade, the calculated 95% time intervals are 3.2 and 15.6 years, respectively, so we characterize the duration indicated by the difference between groups 1–4 and groups 5 and 6 as about 10 ± 5 years.

The duration of all the Giant Crater eruptions is difficult to estimate, because of the absence of secular variation during the emplacement of groups 1–4 and because of such a small angular difference between groups 5 and 6. These minimal directional variations suggest very high effusion rates. Because we do not find evidence of directional variation within groups 1–4 or between groups 5 and 6, we know those eruptions cannot have taken as much as 10 years, the duration of the identifiable gap between them. Therefore we can limit the duration of all the Giant Crater eruptions to <30 years and infer that the true figure is close to the time estimate of the duration of the time gap between them, 10 ± 5 years.

We cannot constrain the total time frame during which the Giant Crater chemical variation was created. On the basis of the model of *Baker et al.* [1991] we conclude that our studies constrain timing of the generation and eruption of the Group 5 and Group 6 lavas, which represent half the erupted volume and manifest about a third of the chemical variation. The *Baker et al.* [1991, p. 21,840] model states that

> after the group 1–4 eruption, another batch of primitive group 6 entered the magma chamber. The primitive group 6 mixed with underlying ferrobasalt and the unerupted remnants of the last mixing event (group 4), and the magma of group 5 was formed. Continued input of group 6 below the mixed group 5 inflated the magma chamber to a critical value and triggered the eruption of groups 5 and 6 (~2.3 km^3), equal in volume to the group 1–4 eruption.

Group 6 primitive lava [*Baker et al.*, 1991, Figure 12e] also mixed with group 3 and ferrobasalt and formed the large volume of group 4 lavas (1.3 km^3). If we postulate that the intrusion of group 6 magma also triggered the beginning of the eruption of group 1, 2 and group 3 of the early eruption

10

episode before erupting the newly mixed group 4 lavas, then our study may time the generation of 3/4 of the volume of erupted lavas, which includes half the total chemical variation. This time frame spans the generation of all tholeiitic lavas in this magmatic system. While this last assumption is logical and parsimonious (fewest number of intrusion episodes), our data cannot prove it.

Conclusions

Lava flows are excellent recorders of the direction of the magnetic field that existed at the time they erupted. Sampled carefully, they can provide very precise mean directions of magnetization. Statistical analysis of multiple paleomagnetic samples of geologically defined units can give information about possible time durations of longer-lived eruptions. Secular variation can be measured accurately enough in undisturbed lavas that paleo-time spans of eruption can be estimated. In the case of the Giant Crater lava field, we have shown that 4.4 km^3 of compositionally zoned magma was erupted in a very brief span of time. A small angular shift recorded in the site mean directions from the lava field indicates a total duration of <30 years. One possible time gap of 10 ± 5 years, between group 4 and 5 lavas is suggested by the data. We consider the Giant Crater lava field to represent a single eruptive event analogous to long-lived Hawaiian eruptions.

Acknowledgments. We gratefully acknowledge the field support of P. Bruggman, K. Champion, J. Ferrari, J. Hamilton, D. McElman, and D. Parks. Reviews by Ed Mankinen, Jon Hagstrum, Monte Marshall, Myrl Beck, and four anonymous reviewers improved and focused the discussion.

References

Baker, M. B., T. L. Grove, R. J. Kinzler, J. M. Donnelly-Nolan, and G. A. Wandless, Origin of the compositional zonation (high-alumina basalt to basaltic andesite) in the Giant Crater lava field, Medicine Lake volcano, northern California, *J. Geophys. Res.*, *96*, 21,819–21,842, 1991.

Bogue, S. W., and R. S. Coe, Paleomagnetic correlation of Columbia River basalt flows using secular variation, *J. Geophys. Res.*, *86*, 11,883–11,897, 1981.

Champion, D. E., Holocene geomagnetic secular variation in the western United States: Implications for the global geomagnetic field, *U.S. Geol. Surv. Open File Rep.*, *80-824*, 326 pp., 1980.

Champion, D. E., and E. M. Shoemaker, Paleomagnetic evidence for episodic volcanism on the Snake River Plain, in Planetary Geology Field Conference on the Snake River Plain, Idaho, Oct. 1977, *NASA Tech. Memo.*, *TM-78436*, 7–8, 1977.

Cox, A., The frequency of geomagnetic reversals and the symmetry of the nondipole field, *Rev. Geophys.*, *13*, 35–51, 1975.

Demarest, H. H., Error analysis for the determination of tectonic rotation from paleomagnetic data, *J. Geophys. Res.*, *88*, 4321–4328, 1983.

Donnelly-Nolan, J. M., D. E. Champion, C. D. Miller, T. L. Grove, and D. A. Trimble, Post-11,000-year volcanism at Medicine Lake volcano, Cascade Range, northern California, *J. Geophys. Res.*, *95*, 19,693–19,704, 1990.

Donnelly-Nolan, J. M., D. E. Champion, T. L. Grove, M. B. Baker, J. E. Taggart Jr., and P. E. Bruggman, The Giant Crater lava field: Geology and geochemistry of a compositionally zoned high-alumina basalt to basaltic andesite eruption at Medicine Lake volcano, California, *J. Geophys. Res.*, *96*, 21,843–21,863, 1991.

Hatheway, A. W., Lava tubes and collapse depressions, Ph.D. thesis, Univ. of Ariz., Tucson, 1971.

Heliker, C., and T. L. Wright, The Pu'u O'o–Kupaianaha eruption of Kilauea, *Eos Trans. AGU*, *72*, 521–526, 1991.

Kuntz, M. A., D. E. Champion, E. C. Spiker, and R. H. Lefebvre, Contrasting magma types and steady-state, volume-predictable, basaltic volcanism along the Great Rift, Idaho, *Geol. Soc. Am. Bull.*, *97*, 579–594, 1986a.

Kuntz, M. A., E. C. Spiker, M. Rubin, D. E. Champion, and R. H. Lefebvre, Radiocarbon studies of latest Pleistocene and Holocene lava flows of the Snake River Plain, Idaho: Data, lessons, interpretations, *Quat. Res.*, *25*, 163–176, 1986b.

McFadden, P. L., and F. J. Lowes, The discrimination of mean directions drawn from Fisher distributions, *Geophys. J. R. Astron. Soc.*, *67*, 19–33, 1981.

McElhinny, M. W., and R. T. Merrill, Geomagnetic secular variation over the past 5 m.y., *Rev. Geophys.*, *13*, 687–708, 1975.

Peddie, N. W., GEOMAG: A geomagnetic field program, *Eos Trans. AGU*, *68*, 530, 1987.

Thordarson, T., and S. Self, The Laki (Skaftar Fires) and Grimsvotn eruptions in 1783–1785, *Bull. Volcanol.*, *55*, 233–263, 1993.

Vestine, E. H., L. Laporte, C. Cooper, I. Lange, and W. C. Hendrix, Description of the Earth's main magnetic field and its secular change, 1905–1945, *Carnegie Inst. Washington Publ.*, *578*, 532 pp., 1959.

Wolfe, E. W., M. O. Garcia, D. B. Jackson, R. Y. Koyanagi, C. A. Neal, and A. T. Okimura, The Puu Oo eruption of Kilauea volcano, episodes 1–20, January 3, 1983 to June 8, 1984, in Volcanism in Hawaii, edited by R. W. Decker, T. L. Wright, and P. H. Stauffer, *U.S. Geol. Surv. Prof. Pap.*, *1350*, 471–508, 1987.

D. E. Champion and J. M. Donnelly-Nolan, U.S. Geological Survey, MS 937, 345 Middlefield Road, Menlo Park, CA, 94025. (e-mail: jdnolan@mojave.wr.usgs.gov).

(Received June 7, 1993; revised March 22, 1994; accepted March 31, 1994.)

JOURNAL OF GEOPHYSICAL RESEARCH, VOL. 96, NO. B13, PAGES 21,843–21,863, DECEMBER 10, 1991

The Giant Crater Lava Field: Geology and Geochemistry of a Compositionally Zoned, High-Alumina Basalt to Basaltic Andesite Eruption at Medicine Lake Volcano, California

JULIE M. DONNELLY-NOLAN,[1] DUANE E. CHAMPION,[1] TIMOTHY L. GROVE,[2] MICHAEL B. BAKER,[3] JOSEPH E. TAGGART, JR.,[4] AND PEGGY E. BRUGGMAN[1]

The Giant Crater lava field consists of >4 km^3 of basaltic lava, compositionally zoned from first-erupted calc-alkaline basaltic andesite to last-erupted primitive high-alumina basalt. On the FeO*/MgO (where FeO* is total Fe calculated as FeO) versus SiO_2 discrimination diagram commonly used to distinguish tholeiitic from calc-alkaline series lavas the compositionally zoned eruption crosses from the tholeiitic field to the calc-alkaline field. The lavas erupted in a brief span of time about 10,500 years ago from several closely spaced vents on the south flank of Medicine Lake volcano in the southern Cascade Range. Six chemical-stratigraphic groups were mapped. Lower K_2O, higher MgO groups always overlie higher K_2O, lower MgO groups. Group 6 lavas erupted last and are aphyric, have high contents of MgO and Ni, and contain as little as 0.07% K_2O. Group 1 lavas are porphyritic and have as much as 1.10% K_2O. Major element contents of primitive group 6 Giant Crater basalt are very similar to a subset of primitive mid-ocean ridge basalts (MORB). Group 6 lava is more depleted in middle and heavy rare earth elements (REE) and Y than is primitive MORB, but it is enriched in large ion lithophile elements (LILE). These LILE enrichments may be a result of fluid from the subducting slab interacting with the mantle beneath Medicine Lake volcano. The group 6 REE pattern is parallel to the pattern of normal-type MORB, indicating a similar although perhaps more depleted mantle source. The location of Medicine Lake volcano in an extensional environment behind the volcanic front facilitates the rise of mantle-derived melts. Modification of the primitive group 6 basalt to more evolved compositions takes place in the upper crust by processes involving fractional crystallization and assimilation. The group 1 calc-alkaline Giant Crater basaltic andesite produced by these processes is similar to other Cascade basaltic andesites, implying that a similar high-alumina basalt may be parental.

INTRODUCTION

The Giant Crater lava field formed by eruptions from several closely spaced vents on the south flank of Medicine Lake volcano (Figure 1) about 10,500 years ago. The eruption began with calc-alkaline basaltic andesite and ended with primitive high-alumina basalt. In this paper we use the term "high-alumina basalt" as used by *Tilley* [1950] to mean aphyric high-MgO basalt with a high content of alumina.

The Giant Crater eruption took place over a brief span of time amounting to as much as a decade (D. E. Champion and J. M. Donnelly-Nolan, A paleomagnetic study of the Giant Crater lava field, submitted to *Journal of Geophysical Research*, 1991; hereinafter referred to as Champion and Donnelly-Nolan, submitted manuscript, 1991) and produced 4.4 km^3 of lava. The lava flows are described and characterized here on the basis of geologic mapping and stratigraphy along with major and trace element chemical compositions. Six chemical-stratigraphic groups have been recognized and mapped (Figure 2). Estimates of the original extent of now-buried flows have been made, and areas and volumes have been calculated. These data are used in a companion paper [*Baker et al.*, this issue] to constrain petrologic models developed to explain the chemical variation.

Medicine Lake volcano is located in the southern part of the Cascade volcanic arc, in an extensional environment behind the volcanic front, about 50 km ENE of Mount Shasta. Primitive high-alumina basalts have erupted throughout the lifespan of this large Quaternary shield volcano [*Donnelly-Nolan*, 1988], although only a few of these older flows may be as primitive as the most primitive samples from the Giant Crater lava field. In this paper the term primitive is used to describe samples with high compatible element contents (e.g., MgO, Ni, and Cr). The most primitive Giant Crater samples are also thought to be primary magmas and thus unmodified since separation from their source residue after being generated as liquids by partial melting in the mantle.

Anderson [1941] mentioned the Giant Crater lavas briefly in his classic study of Medicine Lake Highland. *Greeley and Baer* [1971] reported on the lava tubes in the Giant Crater unit, one of which is 23 km long. *Baer* [1973] included mapping and descriptions of the northern half of the lava field and its lava tubes. He listed one chemical analysis, as did *Mertzman* [1979]. Studies of compositionally zoned basalt flows are relatively uncommon. Some examples include the currently active Puu Oo eruption in Hawaii that began in January 1983 and displayed chemical variability in its early phases [*Wolfe et al.*, 1987], the Saudi Arabian Madinah eruption of 0.5 km^3 of alkali-olivine basalt that shows little variability in silica content but considerable variation in MgO, K_2O, and P_2O_5 [*Camp et al.*, 1987], and the Strawberry Crater flow in the San Francisco volcanic field, Arizona [*Bloomfield and Arculus*, 1989]. Two addi-

[1]U.S. Geological Survey, Menlo Park, California.
[2]Department of Earth, Atmospheric, and Planetary Sciences, Massachusetts Institute of Technology, Cambridge.
[3]Department of Geological and Planetary Sciences, California Institute of Technology, Pasadena.
[4]U.S. Geological Survey, Lakewood, Colorado.

Paper number 91JB01901.
0148-0227/91/91JB-01901$05.00

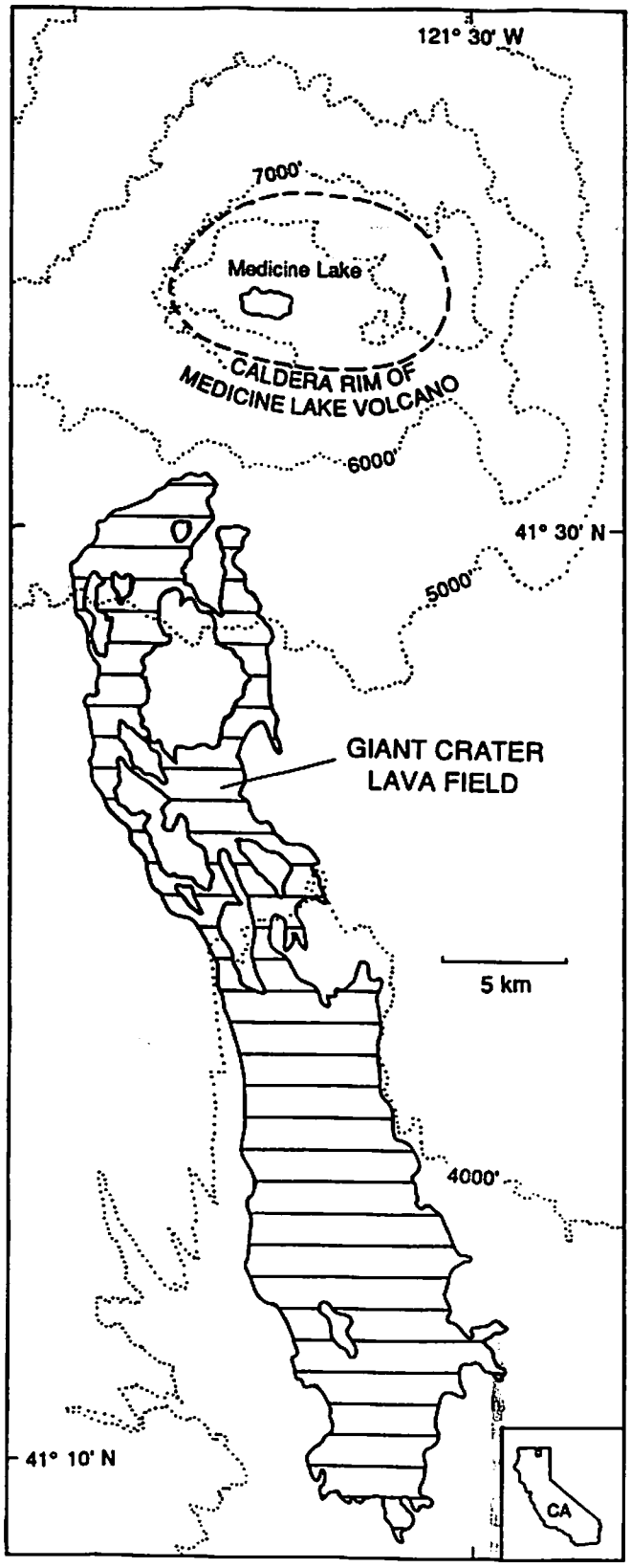

Fig. 1. Location map showing area covered by Giant Crater lava field on south flank of Medicine Lake volcano, northern California. Dotted lines are elevation contours at intervals of ~305 m (1000 feet).

tional compositionally zoned basalt to andesite flows at Medicine Lake volcano are the Mammoth Crater and Callahan units [*Donnelly-Nolan and Champion*, 1987; *Kinzler et al.*, 1989].

THE GIANT CRATER LAVA FIELD AND RELATED UNITS

The Giant Crater lavas were known from *Baer*'s [1973] descriptions and from examination in the field to be petrographically variable. Major element analyses demonstrated the chemical variability of the lavas. In all cases, lower K_2O lava overlies higher K_2O lava even with a group. Six chemical groups were recognized, each stratigraphically distinct. The distribution of the six groups is shown on Figures 2 and 3. Group 1 lavas are the most porphyritic with about 5% of phenocrysts of plagioclase and olivine and an occasional 1–3 mm quartz grain. Plagioclase crystals are as long as 6 cm. Group 2 and 3 lavas contain decreasing amounts of phenocrysts and the plagioclase megacrysts are typically smaller, usually 1–2 cm across in group 3 lavas. The distinctions between groups 1 and 2 and between groups 2 and 3 are difficult to make in the field. Group 4 lavas, however, are distinctive. They are typically massive and aphyric with rare plagioclase megacrysts to 1 cm across. Group 5 lavas are aphyric but diktytaxitic and can be distinguished fairly readily from group 4 lavas but not from group 6. All groups include both aa and pahoehoe lavas.

During the course of mapping, older and younger eruptions closely related in space and time to the Giant Crater lava field were recognized. These include the older basaltic eruptions from vents at Horse Caves and Water Caves, several older spatter vents partly buried within the Double Hole Crater flow, and a younger basalt flow erupted at "vent 5".

Area and Volume Estimates

Areas of groups 1–6 and basalts of Horse Caves-Water Caves and vent 5 are shown in Table 1. Small areas were measured and totaled using a digitizing tablet and commercially available computer software, allowing for variable thickness estimates of different parts of the flows when calculating the volumes. Estimated thicknesses range from 5 to 30 m. Geologic evidence indicates that the southern 25 km of the lava field is confined within a graben, with the floor of the graben tilted down to the east. Thickness estimates were adjusted accordingly. No thickness greater than 30 m was used in the calculations although the eastern part of the graben and some near-vent locations and parts of the tube system may locally have thicknesses of 40 m or more.

Very few data exist for actual flow thicknesses. At the site of sample 1464M a skylight in the major lava tube from Giant Crater indicates that the bottom of the tube is at least 30 m below the surface. Near the eastern edge of the lava field at the location of sample 1465M (Figure 2*b*), a fault scarp exposes 15 m of group 6 lava. Massive interior lava is present at the base of the exposure with no hint that the bottom of the flow is close. The total thickness of Giant Crater lava here may be much greater than 15 m if group 5 lava is also present. Sample 1466M was collected from a small quarry in group 5 lava. Even though the quarry is located at the edge of the flow, the thickness there is at least

10 m. In general, near-vent accumulations and some sections of major lava tubes were estimated to be 30 m thick. Most areas near lava tubes plus ponded areas and flow lobes of higher silica contents (groups 1–3) were estimated to average 20 m thick. Major flow lobes of group 4–6 lava were given thicknesses of 15 m, while areas near flow edges were generally given thicknesses of 10 m, or in some instances 5 m where many patches of underlying units are seen.

Maps used to create the estimates of inferred area in Table 1 are presented in Figure 3. The maps show the sequence and distribution of successive flows. The locations of flow lobes in the northern 20 km of the Giant Crater lava field are controlled by preexisting topography and the general southerly slope of the south flank of Medicine Lake volcano. The major lava tube from Giant Crater was clearly a principal controlling feature in the distribution of group 4, 5, and 6 lavas. The present-day outline of the Giant Crater lava field is shown for reference on each of the maps of Figure 3. All of the units postdate the last glaciation, and no streams are present. Thus no noticeable erosion of the flows has occurred other than minor breakdown of the glassy flow rind and collapse of thin pahoehoe surfaces. Some lava tube collapse has occurred, and flow edges are locally mantled by windblown silt, sand, and in places by scattered pumice from more recent eruptions. In places, the lavas are covered by a thick growth of brush or trees, but the flows are generally well preserved and youthful in appearance, commonly with little vegetation cover.

Eruption History of the Giant Crater Lava Field

Group 1. The eruption began at the uppermost edge of the Giant Crater lava field at an elevation of ~1792 m (~5880 feet) where porphyritic group 1 lava erupted at Chimney Crater and the nearby spatter rampart that includes Shastine Crater (Figure 2). The initial eruption was explosive, producing a small volume of mafic tephra that contains plagioclase megacrysts up to several centimeters across, cumulate inclusions, and partially melted silicic inclusions (see *Baker et al.* [this issue] for chemical analyses of inclusions). The explosive activity was followed by extrusion of a viscous dome of basaltic andesite lava with a veneer of agglutinated cinders. Chimney Crater formed in the center of the dome, perhaps by withdrawal of magma and stoping of the walls of the vent. Nearby to the north, the Shastine Crater spatter rampart forms a N5°E trending rampart of small spatter cones whose trend projects south toward Chimney Crater.

Group 2. Group 2 lava erupted from Chimney Crater and formed a lava tube exiting from the west side of the crater. One kilometer farther south on the same N5°E trend, the large spatter cone of Cousin Cone also erupted group 2 lava. The existence of Cousin Cone indicates that the early part of the eruption involved some explosive activity. The group 2 lava flowed about 6.5 km to the SSW via at least two lava tubes. During the eruption of group 1 and group 2 lavas we assume that Giant Crater, Double Hole Crater, and other vents farther to the southwest did not yet exist. If these vents did erupt group 1 and 2 lavas, all evidence of these eruptions has been buried.

Group 3. The farthest distance traveled by group 3 lavas from the vent at Chimney Crater is about 9 km. They cover a large percentage of the area of group 2 lava. The group 3 lavas were transported by at least two lava tubes from the only known vent at Chimney Crater. Their inferred distribution is drawn to exclude Giant Crater as a vent and provide two lobes of group 3 lava such that a SW trending valley lies between them in the area SW of Giant Crater. By so doing, we can explain the location of the major lava tube that exits from Giant Crater and carries group 4, 5, and 6 basalt. The tube may have followed the topographic crease between northern and southern lobes of group 3 lava.

Group 4. Group 4 lavas erupted from Giant Crater, Double Hole Crater, and adjacent vents after Chimney Crater had ceased activity. Giant Crater is located 1.2 km S55°W of Chimney Crater. Another possible vent ("vent 3") is at a bend in the lava tube from Giant Crater, 1 km further SW in the same S55°W direction. The distinction between real vents and lava vented from a blocked lava tube can be difficult, but the location of vent 3 on the N55°E alignment that also includes "vent 4" suggests that it is a vent fed from a dike that tapped the magmatic system at depth and not from the tube. Double Hole Crater lies 2 km S55°E of Giant Crater, and two small, mostly buried spatter vents for Double Hole lavas lie south of Double Hole Crater. Thus both the location and orientation of vents changed between the eruption of group 3 and group 4 lavas. However, paleomagnetic data (D. E. Champion, unpublished data, 1990) indicate that the lavas of groups 1–4 have the same magnetic direction within analytical error for at least six sites within each group, and thus very little time, much less than a decade, passed during the eruption of these first four groups. Group 4 lavas from Double Hole Crater average slightly higher in K_2O content and lower in MgO (Figure 4) and underlie group 4 lavas from Giant Crater. Figure 4 also shows that near-vent and distal Giant Crater group 4 lavas differ in K_2O and MgO content. Near-vent Giant Crater samples are on average more evolved, although less so than lavas from Double Hole Crater. The implied sequence is the opening of Double Hole Crater and its adjacent vents first, followed by eruptions at Giant Crater and construction of the major lava tube that leaves Giant Crater. The tube trends west and then south for at least 23 km. It carried the distal group 4 lavas that lie as far as 41 km south of Giant Crater. This is twice is far as Double Hole group 4 lavas traveled from their vents, although estimated areas and volumes of Giant Crater and Double Hole group 4 lavas are approximately the same.

Group 5. Paleomagnetic data (D. E. Champion, unpublished data, 1900) indicate the possibility of a brief time gap, perhaps as much as a decade, between eruption of group 4 and group 5 lavas. Group 5 lavas were distinguished from petrographically similar group 6 lavas based on TiO_2 content (Figure 5). Their inferred vent is Giant Crater from which they were presumably transported south via the major lava tube that was built by group 4 lavas along the west edge of the Giant Crater lava field. The lava field's most distal lavas are those of group 5, having flowed 45 km from the vent area to the lowest elevation in the Giant Crater lava field, ~1025 m (3360 feet).

Group 6. Group 6 lavas erupted from three vents, but the Giant Crater vent erupted more than 90% of the volume. One subsidiary vent (vent 4) opened 2.8 km SW of Giant Crater on the same N55°E trend as Chimney Crater, Giant Crater, and vent 3. This is the lowest vent that is indisputably part of the Giant Crater system, at ~1615 m (~5300 feet) in elevation. Another smaller vent 1.2 km S30°E from Giant Crater

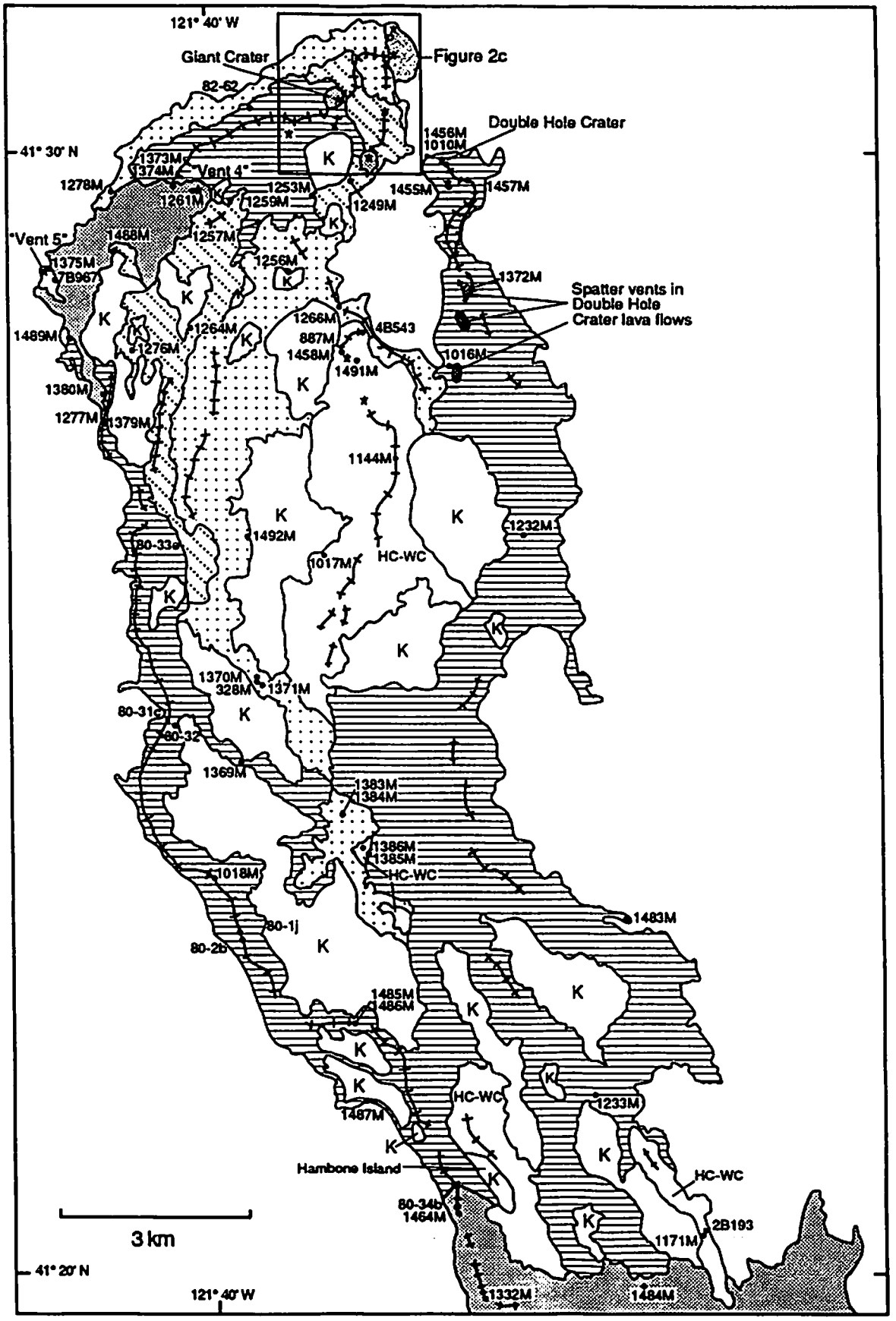

Fig. 2. Geologic map and sample locations, Giant Crater groups 1–6. Related units including the basalt of Horse Caves-Water Caves, spatter vents within Double Hole Crater lava flows, and basalt of vent 5 are also shown. (*a*) Northern half of Giant Crater lava field; (*b*) southern half of lava field; (*c*) (inset) enlarged map of vent area.

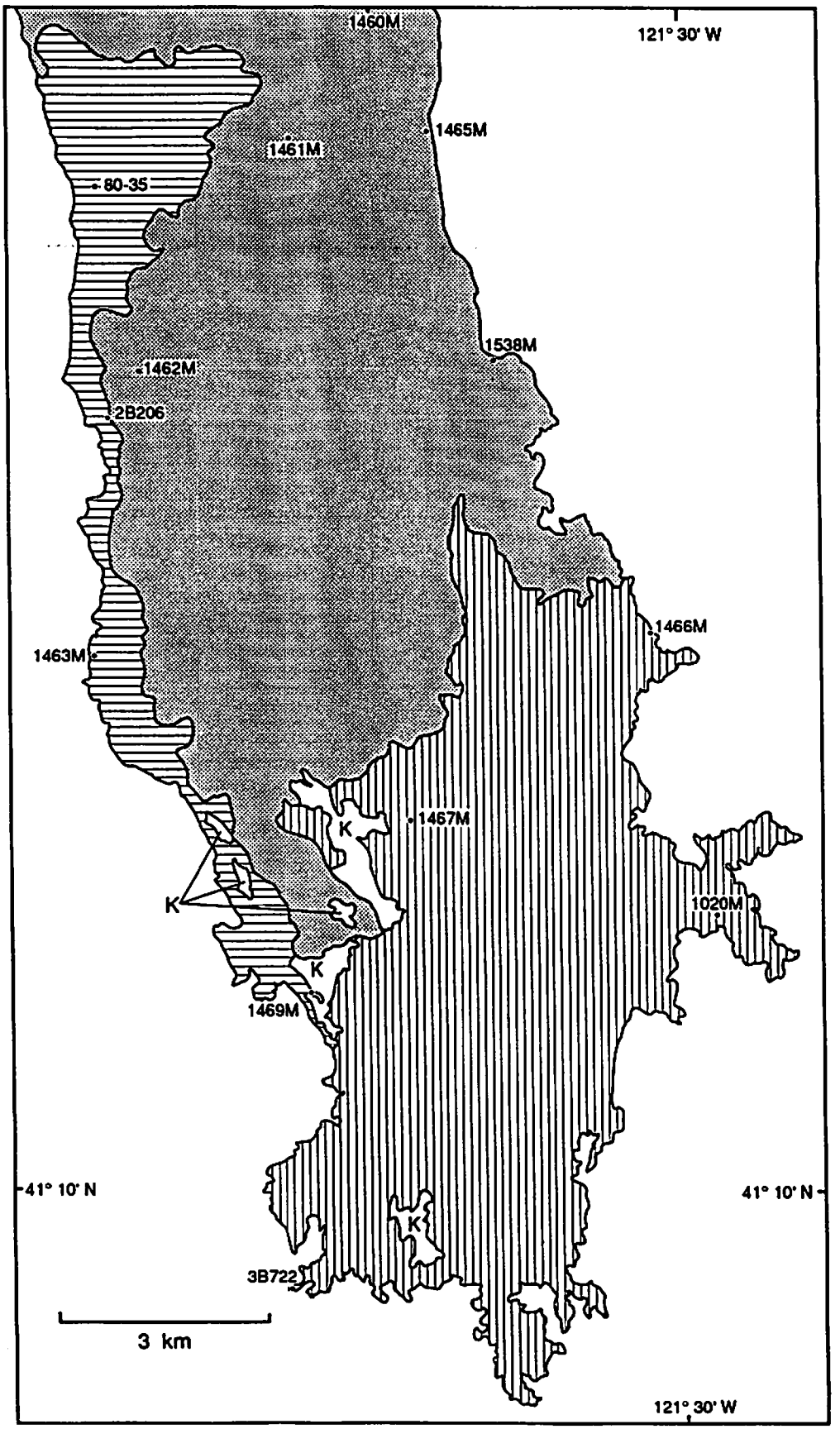

Fig. 2. (continued)

10

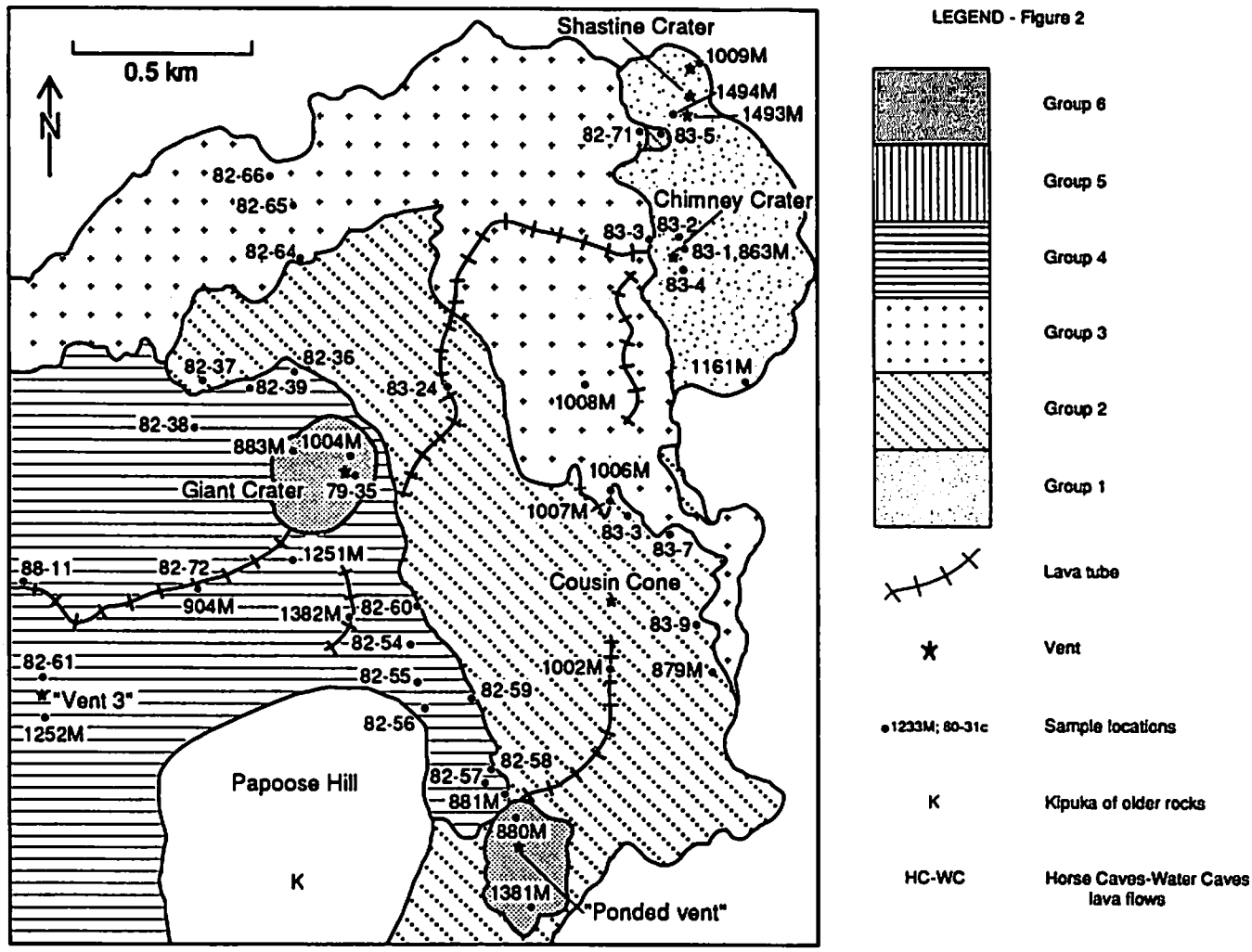

Fig. 2. (continued)

erupted less than 0.001 km^3 of lava. Most of the group 6 lava was transported through the major lava tube that carried the Giant Crater group 4 and 5 lavas.

Basaltic eruptions that preceded the Giant Crater lava field. Several hundred years prior to the Giant Crater eruption, basaltic lava erupted out of vents at Horse Caves and Water Caves. These flows are stratigraphically older but morphologically very similar to Giant Crater flows. They possess paleomagnetic directions that are different from Giant Crater directions, suggesting an interval of several hundred years between these older lavas and Giant Crater eruptions (Champion and Donnelly-Nolan, submitted manuscript, 1991). The Horse Caves-Water Caves lavas are massive and fine grained but petrographically distinctive with a scattering of about 1% of 1-mm olivine phenocrysts. Chemically, these older lavas are compositionally variable and slightly shifted toward higher MgO contents from Giant Crater compositions of similar silica content. None of these lavas is as primitive as Giant Crater group 5 and 6 basalts. Magma remaining in the crust after these eruptions could have been important to the later Giant Crater magmas if it acted as a contaminant or supplied heat of crystallization for melting of crust that became a contaminant.

Several basaltic spatter cones occur partially buried within the group 4 Double Hole lava flows south of Double Hole Crater. Paleomagnetic data (Champion and Donnelly-Nolan, submitted manuscript, 1991) suggest that these eruptions occurred immediately prior to the eruptions that produced Giant Crater groups 1–4. However, the chemical composition of a sample from one spatter cone falls within the group 3 field. The paleomagnetic data have a large analytical error, so it is possible that rather than being precursors, these vents represent sites of eruption of group 3 lavas. If so, the area and volume data for group 3 lavas are underestimates, and Chimney Crater would not be the only vent for this group. The lowest of these potential group 3 spatter vents is at an elevation of ~1539 m (~5050 feet) and would be the lowest vent in the Giant Crater system unless vent 5 is also part of the Giant Crater system (see below).

Basalt of vent 5. This very small basalt flow overlies group 6 lava at the upper west edge of the Giant Crater lava field (Figure 2*a*). The northwest trending rampart of spatter vents lies on the projection of the N55°E vent trend that includes Chimney Crater, Giant Crater, vent 3, and vent 4. This porphyritic basalt is similar in chemical composition and petrographic features to lavas of group 1. Like group 1, it contains melted silicic inclusions and cumulate inclusions. Paleomagnetic and radiocarbon data [*Donnelly-Nolan et al.*, 1990] indicate that the basalt of vent 5 immediately postdates the Giant Crater eruptions. Whether this late porphyritic

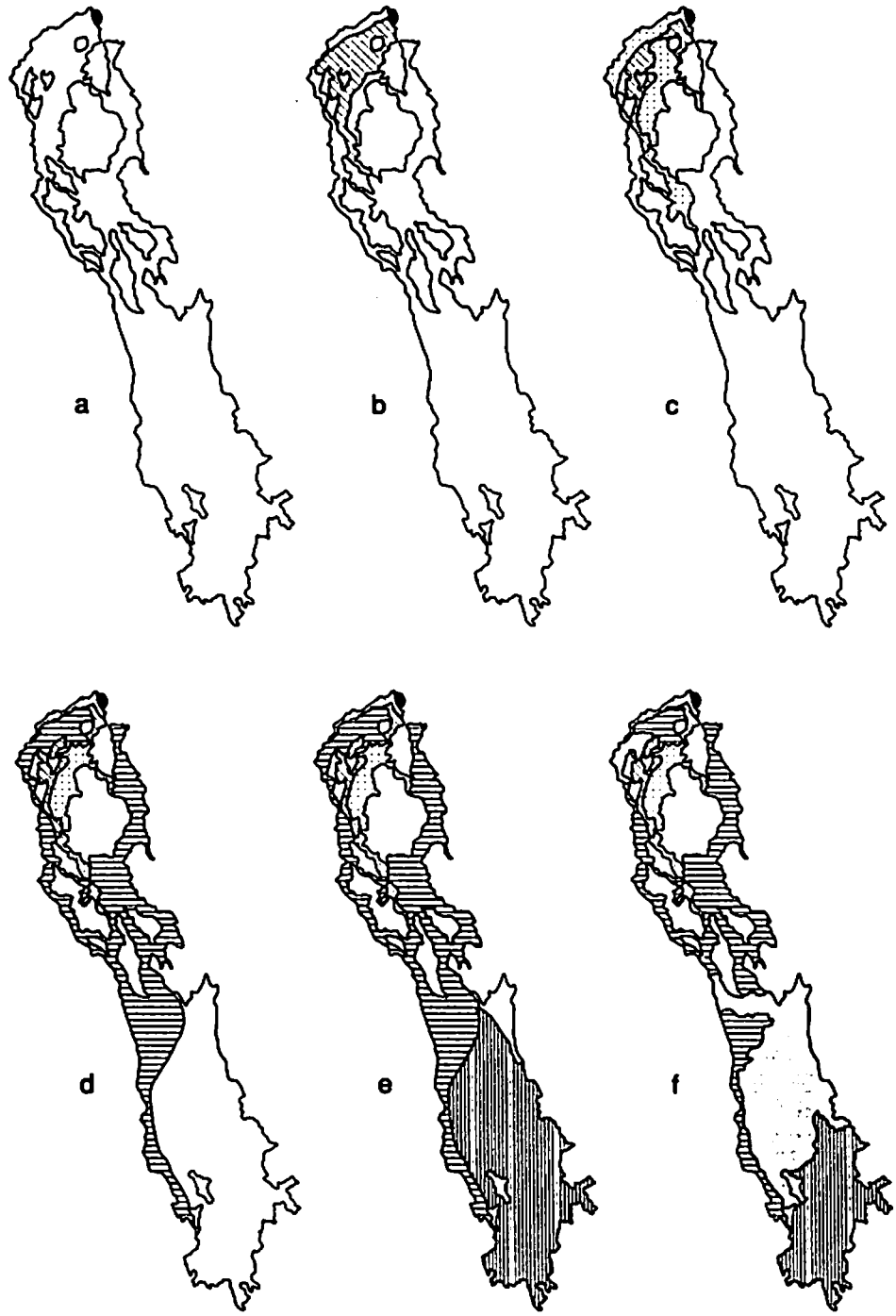

Fig. 3. (*a–f*) Series of small maps shows the sequence of eruptions that produced the Giant Crater lava field, beginning with group 1 and ending with group 6 lavas. Estimated original extents of each group are shown. Outline of lava field is shown for reference. Solid pattern is Group 1 lavas; patterns for other groups are the same as in Figure 2. Group 5 lavas poured out of the lava tube built by group 4 lavas; this same tube was subsequently occupied by group 6 lava. Similarly, part of the group 3 lavas spread out on the surface from a lava tube built by group 2 lava.

lava represents a small leak from the edge of the Giant Crater magma system or constitutes a new pulse of unrelated magma is unknown.

Implications of Vent Data

Medicine Lake volcano lies in an east-west extensional environment east of the main axis of the Cascade Range. Vent trends are typically within 30° of north, as are fault trends. A major east-northeast trending highland of volcanic vents connects across the main axis of the Cascades from Mount Shasta to Medicine Lake volcano and implies a zone of crustal weakness between the two volcanoes. The Giant Crater eruption took place on the southwest flank of Medicine Lake volcano, several hundreds of years after the

TABLE 1. Areas and Volumes of Giant Crater and Related Lavas

Unit	Exposed Area, km^2	Inferred Area, km^2	Total Area Exposed Plus Inferred, km^2	Volume, km^3	Percent of Volume
		Giant Crater Lava Field			
Group 1	0.38	0.05	0.43	0.001	0.02
Group 2	6.41	9.6	16.01	0.31	7
Group 3	13.57	7.5	21.07	0.38	9
Group 4	57.77	16.8	74.57	1.38	31
Group 5	48.46	46.9	95.38	1.32	30
Group 6	66.98		66.98	1.04	23
Total	193.57			4.43	
		Related Lavas			
Horse Caves-Water Caves	10.09	13.3	23.39	0.49	
Vent 5	0.08		0.08	0.001	

eruptions of half a cubic kilometer of basaltic lava from the Horse Caves and Water Caves vents. These earlier vents are aligned N25°W, one of the vent alignments of the later Giant Crater lavas. Several spatter vents that apparently preceded the Giant Crater event by a short time [*Donnelly-Nolan et al.*, 1990] and are nearly buried by the Double Hole flows of group 4 show vent alignments of N15°W and N15°E.

Vent locations are shown on Figure 6, and vent data are summarized in Table 2. During the Giant Crater eruptions, vent trends changed and elevations of the vents lowered as the eruption progressed. Groups 1–3 erupted from vents oriented perpendicular to the dominant regional extension direction. Vent elevations averaged ~1785 m (~5860 feet). These vents closed and several new vents opened during the eruption of the group 4 lavas. Group 4 vents have an average elevation of ~1720 m (~5650 feet), more than 60 m (200 feet) lower than the previous set. The earlier, near-N-S vent direction was preserved at Double Hole Crater and adjacent spatter vents, but Giant Crater and its nearby vent (vent 3) opened on a N55°E trend. The direction from Double Hole Crater to Giant Crater, the two major events for group 4 lava, is N25°W. The change to new vents and new vent directions was also marked by a pronounced compositional gap, but no time gap has been identified between group 3 and group 4 lavas (Champion and Donnelly-Nolan, submitted manuscript, 1991).

Paleomagnetic data (Champion and Donnelly-Nolan, submitted manuscript, 1991) record evidence for a small time gap in the eruption sequence following the eruption of group 4 lavas. No compositional gap exists between group 4 and group 5 basalts (Figure 7). Group 5 lavas are presumed to have erupted at Giant Crater. Group 6 lavas erupted from three vents, Giant Crater and two new vents, with vent trends of N55°E and N30°W, at an average elevation of ~1685 m (~5530 feet), more than 30 m (100 feet) lower than the group 4 vents. The earlier near-N-S vent trend was abandoned, perhaps reflecting the importance of the local stress field in controlling the eruptive sites, following regional control on the initial dike injection and eruption. The N55°E trend that dominated while most of the volume of the system erupted may reflect the importance on this western flank of the volcano of the northeasterly structure that connects across to Mount Shasta.

The small eruption at vent 5 took place shortly after the

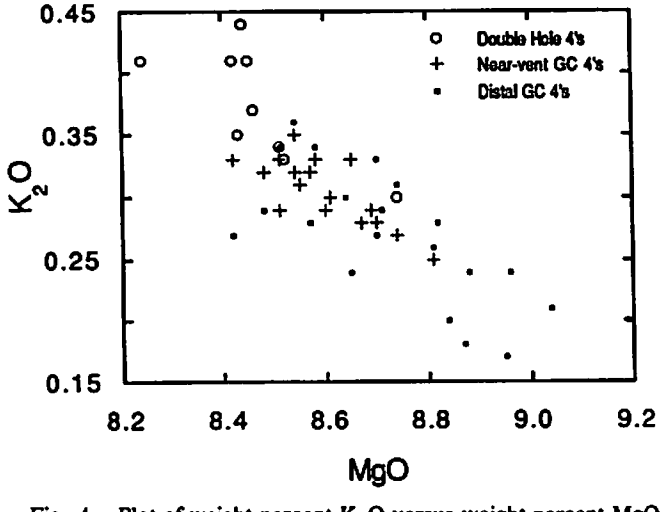

Fig. 4. Plot of weight percent K_2O versus weight percent MgO for group 4 lavas. Symbols identify samples from Double Hole Crater, distal Giant Crater samples, and near-vent Giant Crater samples.

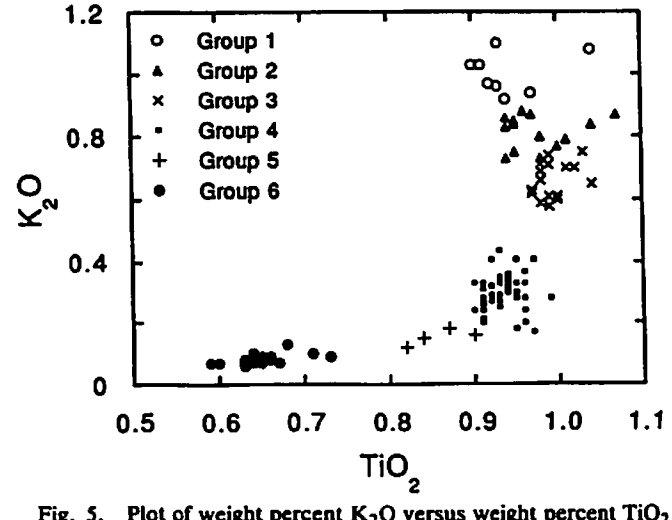

Fig. 5. Plot of weight percent K_2O versus weight percent TiO_2 for the Giant Crater lava field. Group 5 lavas were initially recognized on this plot.

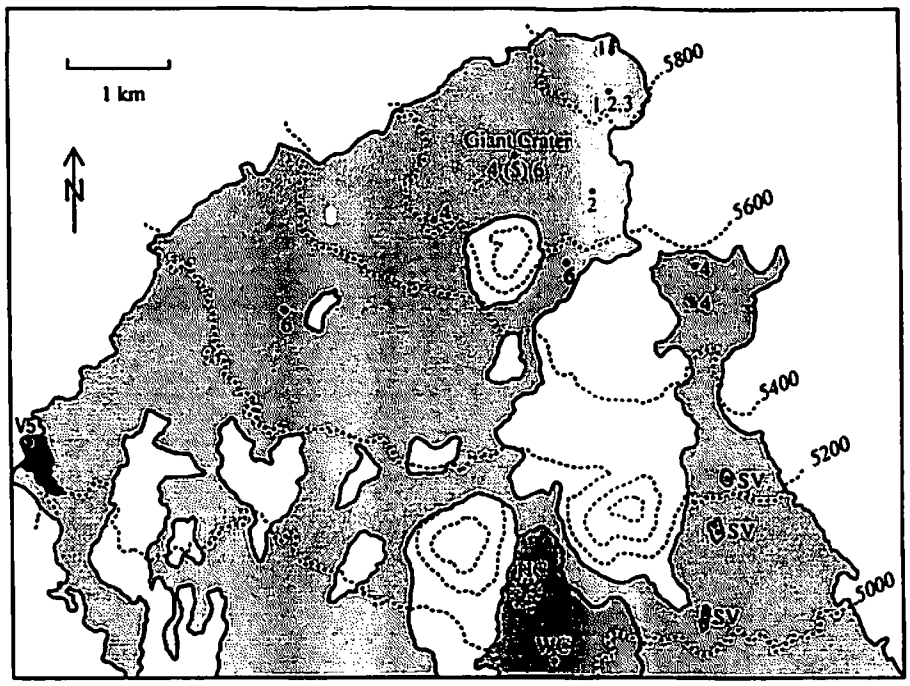

Fig. 6. Map showing vent locations for lava flows of the Giant Crater lava field and related lavas mentioned in text. Vents for groups 1–6 are shown by dots and labeled by group number. The group 5 label is shown in parentheses because Giant Crater is the inferred vent for these lavas. Other vents are indicated as follows: SV for spatter vents within Double Hole flows, HC for Horse Caves vent, WC for Water Caves vent, and V5 for basalt of vent 5. Dotted topographic contours are in feet.

Giant Crater eruptions ceased [*Donnelly-Nolan et al.*, 1990]. It may be coincidental that these new vents are located very near the southwestern projection of the N55°E vent trend. Their elevation is nearly ~150 m (500 feet) lower than the average elevation of group 6 lavas, and the spatter rampart is oriented N25°W, a repeated trend from the Horse Caves-Water Caves eruptions to group 4 and group 6. The vent data and compositional similarity to group 1 lavas suggest that vent 5 lavas may be part of the Giant Crater system, representing a small, late peripheral pulse of contaminated basalt.

Donnelly-Nolan et al. [1990] report that eight mafic eruptions including the Giant Crater event took place across Medicine Lake volcano within a short time interval of a few hundred years about 10,500 radiocarbon years ago. Two have been described above: the spatter vents nearly buried

TABLE 2. Vent Trends and Locations, Giant Crater and Related Lavas

Unit	Vent Names	Approximate Elevation, m (feet)	Vent Trends
Horse Caves-Water Caves		1573 (5160), 1554 (5100)	N25°W
Spatter vents surrounded by Double Hole Crater lava flows		1539 (5050) 1573 (5160) 1585 (5200)	N15°W, N15°E
Giant Crater lavas			
Group 1	Shastine Craters	1792 (5840)	N5°E
	Chimney Crater	1804 (5920)	
Group 2	Chimney Crater	1804 (5920)	
	Cousin Cone	1743 (5720)	N5°E
Group 3	Chimney Crater	1804 (5920)	
Group 4	Giant Crater	1743 (5720)	N55°E (to vent 3)
	vent 3	1725 (5660)	
	Double Hole Crater	1722 (5650)	N-S, N25°W (DH to GC)
	two vents near DH Crater	1701 (5580)	N10°W
Group 5	Giant Crater?	1743 (5720)	
Group 6	Giant Crater	1743 (5720)	
	vent 4	1615 (5300)	N55°E
	ponded vent	1701 (5580)	N30°W (to GC), and location on N5°E trend
Vent 5		1536 (5040)	N25°W

DH is Double Hole; GC is Giant Crater.

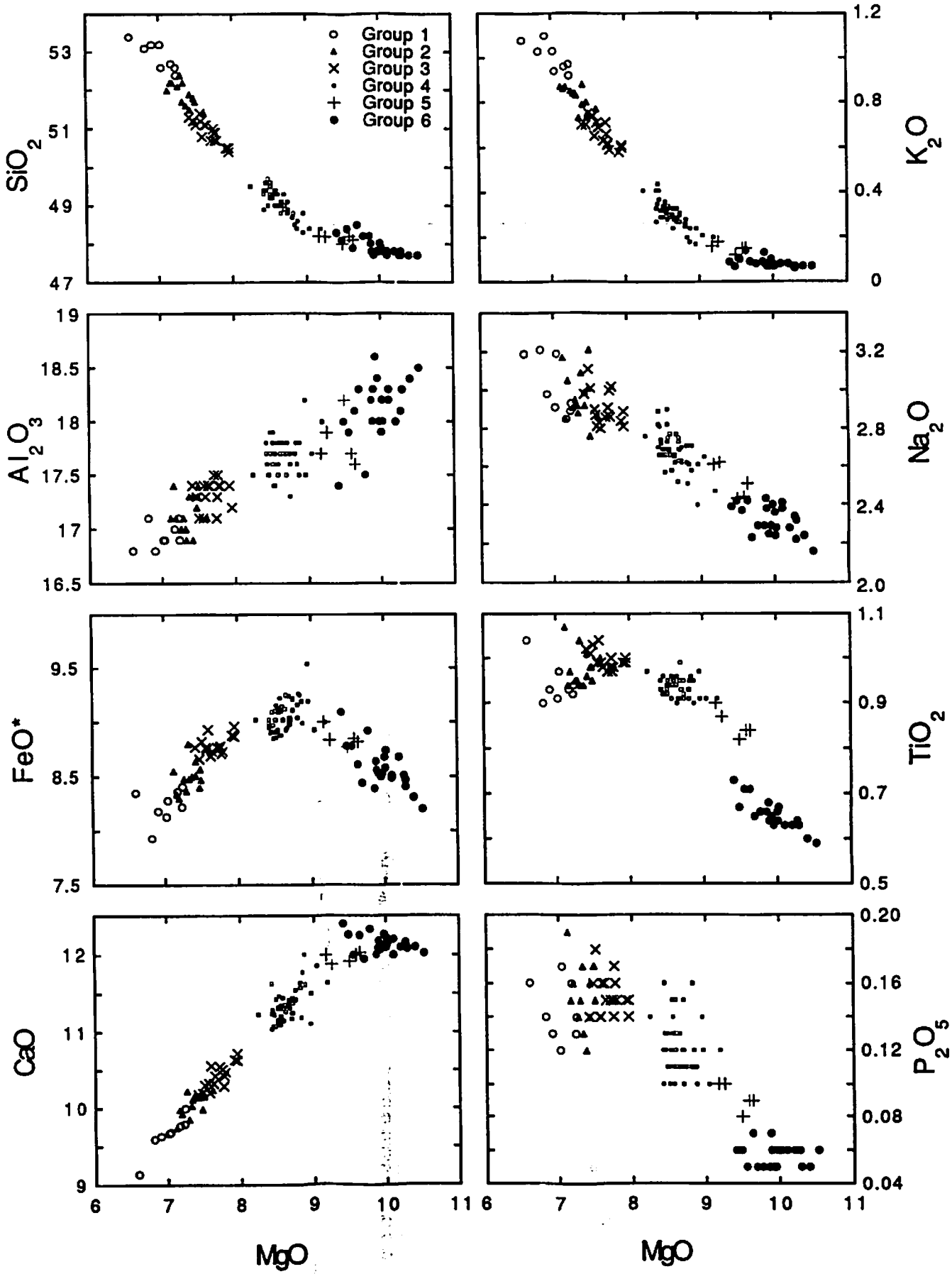

Fig. 7. MgO variation diagrams of major oxides for Giant Crater lavas. All oxides are in weight percent.

TABLE 3. Major and Trace Element Chemical Analyses of Giant Crater and Related Lavas

Sample	SiO_2	Al_2O_3	FeO*	MgO	CaO	Na_2O	K_2O	TiO_2	P_2O_5	MnO	Total[a]	LOI	Rb	Sr	Y	Zr	Ba	Ni	Cr	Latitude[b] N 41°	Longitude[b] W 121°
										Group 1											
83-1	53.1	17.1	7.93	6.82	9.59	3.21	1.03	0.90	0.14	0.15	99.90		28	192	24	122	226	110		30.85	37.66[c]
83-2	53.4	16.8	8.35	6.60	9.14	3.19	1.08	1.04	0.16	0.16	100.06		29	198	29	143	237			30.88	37.68
83-4	52.6	16.9	8.28	7.04	9.68	3.19	0.94	0.97	0.17	0.16	99.78		28	200	26	120	206	110		30.81	37.66
863 M	53.2	16.9	8.13	7.02	9.67	2.91	1.03	0.91	0.12	0.15	100.55	<0.01	31	198	24	120	224	88		30.85	37.66
1009 M	52.6	17.1	8.22	7.23	9.79	2.89	0.97	0.92	0.13	0.15	100.61	0.11	25	201	24	115	219	101		31.13	37.63
1161 M	53.2	16.8	8.18	6.91	9.63	2.98	1.10	0.93	0.13	0.15	100.39	0.34	29	192	24	120	210	105		30.63	37.54
1493 M	52.7	17.0	8.36	7.17	9.77	2.85	0.96	0.93	0.16	0.15	100.53	0.69	26	199	31	116	203	103	121	31.05	37.65[c]
1494 M	52.4	16.9	8.41	7.24	10.00	2.93	0.92	0.94	0.14	0.15	100.24	<0.01	22	201	32	120	210	98	122	31.05	37.68
										Group 2											
82-37	52.0	17.1	8.55	7.12	9.74	3.17	0.87	1.07	0.19	0.16	99.70		19	200	27	133	210	114		30.63	38.62
83-5	51.6	17.3	8.50	7.37	10.19	3.09	0.73	0.94	0.12	0.16	100.04		18	205	24	111	180	124		31.01	37.69
83-7	52.2	17.1	8.30	7.19	9.93	3.05	0.87	0.97	0.16	0.17	99.91		22	195	26	112	185	113		30.40	37.69
83-8	51.8	17.2	8.40	7.47	9.99	3.01	0.80	0.98	0.17	0.16	99.78		21	197	29	121	177	128		30.43	37.69
83-9	52.4	17.1	8.37	7.29	9.85	2.95	0.84	0.95	0.15	0.15	100.08		23	195	24	119	190	120		30.26	37.63
83-24	51.2	17.3	8.57	7.48	10.21	3.21	0.73	0.98	0.17	0.17	100.25		18	200	26	122	167	125		30.60	38.11
879 M	52.2	16.9	8.48	7.33	10.12	2.88	0.83	0.94	0.13	0.15	100.85	0.11	22	200	25	119	202	116		30.19	37.60
1002 M	52.2	17.4	8.34	7.16	9.98	2.85	0.86	0.94	0.15	0.15	100.61	0.95	19	194	25	113	204	112		30.19	37.81[c]
1006 M	51.7	17.4	8.47	7.49	10.16	2.76	0.75	0.95	0.15	0.16	100.68	0.33	16	207	23	108	161	114		30.45	37.81
1249 M	51.4	17.1	8.74	7.61	10.25	2.86	0.77	1.00	0.16	0.16	100.46	<0.01	22	202	28	124	188	110		29.74	38.25[c]
1264 M	52.1	17.0	8.48	7.26	10.23	2.91	0.85	0.95	0.14	0.15	100.76	0.14	20	203	25	120	196	100		28.41	40.13
1276 M	51.7	17.0	8.80	7.32	10.04	2.92	0.84	1.04	0.17	0.16	100.63	0.08	20	208	28	133	191	98		28.21	40.81
1373 M	51.5	17.3	8.64	7.42	10.15	2.92	0.79	1.01	0.16	0.16	100.60	0.16	20	223	29	133	192	111	135	29.72	40.29[c]
1488 M	51.9	16.9	8.51	7.42	10.17	2.99	0.88	0.96	0.14	0.15	100.33	0.09	25	201	33	126	190	104	125	29.12	40.98
										Group 3											
82-64	50.9	17.4	8.71	7.77	10.43	2.86	0.62	0.97	0.16	0.16	99.78		14	201	25	115	154			30.82	38.42
82-65	50.7	17.4	8.73	7.79	10.48	3.02	0.59	0.98	0.15	0.16	99.98		14	200	28	112	168			30.91	38.44
82-66	51.2	17.3	8.66	7.47	10.21	3.11	0.70	1.01	0.16	0.16	100.45		17	202	27	127	169	124		30.95	38.48
82-71	50.7	17.5	8.78	7.76	10.30	3.00	0.61	1.00	0.17	0.16	100.32								152	31.02	37.73
83-3	51.3	17.4	8.77	7.41	10.19	2.98	0.70	1.02	0.14	0.16	99.80		16	207	24	126	173	116		30.85	37.72[c]
328 M	51.2	17.4	8.75	7.57	10.21	2.87	0.74	0.99	0.14	0.16	100.87	<0.01	21	207	27	119	181	105		25.25	39.36
1007 M	51.1	17.4	8.73	7.64	10.43	2.80	0.69	0.98	0.15	0.16	100.66	<0.01	16	207	26	113	175	103		30.46	37.80
1008 M	51.1	17.4	8.69	7.62	10.33	2.83	0.71	0.99	0.16	0.16	100.67	<0.01	14	200	24	116	188	118		30.63	37.86
1256 M	50.7	17.5	8.77	7.71	10.55	2.86	0.63	0.97	0.15	0.16	100.64	0.10	15	201	26	120	147	110		28.92	38.95
1266 M	50.4	17.2	8.96	7.95	10.72	2.81	0.60	1.00	0.15	0.16	100.77	<0.01	16	207	26	121	148	110		28.61	38.38
1278 M	50.8	17.3	8.93	7.59	10.56	2.81	0.65	1.04	0.16	0.16	100.69	0.29	15	213	26	125	164	110		29.66	41.02
1370 M	50.5	17.2	8.87	7.95	10.63	2.89	0.61	0.99	0.14	0.16	100.74	<0.01	11	204	28	124	183	117	135	25.29	39.43
1371 M	51.4	17.1	8.77	7.56	10.33	2.90	0.74	0.99	0.14	0.16	100.71	0.04	19	205	29	122	188	117	128	25.25	39.36
1383 M	50.5	17.4	8.88	7.92	10.64	2.84	0.58	0.99	0.15	0.16	100.63	<0.01	12	210	28	120	172	127	157	24.08	38.46
1384 M	50.9	17.3	8.78	7.75	10.45	2.87	0.66	0.98	0.14	0.16	100.53	<0.01	18	210	27	123	165	126	145	24.08	38.46
1489 M	51.1	17.1	8.82	7.50	10.31	3.01	0.75	1.03	0.18	0.16	100.93	<0.01	18	208	31	130	175	104	124	28.35	41.54
1492 M	51.0	17.1	8.76	7.74	10.51	2.91	0.71	0.98	0.15	0.16	100.86	<0.01	18	199	32	120	159	118	143	26.54	39.47
										Group 4											
2B206	48.3	18.2	9.54	8.95	11.11	2.40	0.17	0.97	0.14	0.17	100.87	1.71							142	16.32	36.05
80-1j	49.1	17.3	9.22	8.74	11.55	2.62	0.31	0.91	0.11	0.17	100.73	0.11							148	23.03	39.65[c]
80-2b	48.4	17.5	9.19	8.87	12.01	2.58	0.18	0.95	0.11	0.16	100.94	<0.01							173	23.00	39.63[c]
80-31c	48.8	17.8	9.25	8.65	11.39	2.62	0.24	0.96	0.13	0.16	100.50	0.24							174	24.89	40.48[c]
80-32	49.0	17.8	9.12	8.64	11.34	2.65	0.30	0.94	0.13	0.16	100.68	<0.01							144	24.87	40.38

TABLE 3. (continued)

Sample	SiO_2	Al_2O_3	FeO*	MgO	CaO	Na_2O	K_2O	TiO_2	P_2O_5	MnO	Total[a]	LOI	Rb	Sr	Y	Zr	Ba	Ni	Cr	Latitude[b] N 41°	Longitude[b] W 121°
										Group 4											
80-33e	49.3	17.4	9.13	8.54	11.35	2.73	0.36	0.94	0.12	0.16	100.61	<0.01							140	26.36	40.80[c]
80-34b	49.3	17.5	9.10	8.58	11.31	2.66	0.34	0.94	0.12	0.16	100.89	<0.01							164	20.60	37.20[c]
80-35	48.8	17.8	9.26	8.82	11.19	2.51	0.28	0.95	0.16	0.17	100.78	0.59							154	18.19	36.19
82-36	49.7	17.7	8.85	8.48	11.08	2.69	0.32	0.92	0.11	0.17	99.99		7	203	25	93	113			30.65	38.44
82-38	49.6	17.8	8.91	8.51	11.13	2.57	0.33	0.93	0.11	0.17	100.37		6	203	25	89	101			30.56	38.64
82-39	49.2	17.8	8.92	8.54	11.10	2.90	0.35	0.94	0.13	0.15	100.28		6	200	24	97	105	140		30.62	38.53
82-54	49.2	17.7	8.93	8.54	11.21	2.82	0.32	0.94	0.15	0.19	99.88		7	199	22	89	93			30.23	30.20
82-55	49.4	17.8	8.88	8.57	11.16	2.69	0.32	0.91	0.10	0.17	100.02		3	203	23	90	98			30.18	38.20
82-56	48.9	17.8	9.02	8.70	11.25	2.73	0.28	0.99	0.15	0.19	99.69		3	201	24	93	94	140		30.14	38.18
82-57	49.1	17.8	8.95	8.67	11.32	2.77	0.28	0.91	0.11	0.15	99.66		4	196	23	91	101			30.03	38.06
82-58	49.3	17.7	8.95	8.42	11.24	2.89	0.33	0.93	0.10	0.16	99.63		3	199	24	90	86			30.05	38.05
82-59	49.4	17.6	8.88	8.58	11.15	2.77	0.33	0.96	0.15	0.18	100.05		9	197	22	91	93	138		30.15	38.08
82-60	49.5	17.9	8.86	8.51	11.16	2.66	0.29	0.92	0.10	0.17	100.29		4	205	21	87	98			30.29	38.20
82-61	49.3	17.6	9.09	8.55	11.21	2.75	0.31	0.94	0.14	0.17	99.64		9	199	23	91	103	145		30.18	38.95
82-62	49.3	17.7	9.02	8.61	11.27	2.58	0.30	0.95	0.11	0.17	100.20		3	196	23	89	98			30.40	39.37
88-11	49.3	17.5	9.24	8.69	11.18	2.52	0.29	0.95	0.12	0.16	100.65	0.31	9	205	26	95	83	146	154	30.32	38.99[c]
881 M	49.1	17.7	8.93	8.65	11.42	2.66	0.33	0.90	0.11	0.16	100.78	<0.01	6	199	24	85	102	135		30.00	38.02
1018 M	49.3	17.6	9.02	8.51	11.32	2.66	0.34	0.93	0.11	0.16	100.78	<0.01	5	201	24	91	94	130		23.53	39.97[c]
1251 M	49.0	17.8	9.14	8.60	11.36	2.58	0.29	0.95	0.13	0.16	100.53	0.09	4	199	23	94	79	140		30.36	38.44
1252 M	49.0	17.9	8.97	8.48	11.43	2.66	0.29	0.92	0.13	0.16	100.75	<0.01	4	197	23	88	87	120		30.12	38.95
1253 M	48.7	17.7	9.16	8.81	11.58	2.62	0.25	0.93	0.11	0.17	101.21	<0.01	5	198	23	88	85	140		29.60	38.64
1257 M	48.5	17.6	9.25	8.84	11.78	2.61	0.20	0.96	0.12	0.17	101.22	<0.01	3	204	23	88	61	150		29.35	39.29
1259 M	48.8	17.5	9.19	8.96	11.51	2.61	0.24	0.91	0.12	0.17	100.90	<0.01	3	207	24	89	78	130		29.56	39.61
1277 M	48.9	17.8	9.02	8.42	11.63	2.70	0.27	0.93	0.12	0.16	100.77	<0.01	5	203	24	89	82	120		27.58	41.16[c]
1369 M	48.9	17.7	9.02	8.71	11.43	2.69	0.29	0.93	0.11	0.16	100.76	<0.01	2	199	23	94	109	139	155	24.55	39.66
1374 M	49.0	17.6	9.22	8.57	11.45	2.68	0.28	0.96	0.11	0.16	100.62	<0.01	7	202	26	94	73	138	164	29.72	40.30[c]
1379 M	48.9	17.8	9.04	8.70	11.45	2.63	0.27	0.91	0.10	0.16	100.52	<0.01	5	207	26	88	87	146	160	27.59	41.11
1382 M	48.9	17.7	9.11	8.74	11.42	2.63	0.27	0.92	0.11	0.16	100.80	<0.01	5	208	24	87	68	156	179	38.33	30.28[c]
1463 M	48.6	17.8	8.99	8.88	11.62	2.71	0.24	0.90	0.10	0.16	100.85	<0.01	3	197	29	83	77	140	157	14.36	36.22
1469 M	48.7	17.7	9.04	8.81	11.64	2.71	0.26	0.91	0.11	0.16	101.51	<0.01	5	209	28	87	59	115	137	11.68	33.99
1485 M	48.4	17.7	8.93	9.04	11.86	2.65	0.21	0.91	0.10	0.16	101.37	<0.01	5	199	24	83	65	123	142	22.23	38.34[c]
1486 M	48.4	18.0	9.00	9.19	11.64	2.47	0.20	0.91	0.12	0.16	101.03	0.35	6	199	28	85	67	147	161	22.23	38.34
1487 M	49.0	17.7	8.98	8.70	11.38	2.75	0.33	0.91	0.12	0.16	101.20	<0.01	5	213	31	98	87	143	156	21.55	38.20
1010 M[d]	48.8	17.6	9.21	8.74	11.43	2.70	0.30	0.95	0.11	0.17	101.65	<0.01	4	204	22	88	75	140		29.92	37.09[c]
1016 M[d]	49.2	17.6	9.10	8.51	11.31	2.69	0.34	0.94	0.11	0.16	100.94	<0.01	7	203	24	94	108	130		28.05	37.10
1232 M[d]	49.5	17.5	9.02	8.24	11.23	2.76	0.41	0.97	0.14	0.16	100.75	<0.01	5	207	24	106	125	120		26.54	36.29
1233 M[d]	49.2	17.4	9.15	8.52	11.47	2.69	0.33	0.95	0.12	0.17	101.32	<0.01	7	208	26	92	88	120		21.59	35.57
1385 M[d]	49.4	17.7	8.99	8.42	11.04	2.82	0.41	0.95	0.12	0.16	100.59	<0.01	6	209	28	106	119	141	161	23.76	38.15
1455 M[d]	49.6	17.5	8.91	8.45	11.24	2.74	0.41	0.92	0.12	0.16	100.63	<0.01	9	200	27	98	92	134	147	29.70	37.11[c]
1456 M[d]	49.4	17.5	9.09	8.46	11.22	2.72	0.37	0.96	0.13	0.16	100.50	0.53	9	203	29	98	102	124	114	29.87	37.09
1457 M[d]	49.4	17.6	8.96	8.43	11.29	2.66	0.35	0.93	0.16	0.16	100.52	0.36	5	203	28	97	82	137	153	29.73	36.81[c]
1483 M[d]	49.6	17.6	8.90	8.44	11.07	2.81	0.44	0.93	0.13	0.16	101.25	<0.01	11	209	34	102	111	115	150	23.17	35.17

Group 5																					
3B722	48.2	17.7	8.85	9.58	12.00	2.44	0.15	0.84	0.09	0.16	101.00	<0.01								9.24	34.23
3B722	48.1	17.6	8.82	9.63	12.03	2.51	0.15	0.84	0.09	0.16	100.72	<0.01	1	196	23	74	44	147	180	9.24	34.23
1020 M	48.0	18.2	8.77	9.49	11.92	2.43	0.12	0.82	0.08	0.16	100.86	0.05	1	196	21	74	65	170		12.32	29.63
1466 M	48.2	17.9	8.84	9.25	11.88	2.62	0.18	0.87	0.10	0.16	101.13	<0.01	4	197	28	77	44	139	133	14.63	30.33
1467 M	48.2	17.7	9.00	9.17	12.00	2.61	0.16	0.90	0.10	0.16	101.04	0.04	2	202	27	80	38	135	159	13.08	32.94
Group 6																					
79-35g	48.2	18.2	8.39	9.86	12.01	2.29	0.09	0.66	0.05	0.16	99.94		<1	177	19	56	60			30.50	38.30[c]
79-35g	47.7	18.6	8.53	9.92	12.07	2.25	0.07	0.65	0.05	0.15	101.24	<0.01	<1	179	17	53	46	198		30.50	38.30[c]
82-72a1	47.8	18.0	8.68	10.20	12.10	2.28	0.08	0.63	0.06	0.16	100.95	<0.01	1	180	17	48	29	185		30.32	38.63[c]
82-72a1-2	48.4	17.9	8.78	9.55	12.00	2.37	0.10	0.71	0.05	0.17	100.03									30.32	38.63[c]
82-72a2-3	48.3	17.4	9.09	9.41	12.40	2.39	0.09	0.73	0.06	0.17	101.05	<0.01	<1	183	18	51	55	140		30.32	38.63[c]
82-72f	47.7	18.5	8.20	10.52	12.02	2.16	0.07	0.59	0.06	0.15	100.72	<0.01	<1	180	17	48	29	245		30.32	38.63[c]
880 M	47.8	18.3	8.41	10.29	12.08	2.22	0.07	0.63	0.05	0.15	101.08	<0.01	2	179	17	50	41	212		29.97	38.00
883 M	48.1	18.0	8.78	9.48	12.26	2.42	0.07	0.67	0.06	0.16	100.52	<0.01	1	178	19	52	34	157		30.52	38.44[c]
904 M	48.2	17.5	8.92	9.77	12.33	2.29	0.08	0.66	0.05	0.16	101.01	0.23	<1	190	21	52	28	161		30.32	38.63[c]
1004 M	47.8	18.2	8.58	10.01	12.21	2.24	0.07	0.64	0.06	0.16	100.90	<0.01	<1	185	17	49	38	189		30.50	38.31[c]
1261 M	47.9	18.0	8.74	10.02	12.15	2.28	0.07	0.67	0.06	0.15	100.70	0.13	<1	183	16	51	32	180		29.64	40.04
1332 M	47.7	18.4	8.31	10.40	12.10	2.24	0.07	0.60	0.05	0.14	100.93	<0.01	<1	185	23	52	11	283	182	19.79	36.89
1380 M	47.8	18.4	8.50	9.95	12.12	2.29	0.07	0.63	0.05	0.15	100.75	<0.01	2	177	21	55	40	262	208	27.80	41.11[c]
1381 M	47.7	18.3	8.47	10.29	12.09	2.32	0.06	0.63	0.05	0.15	101.03	<0.01	1	179	19	53	27	296	205	29.83	37.97
1460 M	47.7	18.2	8.49	10.10	12.20	2.41	0.08	0.63	0.06	0.15	100.96	<0.01	1	180	22	55	39	178	186	19.60	33.32
1461 M	47.8	18.3	8.56	9.89	12.18	2.38	0.08	0.64	0.06	0.15	101.15	<0.01	3	179	25	59	39	161	161	18.57	34.18
1462 M	47.8	18.3	8.51	10.10	12.00	2.38	0.08	0.63	0.06	0.15	101.12	0.16	2	177	22	54	26	177	155	16.63	35.77
1464 M	48.0	18.0	8.64	9.88	12.09	2.43	0.13	0.68	0.07	0.15	101.06	<0.01	3	176	22	61	44	163	178	20.51	37.18
1465 M	47.8	18.0	8.53	9.97	12.26	2.40	0.10	0.64	0.06	0.15	101.27	<0.01	3	186	24	54	44	157	167	18.66	32.68
1484 M	47.7	18.1	8.51	10.27	12.16	2.34	0.07	0.64	0.06	0.15	101.26	<0.01	1	181	22	57	31	192	192	19.87	35.03
1538 M	47.9	18.1	8.61	9.63	12.25	2.42	0.14	0.71	0.07	0.16	101.39	<0.01	4	181	18	61	47	163	172	16.83	31.96
Related Lavas																					
2B193[e]	52.3	17.2	7.97	7.77	9.36	2.99	1.07	1.00	0.18	0.14	100.62	0.36								20.35	34.31
4B543[e]	52.9	17.2	7.72	7.5	9.25	3.04	1.15	0.96	0.16	0.14	100.53	0.05								28.40	38.14[c]
887M[e]	49.9	18.0	8.31	8.65	10.33	2.90	0.62	0.98	0.16	0.15	100.63	<0.01	14	259	23	113	157	139	180	28.20	38.38[c]
1017 M[e]	53.7	17.0	7.55	7.25	8.93	3.04	1.26	0.95	0.16	0.13	100.93	0.28	35	245	24	140	255	120		26.37	38.62
1144 M[e]	53.0	17.1	7.68	7.58	9.24	3.02	1.15	0.93	0.15	0.14	100.59	0.35	33	239	23	128	233	130	164	27.26	37.76[c]
1171 M[e]	52.4	17.3	7.90	7.68	9.41	2.99	1.05	0.98	0.18	0.14	100.36	0.16	26	236	30	132	198	134	156	20.33	34.33
1386 M[e]	52.8	17.3	7.68	7.59	9.36	2.95	1.12	0.93	0.15	0.14	100.62	0.16	27	246	28	131	231	118	142	23.79	38.22[c]
1458 M[e]	52.7	17.2	7.71	7.71	9.30	3.06	1.11	0.94	0.16	0.14	100.68	0.20	27	253	31	135	232	136	121	28.20	38.38[c]
1491 M[e]	53.5	17.0	7.51	7.33	8.99	3.12	1.28	0.95	0.16	0.13	100.52	0.45	35	233	28	138	242	131	133	28.11	38.19[c]
7B967[f]	52.7	17.1	8.02	7.39	9.83	2.91	0.94	0.85	0.13	0.14	100.44	0.26	27	207	31	122	225	122	119	28.89	41.65
1375 M[f]	52.7	17.1	8.06	7.32	9.85	2.84	0.97	0.86	0.12	0.14	100.62	0.18	30	205	29	120	200	108	123	28.94	41.77
1372 M[g]	50.9	17.5	8.91	7.74	10.13	2.78	0.69	1.01	0.17	0.16	100.37	0.71	21	199	30	128	161	125	152	28.77	36.88

LOI is loss on ignition at 900°C; FeO* is total Fe calculated as FeO. Major elements, total, and LOI are in weight percent; trace elements are in parts per million. Major elements were recalculated to 100%, volatile free. Major element analyses without LOI were done at University of Massachusetts, Amherst; those with LOI were done at U.S. Geological Survey, Lakewood, Colorado, by J. Baker, A J. Bartel, R. V. Mendes, D. Siems, K. Stewart, and J. Taggart. Trace element analyses were performed at U.S. Geological Survey, Menlo Park, California, by P. E. Bruggman, T. Frost, B. King, J. R. Lindsay, and D. Vivit. See appendix for analytical methods.

[a] Original total with all iron as Fe_2O_3, plus LOI if determined.

[b] Latitude and longitude measured in minutes using a digitizing tablet.

[c] Indicates that sample was collected within a lava tube, collapse feature, or vent crater.

[d] Group 4 lavas erupted from Double Hole Crater.

[e] Horse Caves-Water Caves lavas.

[f] Vent 5 lavas.

[g] Spatter vent surrounded by Double Hole Crater lava flows.

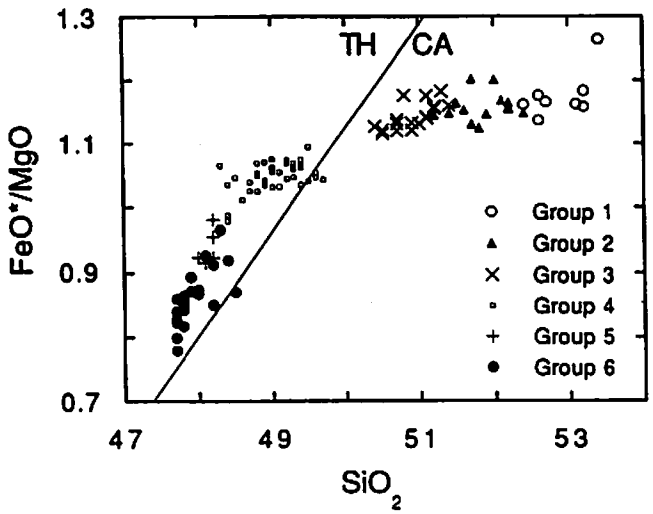

Fig. 8. Plot of FeO*/MgO versus SiO_2 for Giant Crater lavas; oxides are in weight percent. Line dividing tholeiitic (TH) from calc-alkaline (CA) fields is from *Miyashiro* [1974].

by the Double Hole lava flows, and the basalt of vent 5. Two other eruptions occurred on the south flank of the volcano just prior to the Giant Crater eruptions and both display N-S vent alignments, as do the spatter vents for the Tree Molds lava flow on the upper north flank. Farther to the north, the basalt of Valentine Cave erupted from spatter vents aligned N25°W and the basalt of Devils Homestead from vents trending about N25°E. The vents for these eight temporally closely spaced eruptions are distributed over an area about 30 km N-S by 15 km E-W. They indicate to us that a major episode of N-S or near N-S dike intrusions of mafic magma occurred under Medicine Lake volcano about 10,500 years ago.

GEOCHEMISTRY OF THE COMPOSITIONAL ZONED ERUPTION

This discussion is based on chemical analyses presented in Table 3. Analytical methods are described in the appendix.

Major Element Chemical Variations in the Zoned Eruption

The Giant Crater lavas display remarkably regular major element chemical variations over a silica range from 47.7 to 53.2 wt % (Figure 7). One distinct gap in SiO_2 content is present at about 49.7–50.4 wt % (Figures 7 and 8). A common way of distinguishing between calc-alkaline and tholeiitic lavas is the FeO*/MgO versus SiO_2 discrimination diagram of *Miyashiro* [1974]. When the lavas of Giant Crater are plotted on this diagram (Figure 8), they show a transition from calc-alkaline to tholeiitic. Lavas of groups 1–3 are calc-alkaline, whereas groups 4–6 are tholeiitic; the transition coincides with the gap in SiO_2 (Figure 7). The total volume of calc-alkaline lavas of the Giant Crater lava field is estimated at 0.69 km^3, or 16% of the total. Tholeiitic lavas make up 3.66 km^3, 84% of the total estimated eruptive volume. Petrologic modeling by *Baker et al.* [this issue] indicates that group 6 shows the effects of low-pressure near-surface fractional crystallization. Groups 1–5 show evidence of multiple processes including fractional crystallization, assimilation, replenishment, and mixing (FARM) [*Baker et al.*, this issue].

Trace Element Variations

Trace element contents from Table 3 are plotted against K_2O in Figure 9. Trace element concentrations in Giant Crater lavas vary regularly with K_2O, the major element that shows the largest variation, an order of magnitude increase from group 6 to group 1. Ba displays a strong positive correlation with K_2O as does Rb, although the shapes of the two arrays are slightly different, with Ba increasing faster from group 6 to 4 and Rb increasing faster from group 3 to 1. Zr also shows a positive correlation with K_2O, but the initial rapid increase from group 6 to 4 flattens out from group 3 to 1. Sr contents increase rapidly from group 6 to 4, then gradually decline from group 3 to 1. The Y data scatter, but group 6 samples show a smaller average value than the other groups. Ni values are variable in group 6 samples, probably reflecting the effects of olivine fractionation under low-pressure near-surface conditions [*Baker et al.*, this issue]. Ni values then gradually decrease from group 5 to group 1 samples. The trace element variations shown in Figure 9 are consistent with the assimilation-fractional crystallization model proposed by *Baker et al.* [this issue] involving a granitic assimilant.

Primitive Group 6 High-Alumina Basalt: A Primary Magma

The most primitive compositions in the eruption (group 6 lavas) correspond to one of the types of high-alumina basalt that has been described in the literature. *Tilley* [1950] mentioned high-alumina basalt, specifically referring to *Powers* [1932] and *Anderson* [1941] and their descriptions of basalts at Medicine Lake volcano. *Kuno* [1960] in his classic paper cited the aphyric Modoc basalts rich in alumina reported by *Powers* [1932] as examples of high-alumina basalt. Powers had described and analyzed samples of the Warner Basalt of *Russell* [1928] from the lower east flank of Medicine Lake volcano near Tionesta, a unit that is very similar to Giant Crater group 6 basalt. Lavas similar in composition to the Warner Basalt have been referred to by several other names. *Hart et al.* [1984] used the term high-alumina olivine tholeiite to describe primitive basalt flows of the northwestern Great Basin that are similar to mid-ocean ridge and back-arc basin basalts. Low-potassium tholeiite is another term that has been used to describe primitive high-alumina basalts. In this paper we use the original terminology and refer to the Warner Basalt at Tionesta and Giant Crater group 6 basalt as high-alumina basalt.

Crawford et al. [1987] and *Falloon and Green* [1987] recognized that experimentally produced anhydrous partial melts of mantle peridotite were similar in composition to the MgO-rich Warner Basalt. The experimentally produced 10 kbar partial melts of mantle peridotite [*Falloon and Green*, 1987, Table 5] saturated with olivine, orthopyroxene, augite, and spinel are similar to the group 6 high-alumina basalt. *Bartels et al.* [1991] have carried out high-pressure melting experiments on two group 6 lavas, 79-35g and 82-72f, at elevated pressures and anhydrous conditions. 82-72f is the more primitive composition and it is multiply saturated with olivine, orthopyroxene, augite, spinel, and plagioclase within 15°C of its liquidus at 11 kbar. The Mg number of this multiply saturated liquid is 0.70. Therefore we view this

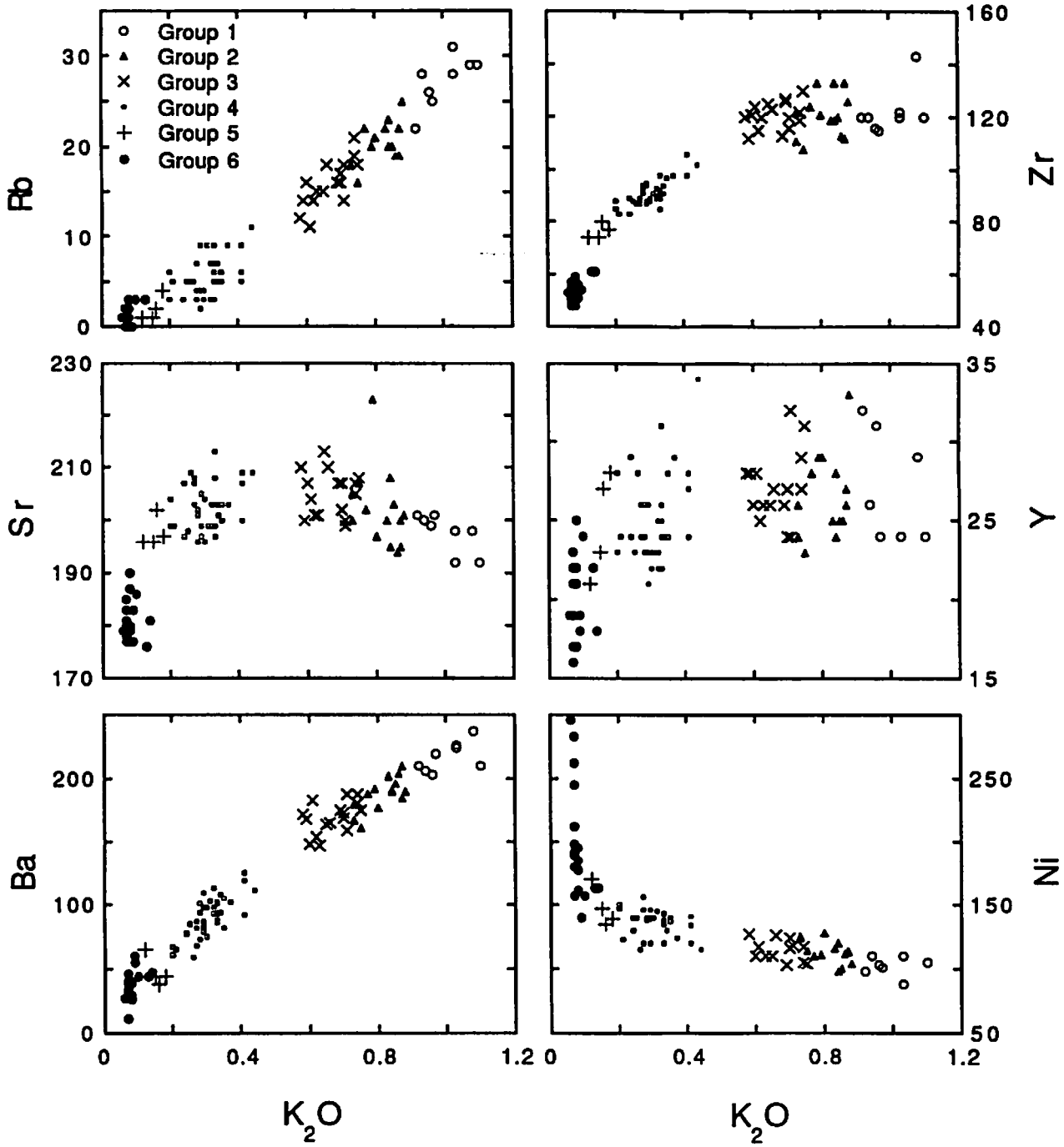

Fig. 9. Contents in parts per million of trace elements for Giant Crater lavas plotted versus weight percent K_2O.

TABLE 4. Rare Earth Element Analyses of Selected Samples From the Giant Crater Lava Field

Sample	Group	La	Ce	Nd	Sm	Eu	Gd	Dy	Er	Yb
1009M	1		17.78	11.00	2.87	1.00	3.51	4.31	2.76	2.74
1232M	4(DH)		13.20	9.15	2.66	1.01	3.48	4.24	2.90	2.62
2B206	4		9.74	7.23	2.31	0.94	3.13	3.85	2.48	2.38
1466M (1)	5	3.17	7.91	6.72	2.22	0.91	2.99	3.71	2.36	2.26
1466M (2)	5	2.84	7.97	6.71	2.22	0.90	2.99	3.73	2.42	2.27
1020M	5		7.50	6.33	2.06	0.86	2.83	3.53	2.24	2.10
880M	6		3.98	3.77	1.34	0.64	2.07	2.76	1.83	1.76
82-72f (1)	6	1.38	3.82	3.56	1.32	0.60	2.04	2.55	1.68	1.56
82-72f (2)	6	1.36	3.83	3.61	1.30	0.61	1.95	2.62	1.79	1.64
82-72f (3)	6	1.23	3.71	3.45	1.24	0.58	1.87	2.46	1.64	1.45

Analyses were performed at U.S. Geological Survey, Menlo Park, California, by isotope dilution mass spectrometry. All analyses except that of 1466M (2) were performed by P. E. Bruggman; 1466M (2) was analyzed by T. D. Bullen. (1), (2), and (3) identify replicate analyses of a single sample. (DH) indicates lava from Double Hole Crater.

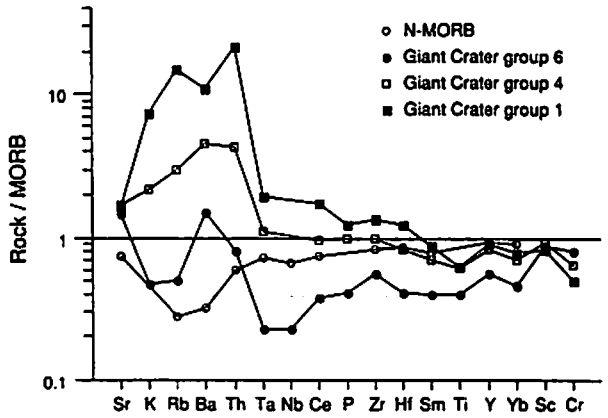

Fig. 10. Spider diagram showing Giant Crater composite group 1, 4, and 6 compositions and normal-type MORB of *Sun and McDonough* [1989] normalized to mid-ocean ridge basalt (MORB) of *Pearce* [1982]. An Nb value of 0.8 ppm was used for Giant Crater group 6 lava (determined by inductively coupled plasma-mass spectroscopy at Washington State University, R. Conrey, unpublished data, 1990). See *Baker et al.* [this issue] for other Giant Crater data not presented in this paper.

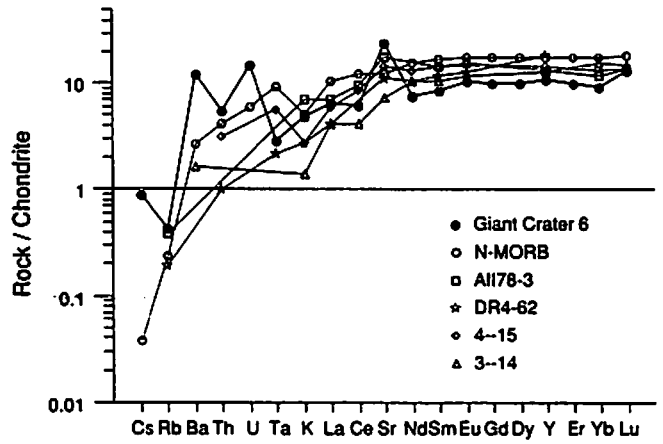

Fig. 12. Compositions of Giant Crater group 6 and five primitive MORB normalized to chondritic values (*Sun and McDonough* [1989] except K value from *Sun* [1980]). Data sources: N-MORB [*Sun and McDonough*, 1989]; Giant Crater [*Baker et al.*, this issue]; AII78-3 [*Bryan et al.*, 1981]; DR4-62 [*Dosso et al.*, 1988]; 4-15 [*Davis and Clague*, 1987]; and 3-14 [*Frey et al.*, 1974].

primitive group 6 basalt as a primary magma derived from mantle peridotite at a depth corresponding to the crust-mantle boundary under Medicine Lake volcano.

Comparisons of Primitive High-Alumina Basalt With MORB and IAB

The primitive group 6 lavas have major and trace element characteristics in common with a subset of primitive mid-ocean ridge basalts (MORB) and primitive island arc basalts (IAB). *Perfit et al.* [1980] have pointed out that primitive MORB and IAB with Mg numbers near 0.70 coincide in major element chemistry. The range of abundances of TiO_2 (0.4–1.2 wt %) and Al_2O_3 (15–18 wt %) overlap, as do abundances of CaO, FeO, and K_2O. A distinctive characteristic of primitive group 6 lavas is their high Al_2O_3 content. A few primitive MORB contain Al_2O_3 > 18 wt %. The average Al_2O_3 content of the 114 primitive MORB tabulated by *Elthon* [1990] is 16.3 wt %, but three of Elthon's primitive MORB contain more than 18 wt % Al_2O_3. Primitive group 6 basalts differ from MORB and resemble IAB in their overabundances of incompatible LILE relative to REE abundances (Figure 10). The Ba/La ratio of the most primitive group 6 lavas is 21, a value that falls at the low end of the range for IAB but is significantly greater than the range for MORB (2–5). These LILE overabundances are diagnostic of subduction zone volcanism and have been attributed to an enrichment process in the mantle source by an aqueous phase derived from the dehydration of the downgoing slab [*Kay*, 1980; *White and Dupré* 1986]. LILE enrichments can also result from crustal contamination, but the experimental evidence for a primary origin of the most primitive Giant Crater basalt is permissive evidence that the LILE enrichments were present in the mantle source.

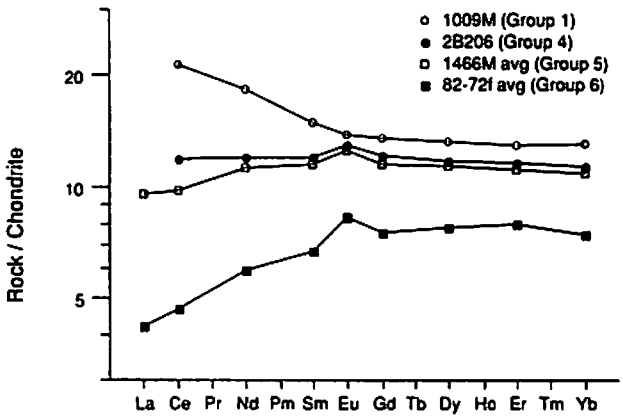

Fig. 11. Chondrite-normalized rare earth element plot using data from Table 4. 1009M is a group 1 sample, 2B206 is a group 4 sample, 1466M avg is the average of two replicate analyses of a single group 5 sample, and 82-72f avg is the average of three replicate analyses of a single group 6 sample. Chondritic values are from *Hanson* [1980, Table 1, column 1].

Rare earth element (REE) data are presented in Table 4. The relative abundances of REE in group 6 lava are similar to those of MORB showing depletion of light REE relative to middle and heavy REE (Figure 11) (La/Sm_{CH} = 0.6 and La/Yb_{CH} = 0.6 where CH indicates chondrite normalization to values of *Hanson* [1980]. IAB from the Lesser Antilles range from light REE enriched to depleted. Depleted IAB were probably derived from a MORB-like source [*Davidson*, 1987]. Primitive group 6 lavas have lower REE abundances than primitive MORB. Figure 12 compares the REE of primitive group 6 lavas with N-MORB of *Sun and McDonough* [1989] and five primitive MORB. The group 6 pattern parallels the MORB patterns and has lower element abundances for REE than any of the MORB but exhibits enrichments in LILE. The five primitive MORB are thought to be near-primary magmas and therefore reflect the oceanic mantle source characteristics. The group 6 REE are more depleted in the middle and heavy REE and Y than are the MORB, suggesting that the source region is slightly more depleted or underwent a larger degree of melting. The relative enrichments of the normal-type MORB and the primitive MORB in REE relative to group 6 could also be caused by modification of these MORB by fractional crystallization after separation from their source. Source char-

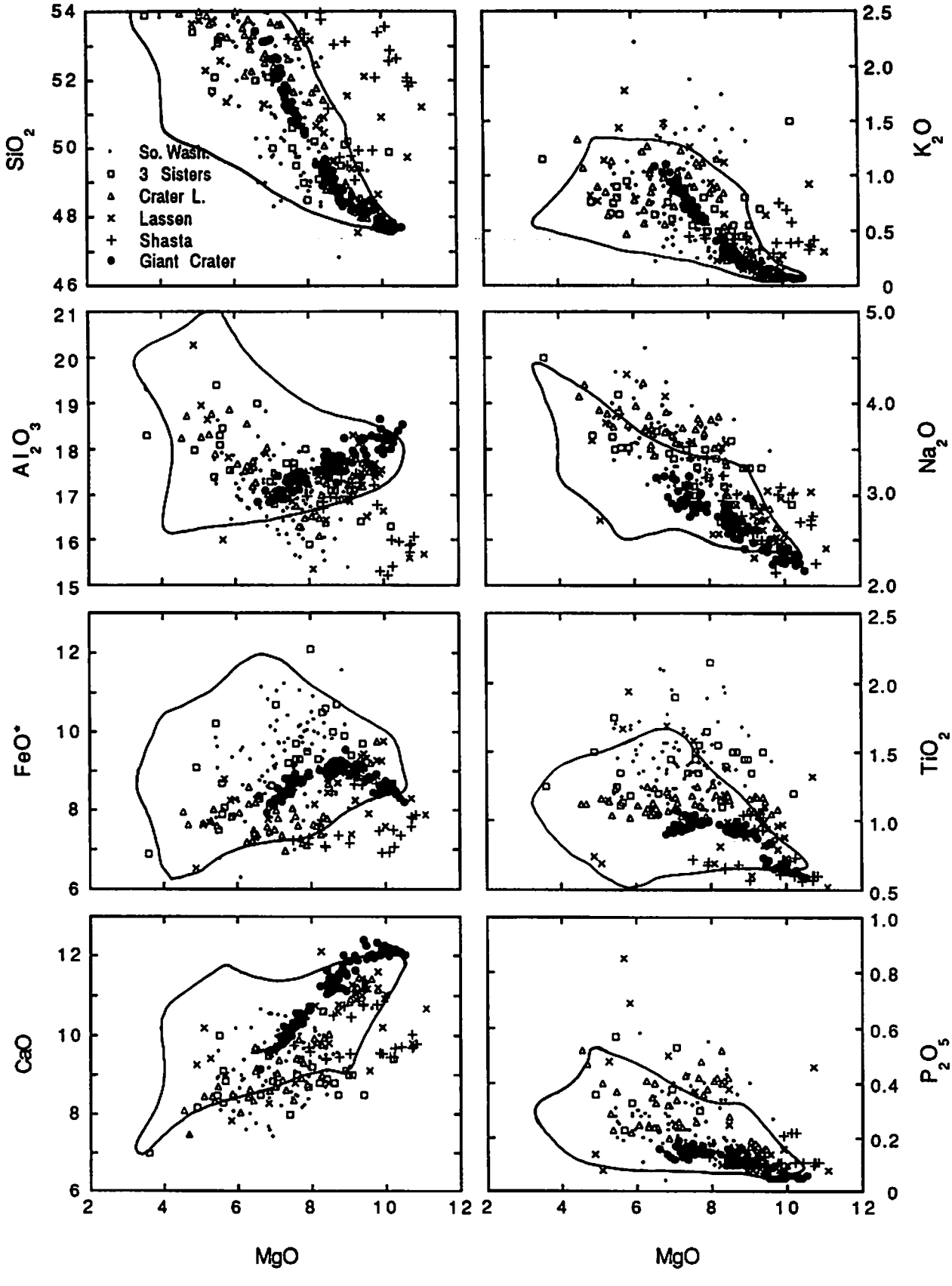

Fig. 13. MgO–major oxide variation diagrams in weight percent showing Cascade lavas with less than 54% SiO_2. Outline indicates field of Medicine Lake lavas other than Giant Crater. Data sources: Southern Washington, *Leeman et al.* [1990] and *Hammond and Korosec* [1983] (includes lavas from Mount St. Helens area, Indian Heaven field, and Mount Adams); Three Sisters area, *Hughes and Taylor* [1986] and *Gardner* [1989]; Crater Lake, *Bruggman et al.* [1989]; Lassen, *Clynne* [1984] and M. A. Clynne and L. J. P. Muffler (unpublished data, 1989); Shasta, *Baker* [1988]; and Medicine Lake (other than Giant Crater), J. M. Donnelly-Nolan (unpublished data, 1989), some Giant Crater Cr analyses from *Baker et al.* [this issue]. All analyses were included regardless of phenocryst content of the rocks.

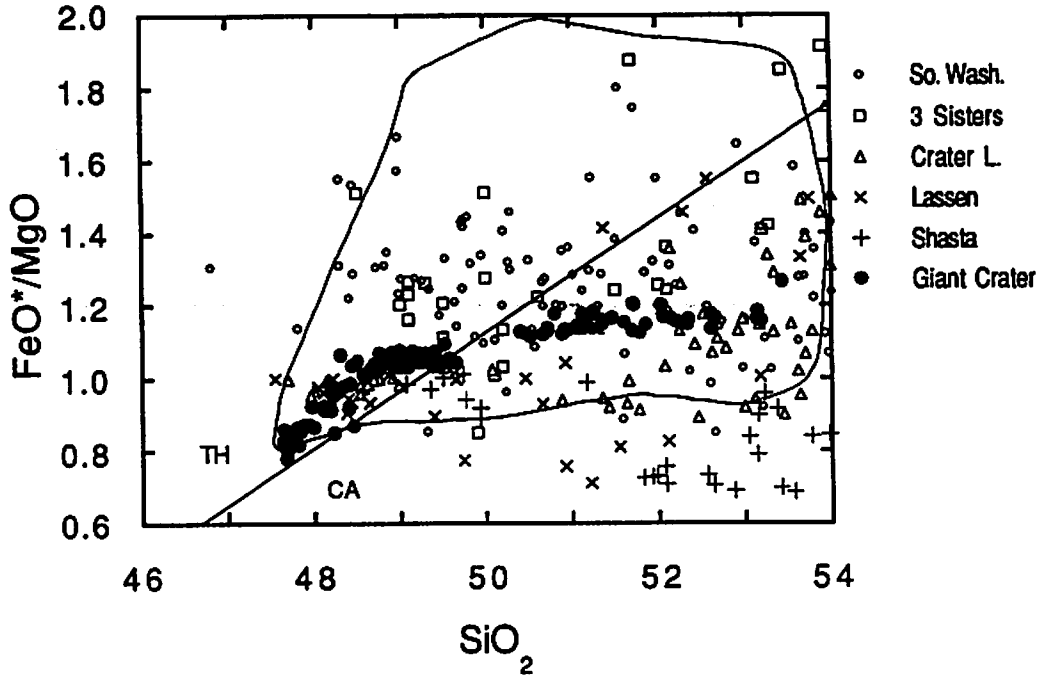

Fig. 14. FeO*/MgO-SiO_2 plot of Cascade lavas with less than 54% SiO_2; oxides in weight percent. Data sources and fields are as in Figure 13, dividing line is from *Miyashiro* [1974].

acteristics or processes may be reflected in the positive Eu anomalies of primitive, aphyric group 6 lavas (Figure 12 and instrumental neutron activation analysis (INAA) data given by *Baker et al.* [this issue]). *Johnson and Kinzler* [1989] found a pronounced negative Eu anomaly in clinopyroxene REE patterns for experiments at mantle pressures and temperatures using clinopyroxene and basaltic liquid. The experiments were done under apparent reducing conditions and may imply that such conditions are present together with clinopyroxene in mantle peridotite under Medicine Lake volcano.

Depletions in the high field strength elements Zr, Hf, Nb, and Ta [*Perfit et al.*, 1980] are a characteristic of IAB. One way to define high field strength element depletions is on a plot of abundance relative to an average rock. On such a plot (Figure 10) the group 6 lava shows depletions in high field strength elements and REE relative to average MORB of *Pearce* [1982] and relative to normal-type MORB of *Sun and McDonough* [1989]. Another way of defining high field strength element depletions is relative to adjacent elements in the plot. In Figure 10 this would show up as a depletion in a high field strength element relative to adjacent REE or LILE. Group 6 basalts do not show this type of depletion for all high field strength elements. The elements Ti and Ta show depletions, Zr shows enrichment, and Hf shows no depletion. In Figure 12, the pattern of primitive Giant Crater group 6 basalt shows a small enrichment in Ta relative to the patterns for primitive MORB. *Bacon* [1990] also shows dichotomous enrichments and depletions in high field strength elements in Crater Lake primitive high-alumina basalts and basaltic andesites.

Comparisons of Evolved Giant Crater Lavas to Other Andesites

The most evolved group 1 Giant Crater lavas are similar to other basaltic andesites of the Cascade range. Figures 13–15 compare Cascade and Medicine Lake lavas including Giant Crater (the fields outlined on Figures 13–15 indicate the range of abundance variations in lavas from Medicine Lake volcano). The trend defined by the Giant Crater lava fields lies in the center of the field defined by Cascade lavas for SiO_2, Al_2O_3, FeO*, K_2O, and TiO_2 on the MgO variation diagrams (Figure 13). The trend defined by the Giant Crater lava field forms the upper limit on the CaO and the lower limit on P_2O_5 and Na_2O variation diagrams. Giant Crater lavas also lie in the center of the field defined by Cascade lavas on the FeO*/MgO versus SiO_2 plot (Figure 14). A comparison of Giant Crater lavas to other Cascade lavas for selected trace elements shows that the most evolved Giant Crater lavas have comparable abundances of Rb, Zr, Ni, and Cr on the K_2O variation diagrams (Figure 15). The trend defined by the Giant Crater lava field defines the lower abundance limits for the Cascade lavas on Sr and Ba, although other Medicine Lake basaltic lavas substantially overlap the compositions of other Cascade lavas.

Group 1 lavas are similar in chemical characteristics to typical calc-alkaline arc basaltic andesites. *Gill* [1981] classified Medicine Lake andesites similar to the group 1 lavas as medium-K calc-alkaline andesites. In Figure 10 the group 1 and group 4 lavas have patterns that show typical arc signatures. In their REE characteristics the group 1 lavas also resemble other medium-K calc-alkaline andesites [*Gill*, 1981, pp. 128–132]. The pattern of the group 1 lavas is light REE-enriched (La/Sm_{CH} = 1.5 and La/Yb_{CH} = 1.9) with a

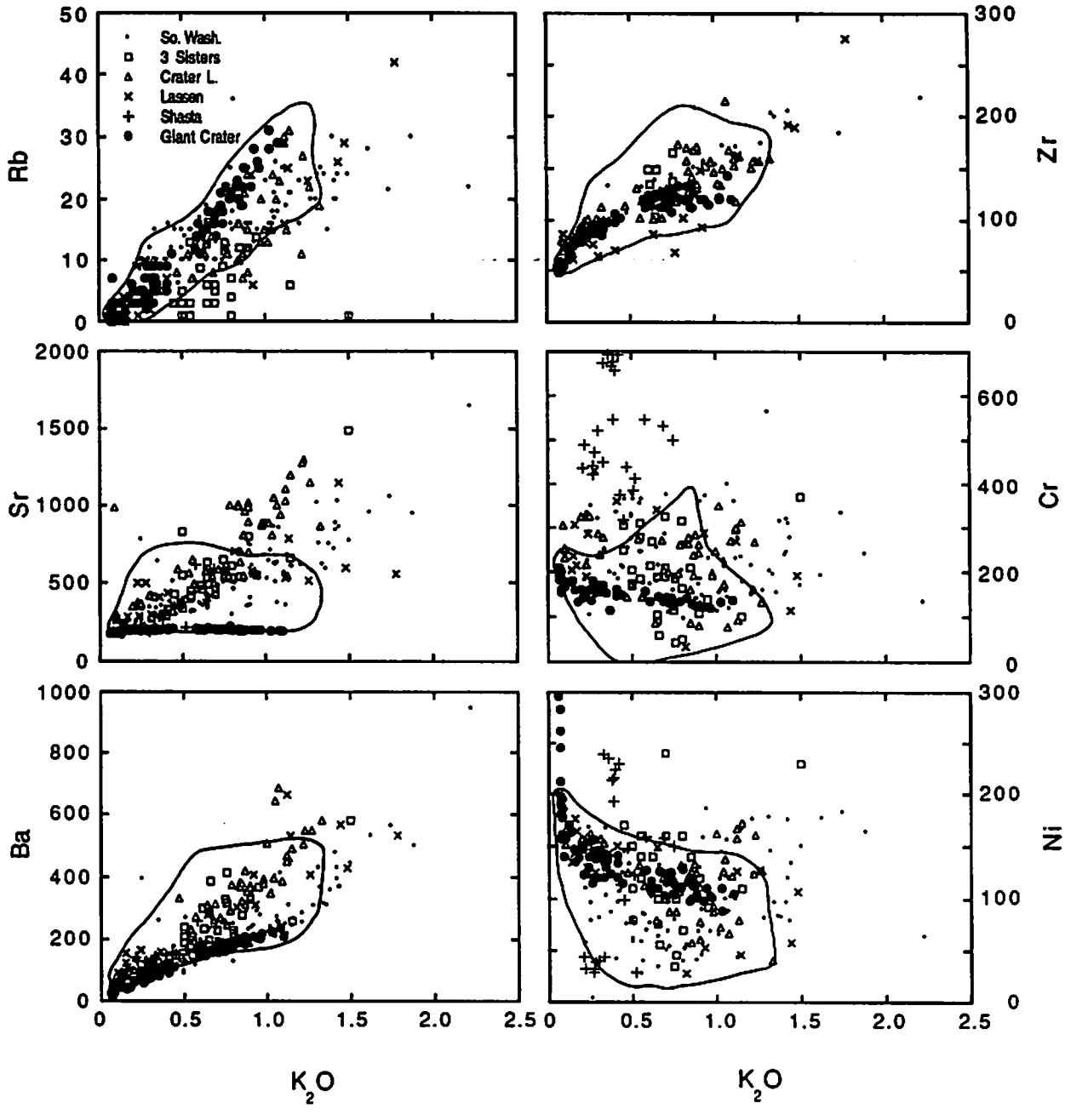

Fig. 15. Selected trace element concentrations in parts per million versus K_2O content in weight percent for Cascade lavas with less than 54% SiO_2. Data sources and fields are as in Figure 13. Analyses of Zr and Rb performed by instrumental neutron activation analysis are not included on plots.

relatively flat pattern for the middle and heavy REE (Figure 11). The light REE-depleted signature of group 6 has been modified to create a light REE-enriched signature in the group 1 lavas. This change in slope in the REE pattern has been brought about by the addition of a granitic crustal melt rich in light REE and depleted in heavy REE, as modeled by *Baker et al.* [this issue].

Giant Crater group 6 lavas are lowest in Sr and Ba and highest in Ni of all Cascade lavas and lowest for their K_2O content in Zr and Cr. As discussed above, the most primitive group 6 lavas are apparently primary magmas produced by melting a depleted MORB-like source that has probably been enriched in LILE by a slab-derived fluid component. Along with the primary high-alumina basalt composition, an MgO-rich basaltic andesite composition plots at the primitive end of the MgO variation diagrams (Figure 13). These high MgO basaltic andesites are higher in SiO_2 (50–52 wt %) and lower in Al_2O_3 (15–16 wt %); they also have high Ni and Cr (Figure 15). High MgO basaltic andesites are found at Mount Shasta [*Baker*, 1988], Lassen [*Fountain*, 1979], and Crater Lake [*Bacon*, 1990], and these lavas are considered to be parental to derivative basaltic andesite and andesite lavas at these volcanic centers. Unlike the group 6 Giant Crater high-alumina basalts, the high MgO basaltic andesites are not multiply saturated with olivine, orthopyroxene, augite, and an aluminous phase at anhydrous or fluid undersaturated conditions and upper mantle pressures [*Baker and Grove*, 1990]. Therefore other processes have modified these basal-

tic andesites after separation from their mantle source region.

The similarity of evolved Giant Crater lavas to basaltic andesites found at other Cascade volcanoes indicates that a primitive magma compositionally similar to Giant Crater group 6 basalt could be parental to other Cascade basaltic andesites. *Waters* [1962] pointed out the close association of high-alumina basalt with the andesitic volcanoes of the Cascades and argued that the andesites were derived from the high-alumina basalt by some process of fractionation or contamination. Relatively primitive high-alumina basalts are found in the Cascades from southern Washington [*Goff*, 1977] to the Crater Lake area in southern Oregon [*Bacon*, 1990]. They are also present in the Lassen area south of Medicine Lake [*Anderson*, 1940]. The abundance and widespread distribution of high-alumina basalt in the Cascades combined with the evidence from Giant Crater linking primitive high-alumina basalt and basaltic andesite adds strength to the proposal that high-alumina basalt may be parental to evolved compositions at other Cascade volcanoes. Primitive high-alumina basalt like the group 6 Giant Crater lavas is an important composition, representing a mantle-derived input to the Cascade volcanic arc.

CONCLUSIONS

Mapping and chemical characterization of the lavas of the Giant Crater field have provided a detailed picture of the geology and geochemistry of a 4.4-km^3 chemically zoned eruptive sequence. The eruptive event began with the most evolved lava composition, a basaltic andesite, and ended with primitive high-alumina basalt. This eruption establishes a direct genetic link between the primitive high-alumina basalt magmas found in the Cascade arc and more evolved basaltic andesite lavas that often constitute the most primitive compositions found at a volcanic center.

APPENDIX: ANALYTICAL METHODS AND SAMPLE COLLECTION

All samples were analyzed for major elements by X ray fluorescence, three quarters at the U.S. Geological Survey (USGS) laboratory in Lakewood, Colorado [*Taggart et al.*, 1987], and one quarter in the laboratory of M. Rhodes, University of Massachusetts, Amherst. The data are presented in Table 3. All the data presented have been recalculated to 100%, volatile free, assuming total iron as FeO and indicated as FeO*. Plots are made from the recalculated data. Original totals and loss on ignition (LOI) at 900°C are presented for the USGS analyses; LOI was not determined for the University of Massachusetts samples. USGS samples were ground in alumina, University of Massachusetts samples in agate.

Separate splits of all sample powders analyzed for major elements were analyzed for Rb, Sr, Y, Zr, Nb, Ba, Cu, Zn, and Ni (and some of the later samples for Cr). The Nb, Cu, and Zn data are not included in Table 3 because they lack precision at these very low concentrations. Measured Nb values for group 1 samples vary from 3 to 7 ppm; for group 6 from 0 to 5 ppm; Cu, from 71 to 105 (group 1) and from 84 to 175 (group 6); Zn, from 43 to 64 (group 1) and from 30 to 58 (group 6). All trace element data listed in Table 3 were obtained by energy-dispersive X ray fluorescence analysis (Kevex) at the USGS analytical chemistry laboratory in Menlo Park, California.

Samples were collected from available outcrops, usually from the most solid material available just below vesicular flow surfaces, and in most cases were chipped on the outcrop to centimeter-size pieces to avoid contamination. A few samples were collected from flow interiors exposed in roadcuts, tube walls, vents, fault scarps, or quarries. LOI in USGS analyses is less than 0.01 wt % in more than half the samples and less than 1.0 wt % in all samples but one, indicating minimal secondary contamination. The one sample with LOI > 1% was originally collected for paleomagnetic analysis.

Acknowledgments. We appreciate the field and laboratory support of W. Loskutoff, J. Hamilton, and O. Guracar, and the computer drafting expertise of E. Lougee. Helpful reviews and comments were provided by C. Bacon, R. Conrey, A. Glazner, G. Goles, W. Hildreth, P. Hooper, P. Michael, R. Tilling, and K. Uto. We are grateful to R. Conrey (Washington State University) for providing unpublished chemical data.

REFERENCES

Anderson, C. A., Hat Creek lava flow, *Am. J. Sci.*, *238*, 477–492, 1940.

Anderson, C. A., Volcanoes of the Medicine Lake Highland, California, *Univ. Calif. Publ. Geol. Sci.*, *25*, 347–422, 1941.

Bacon, C. R., Calc-alkaline, shoshonitic and primitive tholeiitic lavas from monogenetic volcanoes, Crater Lake, Oregon, *J. Petrol.*, *31*, 135–166, 1990.

Baer, R. L., Petrology of Quaternary lavas and geomorphology of lava tubes, south flank of Medicine Lake Highland, California, M.S. thesis, 120 pp., Univ. of N. Mex., 1973.

Baker, M. B., Evolution of lavas at Mt. Shasta volcano, N. California: An experimental and petrologic study, Ph.D. thesis, 430 pp., Mass. Inst. of Technol., Cambridge, 1988.

Baker, M. B., and T. L. Grove, Origin of high-MgO basaltic andesites at Mt. Shasta: An experimental study, (abstract), *Eos Trans. AGU*, *71*, 1714, 1990.

Baker, M. B., T. L. Grove, R. J. Kinzler, J. M. Donnelly-Nolan, and G. A. Wandless, Origin of compositional zonation (high-alumina basalt to basaltic andesite) in the Giant Crater lava field, Medicine Lake volcano, northern California, *J. Geophys. Res.*, this issue.

Bartels, K. S., R. J. Kinzler, and T. L. Grove, High pressure phase relations of a primative high-alumina basalt from Medicine Lake Highland, N. California, *Contrib. Mineral. Petrol.*, in press, 1991.

Bloomfield, A. L., and R. J. Arculus, Magma mixing in the San Francisco Volcanic Field, AZ, *Contrib. Mineral. Petrol.*, *102*, 429–453, 1989.

Bruggman, P. E., C. R. Bacon, J. S. Mee, S. T. Pribble, and D. F. Siems, Chemical analyses of volcanic rocks from monogenetic and shield volcanoes near Crater Lake, Oregon, *U.S. Geol. Surv. Open File Rep.*, *89-562*, 1989.

Bryan, W. B., G. Thompson, and J. N. Ludden, Compositional variation in normal MORB from 22°–25°N: Mid-Atlantic Ridge and Kane Fracture Zone, *J. Geophys. Res.*, *86*, 11,815–11,836, 1981.

Camp, V. E., P. R. Hooper, M. J. Roobol, and D. L. White, The Madinah eruption, Saudi Arabia: Magma mixing and simultaneous extrusion of three basaltic chemical types, *Bull. Volcanol.*, *49*, 489–508, 1987.

Clynne, M. A., Stratigraphy and major element geochemistry of the Lassen Volcanic Center, *U.S. Geol. Surv. Open File Rep.*, *84-224*, 1984.

Crawford, A. J., T. J. Falloon, and S. Eggins, The origin of island arc high-alumina basalts, *Contrib. Mineral. Petrol.*, *97*, 417–430, 1987.

Davidson, J. P., Crustal contamination versus subduction zone enrichment: Examples from the Lesser Antilles and implications

for mantle source compositions of island arc volcanic rocks, *Geochim. Cosmochim. Acta*, *51*, 2185–2198, 1987.

Davis, A. S., and D. A. Clague, Geochemistry, mineralogy, and petrogenesis of basalt from the Gorda Ridge, *J. Geophys. Res.*, *92*, 10,467–10,483, 1987.

Donnelly-Nolan, J. M., A magmatic model of Medicine Lake volcano, California, *J. Geophys. Res.*, *93*, 4412–4420, 1988.

Donnelly-Nolan, J. M., and D. E. Champion, Geologic map of Lava Beds National Monument, northern California, scale 1:24,000, *U.S. Geol. Surv. Misc. Invest. Map*, *I-1804*, 1987.

Donnelly-Nolan, J. M., D. E. Champion, C. D. Miller, T. L. Grove, and D. A. Trimble, Post-11,000-year volcanism at Medicine Lake volcano, Cascade Range, northern California, *J. Geophys. Res.*, *95*, 19,693–19,704, 1990.

Dosso, L., H. Bougault, P. Beuzart, J.-Y. Calvezk, and J.-L. Joron, The geochemical structure of the South-East Indian Ridge, *Earth Planet. Sci. Lett.*, *88*, 47–59, 1988.

Elthon, D., The petrogenesis of primary mid-ocean ridge basalts, *Aquat. Sci.*, *2*, 27–53, 1990.

Falloon, T. J., and D. H. Green, Anhydrous partial melting of MORB pyrolite and other peridotite compositions at 10 kbar: Implications for the origin of primitive MORB glasses, *Mineral. Petrol.*, *37*, 181–219, 1987.

Fountain, J. C., Geochemistry of Brokeoff volcano, California, *Geol. Soc. Am. Bull.*, *90*, 294–300, 1979.

Frey, F. A., W. B. Bryan, and G. Thompson, Atlantic Ocean floor: Geochemistry and petrology of basalts from legs 2 and 3 of the Deep-Sea Drilling Project, *J. Geophys. Res.*, *79*, 5507–5527, 1974.

Gardner, C. A., Geochemical variations of lavas from the Mount Bachelor volcanic chain, *U.S. Geol. Surv. Open File Rep.*, *89-645*, 29–35, 1989.

Gill, J. B., *Orogenic Andesites and Plate Tectonics*, 390 pp., Springer-Verlag, New York, 1981.

Goff, F. E., Vesicle cylinders in vapor-differentiated basalt flows, Ph.D. thesis, 181 pp., Univ. of Calif., Santa Cruz, 1977.

Greeley, R., and R. Baer, Hambone, California and its magnificent lava tubes—preliminary report, *Geol. Soc. Am. Abstr. Programs*, *3*, 128, 1971.

Hammond, P. E., and M. A. Korosec, Geochemical analyses, age dates, and flow-volume estimates for Quaternary volcanic rocks, southern Cascade Mountains, Washington, *Open File Rep. 83-13*, Wash. State Div. Geol. and Earth Resour., Olympia, 1983.

Hanson, G., Rare earth elements in petrogenetic studies of igneous systems, *Annu. Rev. Earth Planet. Sci.*, *8*, 371–406, 1980.

Hart, W. K., J. L. Aronson, and S. A. Mertzman, Areal distribution and age of low-K, high-alumina olivine tholeiite magmatism in the northwestern Great Basin, *Geol. Soc. Am. Bull.*, *95*, 186–195, 1984.

Hughes, S. S., and E. M. Taylor, Geochemistry, petrogenesis, and tectonic implications of central High Cascade mafic platform lavas, *Geol. Soc. Am. Bull.*, *97*, 1024–1036, 1986.

Johnson, K. T. M., and R. J. Kinzler, Partitioning of REE, Ti, Zr, Hf, and Nb between clinopyroxene and basaltic liquid: an ion microprobe study, (abstract), *Eos Trans. AGU*, *70*, 1388, 1989.

Kay, R. W., Volcanic arc magmas: Implications of a melting-mixing model for element recycling in the crust-upper mantle system, *J. Geol.*, *88*, 497–522, 1980.

Kinzler, R. J., T. L. Grove, and J. M. Donnelly-Nolan, The evolution of the Callahan Flow: A chemically zoned basalt-andesite lava flow at Medicine Lake Highland, N. California, (abstract), *Eos Trans. AGU*, *70*, 498, 1989.

Kuno, H., High-alumina basalt, *J. Petrol.*, *1*, 121–145, 1960.

Leeman, W. P., D. R. Smith, W. Hildreth, Z. Palacz, and N. Rogers, Compositional diversity of Late Cenozoic basalts in a transect across the southern Washington Cascades: Implications for subduction zone magmatism, *J. Geophys. Res.*, *95*, 19,561–19,582, 1990.

Mertzman, S. A., Jr., Strontium isotope geochemistry of a low potassium olivine tholeiite and two basalt-pyroxene andesite magma series from the Medicine Lake Highland, California, *Contrib. Mineral. Petrol.*, *70*, 81–88, 1979.

Miyashiro, A., Volcanic rock series in island arcs and active continental margins, *Am. J. Sci.*, *274*, 321–355, 1974.

Pearce, J. A., Trace element characteristics of lavas from destructive plate boundaries: in *Andesites*, edited by R. S. Thorpe, pp. 525–548, John Wiley, New York, 1982.

Perfit, M. R., D. A. Gust, A. E. Bence, R. J. Arculus, and S. R. Taylor, Chemical characteristics of island-arc basalts: Implications for mantle sources, *Chem. Geol.*, *30*, 227–256, 1980.

Powers, H. A., The lavas of the Modoc Lava-Bed quadrangle, California, *Am. Mineral.*, *17*, 253–294, 1932.

Russell, R. J., Basin range structure and stratigraphy of the Warner Range, northeastern California, *Univ. Calif. Publ. Geol. Sci.*, *17*, 387–496, 1928.

Sun, S.-S., Lead isotopic study of young volcanic rocks from mid-ocean ridges, ocean islands and island arcs, *Philos. Trans. R. Soc. London, Ser. A*, *297*, 409–445, 1980.

Sun, S.-S., and W. F. McDonough, Chemical and isotopic systematics of oceanic basalts: Implications for mantle composition and processes, in Magmatism in the Ocean Basins, edited by A. D. Saunders, and M. J. Norry, *Geol. Soc. Spec. Publ. London*, *42*, 313–345, 1989.

Taggart, J. E., Jr., J. R. Lindsay, B. A. Scott, D. V. Vivit, A. J. Bartel, and K. C. Stewart, Analysis of geologic materials by wavelength-dispersive X-ray fluorescence spectrometry, *U.S. Geol. Surv. Bull.*, *1770*, E1–E19, 1987.

Tilley, C. E., Some aspects of magmatic evolution, *Q. J. Geol. Soc. London*, *106*, 37–50, 1950.

Waters, A. C., Basalt magma types and their tectonic associations: Pacific Northwest of the United States, *The Crust of the Pacific Basin*, *Geophys. Monogr. Ser.*, vol. 6, edited by G. A. Macdonald and H. Kuno, pp. 158–170, AGU, Washington, D. C., 1962.

White, W. M., and B. Dupré, Sediment subduction and magma genesis in the Lesser Antilles: Isotopic and trace element constraints, *J. Geophys. Res.*, *91*, 5927–5941, 1986.

Wolfe, E. W., M. O. Garcia, D. B. Jackson, R. Y. Koyanagi, C. A. Neal, and A. T. Okamura, The Puu Oo eruption of Kilauea volcano, episodes 1–20, January 3, 1983 to June 8, 1984, *U.S. Geol. Surv. Prof. Pap.*, *1350*, 471–508, 1987.

M. B. Baker, Department of Geological and Planetary Sciences, California Institute of Technology, Pasadena, CA 91125.

P. E. Bruggman, D. E. Champion, and J. M. Donnelly-Nolan, U.S. Geological Survey, MS 910, 345 Middlefield Road, Menlo Park, CA 94025.

T. L. Grove, Department of Earth, Atmospheric, and Planetary Sciences, Massachusetts Institute of Technology, Cambridge, MA 02139.

J. E. Taggart, Jr., U.S. Geological Survey, MS 973, Box 25046, Denver Federal Center, Denver, CO 80225.

(Received December 19, 1990;
revised July 3, 1991;
accepted July 18, 1991.)

32

APPENDIX 1 - 3A

$^{40}Ar/^{39}Ar$ Dating of Young Low-K Tholeiites: Examples from Northeast California, U.S.A.

Becker, T.A., Sharp, W.D., Renne, P.R., Turrin, B.D., Page, W.D., Wakabayashi, J.

$^{40}Ar/^{39}Ar$ Dating of Quaternary Basalt, Western Modoc Plateau, Northeastern California: Implications to Tectonics

Page, W.D., Renne, P.R.

In Lanphere, M.A., Dalrymple, G.B., and Turrin, B.D., 1994, Abstracts of the Eighth International Conference on Geochronology, Cosmochronology, and Isotope Geology
Berkeley, California, June 5-11, 1994): U.S. Geological Curcular 1107

$^{40}Ar/^{39}Ar$ DATING OF YOUNG LOW-K THOLEIITES: EXAMPLES FROM NORTHEAST CALIFORNIA, U.S.A.

BECKER, T.A., SHARP, W.D., RENNE, P.R., Institute of Human Origins Geochronology Center, 2453 Ridge Road, Berkeley, CA, 94709, U.S.A., TURRIN, B.D. ,U.S. Geological Survey, MS 901, 345 Middlefield Road, Menlo Park, CA, 94025, U.S.A., PAGE, W.D. Pacific Gas and Electric Co., Geosciences Dept., P.O. Box 770000, San Francisco, CA, 94177, and WAKABAYASHI, J. ,Consultant, 1329 Sheridan Lane, Hayward, CA, 94544, U.S.A.

Young low-K (Ca/K ~ 25-40) basalts pose challenges to K-Ar and $^{40}Ar/^{39}Ar$ dating because of their low radiogenic Ar contents and resulting sensitivity to corrections for blanks, mass discrimination, nucleogenic Ar isotopes and trapped Ar of anomalous isotopic composition.

We have developed an automated resistance furnace, employing an infra-red pyrometer, that provides reproducible blanks of $<10^{-16}$ mol for m/e = 40 at 1200 °C. Heating time and residence time in the extraction system for gas purification are adjusted for minimizing blank contibution and optimizing isotope intensity measurement. Full automation of the furnace, along with the extraction line and air pipette, allows unattended operation and makes frequent characterization of procedural blanks and spectrometer discrimination feasible.

Our M.A.P. 215-50C mass spectrometer is configured for a resolution of 450, making $^{40}Ar/^{39}Ar$ ratios of 100 or more acceptable. This allows neutron fluences to be reduced, and in conjunction with thermal neutron shielding and detailed characterization of production ratios, minimizes the effects of nucleogenic Ar isotopes.

Incremental heating produces intermediate-temperature steps with enhanced radiogenic Ar contents and provides data for isochron analysis, revealing subtle anomalous trapped Ar ($^{40}Ar/^{36}Ar$ in the range of 297-305) in many samples. Samples may yield *sensu stricto* plateaux, but have well-defined isochron ages that are significantly younger. Two samples, potentially from different flows, yield distinct plateau ages of 493 ± 22 and 423 ± 7 ka, but give indistinguishable isochron ages of 409 ± 18 and 415 ± 3 ka, with initial $^{40}Ar/^{36}Ar$ of 304.6 ± 1.3 and 301.2 ± 0.9, respectively. Another flow yielded well-defined plateau ages of 1113 ± 81, 921 ± 51, and 907 ± 51 ka from three closely-spaced samples, whereas isochron ages of 889 ± 136, 834 ± 51, and 879 ± 40, and initial $^{40}Ar/^{36}Ar$ of 297.8 ± 1.4, 297.8 ± 1.0 and 296.3 ± 0.9, respectively, were obtained.

Basalts with lower Ca/K (<15) are much less sensitive to slight departures in the trapped Ar from atmospheric air ratio. One such flow yields a plateau age of 68 ± 18 ka and an indistinguishable isochron age of 50 ± 16 ka with initial $^{40}Ar/^{36}Ar$ of 296.8 ± 1.0.

These results indicate that detailed $^{40}Ar/^{39}Ar$ incremental heating analyses are needed for precise and accurate dating of Late Pleistocene low-K basalts.

^{40}AR-^{39}AR DATING OF QUATERNARY BASALT, WESTERN MODOC PLATEAU, NORTHEASTERN CALIFORNIA: IMPLICATIONS TO TECTONICS

PAGE, W. D., Geosciences Department, F22A, Pacific Gas and Electric Company, P. O. Box 770000, San Francisco, CA 94177 and RENNE, P. R., Institute of Human Origins Geochronology Center, 2453 Ridge Road, Berkeley, CA 94709.

The Modoc Plateau has had low seismic activity, yet many faults have displaced the extensive Quaternary "Warner basalts" in this region. In order to help assess the seismic hazards and risks to PG&E's facilities in the region north and northwest of Mt. Lassen, we dated 15 samples from 10 flows by the ^{40}Ar-^{39}Ar, step-heating method. Dating of the rocks proved critical to understanding the tectonics and timing of faulting in the region Discussion of the Ar-Ar results and tectonic implications for the area south of Mt. Lassen are presented in companion abstracts by Becker et al. and by Wakabayashi et al.

Basalts in the Modoc Plateau were mostly contained from spilling to the west and south by the Klamath Mountains and Sierra Nevada as they built up the plateau. The oldest dated basalt flows (~ 2.4 Ma) are small remnants that have been locally weathered to saprolite and are plastered on north flank of the Sierra Nevada. Geomorphic analysis suggests that the older flows may have locally spilled over the divide north of Mt. Lassen. The interconnected, north-striking McArthur, Hat Creek, and Almanor graben now separate the western Modoc Plateau from the mountains to the west and have been a major geomorphic feature for more than a million years.

The west-facing Hat Creek fault zone on the east side of the Hat Creek graben north of the Pit River (Soldier Creek fault) displaces the 1.2 Ma basalt on top of the scarp > 260 m, giving a long-term vertical separation rate of > 0.22 mm/yr. South of the Pit River the Hat Creek fault zone displaces the flow (1.0 Ma) on top of the scarp > 390 m (> 0.38 mm/yr). At the same locality the eastern two faults in the zone displaces the basalt flow west of Hogback Ridge (850 ka) > 85 m (> 0.10 mm/yr). These rates are less than the 1.3 mm/yr (post 15 ka) presented by Muffler et al. (1993 manuscript) for the Hat Creek fault in the near Lost Creek to the south. The Sam Wolfin Spring (800 ka), Rocky Ledge (?) (150 ka) and other flows younger than 1 Ma were deposited within the Hat Creek graben. Extensive diatomite lake beds in the graben underlie the Wolfin Spring flow and hence appear to have been deposited between about 1 Ma and 800 ka.

The Yellow Jacket (?) (840 ka) and the Tuft Creek flows (150 ka) are northwest of Indian Spring Mountain on the northeast side of the McArthur graben. The Mayfield fault displaces the Tuft Creek flow 12 m, down west (0.09 mm/yr). The entire west-facing Mayfield fault zone displaces it about 64 m (0.5 mm/yr). The Fall River Mills basalt (-- ka) and other younger flows partly fill the McArthur graben.

Northwest of Mt. Lassen the northeast-striking Battle Creek fault vertically displaces hypersthene andesite of Brokeoff Mountain flow (550 ka) about 43 m, down south (0.078 mm/yr). The scarp is overlain by the Black Butte basalt (~60 ka) that does not appear to be faulted.

The results of this study strongly indicate that Ar-Ar dating of basalts as young as late Quaternary can provide significant constraints to neotectonic processes.

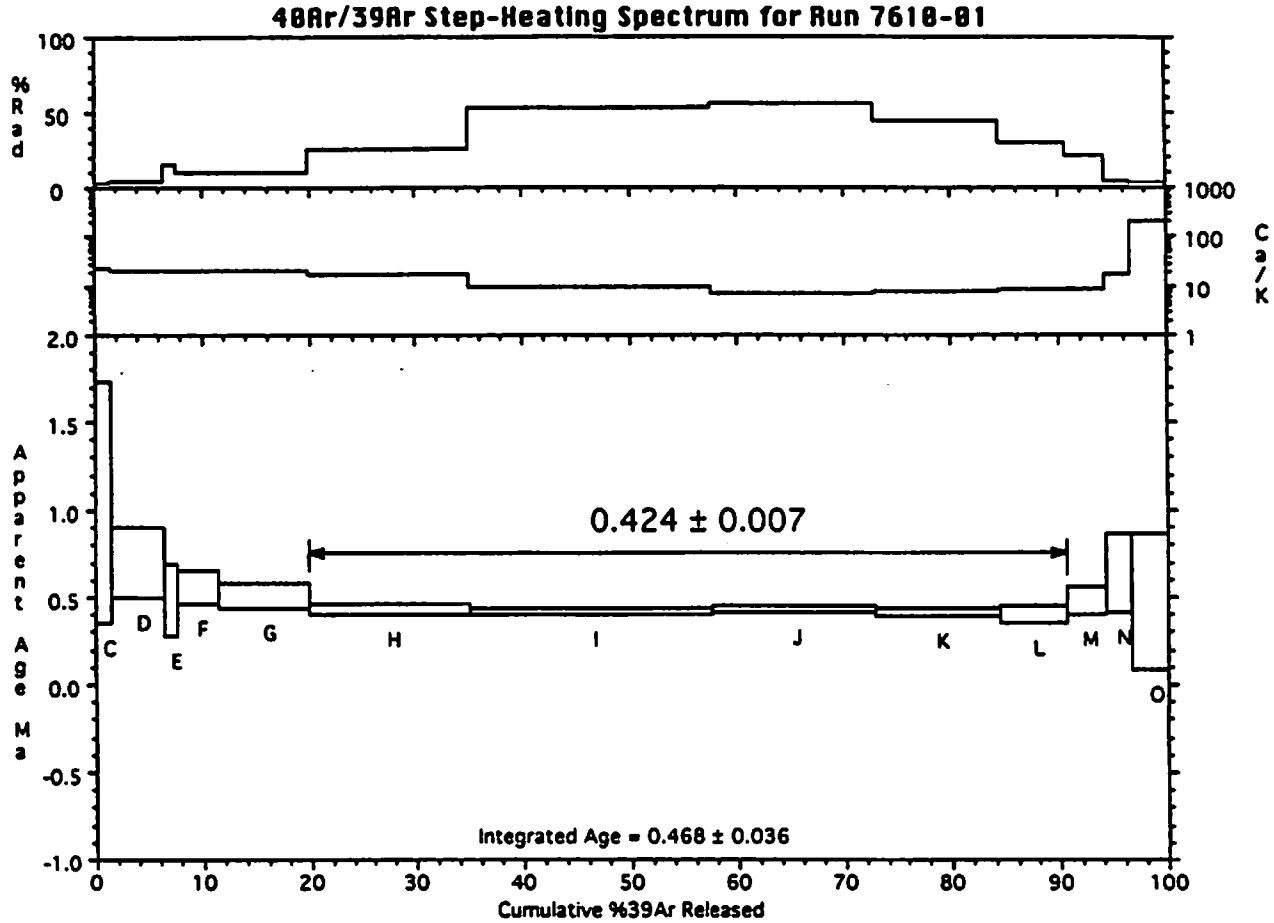
40Ar/39Ar Step-Heating Spectrum for Run 7610-01
% Rad
Ca/K
Apparent Age Ma
0.424 ± 0.007
C
D
E
F
G
H
I
J
K
L
M
N
O
Integrated Age = 0.468 ± 0.036
Cumulative %39Ar Released

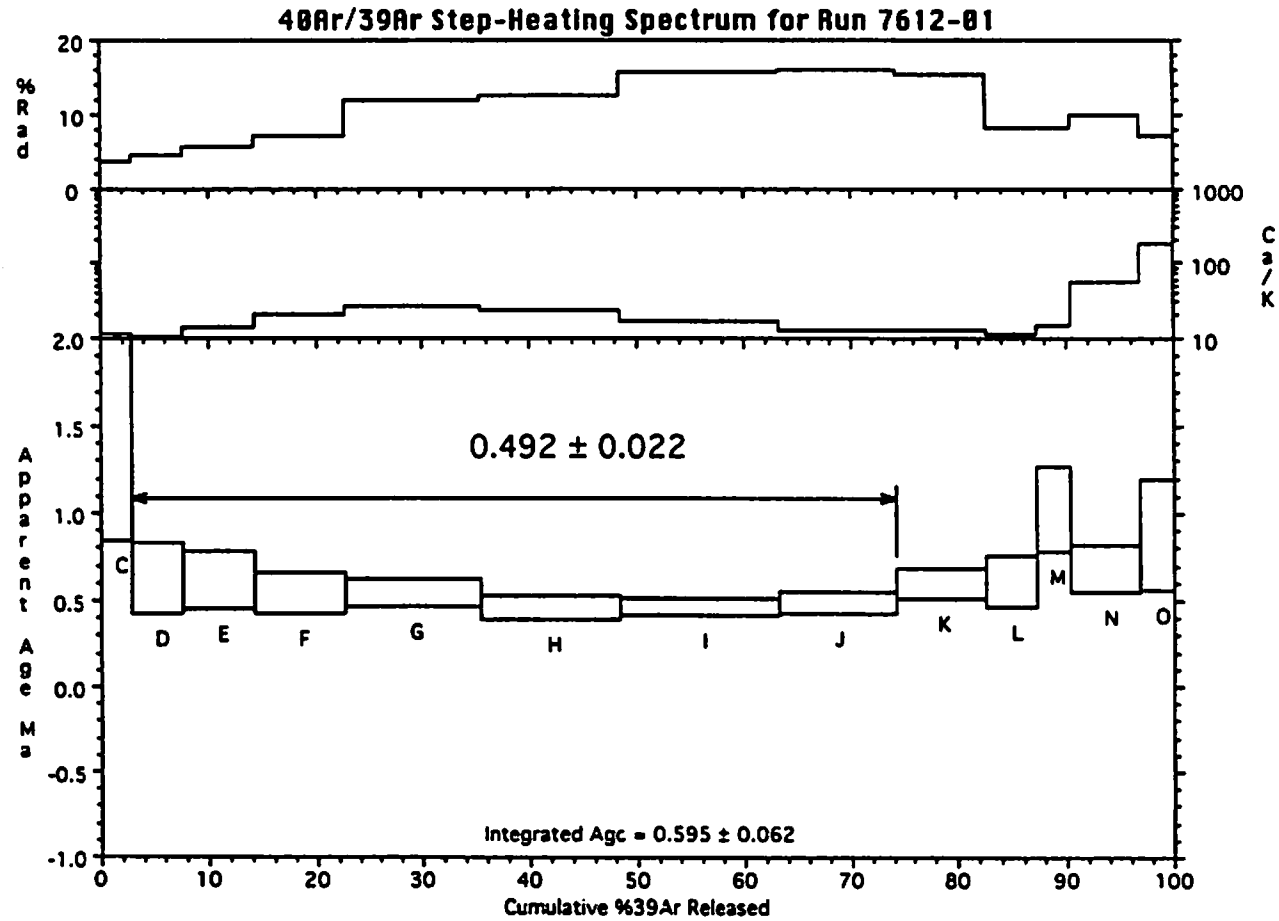
40Ar/39Ar Step-Heating Spectrum for Run 7612-01
% Rad
Ca/K
Apparent Age Ma
0.492 ± 0.022
C
D
E
F
G
H
I
J
K
L
M
N
O
Integrated Age = 0.595 ± 0.062
Cumulative %39Ar Released

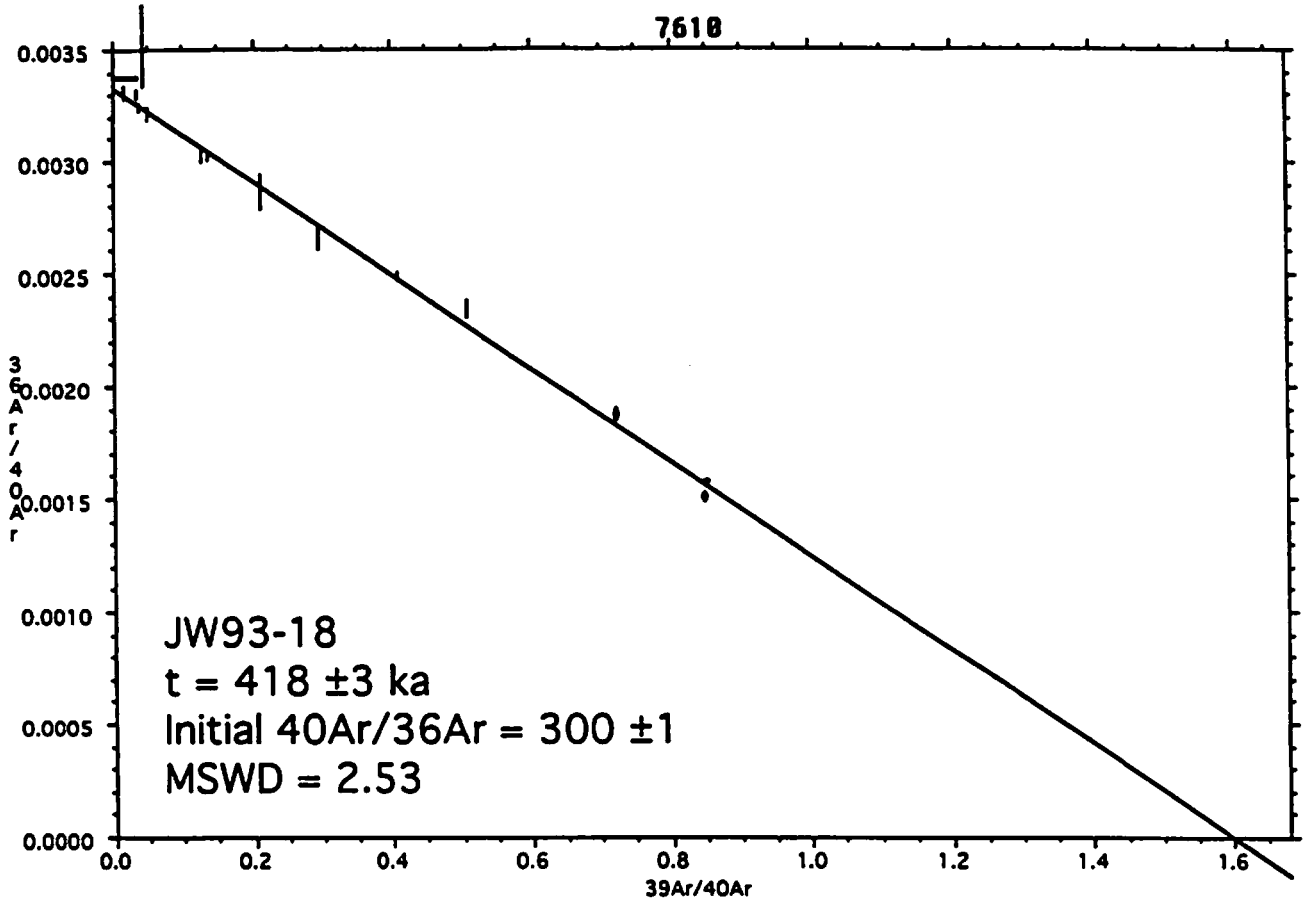
7610
0.0035
0.0030
0.0025
0.0020
0.0015
0.0010
0.0005
0.0000
36Ar/40Ar
0.0
0.2
0.4
0.6
0.8
1.0
1.2
1.4
1.6
39Ar/40Ar
JW93-18
t = 418 ±3 ka
Initial 40Ar/36Ar = 300 ±1
MSWD = 2.53

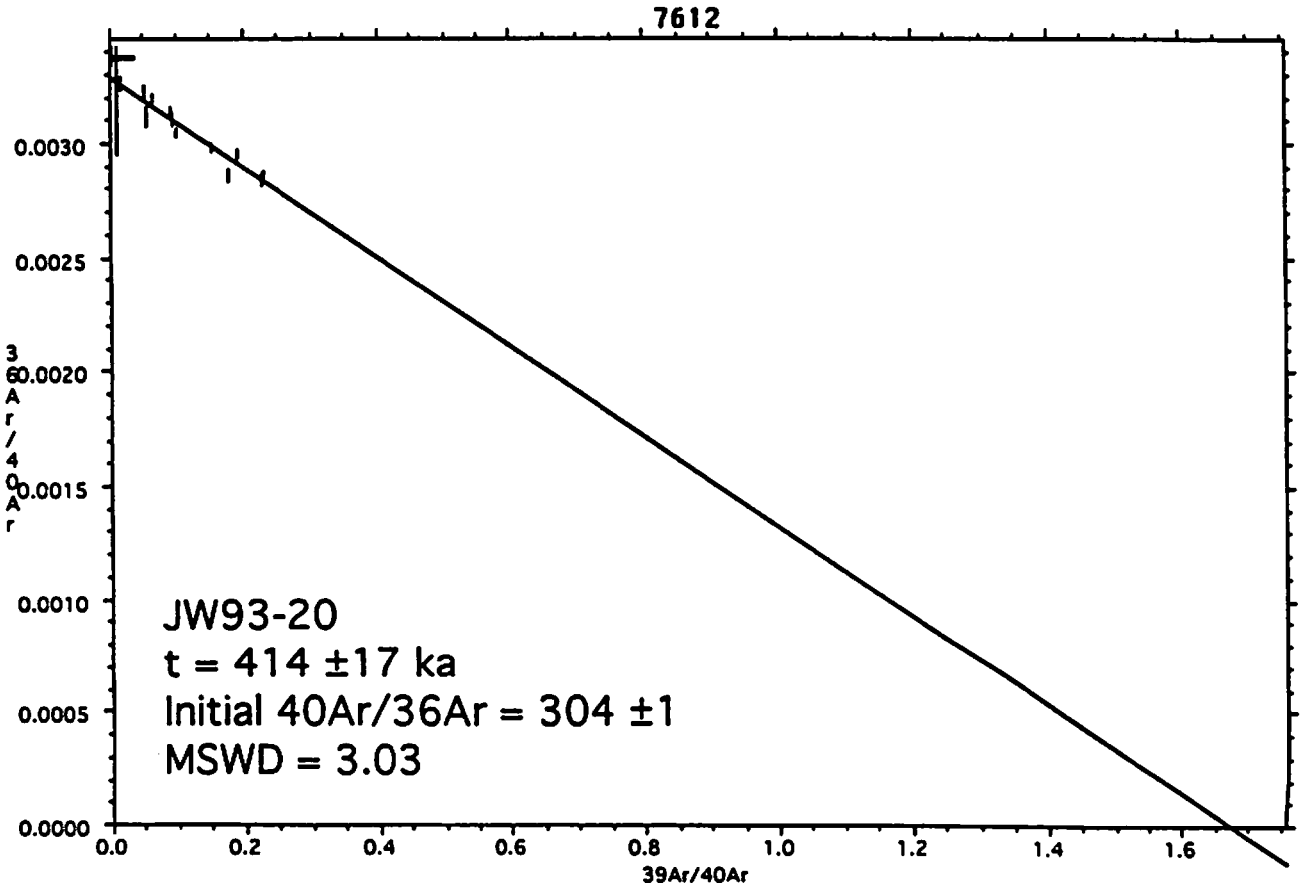
7612
0.0030
0.0025
0.0020
0.0015
0.0010
0.0005
0.0000
36Ar/40Ar
0.0
0.2
0.4
0.6
0.8
1.0
1.2
1.4
1.6
39Ar/40Ar
JW93-20
t = 414 ±17 ka
Initial 40Ar/36Ar = 304 ±1
MSWD = 3.03

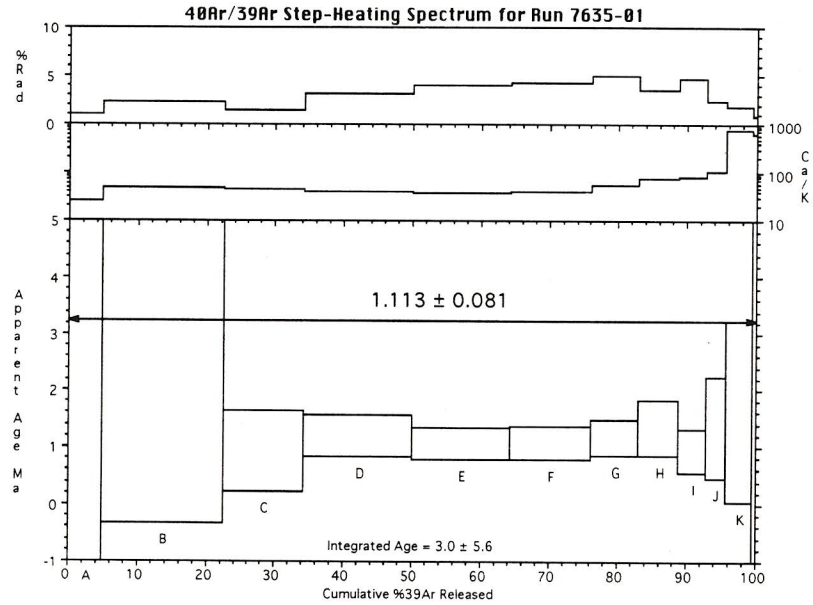
40Ar/39Ar Step-Heating Spectrum for Run 7635-01
% Rad
Ca/K
Apparent Age Ma
1.113 ± 0.081
Integrated Age = 3.0 ± 5.6
Cumulative %39Ar Released

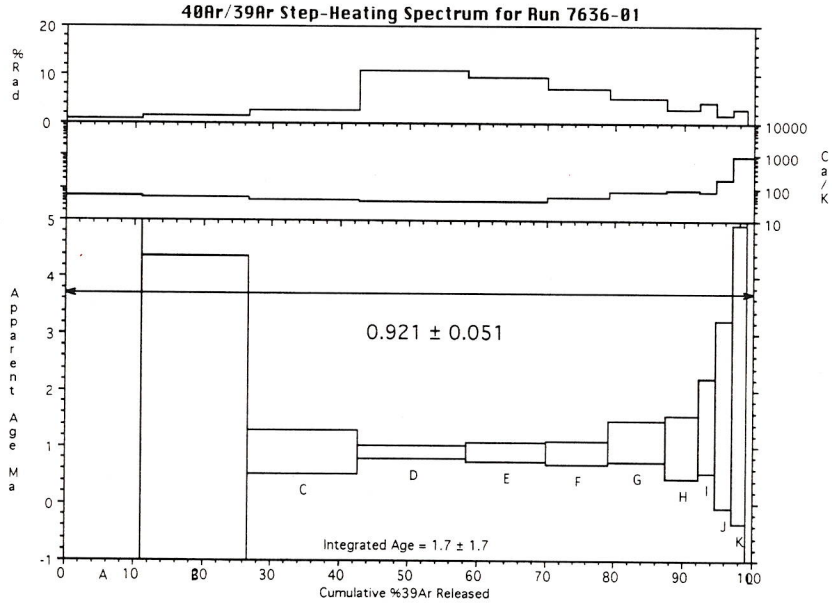
40Ar/39Ar Step-Heating Spectrum for Run 7636-01
% Rad
Ca/K
Apparent Age Ma
0.921 ± 0.051
Integrated Age = 1.7 ± 1.7
Cumulative %39Ar Released

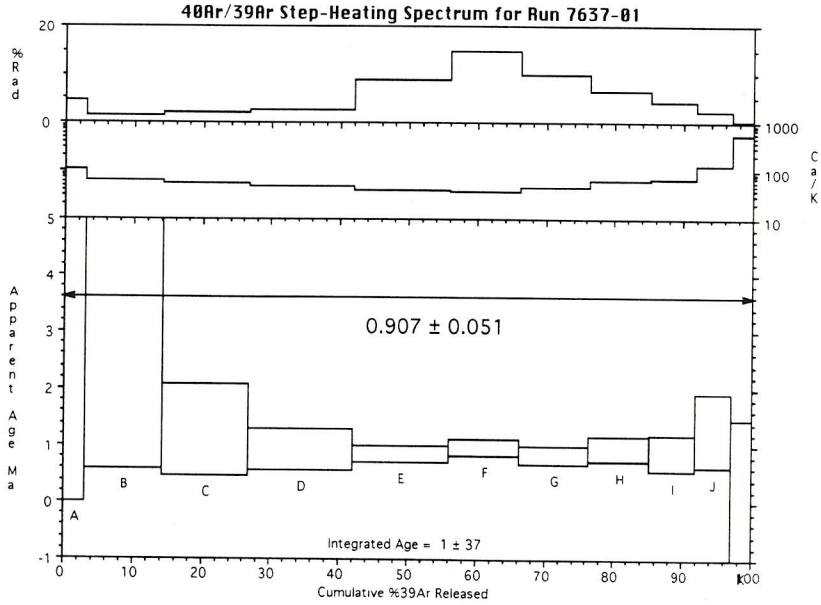
40Ar/39Ar Step-Heating Spectrum for Run 7637-01
% Rad
Ca/K
Apparent Age Ma
0.907 ± 0.051
Integrated Age = 1 ± 37
Cumulative %39Ar Released

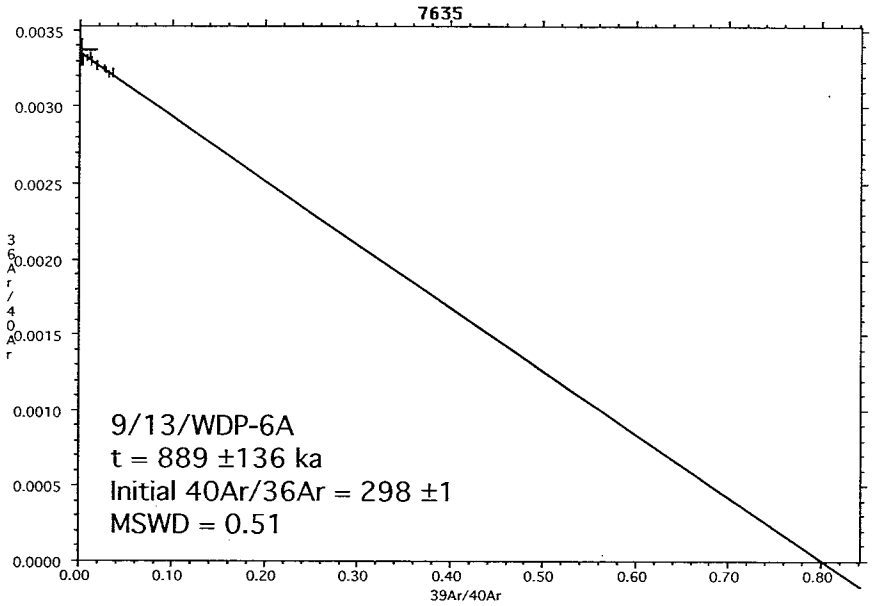
7635
9/13/WDP-6A
t = 889 ±136 ka
Initial 40Ar/36Ar = 298 ±1
MSWD = 0.51
36Ar/40Ar
39Ar/40Ar

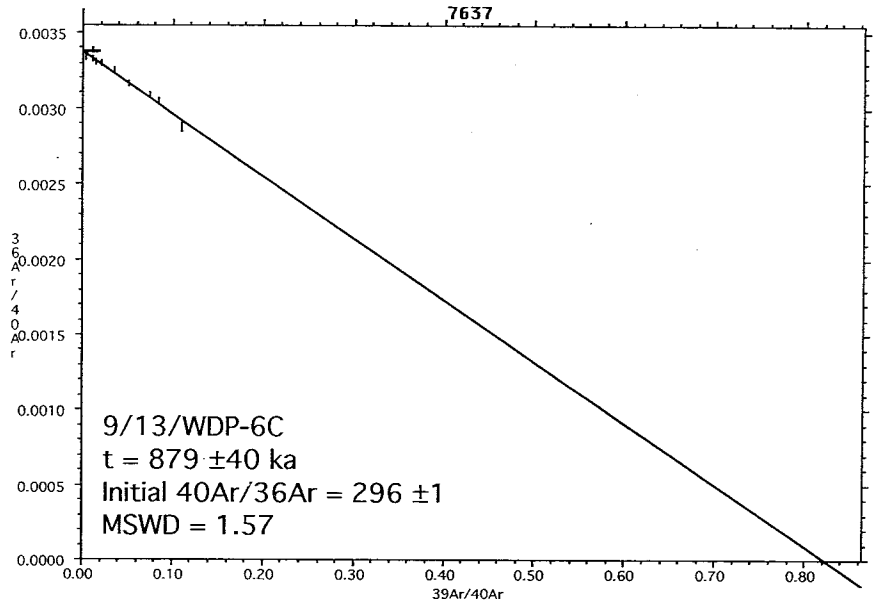
7637
9/13/WDP-6C
t = 879 ±40 ka
Initial 40Ar/36Ar = 296 ±1
MSWD = 1.57
36Ar/40Ar
39Ar/40Ar

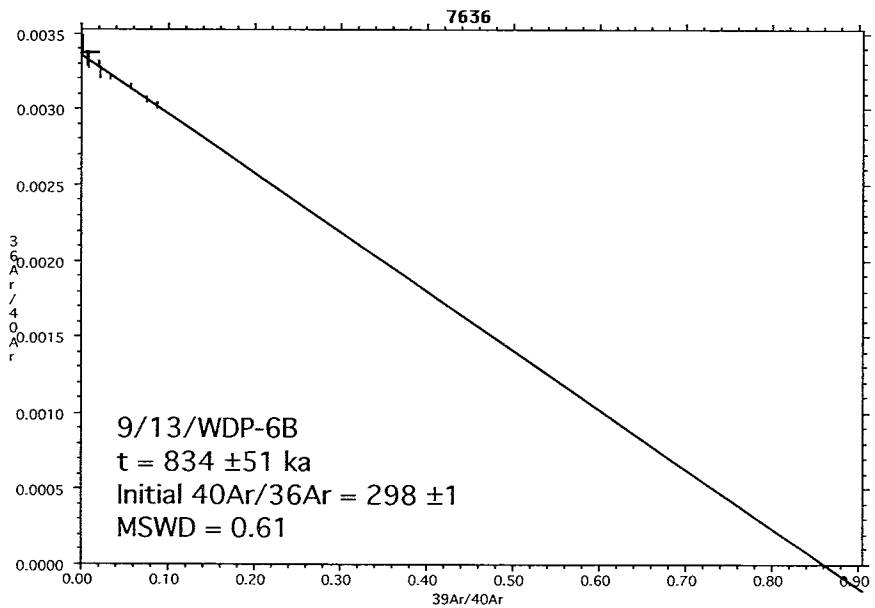
7636
9/13/WDP-6B
t = 834 ±51 ka
Initial 40Ar/36Ar = 298 ±1
MSWD = 0.61
36Ar/40Ar
39Ar/40Ar

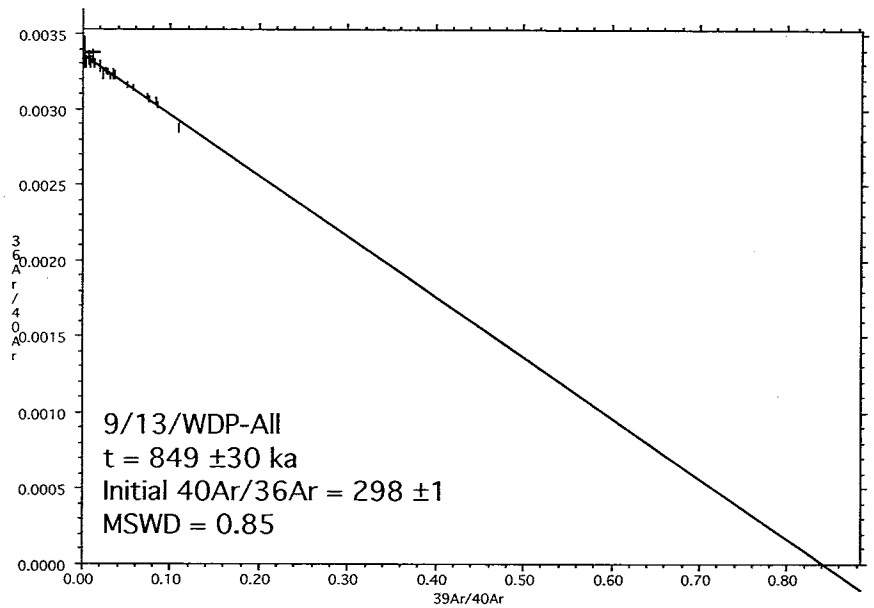
9/13/WDP-All
t = 849 ±30 ka
Initial 40Ar/36Ar = 298 ±1
MSWD = 0.85
36Ar/40Ar
39Ar/40Ar

APPENDIX 1 - 3B

Table 1- Evaluation of faults in the Mayfield, Soldier Mountain, Soldier Creek, and Rodney Ledge fault zones along the PGT pipeline trench, Modoc Plateau, California.
Page, W.D.

Table 2- Dated Basalt flows in the Modoc Plateau Near Burney, California.
Page, W.D.

TABLE 1

EVALUATION OF FAULTS IN THE MAYFIELD, SOLDIER MOUNTAIN, SOLDIER CREEK, AND ROCKY LEDGE FAULT ZONES ALONG PACIFIC GAS TRANSMISSION 401 PIPELINE, MODOC PLATEAU, CALIFORNIA

MP[1]	FAULT OR FEATURE[2]	TYPE OF FAULT	AGE OF MOST RECENT FAULTING (Evaluated from the construction trench; see Figures 1-3-1 and -2, and 1-6-1 and -2)	EST. MAX. VERT. OFFSET[3] (FT)
MAYFIELD FAULT ZONE				
45.61	**Fault east of Indian Spring fault**	Probable normal fault, down on west	Late Pleistocene Air photo lineament in late Pleistocene basalt of Yellowjacket Butte [Y] appears to be due to warping over a fault below the basalt flow. No fault is evident in trench.	< 3
47.27	**Indian Spring Fault**	Normal fault, down on west; .	Late Pleistocene Fault scarp in Tertiary volcanic bedrock [Tv] is moderately degraded; no prominent nick point occurs in Tv on Tuft Creek to south. Possible Holocene shears in Tv in trench, but overlying late Pleistocene colluvium not faulted. Late Pleistocene Yellowjacket Butte basalt flow [Y] that is at the base of the scarp is faulted to southeast of trench; this scarp may be formed by a flow pull-at the trench because it appears to match with similar pull-away scarp in the same basalt at MP 47.6.	< 3
47.72	Air photo linear	Possible antithetic fault or pressure ridge	Late Pleistocene Evidence for a fault here is equivocal. Feature may be a pressure ridge.	< 3 Small displace-ment if feature is fault
48.55	**Tuft Creek Fault**	Normal fault down on west	Holocene Holocene (?) colluvium is in vertical contact with sheared Tertiary volcanic bedrock in trench. The prominent fault scarp in late Pleistocene Yellowjacket Butte basalt flow [Y] is undegraded to weakly degraded and partly vegetated; nick points in basalt in both present channel and in abandoned channel of Tuft Creek attest to multiple displacements in late Pleistocene.	3 to 6
49.03	**Fault north of Julie Glover fault**	Normal fault, down on west	Holocene Thick Holocene (?) colluvium in trench fills the inflection at the base of the slope that is underlain by Tertiary volcanic bedrock; base of slope lies on projection with a fault in late Pleistocene Yellowjacket Butte basalt flow [Y] to the west; fault scarp is weakly to moderately eroded and partly vegetated.	0 ? Fault appears to be dying out to south.

MP[1]	FAULT OR FEATURE[2]	TYPE OF FAULT	AGE OF MOST RECENT FAULTING	EST. MAX. VERT. OFFSET[3] (FT)
49.54	**Julie Glover Fault**	Normal fault, down on west	Holocene Late Pleistocene-Holocene (?) colluvium, which lies on projection of the fault to the trench, is not faulted or sheared. To west of pipeline a fault scarp in the late Pleistocene Yellowjacket Butte flow [Y] is very prominent scarp that is undegraded but covered by lichen, moss and locally trees and brush. The Giant Crater basalt flow, which is C-14 dated at 10,600 BP, is faulted a smaller amount.	< 3 Fault apparently dies out before it reaches pipeline.
50.78 to 50.83	**Mayfield Ice Cave Fault** (north crossing)	Normal fault, down on west	Holocene Giant Crater basalt flow, which is C-14 dated at 10,600 BP, is faulted. The fault scarp in Giant Crater basalt is undegraded, but rocks are covered by lichen and moss.	3 to 6
51.28 to 51.35	**Mayfield Ice Cave Fault** (south crossing)	Normal fault, down on west	Holocene Giant Crater basalt flow, which is C-14 dated at 10,600 BP, is faulted. The fault scarp in Giant Crater basalt is undegraded, but rocks are covered by lichen and moss.	< 3 to 6
58.3	Air Photo lineament near Adobe Flat	Pressure ridge, possible fault, down on east	Holocene The low and weak scarp in Giant Crater basalt flow, which has been C-14 dated at 10,600 BP, is undegraded but rocks are covered by lichen and moss.	< 3
SOLDIER MOUNTAIN FAULT ZONE				
69.19	**Fall River Fault** (east 3 branch of Soldier Mt. zone)	Shear zone	Middle to late Pleistocene (?) Shearing in Pliocene diatomite that is overlain by unfaulted late Pleistocene/Holocene colluvium/alluvium.	< 3
69.48	**Soldier Mountain Fault (east 2 branch)**	Normal fault, down on east	Middle to late Pleistocene (?) Middle to late Pleistocene basalt flow [P] and overlying Pliocene diatomite is sheared and faulted. The overlying late Pleistocene/Holocene colluvium is not faulted.	< 3
69.96	**Soldier Mountain Fault (east 1 branch)**	Normal fault, down on east	Middle to late Pleistocene (?) Middle to late Pleistocene basalt flow [P] is tilted to east over the fault and is faulted.	< 3
70.21	**Soldier Mountain Fault**	Normal fault @ 70.23, down on east; thrust fault @ 70.21, down on east	Middle to late Pleistocene The fault scarp is moderately degraded in Middle Pleistocene basalt flows. Late Pleistocene basalt flow [P] and associated alluvial sediments are sheared and faulted at base and lower part of scarp. Late Pleistocene colluvium over fault is not faulted.	6

MP[1]	FAULT OR FEATURE[2]	TYPE OF FAULT	AGE OF MOST RECENT FAULTING	EST. MAX. VERT. OFFSET[3] (FT)
SOLDIER CREEK FAULT ZONE				
71.38	**Soldier Creek Fault, east 3 branch**	Oblique slip fault, down on west, lateral direction unknown.	Holocene Sheared and faulted late Pleistocene colluvium and soil are exposed in trench. The low fault scarp in early Pleistocene basalt flows (the top flow has an Ar-Ar date of 1.22 ± 0.09 million years) is moderately to highly degraded. The shearing in the soil and basalt suggests that the fault has a significant component of lateral slip.	< 3
71.90	**Soldier Creek Fault, east 2 branch**	Normal fault, down on west	Late Pleistocene Shears and faulting are present in diatomite and older colluvium. Late Pleistocene alluvium and colluvium are not faulted.	< 3
71.99	**Soldier Creek Fault, east 1 branch**	Normal fault, down on east	Late Pleistocene Late Pleistocene colluvium is not faulted. Several faulted and sheared colluvial wedges are evident in road cut to west of trench; these indicate multiple events of 4 to 5 feet each in late Pleistocene.	4 to 5
72.14 to 72.20	**Soldier Creek Fault**	Oblique slip fault, down on west, lateral direction unknown.	Holocene Large, weakly to moderately degraded, fault scarp in Pleistocene volcanic flows attests to multiple events in the late Quaternary. The fault is part of the north extension of the Hat Creek fault zone that is a late Pleistocene and Holocene fault (Muffler and others, 1994). At MP 72.20 the late Pleistocene colluvium and soil exposed at base of slope in trench is sheared, folded and faulted, but vertical displacement is < 3 feet. The shearing suggests that the fault has a significant component of lateral slip. At MP 72.14 late Pleistocene colluvium that overlies a colluvial wedge is not faulted, but vertical displacement there is 4 to 5 feet.	4 to 5
LAKE BRITTON LANDSLIDE				
72.38 to 73.86	**Lake Britton Landslide**	Large landslide (~4 sq. km) The pipeline is in the eastern side of the slide.	Middle to late Pleistocene Late Pleistocene colluvium and soil that is unfaulted overlie the head-scarp faults and occupy the low hollows on the slide, indicating only one slide movement in the late Pleistocene.	

MP[1]	FAULT OR FEATURE[2]	TYPE OF FAULT	AGE OF MOST RECENT FAULTING	EST. MAX. VERT. OFFSET[3] (FT)
ROCKY LEDGE FAULT ZONE				
74.69 to 74.76 ±	**Lake Britton Fault**	Normal fault, down on east	Middle to late? Pleistocene Diatomite that is older than the Rocky Ledge basalt and an older colluvium and alluvium are extensively faulted. Thick late Pleistocene colluvium that overlies the main fault in the adjacent right–of–way cut is unfaulted. Late Pleistocene/Holocene (?) colluvium overlies the northern splays and is unfaulted in the trench. The fault scarp in diatomite and tephra sandstone is severely eroded.	6
75.94	**Arkright Flat Fault**	Normal fault, down on west	Late Pleistocene Fault scarp in Rocky Ledge basalt is weakly degraded. The basalt is tilted at trench. Possible Holocene fracture fill occurs near base of scarp in late Pleistocene colluvial wedge.	< 3; Displacement is 6 feet in older deposits.
76.45	**Cassel Fault**	Normal fault, down on east	Late Pleistocene Fault scarp in Rocky Ledge basalt is weakly degraded. The basalt is tilted at trench. Late Pleistocene colluvial wedge is not faulted or sheared.	6
76.90	**Old Lumber Mill Fault**	Normal fault, down on west	Late Pleistocene Fault scarp in Rocky Ledge basalt is weakly degraded. Possible Holocene fracture fill occurs in late Pleistocene colluvial wedge (2 wedges?).	< 3 Older displacement on fault is about 6 feet.
77.60	**Four Corners East Fault**	Normal fault, down on west	Late Pleistocene Fault scarp in Rocky Ledge basalt is weakly degraded. Possible Holocene fracture fill in late Pleistocene colluvial wedge. The basalt is tilted at trench.	< 3 ? Deformation at fault crossing is mostly warping.
77.96 to 78.00	**Four Corners West Fault**	Normal fault, down on east (main splay @ 77.95; west splay @ 78.0)	Late Pleistocene Fault scarp in Rocky Ledge basalt is weakly degraded. At MP 77.95 late Pleistocene colluvial wedge and fill at base of slope is not faulted or sheared. The basalt is tilted between the main and west splays. At MP 78.0 a graben is present to south of trench. Late Pleistocene colluvial fill is not faulted or sheared in trench.	6
79.35	**Rocky Ledge Fault** (east strand)	Normal fault, down on east	Late Pleistocene/Holocene ? Fault scarp in Rocky Ledge basalt is undegraded to weakly degraded. Possible weak shears occur in late Pleistocene colluvial fill at base of scarp. The basalt is tilted between the east and west strands.	1

MP[1]	FAULT OR FEATURE[2]	TYPE OF FAULT	AGE OF MOST RECENT FAULTING	EST. MAX. VERT. OFFSET[3] (FT)
79.67	**Rocky Ledge Fault** (west strand)	Normal fault, down on east	Late Pleistocene Fault scarp in Rocky-Ledge basalt is undegraded to weakly degraded. Late Pleistocene colluvial fill is not faulted or sheared. The basalt is tilted between the east and west strands.	1

Notes:

1. Mileposts are measured south from the Oregon border near Tule Lake.

2. The names of the faults are those generally those used by the California Division of Mines and Geology. Individual faults within a wider fault zone and new faults identified in this evaluation have been given names from local geographic features.

3. The potential vertical displacement at the crossing is estimated from two factors: the maximum displacement that has generally occurred in late Pleistocene and Holocene on faults in the Modoc Plateau and evidence of displacement from the pipeline trench. The amount varies by fault and by the location of the crossing with respect to the ends or central part of the fault.

TABLE 2

DATED BASALT FLOWS IN THE MODOC PLATEAU NEAR BURNEY, CALIFORNIA

Lava Flow	Type of Date	Date	Reference
Hat Creek Rim flow, top flow	K-Ar K-Ar Ar-Ar (plateau date)	1.645 ±0.35 Ma 4 to 1.8 Ma 1.009 ±0.078 Ma	USGS, Clynne, 1993, oral communication Longshore, 1987 oral communication PG&E Page and Renne, 1994
Top flow, "Plateau" between Saddle Mountain and Soldier Mountain	Ar-Ar (plateau date)	1.219 ±0.89 Ma	PG&E 8/4/92 WDP-1 Page and Renne, 1994
Fall River Mills flow, north of Pit River canyon	Ar-Ar (isochron date)	945 ±46 ka	PG&E Page and Renne, 1994
Flow within Hat Creek graben, Highest inset flow below Hat Creek Rim, southwest of Pit River Canyon	Ar-Ar (isochron date)	889 ±136 ka 834 ±51 ka 879 ±40 ka	PG&E Page and Renne, 1994
Sam Wolfin Spring Flow, second highest flow within Hat Creek graben, below Hat Creek Rim, southwest of Pit River canyon	Ar-Ar (plateau date)	846 ±47 ka	PG&E Page and Renne, 1994
Bidwell Bench flow below rim within graben	K-Ar	920 ±20 ka	USGS, Clynne, 1993, personal communication
Older flow below Tuft Creek flow, top of Indian Spring Mt. fault scarp,	Ar-Ar (plateau date)	840 ±40 ka	PG&E 6/16/92 WDP-3 Page and Renne, 1994
Rocky Ledge flow (?) flow inset into graben east of Burney and north of Highway 299	Ar-Ar (plateau date)	150 ±20 ka	PG&E 6/30/92 GM-5 Page and Renne, 1994
Yellowjacket Butte flow north of Indian Spring Mt.	Ar-Ar (plateau date)	130 ±20 ka	PG&E 7/1/92 WDP-6 Page and Renne, 1994
"Popcorn Cave" flow south of McArthur	Estimate based on comparison of geomorphology with other flows in the Modoc Plateau	< 30 ka < 50 ka	Woodward-Clyde Consultants, 1987 This study
Hat Creek basalt at Lost Creek	Ar-Ar Flow overlain by glacial outwash from Lost Cr. and by lava of Cinder Butte (Ar-Ar dated at 37 ±5 ka)	~30 ka 23 ±16 ka and 89 ±68 ka	Clynne, 1995 written communication

Lava Flow	Type of Date	Date	Reference
West Prospect Peak older flow, east of Mt. Lassen	Flow not glaciated	~15 ka	estimate based on vegetation cover, Woodward-Clyde Consultants, 1987
Giant Crater flow	C-14	10,600 years	Donnelly-Nolan and others, 1989; PG&E
Flow NE of Timbered Crater	Ar-Ar (plateau date)	~20 ±120 ka	Page and Renne, 1994
Baked sediments NE of Timbered Crater	C-14 charcoal from baked soil	10,400 ±60 10,570 ±70	PG&E 6/18/92 WDP-5, WDP-7
Cinder Cone Basalt at Snag Lake	C-14	510 ±160 ka	Luedke and Smith, 1981

Origin and features of Mayfield Ice Cave, Siskiyou County, California

By Janet M. Sowers and Gary D. Simpson

William Lettis & Associates, Inc.
1777 Botelho Drive, Suite 262
Walnut Creek, CA 94596

ABSTRACT

Mayfield Ice Cave is a small fissure cave formed in basalt along the Mayfield fault near the base of the western flank of Indian Spring Mountain in Siskiyou County, California. The cave is approximately 125 feet long, 10 to 20 feet wide, 30 feet deep, and is oriented N 45° E. The cave is formed in basalt of the Giant Crater Flow of the Medicine Lake volcano, along a fissure at the base of the scarp of the Mayfield Fault. The cave passage appears to have developed in the plane of the fault and may owe its existence, at least in part, to movement on the fault. The Mayfield Fault is of Holocene age, and offsets lavas dated at 10,600 years (Donnelly-Nolan and others, 1990). We surveyed and inventoried this cave to assess the potential impact on the cave of Pacific Gas & Electric Company's proposed PGT pipeline that passes a few hundred feet from the cave entrance.

Mayfield Ice Cave was named in 1873 by J. H. Mayfield. Both he (in 1887) and later Julia Glover (in 1892), made attempts to develop the cave for tourists. Ice deposits are a significant feature of the cave. Some ice features, such as icicles, frost, and ice draperies may be seasonal. Others, such as ice pools, are probably permanent features of the cave. The ice is an important resource both as a source of water for wildlife, and as a curiosity for visitors. In the past it may have been used as a source of water for native peoples. The cave contains a compacted deposit, 4 to 7 feet thick, of charcoal, sticks, and stones, which may indicate prehistoric human use of the cave. It also contains a loose pile of larger sticks, stones, and charcoal and a wooden ladder, which indicate historic use.

I. INTRODUCTION

A. Purpose and scope of the investigation

Mayfield Ice Cave is located in a lava plain a few hundred feet west of a Pacific Gas & Electric Company (PG&E) natural gas supply pipeline, constructed in 1993. This study was undertaken in 1991 at the request of PG&E to 1) determine the exact position of the cave relative to the proposed pipeline, 2) identify and characterize the features of the cave, 3) assess the impact of pipeline construction on the cave, and, 4) if necessary, make recommendations for mitigation of impacts resulting from construction or operation of the pipeline.

Our investigation, conducted in May, 1991, included a brief review of existing information, a compass and tape survey from the pipeline to the cave and through the major passages of the cave, and an inventory of geologic, biologic, cultural, and hydrologic features of the cave. This article is a summary of the origin and features of the cave revealed in the course of our investigation.

B. Setting

Mayfield Ice Cave is located in Siskiyou County, California on the south flank of the Medicine Lake Volcano, at the base of Indian Spring Mountain, in the NE 1/4 of Sec 7, T 40 N, R 4 E (Figure 1). The cave is formed in a fissure in a rugged basalt plain of the Giant Crater flow, within the Ponderosa pine woodland of the Modoc National Forest. Other similar deep fissure caves are found in the immediate vicinity, though Mayfield Ice Cave is the largest. In addition, hundreds of lava tube caves are found within the Giant Crater Flow and other basaltic flows of the Medicine Lake volcano. Lava tube caves are the remnants of conduits that carried flowing lava during the eruption. Mayfield Ice Cave does not share this origin.

Mayfield Ice Cave was named in 1873 by J. H. Mayfield who found the cave while searching for one of his cattle. Both he (in 1887) and later Julia Glover (in 1892), made attempts to develop the cave for tourists. Both had planned to build a hotel, but apparently neither plan was carried out. Mr. Mayfield built the Mayfield Road in part to provide access to the cave. Glover had a homestead at Julia Glover Flat. A rough hewn wooden ladder is present in the cave and may date from that period. (McCloud River Pioneer, 1889-1893, and Mt Shasta Herald, 1887).

C. Methods

We conducted a three-dimensional survey of the location and dimensions of the cave relative to mile marker 50-34 of PG&E's existing pipeline 400 (Fig 2). We used a 100-foot fiberglass tape, a Suunto compass, and a Suunto clinometer. At each station we measured the distance from the previous station, the bearing from the previous station, reading both a backsight and a foresight, and inclination from the previous station, both backsight and foresight. In addition, inside the cave we measured passage dimensions and constructed cross sections at most stations. We plotted the line transect and drew in the cave walls and major features as we progressed through the cave. Final drafted maps and profiles are shown in Figures 2, 3, and 4.

Due to problems with the magnetism of the basalt, our backsight and foresight azimuth readings for the above ground portion of the traverse were difficult to match. Taking into account the error determined from maximum and minimum azimuth readings, location of the cave could be off by as much as 8 feet with respect to the pipeline. However, we had little problem inside the cave with basalt magnetism, so the survey within the cave is probably accurate to within 1 foot. Loop closure through the cave itself (Stations 5 through 14) shows

error of 0.1, 0.4, and 0.1 feet in the x, y, and z directions respectively.

To inventory the features of the cave, we used a cave inventory form developed by the first author for evaluation of caves at Lava Beds National Monument. Topics included in the inventory are location, extent, biology, hydrology, geology, cultural resources, paleontology, and visitors.

II. ORIGIN AND FEATURES

A. Physical and geologic features

Mayfield Ice Cave is approximately 125 feet long, 10 to 20 feet wide, and 30 feet deep (Figures 3 and 4), and is oriented in a plane that strikes N 45° W and dips 40-90° to the SE. The cave has three entrances, located along the base of a 20-foot-high, northeast-trending escarpment. The easiest way to enter the cave is through the South Entrance. The Central and North Entrances are steeper and more difficult to traverse. We found that no passages extend beneath the PG&E gas pipeline corridor (Figure 2); all passages lie 200 to 300 feet from the pipeline.

The interior of the cave is basalt, generally devoid of lava formations or secondary mineralization. The NW wall of the cave is primarily a slope of breakdown blocks, and the SE wall is primarily in-place rock. The entire floor of the cave is covered with breakdown. The opening of the fissure may also have exposed a small portion of a lava tube. The southeast wall of the cave at station 7 resembles the wall of an intact lava tube (see station 7 cross section on Figure 4).

B. Biologic, Hydrologic, and Cultural features

The cave is set within the Ponderosa pine, Juniper, and Mountain mahogany woodland. At the entrance to the cave, primitive plants characteristic of moderately high moisture conditions, such as mosses and ferns, are found. Almost all the cave is located in the twilight zone. Total darkness is found only in the extreme lower levels at the northeast end of the cave.

Evidence was seen for only one type of vertebrate, the pack rat (Neotoma), in the cave. This evidence consisted of small amounts of scat on tops of boulders, and an accumulation of organics similar to that typically found beneath pack rat nests located on the slope in the far northeastern chamber. This organic material was coated with about 1 cm of clear ice, so could not be examined closely. We speculate that the nest itself may be located on a ledge in the ceiling. No evidence for use of the cave by bats was seen.

The cave is likely to be important to other wildlife on a seasonal basis. There are few water sources such as streams or lakes in the area, thus, the cave is probably an important source of

water during the summer months. We speculate that the present cover of ice in the cave may be obscuring evidence of summertime animal use. We surveyed the cave in May when much of the winter ice was still present.

We did not conduct an invertebrate survey, however, invertebrate populations are likely to be significant in this cave. The abundant moisture and organic material in this cave would provide an excellent habitat for invertebrates.

The cave contains significant ice deposits, some of which persist in the cave all year. Only a relatively small percentage of the numerous caves in the area contain permanent ice. Cold air is trapped in the cave in the winter and, because the cave is fairly deep and has little air circulation, this cold air is not replaced by warm air in the summer. Thus, water from rain or snow which enters the cave encounters the cold air and freezes. Ice then accumulates on the walls and in pools on the floor of the cave.

Two major pools of ice were noted, totalling about 50 square feet in areal extent. These pools probably persist all year, though they may partially melt in the summer. In addition, the cave contained many icicles, coatings of ice on the floor and slopes, ice draperies, and ice stalagmites. Many of these formations were melting and falling off the walls during our visit, especially in the higher parts of the cave. We expect that these formations are seasonal, except perhaps those in the far northeastern room, which is deeper and has more limited air circulation. We surveyed the cave in May when the ice would be expected to be past its winter maximum.

A thick charcoal deposit may be prehistoric in age and culturally significant. This deposit is located in the southwest part of the cave (at Station 8) and is 4 to 7 feet thick (Figure 4). It consists of compacted fine and coarse charcoal, charred logs and sticks, and stones. The top of the deposit is covered with a thin layer of ice, but the side of the deposit is eroding and cascades down the chute into the lower room beyond Station 9. We speculate that this deposit may represent an accumulation of coals and heated rocks which native peoples placed on the ice to melt it for water. Lack of soot on the ceiling of the cave suggests that the charcoal did not come from fires built inside the cave.

Because there are few surface streams or springs in this region, the cave may indeed have been an important water source. However, if people did obtain water from this part of the cave, this passage must have contained more ice then than it does today. Today the ice in the southwestern part of the cave consists of thin coatings on the floor and icicles, all of which appear to be seasonal. We were informed by Jim Wolff of the US Forest Service in McCloud that an archaeological site record exists for a surface site near the cave. This surface site may be related to prehistoric use of the cave.

A second deposit, immediately NE of Station 9, may be historic or modern in age. It is a loose pile of charred sticks, logs, stones, and chunks of charcoal. Historical or modern age is indicated by its loose character and by the presence of a charred piece of cut lumber.

No paleontologic deposits were noted. However, we cannot rule out the possibility that such deposits exists beneath the ice. Given the age of the basalt, any such deposits would be no older than 10,600 years.

Mayfield Ice Cave is well known locally and easy to find. It is shown on U. S. Geological Survey topographic maps, and a sign and a trail lead to the cave entrance. Ice formations in the winter and cool temperatures in the summer combine to attract visitors. In addition, traversing the cave passages is a fun, adventurous experience for many visitors. Visitors must climb, crawl, and negotiate slippery, or uneven floors in the semi-darkness.

Evidence of use includes trash (soda and beer cans) and yellow spray paint at the North Entrance. Ice covering the floor and walls may have obscured further evidence of use. Regardless, the cave is not heavily vandalized. No signatures or graffiti were noted inside the cave.

C. Geologic Origin

Mayfield Ice Cave is atypical of caves formed in basalt. It is not a lava tube, or former conduit for lava. Rather it formed from the opening of a fissure in the ground. The west side of the fissure is downdropped approximately 20 feet, and the edge of the east side block appears tilted westward along a small fissure above the cave, forming the roof of the cave (Figure 3).

The fissure has two possible origins. First, the fissure may have formed from the drainage of hot lava from beneath an already cooled basalt crust, causing collapse and large extensional fissures to open up in the crust. Such extensional cracks are common in basaltic flows. However, this mechanism alone does not account for the coincidence of the cave passage geometry with the Mayfield fault.

Second, and more plausibly, the fissure may have formed from movement on the Mayfield Fault. The Mayfield Fault is mapped by Donnelly-Nolan (shown on CDMG preliminary special studies zone maps maps, 1990) at the base of the escarpment at the cave entrance. The fault is a striking feature on aerial photos and is significantly more prominent and continuous than extensional cracks seen elsewhere in the flow. The fault escarpment runs NW-SE, parallel to the cave passage, and the cave passages appear to lie in the plane of the fault.

The cave fissure may also have formed from a combination of cracking and faulting. Cracking that formed during lava drainage and collapse could have been enlarged and modified by movement on the Mayfield Fault. Presence of a pre-existing extensional crack could help explain the presence of fissure caves here and not elsewhere along the fault.

IV. SUMMARY

Our findings can be summarized as follows:

1) Mayfield Ice Cave is an excellent example of a fissure cave formed along an active fault.

2) The cave contains permanent ice, a relatively unusual occurrence in caves in the area, and probable important water source for animals and, in the past, for people as well.

3) The cave contains a charcoal deposit that may indicate prehistoric and/or historic human use.

4) The cave is of local historical interest and is a recreational site for cavers and the local population.

Acknowledgements

We thank Pacific Gas & Electric Company for funding this project and for permission to include this report in the Friends of the Pleistocene guidebook. Larry Patskowski of PG&E supervised the project, Bill Lettis provided helpful discussions and reviewed the report, and Carolyn Mosher drafted the figures. Historical information was provided by Jim Wolff. William Lettis & Associates, Inc. provided logistical support.

REFERENCES

California Division of Mines and Geology, 1990, Special studies zones preliminary review map, Indian Springs Mountain quadrangle.

Cave Research Foundation and Lava Beds National Monument, 1990, Cave Inventory Form and Handbook: Lava Beds National Monument, Tulelake, CA.

Donnelly-Nolan, 1990, Post-11,000 year volcanism at Medicine Lake Volcano, Cascade Range, Northern California: Journal of Geophysical Research, v. 95, pp. 19693-19704.

McCloud River Pioneer, Bartle, CA, excerpts, comments, and items of general interest, Aug 24, 1889 to Dec 31, 1893.

Mt. Shasta Herald, September 13, 1887.

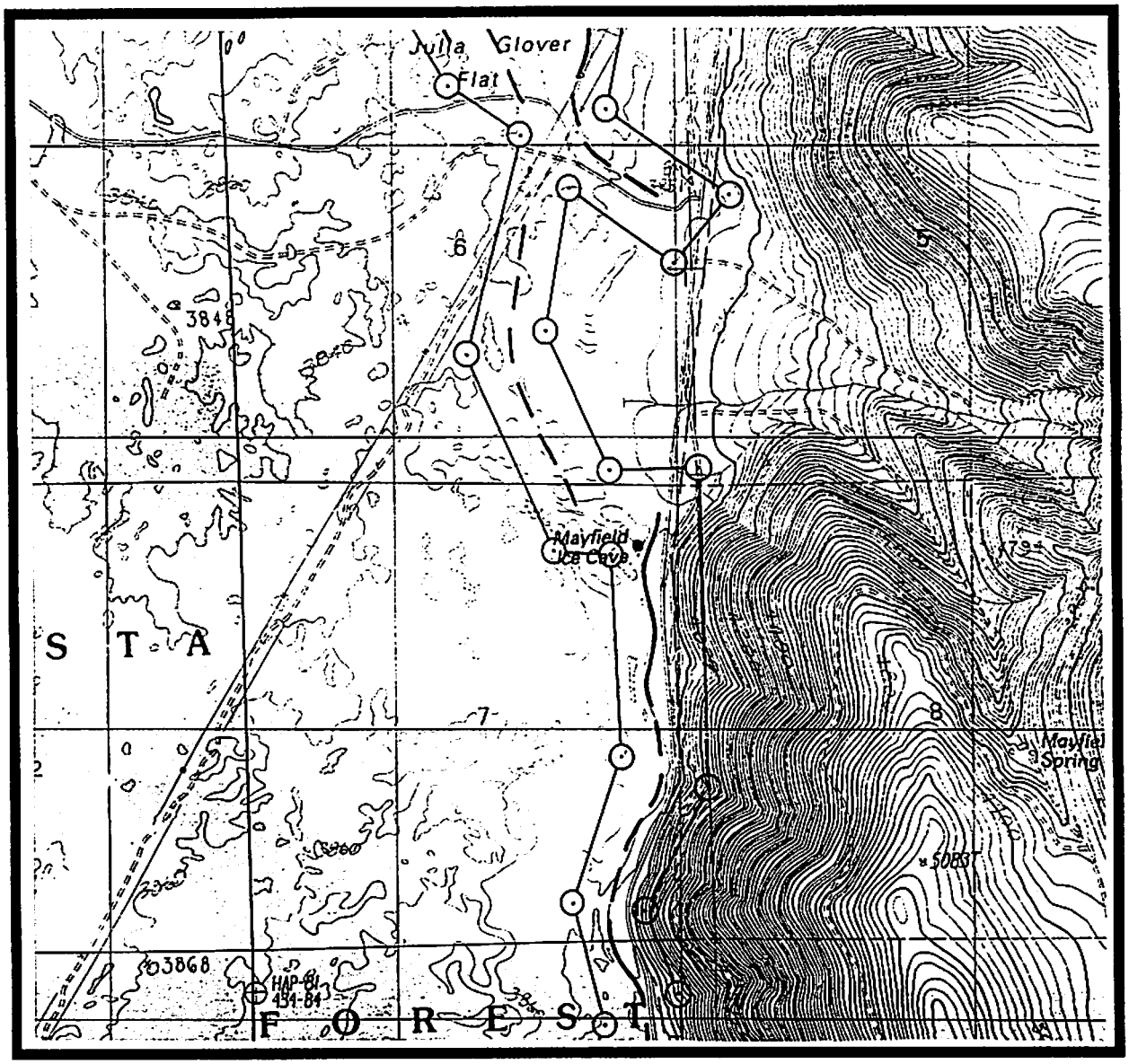

Figure 1: Location of Mayfield Ice Cave showing topography, active faults, and Alquist-Priolo special studies zones. The cave is within the special studies zone along the Mayfield Fault. From CDMG preliminary special studies zone maps, 1990, Indian Spring Mountain 7.5 minute quadrangle. Scale = 1:24,000.

SURVEY AND INVENTORY OF MAYFIELD ICE CAVE PG&E gas pipeline	
William Lettis & Associates	
By: JMS	Date: 6/03/91

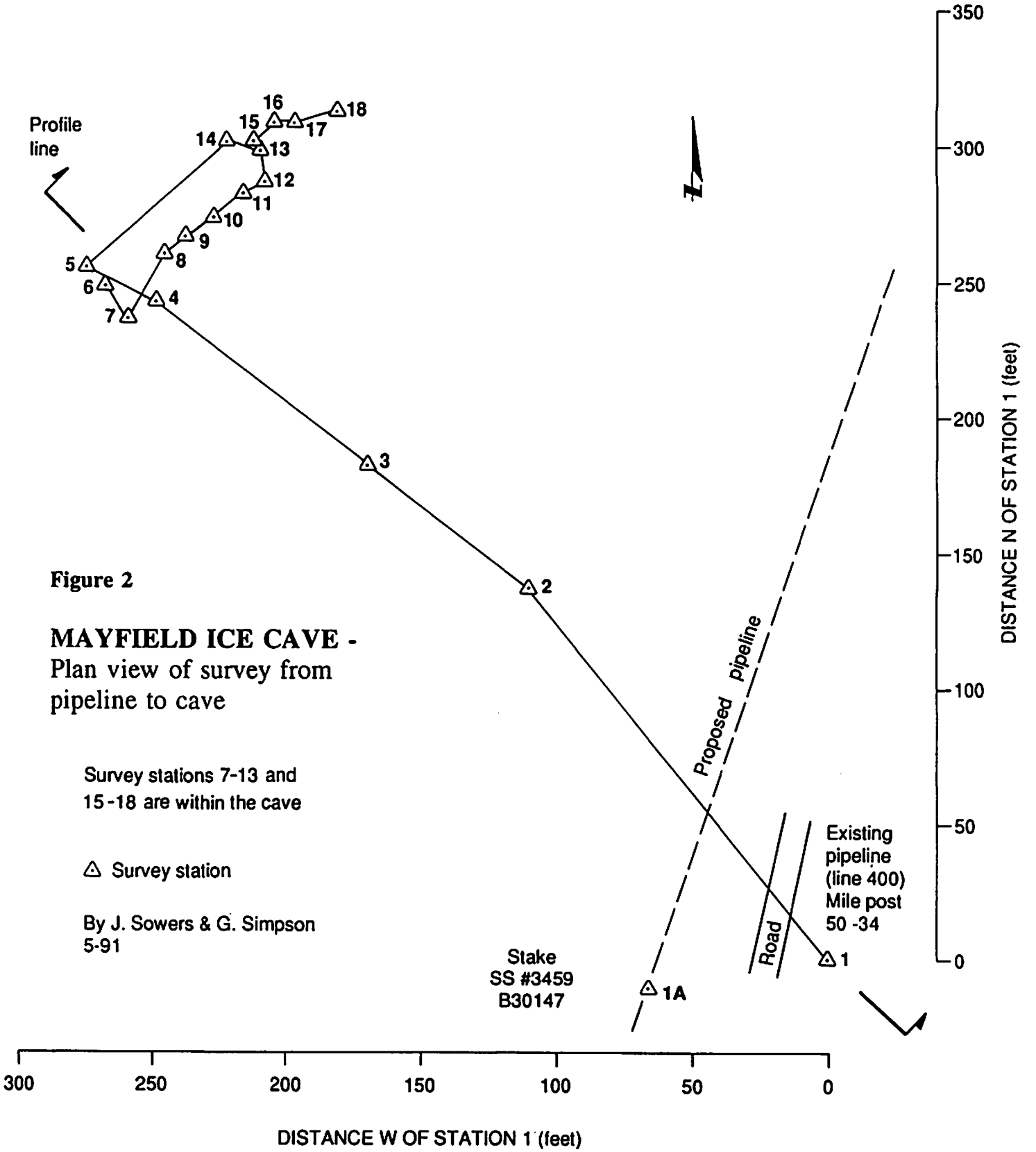

Figure 2

MAYFIELD ICE CAVE -
Plan view of survey from pipeline to cave

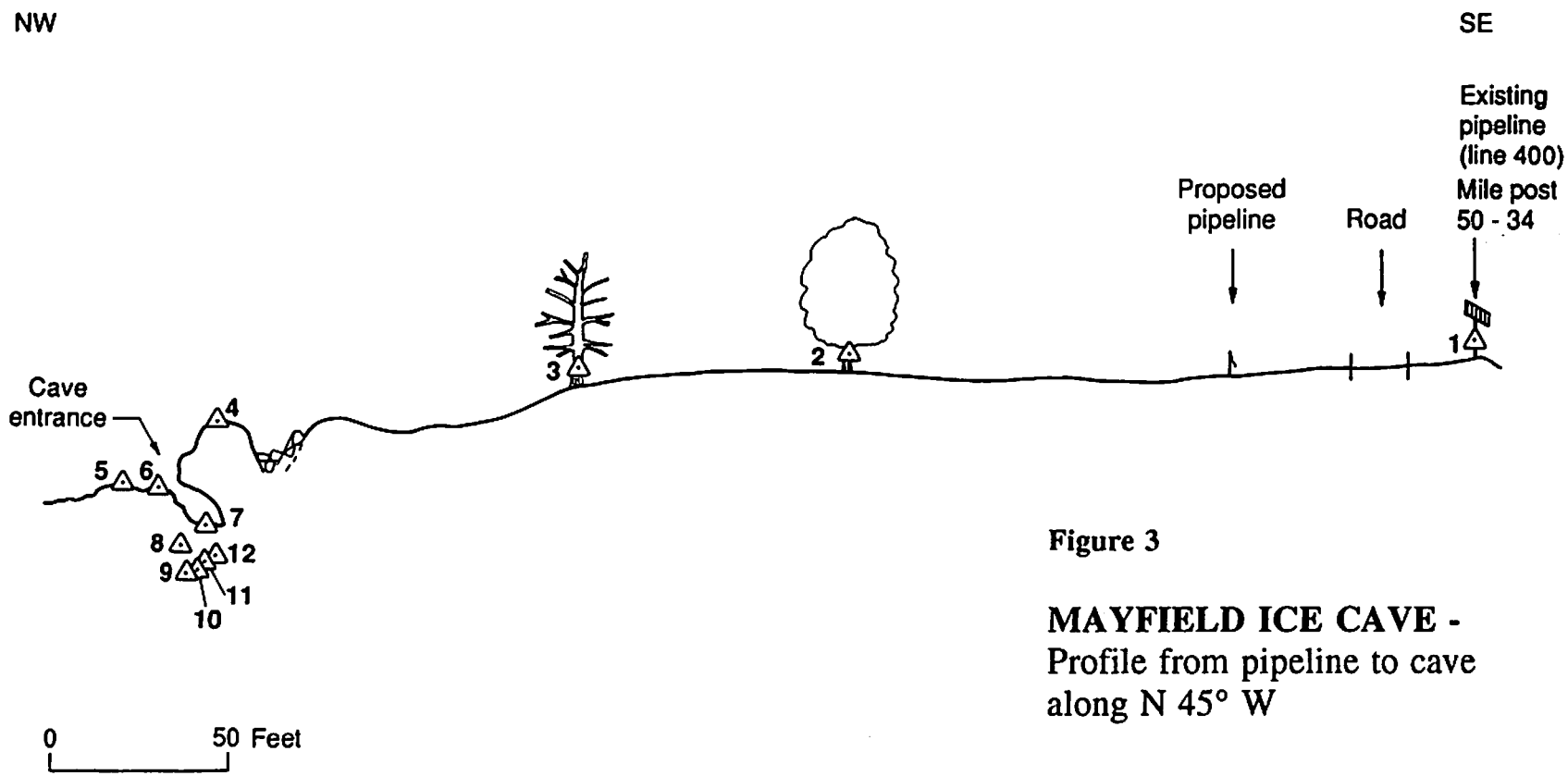

Figure 3

MAYFIELD ICE CAVE -
Profile from pipeline to cave along N 45° W

△ Survey station

By J. Sowers & G. Simpson
5-91

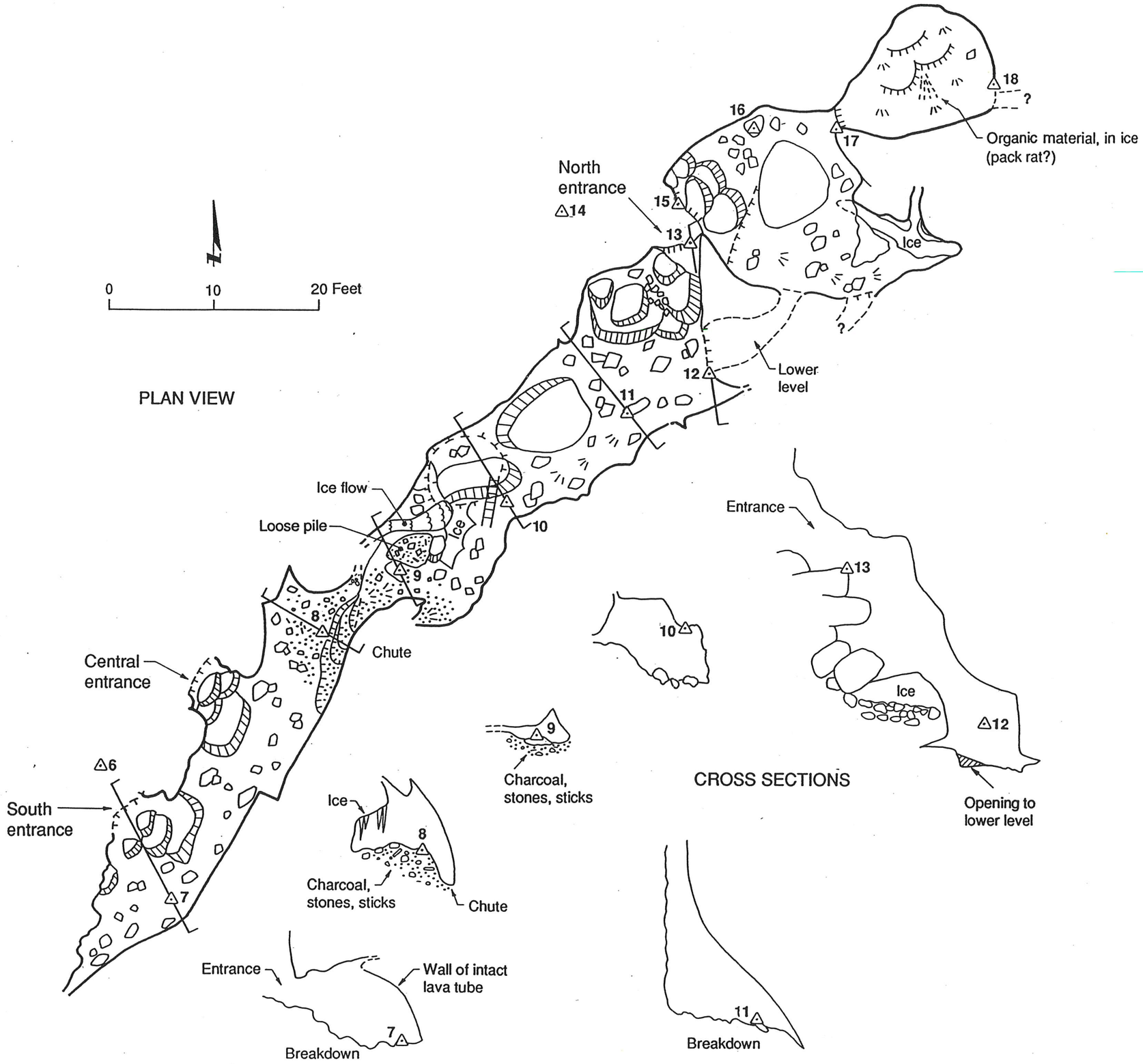

Figure 4

MAYFIELD ICE CAVE
Map and cross sections

- Survey station
- Drop in floor, ticks down
- Drop in ceiling, ticks on lower ceiling
- Sloped floor, lines splay in downslope direction
- Breakdown
- Large breakdown block
- Charcoal
- Wall of underlying passage

Surveyed and drawn May 1991
by J. Sowers and G. Simpson

APPENDIX 1 - 5

A. Evaluation of Risk From Surface Fault Rupture to a Penstock Using the 40Ar/39Ar Dating Technique.

Bachhuber, J., Page, W.D., Renne, P.R.

Evaluation of Risk from Surface Fault Rupture to a Penstock Using the $^{40}Ar/^{39}Ar$ Dating Technique

Jeff Bachhuber, William D. Page, and Paul R. Renne

Introduction

The $^{40}Ar/^{39}Ar$ dating method was applied to assess the risk from fault rupture on the Hat Creek fault to Pacific Gas & Electric Company's (PG&E) Pit 1 penstock in the Modoc Plateau of northeastern California (Figure 1). The 1,700 foot long penstock is a 96 to 129 inch diameter, riveted and welded steel pipe that conveys water from a tunnel to a powerhouse on the Pit River. Geologic mapping for PG&E's penstock safety program identified four subparallel, north-trending faults that crossed under the penstock.

The Pit 1 penstock is located on the east side of the 3 to 5 kilometer-wide Hat Creek graben that is part of the larger tectonic trough separating the Modoc Plateau from the southern Cascade Mountains. Faults crossed by the penstock occur on the east side of the graben along the northernmost part of the Hat Creek fault zone. The Hat Creek fault has down-on-the-west normal displacement and is a major fault that extends for about 40 kilometers from Mount Lassen to just north of the Pit River (Figure 1). South of the Pit River the fault displaces Quaternary and late Pliocene volcanic rocks vertically over 500 meters (Muffler and others, 1994). The California Division of Mines and Geology (CDMG) classifies the Hat Creek fault as Holocene-active south of the Pit River, but has not zoned the faults in the immediate vicinity of the penstock and the Pit River as Holocene-active (Wills, 1991). In the vicinity of the Pit River, scarp heights along the Hat Creek fault decrease northward, and regional strain appears to transfer west (left) to the Soldier Creek fault zone, and east to the McArthur fault (PG&E, 1994).

Hat Creek Fault Near The Penstock

On the north side of the Pit River at the penstock, the traces of the Hat Creek graben faults are defined by linear hillside benches, subtle degraded scarps, aligned topographic saddles, offset Plio-Pleistocene bedrock that is exposed in road cuts and river banks, and vegetation and tonal lineaments (Figure 2). A smaller, 1,500 meter-wide subgraben is nested within the larger Hat Creek graben at the south rim of the Pit River canyon. Fault scarps within the subgraben displace a series of low-potassium, olivine (tholeiite) basalt flows. Three separate flows were differentiated for this study and are designated Q_{v1} (the oldest and highest basalt flow inset within the graben); Q_{v2} (the Sam Wolfin Springs flow); and Q_{v3} (the youngest flow which emanates from the crater field east of Cassel). The individual flows were mapped on air photos and in the field on the basis of variations in vegetation cover, degree of dissection, preservation of flow features, amount of tilting of the flow surfaces, and stratigraphic relationships. Both flows Q_{v2} and Q_{v3} were laterally constrained within the linear subgraben formed by earlier faulting of flow Q_{v1}, indicating that significant displacements had already occurred along the bounding faults prior to extrusion of these later flows (Figures 2 and 3).

The fault splays south of the Pit River are laterally continuous with the faults at the penstock, but are much more pronounced and exhibit greater magnitudes of displacement. The greater prominence of the faults here is partly due to preservation of fault features in the resistant basalt flows as compared to the volcaniclastic rocks north of the river, and in part because the displacements die out northward. Recent channel alluvium and Quaternary stream terrace and landslide deposits in the floor and south wall of the Pit River canyon do not exhibit evidence of fault offsets on air photos.

We measured the cumulative offset across the en-echelon scarps that cut flow Q_{v1} along the east margin of the Hat Creek graben from a profile constructed using 1:24,000-scale topographic maps (Figure 3). The displacement from the Q_{v1} flow surface at the top of the

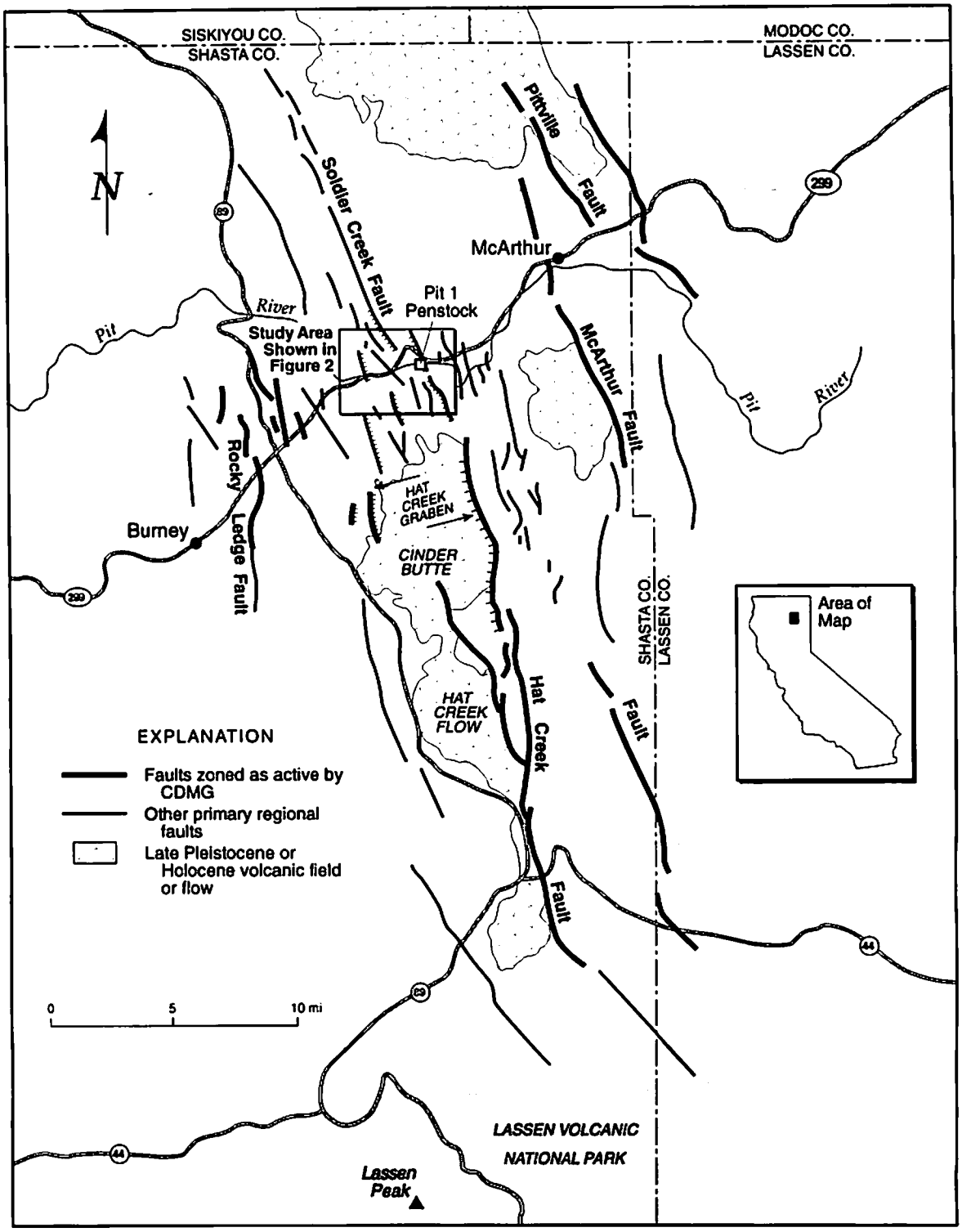

Figure 1. Study area location and regional fault map (modified from Wills, 1991).

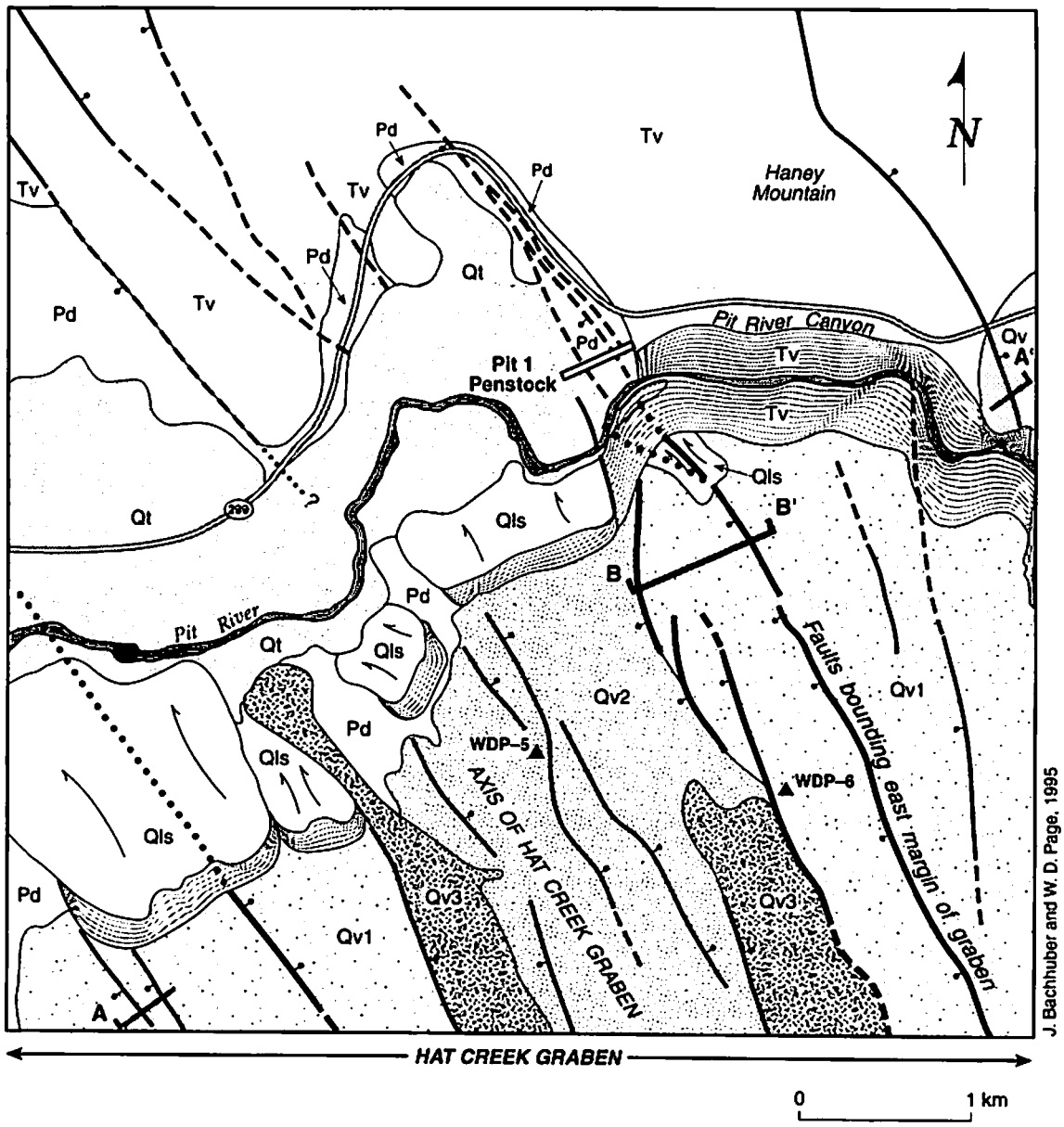

EXPLANATION

Qt – Quaternary stream terraces

Qls – Quaternary landslide (larger features likely Pleistocene)

Qv – Quaternary basalt flows differentiated on basis of geomorphic expression, stratigraphic position, and $^{40}Ar/^{39}Ar$ dates. Approximate dates:

- Qv3 < 0.05 my
- Qv2 ≅ 0.846 my
- Qv1 ≅ 0.867 my
- Qv ≅ 0.945 my

Pd – Pliocene Alturas Formation diatomite and lacustrine/fluvial sediments

Tv – Tertiary volcanic rocks

– Fault, dashed where approximately located, dotted where buried. Ball on downthrown block of fault exhibiting primarily normal displacement. More prominant and active faults are indicated by thicker lines.

WDP-5 – Location of basalt sample submitted for $^{40}Ar/^{39}Ar$ dating

A A' – Location of geologic section

B B' – Location of scarp displacement measured profile

Figure 2. Geologic map of Pit 1 Penstock area and the Hat Creek graben.

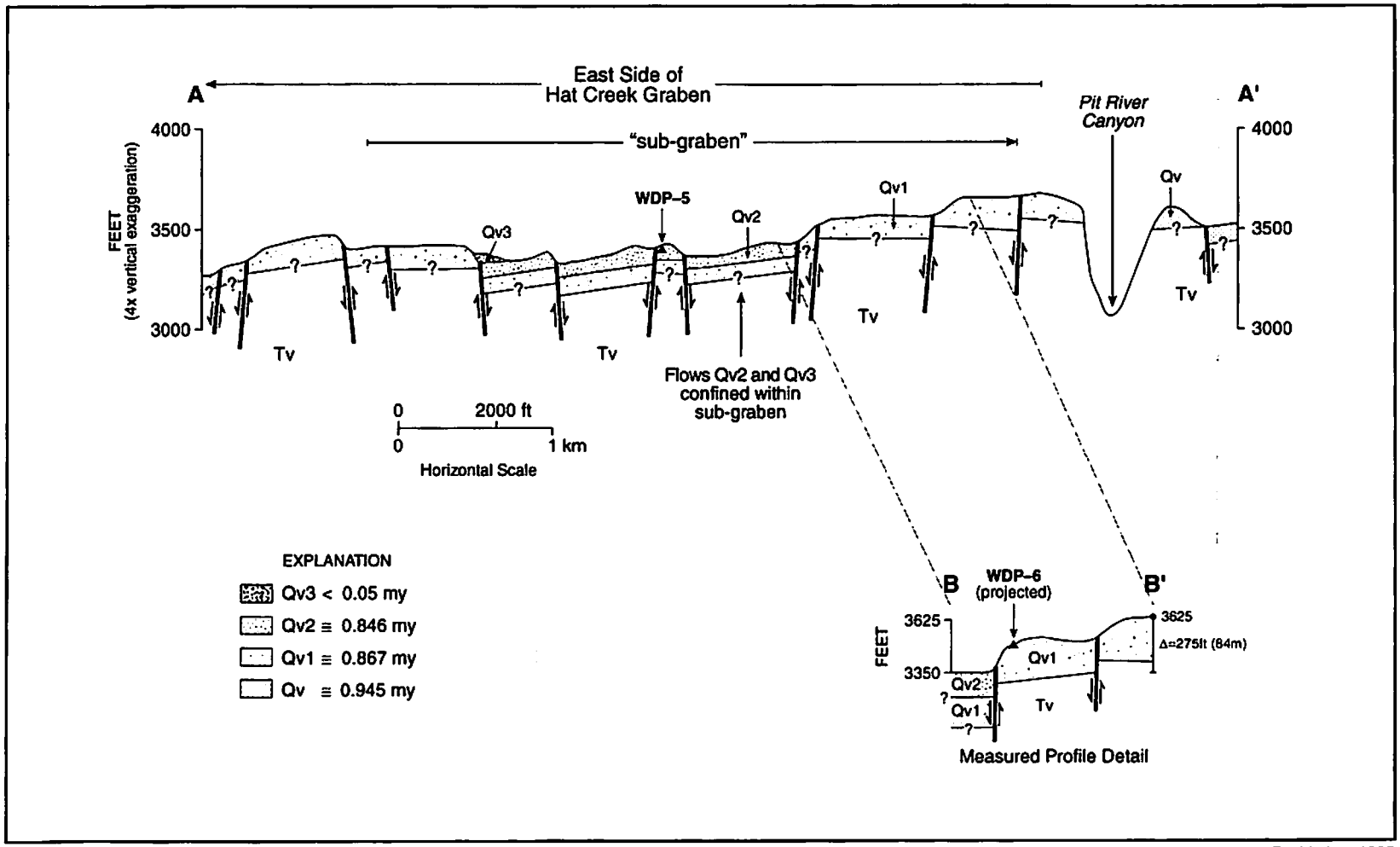

Bachhuber, 1995

Figure 3. Geologic cross sections A–A' and B–B'.

highest west-facing scarp, to the top of flow Q_{v2} at the base of the lowest west-facing scarp, is 84 meters. This is a minimum displacement because the top of flow Q_{v1} is at some depth below the elevation of the base of the exposed scarp, and is covered by flow Q_{v2} that pooled against and obscured the lower portion of the scarp.

$^{40}Ar/^{39}Ar$ Dating Methodology

Previous attempts to date late Quaternary tholeiite basalt flows displaced by the Hat Creek fault using potassium argon (KAr) have not been successful because of the low-potassium content of the flows (Page and Renne, 1994; Muffler and others, 1994). Although thermoluminescence dating of baked soils beneath lavas has proven viable for dating flows at locations elsewhere (Steve Foreman, 1994, personal communication), suitable conditions were not found in the study area to apply this method. Because of these constraints, the $^{40}Ar/^{39}Ar$ method was selected to estimate the ages of the volcanic flows cut by the Hat Creek fault near the Pit River canyon to assess the fault rupture hazard to the Pit 1 Penstock. $^{40}Ar/^{39}Ar$ has been successfully used in other areas to date volcanic rocks, including low-potassium basalts (Renne, this volume).

A suite of hand samples was collected from flows Q_{v1} and Q_{v2} that are exposed near the upper surface of the fault scarps south of the penstock. The samples were selected from layered portions of the flows that exhibited the lowest density of vesicles to minimize potential problems from excessive adsorption of atmospheric Ar. Where present, weathered rinds were removed from the specimens. The samples were labeled in the field and transported to the Berkeley Geochronology Laboratory for analysis.

Sample preparation and analysis followed the procedures outlined by Renne (this volume). Samples were prepared from 40-80 mesh sieve fractions, and were rinsed ultrasonically in HCl and HF baths. Samples were irradiated along with the Fish Canyon sanidine (27.84 Ma) neutron fluence monitor in the cadmium shielded port at the Oregon State University Reactor in Corvallis. Between 50 and 200 mg were incrementally heated in 8-12 steps with either an Ar-ion laser or a double-vacuum resistance furnace. Laser-heated samples used the methods and equipment described by Renne et al. (1993), whereas the furnace heating used methods and equipment outlined by Renne (1995) and Sharp et al. (1995).

Both plateau and isochron dates (see Renne, this volume) were calculated for each sample, along with analytical uncertainties (1σ) that reflect propagation of errors in relative abundances of Ar isotopes, mass discrimination, decay corrections, interfering isotope corrections, air corrections (where applicable), and the determination of the neutron fluence parameter "J". The extremely low K contents of these lavas renders K-Ar-based dating methods particularly sensitive to small amounts of excess ^{40}Ar, and initial $^{40}Ar/^{36}Ar$ only slightly higher than the atmospheric ratio of 295.5 can produce spurious plateau dates, whereas the other hand, in cases where sufficient range in $^{40}Ar/^{36}Ar$ and $^{40}Ar/^{39}Ar$ are not produced by incremental heating, a data array may not be produced that is amenable to isochron regression.

In the present study, most samples yielded isochron dates with acceptable regression dates are indistinguishable from plateau dates. Plateau dates are preferred herein only if the isochron yielded poor statistics by the above criteria.

$^{40}Ar/^{39}Ar$ Dating Results

The results from the $^{40}Ar/^{39}Ar$ dating are shown on Table 1. In addition to the ages determined for the Q_{v1} and Q_{v2} flows, the table also presents results from $^{40}Ar/^{39}$ dating of other basalt flows in the Pit River vicinity to provide a regional framework. A total of four whole rock $^{40}Ar/^{39}Ar$ dates were obtained from flows Q_{v1} and Q_{v2} that are displaced by the graben faults south of the Pit 1 Penstock: three on specimens from the same outcrop and

Table 1. $^{40}Ar/^{39}Ar$ dates of basalt flows near the Hat Creek fault and graben in the vicinity of the Pit River, Modoc Plateau

Basalt Unit	Location	Sample No. and Year	Plateau Age (ka)	Isochron Age (ka)	$(^{40}Ar/^{36}Ar)_0$	MSWD
Hat Creek Graben Highest Inset Flow (Qv1, this study)	Flow exposed at the top of the fault scarps that form the east margin of the graben, south of the Pit River	WDP-6a (1993)-F	1,113 ±81	**889 ±136**	297.8 ±1.4	0.51
		WDP-6b (1993)-F	921 ±51	**834 ±51**	297.8 ±1.0	0.61
		WDP-6b (1993)-F	907 ±51	**879 ±40**	296.3 ±0.9	1.57
		WDP-6 average		**867**		
Sam Wolfin Spring Flow (Qv2, this study)	Flow in the bottom of a small, secondary graben south of the Pit River that appears different from the "Highest Inset" flow	WDP-5 (1993)-F	**846 ±47**	681 ±47	301.0 ±1.4	0.19
Soldier-Saddle Mountain Divide Upper Flow	Flow at the top of the divide between Soldier and Saddle Mountains, north of the Pit River	WDP-1 (1992)-L	**1,219 ±89**	1,360 ±17	292.9 ±1.7	47.92
Hat Creek Rim Uppermost Flow	Flow at the top of the fault scarp, south of the Pit River and east of Cassel	WDP-3 (1993)-F	1,036 ±66	**1,009 ±78**	296.0 ±1.1	0.56
Fall River Mills Flow	Flow exposed in a cut along Highway 299, overlying the top of the Hat Creek Rim flows	WDP-7 (1993)-F	1,056 ±57	**945 ±46**	298.3 ±0.9	0.63
Hat Creek Graben Inset Flow South of Lake Britton	One of the lower flows in the graben south of the Pit River and northwest of Brush Mountain	GM-5 (1992)-L	**150 ±20**	166 ±20	291.8 ±3.4	0.33

stratum of flow Q_{v1} (WDP-6 a,b,c), and one from a specimen of flow Q_{v2} (WDP-5; Figure 2). The isochron dates for the three Q_{v1} specimens were: 834±51 ka, 879±40 ka, and 889±136 ka. The single Q_{v2} sample yielded a plateau date of 846±47 ka. The surface of this flow, as seen on air photos and in the field, appears to be different and slightly younger than that of flow Q_{v1}. The $^{40}Ar/^{39}Ar$ dates support this conclusion. The youngest basalt, Q_{v3}, was not dated because the fresh morphology of the flow suggests that it is less than 50,000 years old, and this flow is not offset by the faults along the east margin of the Hat Creek graben that project northward to the faults near the penstock.

Slip Rate

A long-term, average slip rate of 0.1 millimeters/year (mm/yr) was estimated for the faults along the east margin of the Hat Creek graben by dividing the measured total displacement of flow Q_{v1} (84 meters) by the average $^{40}Ar/^{39}Ar$ isochron age of 867 ka. The 0.1 mm/yr slip rate is considered to be a minimum long-term rate for the canyon rim segments of the Hat Creek fault, because total offset of flow Q_{v1} is likely somewhat greater than that measured across the exposed portions of the scarps. However, 0.1 mm/yr is believed to be a conservatively appropriate rate for the faults at the penstock along strike to the north because their geomorphic expression suggests a significantly lower rate of activity than the segments that were dated.

Muffler and others (1994) report an average slip rate of 1.3 mm/yr for the Hat Creek fault since the late Pleistocene near Lost Creek, 25 kilometers to the south, where regional strain appears to be accommodated by greater magnitude displacements along a single trace of the fault. The lower slip rate estimated for the fault segments at the Pit River by this study is because only part of the fault zone is measured and because the fault displacement is less along the northern portion of the fault.

Recurrence Interval Estimation

Recurrence intervals for varying magnitudes of surface displacement were estimated using a long-term slip rate of 0.1 mm/yr. The recurrence model is based on the assumption that the faults characteristically rupture with near-maximum displacements, and that strain accumulates uniformly along the fault between displacement events. This approach, posited by Schwartz and Coppersmith (1984), has been widely used for fault characterization studies.

Based on our current knowledge of fault mechanics in the Modoc Plateau, and regressions that relate maximum magnitude to surface displacement, maximum single event displacements are estimated to be on the order of 2 to 4 meters for the Hat Creek graben faults south of the Pit River, and about 1 to 2 meters for the faults at the penstock (Page and others, 1987). Table 2 shows the relationship between fault displacement magnitude and estimated recurrence intervals. For displacements of 1 and 2 meters, estimated recurrence intervals range between 10,000 and 20,000 years, respectively.

Table 2. Estimated slip rate and surface rupture displacement per event, recurrence interval, and probability for the northern Hat Creek fault near the Pit 1 penstock

Estimated Slip Rate (mm/yr)	Earthquake Displacement/Event (meters)	Estimated Recurrence Interval (years)	Annual Probability of Surface Rupture	50 Year Probability of Surface Rupture
0.1	1.0	10,000	0.010%	0.50%
0.1	1.5	15,000	0.007%	0.33%
0.1	2.0	20,000	0.005%	0.25%

Fault Rupture Probability And Penstock Risk

The potential hazard to the penstock was assessed by estimating the annual and 50-year probabilities of occurrence for surface displacements between 1 and 2 meters, using recurrence intervals of 10,000 and 20,000 years, respectively. The resulting annual probabilities ranged between 0.01% for 1 meter displacement, to 0.005% per year for a 2 meter displacement. These correspond to 50-year probabilities of occurrence of between 0.5% and 0.25%. The results from this study have suggested that the probability of occurrance for damaging levels of surface fault displacement at the PG&E Pit 1 Penstock is very low, and presents a minimal risk.

References

Becker, T.A., Sharp, W.D., Renne, P.R., Turrin, B.D., Page, W.D., and Wakabayashi, J., 1994, $^{40}Ar/^{39}Ar$ dating of young, low-k tholeiites, examples from NE California: [abs.] 8th International Conference on Geochronology, Cosmochronology, and Isotope Geology, Berkeley.

Hill, B.E., Leslie, B.W., and Connor, C.B., 1993, A review and analysis of dating techniques for Neogene and Quaternary volcanic rocks: Center for Nuclear Waste Regulatory Analyses, San Antonio, Texas, p. 2-14 to 2-20.

Muffler, P.L.J., Clynne, M.A., and Champion, D.E., 1994, Late Quaternary normal faulting of the Hat Creek Basalt, northern California: Geological Society of America Bulletin, v. 106, p. 195-200.

Page, W.D., and Renne, P.R., ^{40}Ar-^{39}Ar Dating of Quaternary basalt, Western Modoc Plateau, northeastern California: Implications to tectonics: [abs.], 8th International Conference on Geochronology, Cosmochronology, and Isotope Geology, Berkeley.

Page, W.D., Hemphill-Haley, M.A., and Wong, I.G., 1987, Exaggerated fault scarps in the Modoc Plateau, northeastern California [abs.]: Geological Society of America Abstracts with Programs, v. 19, no. 7, p. 797.

Renne, P.R., 1995, this volume.

Renne, P.R., Walter, R.C., Verosub, K.L., Sweitzer, M. and Aronson, J.L., 1993, New Data from Hadar (Ethiopia) Support Orbitally Tuned Time Scale to 3.3 Ma: Geophysical Research Letters, v. 20, p. 1067-1070.

Renne, P.R., 1995, Excess ^{40}Ar in Biotite and Hornblende from the Norils'k 1 Intrusion, Siberia: Implications for the Age of the Siberian Traps: Earth and Planetary Science Letters, v. 131, p. 165-176.

Schwartz, D.P., and Coppersmith, K.J., 1984, Fault behavior and characteristic earthquakes, examples from the Wasatch and San Andreas faults: Journal of Geophysical Research, v. 89, p. 5681-5698.

Sharp, W.D., Turrin, B.D., Renne, P.R., and Lanphere, M.A., 1995, $^{40}Ar/^{39}Ar$ and K/Ar Dating of Core from the Hilo Drill Site, Hawaiian Scientific Drilling Project: Journal of Geophysical Research, in press.

Wells, D.L., and Coppersmith, K.J., 1994, Updated empirical relationships among magnitude, rupture length, rupture area, and surface displacement: Seismological Society of America Bulletin, v. 84 (submitted).

Wills, C.J., 1991, Active faults north of Lassen Volcanic National Park, northern California: California Geology-March 1991, California Division of Mines and Geology, p. 51-58.

Woodward-Clyde Consultants, 1987, Pit 1 Forebay Dam (97-110)-evaluation of seismic geology, seismicity, and earthquake ground motions: unpublished report for Pacific Gas and Electric Company.

10

APPENDIX 2 - 1

A. Late Quaternary faulting of the Hat Creek Basalt, Northern California.
Muffler, L., Clynne, M., Champion, D.

B. Vesicle Cylinders in the Warner and Hat Creek Basalts, Northeastern California.
Goff, F.

Late Quaternary normal faulting of the Hat Creek Basalt, northern California

L. J. PATRICK MUFFLER
MICHAEL A. CLYNNE
DUANE E. CHAMPION
U.S. Geological Survey, Menlo Park, California 94025

ABSTRACT

The Hat Creek fault is a major, young, north-striking, normal fault along the western boundary of extensional Basin and Range deformation in the Lassen region of northeastern California. Volcanic rocks of Quaternary and late Pliocene age are displaced a total of >500 m down to the west along west-facing, *en echelon* scarps now retreated to ~35° slopes. Fresh, young scarps as much as 30 m high cut the Hat Creek Basalt (erupted between 15 and ~40 ka) a few tens of meters west of the retreated scarps. Prior to the late 1980s, these young scarps were interpreted as lava slump scarps formed as the Hat Creek Basalt ponded against the older fault scarps and then drained away to the northwest. Numerous pieces of geologic evidence, however, show that the young scarps formed after the Hat Creek Basalt solidified and cooled and are true fault features formed by the youngest displacements of the Hat Creek fault. Structural details are remarkably well preserved along the series of left-stepping scarps cutting the Hat Creek Basalt. Near the central parts of individual segments, the fault is displayed as a single, vertical scarp. Near the ends of the segments, the scarp decreases in height and becomes a monoclinal flexure on which the recent dip separation has been taken up by small-scale offset along columnar cooling joints in the basalt. These monoclinal flexures commonly rotate into east-west monoclines that join adjacent north-south segments. Displacement of outwash gravel overlying the Hat Creek Basalt shows that vertical separation on the Hat Creek fault has averaged ~1.3 mm yr^{-1} for the past 15,000 yr. The Hat Creek fault thus represents a potential earthquake hazard, despite the low level and diffuse nature of modern seismicity in the region.

GEOLOGIC SETTING

The Hat Creek fault is located in the southernmost segment of the Cascade Range (Guffanti and Weaver, 1988), here termed the "Lassen segment." Eruptions from more than 500 volcanic vents in the past 7 m.y. have produced a region that is topographically and geologically separate from the Shasta–Medicine Lake segment to the north (Guffanti and others, 1990). The primary focus of volcanism in the past 700,000 yr in the Lassen segment has been in and around Lassen Volcanic National Park (Clynne and Muffler, 1989; Clynne, 1990), creating a broad volcanic highland (Fig. 1) dominated by Lassen Peak, a dacite dome complex erupted ~20,000 yr ago. Although the Lassen segment is within a broad zone of distributed extension between the Cascadia subduction

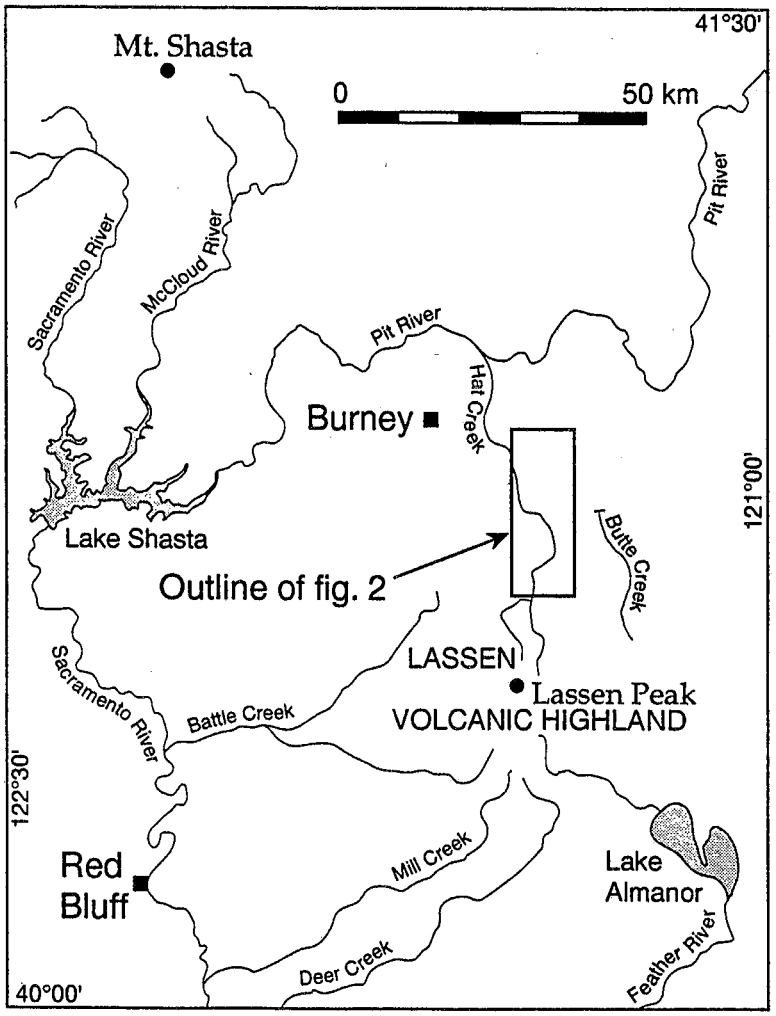

Figure 1. Index map of the southern Cascade range in northeastern California.

Geological Society of America Bulletin, v. 106, p. 195–200, 5 figs., 1 table, February 1994.

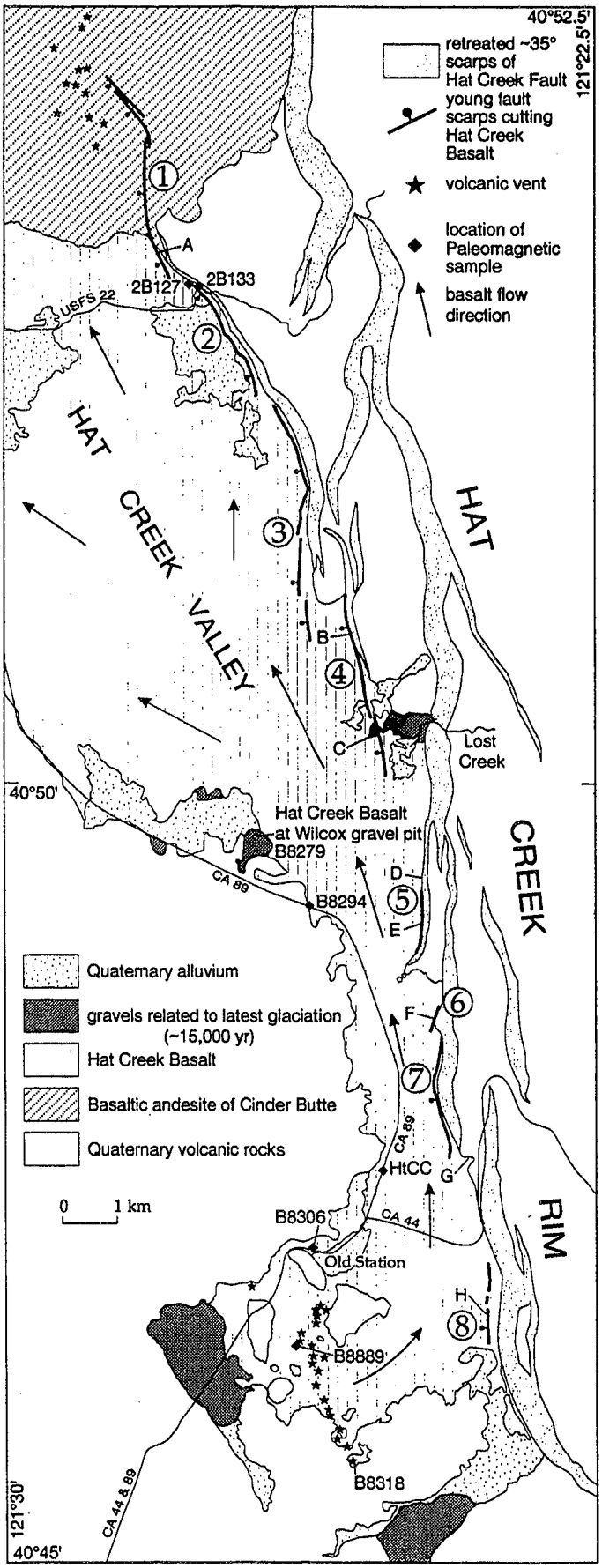

Figure 2. Simplified geologic map of the Hat Creek fault. Circled numbers refer to fault segments, and letters with leaders refer to localities mentioned in text. Solid diamonds with associated numbers designate locations of paleomagnetic samples.

zone and the Basin and Range province (Guffanti and others, 1990), faults are poorly expressed within the volcanic highland, where they are obscured by a combination of volcanism and glaciation. In addition, by analogy with the situation at Medicine Lake (Dzurisin and others, 1991) and in the Long Valley–Mono Lake region of California (Bursik and Sieh, 1989), some of the extension in the Lassen volcanic highland may be accommodated by intrusion and aseismic creep in thermally weakened crust rather than by brittle fracturing.

Normal faulting is conspicuous, however, both south and north of the Lassen volcanic highland. To the south, faults strike approximately northwest, whereas to the north, faults strike north-northwest. This paper focuses on the most prominent and perhaps the youngest of these faults, the Hat Creek fault, which extends for ~35 km south from the Pit River (Page and others, 1987; Woodward Clyde Consultants, 1987; Wills, 1991). The Hat Creek fault displaces Quaternary and late Pliocene volcanic rocks down to the west, forming the Hat Creek Valley, an asymmetric half graben partly filled with Quaternary volcanic rocks (see cover photograph accompanying Wills, 1991). The fault is expressed as left-stepping *en echelon* segments, each several kilometers in length (Fig. 2). Individual fault scarps are as much as 350 m high and are retreated by erosion to ~35° angle of repose. Total vertical displacement from Hat Creek Valley to Hat Creek Rim exceeds 520 m at the latitude of segment 3 (Fig. 2).

Flooring much of the Hat Creek Valley is the Hat Creek Basalt, which erupted from numerous vents southeast of Old Station and flowed north for nearly 30 km (C. A. Anderson, 1940). The original pahoehoe surface of the Hat Creek Basalt has been modified only slightly by erosion, and it thus preserves detailed features of the youngest breaks of the Hat Creek fault.

HAT CREEK BASALT

The Hat Creek Basalt is a low-potassium high-alumina olivine tholeiite (A. T. Anderson and Gottfried, 1971; L.J.P. Muffler and M. A. Clynne, unpub. data) with 0–4% phenocrysts of forsteritic olivine and rare plagioclase in a conspicuously diktytaxitic ground-

TABLE 1. PALEOMAGNETIC DATA FROM THE HAT CREEK BASALT

Site	Lat.	Long.	N/No	Exp.	I	D	α_{95}	k	R	Plat.	Plong.
Structurally stable sites											
HtCC	40.688°	238.580°	12/12	20	65.1°	4.0°	1.4°	956	11.98849	83.0°	261.5°
B8279	40.742°	238.553°	15/15	10	63.0°	5.6°	1.3°	934	14.98502	84.5°	284.7°
B8294	40.731°	238.565°	12/12	5+	64.0°	10.0°	1.3°	1120	11.99018	81.2°	290.9°
B8306	40.676°	238.565°	11/12	5	63.4°	2.0°	1.1°	1753	10.99430	85.5°	257.1°
B8318	40.642°	238.574°	12/12	5+	63.8°	353.3°	2.0°	465	11.97634	83.2°	195.1°
B8889	40.660°	238.562°	11/12	10	65.9°	2.3°	2.4°	377	10.97349	82.4°	250.1°
B8919	40.808°	238.488°	12/12	10	65.5°	0.6°	1.3°	1111	11.99010	83.1°	241.9°
B8931	40.868°	238.452°	12/12	10	63.0°	350.5°	2.0°	350	11.97764	82.1°	179.0°
Mean of 8 sites	40.7°	238.5°	..	..	64.3°	1.0°	2.1°	720	..	84.5°	245.7°
Structurally unstable sites											
2B133	40.830°	238.542°	12/12	20	60.4°	359.5°	1.6°	771	11.98572	89.4°	202.9°
2B127	40.831°	238.539°	6/6	20	46.2°	5.8°	2.4°	601	5.99168	75.9°	37.0°
(Corrected for tilt of block)					(70.8	14.6°)				(72.8°	267.6°)

Site is alphanumeric identifier; Lat. and Long. are latitude and longitude in degrees North and East of each site's location; N/No is the number of cores used compared with the number originally taken at the site; Exp. is the strength of the peak cleaning field; I and D are the remanent inclination and declination; α_{95} is the 95% confidence limit about the mean direction; k is the estimate of the Fisherian precision parameter; R is the length of the resultant vector, and Plat. and Plong. are the locations in degrees North and East of the virtual geomagnetic pole (VGP) calculated from the site mean direction. Sites are located in Figure 2 except for B8919 and B8931, which are along Highway 89 northwest of the area shown in Figure 2.

mass of plagioclase and clinopyroxene. A. T. Anderson (1971) described interstitial ferrodacite and rhyodacite glass, quenched Fe- and Ti-rich residual melt that oozed into cooling cracks, and peralkaline, silica-undersaturated glass as vesicle linings and coatings of segregation veins.

C. A. Anderson (1940) suggested that the Hat Creek Basalt erupted less than 2,000 yr ago. Our geologic mapping, however, shows that the Hat Creek Basalt is overlain by gravel related to the last major glaciation, which ended about 15,000 yr ago (Gerstel, 1989; Gerstel and Clynne, 1989). Furthermore, the flow is incised to a depth of 6 m by Hat Creek itself. The maximum age of the flow is poorly constrained; the well-preserved, rugged surface morphology makes it unlikely that the flow is older than ~40 ka.

The Hat Creek Basalt has not yet been dated by instrumental techniques. We have been unable to find charcoal under the Hat Creek Basalt for ^{14}C dating, and the basalt has ~0.2% K_2O, insufficient for potassium-argon dating of such a young rock. ^{39}Ar-^{40}Ar dating is currently being attempted (Brent W. Turrin, 1993, oral commun.).

Paleomagnetic Studies

Core samples were collected from ten sites (Fig. 2; Table 1) in outcrops of the Hat Creek Basalt. Twelve cores were taken at each site with a water-cooled diamond drill and were oriented in the field using a sun compass. Specimens were demagnetized using alternating field to remove secondary magnetic components. Peak field strengths required to clean specimens were low (5–20 mT), and within-site statistics show that the paleomagnetic data are generally of high quality.

An equal-area diagram of the paleomagnetic directions (Fig. 3) shows that the mean directions of 8 of the 10 sites are closely grouped about a direction of magnetization with an inclination of 64.3° and a declination of 1.0°, suggesting that the Hat Creek Basalt is a single eruptive unit. If the small differences among directions of individual sites are due to secular variation of the magnetic field, the data indicate a ~100-yr time frame for emplacement of the lava field. We were unable to link the declination differences, however, to stratigraphic position.

Paleomagnetic site B8279 was located in basalt at the bottom of the Wilcox gravel pit (Fig. 2) beneath gravel and sand that makes up a unit of glacial outwash derived from the Lassen Volcanic Highlands (Fig. 1). This outwash contains distinctive clasts of quartz-rich dacite of Lassen Peak (erupted ~18,000 to 25,000 yr ago) and thus correlates with the waning stages of the youngest major glaciation in the region, which ended ~15,000 yr ago (Gerstel, 1989; Gerstel and Clynne, 1989). The excellent correspondence of paleomagnetic data from this site with data from our other sites in the Hat Creek Basalt, combined with nearly identical chemical analyses (Muffler and Clynne, 1993), demonstrates clearly that the basalt at B8279 is the Hat Creek Basalt, not an older basalt as suggested by Muffler and Campbell (1984). Use of an algorithm of Bogue and Coe (1981) shows that there is only a 2.4% chance that the Wilcox pit site could be a random sample of geomagnetic secular variation.

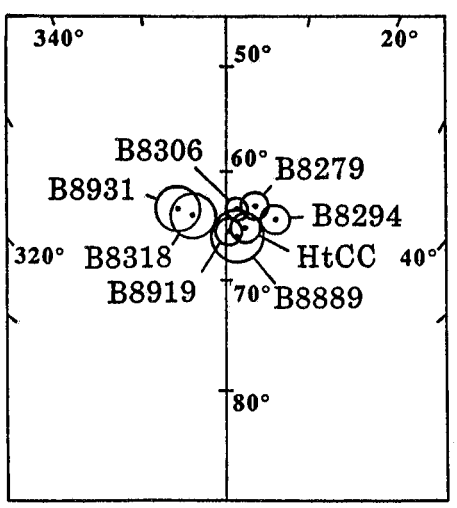

Figure 3. Part of an equal-area stereographic projection (lower hemisphere) showing mean directions and circles of 95% confidence for paleomagnetic directions measured in undisturbed sites of the Hat Creek Basalt. See Figure 2 for sample locations.

Two sites at the north end of segment 2 of the Hat Creek fault (Fig. 2) were located in areas likely to be affected by the late Quaternary faulting. Site 2B133, although within an area of solid basalt, has an azimuth very similar to those of other sites in the Hat Creek Basalt, but a somewhat shallower inclination. This shallowing could be due either to the random dispersions associated with paleomagnetic sampling and analysis or to ~4° rotation down to the south about an N80°E axis. Site 2B127 is in a block that displays originally horizontal flow features now rotated significantly down to the south. Returning these flow features to the horizontal results in a significant improvement in the correspondence with directions from the eight stable sites.

DESCRIPTION OF SCARPS CUTTING THE HAT CREEK BASALT

At the base of the retreated ~35° scarps of the Hat Creek fault, the contact between the Hat Creek Basalt and the older volcanic rocks is depositional, with the Hat Creek Basalt lapping onto older volcanic rocks and their talus. A few meters to tens of meters west of the large ~35° scarps, the Hat Creek Basalt is cut by subvertical scarps as much as 30 m high that mimic in plan view the pattern of the larger, retreated scarps. In many localities, this young faulting produced a conspicuous horizontal bench of Hat Creek Basalt between the young fault scarp and the older ~35° scarps.

The young subvertical scarps cutting the Hat Creek Basalt attain a maximum height of 30 m (Fig. 4) near the central parts of individual segments, but the scarps decrease in height toward the ends of the segments. The scarps along several segments pass into monoclinal flexures on which dip slip has been accommodated by small-scale offsets along vertical columnar cooling joints in the basalt. These monoclinal flexures commonly rotate into east-west–trending monoclines that join adjacent *en echelon* north-south segments. The scarps in the Hat Creek Basalt are morphologically similar to the scarps in the Koae fault system of Kilauea Volcano, Hawaii (Duffield, 1975).

We have grouped the young scarps cutting the Hat Creek Basalt into eight major segments, from north to south (Fig. 2):

Segment 1. This segment cuts lava from Cinder Butte and extends south into the Hat Creek Basalt, where it is expressed as a series of scarps and rotated blocks that form a complex monocline. At locality A, the Hat Creek Basalt laps against talus of Cinder Butte as a horizontal bench, with blocks of Cinder Butte lava included within the Hat Creek Basalt. The scarp bounding this bench on the west exposes the lower contact of the Hat Creek Basalt, which lies with no soil zone directly upon basaltic andesite of Cinder Butte.

Segment 2. This segment begins at the bend in the gravel road (USFS 22) at Stop 7 of Clynne and Muffler (1989). Segments 1 and 2 are joined by a southwest-dipping ramp of rotated blocks separated along cooling joints, whereas 400 m south, segment 2 changes abruptly from a series of cracks and rotated blocks to a nearly vertical scarp as much as 30 m high in Hat Creek Basalt. Along much of the southern half of segment 2, the jointed basalt in the scarp has collapsed to form a steep talus slope.

Segment 3. Most of segment 3 also is a steep talus slope where the jointed Hat Creek Basalt has collapsed. At the left step between segments 3 and 4, the northward-flowing Hat Creek Basalt dammed up against a south-sloping ramp in the older volcanic rocks, resulting in conspicuous, rugged, flow-top topography and east-west–trending pressure ridges in the Hat Creek Basalt.

Segment 4. The northern part of segment 4 is obscured by talus from the older scarp. South of locality B, a bench of Hat Creek Basalt laps onto the ~35° scarp. The elevation of the bench above the Hat Creek Basalt to the west rises from ~10 m at locality B to ~18 m at a point 400 m south. The west side of the bench is marked by a steep broken monocline, with jointed blocks rotated up to 90° west. Beginning 800 m south of locality B, this broken monocline cuts across complex irregular flow topography with many large tumuli. At locality C (Fig. 2), due west of a prominent canyon carved by Lost Creek into a ~35° older scarp of the Hat Creek fault, coarse gravels deposited by Lost Creek overlie the Hat Creek Basalt and are vertically displaced ~20 m along a complex broken monocline that marks the fault trace.

Unlike the gravels at the Wilcox sand and gravel pit, these gravels at Lost Creek were not derived from the headwaters of Hat Creek and therefore do not contain the distinctive dacite clasts from Lassen Peak. Instead, they were derived from the Butte Creek drainage (Fig. 1), where there are large moraines and extensive outwash gravels related to the waning stages of the same young glaciation. Lost Creek is actually the lower stream course of Butte Creek, but modern Butte Creek sinks into the porous volcanic rocks 0.5 mi before reaching Lost Creek. During the waning stages of glaciation, however, Butte Creek had abundant water and flowed north and west into the canyon of Lost Creek, depositing the gravels at the canyon mouth. Like the Wilcox gravels (Gerstel, 1989; Gerstel and Clynne, 1989), the correlative Lost Creek gravels most likely were deposited at the period of maximum retreat of the glaciers, ~15,000 yr ago. Consequently, the 20-m displacement of the Lost Creek gravels along the fault trace yields an average displacement rate of ~1.3 mm yr^{-1}.

Segment 5. For 2 km south of Lost Creek, any young scarp cutting the Hat Creek Basalt is obscured by talus from the ~35° older fault scarp; however, 300 m east of the southern tip of segment 4, a gravel pit exposes sediments deposited in a depressed area caused by eastward rotation of the down-dropped block against a young fault. At locality D, Hat Creek Basalt lapping against the ~35° scarp forms a gentle ramp reaching ~10 m above the general level of the Hat Creek Basalt to the west. 250 m south of locality D, this ramp passes into segment 5, a conspicuous bench ~14 m above the general level of the Hat Creek Basalt to the west. The bench is a broken monocline cut by cracks and displaying slumping and ramping to the west. At locality E, the Hat Creek Basalt is displaced by two scarps; the eastern one is a crack ~11 m

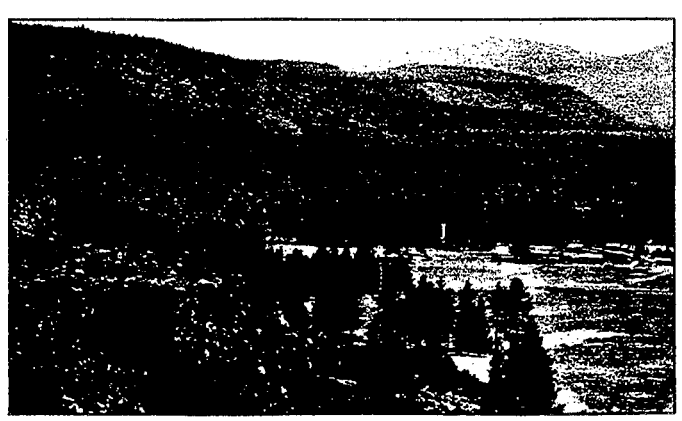

Figure 4. View looking south along the Hat Creek fault from near the north end of segment 2 (Fig. 2). Sparsely forested slope at upper left is one of the old ~35° scarps. Prominent subvertical scarp at its base cuts the Hat Creek Basalt.

deep, with the Hat Creek Basalt downdropped 8 m and displaced westward several meters. The western scarp displaces the Hat Creek Basalt an additional 2 m down to the west. At the southern tip of segment 5, the old ~35° scarp swings southwest and is overlapped in two places by narrow (20-m-wide), unbroken tongues of Hat Creek Basalt flowing over the scarp. One of these tongues displays a lava tube 1 m in diameter.

Segment 6. The northern two-thirds of segment 6 is obscured by talus from the ~35° scarp to the east. At locality F, a bench of Hat Creek Basalt protrudes from the talus ~4 m above the base of the scarp. This bench rises to the south, where it becomes a complex, disjointed monocline, with blocks rotated to the west to high angles. The monocline wraps around the southern terminus of segment 6, becoming a disjointed south-dipping ramp broken by cracks several meters wide and as much as 6 m deep which joins segments 6 and 7.

Segment 7. Directly west of the northern terminus of segment 7, a nearly continuous surface of Hat Creek Basalt displaying conspicuous columnar joints dips ~30° south. At the southern margin of this slope, the surface of the Hat Creek Basalt is at least 10 m lower than it is 300 m to the west along the projection of segment 6. The northern tip of segment 7 is a vertical scarp with a displacement that increases from 0 at the segment tip to about 20 m at a point 100 m to the south. The southernmost 200 m of segment 7 consists of at least two traces marked by basalt rubble and rotated, west-dipping blocks.

Segment 8. Between segments 7 and 8, the Hat Creek Basalt either laps against the older ~35° scarp or is covered by talus from the older scarp. At locality G (Fig. 2), Hat Creek Basalt flowed into a small east-west valley cut in older basaltic andesite. Along segment 8, the Hat Creek Basalt is uplifted to the east to form a bench as much as 10 m higher than the general elevation of the Hat Creek Basalt 50 m west. At the point of maximum vertical displacement (locality H, Fig. 2), the monocline is broken by a 7-m scarp, which passes southward into a V-shaped crack and then into an unbroken monocline.

SCARPS IN THE HAT CREEK BASALT: FAULTS OR LAVA SLUMP SCARPS?

Several previous workers, most notably Finch (1933), C. A. Anderson (1940), and Macdonald (1966), interpreted the steep young scarps in the Hat Creek Basalt as "lava slump scarps," defined by Finch (1933) as scarps produced by subsidence in a lava flow after the feeding source has ceased activity. These authors suggested that the Hat Creek Basalt ponded behind a temporary obstruction in the narrow part of the valley to the northwest; removal or collapse of the obstruction allowed the lava to drain, leaving a "bathtub ring" of solidified basalt along the older ~35° retreated fault scarps. The following observations, however, demonstrate that the young subvertical scarps in the Hat Creek Basalt are true tectonic fault scarps.

(1) The scarps are in inflated tube-fed basalt, a flow type in which lava slump scarps are unknown (R. T. Holcomb, 1982, written commun.).

(2) The scarps lack features such as lava stalactites or ooze-outs that would indicate that the interior of the basalt was molten enough to flow at the time of disruption (Muffler and others, 1989).

(3) Rotation of remanent magnetization in a tilted block (2B127) demonstrates that the basalt was cool at the time of tilting.

(4) The young subvertical scarps exist only adjacent to the conspicuous ~35° fault scarps along the east side of Hat Creek Valley (Fig. 2). No scarps are present in the Hat Creek Basalt where it abuts older volcanic rocks on the west side of the valley.

(5) Stream gravels that overlie the Hat Creek Basalt are displaced vertically as much as 20 m across individual scarps of the fault.

(6) Deep cracks along one of the young scarps (locality D, Fig. 2) expose at least three separate, chemically identical, flow units. A single lava slump scarp should affect only one flow unit.

(7) In segment 1 of the Hat Creek fault (locality A, Fig. 2), a steep scarp extends through the Hat Creek Basalt into the underlying basaltic andesite of Cinder Butte. If this scarp in the Hat Creek Basalt were a lava slump scarp, then it could not extend down into an older unit.

MODEL FOR FORMATION OF THE YOUNG FAULT SCARPS

Prior to emplacement of the Hat Creek Basalt (Fig. 5a), Quaternary and Pliocene volcanic rocks were displaced by the Hat Creek fault, assumed to dip at ~60° as in many Basin and Range faults (Muffler, 1964, p. 71–77; Stewart, 1971; Thompson and Burke, 1973). The fault scarp was modified by erosion to an angle of repose of ~35°, with a talus apron at

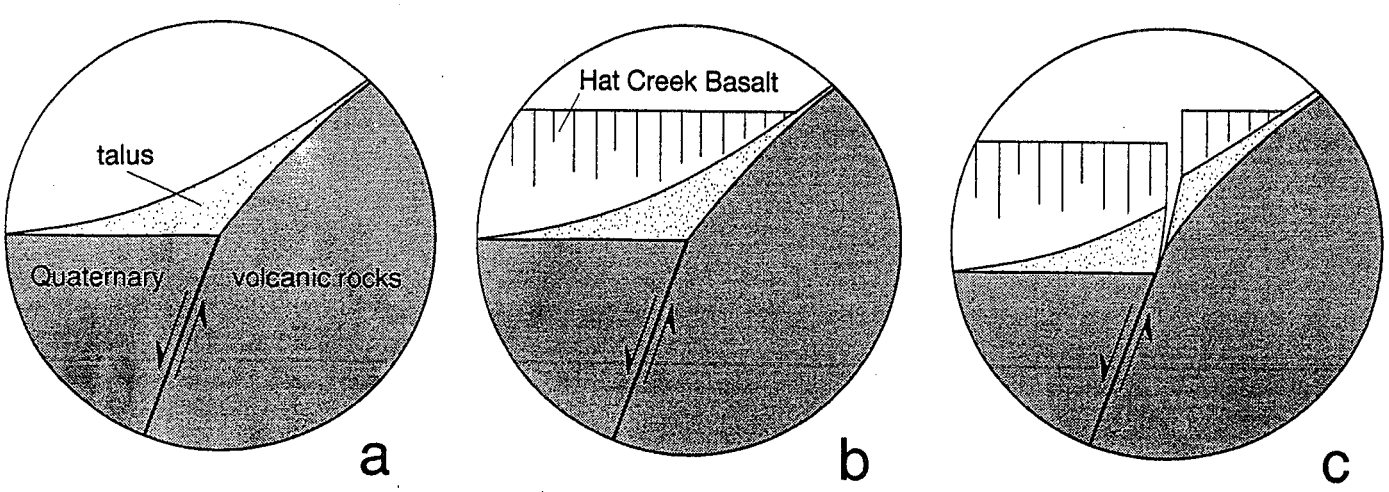

Figure 5. Diagrammatic cross sections of a segment of the Hat Creek fault: (a) prior to emplacement of Hat Creek Basalt, (b) just after emplacement of the Hat Creek Basalt, and (c) after renewed movement of the Hat Creek fault.

its base. Just after emplacement of the Hat Creek Basalt, near-vertical columnar cooling joints developed in at least the upper part of the flow (Fig. 5b). Subsequent renewed movement on the Hat Creek fault followed the 60° fault plane at depth but displaced the Hat Creek Basalt along the pre-existing cooling joints (Fig. 5c), thus creating a near-vertical scarp with some horizontal displacement perpendicular to the fault trace.

Although the scarp in the Hat Creek Basalt lacks lava stalactites and ooze-outs, many joint faces, both along the fault scarp and away from it, display thin glassy selvages, interpreted by A. T. Anderson and Gottfried (1971) and by us as squeezing out of glass from the interstices of the diktytaxitic groundmass. This squeezing out occurred during the last stages of cooling of the flow, after formation of the columnar, cooling joints. Displacement during the subsequent faulting occurred along these pre-existing near-vertical joints, thus exposing the glassy selvages. Because the horizontal component of separation is perpendicular to the fault trace in this extensional tectonic environment, the walls of the cracks did not rub against each other, and thus the selvages were preserved rather than being ground up in a fault gouge or along slickensided fault planes.

CONCLUSIONS

The young scarps of the Hat Creek fault are not lava slump scarps but are true tectonic fault scarps with a displacement of as much as ~20 m since the end of the last major glaciation, about 15,000 yr ago. The youngest volcanic unit cut by the fault is the Hat Creek Basalt, erupted between 15,000 and ~40,000 yr ago. Displacement of outwash gravel overlying the Hat Creek Basalt indicates that the rate of vertical displacement along the fault averaged over the past 15,000 yr has been ~1.3 mm yr^{-1}. The number of individual events along the fault during this time is not known but is being addressed by detailed surface-rupture studies of the young scarps in the Hat Creek Basalt (Marie D. Jackson, 1992, personal commun.), using the techniques and approach of Jackson and others (1992). Modern seismicity in this area is low and diffuse (LaForge and Hawkins, 1986), suggesting that displacement on the Hat Creek fault has been episodic, with significant earthquakes occurring at periods of hundreds or perhaps thousands of years.

ACKNOWLEDGMENTS

The geologic mapping upon which much of this paper is based was carried out by Muffler and Clynne intermittently between 1979 and 1992 as part of regional geologic mapping of more than 2,000 km^2 in Lassen Volcanic National Park and vicinity. Our observations in this paper should be viewed as framework and stimulus for more detailed analyses of the fault scarp, such as those being carried out currently by Marie D. Jackson. We are very grateful to Marie D. Jackson, William R. Lettis, Richard B. Moore, and Christopher W. Wills for helpful reviews of the manuscript.

REFERENCES CITED

Anderson, A. T., 1971, Alkali-rich, SiO_2-deficient glasses in high-alumina olivine tholeiite, Hat Creek Valley, California: American Journal of Science, v. 271, p. 293–303.

Anderson, A. T., and Gottfried, D., 1971, Contrasting behavior of P, Ti, and Nb in a differentiated high-alumina olivine tholeiite and a calc-alkaline andesitic suite: Geological Society of America Bulletin, v. 82, p. 1929–1942.

Anderson, C. A., 1940, Hat Creek lava flow: American Journal of Science, v. 238, p. 477–492.

Bogue, S. W., and Coe, R. S., 1981, Paleomagnetic correlation of Columbia River Basalt flows using secular variation: Journal of Geophysical Research, v. 86, p. 11,883–11,897.

Bursik, M., and Sieh, K., 1989, Range front faulting and volcanism in the Mono Basin, eastern California: Journal of Geophysical Research, v. 94, p. 15,587–15,609.

Clynne, M. A., 1990, Stratigraphic, lithologic, and major element geochemical constraints on magmatic evolution at Lassen Volcanic Center, California: Journal of Geophysical Research, v. 95, p. 19,651–19,669.

Clynne, M. A., and Muffler, L.J.P., 1989, Lassen Volcanic National Park and vicinity, *in* Chapin, C. E., and Zidek, J., eds., Field excursions to volcanic terranes in the western United States, Volume II: Cascades and intermountain West: New Mexico Bureau of Mines and Mineral Resources Memoir 47, p. 183–194.

Duffield, W. A., 1975, Structure and origin of the Koae fault system, Kilauea Volcano, Hawaii: U.S. Geological Survey Professional Paper 856, 12 p.

Dzurisin, D., Donnelly-Nolan, J. M., Evans, J. R., and Walter, S. R., 1991, Crustal subsidence, seismicity, and structure near Medicine Lake volcano, California: Journal of Geophysical Research, v. 96, p. 16,319–16,333.

Finch, R. H., 1933, Slump scarps: Journal of Geology, v. 41, p. 647–649.

Gerstel, W. J., 1989, Glacial chronology and the relationship to volcanic stratigraphy in the Hat and Lost Creek drainages, Lassen Volcanic National Park, California [M.S. thesis]: Arcata, California, Humboldt State University, 89 p.

Gerstel, W. J., and Clynne, M. A., 1989, Glacial stratigraphy in the Lassen Peak area of northern California—Implications for the age of Lassen Peak dacite dome [abs.]: Geological Society of America Abstracts with Programs, v. 21, no. 5, p. 83.

Guffanti, M., and Weaver, C. S., 1988, Distribution of late Cenozoic volcanic vents in the Cascade Range: Volcanic arc segmentation and regional tectonic considerations: Journal of Geophysical Research, v. 93, p. 6513–6529.

Guffanti, M., Clynne, M. A., Smith, J. G., Muffler, L.J.P., and Bullen, T. D., 1990, Late Cenozoic volcanism, subjection, and extension in the Lassen region of California, Southern Cascade Range: Journal of Geophysical Research, v. 95, p. 19,453–19,465.

Jackson, M. D., Endo, E. T., Delaney, P. T., Arnadottir, T., and Rubin, A. M., 1992, Ground ruptures of the 1974 and 1983 Kaoiki earthquakes, Mauna Loa volcano, Hawaii: Journal of Geophysical Research, v. 97, p. 8775–8796.

LaForge, R. C., and Hawkins, F. F., 1986, Seismotectonic study of northernmost California for Shasta, Keswick, Spring Creek Debris, Trinity, Lewiston, and Whiskeytown Dams: U.S. Bureau of Reclamation Seismotectonic Report No. 86-1, 132 p.

Macdonald, G. A., 1966, Geology of the Cascade Range and Modoc Plateau, *in* Bailey, E. H., ed., Geology of northern California: California Division of Mines and Geology Bulletin 190, p. 65–96.

Muffler, L.J.P., 1964, Geology of the Frenchie Creek quadrangle, north-central Nevada: U.S. Geological Survey Bulletin 1179, 99 p.

Muffler, L.J.P., and Campbell, H. W., 1984, Lost Creek roadless area, California: U.S. Geological Survey Professional Paper 1300, p. 283–285.

Muffler, L.J.P., Clynne, M. A., and Holcomb, R. T., 1989, Late Quaternary faulting of the Hat Creek Basalt [abs.]: Eos (American Geophysical Union Transactions), v. 70, no. 43, p. 1310.

Page, W. D., Hemphill-Haley, M. A., and Wong, I. G., 1987, Exaggerated fault scarps in the Modoc Plateau, northeastern California [abs.]: Geological Society of America Abstracts with Programs, v. 19, no. 7, p. 797.

Stewart, J. S., 1971, Basin and Range structure: A system of horsts and grabens produced by deep-seated extension: Geological Society of America Bulletin, v. 82, p. 1019–1044.

Thompson, G. A., and Burke, D. B., 1973, Rate and direction of spreading in Dixie Valley, Basin and Range province, Nevada: Geological Society of America Bulletin, v. 84, p. 627–632.

Wills, C. J., 1991, Active faults north of Lassen Volcanic National Park, northern California: California Geology, v. 44, p. 51–58.

Woodward-Clyde Consultants, 1987, Pit 1 Forebay Dam (97-110)—Evaluation of seismic geology, seismicity, and earthquake ground motions: Unpublished report prepared for Pacific Gas and Electric Company, p. 2-7–2-10.

MANUSCRIPT RECEIVED BY THE SOCIETY APRIL 13, 1992
REVISED MANUSCRIPT RECEIVED MAY 14, 1993
MANUSCRIPT ACCEPTED MAY 24, 1993

Printed in U.S.A.

PAPER FOR APPENDIX

VESICLE CYLINDERS IN THE WARNER AND HAT CREEK BASALTS, NORTHEASTERN CALIFORNIA

Fraser Goff
EES-1, MS D462
Los Alamos National Laboratory
Los Alamos, NM 87545

Vesicle cylinders (segregation pipes or veins) are vertical pipes filled with bubbles and residual melt that differentiate from diktytaxitic basalt flows during crystallization (Goff, 1977; 1996). Lavas containing vesicle cylinders develope a network of interfingering differentiated structures (vesicle sheets and pods) in the upper half of the flows. The cylinders grow from about 0.25 m above the base of the flow to the bottom of the chilled flow top (Fig. 1). Field relations limit growth of the cylinders and virtually all other differentiatied structures to the period between cessation of (most) lava movement and deep penetration of columnar joints. Presence of vesicle cylinders is not linked to flowage of basaltic lavas over wet sediments. Many occurances are documented where stacks of basalt flows and flow units all contain vesicle cylinders or where cylinder-hosted lavas flow over sediments, lavas, and other rocks (Goff, 1977).

Although any type or age of basalt lava can contain vesicle cylinders, they are particularly plentiful in Plio-Plistocene high-alumina tholeiites of the Cascade Range and Modoc Plateau. Several diktytaxitic, high-alumina tholeiites of northeastern California including the Warner and Hat Creek Basalts are well known for their abundence of differentiated structures and textures (Kuno, 1965; Anderson et al, 1984).

Vesicle cylinders, sheets, and pods record a natural process of differentiation (i.e., Bowen, 1928) from a basaltic parent to residual patches of rhyolitic glass. Continuous geochemical and mineralogical changes can be studied within the space of single hand samples. Because the exsolution of volatile components is the ultimate cause of vesicle cylinder formation, studies of the physical differences between cylinders and their enclosing lavas reveals much about the rheology of basalt flows after eruption and during bubble growth and solidification (Goff, 1977; 1996; Manga and Stone, 1994).

Two studied locations in the Warner Basalt and one in the Hat Creek Basalt (Table 1) show most of the features depicted in Fig. 1. The lavas at the two Warner sites overlie volcaniclastic sedimentary rocks (Goff, 1977), whereas the lava at the Hat Creek locality overlies an earlier basalt flow (Muffler et al, 1994). The cylinders and other differentiated structures generally have distinct boundaries with thier host basalt (Fig. 2). Some important physical characteristics of the differentiates and enclosing lavas are listed in Table 2. Although parameters such as eruption temperature and viscosity can be calculated, all lavas containing vesicle cylinders have pahoe-hoe surfaces and other fluid textures suggesting that eruption temperatures were relatively high and that viscosities were relatively low. In addition, all lavas containing vesicle cylinders have diktytaxitic textures (resulting in high porosities) attesting to unusually high volatile contents in the lavas and exsolution of volatiles during the waning stages of crystalization (Fuller, 1931). These features suggest that water contents in the magmas ultimately forming vesicle cylinders and related structures were unusually high before eruption (Goff, 1977; 1996).

Although both whole rock samples of vesicle cylinders and host lava are basaltic, the cylinders are enriched in elements not removed by the initial crystalization of the host: Fe, Mn, Ti, Na, K, and P (Table 3). Where analyses are available, the differentiates are also enriched in many trace elements such as Cl, Rb, Y, Zr, Zn, and Nb (Anderson and Gottfried, 1971; Goff, 1977). High-alumina tholeiite magmas such as the Warner and Hat Creek lavas contain olivine and plagioclase phenocrysts at eruption. Post-eruptive crystals include microphenocrysts of olivine and plagioclase, ophitic augite, Fe-Ti oxides and basaltic glass. Cylinders include these minerals as stoped fragments but also include a higher proportion of more evolved glass, oxides, alkali feldspar, and pyroxene. The last residues to solidify within the cylinders consist of dacitic-rhyolitic glass, Fe-Ti oxide neddles, anorthoclase, apatite ± fayalite blades ± aegerine. Cristobalite spherules commonly cling to the walls of vesicles.

Fe-Ti oxide geothermometry indicates that the cylinders began forming at ~1100°C but ceased crystallizing at ~950°C. Calculated viscosities of host lavas and frothy differentiate at an average cylinder formation temperature of 1075°C are $\leq 10^6$ and $\sim 10^4$ poise, respectively. Because the cylinders have lower viscosity and contain a higher proportion of bubbles (have lower density), they rise as plumes or diapirs through the enclosing lava.

Pre-eruptive, high-temperature, iddingsite alteration of olivine phenocrysts in many lavas containing vesicle cylinders shows that the fO_2 of the magmas was extremely high at eruption ($\sim 10^{-4}$). After eruption, the fO_2 of the lavas fell dramatically (when pressure decreased and volatiles were exsolved) to values of about 10^{-11}. Conditions followed the fayalite-magnetite-quartz buffer to final crystallization. Because the iddingsite forms before eruption, the magmas may become relatively oxidizing by addition of meteoric water late in their evolution. Oxygen-18 analyses of four basalt-differentiate pairs from other localities with vesicle cylinders are consistent with meteoric water addition (Goff, 1996).

Field relations and thermal profiles of cooling lava flows limit the growth period of vesicle cylinders to 1-5 d after a flow of typical thickness (3-10 m) comes to rest (Jaeger, 1961). Although an adequate quantitative model describing growth of vesicle cylinders does not exist, they apparently form by vesicle (bubble) nucleation and resulting density instability above the lower solidification front of the cooling flows (Manga and Stone, 1994). As the bubble aggregates rise, residual liquid from the lava migrates into the diapiric structures to form vesicle cylinders (Fig. 4).

Acknowledgments

This contribution was made possible by an LDRD grant from Los Alamos National Laboratory. The author thanks Marcia McLaren and William Page of Pacific Gas and Electric Company for the opportunity to participate on the field trip and thanks C.J. Janik (U.S. Geological Survey) for helping out with field work on the Hat Creek Basalt.

References

Anderson, A.T., and Gottfried, D., 1971, Contrasting behavior of P, Ti, and Nb in a differentiated high-alumina olivine tholeiite and a calc-alkaline andesitic suite: Geol. Soc. Amer. Bull., v. 82, p. 1929-1942.

Anderson, A.T., Swihart, G.H., Artioli, G., and Geiger, C.A., 1984, Segregation vesicles, gas filter-pressing, and igneous differentiation: Jour. Geol., v. 92, p. 55-72.

Bowen, N.L., 1928, The evolution of the igneous rocks: Princeton, N.J., Princeton Univ. Press, 332 p.

Fuller, R.E., 1931, The geomorphology and volcanic sequence of Steens Mountain in southeastern Oregon: Univ. Wash., Public. in Geol., v. 3, p. 1-130.

Goff, F.E., 1977, Vesicle cylinders in vapor-differentiated basalt flows: Ph.D. thesis, Univ. Calif., Santa Cruz, 181 p.

Goff, F.E., 1996, Vesicle cylinders in vapor-differentiated basalt flows: Jour. Volcanol. Geotherm. Res., in press.

Jaeger, J.C., 1961, The cooling of irregularly shaped igneous bodies: Am. Jour. Sci., v. 259, p. 721-734.

Kuno, H., 1965, Fractionation trends of basalt magmas in lava flows: Jour. Petrol., v. 6, p. 302-321.

Manga, M., and Stone, H.A., 1994, Interactions between bubbles in magmas and lavas: Effects of bubble deformation: Jour. Volcanol. Geother. Res., v. 63, p. 267-279.

Muffler, L.J.P., Clynne, M.A., and Champion, D.E., 1994, Late Quaternary normal faulting of the Hat Creek Basalt, northern California: Geol. Soc. Amer. Bull., v. 106, p. 195-200.

Roeder, P.L., and Emslie, R.F., 1970, Olivine-liquid equilibrium: Contr. Mineral. Petrol., v. 29, p. 275-289.

Shaw, H.R., 1972, Viscosities of magmatic silicate liquids: An empirical method of prediction: Am. Jour. Sci., v. 272, p. 870-893.

TABLE 1: Locations of sites showing good examples of vesicle cylinders, sheets, and pods in the Warner and Hat Creek Basalts, northeastern California.

Name	Location
Warner, A	South side of Highway 395, 6 km NE of Alturas (Kuno, 1965).
Warner, C	Top of grade, west side of Highway 139, 8 km NW of Canby.
Hat Creek	About 15 m above valley floor, W edge of Murken Bench on USFS 22 (site 2 of Muffler et al, 1994); about 12 km N of junction of Highways 44 and 89 (near Old Station).

TABLE 2: Physical characteristics of vesicle cylinder-bearing lavas in the Warner and Hat Creek Basalts, California.[1]

Characteristic	Warner, A	Warner, C	Hat Creek
Vesicle cylinders per square meter[2]	20	20	50
Ave. closest cylinder spacing (cm)[2]	26	24	17
Max. gdmass pheno. dimension, plag (mm)	1.3 x 0.24	1.6 x 0.30	N.M.
Phenocryst content at eruption (%), vesicle free	≤50	≤50	N.M.
Average porosity (%)	12	10	N.M.
Iddingsite alteration of olivine pheno. (%)	30-40	30-40	present
Thickness of flow (m)	8	7	4.5-6
Max. height of VC (m)	6-6.5	5.5	2.5-3
Calc. eruption temperature (°C)[3]	1235	1205	1175
Calc. viscosity of differentiate (poise)[4]	2.3×10^4	2.3×10^4	N.M.

[1]Data from Anderson and Gottfried (1971), Goff (1977) and this study; locations in Table 1. N.M. means not measured or calculated.

[2]Measured 1 m above base for Warner locations and 2 m above base at Hat Creek site.

[3]From olivine-glass geothermometer of Roeder and Emslie (1970).

[4]From Shaw (1972); assumes temperature of 1075°C, water content of 0.5 wt-%, 40% crystals, and 10% bubbles.

TABLE 3: Selected chemical analyses of host basalts and vesicle cylinders in the Warner and Hat Creek Basalts, California.[1]

Site	Warner, A			Warner, C		Hat Creek	
Sample	A	A6C	AS	139-1	139-1C	HC4-0	HC4-6
Type	Flow	Cyl	Cyl	Flow	Cyl	Flow	Cyl (?)
Major Elements (wt-%)							
SiO_2	48.10	49.20	49.52	47.7	49.4	49.4	54.0
TiO_2	0.86	2.47	2.84	1.12	2.38	1.0	2.7
Al_2O_3	16.29	12.54	12.35	17.8	13.8	17.4	13.7
Fe_2O_3	2.82	3.97	6.19	3.72	3.79	1.4	10.6
FeO	7.63	11.38	9.80	6.39	9.24	7.8	2.0
MnO	0.16	0.27	0.23	0.16	0.22	0.21	0.24
MgO	8.97	4.90	3.59	8.68	5.55	8.7	3.6
CaO	11.59	10.11	8.85	11.2	10.7	10.6	6.4
Na_2O	2.43	3.68	4.33	2.94	3.84	2.6	3.6
K_2O	0.23	0.52	0.73	0.26	0.50	0.4	1.3
P_2O_5	0.07	0.34	0.51	0.16	0.37	0.17	0.53
$H_2O(+)$	0.42	--	0.57	--	--	0.35	1.5
$H_2O(-)$	0.25	0.24	0.65	0.14	0.19	0.02	0.00
TOTAL	99.82	99.62	100.16	100.3	100.0	100.0	100.0

[1] Hat Creek analyses from Anderson and Gottfried (1971); others from Goff (1977).

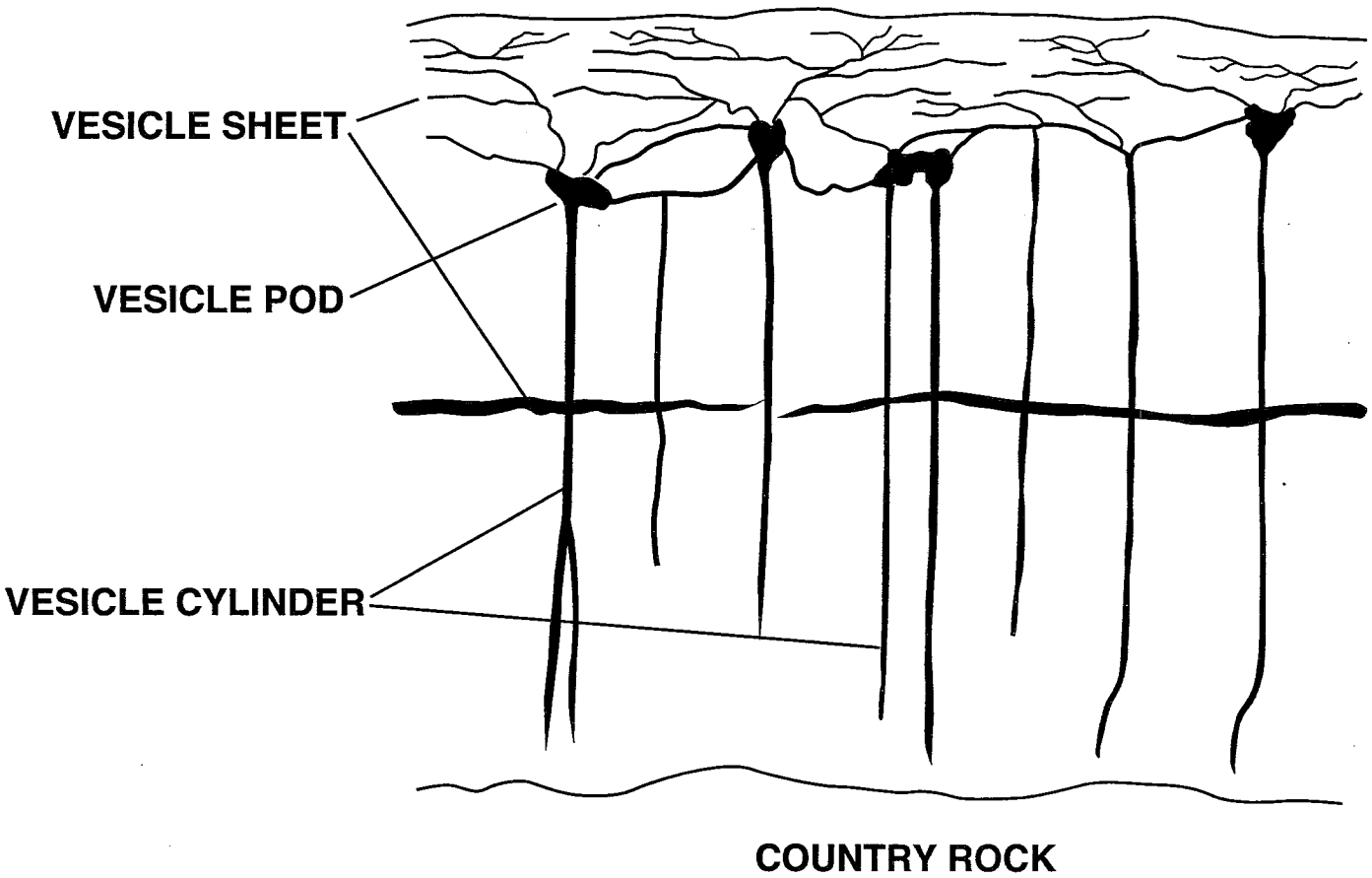

Figure 1: Idealized cross-section of a basalt flow (3-10 m thick) showing the network of vesicle cylinders, pods, and sheets. The country rock may be another flow or flow-unit of basalt. Warped cylinders near base of flow indicate that the cylinders may form when the flow is still plastic enough to creep.

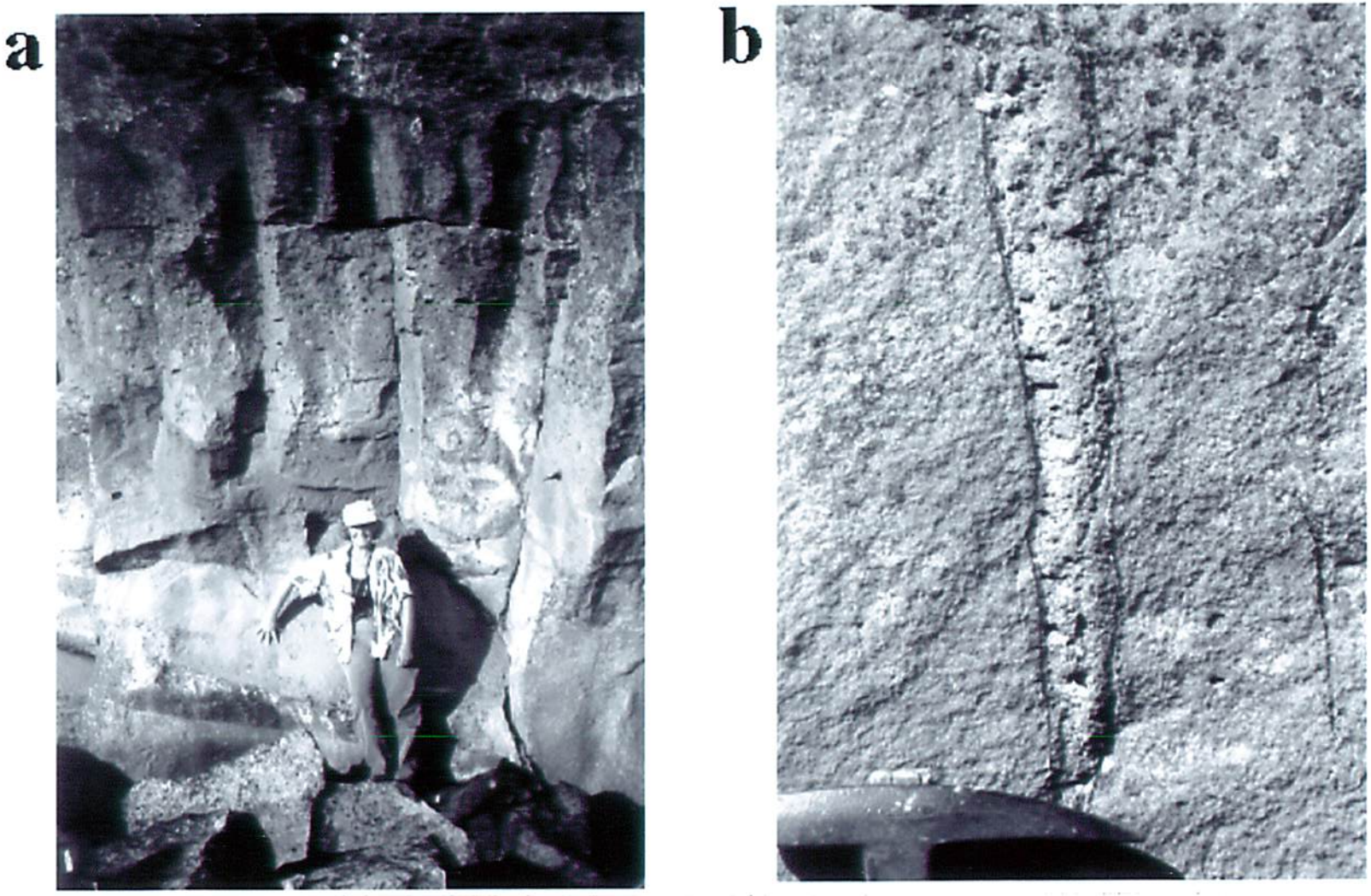

Figure 2: Photos of the Hat Creek Basalt at Murken Bench, California: **a.** Lava flow is about 4.5 to 6 m thick and contains a variety of vesicle cylinders, sheets, and pods. Right hand of geoscientist is pointing at the three vesicle cylinders shown in the photo of Stop 2-1. **b.** Vesicle cylinder exposed in vertical face near photo a; cylinders are more vesiculated and contain more evolved glass and mineral compositions than host lava.

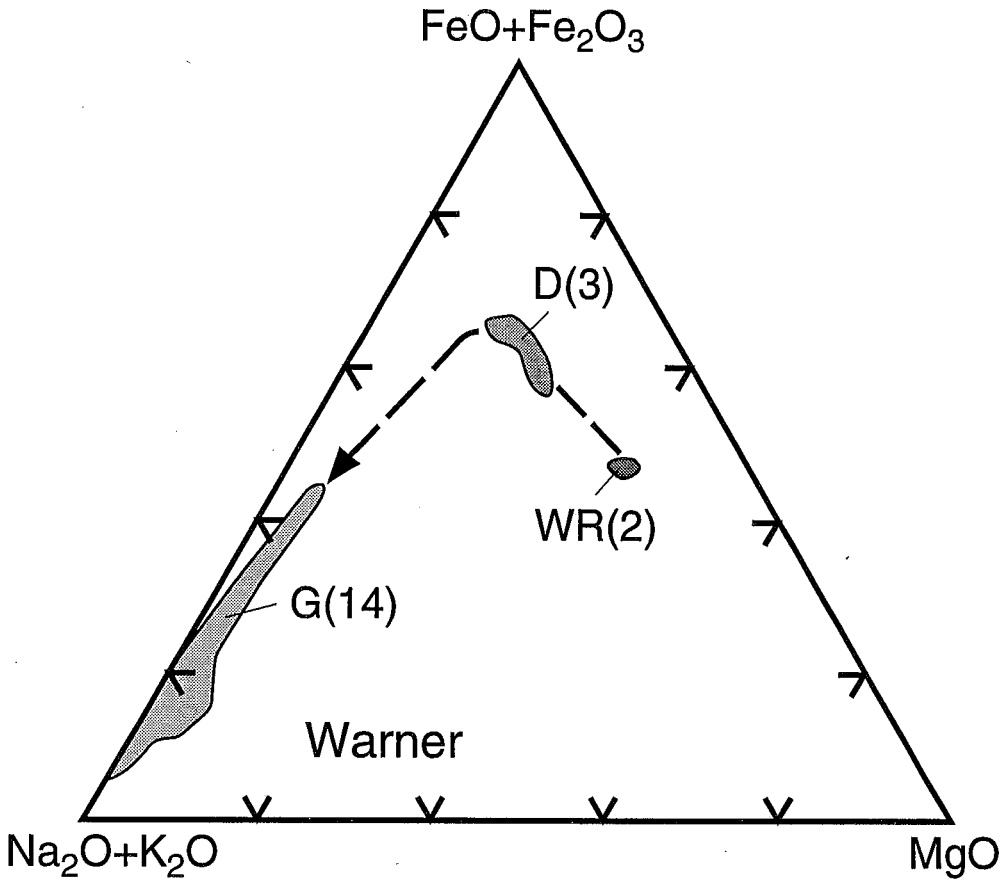

Figure 3: AFM diagram of analyses for whole rock basalts (WR), differentiates (D), and residual glasses (G) in the Warner Basalt, California. Numbers in paraentheses are numbers of analyses. The line connecting the data clouds follows a classic differentiation trend. Data from Goff (1977).

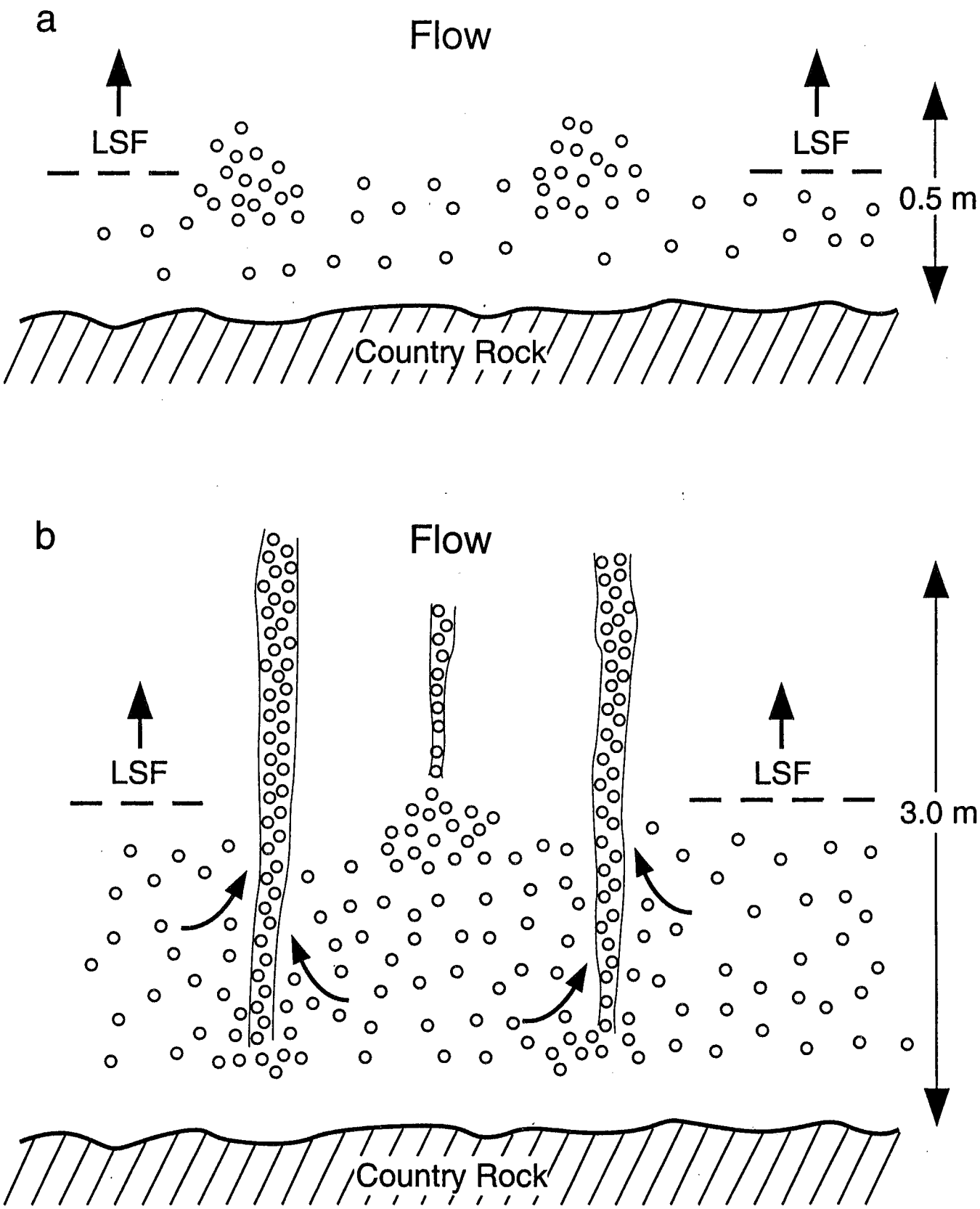

Figure 4: Cartoons dipicting the formation of vesicle cylinders from **a.** coalescing clusters of bubbles at the lower solidifcation front (LSF) of a basalt flow (Manga and Stone, 1994). **b.** Once a cluster of bubbles begins to rise, residual melt in the enclosing lava migrates into the low pressure region created by this disturbance. The cylinders accumulate gases and differentiate as they rise and the diameters of the cylinders increase as they move upwards toward the chilled top crust. Upward migration of the soidification front causes formation of new cylinders (Goff, 1996).

APPENDIX 2 - 3

A. Volcanic and Glacial Stratigraphy in the Hat and Lost Creek Drainages and the Age of Lassen Peak.
Gerstel, W.J., Clynne, M.A.

B. Stratigraphic, Lithologic, and Major Element Geochemical Constraints on Magmatic Evolution at Lassen Volcanic Center, California.
Clynne, M.A.

C. Late Cenozoic Volcanism, Subduction, and Extension in the Lassen Region of California, Southern Cascade Range.
Guffanti, M., Clynne, M.A., Smith, J.G., Muffler, L.J.P., Bullen, T.D.

VOLCANIC AND GLACIAL STRATIGRAPHY IN THE HAT AND LOST CREEK DRAINAGES AND THE AGE OF LASSEN PEAK

By Wendy J. Gerstel and Michael A. Clynne

Volcanic activity on a regional scale in the southern Cascade range is predominantly basaltic to andesitic, forming dispersed, relatively small, short-lived volcanoes. Superimposed on the regional volcanoes are a few, longer-lived, much larger volcanic centers, including the Lassen Volcanic Center, where eruptions between 0.65 and 0.40 Ma produced the predominantly andesitic Brokeoff stratovolcano (ancient Mount Tehema). Eruptions of at least 50 km^3 of rhyolitic magma and consequent formation of a small caldera at 0.4 Ma initiated a dacitic dome field on the northern flank of the Brokeoff cone. Subsequent activity has been concentrated in two major sequences of primarily dacitic volcanism at about 0.25-0.20 Ma and at less than about 0.1 Ma, infilling the caldera. In addition, hybrid andesite consisting of mixed mafic and silicic magma, including the dome Lassen Peak, has erupted intermittently from the margins of the dacitic dome field since about 0.3 Ma.

Lassen Peak is the largest and most prominent feature among scores of dacitic and rhyodacitic domes, lava flows and pyroclastic deposits on the north flank of the Lassen Volcanic Center (Clynne, 1990, 1993). These domes were emplaced in several episodes over the past 400 ka, the most recent major episode producing 6 volcanic domes and related pyroclastic deposits of Chaos Crags, about 1 ka in age. Lassen Peak, a single large dome somewhat older than Chaos Crags (Figure 1, and Tables 1a and 1b), represents the youngest previous eruptive episode. The summit of Lassen Peak was also the site of a relatively minor eruptive episode in 1915-1917. During that episode, between May, 14 and May 22, 1915, a small dacite dome and flow were emplaced at the summit of Lassen Peak, and avalanches, pyroclastic flows, and debris-flows occurred on its northeastern side (Christiansen and Clynne, 1987).

The most commonly cited age for Lassen Peak has been that of Crandell (1972), who suggested that the dome was emplaced about 11,000 years ago. This suggestion was based on the extensive talus slopes draping the dome which were thought to demonstrate that the dome was largely unglaciated, and that any post-dome-emplacement glacial ice would have removed this talus. It appears that much of the original hot emplacement dome material has been removed, and that over 95% of the remaining talus is erosional, not part of the original dome carapace.

During the mapping of the volcanic stratigraphy in the Lassen area in the early 1980's, Clynne noted clasts of dacite of Lassen Peak in lateral moraines on the north side of Lassen Peak. These moraines had been mapped by Crandell (1972) as (late) Tioga age, using Sierra Nevada nomenclature, and were thought to pre-date the emplacement of Lassen Peak.

The initial approach used by Gerstel in interpreting the glacial chronology was to differentiate glacial deposits in the Hat and Lost Creek drainages based on constituent clast lithology. Available geochronology of volcanic flows and associated pyroclastic deposits outcropping in the Hat and Lost Creek drainages (Table 1a), offered the possibility of bracketing the ages of several episodes of glaciation (Gerstel, 1989).

A dacite lava flow, dacite of Kings Creek, erupted from a vent now covered by Lassen Peak, is overlain by glacial deposits and in turn overlies peat and glacial

deposits devoid of dacite of Lassen Peak (Fig. 2, site 59e). The peat yields a radiocarbon age of 31,280 +/- 2000 BP (USGS #1849). This date provides a maximum age for the Lassen Peak dome. Andesites of Hat Mtn., Raker Peak, Badger Mtn. and dacites and rhyodacites of Reading Peak and Crescent Crater also provided stratigraphic control for the study (Fig. 3).

As it turned out, differences in till clast lithologies permitted the distinction of only two time stratigraphic units (Fig. 3). The older, more extensive deposits lacking clasts of dacite of Lassen Peak and were informally assigned to the Reading Peak episode of glaciation. The younger deposits, where dacite of Lassen Peak is a major constituent (>85%), were informally assigned to the Lassen Peak episode of glaciation.

Further differentiation of glacial deposits within the Reading Peak and Lassen Peak groupings was based on modifications of the classic relative dating (RD) techniques (Burke and Birkeland, 1979); weathering rind thickness, soil profile development, relative topographic/geographic position, and morphologic expression (Table 2). Modifications to the standard RD techniques were made as it became apparent that in this setting with repeated volcanic activity, episodic input of debris flows and tephra (primary and reworked) eliminated the opportunity for boulder frequency counts, affected soil profile development, and distorted the results of weathering rind data.

Weathering rind measurements were problematic where clay coatings were observed on till stones. The coatings apparently slow the process of weathering-rind formation. When the measurements on coated stones were eliminated from the data set, two age populations could be distinguished (Figs. 4a and 4b). Furthermore, weathering rind thicknesses could only reliably be measured on andesite stones, precluding the use of dacite stones, a major constituent of the younger deposits, because of their granular texture.

Using the available radiocarbon dating, the Reading Peak episode deposits were correlated to Oxygen Isotope Stage 4. The younger, Lassen Peak episode deposits were correlated to Oxygen Isotope Stage 2. Based on the modified RD techniques, 2 phases of glaciation were identified in the deposits of the Reading Peak episode, and 4 phases in the deposits of the Lassen Peak episode (Table 1b and Fig. 5).

Proposed regional correlations of the Hat and Lost Creek glacial stratigraphy with that in the Sierra Nevada, Trinity Alps and southern and central Oregon Cascades are shown in Table 3.

The sequence of lateral moraines on the west side of Badger Mtn. marks a position of the valley glacier some time during the Reading Peak episode of glaciation. Although no end moraines associated with this episode were observed within the study area, it is possible that they are buried under the younger Lassen Peak episode outwash and debris flows. The ice source during the Reading Peak episode must have been the Brokeoff Volcano and Bumpass group domes including Reading Peak, Ski Heil, Bumpass Mtn., Mt. Helen, and others. At its maximum, ice of the Lassen Peak episode, emanating from Lassen Peak, extended approximately 8 km into the Hat Creek drainage and 6.5 km in to the Lost Creek drainage, to an elevation in both drainages of about 1650m (5400ft.) (Fig. 1).

Evidence for the pre-maximum Oxygen Isotope Stage 2 existence of Lassen Peak lies partially in the geographic extent of Lassen Peak episode deposits in the Hat

and Lost Creek drainages. Additional evidence is found in the striations surrounding Lassen Peak, particularly those radiating from the southeast flank on the surface of the rhyodacite of Kings Creek (with a date of approx. 32 ka). These striations suggest a carapace ice source model for the Lassen area during the waning of the Lassen Peak episode of glaciation (Fig. 6).

A deposit north of Raker Peak and deposits found since Gerstel's work and located along the southwest base of Badger Mtn., lend additional strong evidence to the hypothesis that Lassen Peak existed prior to maximum stage 2 glaciation. These deposits consist of angular clasts of dacite of Lassen Peak in a sandy matrix. We interpret them as rockfall deposits carried to this location on the surface of the ice.

So, with the peat deposit beneath the rhyodacite flow of Kings Creek providing a maximum age for Lassen Peak dome emplacement of approximately 31 ka, and the timing of the maximum Stage 2 glaciation providing a minimum age of approximately 18-20 ka, we suggested an age for Lassen Peak of 23-28 ka (Gerstel and Clynne, 1989). This age estimate has been confirmed by a recent $^{40}Ar/^{39}Ar$ date of 27.1±2.8 ka (Turrin, et al.).

REFERENCES CITED

Burke, R.M., and Birkeland, P.W., 1979, Re-evaluation of multiparameter relative dating techniques and their application to glacial sequences along the eastern escarpment of the Sierra Nevada, Calif., Quaternary Research, v. 11, p. 21-51.

Christiansen, R.L., and Clynne, M.A., 1986, The climactic eruptions of Lassen Peak, California, in May 1915, abs. EOS, Transactions American Geophysical Union, vol. 67, no. 44, p. 1247.

Clynne, M.A., 1990, Stratigraphic, lithologic, and major element geochemical constraints on magmatic evolution at Lassen volcanic center, California, Journal of Geophysical Research, vol. 95, no. 2, p. 19,651-19,669.

Clynne, M.A., 1993, Geologic studies of the Lassen volcanic center, Cascade Range, California, Ph.D. Dissertation, University of California, Santa Cruz, 413 p.

Crandell, D.R., 1972, Glaciation near Lassen Peak, northern California: U.S. Geological Survey Professional Paper 800-c, p.c179-c188.

Eppler, D.B., 1984, Characteristics of volcanic blasts, mudflows and rock-fall avalanches in Lassen Volcanic National Park, California, Ph.D. Thesis, Arizona State University, 332 p.

Gerstel, W.J., 1989, Glacial chronology and the relationship to volcanic stratigraphy in the Hat and Lost Creek drainages, Lassen Volcanic National Park, California, MSc Thesis, Humboldt State University, 89 p.

Gerstel, W.J., and Clynne, M.A., 1989, Glacial stratigraphy in the Lassen Peak area of Northern California; implications for the age of Lassen Peak dacite dome, Abs. Geological Society of America 42nd annual meeting, vol. 21, no. 5, p. 83.

Turrin, B.D., Clynne, M.A., Christiansen, R.L., Muffler, L.J.P., Gerstel, W.J., Champion, D.E., and Trimble, D.A., (in press), $^{40}Ar/^{39}Ar$ Ages from Lassen Peak, California: Dating a young heterogeneous dacite dome, and implications for the age of latest Pleistocene glaciation in the southern Cascade Range.


Andesite of Raker Pk
27
405 QR1
Qbf
QR2
Emigrant Bord Campground
Andesite of Badger Mtn
Badger Mountain
430
431
QR1
Andesite of Raker Peak
QL1
QL1a
385
Mobles
Chaos Jumbles
Manzanita Lake
Chaos Crags
Andesite of Hat Mtn
QL1
QL2
415
Hot Mud Flow
Hot Mountain
Crescent Mud Flow
Crater
1915 Mud Flow
400
QL2
QL3
QL2
LASSEN PEAK
Lassen Peak
Rhyodacite of Kings Creek
Rhyodacite of Reading Pk
QL1
Brokeoff Volcano
Ridge Lake
Kings Creek
Cold Boiling
Hemlock Lake
1 MILE
FIGURE 1

Glacial Units

Early-Holocene	Late-Holocene	QL4	- Youngest deposits of the Lassen Peak episode a,b show nested moraines of the "mini-glacier" w, m, e show protalus ramparts on Reading Peak.
		QL3	- Sharp-crested moraines located at 2500-2700m surrounding Lassen Peak. Oxidized to <1 m.
Late-Wisconsin	Oxygen Isotope Stage 2	Qbfs	- Small debris fan exiting from abandoned Hat Creek channel, associated with deglaciation of QL1 or QL2 phase. Contains >60 % dacite of Lassen Peak.
		Qbf	- Large debris fan exiting from abandoned Hat Cr channel, associated with retreat of Central Plateau ice. Contains 98% andesite of Badger Mtn.
		QL2	- Lateral moraines of Lost Creek on Lassen Peak terminating at 1950 m; ground moraine n. of Reading Peak, Lake Helen moraine. All show oxidation to <1m.
		QL1	- Oldest deposits of the Lassen Peak episode, oxidation to 0.5-1.0 m. At least two recessional positions in Lost Cr.
Mid(?)- Wisconsin	Oxygen Isotope Stage 4	QR2	- Younger deposits of Reading Peak episode. Lateral moraines 10 1550 m well preserved in Hat Cr. Oxidation to >2 m. Contain no dacites of Lassen Pk.
		QR1	- Older deposits of Reading Peak episode. No morainal morphology. Oxidation to >2 m. Contain no dacites of Lassen Peak.

Fig. 1 (cont'd)

Table 1a. List of lithologic units found in till deposits of the Hat and Lost Creek drainages, determined or estimated ages, and area of outcrop. Dates are from USGS.

Unit Name as appears on Plate 1	Age and dating technique	Area of exposure/ outcrop
rhyodacite, pyroclastics, and airfall of Chaos Crags	1000-1100 BP/ 14C on charred wood	2-4 km north of Lassen Pk west of Lost Cr.
dacite of Lassen Peak	15-29 ka/ stratigraphic correlation	headwaters of Lost Cr., West Fork Hat Cr.
rhyodacite of Kings Creek	31±2 ka/ 14C on underlying peat deposit	headwaters of West Fork Hat Cr.
dacite of Sunflower Flat	35±2 ka/ 14C on charred wood	4-6 km north of Lassen Pk, west side Lost Cr.
andesite of Hat Mountain	25±21 ka/ K-Ar	east side Hat Cr. n. of Hat Lake, Central Plateau
dacite of Krummholz Dome	>30 ka, <~100 ka/ stratigraphic corr.	headwaters of Lost Cr.
dacite of Crescent Crater	>30 ka, <~100 ka/ stratigraphic corr.	west side of headwaters of Lost Cr.
dacite of Reading Peak	212±2 ka/ K-Ar	headwaters East and West Fork Hat Cr.
diktytaxic basalt	>~100 ka, <270 ka/ stratig. corr./K-Ar	Hat Cr. north of Hat Lake
andesite of Raker Peak	270±18 ka/ K-Ar	Raker Pk and flows to north, west of Hat Cr.
andesite of Brokeoff Stage II	~400 ka/ K-Ar, fission track on Rockland Tephra	Isolated outcrops upper Hat and Lost Cr.
andesite of Badger Mountain	708 ± 21 Ka/K-Ar	east side Hat Cr. 12 km north of Lassen Peak

Table 1b -- Sequence and timing of glacial and volcanic events in the Hat and Lost Creek drainages, north of Lassen Peak.

Age	Unit	Description
80 y	1915 deposits	Flows, dome, pyroclastic flows, debris flows
300-200+?	QL4 deposits	Moraines of mini-glacier (se side Lassen Pk), and pro-talus ramparts north side of Reading Pk
1100-1000 ^{14}C	Dacite of Chaos Crags	Domes, pyroclastic flows, fallout pumice
8130±110 ^{14}C	no designation	Debris flows associated with deglaciation of the QL3 advance
	QL3 deposits	Moraines at 2600-2900 m elev. on Lassen Peak and Reading Pk
	QL2 deposits	Moraines at 2100-2400 m elev. in upper Lost Cr. (Survivor Ridge)
	QL1 deposits	Moraines at 1800-2100 m in Lost and Hat Creeks (e.g., on Raker Peak, on Hill 6103', and along Sunflower Flat domes)
27.3±2.3 Ar/Ar	Dacite of Lassen Pk	Dome of Lassen Pk and dome-collapse avalanche deposits in upper Lost Cr.
	Dacite of Kings Cr	Pyroclastic flows and lava flow in upper Hat Cr.
31,180±200 ^{14}C	peat deposit	Silty, quiet-water sediments interbedded with sand and gravel in Hat Cr below Hat Lake
34,360±360 ^{14}C	Dacite of Sunflower Flat	Domes and pyroclastic flows

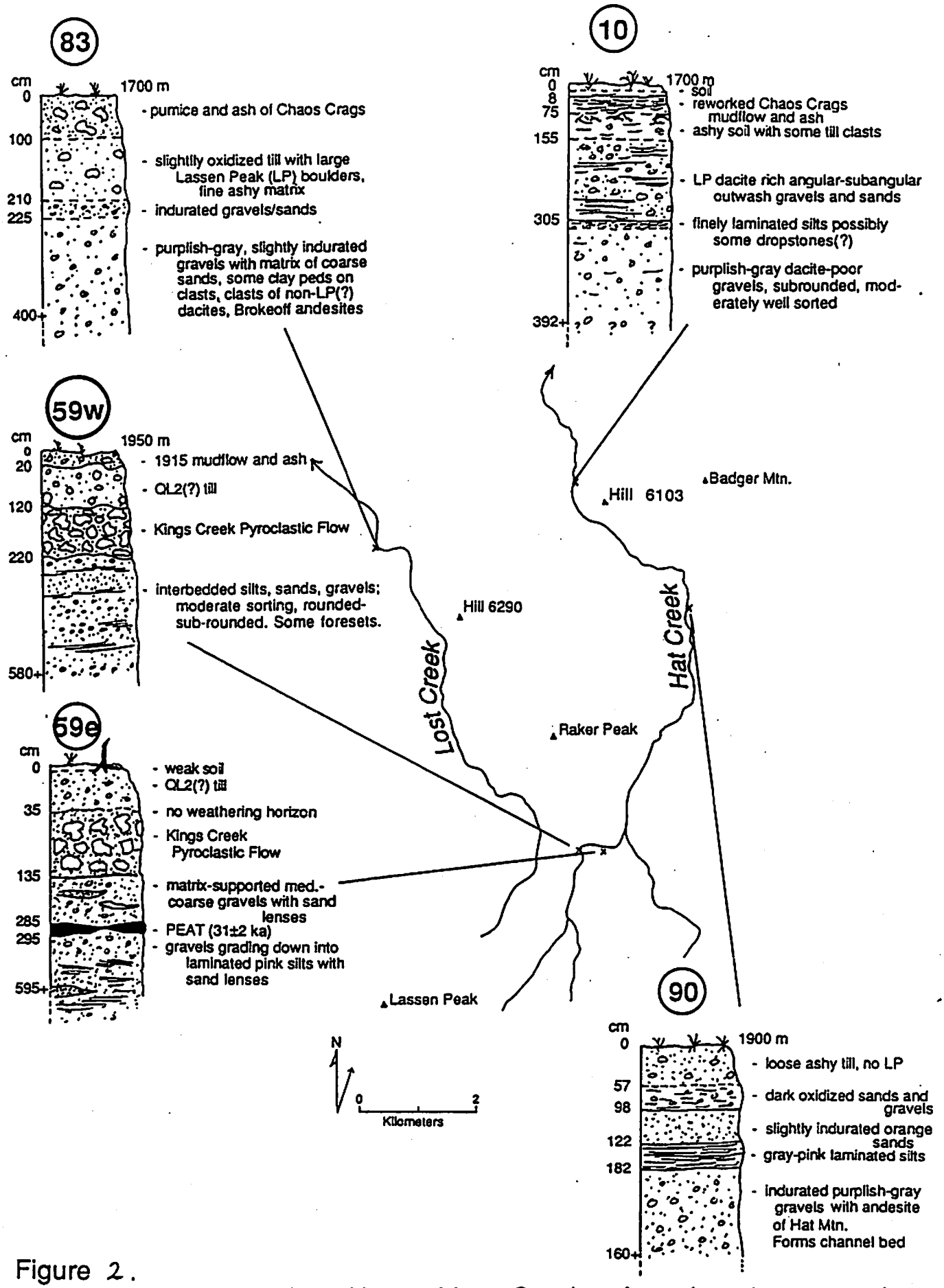

Figure 2.

Key sections along Hat and Lost Creeks of stratigraphy suggesting jökulhlaup events and periodic damming of Hat Creek. Circled numbers are site localities refered to in text or photographs. LP= dacite of Lassen Peak.

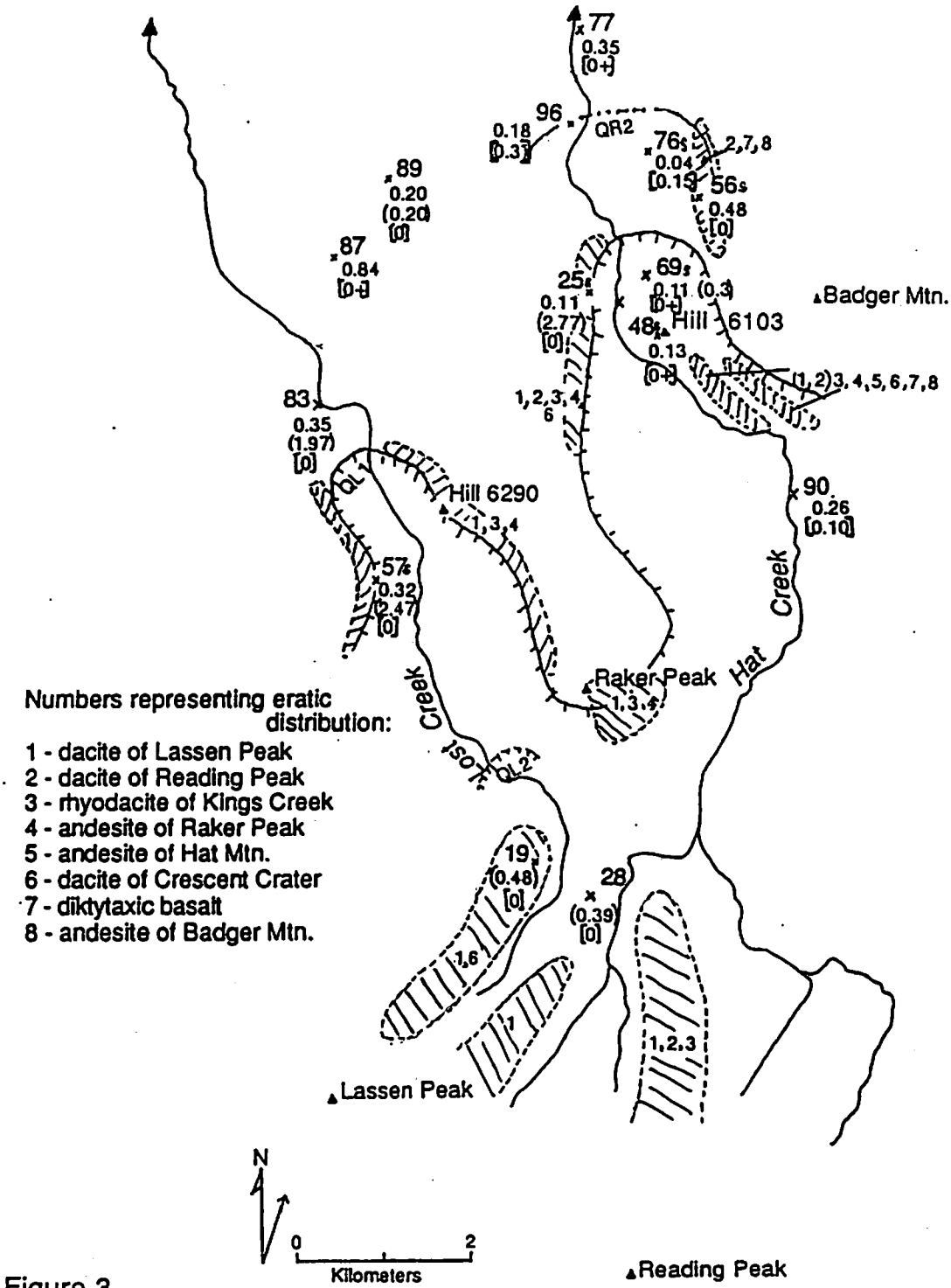

Figure 3.
Site localities and mean thicknesses for weathering rind measurements on andesite till stones. S indicates pits with soil profile descriptions, indicates maximum ice limit for the Q_{L1} phase of the Lassen Peak episode, ( ) show mean rind thickness on dacite stones, [ ] show mean thickness of silt/clay coatings. All measurements are in mm. Number codes show distribution of lithologies in till deposits, as listed above.

Table 2. Criteria used to differentiate till deposits in the Hat and Lost Creek drainages, and some limitations with respect to local application.

Technique	Local Application	Advantages and Limitations
Stratigraphic sequence	described in bankcuts, soil profiles, outcrops	useful in bankcuts as indicative of depositional environments and relative timing of events, only isolated outcrops of unit contacts
Geographic position	applied in both Hat and Lost Cr drainages	most useful for Lassen Pk episode tills
Weathering rind formation	used on all deposits to support distinction by lithologic constituent	problems with silt/clay coatings, variable lithologies and textures-cautious application still useful
Soil profile development	investigated in all till deposits not buried by 1915 mud and debris flows	limited use as relative-dating tool, lack of good chronosequence with age controls, lack of complete profiles due to logging`
Hydration rinds on volcanic glass	used on rhyodacite of Kings Creek and clasts of same in tills of QL1	porphyritic nature of flow makes chemical determination of glass difficult, good potential for relative dating
Progressive landform modification	applied in both drainages	useful tool for all deposits taking into account lack of original well-defined morphology
Surface boulder counts	considered but not used	not applicable due to cover of Chaos Crags airfall to variable thickness
Tephrochronology	looked for in riverbank exposures and soil profiles	no critical stratigraphic marker beds found, only deposits younger that glacial deposits
Paleomagnetism	used to envestigate timing of emplacement of Lassen Pk dome	need more data for development of local curve for calibration
Lichenometry	north side Reading Pk used to distinquish QL3 and QL4 deposits	revised technique of percent cover worked well
Dendrochronology	attempted on early QL4 deposits below "mini-glacier".	near tree-line, too much time between glacial deposition and colonization of mtn hemlock

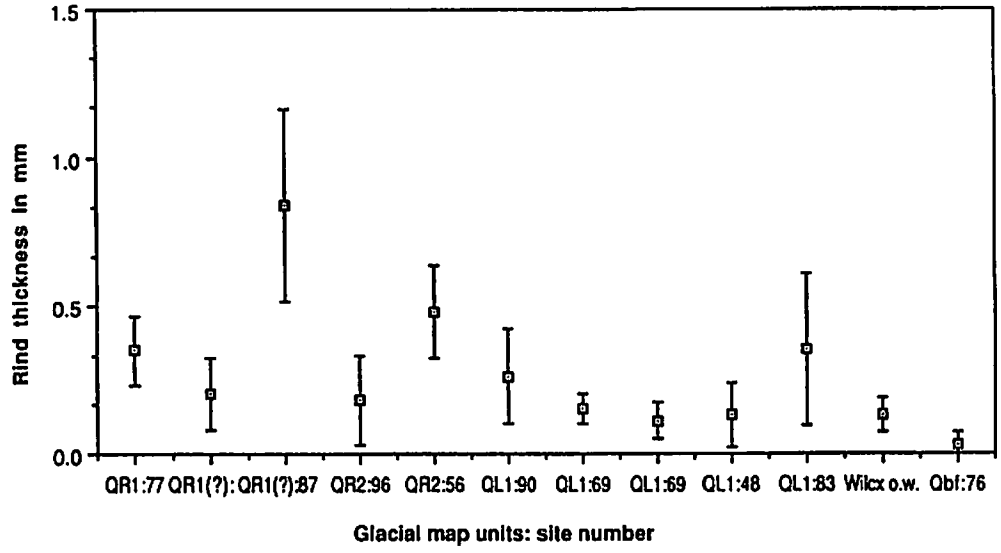

Figure 4a. Plot of weathering rind thicknesses ± 1 standard deviation measured on andesite till stones from localities shown on Plate 1.

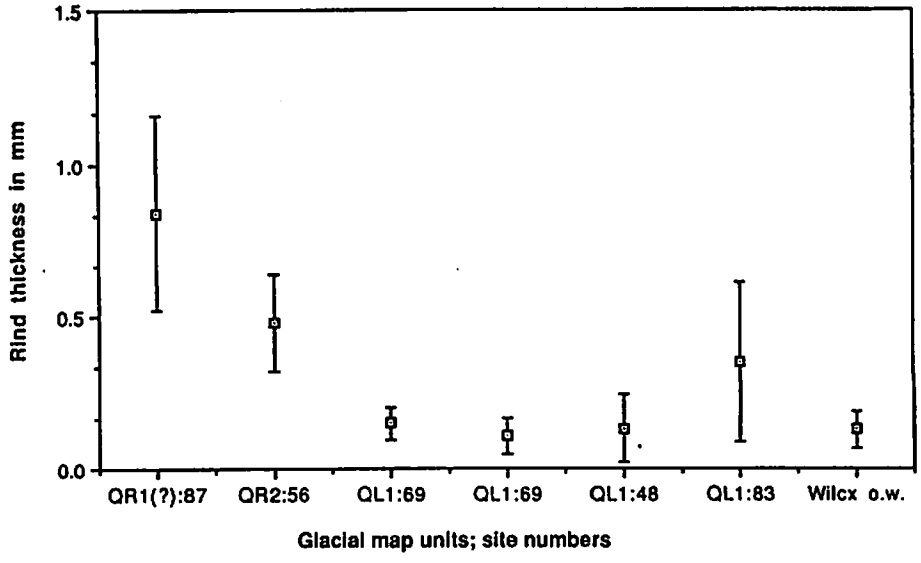

Figure 4b Plot of weathering rind thicknesses ± 1 standard deviation measured on andesite till stones from pits where no silt/clay coating were observed.

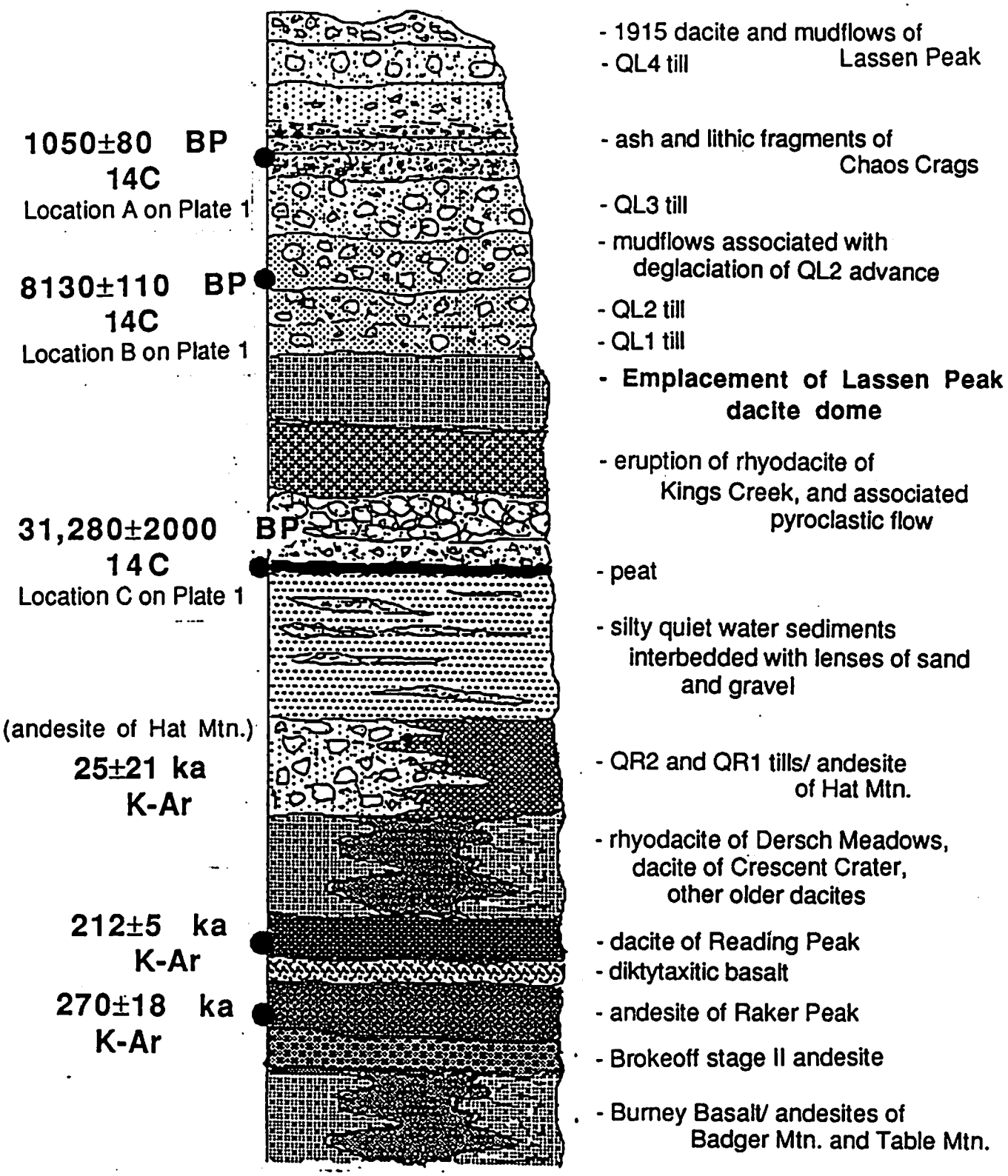

Figure 5.
Idealized composite section of the glacial and volcanic stratigraphy in the Hat and Lost Creek drainages. ● indicates dated units. Age and dating technique are listed to the left of the diagram. All dates are provided by USGS.

Table 3. Regional correlation of glacial stratigraphy.

Age	References				
	Gerstel, this report	Carver (1972)	Scott (1972)	Sharp (1960)	Burke and Burkeland (1979)
	QL4 *1000 BP	Neoglacial II *500 BP *2000 BP Neoglacial I	Jefferson Park (phase 1 & 2)		
*6600BP		MAZAMA "O"			
oxygen isotope Stage 2	QL3 *8800 BP	Zephyr Lake *9400 BP	Canyon Cr advance		Tioga
			Cabbot Creek Glaciation		late
	QL2	*13 Ka Waban drift		Morris Meadows	
	QL1	(extensive with numerous recessionals)	Suttle Lake advance		middle
					early
	* 31±2 ka				
oxygen isotope Stage 4	QR2	Varney Creek	Jack Creek (40-80 ka) or (120-200 ka)	Rush Creek	
	QR1				
oxygen isotope Stage 5e or 6				Alpine Lake (?)	Tahoe
			Abbot Butte (200-900 ka)		
				Swift Creek (pre-Wisc.)	

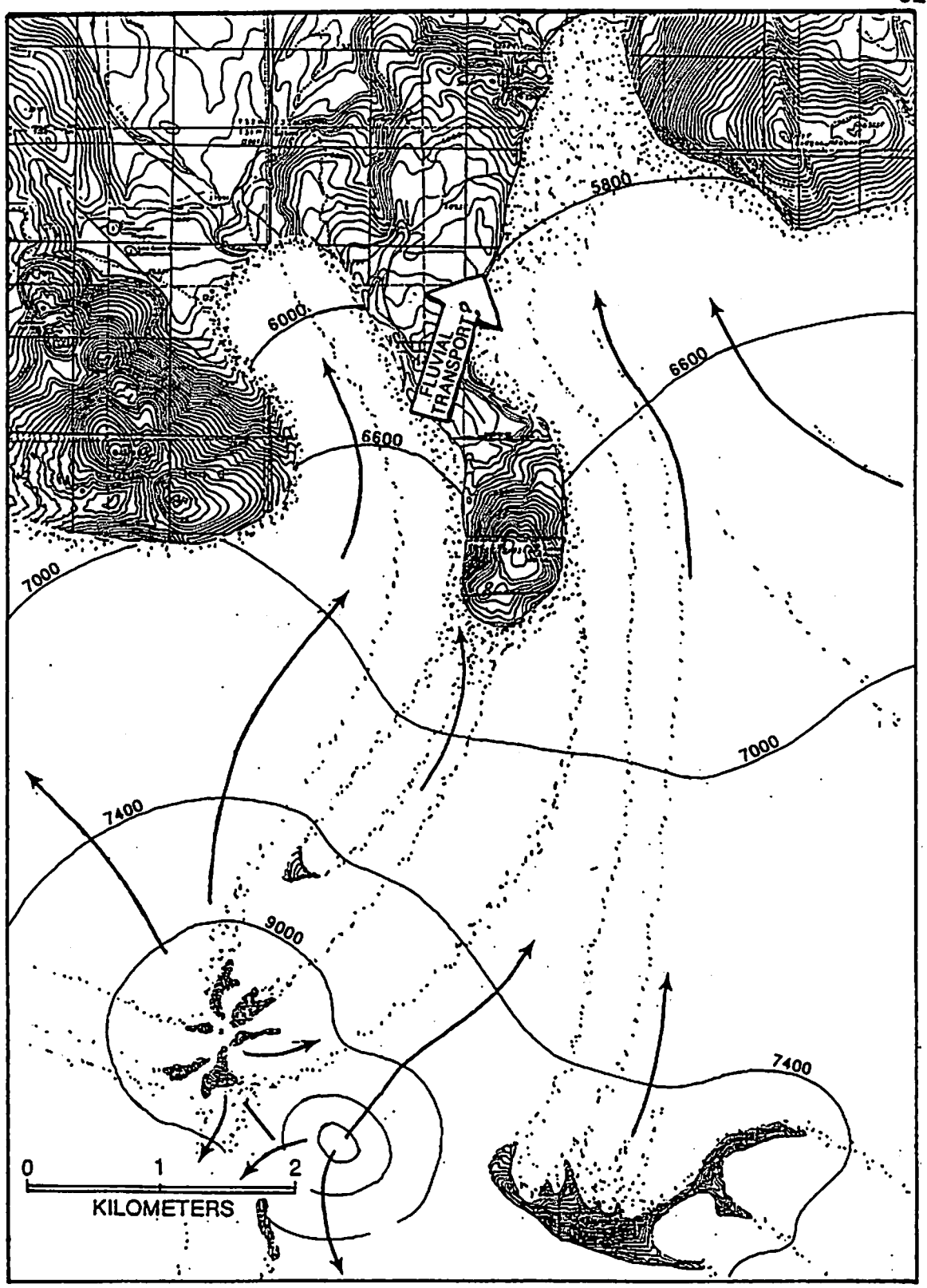

Figure 6. Reconstruction of ice sheet showing maximum extent of ice cover during the Q_{L1} phase of the Lassen Peak episode. Arrows indicate ice flow direction, stipple pattern indicates eratic transport lines.

JOURNAL OF GEOPHYSICAL RESEARCH, VOL. 95, NO. B12, PAGES 19,651–19,669, NOVEMBER 10, 1990

Stratigraphic, Lithologic, and Major Element Geochemical Constraints on Magmatic Evolution at Lassen Volcanic Center, California

MICHAEL A. CLYNNE

U.S. Geological Survey, Menlo Park, California

The Lassen volcanic center is the most recent of several long-lived volcanic centers in the southernmost Cascade Range. These centers have erupted products ranging from basaltic andesite to rhyolite and are superimposed on a background of regional basaltic to andesitic volcanism. The evolution of the Lassen volcanic center is described in three stages. Stages I and II comprise the Brokeoff volcano, and 80 km^3 andesitic stratocone, active from 600 to 400 ka. Brokeoff volcano is compositionally equivalent to the regional basaltic andesite to andesite volcanism in the Lassen region and is the result of structurally controlled focusing of the diffuse regional mafic magmatism. Stage III comprises a silicic dome field and adjacent area of hybrid andesites and has a total volume of about 100 km^3. Volcanism during stage III was episodic and is subdivided into four sequences of lithologically and temporally distinct lavas. Stage III began at 400 ka with a rhyolitic, caldera-forming pyroclastic eruption and chemically related lavas. Additional sequences of dacite erupted between 250–200 ka and 100–0 ka. Hybrid andesites erupted adjacent to the silicic dome field between 300 and 0 ka. Porphyritic andesite and dacite with high Al_2O_3, low TiO_2, medium K_2O and FeO/MgO ratios of 1.5–2.0 are the most abundant rock types in the Lassen volcanic center. However, the single most voluminous unit is sparsely phyric rhyolite pumice. In general, the lavas of Lassen volcanic center form a single coherent trend on major element variation diagrams and in pseudo-quaternary phase space, consistant with an origin either by fractional crystallization or magma mixing. In detail, however, the lack of systematic temporal change in silica and subtly crossing trends indicate a complex origin. A variety of statistically successful fractional crystallization models can be constructed that derive Brokeoff andesites from regional magmas. An important conclusion of the modeling is that if fractional crystallization is the process responsible for generation of Brokeoff andesite, then the parent magma must be low to medium K in geochemical affinity in order to explain the variation in K_2O. However, although major element variation can be modeled by fractional crystallization, petrographic and stratigraphic evidence indicates that magma mixing is an important but subtle process in Brokeoff lavas and suggests that lavas evolved in small independent batches. Lavas erupted during stage III, while predominantly silicic, range from 53 to 75% SiO_2. Disequilibrium mineral assemblages in the stage III lavas indicate that they are not directly derived from Brokeoff andesite by fractional crystallization. Mixing of silicic magma with regional mafic magma and disaggregation of andesitic quenched magmatic inclusions play dominant roles in the compositional diversity of stage III lavas.

INTRODUCTION

Multidisciplinary integrated studies of volcanic centers can lead to more thorough understanding of the origin and evolution of their magmatic systems. This paper describes regional geologic background, generalized geochronology, stratigraphy, lithologies, and major element geochemistry of the Lassen volcanic center. These data provide important constraints on the interpretation of trace element and isotopic data presented by *Bullen and Clynne* [this issue] and allow the development of a model for the origin of the Lassen volcanic center magmas.

Least squares modeling of the major element geochemical data presented here indicates that andesites of Brokeoff volcano can be derived by fractional crystallization of low- to medium-K_2O basalt found in the Lassen region of the Cascade Range. However, a more rigorous interpretation of the geochemical data, in light of the lithologic, stratigraphic, and geochronological data indicates that magma mixing is the predominant process in all stages of the development and magmatic evolution of the Lassen volcanic center.

Paper number 90JB01731.

REGIONAL GEOLOGY

The Cascade Range is the volcanic expression of subduction zone magmatism resulting from interaction of the Juan de Fuca, Explorer, and Gorda plates with the North American plate. Subduction is strongly oblique, and young relatively warm oceanic crust is being subducted. At the southern end of the Juan de Fuca plate system, although a well-defined Benioff Zone is lacking and the Gorda South plate has recently stopped being subducted [*Riddehough*, 1984], the general character and composition of volcanism are similar to magmatism in the rest of Cascade Range.

Volcanism in the southernmost Cascade Range can be characterized on two scales. Detailed [*Muffler and Clynne*, 1989, also unpublished data, 1989] and reconnaissance [*Guffanti et al.*, this issue; T. L. T. Grose, written communication, 1989; J. G. Smith, written communication, 1989] geologic mapping show that on the regional scale, volcanism is predominantly basaltic to andesitic, and hundreds of coalescing volcanoes have small volumes in the range 10^{-3} to 10^2 km^3 and lifetimes that are relatively short. Individual volcanoes range from monogenetic cinder cones of basalt and basaltic andesite to larger lava cones and shields of basaltic to andesitic composition. Rocks with greater than 60% SiO_2 are sparse. Superimposed on this regional mafic to intermediate volcanism are a few long-lived, much larger volcanic centers that have erupted products spanning a wide compositional range from basaltic andesite to dacite or

rhyolite. Each of the larger centers consists of a basaltic andesite to andesite composite cone and flanking silicic domes and flows.

Five centers younger than about 3 Ma have been recognized in the Lassen Volcanic National Park area, but older unrecognized centers undoubtedly exist. In order of decreasing age, these five are the Snow Mountain (J. G. Smith, personal communication, 1989), Dittmar [*Clynne*, 1985], Yana [*Lydon*, 1968], Maidu [*Wilson*, 1961], and Lassen [*Clynne*, 1984] volcanic centers. Detailed and reconnaissance geologic mapping and reinterpretation of the literature provide a basis for development of a general evolutionary model of the geologic history of a given volcanic center. Early in the life of the composite cone, basaltic andesite to dacite are erupted as thin lava flows and pyroclastic deposits. This part of the history is characterized by heterogeneity in composition and lithology. Later history of the cone is dominated by eruption of thick lava flows of silicic andesite to dacite, characterized by compositional and lithologic homogeneity. Growth of the composite cone is followed by a period of silicic volcanism on its flanks. The silicic magma system provides a shallow heat source for a hydrothermal system that develops within the core of the main cone. Alteration of permeable rocks of the cone facilitates glacial and fluvial erosion of the central part of the volcano. The result is selective preservation of a resistant rim of thick cone-building lava flows and flanking silicic rocks around a central depression, which replaces the altered and eroded core of the composite cone.

The four older volcanic centers in the Lassen area have reached the terminal stage, and their hydrothermal systems are extinct. The youngest, the Lassen volcanic center, has likewise progressed into the terminal stage but hosts active silicic volcanism and a well-developed hydrothermal system, including the thermal features in Lassen Volcanic National Park and Mill Canyon. The Lassen volcanic center is the best preserved of the volcanic centers and can be used as a general model of center-type volcanism in the Lassen area.

Lassen Volcanic Center

The Lassen volcanic center is located in northeastern California at the southern end of the Cascade range (Figure 1) and occupies the western and central parts of Lassen Volcanic National Park. The distribution of rock units is shown in Figure 2, a generalized geologic map of Lassen Volcanic National Park and vicinity. The evolution of the Lassen volcanic center is described in the three stages: stages I and II represent the growth of the composite cone, Brokeoff volcano, and stage III represents the subsequent, dominantly silicic volcanism on the flanks of Brokeoff volcano. The details of the stratigraphy are outlined by *Clynne* [1984]. The chemical evolution of the Lassen volcanic center is illustrated schematically in Figure 3, and pertinent lithologic aspects of the Lassen volcanic center are summarized in Table 1. In Table 1 and all subsequent descriptions the following divisions between rock types are used: basalt (less than 53 wt % SiO_2), basaltic andesite (53–57 wt % SiO_2), andesite (57–63 wt % SiO_2), dacite (63–72 wt % SiO_2), and rhyolite (greater than 72 wt % SiO_2).

K-Ar ages (G. B. Dalrymple, written communication, 1989) in combination with other geochronologic data [*Meyer et al.*, 1980; *Trimble et al.*, 1984; also unpublished radiocarbon ages, 1989; C. E. Meyer, written communication, 1989] provide a general geochronology of the Lassen volcanic center. Brokeoff volcano was active for about 200 ka: stage I from about 600 to 470 ka and stage II from 470 to 400 ka. Three subsequent sequences of silicic lavas correspond to pulses of volcanism that occurred at 400 (Rockland sequence), 250–200 (Bumpass sequence), and 100–0 ka (Loomis sequence). The Twin Lakes sequence of hybrid intermediate lavas was emplaced intermittently during the time span from 300 to 0 ka.

Brokeoff Volcano

The evolution of the Lassen volcanic center began with the construction of Brokeoff volcano, an andesitic stratocone. The best evidence of the stratigraphic record at Brokeoff volcano lies in the well-exposed sections of lavas in deep glacial canyons on the south and west flanks. The exhumed core of Brokeoff volcano consists of thin, glassy, basaltic andesite to andesite lava flows and abundant, fragmental rocks that erupted from summit vents. The flanks consist primarily of thicker, more crystalline, silicic andesite lava flows with sparse fragmental rocks, probably erupted from vents on the flanks of the volcano. Geologic mapping indicates that Brokeoff volcano had a basal diameter of approximately 12 km. Reconstruction of Brokeoff volcano by projecting the radial dips of its preserved lavas suggests that at its maximum the summit was approximately 3350 m high [*Williams*, 1932]. The base of the Brokeoff volcano is exposed at about 1700 m in Mill Creek and 1950 m in Bailey and Blue Lake canyons. The reconstructed total volume of Brokeoff volcano is estimated to be about 80 km^3.

Early Brokeoff lavas are porphyritic olivine-augite basaltic andesites and olivine-augite, olivine-hypersthene-augite, and hypersthene-augite andesites. Minor hornblende-pyroxene dacites appear sporadically throughout the lower part of Brokeoff volcano. Phenocryst abundance in the basaltic andesites and andesites is variable from 5 to 40%, and the phenocrysts are generally less than a few millimeters in size. Plagioclase is ubiquitous and usually the dominant phenocryst phase. A conspicuous feature of the early Brokeoff lavas is their lithologic diversity. Adjacent flow often have different phenocryst assemblages and radically different phenocryst abundances. Olivine-bearing basaltic andesites and andesites are more common, and olivine is more abundant in lavas from the lower part of the section [*Clynne*, 1984].

Textural evidence for disequilibrium in early Brokeoff lavas is common. Multiple populations of phenocryst phases are often present. Plagioclase phenocrysts often occur as two distinct populations, one of which is strongly to weakly resorbed. Olivine is usually rimmed by pyroxene. Augite jacketed by bronzite or hypersthene (or vice versa) commonly coexists with unjacketed pyroxene phenocrysts. Microprobe analyses of mafic phenocrysts (M. A. Clynne, manuscript in preparation, 1990) confirm the common presence of disequilibrium assemblages in early Brokeoff lavas. Reverse and normally zoned pyroxenes coexist in some lavas, and compatible-element spikes in phenocryst zoning profiles are common. Some lavas contain two populations of pyroxene that appear to be in textural equilibrium but in which one population is more magnesian and has high compatible-element content (e.g., up to 0.5 wt % Cr_2O_3). Many lavas contain pyroxenes with rims more magnesian

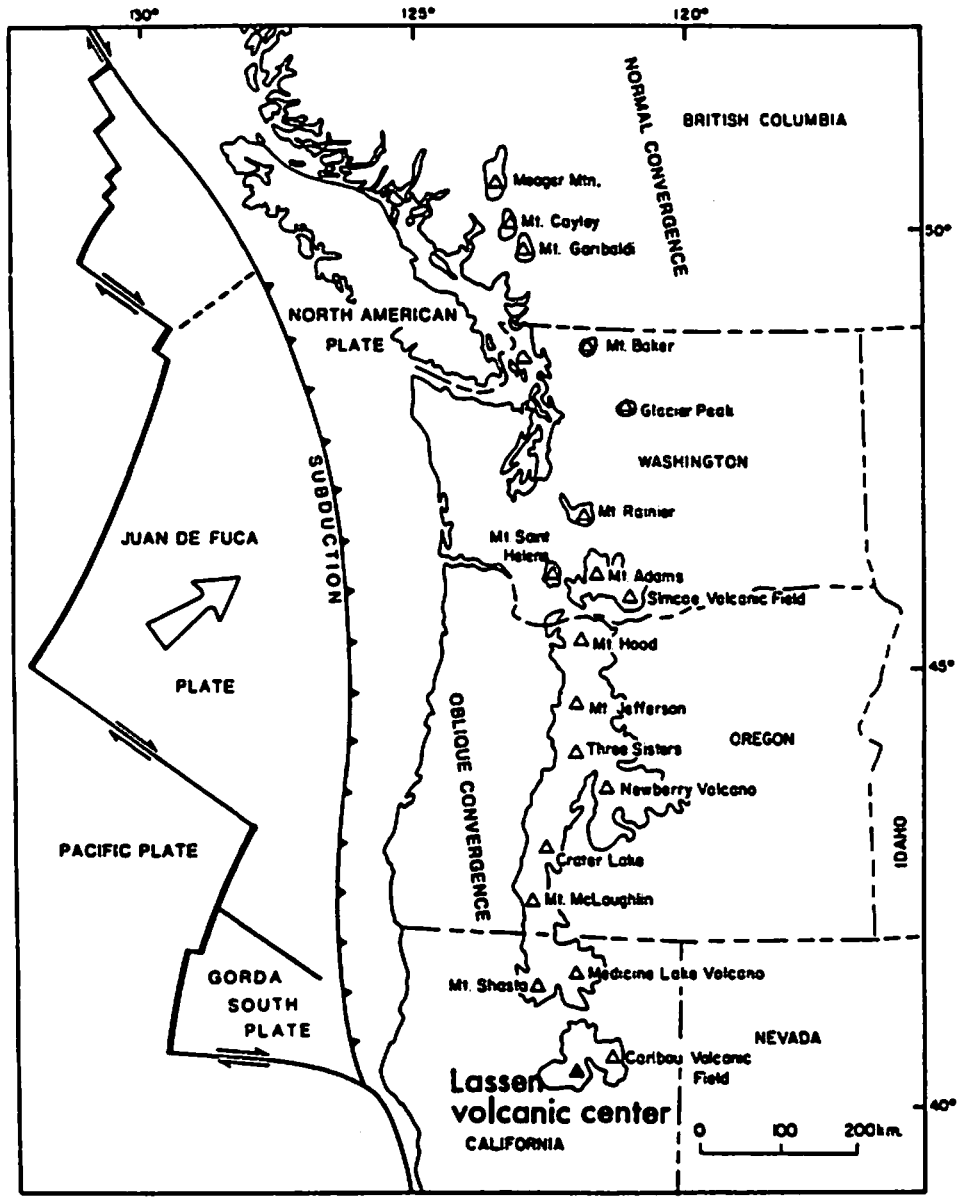

Fig. 1. Location map showing the tectonic framework of the Cascade Range and the relationship of the Lassen volcanic center to other Cascade volcanoes. Solid line denotes extent of Quaternary volcanic rocks.

than their cores by 5–10 mol % En. These could result from decompression [*Ewart et al.*, 1975], an increase in f_{O_2}, magma mixing, or a combination of processes.

The latter part of the history of Brokeoff volcano consists of porphyritic augite-hypersthene silicic andesite lava flows erupted from flank vents. These lavas dip away from the volcano on the outer flanks of the major remnants, are usually 30 m or more thick and lack intercalated fragmental rocks. In contrast to the early Brokeoff lavas, the phenocryst assemblage and content of late Brokeoff lavas are homogeneous. Late Brokeoff andesites contain 30–40% phenocrysts of plagioclase, hypersthene, augite, and titanomagnetite that are larger (e.g., plagioclase usually about 5 mm) than phenocrysts in early Brokeoff andesites. Partially resorbed olivine is often present but sparse. Hornblende is rarely present. Textural and compositional features of the phenocrysts suggestive of disequilibrium are less common and less pronounced than in the early Brokeoff lavas.

A conspicuous feature of the late Brokeoff andesite lavas is the ubiquitous presence of abundant, small (5 mm to a few centimeters) glomeroporphyritic clots with hypidiomorphic to allotriomorphic granular texture. Cumulate-textured xenoliths also are present but uncommon. The mineral assemblage of the clots (plagioclase + augite + hypersthene + Fe-Ti oxide ± olivine) is the same as that of the host lavas. Microprobe analyses (M. A. Clynne, manuscript in preparation, 1990) indicate that the mineral compositions are similar to those in the host lavas, although subtle differences (more magnesian and compatible element-rich compositions) occur in the clots. However, textural features indicative of recrystallization (orthopyroxene poikilitically enclosing anhedral olivine, patchy zoned plagioclase, vermicular oxide, and exsolution lamellae in clinopyroxene and orthopyroxene) preclude them from being simply clots of the host lava phenocrysts. Similar textural features have been observed in plutonic rocks and have been interpreted as cumulates fractionated from primitive magmas in the roots of island arcs [*Beard*, 1986; *Burns*, 1985; *DeBari and Coleman*, 1989].

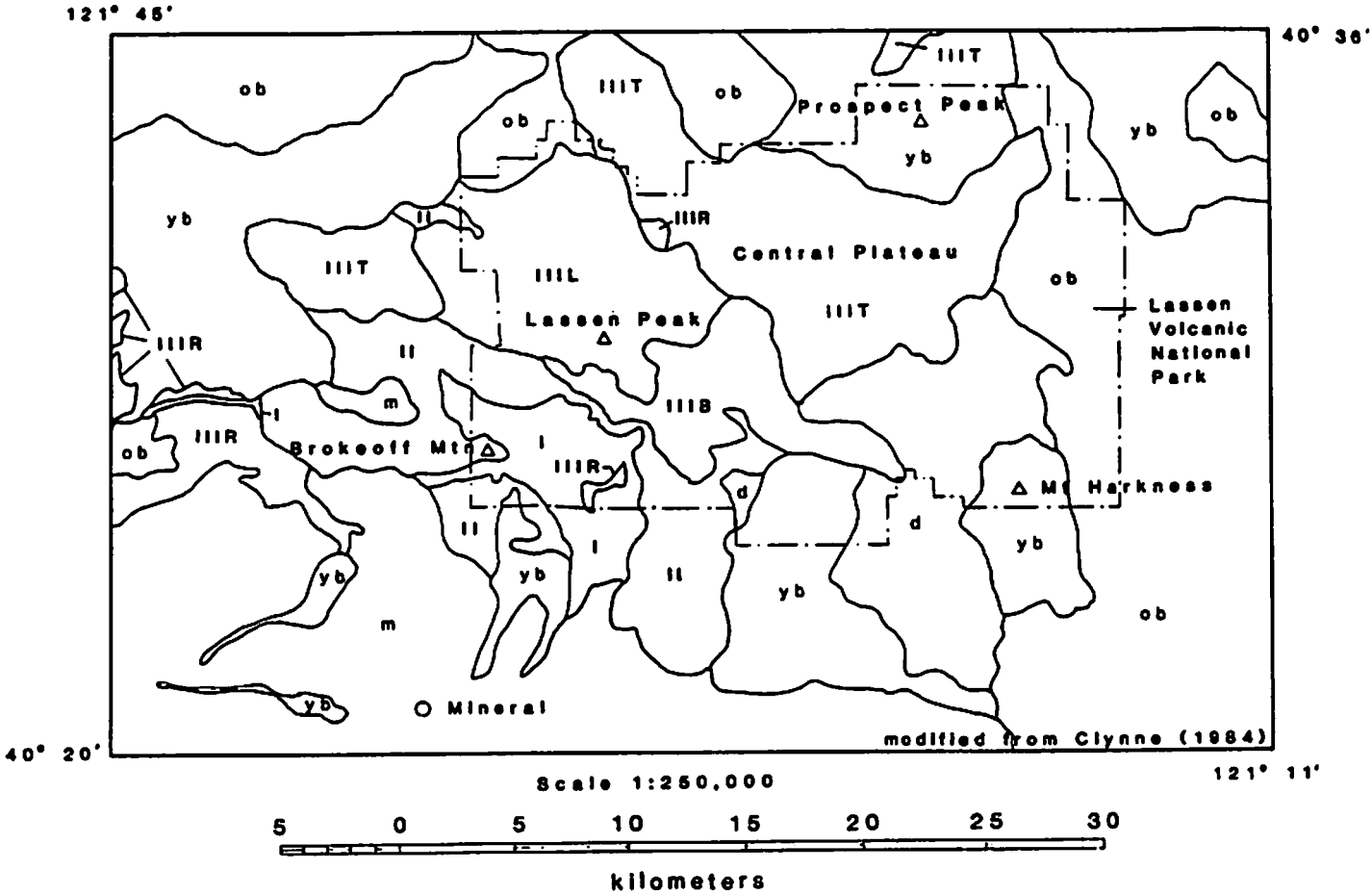

EXPLANATION

VOLCANIC CENTERS

LASSEN VOLCANIC CENTER

STAGE III

- IIIT — Twin Lakes sequence; hybrid andesites; lava shields and cones; augite andesite and olivine andesite; 300-0 ka
- IIIL — Loomis sequence; silicic domefield; lava domes and flows and pyroclastic flows; hornblende-biotite dacite and rhyodacite; 100-0 ka
- IIIB — Bumpass sequence; silicic domefield; lava domes and flows; 2-pyroxene-hornblende dacite; 250-200 ka
- IIIR — Rockland sequence; airfall and ashflow tephra, lava dome and flows, and debris flows; hypersthene-hornblende rhyolite, hornblende-biotite rhyolite and rhyodacite; 400 ka

STAGE II

- II — Brokeoff volcano; lava flows; augite-hypersthene andesite; 470-400 ka

STAGE I

- I — Brokeoff volcano; lava flows; 2-pyroxene-hornblende dacite; 470 ka; lava flows and stratified pyroclastic deposits; olivine-augite andesite; pyroxene andesite; 600-470 ka

MAIDU VOLCANIC CENTER

- m — composite cone; basaltic andesite to andesite; silicic domefield; rhyolite flows; 0.8 - 2.0 Ma

DITTMAR VOLCANIC CENTER

- d — composite cone; basaltic andesite to dacite and peripheral silicic rocks; 1.4 - 2.0+ Ma

REGIONAL VOLCANISM

- yb — Younger basalts to andesites; shield volcanoes and cinder cones
- ob — Older basalts to andesites; shield volcanoes and cinder cones

Fig. 2. Generalized geologic map of the Lassen volcanic center.

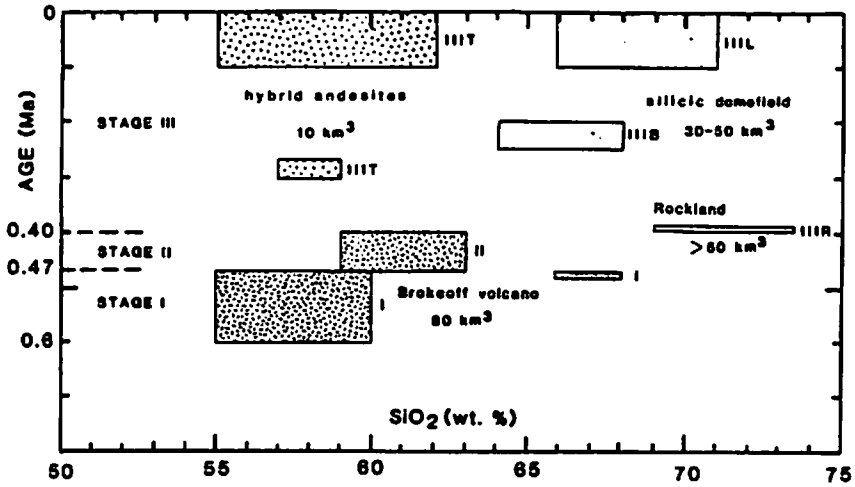

Fig. 3. Evolution of the Lassen volcanic center. All volumes are approximate (informally designated Rockland tephra of *Sarna-Wojcicki et al.* [1983] not recalculated to dense rock equivalent). Compositional ranges are generalized to reflect the majority of analyzed samples. Some undated units in the Loomis and Twin lakes sequences may fall outside the indicated age ranges. Unit symbols correspond to legend of Figure 2.

Given this lithologic framework, the evolution of the Brokeoff volcano can be described in two stages that correspond to the early (stage I) and late (stage II) Brokeoff lavas. The bulk of Brokeoff volcano consists of stage I deposits. A few lavas near the boundary of the stages resemble those of the other stage; however, the key characteristic in distinguishing the stages is the heterogeneity of adjacent flows in stage I and the homogeneity of adjacent flows in stage II. A small-volume but widespread eruption of a distinctive hornblende-pyroxene dacite lava (dacite of Twin Meadows) is a convenient stratigraphic boundary between stages I and II. *Clynne* [1984] reported an unconformity between the stages; however, the time interval represented by the unconformity is unresolvable by the K-Ar dating technique and must be short (G. B. Dalrymple, written communication, 1989).

STAGE III OF THE LASSEN VOLCANIC CENTER

Fundamental changes in the character of volcanism at the Lassen volcanic center mark the break between stage II and the more silicic phase of volcanism, or stage III. The locus of volcanism shifted to the northern flank of Brokeoff volcano,

TABLE 1. Generalized Petrographic and Petrologic Characteristics of the Lassen Volcanic Center

	Brokeoff Volcano			Stage III				
	Stage I	Stage I	Stage II	Rockland Sequence	Bumpass Sequence	Loomis Sequence	Twin Lakes Sequence	quenched Inclusions
Rock type	ol-augite and hyp-aug andesite	2-px-hb dacite	augite-hyp andesite	hyp-hb rhyolite	2-px-hb dacite	hb-bio dacite	ol-aug andesite	andesitic
Mineralogy								
Phenocrysts	10–30%, 2 mm	8–15%, 2 mm	30–40%, 5 mm	10%, 2 mm	10%, 5 mm	15–40%, 5 mm	5–10%, 1–5 mm	sparse, 2 mm
	plag aug ol hy	plag hb px	plag hyp aug	plag hb hyp	plag hb hyp aug	pl bio hb hyp qtz	pl bio hb hyp qtz	ol aug plag hyp hb bio qtz
	disequilibrium	disequilibrium	disequilibrium	equilibrium	disequilibrium	disequilibrium	disequilibrium	disequilibrium
Groundmass	hyalopilitic, pilotaxitic	hyalopilitic	hyalopilitic	holohyaline	hyalopilitic	holohyaline	holohyaline	hyalopilitic
Glomeroporphyritic clots	sparse	sparse	abundant	absent	sparse	absent	absent	absent
quenched inclusions	absent	abundant	sparse	sparse	sparse to abundant	sparse to abundant	sparse	
Chemistry								
SiO_2	55–64%	66–68%	59–63%	69–74%	64–68%	66–71%	54–65%	53–60%
MgO	2.5–8.0%	1.0–1.5%	3.0–4.0%	0.8–1.2%	1.7–2.8%	0.8–2.8%	2.5–8.5%	2.5–5.0%
K_2O	0.8–2.2%	3.0%	1.5–2.5%	2.7–3.4%	1.8–2.7%	1.8–3.0%	1.1–2.3%	0.7–1.4%
FeO/MgO	0.8–2.0	2.4–3.0	1.3–1.8	2.2–2.9	1.5–2.0	1.5–2.4	0.7–1.2	1.4–1.8
Morphology	thin flows, interbedded pyroclastics	thick flows	thick flows	ash flow tuff, dome, flows	domes, thick flows	domes, flows, pyroclastic flows	thick flow complexes	inclusions
Age, ka	600–470	470	470–400	400	250–200	100–0	300–0	

where the silicic dome field and Central Plateau of Lassen Volcanic National Park were constructed. The lavas of stage III are generally more silicic than those of Brokeoff volcano and are divided into four sequences with stratigraphic and lithologic distinction. A silicic dome field and associated pyroclastic deposits comprise the Rockland, Bumpass, and Loomis sequences which are dacite to rhyolite in composition. The Twin Lakes sequence formed the Central Plateau and is primarily basaltic andesite to andesite in composition.

At about the time Brokeoff volcano became extinct, stage III began with the eruption of the Rockland sequence. Dacite lava flows (dacite of Mount Conard) and a rhyolite dome (rhyolite of Raker Peak) probably preceded the eruption of at least 50 km^3 [*Sarna-Wojcicki et al.*, 1983] of dacitic to rhyolitic tephra as air fall and ash flows. Tephra of the Rockland sequence is sparsely phyric hypersthene-hornblende rhyolite. Domes and flows of the Rockland sequence are sparsely phyric hornblende-biotite rhyolite and porphyritic hornblende-biotite dacite.

Eruption of a magma volume as large as the Rockland ash flow universally results in structural subsidence [*Smith*, 1960] and probably produced a caldera of approximately 6 km diameter on the northern flank of Brokeoff volcano. Subsequent silicic volcanism and repeated glaciation have obscured topographic and structural expression of the caldera. However, four lines of evidence lend credence to the caldera-forming event: (1) Raker Peak appears to be truncated on its southern margin, and the vents for the dacite lava flows of Mount Conard have been downfaulted and removed, (2) Brokeoff lavas are missing in the northern quadrant of Brokeoff volcano and appear to be truncated in Upper Manzanita Creek and Hat Creek and below Raker Peak, (3) andesites that correlate to Brokeoff volcano are a major component of the lithic-fragment population of the Rockland tephra, and (4) domes of the Bumpass sequence erupted in a semicircle that forms the contact between Brokeoff volcano lavas and the dacite dome field.

The subsequent Bumpass and Loomis sequences comprise the bulk of the lavas of the silicic dome field and total about 30–50 km^3. The Bumpass sequence, which forms the southern part of the silicic dome field, consists of a group of 12 domes and flows of sparsely phyric to porphyritic 2-pyroxene-hornblende dacite. The lavas contain 5–20% phenocrysts. Plagioclase is the dominant phenocryst and usually present in two populations, one weakly to strongly resorbed and one unresorbed. Magnesian hornblende is the characteristic femic phase in Bumpass sequence lavas, orthopyroxene occurs in most rocks, and Fe-Ti oxides are ubiquitous. Large crystals (to 5 mm) of clinopyroxene optically resembling those in regional mafic lavas are common in some Bumpass sequence lavas. Magnesian olivine, biotite, and quartz occur in small amounts in some rocks, usually as resorbed crystals.

The Loomis sequence, which forms the northern and western parts of the silicic dome field, consists of porphyritic hornblende-biotite dacite erupted as domes, lava flows, and pyroclastic flows in at least 12 episodes during the past 100 kyr. Vents of the youngest domes and flows (35 ka to 1050 years) form a NNW linear array [*Guffanti et al.*, this issue] that suggests regional tectonic control of vent locations rather than the perturbing influence of a large, shallow magma chamber [*Bacon*, 1985].

Lavas of the Loomis sequence are porphyritic, hornblende-biotite dacite usually containing 20–30% phenocrysts. Plagioclase phenocrysts are large (often up to 1 cm), oscillatory or patchy zoned in the range An_{25-45}, and occasionally contain anhedral cores as calcic as An_{80}. Most lavas contain both resorbed and unresorbed plagioclase phenocrysts. Resorbed plagioclase phenocrysts have normally zoned overgrowth rims of An_{70-50}. Hornblende and biotite are the characteristic femic phases, and orthopyroxene and Fe-Ti oxides are usually present in minor amounts. Quartz is usually present but rarely comprises more than a few percent of the rock.

Evidence of magma mixing is abundant in lavas of the silicic dome field. The lavas of the Bumpass sequence usually contain resorbed phenocrysts such as quartz, biotite, and amphibole that are characteristic of more silicic magma, whereas the lavas of the Loomis sequence contain femic phenocrysts (magnesian olivine and augite and calcic plagioclase) that are characteristic of more mafic magma. Complex zoning of phenocrysts and multiple phenocryst populations are characteristic of both sequences. The dacite of Lassen Peak, a Loomis Sequence lava described by *Clynne* [1989] serves as an example. The dacite of Lassen Peak contains oscillatory zoned plagioclase of An_{25-35} composition which lack resorption textures and calcic rims. A second population of plagioclase phenocrysts is strongly resorbed (sometimes with small preserved cores of An_{25-35} composition) and thin, strongly normally zoned rims (An_{80-50}). A third population of plagioclase phenocrysts has An_{85-90} cores and strongly zoned rims like those on the resorbed phenocrysts. Plagioclase microlites in the dacite of Lassen Peak have zoning that also matches that on the rims of the resorbed phenocrysts. Also present in the dacite are multiple populations of other phases that can be distinguished on the basis of composition and texture. For example, three populations of amphibole, two populations of biotite, two populations of quartz, two populations of clinopyroxene, two populations of orthopyroxene, two populations of titanomagnetite, and single populations of ilmenite and magnesian olivine are observed [*Clynne*, 1989].

A conspicuous feature of silicic lavas at the Lassen volcanic center is the presence of fine-grained mafic inclusions of basaltic andesite to andesite composition. These are typically 10–20 mm in diameter but range from a few millimeters to 1 m in size. They are ellipsoidal to spheroidal in shape with crenulate margins convex toward the host rock. They are thought to represent mafic magma injected into and quenched by the silicic magma system and to be formed when the ratio of mafic to silicic magma is small [*Bacon*, 1986]. The inclusions vary in abundance from negligible to about 20%. Multiple populations of inclusions containing variable phenocryst assemblages and exhibiting variable degrees of recrystallization suggest that multiple inclusion-forming events are recorded in some lavas. The complexity of the phenocryst assemblage in the dacite of Lassen Peak described above is attributed to mixing of mafic and silicic magmas and the formation and subsequent disaggregation of quenched inclusions [*Clynne*, 1989, also manuscript in preparation, 1990]. Disaggregation of inclusions plays an important role in the origin of multiple and disequilibrium phenocryst populations and extends the range of silicic lavas at the Lassen volcanic center toward more mafic compositions.

Further evidence for the importance of magma mixing

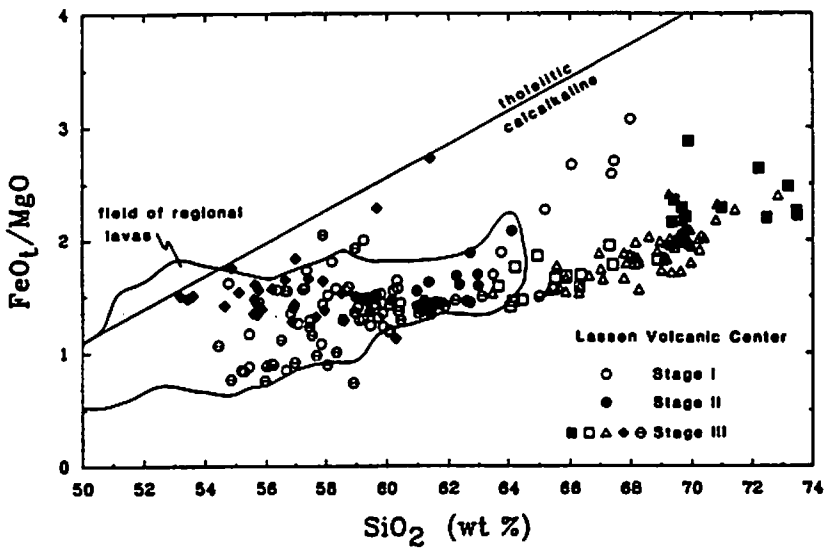

Fig. 4. FeO_t/MgO versus SiO_2 for rocks of the Lassen volcanic center. The lavas are strongly calc-alkaline as defined by lack of iron enrichment. Calc-alkaline-tholeiitic line after *Miyashiro* [1974]. Symbols for stage III lavas as in Figure 5 and field as in Figure 5.

during stage III lies in the unusual petrographic character of the Twin Lakes sequence, which consists of about 10 km^3 of hybrid andesite erupted peripheral to the dacite dome field throughout the span of stage III. The 10 lava flows thus far identified in this diverse sequence all have disequilibrium phenocryst assemblages characterized by the coexistence of magnesian olivine (Fo_{80-88}) and quartz. The rocks are porphyritic, black, glassy, olivine and augite and sometimes calcic plagioclase bearing and range in composition from basaltic andesite to dacite but are mostly andesite. They also contain abundant strongly resorbed felsic phenocrysts (sodic plagioclase, amphibole, biotite, and quartz) that resemble those in the dacites of the silicic dome field. Unresorbed felsic phenocrysts are absent. Quenched inclusions similar to those in the dome field lavas are often present, but they are small and sparse. Some of the lava flows are zoned in composition or phenocryst abundance and degree of resorption or contain flow units that are either more mafic or more silicic than the main part of the flow.

The mafic phenocryst assemblage of Twin Lakes lavas suggests that the mafic component was magma similar to that of the regional mafic volcanism. The silicic component was most likely dacitic magma similar to that of the silicic dome field. The predominately andesite compositions, lack of quenched inclusions, and degree of resorption of the felsic phenocrysts all suggest a large proportion of mafic magma in the Twin Lakes lavas. The abundance of femic and resorbed felsic phenocryst populations are variable but on the whole support an important role for the mafic component. Thermal modeling [*Sparks and Marshall*, 1986] suggests that relatively thorough mixing of this type will occur when the masses of the silicic and mafic mixing components are subequal or the mafic component is dominant.

MAJOR ELEMENT GEOCHEMISTRY

Porphyritic andesite and dacite with high Al_2O_3, low TiO_2, medium K_2O contents, and FeO/MgO ratios of 1.5–2.0 are the most abundant rock types (Table 1) in the Lassen volcanic center. However, the single most voluminous unit is sparsely phyric rhyolite pumice [Rockland ash flow). Early basaltic andesite and hybrid andesite are subordinate in abundance. Rocks of the Lassen volcanic center are similar in geochemistry and mineralogy to other medium-K_2O, calc-alkaline volcanic rocks emplaced through moderately thick crust on continental fragments or margins (e.g., Japan, New Zealand, and Central America) [*Ewart*, 1979, 1982; *Gill*, 1981].

Major element Harker variation diagrams (Figures 4–7) for the Lassen volcanic center show continuous trends from 53 to 74% SiO_2 (see *Clynne* [1984] and *Bullen and Clynne* [this issue] for tables of chemical data). The lavas of the Lassen volcanic center are strongly calc-alkaline as defined by lack of iron enrichment. FeO/MgO remains almost constant with increasing SiO_2 in stages I and II, except for a small increase in the dacites of Twin Meadows (Figure 4). Stage III lavas show a similar behavior with little increase in FeO/MgO even in the most silicic lavas. Broadly speaking, MgO, Al_2O_3, FeO, CaO, TiO_2, and P_2O_5 correlate negatively with SiO_2, whereas K_2O and Na_2O correlate positively with SiO_2 (Figures 5–7). Most major element oxides show considerable scatter at the low-silica end of the array and relative consistancy at the high-silica end. The details of the major element geochemical variation of Lassen volcanic center lavas is discussed below using MgO and K_2O variation with SiO_2 (Figures 6 and 7) to illustrate the behavior of compatible and incompatible elements respectively. Trace elements in rocks of Lassen volcanic center show distributions similar to their geochemically similar major elements [*Bullen and Clynne*, this issue].

The overall compositional evolution of the Lassen volcanic center is from andesite in Brokeoff volcano to dominantly silicic in stage III. Except for rare dacite lavas, SiO_2 in stage I and stage II (Brokeoff) lavas is restricted to the range from basaltic andesite to silicic andesite. With time the lavas of Brokeoff volcano evolve toward increasing silica and decreasing compatible major element diversity while

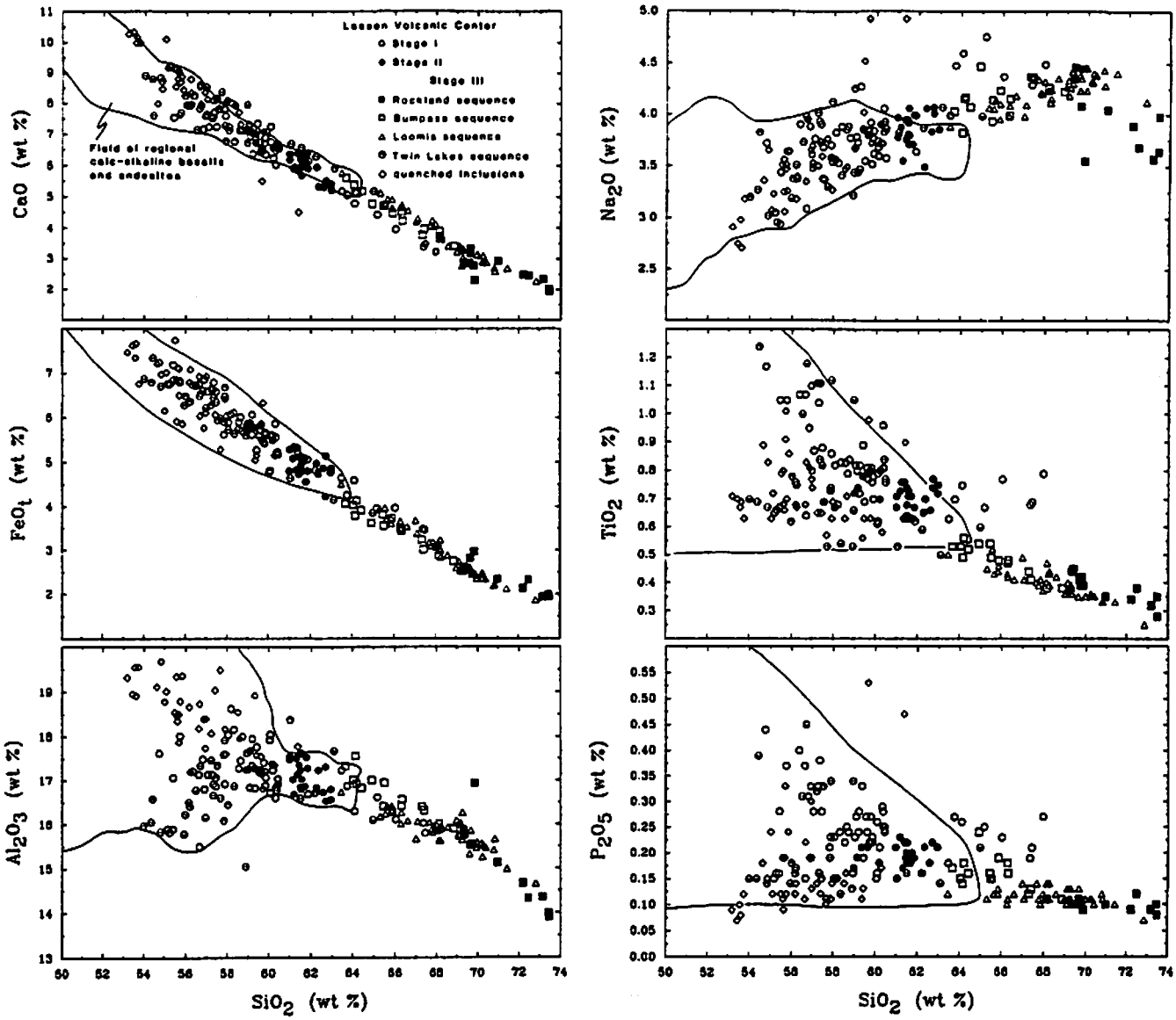

Fig. 5. Harker variation diagrams for CaO, FeO_t, Al_2O_3, Na_2O, TiO_2, and P_2O_3. Symbols on CaO plot. Solid lines enclose the compositional fields of calc-alkaline mafic to intermediate lavas found in the area surrounding the Lassen volcanic center. Most of these regional lavas are younger than 1 Ma and are contemporaneous with the Lassen volcanic center.

simultaneously maintaining diverse incompatible major element signatures. Stage III lavas range in composition from basaltic andesite to rhyolite. The silicic lavas are volumetrically dominant with dacite and rhyolite approximately subequal in volume. The evolution in stage III is not that of progressively increasing SiO_2 (see Figure 3). During stage III the most silicic lavas were erupted first (Rockland sequence), then the least silicic dacites were emplaced (Bumpass sequence). Finally, the Loomis sequence, with compositions generally intermediate to the other two sequences, was emplaced. The mixed lavas of the Twin Lakes sequence were emplaced throughout stage III, but most are coeval with the Loomis sequence.

Also shown on Figures 4–6 are fields for the range of composition observed in a suite of more than 200 calc-alkaline lavas from basaltic to andesite monogenetic cinder cones, small lava cones, and shield volcanoes in the southernmost Cascade Range [*Clynne*, 1984, also unpublished data, 1989]. The majority of the regional lavas have SiO_2 contents ranging from about 50 to about 64 wt %. Lavas with SiO_2 greater than 64 wt % are rare and are not shown. Regional lavas with SiO_2 content that overlaps the range observed in Brokeoff volcano display a range of major element composition nearly identical to Brokeoff volcano lavas (Figures 4–6).

Brokeoff Volcano

In addition to the lithologic diversity of stage I lavas of Brokeoff volcano, the chemistry is equally diverse within a limited range of SiO_2 (Figures 6*a* and 6*b*). The most magnesian lavas have 55–57 wt % SiO_2 and 7.5–8 wt % MgO. MgO decreases with SiO_2 and converges on the most abundant composition, which has about 59.5 wt % SiO_2 and about 4 wt % MgO. The dacite of Twin Meadows has 1–1.5 wt % MgO at 66–68 wt % SiO_2. The other dacites sparsely fill the gap between the dacite of Twin Meadows and the andesites. K_2O in Brokeoff andesites varies from 0.8 to 1.6 wt % at 55

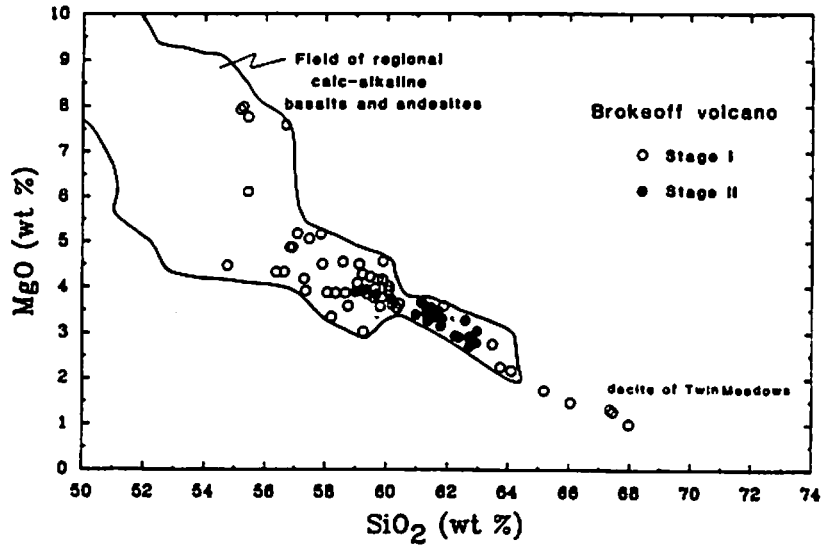

Fig. 6*a*. MgO versus SiO_2 for lavas of the Brokeoff volcano. Field as in Figure 5.

wt % SiO_2 and from 1.0 to 2.2 at 60 wt % SiO_2. K_2O variation with SiO_2 in the stage I lavas indicates the presence of two chemically distinct groups, one having markedly less K_2O than the other. The lower-K_2O group includes all the lavas with greater than 7 wt % MgO, and the lower-K_2O lavas, in general, tend to have slightly higher MgO at equivalent SiO_2 than the higher-K_2O group lavas. The lower-K_2O lavas are randomly distributed in both time and space within the stage I section. K_2O in the stage I dacites increases irregularly with increasing SiO_2.

The stage II andesites are chemically more restricted than those of stage I. They range from 58 to 64 wt % SiO_2, but the majority of samples contain 61–63 wt % SiO_2 (Figures 6*a* and 6*b*), and thus the SiO_2 content of stage II lavas is higher than the majority of stage I lavas. MgO ranges from 3.9 wt % at 59 wt % SiO_2 to 2.2 wt % at 64 wt % SiO_2. K_2O shows a large range (1.5–2.6%) at 61–62% SiO_2 and a poor correlation of increasing K_2O with increasing SiO_2. Stage II andesites are intermediate in major element composition between stage I andesites and the dacite of Twin Meadows.

Stage III

Stage III rocks, although predominantly silicic, range from 53 to 74% SiO_2 (Figures 5 and 7). For most elements, the silicic sequences (Rockland, Bumpass, and Loomis) overlap and form continuous trends versus silica. Relatively low Na_2O in the Rockland sequence is an example of an exception to the regular variation. The mixed lavas of the Twin Lakes sequence and the quenched inclusions have diverse compositions at the low-SiO_2 end of the array, and a few compositions fall slightly outside the range of Brokeoff volcano and the regional lavas.

Several differences between stage III lavas and Brokeoff lavas are apparent from Figures 6 and 7: (1) At equivalent SiO_2, the stage III silicic lavas have a higher MgO content and the quenched inclusions a slightly lower MgO content than the majority of Brokeoff volcano lavas, (2) at equivalent SiO_2 most stage III silicic compositions have lower K_2O content than stage II lavas of the Brokeoff volcano, (3) the majority of the quenched inclusions have K_2O contents

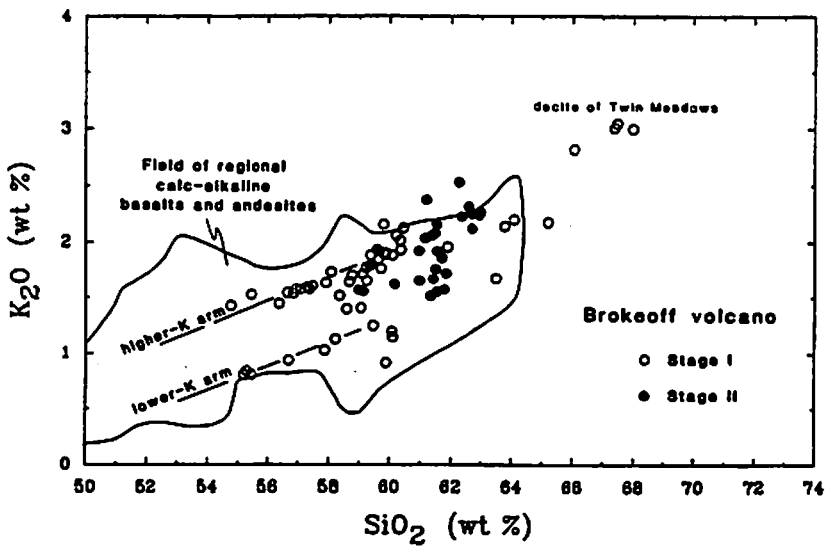

Fig. 6*b*. K_2O versus SiO_2 diagram for lavas of Brokeoff volcano. Field as in Figure 5.

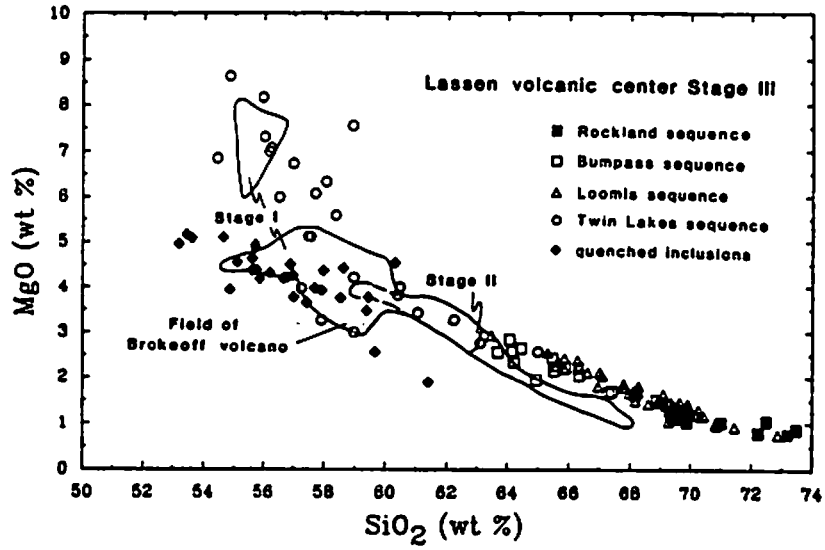

Fig. 7*a*. MgO versus SiO_2 for rocks of stage III of the Lassen volcanic center. Symbols as in Figure 6*a*. Solid line denotes the field of Brokeoff volcano lavas on Figure 6*a*, and the dashed line encloses the field of Stage II lavas on Figure 6*a*.

intermediate between the lower- and higher-K_2O arms of Brokeoff volcano andesites, and (4) Twin Lakes sequence lavas have variable compositions, but many have relatively high MgO compared to the majority of Brokeoff volcano lavas.

CMAS SYSTEMATICS OF LASSEN VOLCANIC CENTER LAVAS

Pseudoquaternary phase proportions (An-Di-Ol-Si) were calculated for all lavas of the Lassen volcanic center using the method of *Bullen* [1986, 1990] and plotted as the Di-Ol-Si components projected from anorthite in Figures 8*a* and 8*b*. Included in this diagram are the experimentally determined 1-atm cotectics [*Walker et al.*, 1979; *Grove et al.*, 1982; *Grove and Bryan*, 1983], fields for anhydrous liquids in equilibrium with olivine, orthopyroxene, clinopyroxene, ±plagioclase at 5 and 10 kbar [*Falloon et al.*, 1988; *Takahashi and Kushiro*, 1983; *Jacques and Green*, 1980; *Fujii and Scarfe*, 1985], and a cotectic describing the compositions of more silicic liquids (bold line) produced by melting of basalt at $P_{H_2O} = P_{total} = 5$ kbar [*Helz*, 1976]. Projections of this type that consider all the major elements together are useful for identification of petrogenetic processes that may have affected a magma suite. The projection from anorthite is particularly useful in this case because all Lassen volcanic center lavas contain plagioclase.

The data set forms a broad band that crosses primary 1-atm phase volumes and therefore is not compatible with crystal fractionation of olivine, pyroxenes, and plagioclase at low pressure. However, the data are compatible with at least two interpretations. On one hand, with increasing pressure the primary phase volume of clinopyroxene ex-

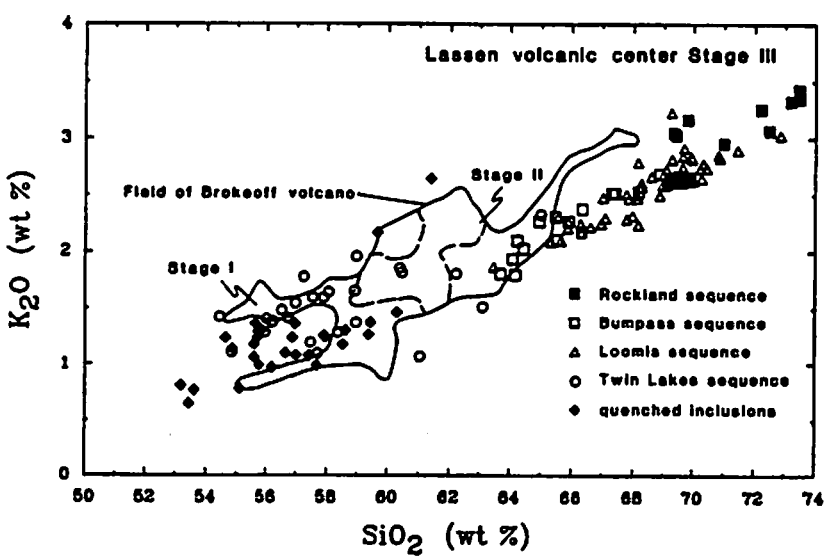

Fig. 7*b*. K_2O versus SiO_2 diagram for rocks of stage III of the Lassen volcanic center. Symbols as in Figure 6*b*. Solid line denotes the field of Brokeoff volcano lavas on Figure 6*b*, and the dashed line encloses the field of stage II lavas on Figure 6*b*.

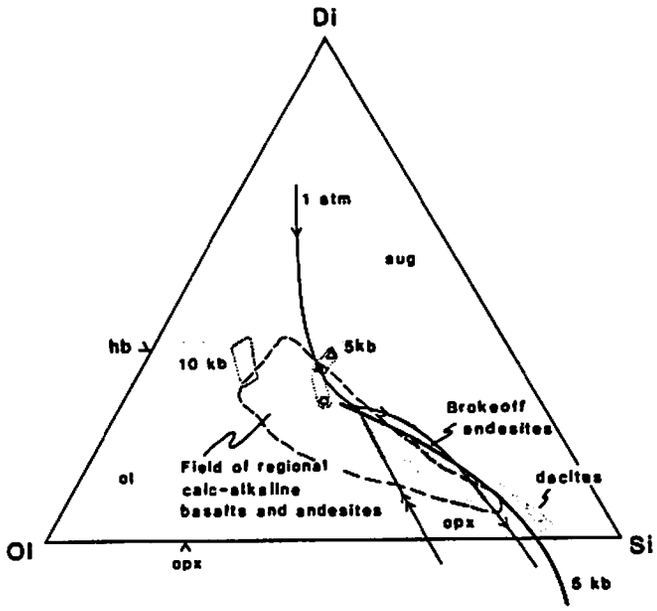

Fig. 8*a*. Pseudoquaternary phase proportions (An-Di-Ol-Si) plotted as the Di-Ol-Si components projected from anorthite for Brokeoff volcano andesites and dacites and regional basalt to andesite lavas. Also shown are fields for experimentally derived liquids in equilibrium with peridotite at 5 and 10 kbar (see text for references). The 5-kbar field based on equilibria of *Falloon et al.* [1988] (diamonds) and *Takahashi and Kushiro* [1983] (circle). See text for reference data for 1-atm cotectic. Bold line labeled 5 kbar is a plagioclase-saturated 2-px cotectic based on melting of basalt [*Helz*, 1976]. Field for regional calc-alkaline basalts and andesites corresponds to that shown in Figures 4–6. See text for further explanation.

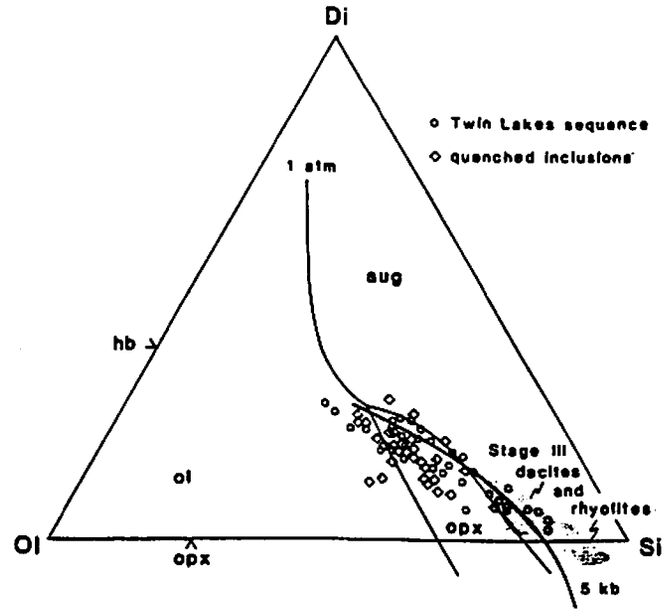

Fig. 8*b*. Pseudoquaternary phase proportions (An-Di-Ol-Si) plotted as the Di-Ol-Si components projected from anorthite for stage III lavas. Cotectics as in Figure 8*a*.

pands at the expense of olivine so that the ol-cpx-opx triple point moves closer to the olivine-diopside junction [*Jaques and Green*, 1980]. At the same time, the 2-px-plagioclase cotectic probably pivots to a flatter slope similar to the data array, although there are no experimental data to rigorously defend this contention. However, based on the relative positions of orthopyroxene and hornblende in this diagram, a two-pyroxene cotectic is likely to have a flatter slope than the hornblende-clinopyroxene cotectic defined by the hydrous melts of basalt. Thus, in principle, the data set for the Lassen volcanic center appears to be consistant with crystal fractionation of a 2-px-plagioclase assemblage at moderate pressures (e.g., 5–10 kbar) and agrees with the interpretation of *Grove and Baker* [1984] for calc-alkaline series rocks.

On the other hand, the data are compatible with mixing of any of a variety of compositions that occur along or at the ends of the array. To illustrate the validity of this interpretation, the compositions of various eruptive units of the Twin Lakes sequence, clearly a group of mixed lavas, are plotted in Figure 9. Each unit of this group plots along a separate linear array. The arrays in Figure 9 project toward a common silicic end member and variable mafic end members. The group of arrays mimics the entire Lassen volcanic center data set (Figures 8*a* and 8*b*), thus suggesting that the variation observed in the entire Lassen suite could be due to mixing.

CRYSTAL FRACTIONATION MODELING OF BROKEOFF VOLCANO MAGMAS

The CMAS relations indicate that the major element variations observed at Lassen volcanic center are consistant with an origin by fractional crystallization and/or mixing. Considering that crystal fractionation from calc-alkaline basalt is believed to be the most common process by which calc-alkaline andesites are produced [*Gill*, 1981], the purpose of this section is to attempt to rigorously constrain a fractional crystallization model for Brokeoff volcano magmas. The fact that Brokeoff andesites are mineralogically similar and temporally related to regional volcanism suggests that the mafic input to Brokeoff volcano may be magma similar to that producing the regional volcanism. The range of major

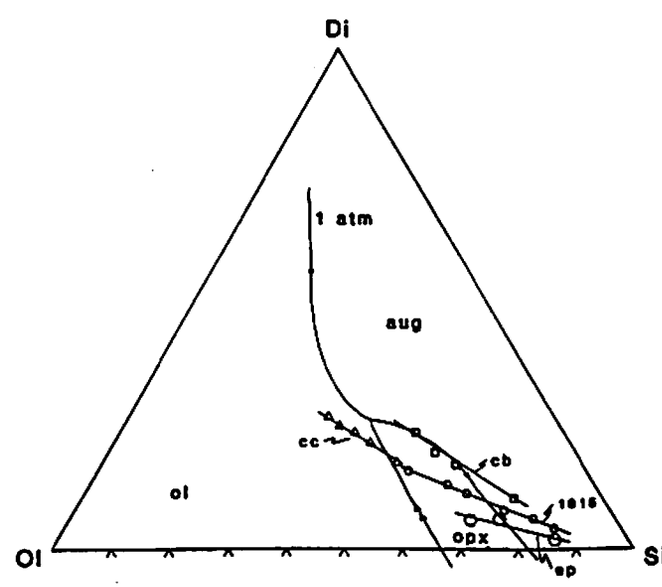

Fig. 9. Pseudoquaternary phase proportions (An-Di-Ol-Si) plotted as the Di-Ol-Si components projected from anorthite for several lava flows of the Twin Lakes sequence. Lines connect samples from the same unit. Each unit plots on a mixing line pointing toward a common silicic component and a variable mafic component. Symbols are Cinder Cone (cc); pumice and lava from the 1915 eruption of Lassen Peak (1915); Crater Butte (cb); Eagle Park (ep). Cotectics as in Figure 8*a*.

TABLE 2. Mineral Compositions Used in Crystal Fractionation Models

	Olivine	Clinopyroxene			Orthopyroxene	
	Fo_{85}	537 cpx 6	436B cpx 2	182 cpx 12	436B opx 11	182 opx 10
SiO_2	40.03	51.12	52.36	52.35	54.99	53.31
Al_2O_3	0.00	3.40	2.17	1.42	1.35	0.68
MgO	45.66	16.04	17.26	15.14	28.47	24.69
FeOt	13.88	6.11	6.58	8.76	12.48	18.64
CaO	0.19	21.53	20.22	20.77	1.93	1.32
Na_2O	0.00	0.33	0.27	0.36	0.00	0.05
TiO_2	0.00	0.73	0.36	0.46	0.21	0.23
MnO	0.27	0.16	0.18	0.29	0.28	0.55

element composition of regional calc-alkaline basaltic andesite to andesite lavas from monogenetic to short-lived polygenetic volcanoes in the Lassen region is similar to that of Brokeoff volcano. Furthermore, at a given silica content, mineral assemblages of regional andesites and Brokeoff andesites are the same. Therefore modeling can be attempted that utilizes regional basalt as real data for input as parental starting compositions.

Crystal fractionation modeling was performed with the computer program XLFRAC [*Stormer and Nicholls*, 1978] in order to determine (1) whether the basaltic andesites of Brokeoff volcano can be derived from regional mafic lavas by fractional crystallization and (2) whether crystal fractionation is a viable process for relating the range of magma compositions within Brokeoff volcano as suggested by the CMAS relations. The rationale behind the modeling was to determine the range of parental compositions that can produce the major element variations observed in Brokeoff lavas by a fractional crystallization mechanism. The range of sucessful parent compositions and the required mineral assemblages were then compared to the observed range of regional lavas and the assemblages observed in Brokeoff lavas in order to test the validity of the modeling. In addition, the mineral proportions and the extents of fractionation required are used by *Bullen and Clynne* [this issue] to test the validity of the fractional crystallization mechanism using trace-element constraints.

MINERAL AND ROCK COMPOSITIONS

If fractional crystallization was an important process at Brokeoff, then the lithologic and geochemical diversity of Brokeoff lavas, the long length of time involved in producing Brokeoff lavas, and the range of composition observed in the regional mafic suite all suggest that the mafic input to Brokeoff was of variable composition and/or that the P-T path of the derivative magmas was variable. Consequently, pairs of lavas selected at random might have little chance of producing successful models, and it is possible that successful models will be fortuitous. Nevertheless, some generalities derived from the modeling provide constraints on interpretation of the geochemical data.

Based on the petrographic characteristics, derivation of silicic andesite from regional mafic magma by fractional crystallization would involve a changing mineral assemblage over a large range of silica. Consequently, crystal fractionation modeling was done in three steps or silica intervals corresponding to changes in the fractionating assemblage. These were 50–56% SiO_2, 56–60% SiO_2, and 60–62% SiO_2. In these three silica ranges, real rocks tend to have the mineral assemblages (without regard to relative abundance) ol-plag-cpx, ol-plag-cpx-opx, and opx-cpx-plag, respectively.

In the regional mafic suite, phases are observed to enter the crystallization assemblage in the order olivine, then clinopyroxene or plagioclase. Phenocrysts of Fe-Ti oxide also begin precipitating early, so that most lavas with between 53 and 56% SiO_2 contain the four-phase assemblage. Orthopyroxene replaces olivine in the assemblage at about 56% SiO_2, and the resultant plag-cpx-opx-ox assemblage remains constant through the andesitic composition range. Clinopyroxene is the dominant pyroxene in andesites, and orthopyroxene is the dominant pyroxene in silicic andesites. Mineral compositions obtained by microprobe analysis (Table 2) were used whenever possible in the modeling. When they were not available, a combination of natural and stoichiometric compositions was used.

Two primitive regional basalts, one with low-K and one with medium-K were selected as prospective Brokeoff parents. The low-K basalt, LC88-1308, has 0.41% K_2O, 9.10% MgO, an Mg # of 73, and 166 ppm Ni and contains 5% phenocrysts of Fo_{89-88} olivine with inclusions of Cr spinel. The medium-K basalt, LC82-905, has 0.65% K_2O, 8.4% MgO, an Mg # of 69, and 150 ppm Ni and contains a few percent phenocrysts of Fo_{88-86} olivine with inclusions of Cr spinel. In addition, representative compositions were calculated for the lower- and higher-K Brokeoff basaltic andesites with 56% SiO_2 (Bv56lk and Bv56hk) by averaging lavas that have about 56% SiO_2. Compositions were similarly derived for 60% SiO_2 (Bv60lk and Bv60hk) and 62% SiO_2 (Bv62lk and Bv62hk). Models were determined that attempted to relate compositions within and between the lower- and higher-K arrays.

RESULTS

A variety of successful models were generated. Solutions derived using the averaged compositions of Brokeoff lavas are shown in Table 3 and graphically summarized in Figure 10 and are representative of solutions involving real lava compositions. Most solutions shown in Table 3 have sums of squares of the residuals about 0.1 or less, lower than those for models generally accepted to be successful [*Stormer and Nicholls*, 1978]. However, in some models the residuals for certain elements do not fall within the analytical uncertainties for these elements. These discrepancies are discussed below.

Step 1 in the crystal fractionation process, the attempt to

TABLE 3. Crystal Fractionation Models of Averaged Compositions

	Solution 1: Low-K Regional Basalt to Bv561k					
	Initial Magma LC88-1308	Final Magma Bv561k	Calculated Magma	Residual	Weight Percent of Initial Magma	Weight Percent of All Phases
SiO_2	51.61	55.76	55.77	−0.01		
Al_2O_3	16.87	15.83	15.84	−0.01		
MgO	9.12	7.87	7.88	−0.01		
FeOt	7.40	6.71	6.72	−0.01		
CaO	11.28	9.07	9.07	0.00		
Na_2O	2.47	3.01	2.99	0.02		
K_2O	0.41	0.85	0.79	0.06		
TiO_2	0.60	0.65	0.65	0.00		
P_2O_5	0.08	0.15	0.15	0.00		
MnO	0.16	0.10	0.15	−0.05		
Sum of squares of the residuals				0.007		
Phase subtracted as						
ol Fo_{85}					6.17	13.20
537 cpx 6					13.03	27.88
$An_{70}Or_{0.5}$					25.19	53.90
Usp_{15}					2.34	5.02
Total					46.74	100.00

	Solution 2: Medium-K Regional Basalt to Bv56hk					
	Initial Magma LC82-905	Final Magma Bv56hk	Calculated Magma	Residual	Weight Percent of Initial Magma	Weight Percent of All Phases
SiO_2	50.46	56.00	55.97	0.03		
Al_2O_3	17.76	17.75	17.71	0.04		
MgO	8.45	5.00	4.98	0.02		
FeOt	8.45	6.40	6.37	0.03		
CaO	9.81	8.50	8.48	0.02		
Na_2O	3.03	3.50	3.54	−0.04		
K_2O	0.65	1.50	1.46	0.04		
TiO_2	0.99	1.00	0.97	0.03		
P_2O_5	0.25	0.25	0.39	−0.14		
MnO	0.16	0.10	0.14	−0.04		
Sum of squares of the residuals				0.031		
Phase subtracted as						
ol Fo_{85}					10.49	18.17
537 cpx 6					9.74	16.87
$An_{60}Or_1$					33.23	57.55
Usp_{35}					4.28	7.41
Total					57.74	100.00

	Solution 3: Bv561k to Bv601k					
	Initial Magma BV561k	Final Magma Bv601k	Calculated Magma	Residual	Weight Percent of Initial Magma	Weight Percent of All Phases
SiO_2	55.76	59.96	59.88	0.08		
Al_2O_3	15.83	17.72	17.67	0.05		
MgO	7.87	4.20	4.19	0.01		
FeOt	6.71	5.11	5.03	0.07		
CaO	9.07	7.26	7.21	0.05		
Na_2O	3.01	3.65	3.68	−0.03		
K_2O	0.85	1.15	1.37	−0.22		
TiO_2	0.65	0.65	0.65	0.00		
P_2O_5	0.15	0.20	0.25	−0.05		
MnO	0.10	0.10	0.07	0.03		
Sum of squares of the residuals				0.069		
Phase subtracted as						
$An_{55}Or_{1.5}$					22.78	45.21
436B cpx 2					13.20	26.19
436B opx 11					12.30	24.40
Usp_{35}					2.12	4.20
Total					50.39	100.00

14-35

TABLE 3. (continued)

	Solution 4: Bv561k to Bv60hk					
	Initial Magma Bv561k	Final Magma Bv60hk	Calculated Magma	Residual	Weight Percent of Initial Magma	Weight Percent of All Phases
SiO_2	55.76	59.98	60.00	−0.02		
Al_2O_3	15.83	17.29	17.31	−0.02		
MgO	7.87	3.80	3.80	0.00		
FeOt	6.71	5.60	5.62	−0.02		
CaO	9.07	6.54	6.55	−0.01		
Na_2O	3.01	3.80	3.77	0.03		
K_2O	0.85	1.90	1.82	0.08		
TiO_2	0.65	0.80	0.78	0.02		
P_2O_5	0.15	0.20	0.26	−0.06		
MnO	0.10	0.10	0.08	0.02		
Sum of squares of the residuals				0.013		
Phase subtracted as						
$An_{55}Or_{1.5}$					25.79	47.07
436B cpx 2					14.36	26.20
436B opx 11					12.80	23.36
Usp_{35}					1.85	3.37
Total					54.80	100.00

	Solution 5: Bv56hk to Bv60hk					
	Initial Magma Bv56hk	Final Magma Bv60hk	Calculated Magma	Residual	Weight Percent of Initial Magma	Weight Percent of All Phases
SiO_2	56.00	60.00	59.85	0.15		
Al_2O_3	17.75	17.30	17.24	0.06		
MgO	5.00	3.80	3.78	0.02		
FeOt	6.40	5.60	5.46	0.14		
CaO	8.50	6.50	6.42	0.08		
Na_2O	3.50	3.80	3.78	0.02		
K_2O	1.50	1.90	2.21	−0.31		
TiO_2	1.00	0.80	0.83	−0.03		
P_2O_5	0.25	0.20	0.33	−0.13		
MnO	0.10	0.10	0.09	0.01		
Sum of squares of the residuals				0.169		
Phase subtracted as						
$An_{55}Or_{1.5}$					25.27	61.59
436B cpx 2					8.77	21.38
436B opx 11					4.41	10.75
Usp_{50}					2.58	6.29
Total					41.03	100.00

	Solution 6: Bv601k to Bv621k					
	Initial Magma Bv601k	Final Magma Bv621k	Calculated Magma	Residual	Weight Percent of Initial Magma	Weight Percent of All Phases
SiO_2	59.96	61.65	61.71	−0.06		
Al_2O_3	17.72	17.45	17.48	−0.03		
MgO	4.20	3.35	3.35	−0.00		
FeOt	5.11	4.78	4.81	−0.03		
CaO	7.26	6.28	6.30	−0.02		
Na_2O	3.65	3.93	3.87	0.05		
K_2O	1.15	1.64	1.44	0.20		
TiO_2	0.65	0.65	0.71	−0.06		
P_2O_5	0.20	0.19	0.24	−0.05		
MnO	0.10	0.08	0.08	0.00		
Sum of squares of the residuals				0.053		
Phase subtracted as						
$An_{60}Or_1$					11.67	61.09
182 cpx 12					3.17	16.59
182 opx 10					4.06	21.23
Usp_{50}					0.21	1.09
Total					19.10	100.00

TABLE 3. (continued)

	Solution 7: Bv60hk to Bv62hk					
	Initial Magma Bv60hk	Final Magma Bv62hk	Calculated Magma	Residual	Weight Percent of Initial Magma	Weight Percent of All Phases
SiO_2	60.00	62.00	61.94	0.06		
Al_2O_3	17.30	16.80	16.77	0.03		
MgO	3.80	3.30	3.30	0.00		
FeOt	5.60	4.90	4.84	0.06		
CaO	6.50	6.00	5.97	0.03		
Na_2O	3.80	3.90	3.89	0.01		
K_2O	1.90	2.10	2.24	−0.14		
TiO_2	0.80	0.70	0.73	−0.03		
P_2O_5	0.20	0.20	0.23	−0.03		
MnO	0.10	0.10	0.09	0.01		
Sum of squares of the residuals				0.03		
Phase subtracted as						
$An_{55}Or_{1.5}$					11.71	67.26
182 cpx 12					0.94	5.40
182 opx 10					3.74	21.51
Usp_{50}					1.02	5.84
Total					17.41	100.00

Mineral compositions: stoichiometric compositions used for plagioclase and Fe-Ti oxides. Olivine and pyroxene compositions are given in Table 2.

derive Brokeoff basaltic andesites, Bv56lk and Bv56hk from regional basalts is illustrated in Table 3 (solutions 1 and 2). Crystal fractionation of the assemblage olivine (Fo_{85}), clinopyroxene, plagioclase ($An_{70}Ab_{29.5}Or_{0.5}$), and Fe-Ti oxide (Usp_{15}) in the weight proportions (13:28:54:5) successfully predicts the composition of Bv56lk after 47% crystallization of the regional basalt LC88-1308. Crystal fractionation of the assemblage olivine (Fo_{85}), clinopyroxene, plagioclase ($An_{60}Ab_{39}Or_1$), and Fe-Ti oxide (Usp_{35}) in the weight proportions (18:17:58:7) successfully predicts the composition of Bv56hk after 58% crystallization of the regional basalt LC82-905. The fractionating phases and their relative proportions are similar to those observed in Brokeoff basaltic andesites and many regional mafic lavas. Relative to the low-K basalt to Bv56lk solution, the medium-K basalt to Bv56hk solution has an increased role for olivine relative to clinopyroxene, less calcic plagioclase, and a greater amount of more titaniferous Fe-Ti oxide removed.

The next step attempts to relate lavas within the stage I Brokeoff array. Solutions were developed using the phases olivine, clinopyroxene, orthopyroxene, plagioclase, and Fe-Ti oxide along both the lower-K and higher-K arms of the Brokeoff array and between Bv56lk and Bv60hk compositions.

Crystal fractionation modeling to relate Bv56 and Bv60 compositions within the lower-K and between the lower-K and higher-K lavas was successful (solutions 3 and 4 in Table 3). Crystal fractionation in this silica interval is dominated by

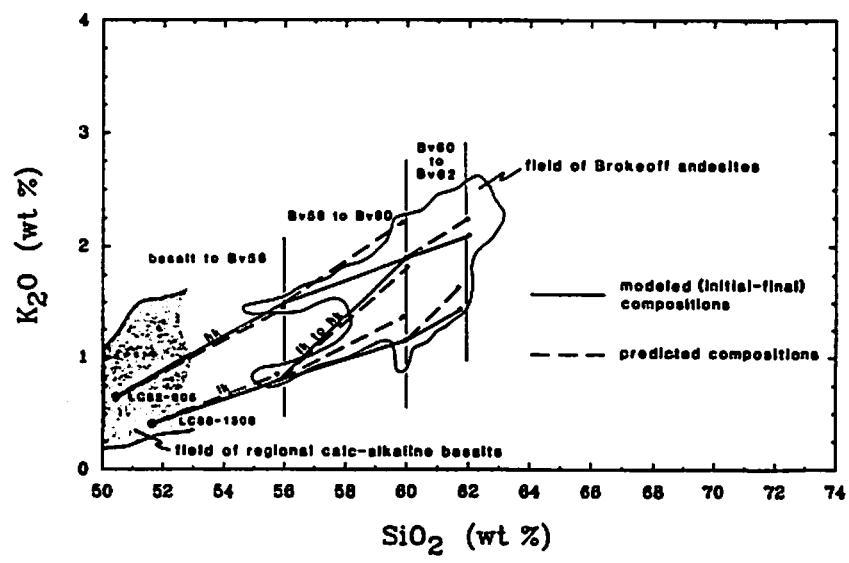

Fig. 10. Graphical summary of the K_2O versus SiO_2 variation of the modeled Brokeoff andesite compositions.

removal of plagioclase. The composition of the plagioclase is An_{55}, matching that in the lavas. Clinopyroxene and orthopyroxenes are removed in subequal amounts. A variety of pyroxene compositions was tried, and the best fits were obtained with pyroxene compositions that are among the most magnesian analyzed in Brokeoff volcano lavas. However, varying the pyroxene composition has only a minor effect on the solution; the relative proportions of phases and the total amount of fractionation are not significantly affected. Fe-Ti oxide fractionation is required but is of diminished importance compared to the basalt to BV56 interval. Substitution of olivine for orthopyroxene in the fractionating assemblage results in similar to slightly better solutions. Approximately 50–55% crystals must be removed to relate compositions within the lower-K arm and between the lower- and higher-K arms.

Crystal fractionation modeling within the higher-K arm of the Brokeoff array was marginally successful. The best solution has the sum of the squares of the residuals greater than 0.1 (solution 5 in Table 3). The differences between this and the other Bv56 to Bv60 solutions include (1) an increase in the role of plagioclase, (2) an increase in the amount of clinopyroxene relative to orthopyroxene, and (3) an increased importance of Fe-Ti oxide in the fractionating assemblage. In addition, the Ti content of the oxide composition required (Usp_{50}) is at the upper end of the range (Usp_{20-50}) normally observed in calc-alkaline andesites [*Gill*, 1981].

The last step in the crystal-fractionation modeling attempts to relate stage I and stage II andesites. Average stage II andesites, Bv62lk and B62hk, can be derived from Bv60lk and Bv60hk compositions respectively, with a 2-pyroxene, plagioclase, Fe-Ti oxide assemblage (solutions 6 and 7 in Table 3). Successful models are plagioclase-dominated; the amount of orthopyroxene relative to clinopyroxene is increased over that in the 56–60% silica range. About 20% crystal fractionation is required to relate the two silica ranges.

DISCUSSION OF CRYSTAL FRACTIONATION MODELING AND THE ORIGIN OF BROKEOFF VOLCANO ANDESITES

Crystal fractionation modeling provides several important constraints on the origin and evolution of Brokeoff lavas. First, even considering the variation in intensive parameters during crystallization (e.g., water content, oxygen fugacity, and total pressure) that could be expected within this large suite of lavas, reasonable models can be constructed that satisfy the range of Brokeoff lavas using the mineral assemblages and compositions observed. Second, the most mafic Brokeoff andesites can be derived from regional basalts, at least in terms of major elements, by fractionation of the mineral assemblage observed in the basalts. Furthermore, each successive step in the derivation of the range of Brokeoff andesites can be modeled using the mineral assemblages observed in those rocks. Third, the model fractionating assemblages for all silica intervals are plagioclase dominated. Fourth, after andesitic compositions are reached, olivine, if involved at all, is not an important phase. Fifth, an oxide phase is required in the fractionating assemblage in all three silica intervals. Sixth, residuals are minimized by use of relatively calcic plagioclase, magnesian pyroxenes, and Ti-rich oxides. Seventh, approximately 50–60% crystal fractionation is required to derive Brokeoff basaltic andesite from regional basalt, 35–50% to derive Brokeoff andesite from basaltic andesite, and 15–20% to derive silicic andesite from andesite. Therefore, if Brokeoff silicic andesites are derived from regional basalt by fractional crystallization, about 80% crystal removal is required.

As is often the case in crystal fractionation models, the major discrepancies between the predicted and actual Bv56lk to Bv60lk, Bv56hk to Bv60hk, Bv60lk to Bv62lk, and Bv60hk to Bv62hk compositions are the conserved elements K_2O and P_2O_5. However, contrary to the normal situation [*Gill*, 1981], K_2O in the real lavas does not increase as fast as the models predict (except for the Bv60lk to Bv62lk solution). The models also predict an increase in P_2O_5, but P_2O_5 continually decreases with increasing SiO_2 in the Brokeoff lavas. As little as 0.2% apatite in the fractionating assemblage, however, would alleviate the discrepancy, and indeed, small amounts of apatite have been observed as inclusions in plagioclase phenocrysts in Brokeoff andesites.

Perhaps more importantly, by starting with a low-K parent, the entire range of major element variation observed in Brokeoff andesites can be modeled by crystal fractionation, without addition of another component. The rate of increase of K_2O versus SiO_2 in all models is primarily a function of the composition and proportion of plagioclase removed from the parent. The range of possible rates of increase of K_2O with SiO_2 at Brokeoff is approximately bounded by the Bv56lk to Bv60lk solution (3) and the Bv56lk to Bv60hk solution (4). The solution between Bv56lk and Bv60hk is remarkably good. The predominance of Bv60hk-type lavas at Brokeoff suggests that this would be the most common path if crystal fractionation is the process controlling Brokeoff-andesite compositions.

Although modeling of crystal fractionation along both arms produces statistically acceptable results overall, the models do not produce acceptable results for K_2O, which is generally overpredicted. Consequently, in order to explain the K_2O variation of Brokeoff lavas by crystal fractionation it is necessary to start with low-K to medium-K parents (i.e., basalts with less than about 0.75 wt % K_2O) to generate the basaltic andesites. Medium-K basaltic lavas with greater K_2O are present in the Lassen area (Figures 6*b* and 10) but cannot be the parents of Brokeoff andesites through crystal fractionation of the observed phase assemblages. The lack of involvement of the relatively K-rich medium-K basalts in the origin of Brokeoff andesites is supported by the nearly exclusive spatial distribution of this lava type to the east of the arc axis in the Lassen region [*Bullen and Clynne*, 1989].

The fractional crystallization modeling is useful for determination of appropriate crystallization assemblages and to provide estimates of the degree of fractionation as a basis for interpretation of trace element and isotopic data. However, when one considers the petrographic, stratigraphic, and chemical complexity of Brokeoff lavas, a simple fractional crystallization model involving a single parent is clearly unrealistic. The phase assemblage, crystal content, and major element diversity of Brokeoff lavas can be reconciled if the majority of them are produced by fractional crystallization of regional mafic magma in small independent batches. Consequently, the chemical diversity of Brokeoff andesites arises at least in part from the diversity within the low to medium-K mafic parent. Magma mixing of variously fractionated batches of andesite explains the petrographic

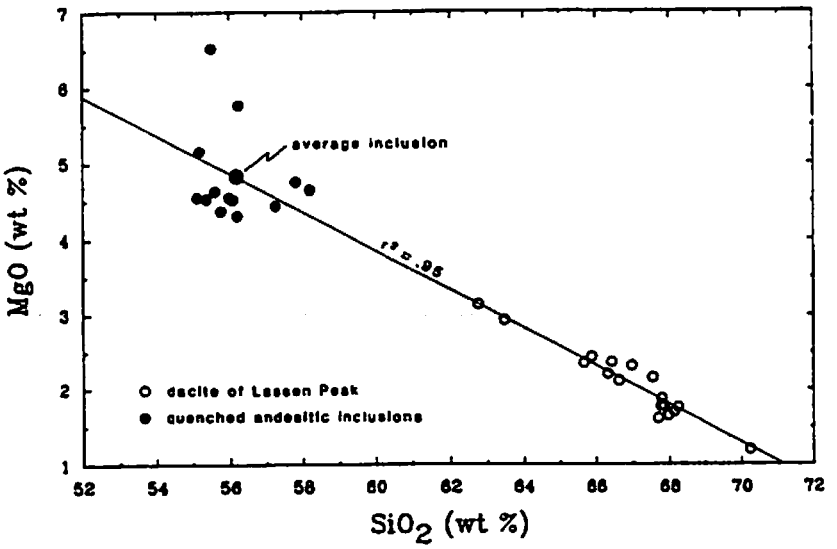

Fig. 11. MgO versus SiO_2 for the lavas and quenched andesitic inclusions of the dacite of Lassen Peak. The average SiO_2 and MgO content of all the quenched inclusions plots on the least squares regression line of all the dacites and inclusions. The range of compositions of the dacite of Lassen Peak nearly equals the entire range seen in stage III silicic lavas.

diversity without causing major element compositions to deviate from the fractionation envelope.

The lavas of Brokeoff volcano have compositions similar to the more evolved regional lavas, suggesting that they have similar sources and evolutionary histories. However, the difference between Brokeoff volcano and the regional volcanism is the larger-volume and long-lived locus of volcanism at Brokeoff volcano. Basalts are not present in Brokeoff volcano, although the presence of mafic minerals with compositions consistent with crystallization from basalt indicate that basalt or basaltic andesite are entering the magmatic system. The similarities suggest that Brokeoff volcano represents a focusing of the regional volcanism, probably with increased average residence time and interaction of magma batches in the crust.

Control of focusing is probably structural or related to a local increase in the magma supply rate. The Lassen volcanic center (and the older volcanic centers in the area) are located on the edge of a regional gravity low [*Blakely et al.*, 1985]. The gravity low is probably in part an expression of (1) near-surface low-density volcanic rocks and (2) Quaternary plutonic rocks beneath the volcanic field [*Pakiser*, 1964; *LaFehr*, 1965]. *Blakely and Jachens* [this issue] suggest that the gravity low also reflects a structural depression and that large volcanic centers are located around the margins of the depression because boundary faults facilitate ascent of magma to the surface. This effect may allow the development of complex magmatic plumbing systems and would focus the regional volcanism into large, long-lived volcanic centers.

VARIATION IN STAGE III MAGMAS

Although it is intriguing to envision stage III silicic lavas as evolved Brokeoff magmas, several features of stage III magmas are inconsistent with an origin by crystal fractionation from Brokeoff andesites: (1) The volume of stage III volcanism exceeds that of the Brokeoff volcano, (2) a large compositional gap exists between nearly contemporaneous latest Brokeoff andesites and the Rockland sequence, (3) the decreasing geochemical diversity as more silicic compositions are reached (Figures 5–7) cannot be explained by simple closed-system crystal fractionation, (4) the abrupt change from a 2-pyroxene-plagioclase-dominated phenocryst assemblage in Brokeoff andesites to a plagioclase-hornblende-biotite-quartz-dominated and strongly disequilibrium phenocryst assemblages in stage III lavas is inconsistent with an origin by crystal fractionation alone, and (5) attempts at least squares modeling using the phenocryst assemblage and compositions present in the lavas fail to predict the observed compositional variation. The compatible components are underpredicted, and the incompatible components are overpredicted. Acceptable solutions invariably require the addition of a mafic component at the same time as phenocrysts are being subtracted.

The origin of variation in stage III lavas, however, can be better explained by mixing between mafic to intermediate magma and rhyolitic magma. Furthermore, formation and disaggregation of quenched andesitic inclusions probably plays a significant role in the mixing origin of stage III compositional variation. The compositional variation observed in dacite of Lassen Peak provides the clearest example of the process and its significance on magma composition. The dacite dome of Lassen Peak appears to be a single eruptive unit emplaced over a short time interval. No internal contacts have been found, and eight paleomagnetic sampling sites covering all flanks of the dome give a single magnetic direction (D. E. Champion, written communication, 1989). The complex phenocryst assemblage in this lava was described in a previous section. The textural details and electron microprobe analyses of the mineral populations demonstrate that the origin of the complex phenocryst assemblage is by disaggregation of quenched inclusions into the host lava [*Clynne*, 1989; also manuscript in preparation, 1990]. The effect of this process on bulk composition of the host lava is illustrated in Figure 11. The compositions of dacite of Lassen Peak fall on a mixing line between the average of the quenched inclusions and the most silicic dacite. The composition of the dacite of Lassen Peak spans

nearly the entire range of compositions found in stage III silicic lavas.

Quenched inclusions themselves are mixed. They often contain femic phenocrysts rich in compatible elements such as Ni and Cr, indicating a basaltic or basaltic andesite parent [*Clynne and Christiansen*, 1988; *Clynne*, 1989], but even the lowest silica inclusions contain relatively low MgO (Figure 7*a*). Most inclusions are andesitic and contain resorbed salic phenocrysts derived from their host at the time of inclusion formation. Thus the quenched inclusions record a history of fractionation and mixing, and thus their compositions do not represent the unmodified regional mafic input to the silicic magma system.

The range of compositions exhibited by the dacite of Lassen Peak requires nearly 50–50 mixing to produce the least silicic compositions. The ability of mixing to effect so profoundly the composition of the silicic magma suggests that the silicic magma reservior is small and may explain why geophysical studies have been unable to detect a magma chamber beneath the Lassen volcanic center [*Berge and Monfort*, 1986; *Berge and Stauber*, 1987; *Iyer*, 1984]. However, the long-lived nature and coherent compositional variation of silicic volcanism do suggest an organized, albeit complex, magmatic system beneath the Lassen volcanic center.

SUMMARY

The data and discussion presented above lead to several conclusions that must be considered in any model of the petrogenesis of the Lassen volcanic center. The stratigraphy, lithology, and chronology of the products of the Lassen volcanic center indicate a complex magmatic system. The voluminous, long-lived edifice of Brokeoff volcano was the result of focusing of diffuse regional mafic volcanism. The location and long lifespan of Brokeoff volcano are probably controlled by structures in the crust and may be enhanced by a local increase in the magma supply rate. The compositional diversity of Brokeoff volcano is identical to that displayed by regional lavas with similar SiO_2 content.

Crystal fractionation of low-K to medium-K regional basalt can derive Brokeoff basaltic andesites, and fractional crystallization models satisfactorily reproduce the compositional array of Brokeoff andesites. The fractionating assemblages are plagioclase dominated, and the clinopyroxene to orthopyroxene ratio increases with increasing silica, as observed in the lavas. The rate of change of K_2O with SiO_2 is variable and controlled primarily by the composition and proportion of plagioclase in the fractionating assemblage.

However, variations along the lower- and higher-K arms (Figures 6*b* and 10) are not modeled for K, which is overpredicted. Therefore a process other than fractional crystallization must be invoked to account for the origin of the arms. Furthermore, stratigraphic, lithologic, and petrographic evidence suggest that stage I Brokeoff magmas were produced in small independent batches and that mixing between batches of andesite of not too dissimilar composition and temperature was probably common. It is unlikely that a long-lived magma chamber existed at this time. Stage II rocks are very homogeneous in compatible major elements, but trace element and isotope data show that these magmas were also formed in independent batches [*Bullen and Clynne*, this issue].

Stage III lavas are not directly related to Brokeoff volcano lavas by any simple process. Partial melting of young mafic crust appears to be the origin of the silicic magmas at the Lassen volcanic center [*Bullen and Clynne*, this issue]. Hybrid andesites and ubiquitous quenched inclusions provide abundant evidence for the interaction of mafic and silicic magma. Disaggregation of quenched andesitic inclusions plays an important role in the increased compositional diversity in stage III lavas. Finally, the compositional diversity of the Twin Lakes sequence results from mixing with regional mafic magma of diverse composition. Regional mafic magma provides the fundamental heat and material input to the magmatic system.

Acknowledgments. This paper is an outgrowth of a project proposed and supported at all stages by Pat Muffler, and I am grateful for the opportunity to have worked with him. The cooperation of Richard Vance, Chief Naturalist at Lassen Volcanic National Park, was essential in gaining access to public land. Debbie Trimble and Lars Borg provided assistance in the field. Joe Taggert and crew provided major element analytical support. Brent Dalymple provided K-Ar and Debbie Trimble provided radiocarbon geochronological support. Discussion with Tom Bullen and Jim Gill helped to refine the ideas presented herein. Thoughtful reviews by Patrick Muffler, Tom Bullen, Bill Hart, and Al Brandon greatly improved the manuscript in form and substance.

REFERENCES

Bacon, C. R., Implications of silicic vent patterns for the presence of large crustal magma chambers, *J. Geophys. Res.*, *90*, 11,243–11,252, 1985.

Bacon, C. R., Magmatic inclusions in silicic and intermediate volcanic rocks, *J. Geophys. Res.*, *91*, 6091–6112, 1986.

Beard, J. S., Characteristic mineralogy of arc-related cumulate gabbros: Implications for the tectonic setting of gabbro plutons and for andesite genesis, *Geology*, *14*, 848–851, 1986.

Berge, P. A., and M. E. Monfort, Teleseismic residual study of the Lassen Volcanic National Park area, northern California, *U.S. Geol. Survey Open File Rep.*, *86-252*, 71 pp., 1986.

Berge, P. A., and D. A. Stauber, Seismic refraction study of the upper crustal structure of the Lassen Peak area, northern California, *J. Geophys. Res.*, *92*, 10,571–10,579, 1987.

Blakely, R. J., and R. C. Jachens, Volcanism, isostatic residual gravity, and regional tectonic setting of the Cascade volcanic province, *J. Geophys. Res.*, this issue.

Blakely, R. J., R. C. Jachens, R. W. Simpson, and R. W. Couch, Tectonic setting of the southern Cascade Range as interpreted from its magnetic and gravity fields, *Geol. Soc. Am. Bull.*, *96*, 43–48, 1985.

Bullen, T. D., Magmagenesis in the Devils Garden lava field: Implications for the nature of the sub-continental lithosphere at an active continetal margin, Ph.D. Dissertation, Univ. of Calif., Santa Cruz, 1986.

Bullen, T. D., Petrogenetic implications of compositional trends in phenocrysts from N.E. California high-alumina basalts, *J. Petrol.*, in press, 1990.

Bullen, T. D., and M. A. Clynne, Coupled spatial, chemical, and isotopic characteristics of primitive lavas from the Lassen region, California, (abstract), *Bull. N. M. Bur. Mines Miner. Resour.*, *131*, 33, 1989.

Bullen, T. D., and M. A. Clynne, Trace element and isotopic constraints on magmatic evolution at Lassen volcanic center, *J. Geophys. Res.*, this issue.

Burns, L. E., The Border Ranges ultramafic and mafic complex, south-central Alaska: cumulate fractionates of island arc volcanics, *Can. J. Earth Sci.*, *22*, 1020–1038, 1985.

Clynne, M. A., Stratigraphy and major-element geochemistry of the Lassen Volcanic Center, California, *U.S. Geol. Surv. Open File Rep.*, *84-224*, 168 pp., 1984.

Clynne, M. A., Quaternary volcanism in the southernmost Cascade Range, California, Proceedings of the Workshop on Geothermal

Resources of the Cascade Range, edited by L. J. P. Muffler and M. Guffanti, *U.S. Geol. Surv. Open File Rep.*, *85-521*, 24–30, 1985.

Clynne, M. A., Disaggregation of quenched magmatic inclusions contributes to chemical diversity in silicic lavas of Lassen Peak, California (abstract), *Bull. N. M. Bur. Mines Miner. Resour.*, *131*, 54, 1989.

Clynne, M. A., and R. L. Christiansen, Magma mixing and the devastating eruptions of May 1915 at Lassen Peak, paper presented at Hawaiian Symposium on How Volcanoes Work, AGU, Hilo, Hawaii, Jan. 19–25, 1987.

DeBari, S. M., and R. G. Coleman, Examination of the deep levels of an island arc: Evidence from the Tonsina ultramafic-mafic assemblage, Tonsina, Alaska, *J. Geophys. Res.*, *94*, 4373–4391, 1989.

Ewart, A., A review of the mineralogy and chemistry of Tertiary-Recent dacitic, rhyolitic and related salic volcanic rocks, in *Trondhjemites, Dacites and Related Rocks*, edited by F. Barker, pp. 13–121, Elsevier, New York, 1979.

Ewart, A., The mineralogy and petrology of Tertiary-Recent orogenic volcanic rocks: With special reference to the andesitic-basaltic compositional range: in *Andesites: Orogenic Andesites and Related Rocks*, edited by R. S. Thorpe, pp. 25–95, John Wiley, New York, 1982.

Ewart, A., W. Hildreth, and I. S. E. Carmichael, Quaternary acid magma in New Zealand, *Contrib. Mineral. Petrol.*, *51*, 1–27, 1975.

Falloon, T. J., D. H. Green, C. J. Hatton, and K. L. Harris, Anhyrous partial melting of a fertile and depleted peridotite from 2 to 30 kb and application to basalt petrogenesis, *J. Petrol.*, *29*, 1257–1282, 1988.

Fujii, T., and C. M. Scarfe, Composition of liquids coexisting with spinel peridotite at 10 kb and the genesis of MORBs, *Contrib. Mineral. Petrol.*, *90*, 18–28, 1985.

Gill, J. B., *Orogenic Andesites and Plate Tectonics*, Springer-Verlag, New York, 1981.

Grove, T. L., and M. B. Baker, Phase equilibrium controls on the tholeiitic versus calc-alkaline differentiation trends, *J. Geophys. Res.*, *89*, 3253–3274, 1984.

Grove, T. L., and W. B. Bryan, Fractionation of pyroxene phyric MORB at low pressure: An experimental study, *Contrib. Mineral. Petrol.*, *84*, 293–309, 1983.

Grove, T. L., D. C. Gerlach, and T. W. Sando, Origin of calc-alkaline series lavas at Medicine Lake Volcano by fractionation, assimilation, and mixing, *Contrib. Mineral. Petrol.*, *80*, 160–182, 1982.

Guffanti, M., M. A. Clynne, J. G. Smith, L. J. P. Muffler, and T. D. Bullen, Late Cenozoic volcanism, subduction, and extension in the Lassen region of California, southern Cascade Range, *J. Geophys. Res.*, this issue.

Helz, R. T., Phase relations of basalts in their melting ranges at P_{H_2O} = 5 kb, part II, Melt compositions, *J. Petrol.*, *17*, 139–193, 1976.

Iyer, H. M., Geophysical evidence for the locations, shapes and sizes, and internal structures of magma chambers beneath regions of Quaternary volcanism, *Philos. Trans. R. Soc. London, Ser. A*, *310*, 473–510, 1984.

Jaques, A. L., and D. H. Green, Anhyrous melting of peridotite at 0–15 kb pressure and the genesis of tholeiitic basalts, *Contrib. Mineral. Petrol.*, *73*, 287–310, 1980.

LaFehr, T. R., Gravity, isostasy, and crustal structure in the southern Cascade Range, *J. Geophys. Res.*, *70*, 5581–5597, 1965.

Lydon, P. A., Geology of the Butt Mountain area, a source of the Tuscan Formation in northern California, Ph.D. dissertation, 230 pp., Univ. of Oreg., Eugene, 1968.

Meyer, C. E., M. J. Woodward, A. M. Sarna-Wojcicki, and C. W. Naeser, Zircon fission-track age of 0.45 million years on ash in the type section of the Merced Formation, west-central California, *U.S. Geol. Surv. Open File Rep.*, *80-1071*, 9 pp., 1980.

Miyashiro, A., Volcanic rock series in island arcs and active continental margins, *Am. J. Sci.*, *274*, 321–355, 1974.

Muffler, L. J. P., and M. A. Clynne, Geologic map of the Lassen region, Cascade Range, USA (abstract), *Bull. N. M. Bur. Mines Miner. Resour.*, *131*, 199, 1989.

Pakiser, L. C., Gravity, volcanism, and crustal structure in the southern Cascade Range, California, *Geol. Soc. Am. Bull.*, *75*, 611–620, 1964.

Riddehough, R., Recent movements of the Juan de Fuca plate system, *J. Geophys. Res.*, *89*, 6980–6994, 1984.

Sarna-Wojcicki, A. M., C. E. Meyer, H. R. Bowman, N. T. Hall, P. C. Russell, M. J. Woodward, and J. L. Slate, Correlation of the Rockland ash bed, a mid-Pleistocene stratigraphic marker in northern and central California and western Nevada and implications for the middle Pleistocene paleogeography of central California, *Quat. Res.*, *23*, 236–257, 1983.

Smith, R. L., Ash flows, *Geol. Soc. Am. Bull.*, *71* 795–842, 1960.

Sparks, R. S. J., and L. A. Marshall, Thermal and mechanical constraints on mixing between mafic and silicic magmas, *J. Volcanol. Geotherm. Res.*, *29*, 99–124, 1986.

Stormer, J. C., and J. Nicholls, XLFRAC: A program for the interactive testing of magmatic differentiation models, *Comput. Geosci.*, *4*, 143–159, 1978.

Takahashi, E., and I. Kushiro, Melting of a dry peridotite at high pressures and basalt magma genesis, *Am. Mineral.*, *68*, 859–879, 1983.

Trimble, D. A., M. A. Clynne, and S. W. Robinson, The application of uranium-thorium systematics to rocks from the Lassen Dome Field, California, *U.S. Geol. Surv. Open File Rep.*, *84-371*, 92 pp., 1984.

Walker, D., T. Shibata, and S. F. DeLong, Abyssal tholeiites from the Oceanographer Fracture Zone, II, Phase equilibria and mixing, *Contrib. Mineral. Petrol.*, *70*, 111–125, 1979.

Williams, H., Geology of the Lassen Volcanic National Park, California, *Univ. Calif. Publ. Geol. Sci.*, *21*, 195–385, 1932.

Wilson, T. A., The geology near Mineral, California, M.S. thesis, 92 pp., Univ. of Calif., Berkeley, 1961.

M. A. Clynne, U.S. Geological Survey, 345 Middlefield Road, MS 910, Menlo Park, CA 94025.

(Received July 27, 1989;
revised July 31, 1990;
accepted July 31, 1990.)

JOURNAL OF GEOPHYSICAL RESEARCH, VOL. 95, NO. B12, PAGES 19,453–19,464, NOVEMBER 10, 1990

Late Cenozoic Volcanism, Subduction, and Extension in the Lassen Region of California, Southern Cascade Range

MARIANNE GUFFANTI

U.S. Geological Survey, Reston, Virginia

MICHAEL A. CLYNNE, JAMES G. SMITH, L. J. P. MUFFLER, AND THOMAS D. BULLEN

U.S. Geological Survey, Menlo Park, California

Hundreds of short-lived, small- to moderate-volume, mostly mafic volcanoes occur throughout the Lassen region of NE California and surround five longer-lived, large-volume, intermediate to silicic volcanic centers younger than 3 Ma. Volcanic rocks older than 7 Ma are scarce in the Lassen region. We identify 537 volcanic vents younger than 7 Ma, and we classify these into five age intervals and five compositional categories based on SiO_2 content. Maps of vents by age and composition illustrate regionally representative volcanic trends. By 2 Ma, the eastern limit of volcanism had contracted westward toward the late Quaternary arc. Late Quaternary volcanism is concentrated around and north of the silicic Lassen volcanic center. The belt of most recent volcanism (25–0 ka) has been active since at least 2 Ma. Most mafic volcanism is calcalkaline basalt and basaltic andesite. However, lesser volume of low-potassium olivine tholeiite (LKOT), a geochemically distinctive basalt type found in the northern Basin and Range province, also has erupted throughout the Lassen segment of the Cascade arc since the Pliocene. Thus models of the mantle source and tectonic control of LKOT magmatism should be applicable both within and behind the subduction-related arc. Normal faults and linear groups of vents are evidence of widespread crustal extension throughout most of the Lassen region. NNW alignments of these features indicate NNW orientation of maximum horizontal stress (ENE extension), which is similar to the stress regime in the adjacent northwestern Basin and Range and northern Sierra Nevada provinces. The large, long-lived volcanic centers developed just west of a zone of closely spaced NNW trending normal faults. Within that zone of faulting, pervasive ENE extension has precluded growth of large, long-lived crustal magma systems. We interpret the western limit of the zone of NNW trending normal faults as the western boundary of the Basin and Range province where it overlaps the Lassen segment of the Cascade arc. In our view, the Lassen volcanic region occurs above the subducting Gorda North plate but also lies within a broad zone of distributed extension that occurs in the North American lithosphere east and southeast of the present Cascadia subduction zone. An episode of ENE extension that began in the late Miocene in the northwestern Basin and Range province appears to have triggered widespread late Miocene to Quaternary mafic volcanism in the Lassen region. The scarcity of volcanic rocks older than 7 Ma suggests that a more compressive lithospheric stress regime prior to the late Miocene extensional episode may have suppressed volcanism, even though subduction probably was occurring beneath the Lassen region.

INTRODUCTION

The volcanic arc associated with Cenozoic subduction beneath the North American plate has contracted northward since the Miocene, in conjunction with northward migration of the Mendocino triple junction [*Dickinson and Snyder*, 1979]. At 20 Ma, the arc was active as far south as Las Vegas. Since the late Pliocene, the southern terminus of the arc has been located in the vicinity of the Lassen region in northeastern California (Figure 1). In its position at the southern end of the Cascade arc, the Lassen volcanic region lies near the junction of three active tectonic regimes: (1) a subduction regime to the north resulting from thrusting of the Juan de Fuca plate system under the North American plate; (2) a transform regime to the south resulting from the relative motion of the North American and Pacific plates; and (3) an extensional regime to the east in the Basin and Range province (Figure 1). In this paper, we consider the effects of the adjacent tectonic environments on volcanism in the subduction environment of the Lassen region.

The Lassen region, separated from the Mount Shasta and Medicine Lake volcanic centers to the north by an area in which there are no recognized Quaternary volcanic vents, forms a distinct segment of the Cascade arc [*Guffanti and Weaver*, 1988]. Within the Lassen region (120°30′ to 122°10′W and 40°15′ to 41°N, an area of approximately 10,000 km^2), the volcanic record is overwhelmingly younger than 7 Ma. Hundreds of short-lived, small- to moderate-volume, mostly mafic volcanoes surround a few long-lived, large-volume, intermediate to silicic volcanic centers younger than 3 Ma (Figure 2).

In order to characterize volcanic activity on a regional scale, we located as many volcanic vents as we could in the Lassen region (537 vents) and assigned each one to an age category and a compositional category using a variety of geochemical and geochronological data. We present maps of vents by age and composition to illustrate regionally representative volcanic trends.

We propose that some of the volcanic and tectonic features of the Lassen region are best understood as resulting from the spatial overlap of the extensional Basin and Range province on the subduction-related arc. Basin and Range influence on the Cascade Range previously has been suggested by others, for example, *Magill et al.*, [1982], *Priest et*

Paper number 90JB00246.

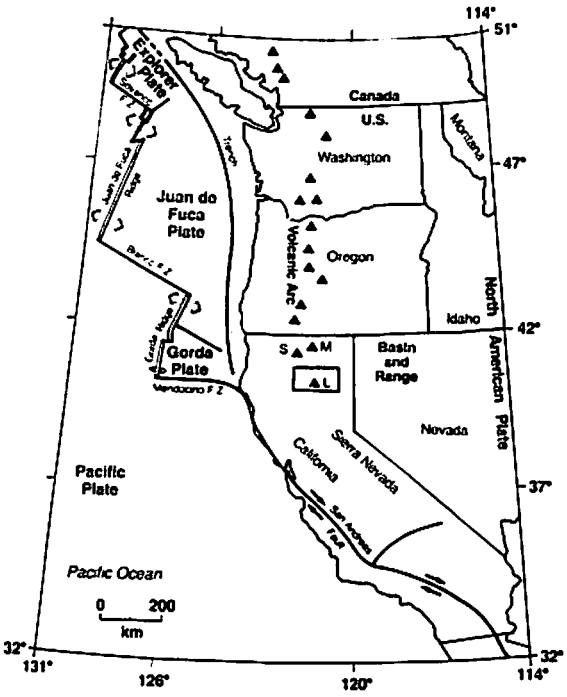

Fig. 1. Plate tectonic setting of the Lassen volcanic region. Triangles indicate major Quaternary volcanic centers of the Cascade Range. Small rectangle encloses Lassen region. S, Mount Shasta; M, Medicine Lake volcano. (Modified from *Mooney and Weaver* [1989].)

al. [1983], *Smith and Luedke* [1984], and *Guffanti and Weaver* [1988]; in this paper, we attempt to enlarge upon their insights in the southern Cascades.

GEOLOGIC AND TECTONIC SETTING

The Lassen region is distinctive because the record of volcanism prior to the late Miocene is very sparse. Thick sections of early Oligocene to middle Miocene volcanogenic rocks of the Western Cascade Range are widely exposed from west of Mount Shasta north to Mount Rainier. In contrast, Oligocene and early Miocene rocks are not evident south of Mount Shasta, and only a few small areas of middle Miocene (~15 Ma) rocks deposited on Mesozoic and Paleozoic basement are exposed in the western part of the Lassen region. The time span from 17 to 7 Ma appears to be an interval of relative volcanic quiescence in the Cascades in Washington as well as in northern California, although not in central Oregon [*Smith*, 1989; *Sherrod and Smith*, 1989].

Whereas nearly all volcanic rocks within the Lassen region are younger than 7 Ma, volcanic rocks east of the Lassen region are mostly older than 7 Ma. Adjacent to the east of the study area and north of Honey Lake, widely scattered stratovolcanoes are Miocene in age, commonly about 10 Ma [*Grose and McKee*, 1986]. Decrease in age of volcanic rocks from east to west occurred during the late Miocene near Susanville, on the eastern edge of the Lassen region [*Grose and McKee*, 1982; *Grose*, 1985].

The Lassen volcanic region is associated with subduction of the Gorda North plate, part of the Juan de Fuca plate system. Contours of estimated plate depth and locations of recognized volcanic vents are shown in Figure 2. Most vents in the Lassen region lie over the subducting plate where its upper surface is estimated to be between 80 km and at least 130 km deep. Subcrustal earthquake hypocenters along a Wadati-Benioff zone west of the Lassen region define slab dip of 25° between depths of 50–90 km [*Walter*, 1986; *Cockerham*, 1984]. Subcrustal earthquakes, however, have not been detected at depths greater than 90 km beneath the Lassen segment of the Cascade arc. We estimate contours of plate depth greater than 90 km by continued eastward projection of the 25° plate dip, recognizing that actual plate dip may be steeper than that.

The southern edge of the subducting slab is a function of the position of the northward migrating Mendocino triple junction [*Dickinson and Snyder*, 1979]. At present, the subducting slab extends as far south as about 39°45'N [*Jachens and Griscom*, 1983; *Wilson*, 1986]. Migration of the Mendocino triple junction has been correlated with extension in the northern California Coast Ranges [*McLaughlin*, 1981] and the Sacramento Valley [*Harwood*, 1984] but not correlated with extension farther east in the Lassen region.

Geophysical studies in the Lassen region suggest that a few kilometers of late Cenozoic volcanic rocks are underlain by granitic crust. The thickness of the crust beneath the Lassen region is 38 ± 4 km [*Mooney and Weaver*, 1989]. *Berge and Stauber* [1987] concluded from a two-dimensional seismic refraction study that volcanic rocks in the Lassen region range from about 1 to 4 km in thickness and that Sierra Nevada basement probably underlies the volcanic rocks at least as far northwest as Lassen Peak. This conclusion is compatible with the fact that fault blocks of Sierran granitic rock are exposed southeast of Eagle Lake (Figure 2). *Blakely et al.* [1985, Figure 7, feature F] suggested that an aeromagnetic anomaly in the northern part of the Lassen region may represent an isolated fragment of mafic or ultramafic rocks at shallow depth in the crust. This aeromagnetic feature could be part of either the Trinity ophiolite complex of the Klamath Mountains or an ultramafic body in the Sierra Nevada basement complex. Thus a transition from Sierran to Klamath basement may occur beneath the northern part of the Lassen region.

Evidence from gravity modeling indicates that upper crustal structure in the Basin and Range continues into the Lassen region. *Blakely and Jachens* [this issue] describe a NE trending gravity depression that extends from the Lassen region hundreds of kilometers into Nevada. Similar NE trending gravity features occur throughout Oregon into Washington and largely correlate with the Cascade arc segmentation of *Guffanti and Weaver* [1988]. *Blakely and Jachens* [this issue] proposed that the NE trending features reflect upper crustal structures that have actively influenced the locus of more recent volcanism.

Voluminous, intermediate to silicic volcanism has occurred in the Lassen region at four, large, late Pliocene to Quaternary centers, Dittmar, Snow Mountain, Maidu, and Lassen (Figure 2). A fifth large center, Yana, of late Pliocene age [*Lydon*, 1968] lies just outside the study area to the south. These centers are located in the western part of the volcanic region where the upper part of the subducting slab is projected to lie between depths of approximately 85 and 110 km. The centers are long-lived, of the order of hundreds of thousands of years, compared to smaller volcanoes in the surrounding region. The youngest large center is Lassen volcanic center (<0.6 Ma), which lies largely within Lassen Volcanic National Park [*Clynne*, this issue; *Bullen and*

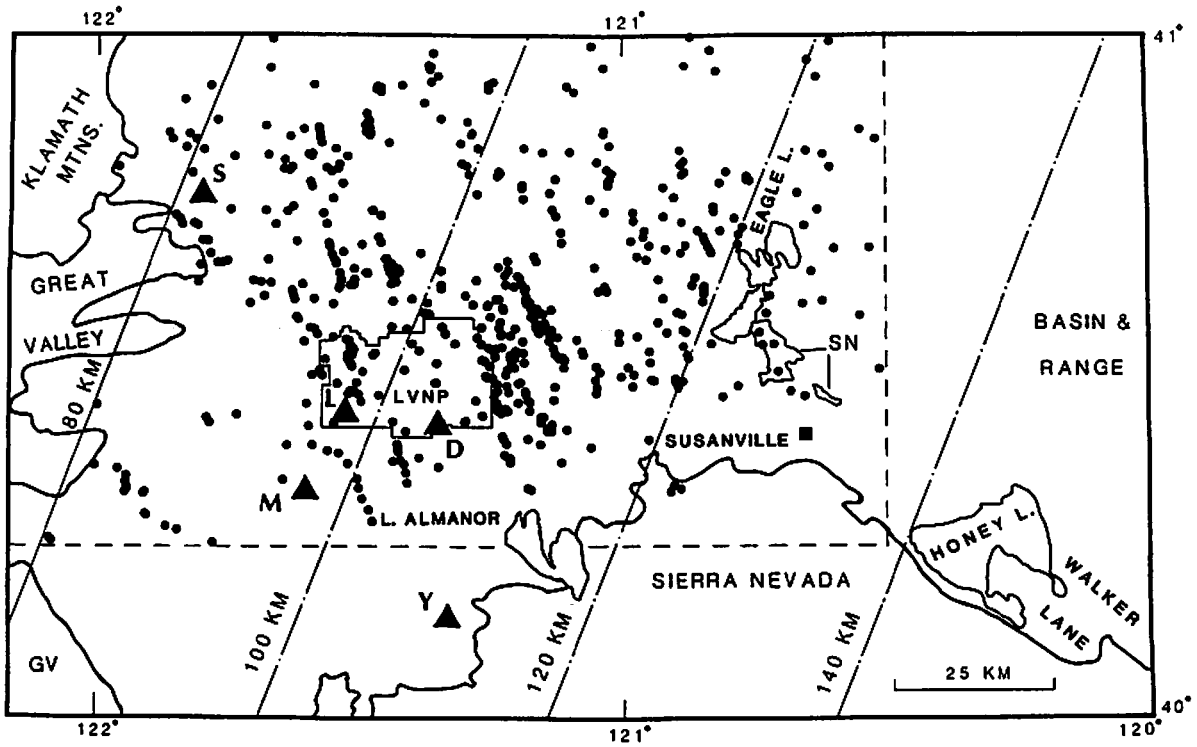

Fig. 2. Regional geologic setting of the Lassen volcanic region. Solid dots depict 537 volcanic vents younger than 7 Ma. Solid triangles indicate major volcanic centers younger than 3 Ma: Y, Yana; D, Dittmar; M, Maidu; L, Lassen; S, Snow Mountain. Estimated depth to the subducting plate shown by NE trending lines. LVNP, Lassen Volcanic National Park. SN, Sierra Nevada outcrops. GV, Great Valley. Dashed rectangle is area shown in Figures 4–10.

Clynne, this issue]. Lassen volcanic center, having produced about 100 km^3 of silicic (>63% SiO_2) rocks (roughly half of its total eruptive volume) is the largest Quaternary silicic magma system in the Cascades.

Faults are more abundant in the Lassen region than elsewhere in the Cascade Range except, perhaps, around Medicine Lake volcano. Many faults have vents along them, although not all magma rose along faults observable on the surface. In the northern part of the region, normal faulting is concentrated in zones of closely spaced individual faults having separations of about 0.8 km; other areas lack closely spaced faults. On the westernmost side of the Lassen region is the Battle Creek fault zone of ENE trending, late Quaternary, dominantly normal faults [*Helley et al.*, 1981]. The westward limit of NNW trending normal faults within the Lassen region is delineated on Figure 3. The four large-volume volcanic centers occur along or west of this boundary.

VOLCANIC TRENDS

Data Sources

We identified 537 volcanic vents in the Lassen region and assigned them to age and compositional categories. We created the vent data set based on published geologic maps [*Lerch*, 1987; *Clynne*, 1984; *Hazlett*, 1984; *Helley et al.*, 1981; *Tuppan*, 1981; *Bean*, 1980; *Youngkin*, 1980; *MacDonald and Lydon*, 1972; *MacDonald*, 1965, 1964, 1963; *Lydon et al.*, 1960] and unpublished mapping by T. L. T. Grose (contract mapping to the U.S. Geological Survey (USGS), in preparation, 1990) and the authors.

The compositional categories are based on SiO_2 content: basalt, 48–53%; basaltic andesite, 53–57%; andesite, 57–63%; dacite, 63–70%; rhyolite, >70%. The basalt category is subdivided into low-potassium (<0.3%) olivine tholeiite basalt (LKOT) and calcalkaline basalt. Compositions are determined on the basis of chemical analyses or estimated from thin sections and hand samples. LKOT is aphyric to sparsely phyric and commonly has diktytaxitic texture; flows from all identified LKOT vents have been chemically analyzed. The distinction between calcalkaline basalt and basaltic andesite is subtle in hand sample identification; compared to calcalkaline basalt, the matrix texture of basaltic andesite typically is aphanitic, and clinopyroxene usually is present in the phenocryst assemblage.

Age categories are slightly modified from those of *Smith* [1989]: 7–2 Ma, 2–0.73 Ma, 730–120 ka, 120–25 ka, and 25–0 ka. Age determinations are based on unpublished K-Ar determinations by G. B. Dalrymple, A. L. Cook, L. B. Pickthorn, and J. G. Smith, ^{14}C dates by D. A. Trimble and S. W. Robinson, published ages of *Clynne* [this issue], *Grose and McKee* [1986], *Sarna-Wojcicki et al.* [1985], *Trimble et al.* [1984], *Crandell et al.* [1974], *Crandell* [1972], and *Ruben and Alaxander* [1960], paleomagnetic determinations by D. E. Champion, glacial and volcanic stratigraphy, and geomorphological characterization by the authors.

For various spatial distributions of vents by age and composition, we selected vent alignments based on visual inspection and judgement rather than quantitative methods [cf. *Wadge and Cross*, 1988]. The criteria we used to select alignments are the following: (1) groups of vents are roughly coeval, (2) vents are in groups of three or more, and (3) vents

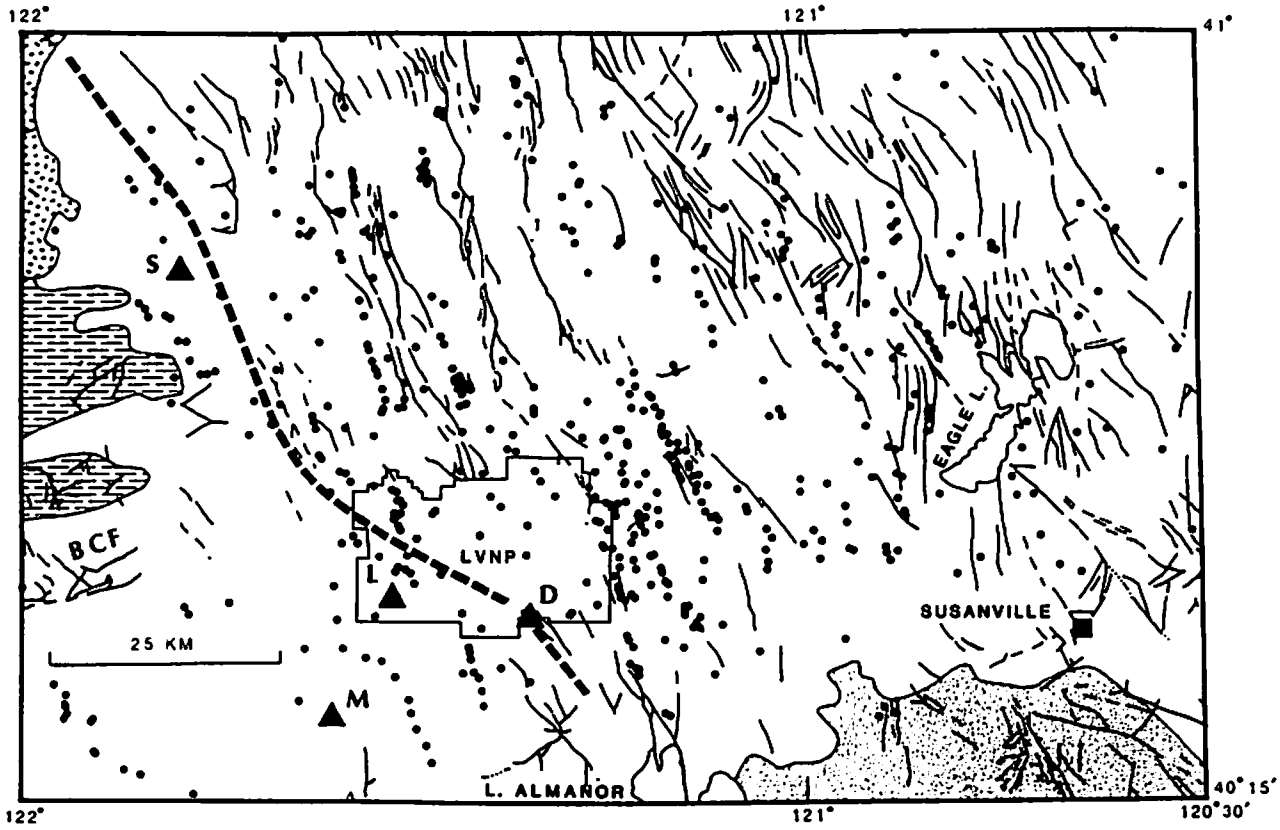

Fig. 3. Volcanic vents less than 7 Ma (solid dots) and faults (thin lines; modified from *Lydon et al.* [1960]). Thick dashed line is western limit of closely spaced normal faults. Large solid triangles indicate major volcanic centers: D, Dittmar; M, Maidu; L, Lassen; S, Snow Mountain. LVNP, Lassen Volcanic National Park. BCF, Battle Creek fault. Stipple pattern, Sierra Nevada; horizontal dash pattern, Great Valley; random dash pattern, Klamath Mountains.

are closely spaced or, if more widely spaced, are thought to be genetically related. We typically did not choose an alignment where a group of vents exhibits a variety of possible linear orientations; rather, we selected those groups that display an obvious, unambiguous alignment direction.

Basalt Types

Both calcalkaline basalt and low-potassium olivine tholeiitic basalt (LKOT) occur in the Lassen region. Mafic volcanism is predominantly calcalkaline basalt and basaltic andesite, which builds small shield volcanoes and cinder cones. LKOT produces fluid, far-traveled but thin flows and very low shields. LKOT lavas are volumetrically minor compared to calcalkaline basalt and basaltic andesite.

Geochemical characteristics of Lassen calcalkaline basalt and Lassen LKOT are given in Table 1. Lassen LKOT is characterized by low K_2O content (<0.3%) and high FeO*/MgO (0.9–1.2%) at low silica values (48–50%). Many calcalkaline and most LKOT lavas are primitive in composition. Both types of primitive basalt typically are sparsely phyric, are singly saturated (olivine ± spinel), have high combatible-element (Ni, Cr, Sc) abundances, and have incompatible-element (K, Rb) abundances that do not correlate with isotopic signatures expected from crustal contamination [*Bullen and Clynne*, 1989].

LKOT in the Lassen region is similar in major and trace element composition to many low-potassium, high-alumina olivine tholeiites found at Medicine Lake volcano [*Mertzman*, 1979], throughout the northern Basin and Range province [*Hart et al.*, 1984; *McKee et al.*, 1983], and in the central Oregon High Cascades [*Smith et al.*, 1987]. *Hart et al.* [1984] considered this basalt type to be a distinctive regional geochemical unit of the Basin and Range (see Table 1) and named it HAOT, the acronym for high-alumina olivine

TABLE 1. Ranges of Selected Major and Trace Elements at Average SiO_2 Contents for Lassen Calc-alkaline Basalt (CAB) and Low-Potassium Olivine Tholeiite (LKOT), Compared to Average High-Alumina Olivine Tholeiite (HAOT) From the Northwestern Basin and Range Province

	Lassen CAB	Lassen LKOT	B and R HAOT[a]
SiO_2, wt %	52.0[b]	48.7[b]	48.2
AlO_2, wt %	15.0–18.5	17.2–18.2	17.1
K_2O, wt %	0.30–1.90	0.10–0.30	0.23
TiO_2, wt %	0.50–1.80	0.80–1.10	1.01
Na_2O, wt %	2.50–4.50	2.50–3.00	2.56
FeO*/MgO	0.70–1.60	0.90–1.20	1.09
Rb, ppm	5–40	1–6	2.1
Sr, ppm	400–1200	200–400	255
Ba, ppm	150–600	100–200	141
Zr, ppm	60–100	60–100	95
Y, ppm	15–30	20–30	20
Number of samples	~300	~60	50

[a]From *Hart et al.* [1984].
[b]Average.

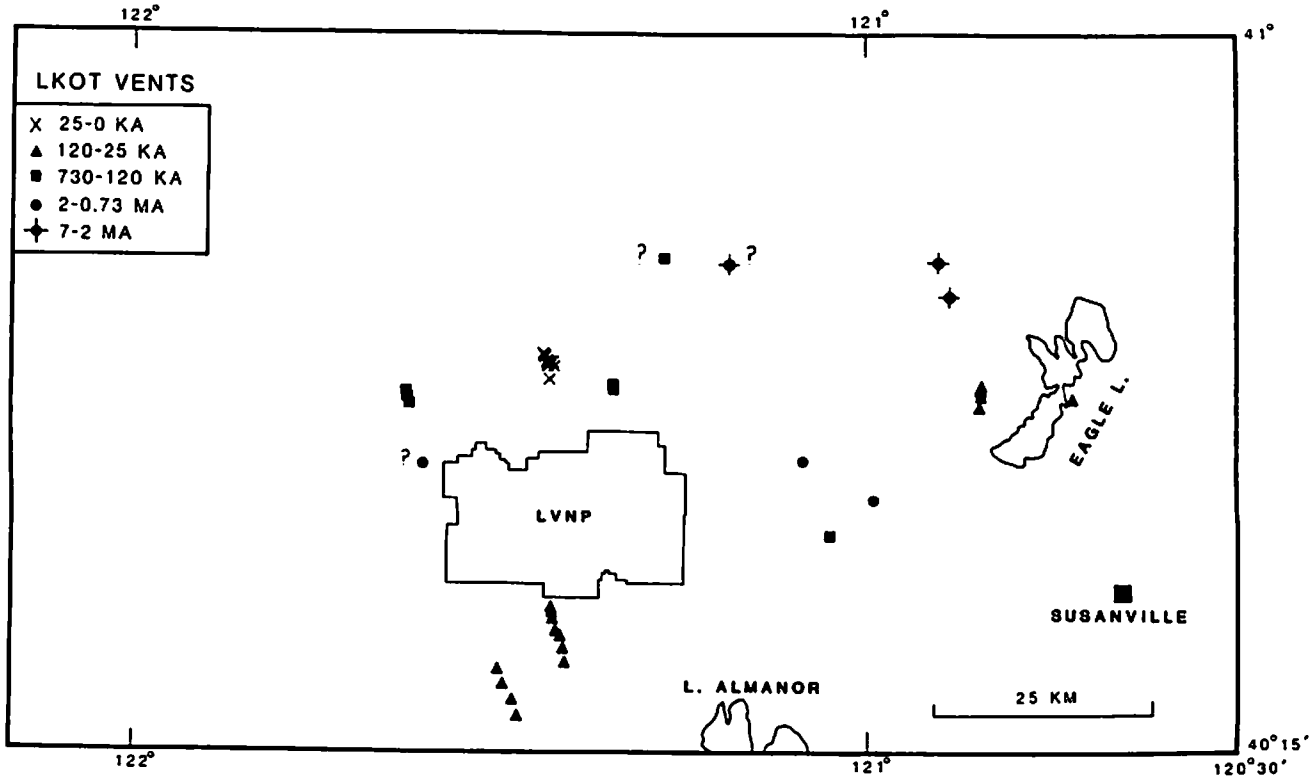

Fig. 4. Forty-one vents of low-potassium olivine tholeiite (LKOT). Symbols indicate age categories. For three LKOT vents, inferred vent locations are shown by queried symbols. LVNP, Lassen Volcanic National Park.

tholeiite. We prefer the acronym LKOT because low potassium, rather than high alumina, is the distinctive feature of these tholeiites.

Vent Distributions

LKOT lavas have erupted sporadically in the Lassen region since the Pliocene (Figure 4). Although the majority of LKOT flows have identified vents, some flows without recognizable vents are not represented on Figure 4. The oldest identified LKOT vents are Pliocene in age and occur in the eastern part of the Lassen region. Among vents younger than 2 Ma, no strong temporal/spatial trend is apparent; the youngest LKOT vents are not the farthest west, and both Pliocene and late Pleistocene vents are located within 15 km of each other west of Eagle Lake. Many Quaternary LKOT lavas erupted from NNW trending alignments of vents. The youngest group of LKOT vents, north of Lassen Volcanic National Park, erupted about 15 ka to form the Hat Creek basalt flow; these vents are located close to calcalkaline andesite and basalt vents younger than 120 ka.

Maps of all vents by age and composition are shown for five time intervals in Figures 5–9. These figures incorporate LKOT vents from Figure 4. For each interval since 2 Ma, the area within which most vents are concentrated is outlined.

Most late Miocene and Pliocene (7–2 Ma) vents are found east of 121°15′ (Figure 5). The eastern extent of vents in this time period is just outside the study area to the east. The apparent absence of vents west of 121°15′ probably is due in large part to burial of older vents by flows younger than 2 Ma. Vents also are sparse within the Pliocene Tuscan Formation, an extensive volcaniclastic apron west and southwest of Lassen Volcanic National Park [*Lydon*, 1968; *Helley et al.*, 1981]. Lavas erupted in this time period are dominantly mafic; basalt and basaltic andesite comprise 72% of all vents, andesite 21%, and dacite 7%. The Snow Mountain center (J. G. Smith, unpublished data, 1988) and the Dittmar center [*Clynne*, 1984, 1985] were active during the end of this time interval, circa 2 Ma. NNW trending groups of vents are evident near Eagle Lake.

By 2 Ma, the eastern extent of the volcanic field had shifted westward. All but one of the vents formed between 2 and 0.73 Ma occur west of 120°55′ (Figure 6). Andesite is more common (41% of vents) than in the previous group, although the percentage of silicic vents (5%) is about the same. The Maidu center [*Wilson*, 1961] became active during this period, whereas the Dittmar and Snow Mountain centers continued to be active during the early part of the period. A few, mostly NNW trending vent alignments are apparent; one ENE alignment occurs on the west side of the volcanic area.

The area of volcanism is smaller from 730 to 120 ka (Figure 7) than during previous time intervals. Basalt and basaltic andesite form 83% of the vents, andesite 8%, and dacite 9%. The Lassen volcanic center became active during this time interval [*Clynne*, 1984, this issue], whereas volcanism at the Maidu and Snow Mountain centers ended. An approximately E-W alignment occurs within Lassen volcanic center along the boundary between an andesitic stratovolcano (Brokeoff volcano, represented by the large triangle in Figure 7) and younger dacitic vents. Elsewhere, alignments are oriented NNW. A particularly well-developed vent align-

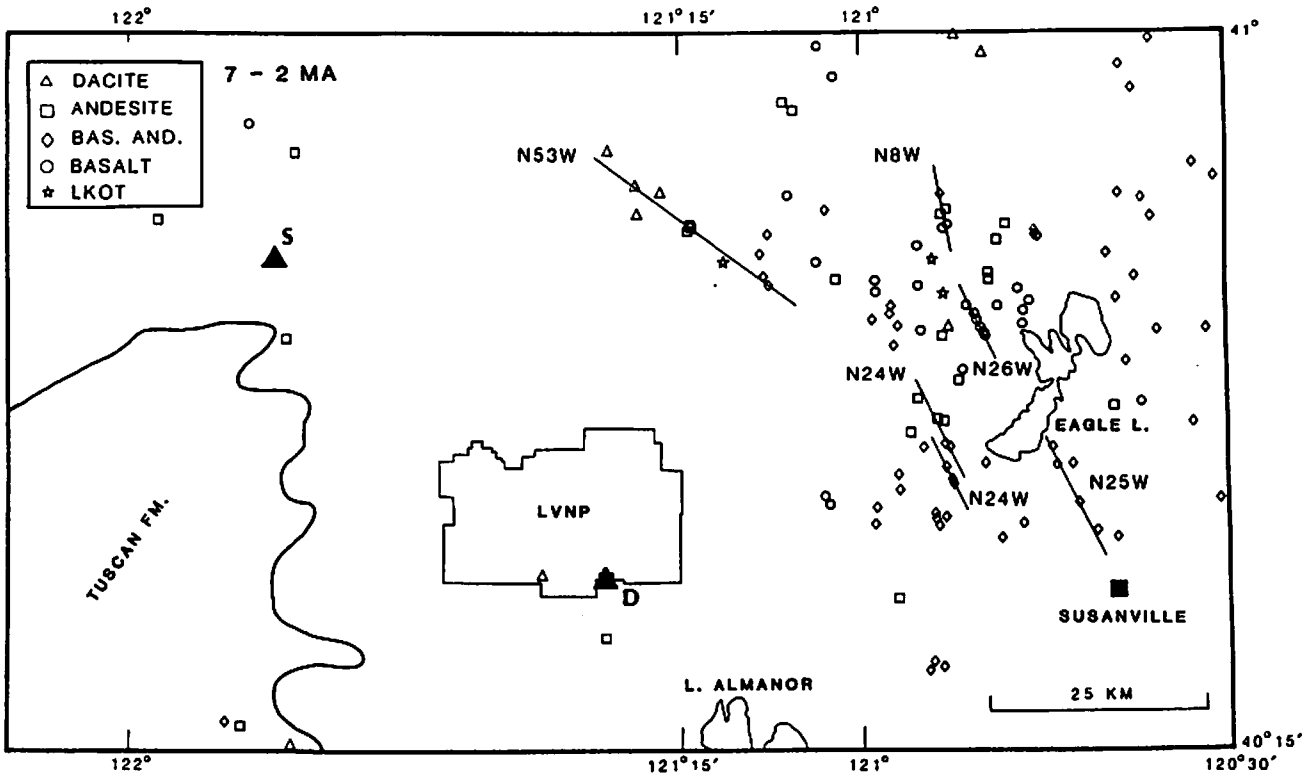

Fig. 5. One hundred and twenty-one volcanic vents formed from 7 to 2 Ma. Symbols indicate compositional categories. Vent alignments shown by oriented lines. Volcanic centers: S, Snow Mountain; D, Dittmar. (Yana center off map to the south.) LVNP, Lassen Volcanic National Park.

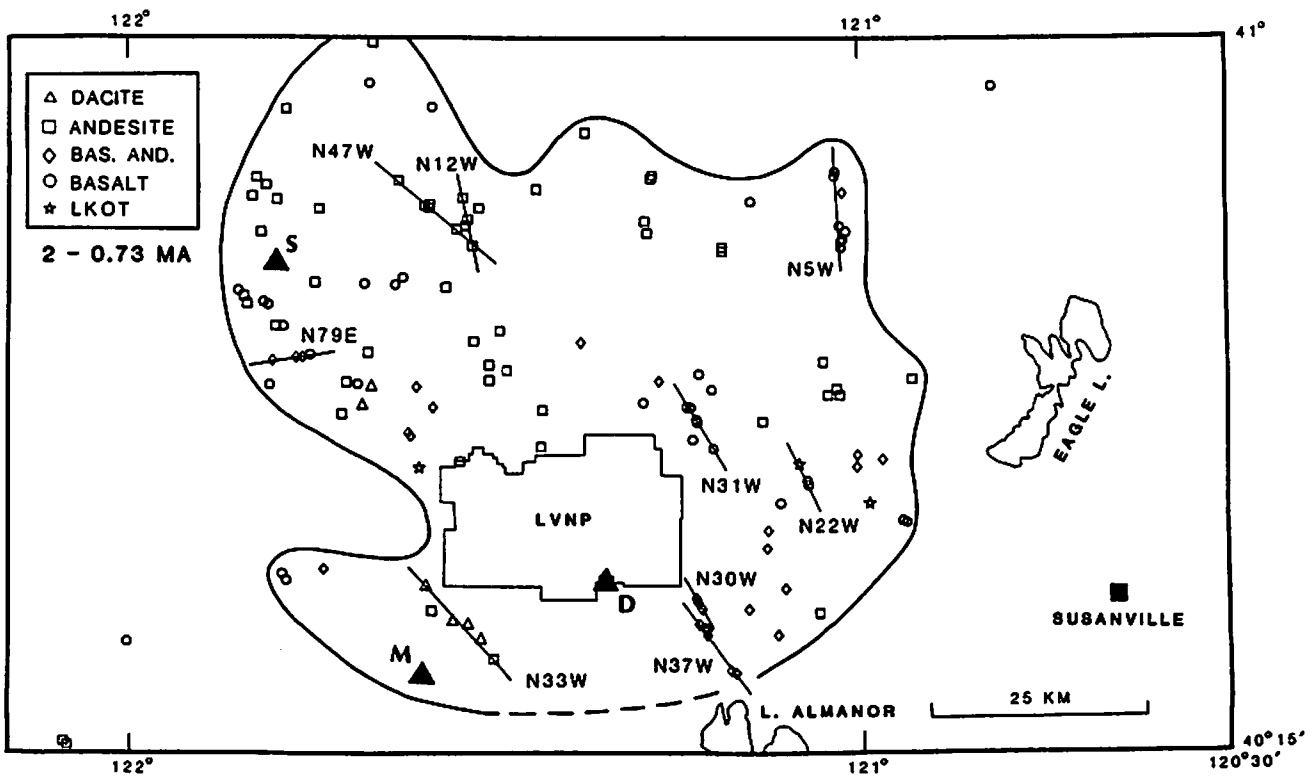

Fig. 6. One hundred and twenty-eight vents formed from 2 to 0.73 Ma. Symbols indicate compositional categories. Irregular line encloses main vent field. Vent alignments shown by oriented lines. Volcanic centers: S, Snow Mountain; D, Dittmar; M, Maidu. LVNP, Lassen Volcanic National Park.

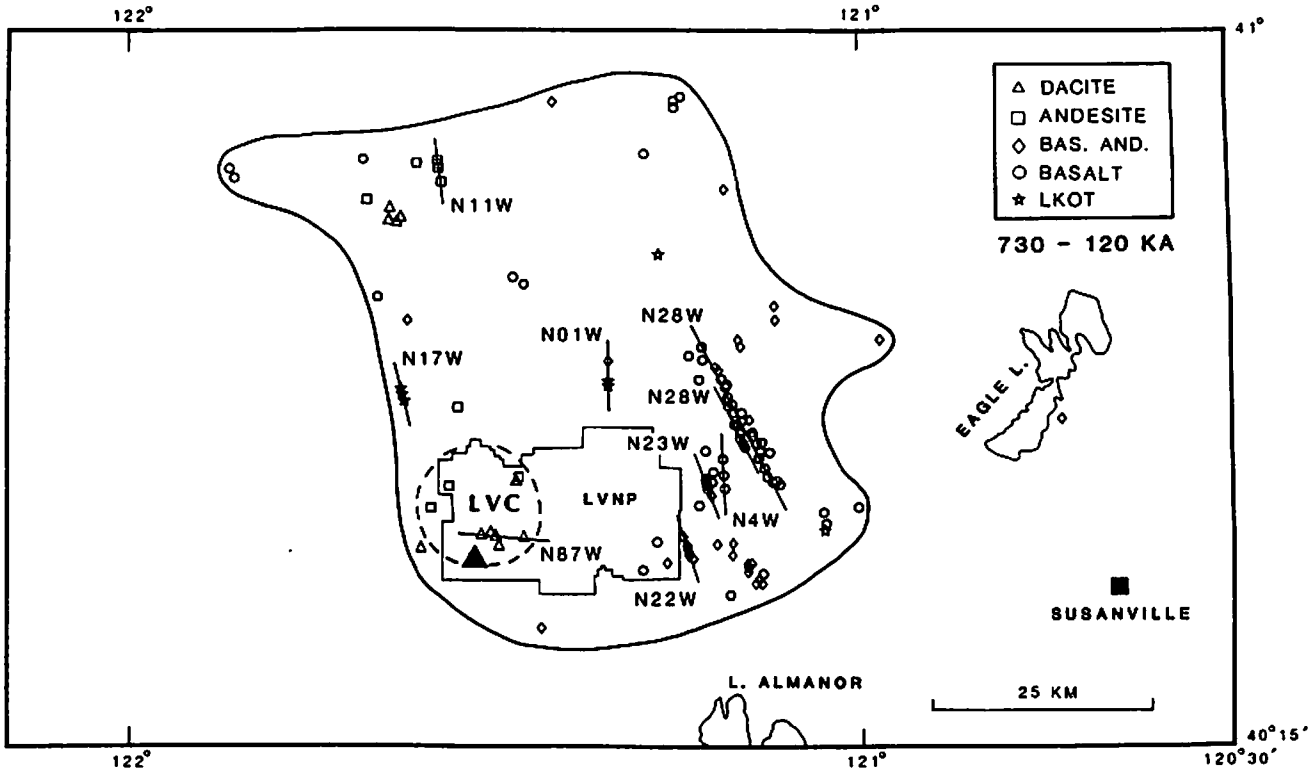

Fig. 7. One hundred and twenty-two vents formed from 730 to 120 ka. Symbols indicate compositional categories. Irregular line encloses main vent field. Vent alignments shown by oriented lines. Dashed circle encloses vents of Lassen volcanic center (LVC). LVNP, Lassen Volcanic National Park.

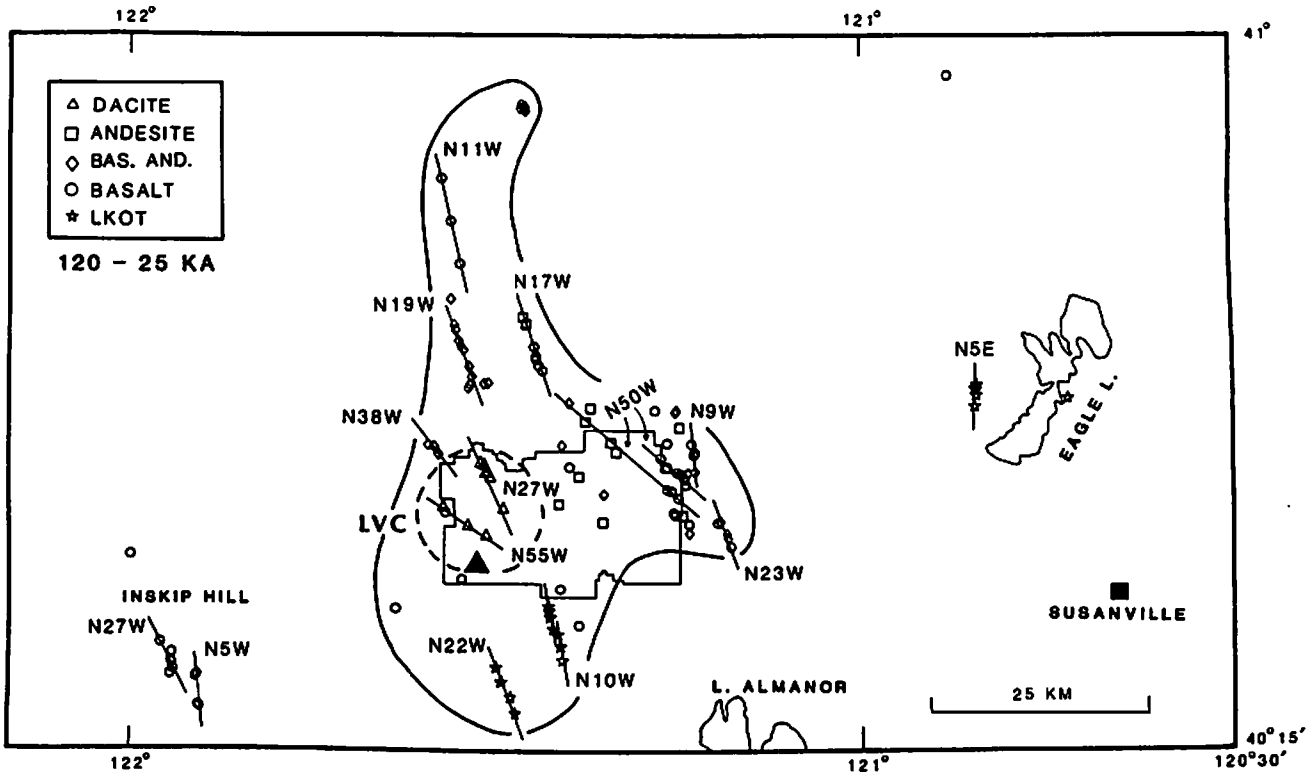

Fig. 8. One hundred and fourteen vents formed from 120 to 25 ka. Symbols indicate compositional categories. Irregular line encloses main vent field. Vent alignments shown by oriented lines. Dashed circle encloses vents of Lassen volcanic center (LVC). LVNP, Lassen Volcanic National Park.

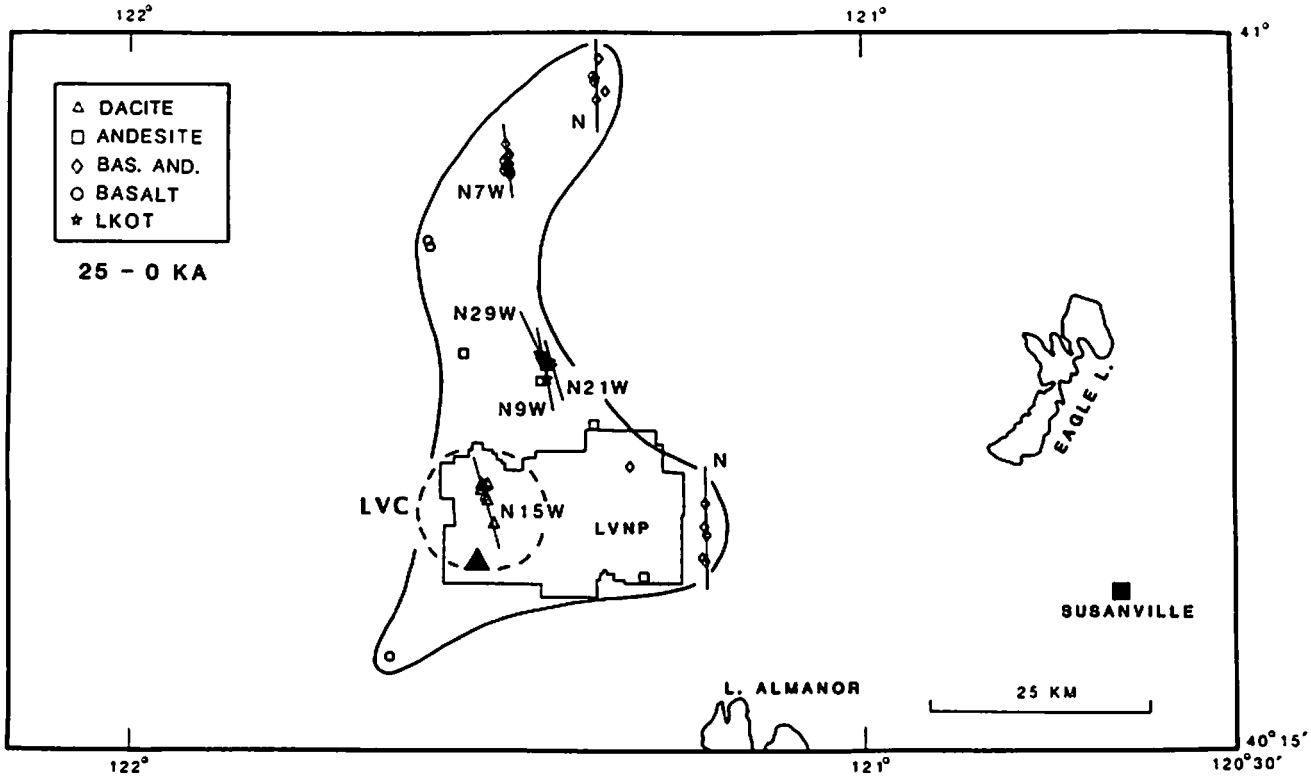

Fig. 9. Fifty-two vents younger than 25 ka. Symbols indicate compositional categories. Irregular line encloses main vent field. Vent alignments shown by oriented lines. Dashed circle encloses vents of Lassen volcanic center (LVC). LVNP, Lassen Volcanic National Park.

ment oriented N28°W occurs NE of Lassen Volcanic National Park.

From 120 to 25 ka (Figure 8), most vents are concentrated around and north of Lassen Volcanic National Park. Exceptions are vents of the Inskip Hill group [*Helley et al.*, 1981], 35 km southwest of the Lassen volcanic center, and LKOT vents near Eagle Lake. The Inskip Hill vents erupted primitive calcalkaline basalt notable for its low K_2O (<0.3%) content [*Bullen and Clynne*, 1989]. The Eagle Lake area is a structural depression comprising N and NW trending Plio-Pleistocene normal faults and is anomalous in the Lassen region for its overall NE trend [*Youngkin*, 1980]. In this time interval, vents are present in about the same compositional proportions as in the previous interval: basalt and basaltic andesite 82%; andesite 10%; dacite 8%. Numerous vent alignments range from NNW to NW, except for one NNE trend of LKOT vents.

Volcanism younger than 25 ka (Figure 9) is confined to a north trending belt less than 35 km wide. Compared to previous vent distributions, the area of volcanism has narrowed westward and eastward. Basalt and basaltic andesite form 79% of the vents and andesite 8%. Dacitic vents, all within Lassen volcanic center, constitute 13% of the total number of vents. Most vents younger than 25 ka form north to NNW trending alignments. Azimuths of these vent alignments are somewhat more northerly than in previous time periods.

In summary, comparison of the spatial distribution of vents formed since 2 Ma to that of vents formed from 7 to 2 Ma (Figure 10) shows that by 2 Ma volcanism had contracted or shifted westward. The main vent field outlined for the interval from 2 to 0.73 Ma (Figure 6) encompasses the main vent fields outlined for the three younger time intervals; since 0.73 Ma progressive decrease in the areas of the vent fields may be an artifact of sampling within successively shorter time intervals. The locus of most recent volcanism (25–0 ka, Figure 9) has been active in all time periods since at least 2 Ma. Basalt and basaltic andesite have constituted the majority of vents in all time periods. No silicic volcanism younger than 100 ka occurs outside of Lassen volcanic center.

Vent alignments and normal faults have tectonic significance because they trend parallel to the direction of maximum horizontal stress [*Nakamura*, 1977]. Alignments of vents from Figures 5–9 are shown on Figure 10. Azimuths of 48 vent alignments range from N79°E to N87°W; 79% of the azimuths are from N4°W to N38°W. Most faults in the volcanic region are NNW striking normal faults (Figure 3). The trends of vent alignments and normal faults thus indicate that the approximate direction of maximum horizontal stress (S_2) throughout most of the Lassen region is NNW since the Pliocene. The corresponding direction of least principal stress (extension) is horizontal and oriented ENE.

West of the zone dominated by NNW trending normal faults and vent alignments, the ENE trending Battle Creek fault zone is the major structural feature (Figure 3). This zone of normal faulting indicates that the direction of maximum horizontal stress (S_2) there is ENE, approximately 90° different from the NNW direction in the volcanic region to the east.

Within Lassen volcanic center, alignments of dacite vents have changed orientation with time. Field relationships

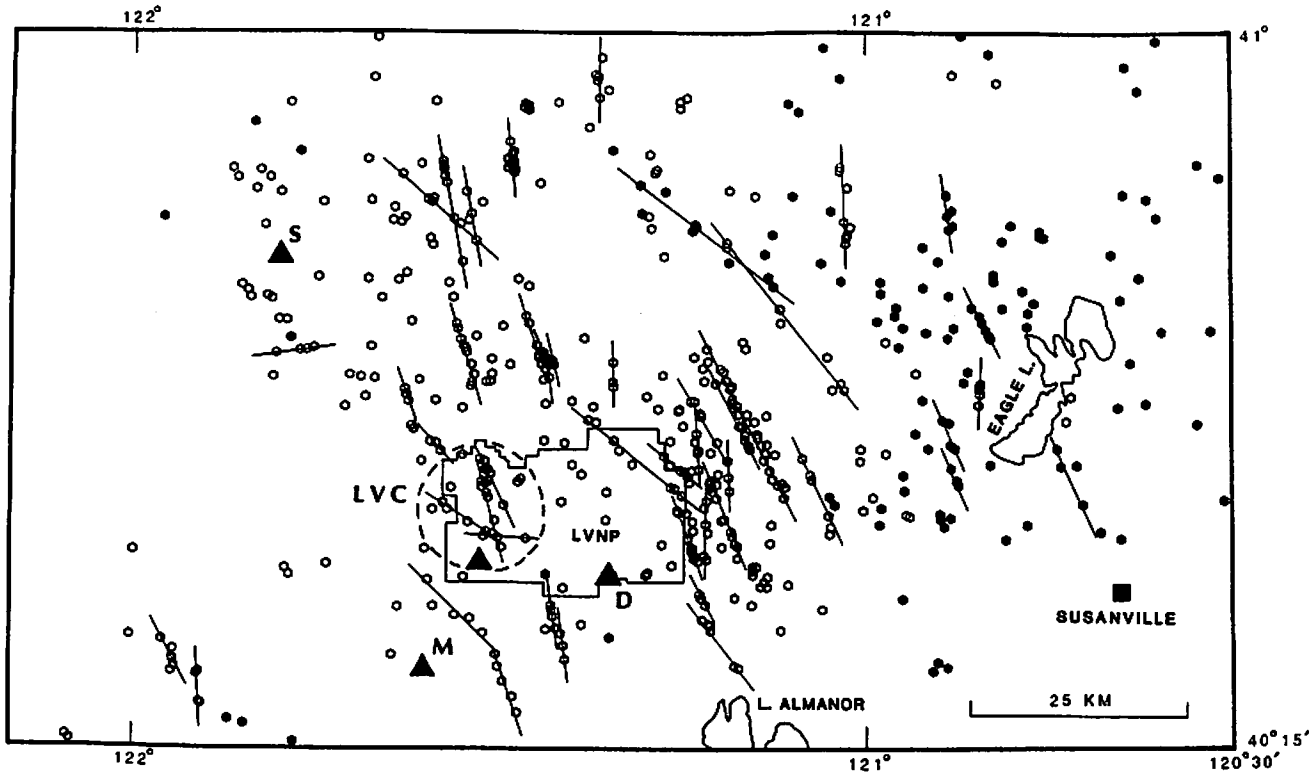

Fig. 10. Five hundred and thirty-seven volcanic vents younger than 7 Ma. Symbols indicate age categories: open symbol, 2-0 Ma; solid symbol, 7-2 Ma. Large triangles are major volcanic centers: M, Maidu; D, Dittmar; S, Snow Mountain. Dashed circle encloses vents of Lassen volcanic center (LVC). Short thin lines show vent alignments. LVNP, Lassen Volcanic National Park.

[*Muffler and Clynne*, 1989] indicate that a nearly E-W vent alignment formed within the interval from 730 to 120 ka (Figure 7) is coincident with the weakened boundary zone between the waning plumbing system of an older andesitic stratovolcano (Brokeoff volcano) and an evolving, generally silicic magma body. Orientation of younger alignments changes to NW during the interval from 120 to 25 ka (Figure 8) and to NNW since 25 ka (Figure 9). The vent alignments formed since 120 ka indicate the recent imprint of regional tectonic stress on the silicic center rather than the perturbing effect of a young, large, shallow, magma body [cf. *Bacon*, 1985; *Nakamura*, 1977].

DISCUSSION

A volcano-tectonic model of the Lassen region should explain the following observations: (1) volcanism prior to the late Miocene is sparse, whereas mafic to intermediate volcanism younger than 7 Ma is abundant; (2) the majority of vent alignments and normal faults in the Lassen region trend NNW; (3) primitive magmas include both calcalkaline and low-potassium olivine tholeiite (LKOT) basalt; (4) large-volume intermediate to silicic volcanic centers developed just west of a zone of closely spaced NNW trending normal faults; and (5) by 2 Ma, the eastern limit of volcanism had contracted westward. We suggest that most of these observations can be explained by the overlap of two tectonic regimes, the Cascade volcanic arc and the Basin and Range province. However, this interpretation does not adequately explain the westward contraction of volcanism by 2 Ma in the Lassen region.

The overall spatial distribution of vents in the Lassen region fits the generally accepted model of active arc volcanism in which vents are located between 90 and 150 km above a subducting slab (Figure 2). The Lassen region, however, also lies on the western edge of a broad zone of lithospheric extension that occurs in the North American plate well east and southeast of the present Cascadia subduction zone. We interpret the western limit of closely spaced NNW trending normal faults (Figure 3) as the western boundary of the extensional Basin and Range province where it overlaps the Lassen segment of the Cascade arc. Accordingly, we consider ENE extension in the Lassen region primarily to result from Basin and Range tectonism.

The NNW direction of maximum horizontal stress throughout most of the Lassen region is similar to that of the northwestern margin of the Basin and Range province as shown by similar fault trends. NNW-trending normal faults characterize the northwestern margin of the Basin and Range province [*Nakata et al.*, 1982] in southeastern Oregon and northeastern California. An episode of extension that began about 8 Ma in the northwestern Basin and Range province took place along several zones of closely spaced, NNW-trending normal faults that cut across the previous NE structural trend [*Rytuba*, 1989]. One of these zones, the Honey Lakes zone, occurs adjacent to the Lassen region.

In addition, the NNW direction of maximum horizontal stress in the Lassen region is similar to that in the northern Sierra Nevada province. *Zoback and Zoback* [1980] inferred an extensional regime having least principal stress direction of N77°E (i.e., ENE) for the northern Sierra Nevada. The

Sierra Nevada province marks a tectonic transition from predominantly strike-slip movement along the San Andreas fault zone to extensional deformation of the Basin and Range province [*Zoback et al.*, 1987].

Weaver [1989] reported that crustal earthquake activity of each segment of the Cascade Range (as defined by *Guffanti and Weaver* [1988]) generally is characteristic of the crustal earthquake activity of the adjacent geological province to the east. In the Lassen segment, the spatial distribution and rate of crustal seismicity resembles that in the adjacent Basin and Range.

We propose that the onset of the episode of late Miocene ENE extension in the northwestern Basin and Range province triggered widespread mafic volcanism in the Lassen region. A more compressive lithospheric stress regime in the continental plate prior to the late Miocene extensional episode may have suppressed the surface expression of arc magmatism, even though subduction was occurring under the Lassen region. Consequently, the volcanic record prior to the late Miocene is sparse.

The large, long-lived volcanic centers in the Lassen region occur where the subducting plate is >80 km deep and also west of the area in which NNW trending normal faults indicate ENE extension. In contrast, within the area dominated by NNW trending normal faults only volcanoes that are small and not highly evolved occur. Thus pervasive ENE crustal extension that is characteristic of the northwestern margin of the Basin and Range province may preclude growth of the long-lived crustal magma systems required for large volcanic centers.

The influence of extension on late Miocene volcanism adjacent to the northwestern Basin and Range province also is evident in the central Oregon Cascades. Extension-related volcanism dominated by basalt and basaltic andesite also began about 7 Ma in the Three Sisters to Mount Jefferson area, near the intersection of the Cascade arc and the northern margin of the Basin and Range province [*Smith et al.*, 1987; *Hughes and Taylor*, 1986, *Taylor*, this issue]. There, as in the Lassen region, north to NNW trending faults and vent alignments indicate intra-arc extension, and LKOT and calcalkaline basalt younger than 7 Ma are intermingled. *Smith et al.* [1987] and *Hughes and Taylor* [1986] consider the mechanism of intra-arc extension in central Oregon to result from the plate margin process of slow, oblique subduction.

At about the same time that extension along the northwestern margin of the Basin and Range province may have triggered Lassen volcanism, the Sierra Nevada province south of Lassen also underwent extension-related changes. Using a gravity model for isostatic adjustment of the batholith, *Chase and Wallace* [1986] argue that between 5 and 10 Ma Basin-and-Range extension broke the lithosphere along the eastern side of the Sierra Nevada, which allowed sudden uplift of the batholith to occur.

The distributions of LKOT and calcalkaline basalt in the Lassen region overlap in space and time. Calc-alkaline basalt is dominant in both number of vents and total volume of volcanic material. Calc-alkaline basalt is similar to orogenic lavas from continental and mature island arcs [*Gill*, 1981] and thus appears to be closely related to subduction. LKOT is not an important eruptive component of the large volcanic centers of the Lassen region but contributes to the regional mafic volcanism and is found throughout the Basin and Range province since the middle Miocene. Accordingly, models of the mantle source and tectonic control of LKOT magmatism must be appropriate both within and behind the subduction-related arc.

Petrologic modeling by *Bullen and Clynne* [1989] indicates that LKOT and primitive calcalkaline basalt cannot be derived from a single primary magma type or by variable degrees of melting of chemically homogeneous mantle. Thus intermingled LKOT and calc-alkaline basalt magmatism in the Lassen region reflects small-scale geochemical heterogeneity in the composition of the underlying mantle wedge. Lithospheric extension in the North American plate may allow adiabatic decompressive melting of mantle to generate both primitive magmas, as well as provide access to the surface.

We conclude that the Lassen segment of the Cascades and adjacent margin of the Basin and Range province share a common stress regime, and we suggest that the tectonic origin of extension is similar in both provinces. Various models for the origin of extension have been proposed for the two provinces. Slow, oblique subduction acting on the central Oregon Cascade arc has been suggested by *Smith et al.* [1987] and *Hughes and Taylor* [1986]. Gravitational instability of thickened lithosphere [*Wernicke et al.*, 1987] and distributed shear due to North American–Pacific plate transform motion [*Atwater*, 1970] have been proposed for the Basin and Range province. Although we do not specify an extensional mechanism for the Lassen region, we do suggest that any model formulated for the southern Cascades also should be applicable to the adjoining margin of the Basin and Range province, and vice versa.

SUMMARY

A spectrum of widespread volcanic activity in the Lassen region is represented by 537 mostly mafic volcanic vents formed during the past 7 million years. ENE-WSW extension of the upper crust produced NNW trending vent alignments and normal faults throughout much of the Lassen region. Four long-lived, large, late Pliocene to Quaternary volcanic centers formed immediately west of the area cut by closely spaced NNW trending normal faults. The eastern limit of volcanic activity in the Lassen region had contracted westward by 2 Ma. Late Quaternary volcanism is concentrated around and north of the silicic Lassen volcanic center.

The Lassen volcanic region occurs above the subducting Gorda North plate but also lies on the western edge of a broad zone of distributed extension that exists within the North American lithosphere east and southeast of the present Cascadia subduction zone. Tectonism and magmatism of the Basin and Range province overlap the subduction-related arc in the Lassen region. The onset of an episode of late Miocene lithospheric extension in the northwestern Basin and Range province appears to have triggered onset of widespread volcanism in the Lassen region. Large crustal magma systems that produced long-lived differentiated volcanoes developed west of the zone of NNW normal faults which are characteristic of the ENE extension of the northwestern Basin and Range province.

Low-potassium olivine tholeiite is a geochemically distinctive basalt type of the Basin and Range province that also occurs in the Lassen segment of the Cascade arc. The mantle source and process of magma generation of this basalt type apparently are the same across the two environments.

Acknowledgments. We appreciate reviews by Cathy Hickson, Robert Jachens, James Rytuba, and Gary Smith. This work was supported by the Geothermal Research and Volcano Hazards programs of the U.S. Geological Survey.

REFERENCES

Atwater, T., Implications of plate tectonics for the Cenozoic tectonic evolution of western North America, *Geol. Soc. Am. Bull.*, *81*, 3513–3536, 1970.

Bacon, C. R., Implications of silicic vent patterns for the presence of large crustal magma chambers, *J. Geophys. Res.*, *90*, 11,243–11,252, 1985.

Bean, S. M., Volcanotectonics and geothermal potential in the Big Jack Lake area, Lassen County, California, M.S. thesis, 103 pp., Colo. Sch. of Mines, Golden, 1980.

Berge, P. A., and D. A. Stauber, Seismic refraction study of upper crustal structure in the Lassen Peak area, northern California, *J. Geophys. Res.*, *92*, 10,571–10,579, 1987.

Blakely, R. J., and R. C. Jachens, Volcanism, isostatic residual gravity, and regional tectonic setting of the Cascade volcanic province, *J. Geophys. Res.*, this issue.

Blakely, R. J., R. C. Jachens, R. W. Simpson, and R. W. Couch, Tectonic setting of the southern Cascade Range as interpreted from its magnetic and gravity fields, *Geol. Soc. Am. Bull.*, *96*, 43–48, 1985.

Bullen, T. D., and M. A. Clynne, Coupled spatial, chemical, and isotopic characteristics of primitive lavas from the Lassen region, California (abstract), *Bull. 131*, p. 33, N. M. Inst. of Min. and Technol., Socorro, 1989.

Bullen, T. D., and M. A. Clynne, Trace element and isotopic constraints on magmatic evolution at Lassen volcanic center, California, *J. Geophys. Res.*, this issue.

Chase, C. G., and T. C. Wallace, Uplift of the Sierra Nevada of California, *Geology*, *14*, 730–733, 1986.

Clynne, M. A., Stratigraphy and major-element geochemistry of the Lassen Volcanic Center, California, *U.S. Geol. Surv. Open File Rep.*, *84-224*, 168 pp., 1984.

Clynne, M. A., Quaternary volcanism in the southernmost Cascade Range, California, *U.S. Geol. Surv. Open File Rep.*, *85-521*, 24–30, 1985.

Clynne, M. A., Stratigraphic, lithological, and major element geochemical constraints on magmatic evolution at Lassen volcanic center, California, *J. Geophys. Res.*, this issue.

Cockerham, R. S., Evidence for a 180-km-long subducted slab beneath northern California, *Bull. Seismol. Soc. Am.*, *74*, 569–576, 1984.

Crandell, D. R., Glaciation near Lassen Peak, northern California, *U.S. Geol. Surv. Prof. Pap.*, *800-C*, C179–C188, 1972.

Crandell, D. R., D. R. Mullineaux, R. S. Sigafoos, and M. Ruben, Chaos Crags eruptions and rock-fall avalanches, Lassen Volcanic National Park, *J. Res. U.S. Geol. Surv.*, *2*, 49–59, 1974.

Dickinson, W. R., and W. S. Snyder, Geometry of subducted slabs related to San Andreas transform, *J. Geol.*, *87*, 609–627, 1979.

Gill, J. B., *Orogenic Andesites and Plate Tectonics*, 390 pp., Springer-Verlag, New York, 1981.

Grose, T. L. T., Volcanotectonic evidence for stress field changes since late Miocene in Basin and Range-Cascade boundary zone (Walker Lane) of northeastern California (abstract), *Eos Trans. AGU*, *66*, 1091, 1985.

Grose, T. L. T., and E. H. McKee, Late Cenozic westward volcanic progression east of Lassen Peak, northeastern California (abstract), *Eos Trans. AGU*, *63*, 1149, 1982.

Grose, T. L. T., and E. H. McKee, Potassium-argon ages of late Miocene to late Quaternary volcanic rocks in the Susanville-Eagle Lake area, Lassen County, California, *Isochron West*, *45*, 5–11, 1986.

Guffanti, M., and C. S. Weaver, Distribution of late Cenozoic volcanic vents in the Cascade Range: Volcanic arc segmentation and regional tectonic considerations, *J. Geophys. Res.*, *93*, 6513–6529, 1988.

Hart, W. K., J. L. Aronson, and S. A. Mertzman, Areal distribution and age of low-K, high-alumina olivine tholeiite magmatism in the northwestern Great Basin, *Geol. Soc. Am. Bull.*, *95*, 186–195, 1984.

Harwood, D. S., Evidence for late Cenozoic east-west compressive tectonism in the Sacramento Valley, in Tectonics and sedimentation along the California Margin, *Publ. 38*, edited by J. K. Crouch and S. B. Bachman, pp. 87–100, Pacific Section, Society of Economic Paleontologists and Mineralogists, Los Angeles, Calif., 1984.

Hazlett, D. P., A volcanotectonic and paleomagnetic investigation in the Hayden Hill area, M.S. thesis, 155 pp., Colo. Sch. of Mines, Golden, 1984.

Helley, E. J., D. S. Harwood, J. A. Barker, and E. A. Griffin, Geologic map of the Battle Creek fault zone and adjacent parts of the northern Sacramento Valley, California, scale 1:62,500, *U.S. Geol. Surv. Misc. Field Stud. Map*, *MF-1298*, 1981.

Hughes, S. S., and E. M. Taylor, Geochemistry, petrogenesis, and tectonic implications of central High Cascade mafic platform lavas, *Geol. Soc. Am. Bull.*, *97*, 1024–1036, 1986.

Jachens, R. C., and A. Griscom, Three-dimensional geometry of the Gorda plate beneath northern California, *J. Geophys. Res.*, *88*, 9375–9392, 1983.

Lerch, F. G., Geology of the Red Cinder 7.5-minute quadrangle, Lassen and Plumas counties, California, M.S. thesis, 274 pp., Colo. Sch. of Mines, Golden, 1987.

Lydon, P. A., Geology and lahars of the Tuscan Formation, northern California, *Mem. Geol. Soc. Am.*, *116*, 441–475, 1968.

Lydon, P. A., T. E. Gay, Jr., and C. W. Jennings, Geologic map of California, Westwood (Susanville) sheet, scale 1:250,000, Div. of Mines and Geol., San Francisco, Calif., 1960.

MacDonald, G. A., Geology of the Manzanita Lake quadrangle, scale 1:62,500, *U.S. Geol. Surv. Geol. Quad. Map*, *GQ-248*, 1963.

MacDonald, G. A., Geology of the Prospect Peak quadrangle, scale 1:62,500, *U.S. Geol. Surv. Geol. Quad. Map*, *GQ-345*, 1964.

MacDonald, G. A., Geologic map of the Harvey Mountain quadrangle, scale 1:62,500, *U.S. Geol. Surv. Geol. Quad. Map*, *GQ-443*, 1965.

MacDonald, G. A., and P. A. Lydon, Geologic map of the Whitmore quadrangle, scale 1:62,500, *U.S. Geol. Surv. Geol. Quad. Map*, *GQ-993*, 1972.

Magill, J. R., R. E. Wells, R. W. Simpson, and A. V. Cox, Post 12 m.y. rotation of southwest Washington, *J. Geophys. Res.*, *87*, 3761–3776, 1982.

McKee, E. H., W. A. Duffield, and R. J. Stern, Late Miocene and early Pliocene basaltic rocks and their implications for crustal structure, northeastern California and south-central Oregon, *Geol. Soc. Am. Bull.*, *94*, 292–304, 1983.

McLaughlin, R. J., Tectonic setting of pre-Tertiary rocks and its relation to geothermal resources in the Geysers-Clear Lake area, *U.S. Geol. Surv. Prof. Pap.*, *1141*, 3–23, 1981.

Mertzman, S. A., Jr., Strontium isotope geochemistry of a low potassium olivine tholeiite and two basalt-pyroxene andesite magma series from Medicine Lake Highland, California, *Contrib. Mineral. Petrol.*, *70*, 81–88, 1979.

Mooney, W. D., and C. S. Weaver, Regional crustal structure and tectonics of the Pacific coastal states: California, Oregon, and Washington, Geophysical Framework of the Continental United States, *Mem. Geol. Soc. Am.*, *172*, 129–162, 1989.

Muffler, L. J. P., and M. A. Clynne, Geologic map of the Lassen region, Cascade Range, USA (abstract), *Bull. 131*, p. 199, N. M. Inst. of Min. and Technol., Socorro, 1989.

Nakamura, K., Volcanoes as possible indicators of tectonic stress orientation, *J. Volcanol. Geotherm. Res.*, *2*, 1–16, 1977.

Nakata, J. K., C. M. Wentworth, and M. N. Machette, Quaternary fault map of the Basin and Range and Rio Grande Rift provinces, western United States, scale 1:2,500,000, *U.S. Geol. Surv. Open File Rep.*, *82-579*, 2 sheets, 1982.

Priest, G. R., N. M. Woller, G. L. Black, and S. H. Evans, Overview of the geology of the central Oregon Cascade Range, *Spec. Pap. State Oreg. Dep. Geol. Miner. Ind.*, *15*, 3–28, 1983.

Ruben, M., and C. Alaxander, U.S. Geological Survey radiocarbon dates V, *Am. J. Sci. Radiocarbon Suppl.*, *2*, 129–185, 1960.

Rytuba, J. J., Volcanism, extensional tectonics, and epithermal mineralizaton in the northern Basin and Range province, California, Nevada, Oregon, and Idaho (extended abstract), *U.S. Geol. Surv. Circ.*, *1035*, 59–61, 1989.

Sarna-Wojcicki, A. M., C. E. Meyer, H. R. Bowman, N. T. Hall, P. C. Russell, M. J. Woodward, and J. L. Slate, Correlation of the Rockland ash bed, a mid-Pleistocene stratigraphic marker in

northern and central California and western Nevada, *Quat. Res. J.*, *23*, 236–257, 1985.

Sherrod, D. R., and J. G. Smith, Preliminary geologic map of upper Eocene to Holocene volcanic and related rocks in the Cascade Range, Oregon, scale 1:500,000, *U.S. Geol. Surv. Open File Rep.*, *89-14*, 1 sheet, 1989.

Smith, G. A., L. W. Snee, and E. M. Taylor, Stratigraphic, sedimentologic, and petrologic record of late Miocene subsidence of the central Oregon High Cascades, *Geology*, *15*, 389–392, 1987.

Smith, J. G., Preliminary geologic map of upper Eocene to Holocene volcanic related rocks in the Cascade Range, Washington, scale 1:500,000, *U.S. Geol. Surv. Open File Rep.*, *89-311*, 61 pp., 1989.

Smith, R. L., and R. G. Luedke, Potentially active volcanic lineaments and loci in western conterminous United States, in *Explosive Volcanism: Inception, Evolution, Hazards*, pp. 47–66, National Academy Press, Washington, D. C., 1984.

Taylor, E. M., Volcanic history and tectonic development of the central High Cascade Range, Oregon, *J. Geophys. Res.*, this issue.

Trimble, D. A., M. A. Clynne, and S. W. Robinson, The application of uranium-thorium systematics to rocks from the Lassen dome field, California, *U.S. Geol. Surv. Open File Rep.*, *84-371*, 100 pp., 1984.

Tuppan, E. J., The volcanics and tectonics of the Slate Mountain area, Lassen County, California, M.S. thesis, 130 pp., Colo. Sch. of Mines, Golden, 1981.

Wadge, G., and A. Cross, Quantitative methods for detecting aligned points: An application to the volcanic vents of the Michoacan-Guanajuato volcanic field, Mexico, *Geology*, *16*, 815–818, 1988.

Walter, S. R., Intermediate-focus earthquakes associated with Gorda plate subduction in northern California, *Bull. Seismol. Soc. Am.*, *76*, 583–588, 1986.

Weaver, C. S., Seismicity of the Cascade Range and adjacent areas, *U.S. Geol. Surv. Open File Rep.*, *89-178*, 74–93, 1989.

Wernicke, B. P., R. L. Christiansen, P. C. England, and L. J. Sonder, Tectonomagmatic evolution of Cenozoic extension in the North American Cordillera, in Continental Extensional Tectonics, edited by M. P. Coward, J. F. Dewey, and P. L. Hancock, *Geol. Soc. Spec. Publ. London*, *28*, 203–221, 1987.

Wilson, D. S., A kinematic model for the Gorda deformation zone as a diffuse southern boundary of the Juan de Fuca plate, *J. Geophys. Res.*, *91*, 10,259–10,269, 1986.

Wilson, T. A., The geology near Mineral, California, M.S. thesis, 92 pp., Univ. of Calif., Berkeley, 1961.

Youngkin, M. T., Upper Cenozoic volcanotectonics of the Eagle Lake in the southeastern Cascade Range, Lassen County, California, M.S. thesis, 106 pp., Colo. Sch. of Mines, Golden, 1980.

Zoback, M. D., M. L. Zoback, V. S. Mount, J. Suppe, J. P. Eaton, J. H. Healy, D. Oppenheimer, P. Reasenberg, L. Jones, C. B. Raleigh, I. G. Wong, O. Scotti, and C. Wentworth, New evidence on the state of stress of the San Andreas fault system, *Science*, *238*, 1105–1111, 1987.

Zoback, M. L., and M. Zoback, State of stress in the conterminous United States, *J. Geophys. Res.*, *85*, 6113–6156, 1980.

T. D. Bullen, M. A. Clynne, L. J. P. Muffler, and J. G. Smith, U.S. Geological Survey, 345 Middlefield Road, MS 910, Menlo Park, CA 94025.

M. Guffanti, U.S. Geological Survey, 922 National Center, Reston, VA 22092.

(Received August 30, 1989;
revised January 19, 1990;
accepted November 18, 1989.)

APPENDIX 2 - 6

A. Displacement of late Pleistocene glacial moraines by the Almanor fault, Plumas County, California.

Kelson, K.I., Hitchcock, C.S., Zeeb, R.B., and Lettis, W.R.

Displacement of Late Pleistocene Glacial Moraines by the Almanor fault, Plumas County, CA

Keith I. Kelson, Christopher S. Hitchcock, Richard B. Zeeb, and William R. Lettis
William Lettis & Associates, Inc.
1777 Botelho Drive, Suite 262
Walnut Creek, CA 94596

William D. Page
Geosciences Department
Pacific Gas and Electric Company
Mail Code F22A
P.O. Box 770000
San Francisco, California 94177

ABSTRACT

North of Lake Almanor, the north-northwest-striking Almanor fault displaces glacial moraine crests associated with three distinct late Pleistocene glacial advances. Moraine crests from these advances were mapped in the Benner Creek drainage, where the fault traverses glaciated terrain. These deposits are informally designated the Last Chance Springs (possible pre-Tahoe correlative), Black Cinder Rock (probable Tahoe correlative), and East Benner Creek (probable Tioga correlative) deposits. Displacement by the fault is progressively greater for the older crests. Each of the crests displays evidence of left-lateral offset, as well as a comparable but generally lesser component of west-down displacement. The ratio of lateral to vertical components of slip is approximately 1 to 2 for each of the moraine crests. Assuming deposit ages based on regional glacial chronologies, the net slip on the Almanor fault ranges from about 1 to 3 mm/yr over the past approximately 200,000 years. The fault also displaces post-East Benner Creek fluvial terraces, suggesting that the most recent earthquake occurred during the latest Pleistocene or Holocene.

INTRODUCTION

The Almanor fault extends 38±5 km from the southern shore of Lake Almanor to a complex intersection with the Hat Creek fault near Butte Lake. The central part of the Almanor fault consists of two subparallel primary strands that strike north-northwest along the western margin of the Almanor Peninsula and the Mud Creek Rim, respectively (Figure 1; PG&E, 1994). Each of these two strands is associated with an escarpment in 2.2 to 2.4 million-year-old basalts (M. Clynne, personal communication, 1995). The cumulative height of these escarpments is more than 360 m (1,200 ft). At the northern end of these escarpments, glacial deposits derived from three distinct ice advances lie across the fault traces. These deposits include lateral moraines, terminal moraines, recessional moraines, glacial till, and glacial outwash. In this study, we conducted detailed mapping in selected areas to assess whether there has been surface faulting during the past 50,000 years. The locations and orientations of glacial moraine crests were used to evaluate the presence or absence of faulting, the amount of displacement from faulting, the sense of slip along the fault, and the fault slip rate.

Our geologic mapping consisted primarily of delineating surficial deposits in areas considered critical to assessing the late Pleistocene history of the Almanor fault. The focus

of this mapping was on glacial moraines in two areas informally named the Dead Tree Swale and Coring Meadow areas (Figure 1). This brief paper summarizes the results and conclusions from the Dead Tree Swale area, which will be visited during this field trip, that are relevant to assessment of the characteristics of the Almanor fault. Other papers within this volume summarize the geologic, tectonic, and seismologic setting of the Almanor area, and the reader is referred to these papers for more regional information.

REGIONAL GLACIAL STRATIGRAPHY

Glacial deposits within the Lassen Volcanic National Park area have been mapped by Crandell (1972), Kane (1975, 1982), Gerstel (1989), and P. Muffler and M. Clynne (unpublished data, 1995). In addition, Colman and Pierce (1981) analyzed weathering rinds on clasts sampled from glacial deposits mapped by previous workers. Reconnaissance-level mapping by Crandell (1972) shows the presence of three groups of deposits correlated to the glacial chronology of the Sierra Nevada region, including pre-Tahoe-, Tahoe-, and Tioga-equivalent deposits (Table 1). Crandell (1972) also divided the Tioga-age deposits into early, middle, and late Tioga deposits. Age differentiations were based on soil characteristics (i.e., depth of oxidation, presence of textural B horizons, soil color) and the thickness of weathering rinds on clasts. Kane (1975) identified a similar, five-fold grouping of glacial deposits, and provided evidence of a large ice cap during the pre-Tahoe and Tahoe glaciations that covered much of the Lassen Volcanic National Park area, including the area traversed by the northern part of the Almanor fault north of Lake Almanor. Colman and Pierce (1981) show that weathering rinds on clasts support the deposit subdivisions of Kane (1975), with rind thicknesses increasing on clasts from the Tioga-, early Tioga-, and Tahoe-equivalent deposits.

Gerstel (1989) mapped the Hat Creek and Lost Creek drainages in the western part of the Lassen Volcanic National Park area, and identified two major glacial advances on the basis of the relative topographic position and morphologic expression of glacial deposits, relative soil development, and thickness of weathering rinds on andesite clasts in till. The younger advance is informally designated the Lassen Peak episode, and is tentatively correlated to oxygen isotope stage 2 (Table 1). Gerstel (1989) identified four phases within the Lassen Peak episode, and shows that the youngest two phases are younger than about 8,800 years BP. The older advance is informally designated the Reading Peak episode, and is tentatively correlated to oxygen isotope stage 4 (Table 1; Gerstel and Clynne, 1989). Two phases are identified within this episode. Importantly, Gerstel (1989) shows that the glacial deposits of the Lassen Peak episode contain clasts of the Lassen Peak dacite, whereas the Reading Peak deposits do not. These relations suggest that the development of Lassen Peak itself occurred after the Reading Peak glacial advance but prior to or during the most-recent major glacial advance (Gerstel and Clynne, 1989).

P. Muffler, M. Clynne, and D. Champion of the U.S. Geological Survey are actively refining the volcanic and glacial mapping in the Lassen Volcanic National Park and Almanor region, and have identified glacial deposits in the area traversed by the Almanor fault. In general, these workers identify Tioga- and Tahoe-equivalent deposits in the Almanor region on the basis of morainal morphology and soil characteristics (P. Muffler, personal communication, 1995). Recent radiometric dating of the dacite of Lassen Peak yields an age-estimate of about 27 ka for the development of the dacite dome (M. Clynne and P. Muffler, personal communication, 1995). These workers also suggest that the development of the dacite dome was contemporaneous with the earlier phase of the Lassen Peak glacial advance (QL1, Table 1), which therefore provides a maximum-limiting age of about 27 ka for the Tioga-equivalent deposits in the Lassen Volcanic National Park and Almanor region. A minimum-limiting age of about 8.8 ka for the middle Tioga-equivalent

Table 1. Correlation of glacial stratigraphy in the Lassen Peak and Sierra Nevada regions.

	Age (ka)	Lassen Peak Region: This Report	Muffler and Clynne (unpubl.)	Gerstel (1989)	Kane (1975)	Crandell (1972)	Sierra Nevada Region: Bursik and Gillespie (1993)	Phillips et al. (1990)	Burke and Birkeland (1979)
		not mapped		QL4					
				1 ka					
				QL3					
				8.8 kyr BP					
		> 4 kyr BP							
Oxygen isotope stage 2	13	East Benner Creek	Tioga (Qgt2)	Lassen Peak 2 (QL2)	Tioga	Tioga	Tioga 22.2 ± 2.0 kyr BP to 25.2 ± 2.5 kyr BP	Tioga >20.4 to 23.1 kyr BP	late Tioga
				Lassen Peak 1 (QL1) 27 ka*					middle Tioga
	30			31 ± 2 kyr BP	Early Tioga				early Tioga
							Tenaya >30.7 ± 2.7 kyr BP	Tenaya >23.3 to 25.5 kyr BP	
Oxygen isotope stage 4	58	Black Cinder Rock	Tahoe (Qgt1)	Reading Peak 2 (QR2)	Tahoe	Tahoe	Tahoe <118 ± 7 kyr BP	Tahoe >55.9 to 65.8 kyr BP	
	73			Reading Peak 1 (QR1)					
Oxygen isotope stage 6	130	Last Chance Springs		not mapped	pre-Tahoe	pre-Tahoe	Mono Basin >131 ± 10 kyr BP	Mono Basin >92 to 119 kyr BP	Tahoe
	190								

* Ar/Ar date on Lassen Peak dacite, contemporaneous with QL1 glaciation (M. Clynne and P. Muffler, pers. comm., 1995)

displacement of about 65 m across the eastern trace (Figure 4), for a total of 71 ± 10 m of displacement across both primary fault traces.

Table 2. Estimated amounts of displacement of moraine crests across the Almanor fault

	Vertical	Lateral	Lateral/Vertical	Net
East Benner Creek (15 to 28 ka)	23 ± 5 m	34 ± 7 m	1.5 ± 0.4	41 ± 9 m
Black Cinder Rock (58 to 75 ka)	71 ± 10 m	> 45 ± 10 m#	> 0.6 ± 0.2@	> 84 ± 14 m@
Last Chance Springs (130 to 190 ka)	110 ± 10 m*	90 ± 90 m*	0.8 ± 0.8*	> 142 ± 90 m*

Data for western trace only, value is minimum for entire fault zone.
@ Lateral data from western trace only, value is minimum for entire fault zone.
* Data for eastern trace only, values are minima for entire fault zone.

Table 3. Estimated slip rates for the Almanor fault based on displacement of moraine crests.

	Vertical (mm/yr)	Lateral (mm/yr)	Net (mm/yr)
East Benner Creek (15 to 28 ka)	0.6 to 1.9	1.0 to 2.7	1.1 to 3.3
Black Cinder Rock (58 to 75 ka)	0.8 to 1.4	> 0.5 to 0.9#	> 0.9 to 1.7@
Last Chance Springs (130 to 190 ka)	>0.5 to 0.9*	>0 to 1.4*	> 0.5 to 1.8*

Data for western trace only, value is minimum for entire fault zone.
@ Lateral component from western trace only, value is minimum for entire fault zone.
* Data for eastern trace only, values are minima for entire fault zone.

Assessment of the amount of lateral offset exhibited by the Black Cinder Rock deposits is hindered by the discontinuity of the Black Cinder Rock moraine crest on the upthrown side of the eastern trace. However, we measured 45 ± 10 m of left-lateral offset of the Black Cinder Rock crest across the western trace, via an electronic topographic survey. We estimate a minimum net slip across the Almanor fault of about 84 m (Table 2). Considering a range in age estimates of 58 to 73 ka for the Black Cinder Rock deposits (Table 1), these data suggest a minimum net slip rate of 0.9 to 1.7 mm/yr (Table 3).

7

The East Benner Creek moraine crest is continuous and well-preserved across the eastern trace of the Almanor fault (Figure 2). As noted above, the width of the crest is less than 3 m and is very well-defined in the field and on topographic maps. There is approximately 23 m of net vertical tectonic displacement across the eastern trace of the fault (Figure 5, Table 2). We observed no evidence of displacement of the East Benner Creek deposits or moraine crest across the western trace of the fault.

The amount of lateral offset of the East Benner Creek moraine is estimated based on the topographic contours from the USGS Red Cinder quadrangle and a field hand-level survey (Figure 6). These data sets suggest a cumulative left-lateral deflection of the East Benner Creek moraine crest of 34 $\pm$ 7 m, and a net slip across the Almanor fault of about 41 m (Table 2). Considering the estimated vertical and lateral displacements of the East Benner Creek moraine crest, we calculate a ratio of lateral to vertical slip of about 1.5 (Table 2). Based on a range in age estimates of 15 to 28 ka for the East Benner Creek deposits (Table 1), these data suggest a net slip rate of 1.1 to 3.3 mm/yr (Table 3).

In summary, the surficial mapping of glacial deposits in the eastern branch of Benner Creek demonstrate recurrent tectonic displacement along the Almanor fault within the past approximately 200,000 years. Assessment of the displacement of moraine crests suggests a substantial left-lateral component of slip, with approximately equal amounts of left-lateral and vertical displacement. Estimated vertical slip rates range from >0.5 to 1.9 mm/yr, and estimated net slip rates range from >0.5 to 3.3 mm/yr. Within uncertainties, the relative ratios of lateral to vertical slip and the rates of slip are consistent for three time intervals during the late Quaternary (post-Last Chance Springs, post-Black Cinder Rock, and post-East Benner Creek deposits).

DEAD TREE SWALE INVESTIGATION AREA

In order to better document the presence of late Pleistocene activity along the Almanor fault, we conducted detailed mapping and topographic surveying at the Dead Tree Swale investigation area. This area is located at the northern end of the eastern escarpment of the Almanor fault, where the fault crosses Black Cinder Rock deposits and an East Benner Creek lateral moraine crest (Figure 2). On the basis of analysis of aerial photography and aerial reconnaissance of the Almanor fault, we identified several lineaments that extend from the base of the eastern escarpment of the Almanor fault across the sharp-crested East Benner Creek lateral moraine (Figure 2). Our tasks at the Dead Tree Swale investigation area consisted of geologic mapping at a scale of 1:6,000, electronic surveying of a scarp developed in Black Cinder Rock glacial deposits, a hand-level survey of the East Benner Creek moraine crest, and detailed electronic surveying of the part of the East Benner Creek moraine crest crossed by the prominent vegetation lineament. These tasks show that the Almanor fault has had multiple surface-rupture earthquakes within the past approximately 30 ka.

The Dead Tree Swale area contains evidence of multiple paleoearthquakes along the eastern trace of the Almanor fault since deposition of the Black Cinder Rock deposits. The Black Cinder Rock deposits are preserved within the swale where the fault traverses the site from northeast to southwest (Figure 2). Black Cinder Rock deposits, which are composed of subrounded basalt and andesite boulders and are associated with a moderately developed soil, make up the floor and eastern margin of the swale. There is a prominent north-northwest-trending topographic scarp across the swale along the fault trace (Figure 2). In the vicinity of the scarp, the deposit contains little or no matrix between individual boulders, and the clasts are angular and fractured. At the southern end of the swale, the base of the scarp is associated with a small trough within the coarse boulder deposit. This

CONCLUSIONS

Deposits related to three glacial advances are located across the central part of the Almanor fault and are displaced by the two major fault traces north of Lake Almanor. The ages of these deposits are estimated based on comparison to glacial chronologies developed in the Lassen and Sierra Nevada regions. Displaced moraine crests from each of these deposits provide the following data on the net slip, net slip rate, and ratios between the lateral and vertical components of slip:

	Net Slip (m)	Net Slip Rate (mm/yr)	Left-Lateral/Vertical Ratio
East Benner Creek (15 to 28 ka)	41 ± 9	1.1 to 3.3	1.5 ± 0.4
Black Cinder Rock (58 to 75 ka)	$> 84 \pm 14$@	> 0.9 to 1.7@	$> 0.6 \pm 0.2$@
Last Chance Springs (130 to 190 ka)	$> 142 \pm 90$*	> 0.5 to 1.8*	0.8 ± 0.8*

@ Lateral component from western trace only, value is minimum for entire fault zone.
* Data for eastern trace only, values are minima for entire fault zone.

Each of the moraine crest exhibits evidence of left-lateral and west-down displacement, with progressively older deposits showing greater amounts of displacement. In addition, several fluvial terraces post-dating the East Benner Creek glacial advance show evidence of fault displacement, suggesting latest Pleistocene and probably Holocene movement on the fault.

ACKNOWLEDGMENTS

We thank Pacific Gas and Electric Company for providing the opportunity to conduct this study. We gratefully acknowledge discussions of regional geology and glacial features with Mike Clynne and Patrick Muffler of the U.S. Geological Survey; Jay Noller, Jeff Unruh, Tom Sawyer, Keith Knudsen, and Patrick Drouin of William Lettis & Associates; Marek Zreda of the University of Arizona; and Wendy Gerstel of the Washington Department of Conservation. However, omissions and misinterpretations are the sole responsibility of the senior author.

REFERENCES

Colman, S. M., and Pierce, K. L., 1981, Weathering rinds on andesitic and basaltic stones as a Quaternary age indicator, western United States: U.S. Geological Survey Professional Paper 1210, 56 p.

Crandell, D. R., 1972, Glaciation near Lassen Peak, Northern California, U.S. Geological Survey Professional Paper 800-C, p. C179-C188.

Gerstel, W. J., 1989, Glacial chronology and the relationship to volcanic stratigraphy in the Hat and Lost Creek drainages, Lassen Volcanic National Park: Master's Thesis, University of Washington, 89 p.

Gerstel, W. J., and Clynne, M. A., 1989, Glacial stratigraphy in the Lassen Peak area of northern California - implications for the age of Lassen Peak dacite dome [abs]: Geological Society of America Abstracts with Programs, v. 21, no. 5, p. 83.

Kane, P. S., 1975, The glacial geomorphology of the Lassen Volcanic National Park area, California: Dissertation, University of California Berkeley, 224 p.

Kane, P. S., 1982, Pleistocene glaciation: Lassen Volcanic National Park: California Geology, May, p. 95-105.

Pacific Gas & Electric, 1994, Identification of potential seismic sources: Lake Almanor Dam: Draft Report, FERC Project 2105-CA, June, 48 p.

Shackelton, N. J., and Opdyke, N. D., 1976, Oxygen isotope and paleomagnetic stratigraphy of Equatorial Pacific core V28-239, Late Pliocene to Latest Pleistocene: *in* Cline, R.M., and Hays, J.D., eds., Investigation of Late Quaternary paleo-oceanography: Geological Society of America Memoir 145, p. 449-64

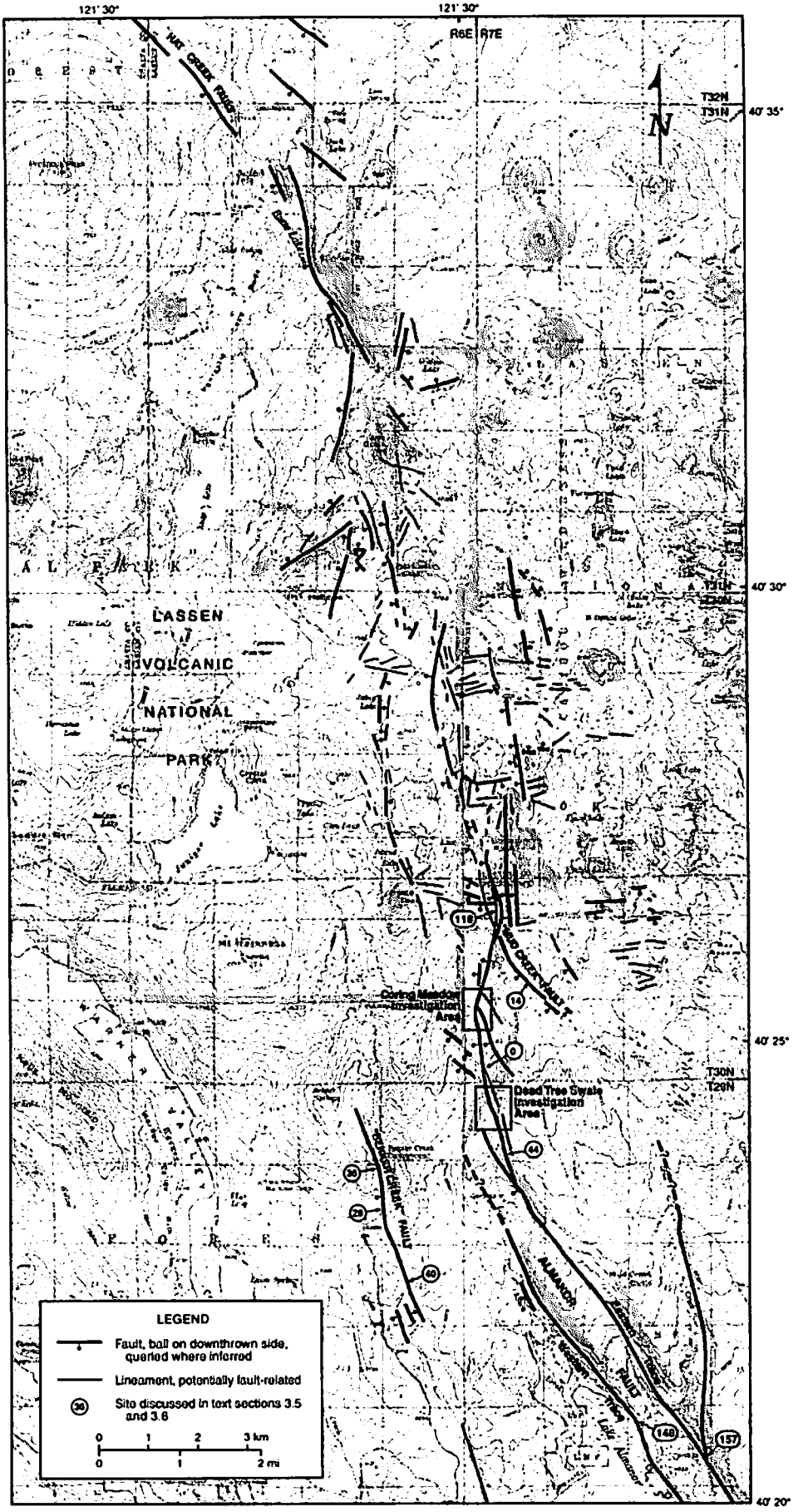

Figure 1. Map of strands of the Almanor fault and potentially fault-related lineaments between Lake Almanor and Butte Lake.

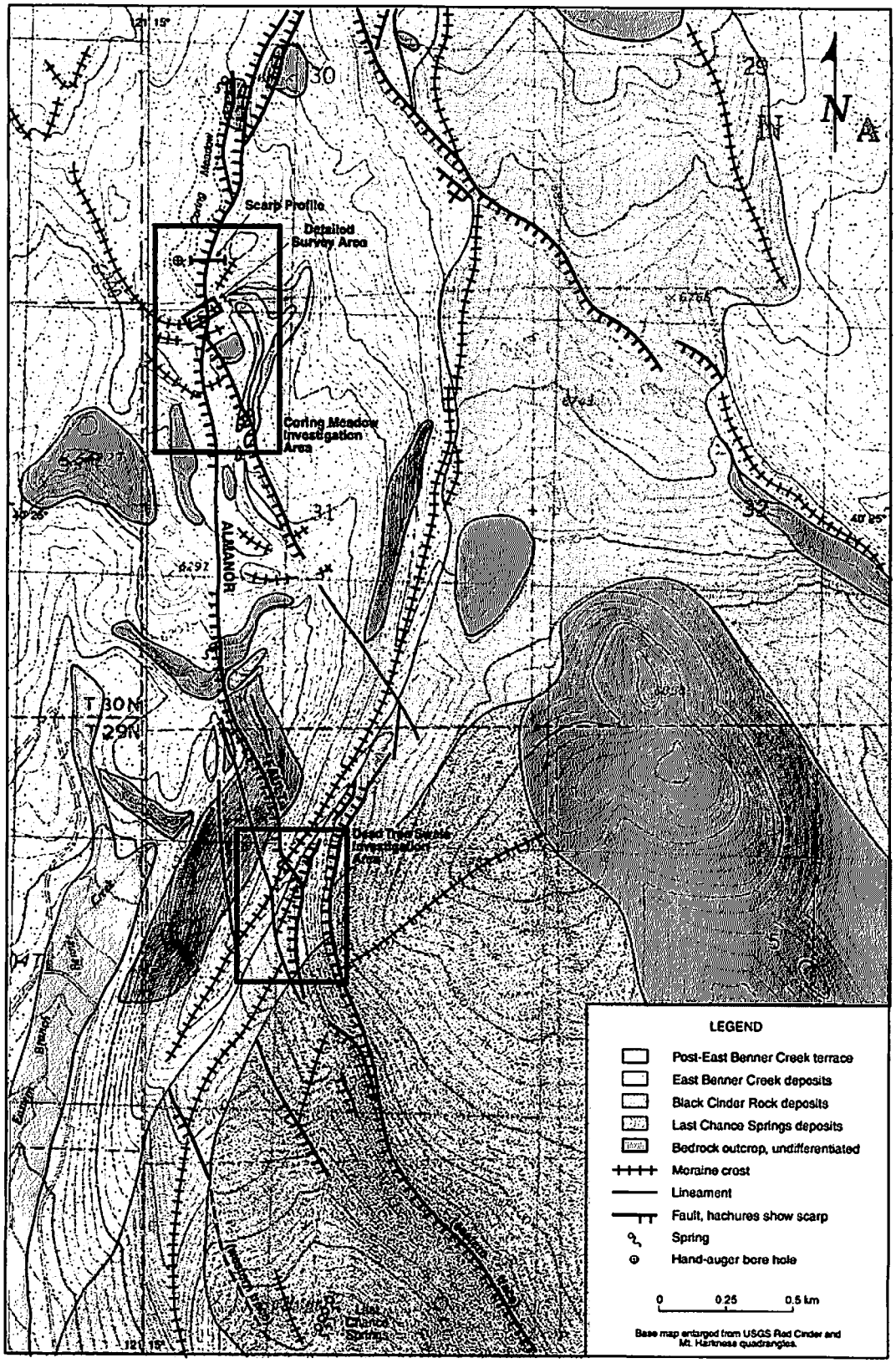

Figure 2. Map of glacial deposits, moriane crests and fault-related features along the Almanor fault between Lake Almanor and Lassen Volcanic National Park.

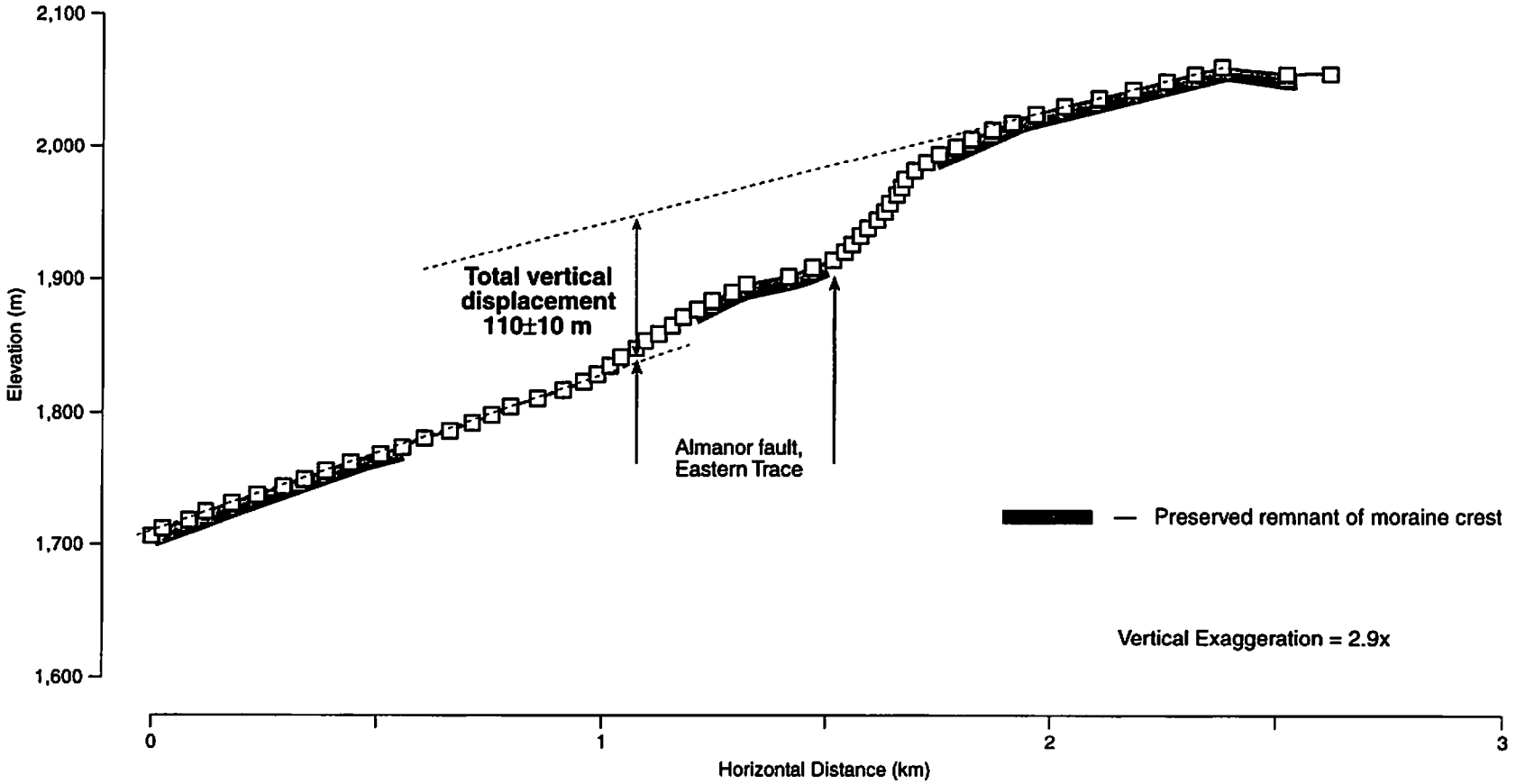

Figure 3. Topographic profile of the Last Chance Springs moraine crest, showing net vertical displacement across the Almanor fault.

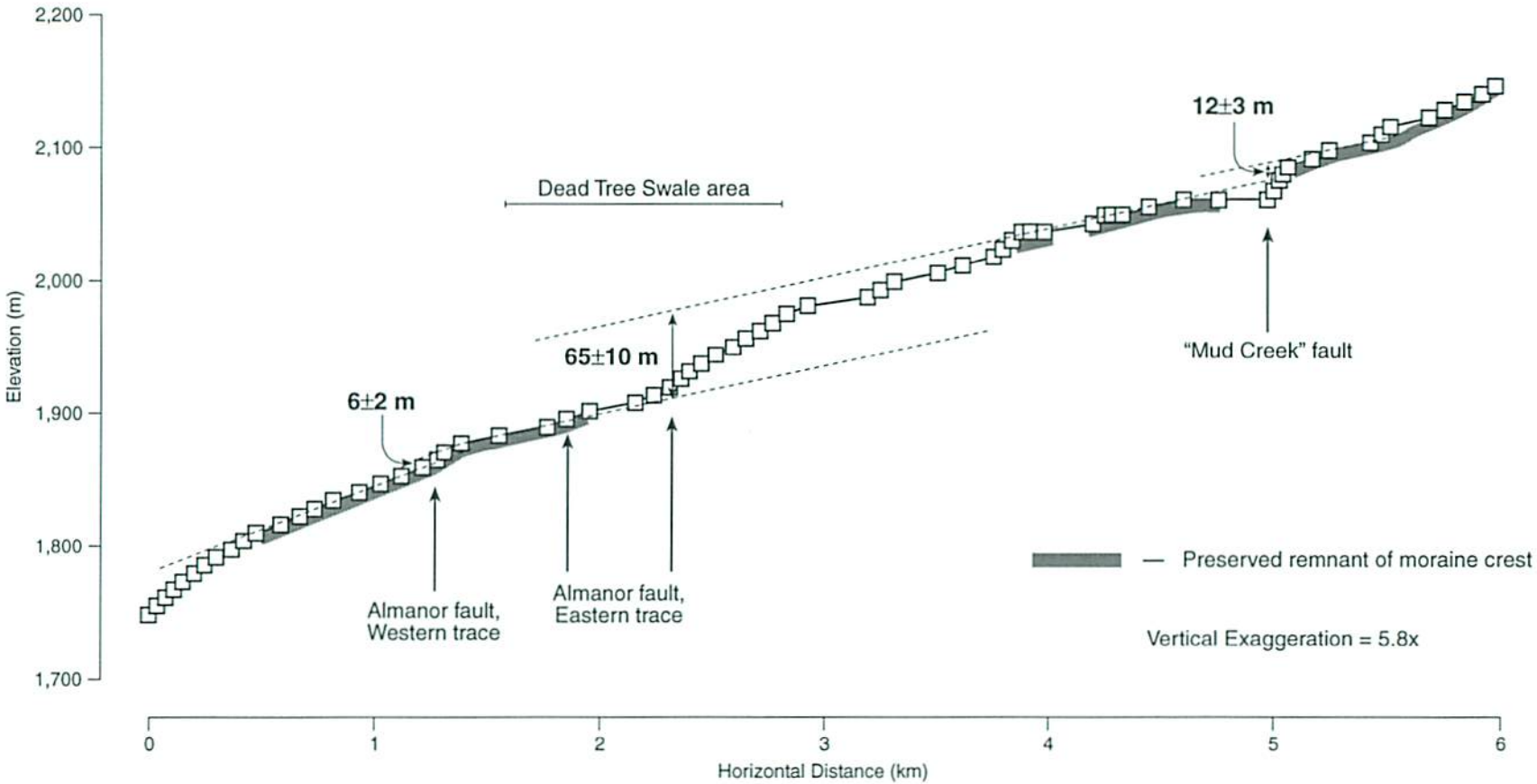

Figure 4. Topographic profile of the Black Cinder Rock moraine crest, showing net vertical displacement across the Almanor fault.

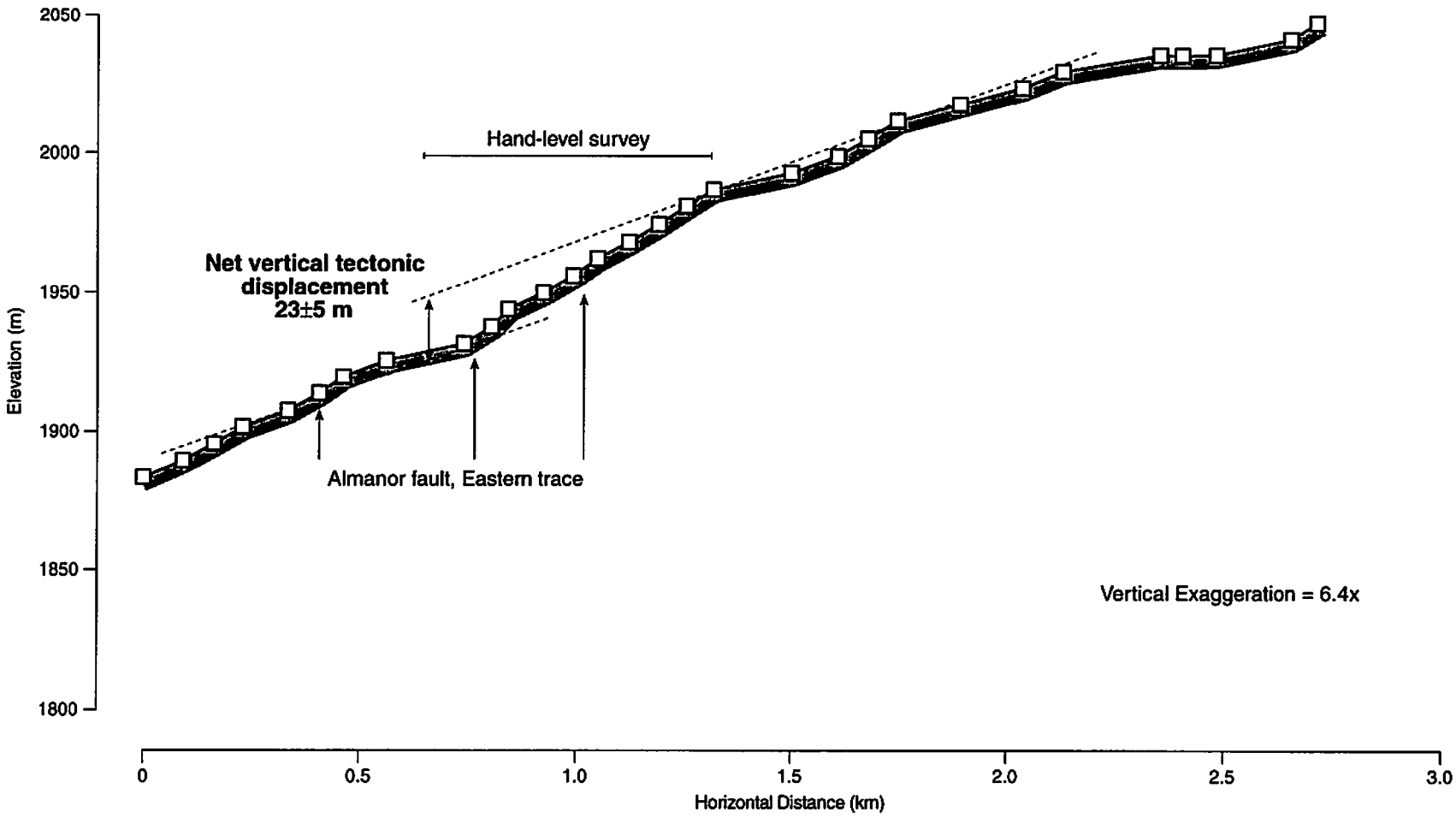

Figure 5. Topographic profile of the East Benner Creek moraine crest, showing net vertical displacement across the Almanor fault.

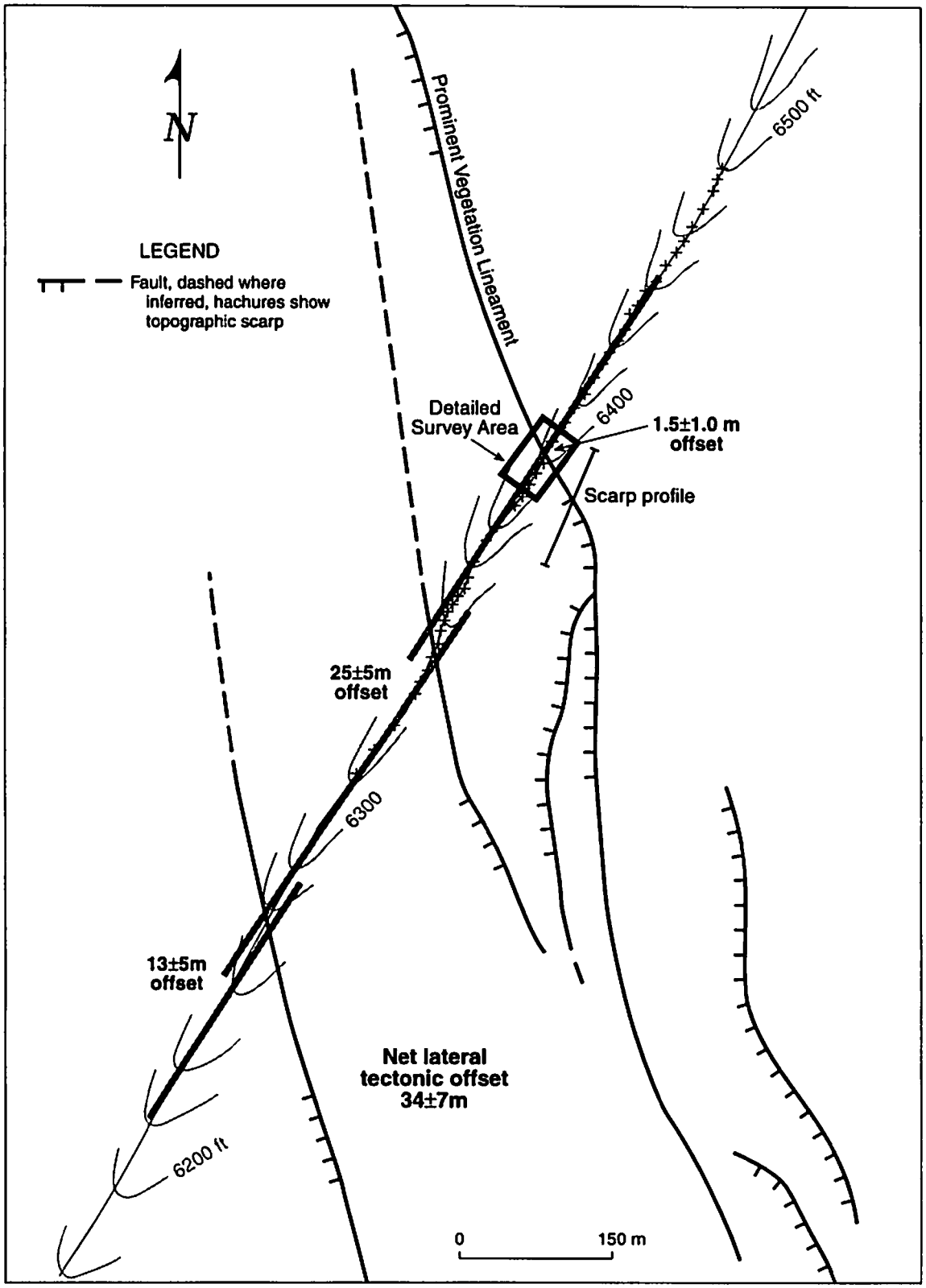

Figure 6. Map of the Dead Tree Swale site, showing the East Benner Creek moraine crest (thin solid line) based on contours from 1:24,000-scale, 20 ft. contour interval topographic map and field hand-level survey (small crosses).

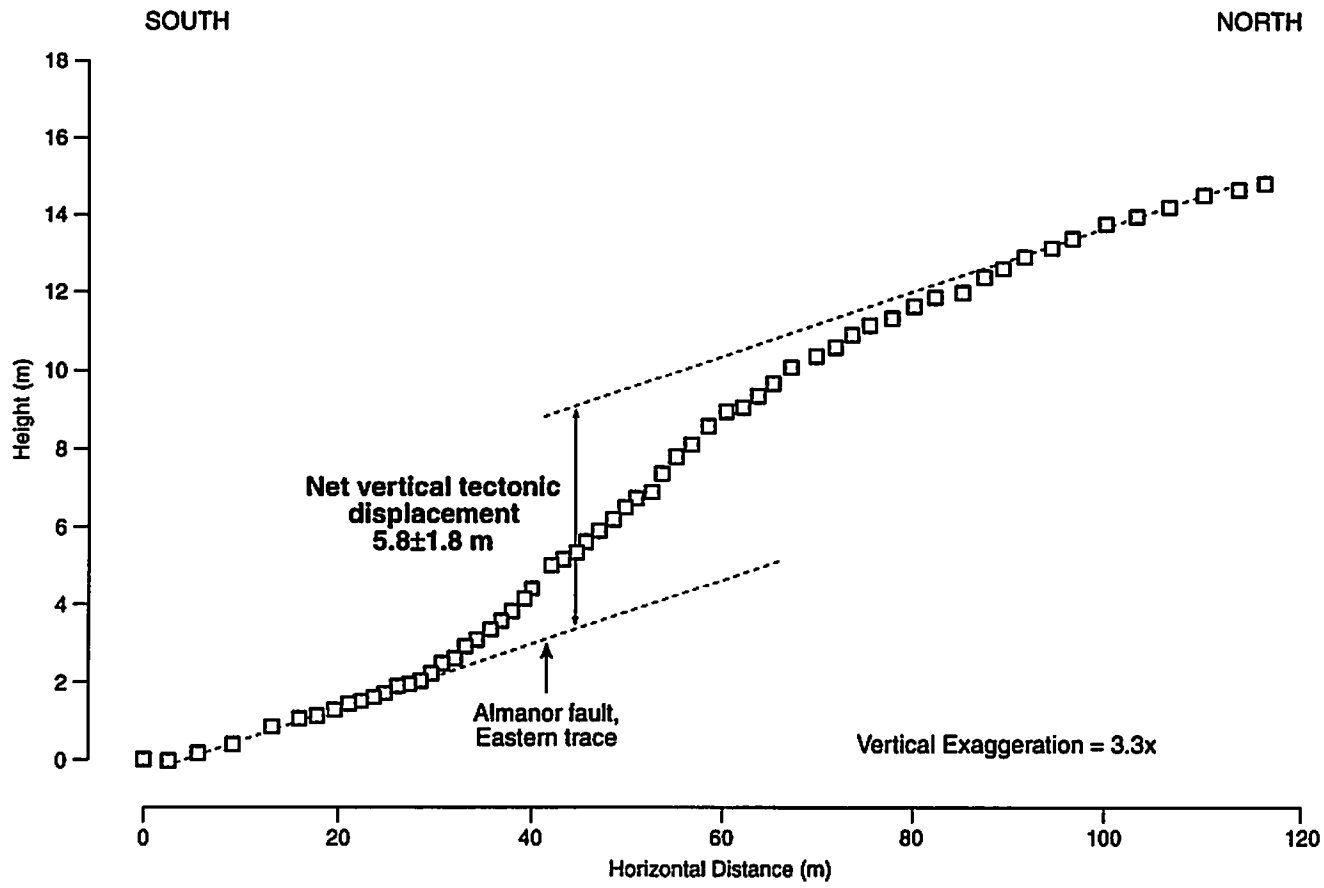

Figure 7. Topographic profile of scarp developed in Black Cinder Rock glacial deposits, Dead Tree Swale site.

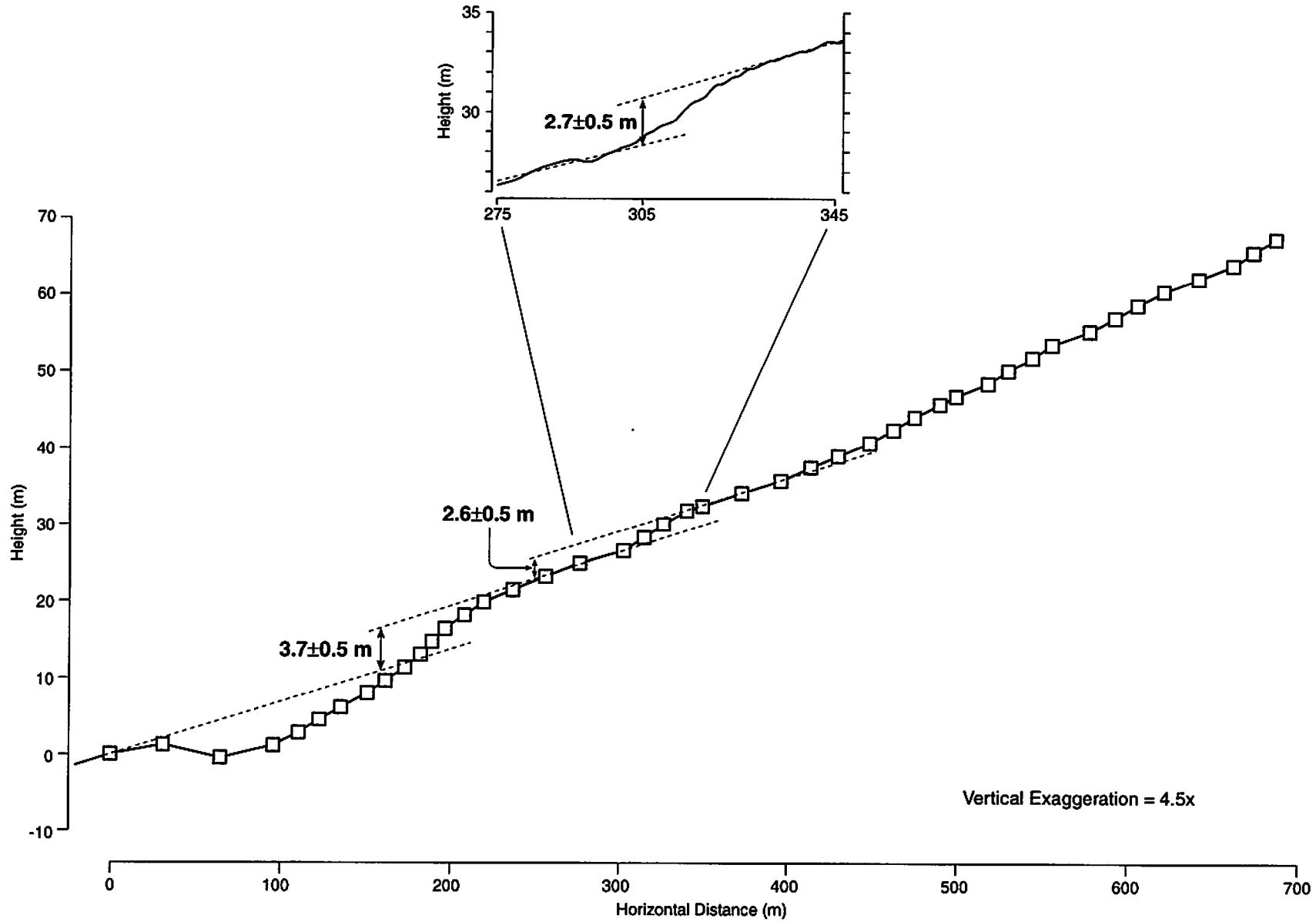

Figure 8. Topographic profiles of the East Benner Creek moraine crest at the Dead Tree Swale site, showing net vertical tectonic displacement. Upper profile derived from detailed electronic survey; lower profile from hand-level survey.

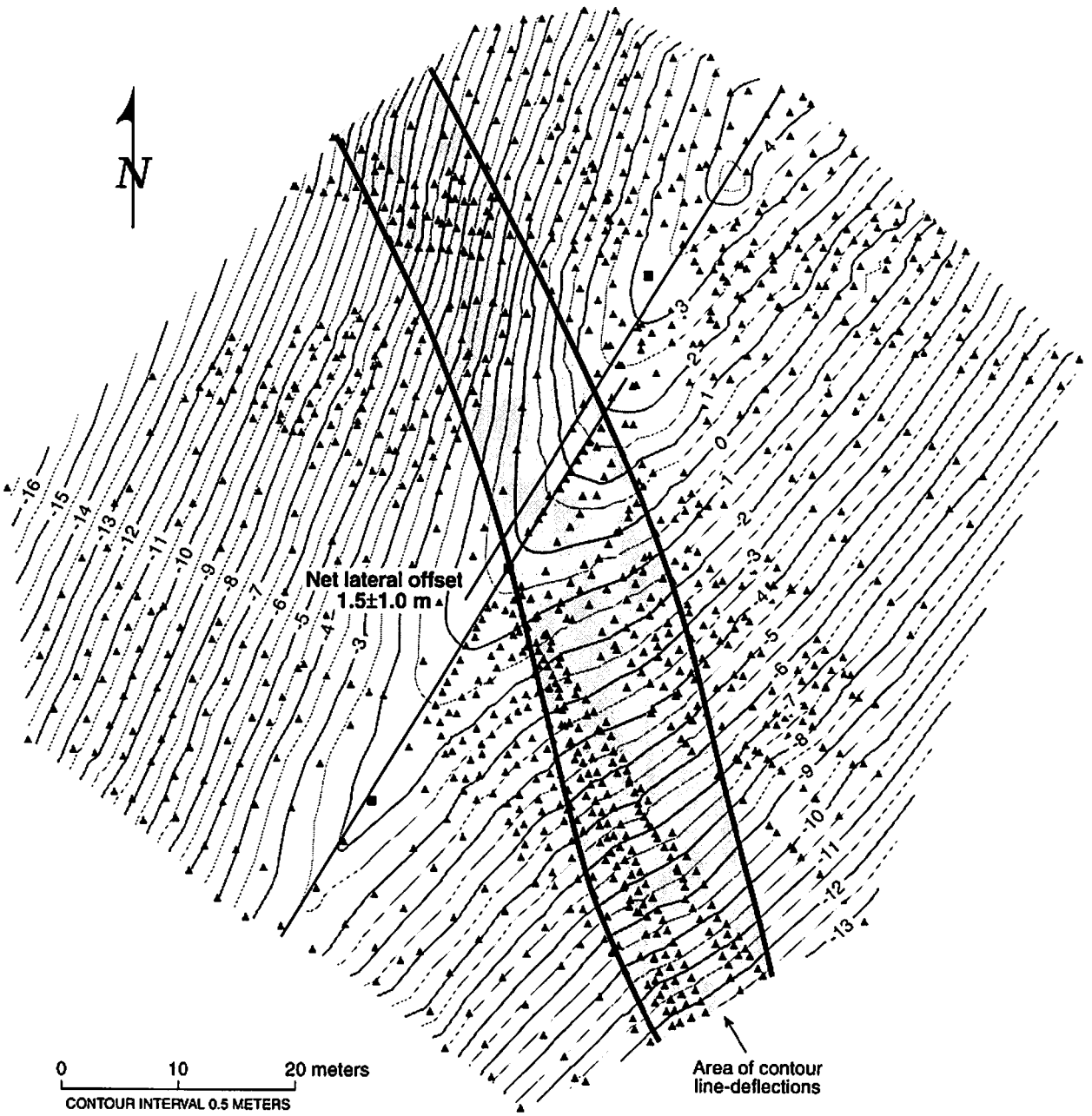

Figure 9. Topographic map of the East Benner Creek moraine crest at the Dead Tree Swale site. Area of contour-deflections coincides with prominent vegetation lineament.

APPENDIX 3 - 1 A

A. The Muleshoe Mine Fault at the Prattville Trench Site

Sawyer, T.L., Hitchcock, C.H., Crampton, T., Sowers, J.M., Caskey, and J.S., Sawyer, J.E.

Appendix 3 - 1 A

FRIENDS OF THE PLEISTOCENE
PACIFIC CELL 1995 FIELD TRIP

The Muleshoe Mine Fault at the Prattville Trench Site

Sawyer, Thomas L., Consultant, 10455 San Fernando Road, Reno, NV 89506
Hitchcock, Christopher S., William Lettis & Associates, Inc., 1777 Botelho Drive, Walnut Creek, CA 94596
Crampton Todd, Geomatrix, Inc., 100 Pine Street, San Francisco, CA 94111
Sowers, Janet M., William Lettis & Associates
Caskey, John S., Center for Neotectonic Studies, University of Nevada, Reno, 89557
Sawyer, Janet E., Consultant, 10455 San Fernando Road, Reno, NV 89506

INTRODUCTION

The Muleshoe Mine fault forms the eastern margin of the Butt Creek fault zone between the North Fork Feather River and Lake Almanor. At each end, the fault offsets Quaternary volcanic deposits of the 520 to 730 ka basalt of Warner Valley and the 1.1 Ma to 1.2 Ma basalt of Rock Creek. The vertical separation of the 2.8 to 2.9 Ma Yana (?) Formation is comparable to the separation of the Quaternary volcanic rocks, suggesting that movement began during the middle Pleistocene on the Muleshoe Mine fault (a reactivated bedrock structure). Thus, the Prattville study supports similar observations by Page and Wakabayashi (PG&E, 1994) along the fault at the North Fork of the Feather River.

In this study, we conducted detailed geologic and geomorphic mapping of the fault trace, excavated and examined structural and stratigraphic relationships in two parallel trenches and a number of test pits, and conducted magnetometer and paleomagnetic measurements to evaluate the seismic hazards associated with the Muleshoe Mine fault. Objectives of the study were to:

- Identify the location and style of faulting;
- Assess the recency of activity of any identified fault strand(s); and
- Identify the number and frequency of surface-faulting events.

Results of these studies show that the Muleshoe Mine fault is potentially active. The fault is prominently expressed as a geomorphic feature north of the range that forms the east wall of Butt Valley. In this area, the fault is delineated by a 15 m down-on-the-west separation of the Pliocene Yana (?) Formation (Figure 1), a prominent 9 m- to 14 m-high west-facing fault scarp on basalt of Rock Creek (verniered by colluvial and alluvial deposits) (e.g., Figure 4) and basalt of Warner Valley, and an elongate poorly drained alluvial valley along the base of the scarp. Trench exposures show that the fault offsets late Pleistocene deposits about 100,000 years old.

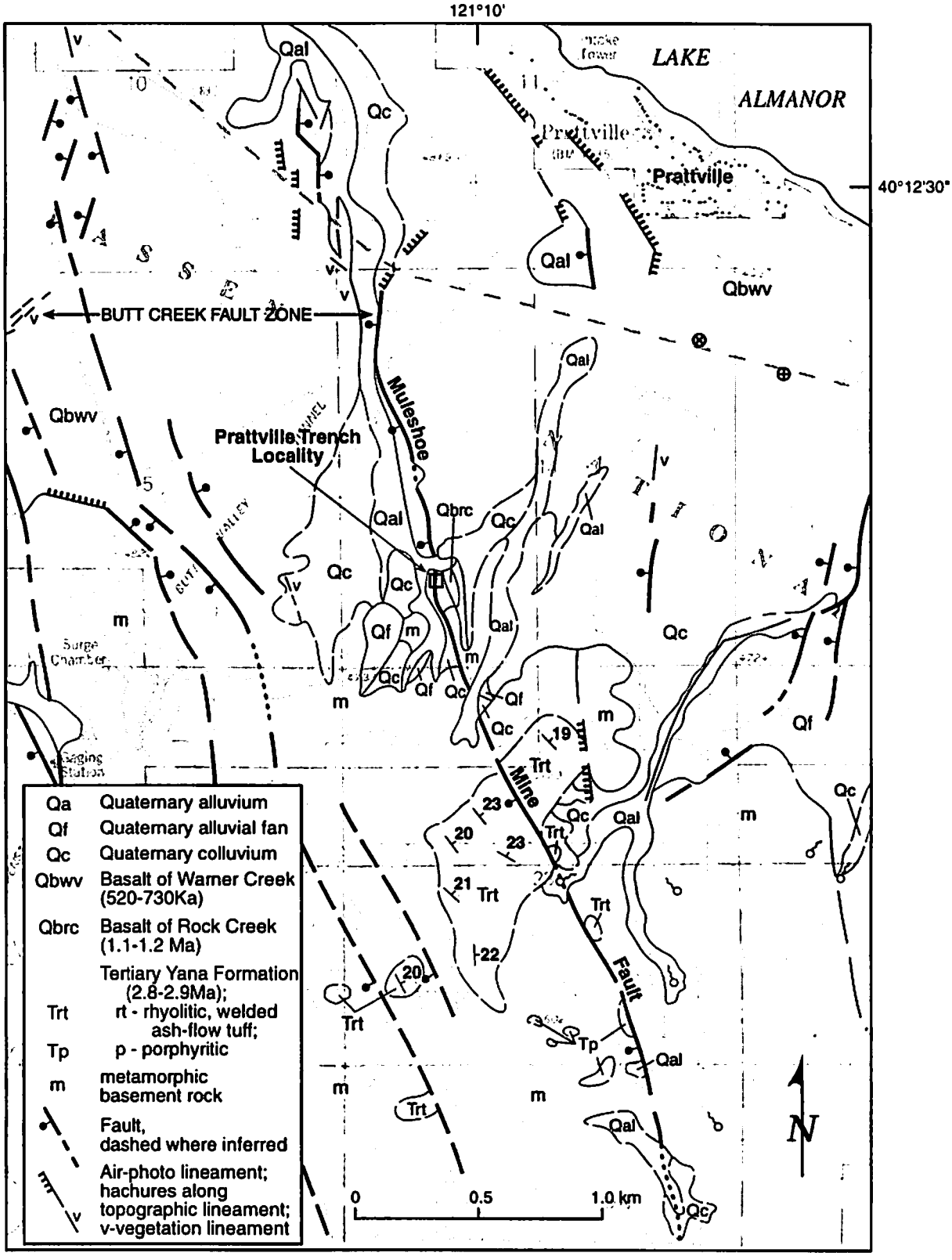

Figure 1. Geologic settting of the Prattville trench locality showing the Muleshoe Mine fault and other faults of the Butt Creek fault zone and showing Pliocene and Quaternary deposits.

ACKNOWLEDGMENTS

This ongoing study is being conducted by William Lettis & Associates Inc. (WLA) as part of Pacific Gas & Electric Company's (PG&E) "Seismic Source Characterization for the Stability Evaluation of Lake Almanor and Butt Valley Dams". Drs. William R. Lettis of William Lettis & Associates and William D. Page of PG&E's Geosciences Department managed and supervised the technical aspects of the study. Technical peer review was provided by Katherine L. Hanson of Geomatrix, Clarence R. Allen geologist retired from U.C. Davis, Alan R. Ramelli of the Nevada Bureau of Mines and Geology, and William Fraser and Jeff Howard of the Division of Dam Safety. We have appreciated their comments and suggestions during the project as it progressed.

RATIONALE FOR TRENCH LOCATION

Two trenches were excavated across a prominent escarpment along the northern Muleshoe Mine fault (SW1/4 Sec. 14, T27N, R7E), 2 km south-southwest of the community of Prattville (Figure 1). The trench site (Figures 2, 3) was selected based on the presence of an escarpment of presumed tectonic origin on middle to late Pleistocene colluvial deposits and on the presence of an alluvial basin along the base of the escarpment that would likely contain stratified late Pleistocene deposits. The main trench (PRT-1) was located based on the following considerations:

- To cross the linear escarpment along the northern Muleshoe Mine fault;
- To cross the surficial colluvial/alluvial contact along the eastern margin of the alluvial basin; and
- To identify a site with a thick sequence of late Quaternary deposits overlying the fault trace from which to assess recency of fault activity.

In order to independently assess the recency of faulting, a second trench (PRT-2) was excavated on the escarpment 10 m south of trench PRT-1.

We considered trenching the southern Muleshoe Mine fault where it crosses metamorphic bedrock in Ohio or Clear Creek valleys. However, because erosion rates in the basement terrain are significantly higher than faulting rates, geomorphic features indicative of youthful faulting are absent. For example, the North Fork of the Feather River has been downcutting at an average rate of 0.21 to 0.43 mm/yr during the past approximately 1,000,000 years, whereas the average slip rate of the Muleshoe Mine fault is only 0.04 to 0.05 mm/yr (PG&E, 1994). Thus, erosion rates are 5- to 8-times higher than faulting rates.

SITE DESCRIPTION AND APPROACH

The Prattville trench site is located on a well-defined west-facing escarpment along the eastern margin of a wet grassy meadow (Figure 2). The site is directly south of a small drainage that is incised obliquely into the escarpment. The escarpment reflects cumulative offset of the 1.1 Ma basalt of Rock Creek. At the site, the basalt escarpment is veneered by colluvial and alluvial deposits derived from a metasedimentary bedrock ridge to the south. North of the drainage the escarpment exposes basalt and is moderately-well defined. A short somewhat subdued east-facing escarpment coincides with the western margin of the meadow, directly opposite of the trench site (Figures 2, 3). This escarpment is likely the trace of an antithetic down-to-the-east fault. This interpretation is supported by a magnetometer survey traversing the Prattville site that shows a significant anomaly

Figure 2. Oblique aerial photograph of the Prattville trench site.

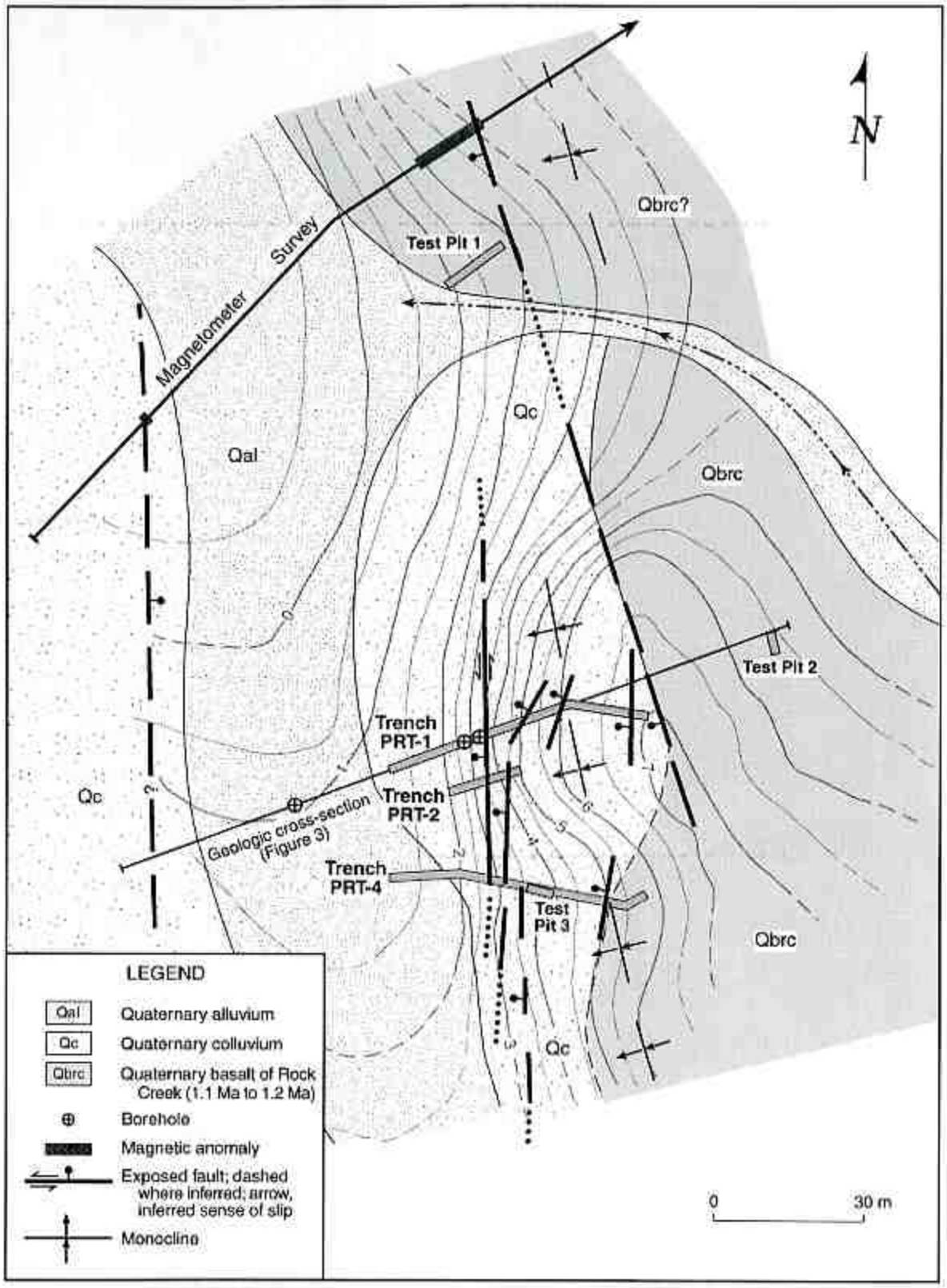

Figure 3. Geologic map of the Prattville trench site showing faults exposed in Prattville trenches and inferred fault traces through the site.

coinciding with both the west- and east-facing escarpments. Hence, in the trench site area the Muleshoe Mine fault forms a graben, occupied by a poorly drained alluvial valley. To the north the east-facing escarpment dies out and the fault appears to form an east-tilted half-graben.

To assess the activity of the Muleshoe Mine fault, we excavated and examined stratigraphic and structural relations in two adjacent trenches (PRT-1, PRT-2), five test pits, and three hand-auger holes on and near the west-facing scarp at the Prattville site. These studies were supported by paleomagnetic measurement on basalt exposed in trench PRT-1 (written communication, D. Champion, 1995), a magnetometer survey transversing the site, and soil-stratigraphic studies conducted in trench PRT-1. We anticipate that we will be able to place numerical-age constrains on the trench stratigraphy by radiocarbon dating of charcoal collected from alluvial and colluvial stratigraphy, luminescence (OSL) dating of bulk colluvial-wedge samples, Ar-Ar dating of minerals separated from a faulted tephra layer, and paleomagnetic measurements on oriented-cubes of the trench stratigraphy (attempting to constrain the stratigraphic position of paleomagnetically reversed strata).

Trench PRT-1 was located across the a well-defined 9.3-m-high escarpment (Figure 4). Four of the test pits were subsequently excavated in an attempt to identify young (late Pleistocene and Holocene) deposits overlying the fault from which to assess the timing of the most recent surface-faulting event. The fifth test pit (TP-2) was excavated 25 m east of the east end of trench PRT-1 to identify the elevation of the surface on the basalt of Rock Creek relative to that exposed in trench PRT-1. The basalt surface is 2.3 m higher in test pit TP-2 than in the east end of trench PRT-1 (Figure 4), suggesting the presence of down-to-the-west faulting (or folding) located between these two excavations; although there is no geomorphic evidence to support the presence of the inferred fault. Trench PRT-2 was excavated on the west-facing escarpment approximately 10 m south of the trench PRT-1 to provide a second exposure of the fault from which to independently assess the timing of the most-recent-faulting event. Two of the three hand-auger holes were bored into the floor of trench PRT-1 to assess the amount of vertical separation of the flow surface on the basalt of Rock Creek; the third auger-hole was bored into the lowest part of the poorly drained alluvial valley, along the projection of trench PRT-1 (Figure 4). This auger hole was bored to a total depth of 1.9 m and encountered fine-grained, reduced "meadow-like" deposits overlying coarse, oxidizided colluvium at a depth of about 50 cm. The borehole shows that a thick sedimentary basin is absent at the site, showing instead that the present drainage base-level is as low at the present as at any time in the past and that regional colluvial/alluvial apron has been down-dropped within the graben.

Trench PRT-1 extended for 53 m and exposed the basalt of Rock Creek overlain by four colluvial and two alluvial deposits in the eastern two-thirds of the trench (Figure 5). The western third of the trench exposed a minimum of six colluvial deposits, the upper three are noticeably more gravely than the other trench deposits, but did not expose the basalt which was at least 2 meters below the reach of the excavation equipment based on an auger borehole in the base of the trench. Due to excavation limitations imposed by shallow ground water conditions in July of 1995, the trench also did not cross the alluvial/colluvial contact at the eastern margin of the meadow. Trench PRT-2 extended for 14 m and exposed the same sequence of colluvial and alluvial deposits.

RESULTS

Results of detailed field mapping in the Prattville trench site area (Figure 1) indicate that the Muleshoe Mine fault is probably a reactivated Mesozoic bedrock structure, the Clear Creek fault of Jayko (1988). Reactivation of the fault has occurred relatively recently, within the last 500,000 years. This is based on the similar amounts of vertical separation of the

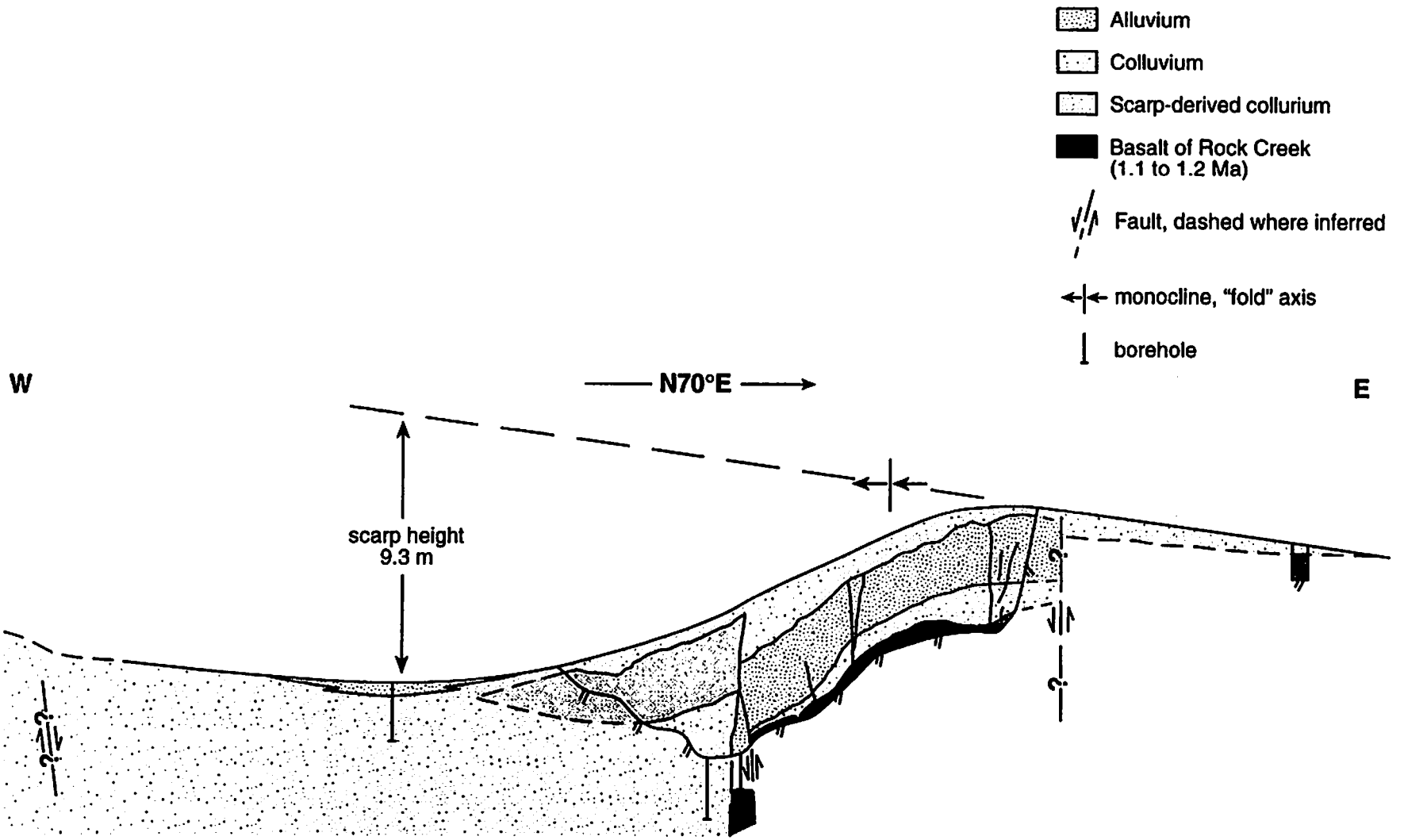

Figure 4. Geologic cross-section of the Prattville trench locality schematically displaying faults and Quaternary stratigraphy exposed in Prattville excavations.

Yana (?) Formation (2.8-2.9 Ma) (Figure 1), basalt of Rock Creek (1.1-1.2 Ma) (Figure 4), and basalt of Warner Valley (550 ka). The middle-Quaternary timing of fault reactivation is consistent with the post-basalt-of-Warner-Valley onset of movement on the Muleshoe Mine fault determined by PG&E (1994) at the North Fork of the Feather River.

Results of the trench investigation at the Prattville site provide evidence of recurrent middle to late Quaternary faulting. The evidence includes several scarp-derived colluvial and fissure-fill deposits and the upward truncations and terminations of faults, fractures, fissures and shear fabric at different stratigraphic levels. Collectively, these data support a minimum of eleven to thirteen surface-faulting events along the northern Muleshoe Mine fault in the past 500,000 years. Thus, the long-term average recurrence interval is 40,000 to 45,000 years or less. Evidence of faulting extends to the base of the modern bioturbation zone, to within 50 cm of the present ground surface. The time of the most-recent-faulting event is not known. However, a colluvial deposit believed to be 100 $\pm$ 50 ka, based on the degree of soil development, is a product of the penultimate event and was faulted during the last event. Hence, it is our judgment that the most-recent faulting has occurred since 100,000 years ago and probably occurred within the past 50,000 years, based on the upward termination of the fault into the modern bioturbation zone.

Bedrock

Basalt of Rock Creek. The flow surface on the basalt of Rock Creek was exposed near the base of the eastern two-thirds of trench PRT-1 and in test pits TP-1, TP-2, and TP-5. Ar-Ar incremental heating analysis shows that the basalt is 1.1 to 1.2 million years old (PG&E, 1994). Paleomagnetic analyses on core samples collected from trench PRT-1 shows that the basalt is magnetically reversed, consistent with the basalt of Rock Creek (D. Champion, personal communication, 1995).

Quaternary Stratigraphy

Eleven colluvial units and two alluvial units, one containing an air-fall ash, were interpreted from the exposures at the Prattville trench locality (Figures 5, 6, 7). Two distinctly different stratigraphic sections are juxtaposed by the main fault zone in trench PRT-1 (fault zone FZ-4) (Figure 5); the same relationship occurs across the continuation of this fault in trench PRT-2 (fault zone FZ-6) (Figure 7). Differentiation and correlation of trench units and sub-units is based primarily on differences in gravel content and lithology, degree of weathering of gravel clasts (relative competence), and soil properties (e.g., color, clay films, consistence, structure). Stratigraphic contacts within and along the base of the alluvial units are generally clear and locally sharp. Basal contacts of colluvial units are uniformly diffuse and, in the near surface, are irregular because of bioturbation. Most of the contacts between units identified in the trench exposures are unconformities. With the exception of the lowermost colluvial unit in the eastern two-thirds of trench PRT-1 (unit C-7), all of the deposits are primarily derived from metasedimentary (schist) bedrock with minor amounts of basalt. Unit C-7 is primarily derived from the basalt of Rock Creek and contains minor schist clasts. Several of the units contain incipient, relict and buried soils, related to periods of landscape stability and soil formation. However, there is little variation in the degree of weathering from the surface to the bottom of the trench. This similarity suggests that the periods of landscape stability and soil formation, intermittent with alluvial and colluvial deposition, were brief relative to the major episode of weathering and soil formation that has subsequently engulfed the entire stratigraphic sequence at the trench site.

The Quaternary soil-stratigraphy of the Prattville trench locality is described below from the stratigraphically youngest unit to the oldest unit.

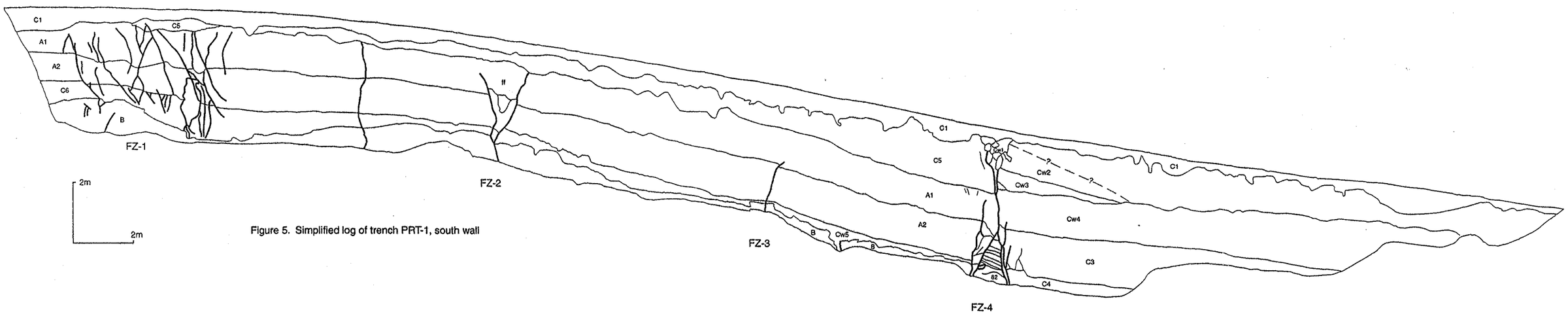

Figure 5. Simplified log of trench PRT-1, south wall

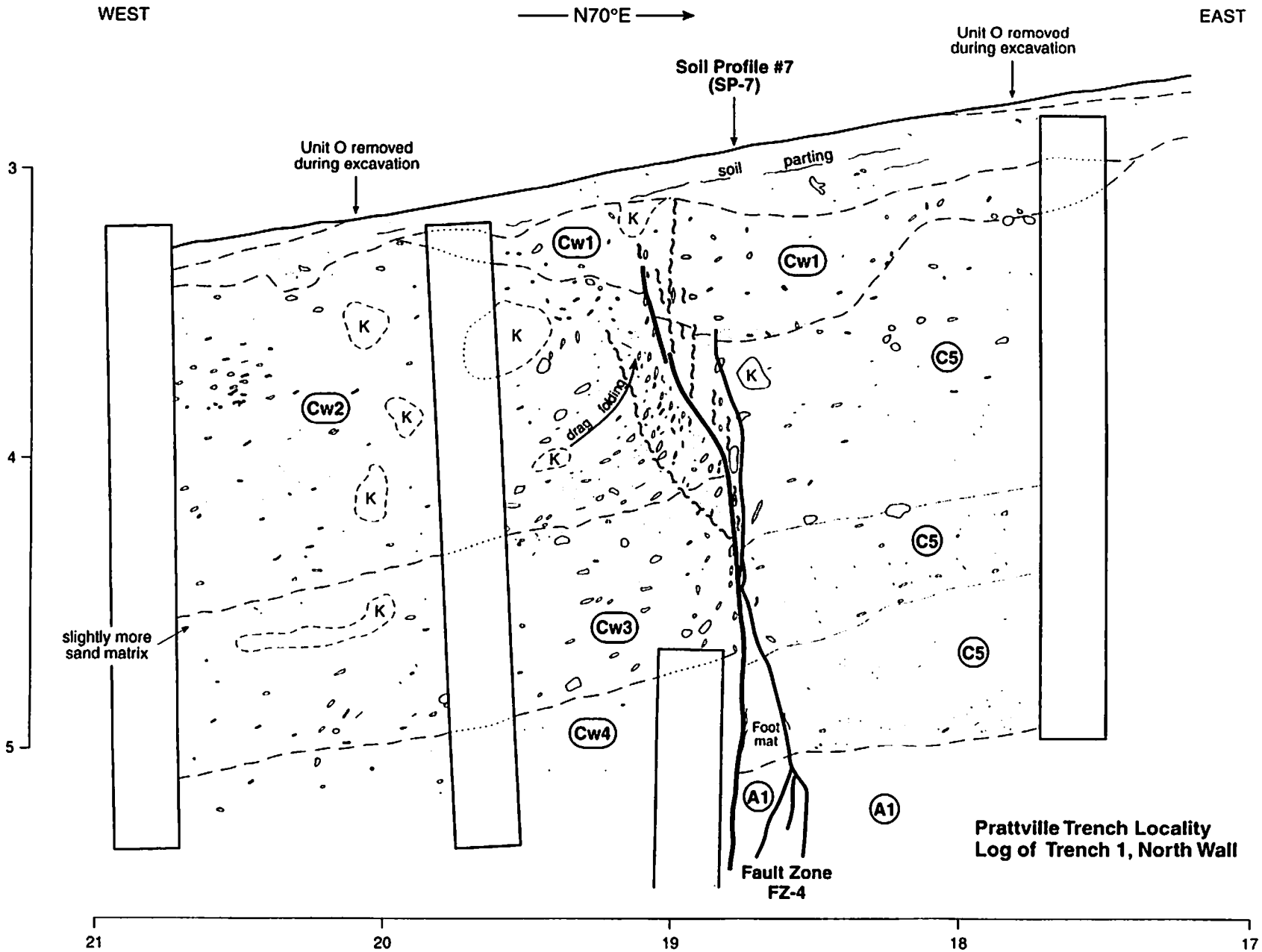

Figure 6 Log of the north wall of Pratville trench PRT-1 showing upper part of fault zone FZ-4. Note fault and subtle shear fabric within colluvial-wedge CW-1 and vertical separation of the base of this unit. See text for map explanation.

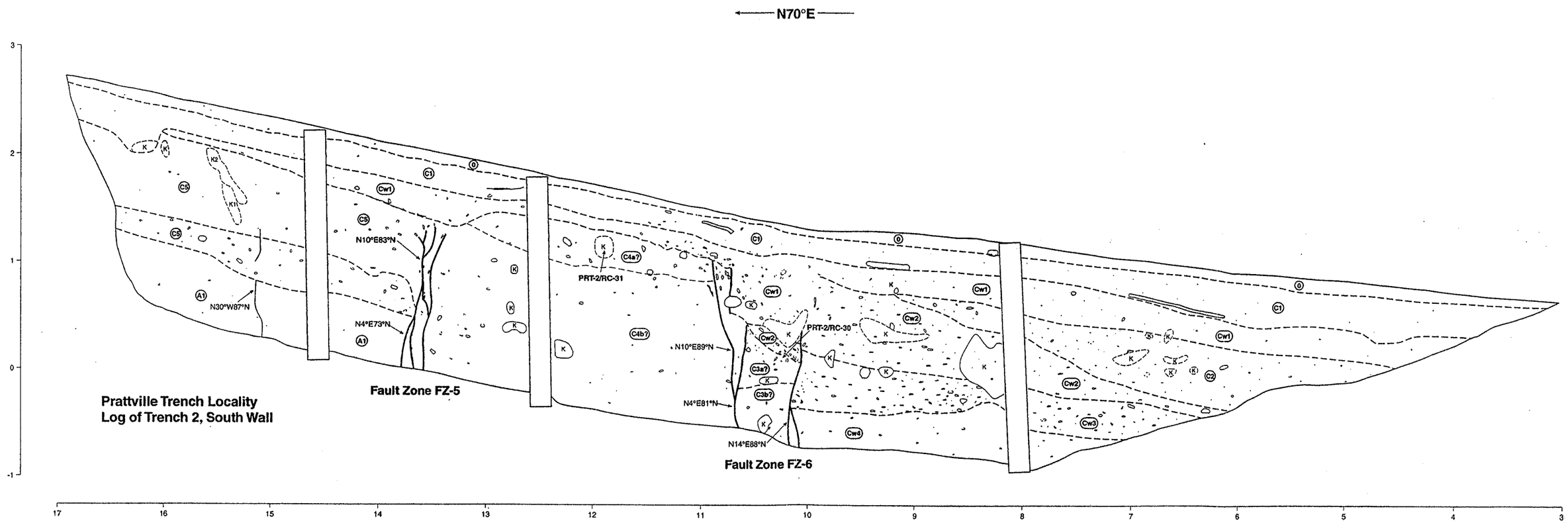

Figure 7 Log of south wall of trench PRT-2. See text for map explanation.

Colluvium C-1. Colluvium C-1 is a 30- to 75-cm-thick brown to dark brown sandy loam exhibiting relatively weak soil properties. This is the only unit to span the full length of both trench PRT-1 and trench PRT-2. The unit represents the upper part of the surficial soil and the zone of active bioturbation; locally at least unit C-1 is a separate stratigraphic deposit. Unit C-1 can be differentiated into two sub-units based on soil structure and humus content. Upper sub-unit O, which was locally removed during excavation, is characterized by many fine to medium roots and abundant humus. Sub-unit C-1 is characterized by moderately distinct granular and platy structure and little humus. Both sub-units contain tabular schist clasts and rounded reddish concretions.

Colluvium Cw-1. Colluvium Cw-1 is a light yellowish brown, silty clay loam exhibiting moderately distinct to distinct subangular blocky structure. Developed within the unit is a sticky, plastic Bt horizon that contains manganese patches on ped faces and clasts. The exteriors of peds are a lighter color than are the interiors, resulting from leaching of clay and/or iron oxides. These soil properties indicate polygenic soil formation, probably resulting from lowering of the modern soil profile due to surficial erosion. The unit, which is up to 25 cm thick, is interpreted to be a colluvial wedge and/or fissure-fill material derived from degradation of the penultimate-event fault scarp.

Colluvium C-2. Colluvium C-2 is a 65-cm-thick or less, brown to strong brown, sandy clay loam exhibiting relatively weak soil properties. Unit C-2 was only locally exposed near the western end of trench PRT-2, where it appears to be inset within colluvial-wedge unit Cw-2. Unlike unit Cw-2 and other exposed scarp-derived colluvial deposits, colluvium C-2 thickens, rather than thins, away from the scarp. Bioturbation has extensive modified parts of this unit.

Colluvium Cw-2. Colluvium Cw-2 is a gravely, sandy clay loam to a gravely, clay loam (i.e., very poorly sorted) that is up to 1.1 m thick. Unit Cw-2 is present only west of the main fault. The unit contains considerably more clasts than the overlying units and the clasts are less weathered then in the subjacent unit (Cw-3). The clasts are moderately to strongly imbricated; the dip of clasts progressively decrease away from the main fault (fault F-4) on both the north (Figure 6) and south walls of trench PRT-1. Proximal to the fault, clasts dip steeper than the angle of repose suggesting that the unit has been tectonically deformed (drag folded?). The unit is interpreted to be a colluvial wedge largely derived from a degrading fault scarp produced by movement along the main fault (fault zones FZ-4 and FZ-6). Unit Cw-2 contains the Bt horizon of the surficial soil and has been divided into three sub-horizons based primarily on percent gravel, weak colluvial bedding, and on the presence of clay films (Appendix 2). All three sub-horizons exhibit moderately distinct subangular blocky structure, but only the two lower sub-horizons contain clay films. The boundary between the lower two sub-horizons coincides with a diffuse contact between sub-units Cw-2a and Cw-2b.

Colluvium Cw-3. Colluvium Cw-3 is a strong brown, coarse to medium, sandy clay loam that exhibits moderately distinct angular blocky structure. The unit, which is up to 80 cm thick, is present only west of the main fault (Figure 7). Unit Cw-3 can be differentiated into two sub-units based on percent gravel and clast orientation. Sub-unit Cw-3a is characterized by about 75 percent clasts and gently dipping to horizontal clast imbrication. In contrast sub-unit Cw-3b contains about 90 percent clasts that are steeply inclined (up to 39°) towards the west. Unit Cw-3 in trench PRT-1 is the best example of what we interpret to be scarp-derived colluvium at the Prattville trench locality; sub-unit Cw-3a is the distal wash facies and sub-unit Cw-3b is the proximal collapse facies of a colluvial wedge. Unit CW-3 contains a Bt horizon of a stripped buried soil.

Colluvium Cw-4. Colluvium Cw-4 is a brown to strong brown, clay loam with

moderately distinct angular blocky structure that is up to 75 cm thick. The unit exhibits fewer clasts that are considerably more weathered (i.e., less competent) than those of overlying unit (unit Cw-3) and it is slightly darker in color (lower value), with an increase in chroma. Unit Cw-4 is present only west the main fault in both trenches and likely is scarp-derived colluvium; although the internal fabric of this unit is difficult to identify due to relatively sparse clasts and because many of the clasts are weathered to mush. The basal contact of this unit, like unit Cw-2, is most distinct adjacent to the main fault and becomes perceptibly less distinct to indistinct away from it; for example, the contact could not be identified more than 31/2 meters to the west of the fault in trench PRT-1. We interpret the unit to contain the upper Bt horizon of a stripped buried soil that extends to the bottom of the trench exposure.

Colluvium C-3. Colluvium C-3 is a 2-m-thick, dark brown to strong brown, clay loam that is massive to having weak angular blocky structure. This unit was divided into three sub-units, C-3a, C-3b and C-3c, based on subtle color and textural changes and on the presence of a stoneline proximal to the main fault. Sub-unit C-3b is 60 to 75 cm thick, extends only west of the main fault, has a basal concentration of clasts, and has a lower contact that becomes progressively less distinct to indistinct away form the main fault. This sub-unit, therefore, is similar to the character of unit Cw-4 suggesting that it too may be scarp-derived colluvium.

Colluvium C-4. Colluvium C-4 is a brown to strong brown clay loam to silt loam with weak angular blocky structure. The unit is present only west of the main fault and was divided into two sub-units (Figure 7) based on a change in texture and percent gravel. Sub-unit C-4a is a clay loam with up to 25 percent clasts and sub-unit C-4b is a silt loam with relatively few clasts. Clasts in both sub-units are highly weathered and can be easily crushed between thumb and forefinger. A hand-auger hole was bored into the floor of the trench to a total depth of 209 cm. Materials recovered from the upper approximately 170 cm of the hole were quite similar to sub-unit C-4b, suggesting that colluvium C-4 may be up to 2.3 m thick.

Colluvium C-5. Colluvium C-5 is a strong brown to yellowish brown, coarse sandy clay loam with moderately distinct angular blocky structure. In trench PRT-1 the unit extends from near the east end of the trench, where it has been removed by erosion, to the main fault (fault zone FZ-4) where it is 1.5 m thick; in trench PRT-2 the colluvium is present from the east end to the eastern fault (fault zone FZ-5)(Figure 7). The unit has moderate clast imbrication within generally clast-supported gravel lenses. The clasts are dominantly tabular fragments of schist and approximately 75 percent of them have been weathered to the point where they can be broken by hand and easily cut with a knife. Unit C-5 is engulfed by the lower Bt sub-horizon of the surficial soil, east of the main fault in trench PRT-1.

Alluvium A-1. Alluvium A-1 is a 1.0- to 1.5-m-thick, strong brown, coarse sandy clay loam to silty clay loam with moderately imbricated gravel lenses. The unit extends from the east end of both trenches to the main fault in trench PRT-1 and to the easternmost fault in trench PRT-2. The stratigraphic unit contains a buried Bt horizon that was divided into three sub-horizons based on gravel content, texture, and structure. The upper two sub-horizons have distinct angular blocky structure and are clay loams. The lower sub-horizon is a silty clay loam that is massive to exhibiting moderately distinct angular block structure.

Alluvium A-2. Alluvium A-2 is a 0.7- to 1.4-m-thick, light yellowish brown to yellowish brown, silty clay to a coarse, sandy clay loam. The unit extends from the east end of trench PRT-1 to the main fault. The basal unit contains three well-defined beds or sub-units presumably comprised of tephra with the uppermost bed (sub-unit 1) being up to 30

cm thick and composed of primary air-fall ash. Stratigraphic unit A-2 contains a Bt horizon related to the second buried soil. The Bt horizon was divided into four sub-horizons primarily based on sand content. Manganese forms nearly continuous coatings on fractures and ped faces in the upper two sub-horizons and forms patches on ped faces in the lower two sub-horizons. The unit contains gravel stringers and lenses; clasts are soft and can be broken by hand and easily cut with a knife.

Colluvia Cw-5 and C-6. Colluvial units Cw-5 and C-6 occupy the same stratigraphic position, have nearly identical in their appearance (i.e., color, texture, structure), and differ from the overlying units in that they contain cobbles of basalt. We correlate the two units based on these similarities. The units are composed of brown to dark brown, cobbly silty loam with moderately distinct angular block structure. Unit Cw-5 is up to 0.4 m thick and extends about 4.5 m west from the easternmost fault within fault zone FZ-3. This unit is interpreted to be derived from degradation of a scarp produced by movement along fault zone FZ-3. Unit C-6 is up to 0.9 m thick and extends approximately 12 m from the east end of the trench; it too may be related to movement along an inferred fault located between the east end of trench PRT-1 and test pit TP-2 (Figure 3).

Colluvium C-7. Colluvium C-7 is a brown, gravely, silty clay loam that contains weathered cinders and basalt clasts. Clasts range in competence from soft to moderately hard. The colluvium is up to 40 cm thick and locally has been removed by erosion. The unit directly overlies the basalt of Rock Creek from the east end of trench PRT-1 to the main fault zone (FZ-4)(Plate 1); the unit was encountered in a hand-auger hole within main fault zone at a depth of about 1.1 m below the trench floor. The unit contains the third and lowermost buried soil within the stratigraphic sequence east of the main fault. Unit C-7 is pervasively fractured (sheared?); vertical fractures occur about 1 cm apart.

Age of Quaternary Deposits. The basalt of Rock Creek, dated by Ar-Ar at 1.1 Ma to 1.2 Ma (PG&E, 1994), underlies the entire soil/stratigraphic sequence. Thus, the entire sequence at the Prattville trench is younger than 1.1 to 1.2 Ma. The antiquity of the trench deposits is indicated by several factors, including:

- All of the deposits are deeply weathered and display mature soils having significant accumulations of pedogenic clay and prominent to distinct clay films. The homogenous character indicates a prolonged period of weathering and soil formation;
- All but the colluvial-wedge deposits currently are removed from their source, the metamorphic bedrock ridge south of the trench site, by moderately extensive drainage dissection;
- Relict soils on the escarpment have been stripped by surficial erosion (e.g., colluvium Cw-1), thus exposing Bt horizons (originally accumulation zones of clay and/or iron oxides) to leaching. Such polygenetic soil formation requires considerable evolution of the landscape.
- All but the one or two youngest trench deposits contain deeply weathered schist and basalt clasts that presently would not remain intact during either colluvial or alluvial transportation processes;
- The colluvial units do not thicken downslope, a common observation on colluvial slopes (e.g., the colluvial slope at the Butt Valley Dam trench site; WLA, 1995a), and the colluvial/alluvial bedding is oriented sub-parallel to the present escarpment, not flat-lying to gently sloping as originally deposited. These observations indicate that the trench units were not deposited on the present escarpment.

Based on soil-profile development unit C-2 is at least 100,000 years old and may be older.

The three subjacent (buried) soils incompletely represent soil formation between about 100,000 and 1,200,000 years ago, with the lowermost soil likely dating from or near the maximum-date within this time period. Additional constraints may be placed on the age of the colluvial and alluvial deposits, if the weathered tephra in the basal part of unit A-2 can be correlated with a tephra of known age or if minerals separated from the tephra can be directly dated by Ar-Ar.

Age constraints for trench units west of the main fault zone (fault zones FZ-4 and FZ-6) are similar to those east of the fault zone. The entire stratigraphic sequence must be younger than the basalt of Rock Creek (i.e., 1.1 Ma to 1.2 Ma). In addition, the sequence must be younger than the entire sequence east of the main fault zone, given the down-to-the-west displacement that characterizes the long-term character of the northern Muleshoe Mine fault. The age of the youngest colluvium, based on soil-profile development, is probably greater than 50,000 years. Thus the two underlying buried soils developed between a minimum of 100,000 and 1,200,000 years ago.

In addition to age estimates based on soil development, we have collected charcoal samples for radiocarbon dating and bulk samples of colluvial-wedge deposits (units Cw-1, Cw-2, Cw-3) for analysis by luminescence dating techniques. However, most of the charcoal in the trench occurs in secondary infillings (e.g., krotavina) and therefore will likely provide minimum ages for trench deposits. Lastly, oriented-cube samples will be collected from colluvial and alluvial trench deposits and submitted for paleomagnetic measurements.

Faults and Style of Deformation

The Muleshoe Mine fault is at least 50 m wide at the Prattville trench site. Faulting (or possibly folding) is inferred to be present east of trench PRT-1, because the flow surface on the basalt of Rock Creek is 2.3 m higher in test pit TP-2 than in the east end of the trench (Figure 4). In addition, an antithetic fault is inferred to coincide with a east-facing escarpment at the western margin of the meadow (Figures 3, 4). Hence the zone of faulting may be as much as 110 m wide at the trench site.

Six faults or narrow fault zones were identified in the trenches at the Prattville trench locality; the western fault in trench PRT-2 (fault zone FZ-6) is believed to be the continuation of the main fault zone in trench PRT-1 (fault zone FZ-4) based on similar stratigraphic and structural relationships, their nearly identical attitudes, and that a line connecting these faults is parallel to their strike. Nearly all of the faults exposed at the site are near vertical to steeply west dipping and several tend to "flower" towards the surface. Along a few faults there are changes in the amount (i.e., increase) and sense of vertical separation upsection. Subhorizontal slickensides and mullions on the main fault and along several subsidiary faults in trench PRT-1 indicate that the most-recent movement along the Muleshoe Mine fault was dominantly strike-slip. These slip indicators generally plunge to the north. The presence of several scarp-derived colluvial deposits (e.g., unit Cw-3), a west-facing escarpment, and an elongate alluvial valley along the escarpment suggest a long-term component of down-to-the-west vertical separation. The flow surface on the basalt of Rock Creek is vertically separated between test pit TP-2 and the lower end of trench PRT-1 a minimum of 8.1 m (Figure 4), and probably considerably more, down to the west. Most faults and fractures in both trenches strike more easterly than the trend of the escarpment, thus forming a left-stepping pattern. The attitude of slip indicators, presence of an alluviated valley, and the pattern of faulting suggest that the Muleshoe Mine fault is a right-oblique-normal fault; characterized by right-lateral slip with a subsidiary component of down-to-the-west vertical displacement.

The presence of scarp-derived colluvial and fissure-fill deposits, exhibiting varying degrees

of weathering and soil formation, and the upward truncations and terminations of faults, fissures and fractures at different stratigraphic levels are considered to be strong evidence of recurrent middle to late Quaternary faulting. Collectively these data support a minimum of 11 or 13 surface-faulting events since deposition of the basalt of Rock Creek (1.1 Ma to 1.2 Ma). Therefore, the average recurrence interval for surface-faulting events on the Muleshoe Mine fault is less than 85,000 years to 120,000 years.

PG&E (1994), working on the southern part of the fault at the North Fork of the Feather River, concluded that movement on the Muleshoe Mine fault initiated after deposition of the 570 ka basalt of Warner Valley. This conclusion is supported by our mapping of volcanic rocks along the fault in the trench site area. Specifically the base of a Pliocene ash-flow tuff (Yana Formation?) on the bedrock ridge south of the Prattville site, is vertically separated 15 m, down to the west. This amount of separation is comparable to the separation of the basalt of Rock Creek at the site (more than 8.1 m) and the height of scarps on the basalt of Warner Valley (up to about 12-14 m), north of the site. Thus, the average recurrence interval on the Muleshoe Mine fault may be less than 40,000 to 60,000 years.

In addition to clear evidence of faulting, monoclinal folding is also present east of the main fault (fault zone FZ-4) in trench PRT-1 (Figure 5, Plate 1). Rather than actual plastic or non-brittle deformation, the observed "folding" likely is the result of highly distributed brittle deformation accommodated by minute displacements along cooling joints pervasive in basalt flows, for example the basalt of Rock Creek. Therefore, it is possible that much or all of the deformation east of the main fault (fault zone FZ-4) in trench PRT-1 is secondary, resulting from bending-moment stresses produced above a brittlely deforming monocline; similar at a regional scale to the Chico monocline.

Fault Zone FZ-1. Fault zone FZ-1 is the easternmost fault exposed in trench PRT-1 (Plate 1). It is a 6.1-m-wide zone of several closely spaced, high-angle faults and fractures. The structures have a range of strikes from N62°E to N62°W, but generally have northerly strikes. Fracture orientations suggest three groupings or fracture sets; northerly striking, northeast-striking, and west-northwest-striking sets. Evidence of recurrent middle to late Quaternary faulting includes:

- A few faults in the basalt of Rock Creek are truncated at the base of unit C-7 (Plate 1)(FZ-1 event(s) Z, Figure 8);
- Most of the closely spaced (about 1 cm) vertical fractures within unit C-7 are truncated at the base of unit C-6 (event V);
- Several fractures and possibly a fault terminate at the base of unit A-2 or within the basal part of unit A-2 (event T);
- Two fractures were identified to terminate just below the base of unit A-1 (possible event R);
- Numerous fractures terminate in the upper part of unit A-1 (event P); and
- Five fractures and a fault, near the middle of the fault zone, terminate at the top of unit A-1 or extend through unit C-5, to within 50 cm of the ground surface, where they have been truncated by a krotavina (event N); these features extend to the base of active zone of bioturbation.

The easternmost fault within fault zone FZ-1 strikes N-S to N5°W and dips from 51°W to 80°W. Well-developed slickensides and mullion along this fault plane plunge 51°S. The vertical separation of the contact between unit C-6 and unit C-7 (approximately 2 cm, down-to-the-west) is considerably less than that of the overlying contact between unit A-2 and unit C-6 (approximately 11 cm, down-to-the-west). The increase in the amount of apparent vertical offset at higher stratigraphic levels is strong evidence of strike-slip displacement. The westernmost fault within fault zone FZ-1 strikes N3°E and dips 67°N.

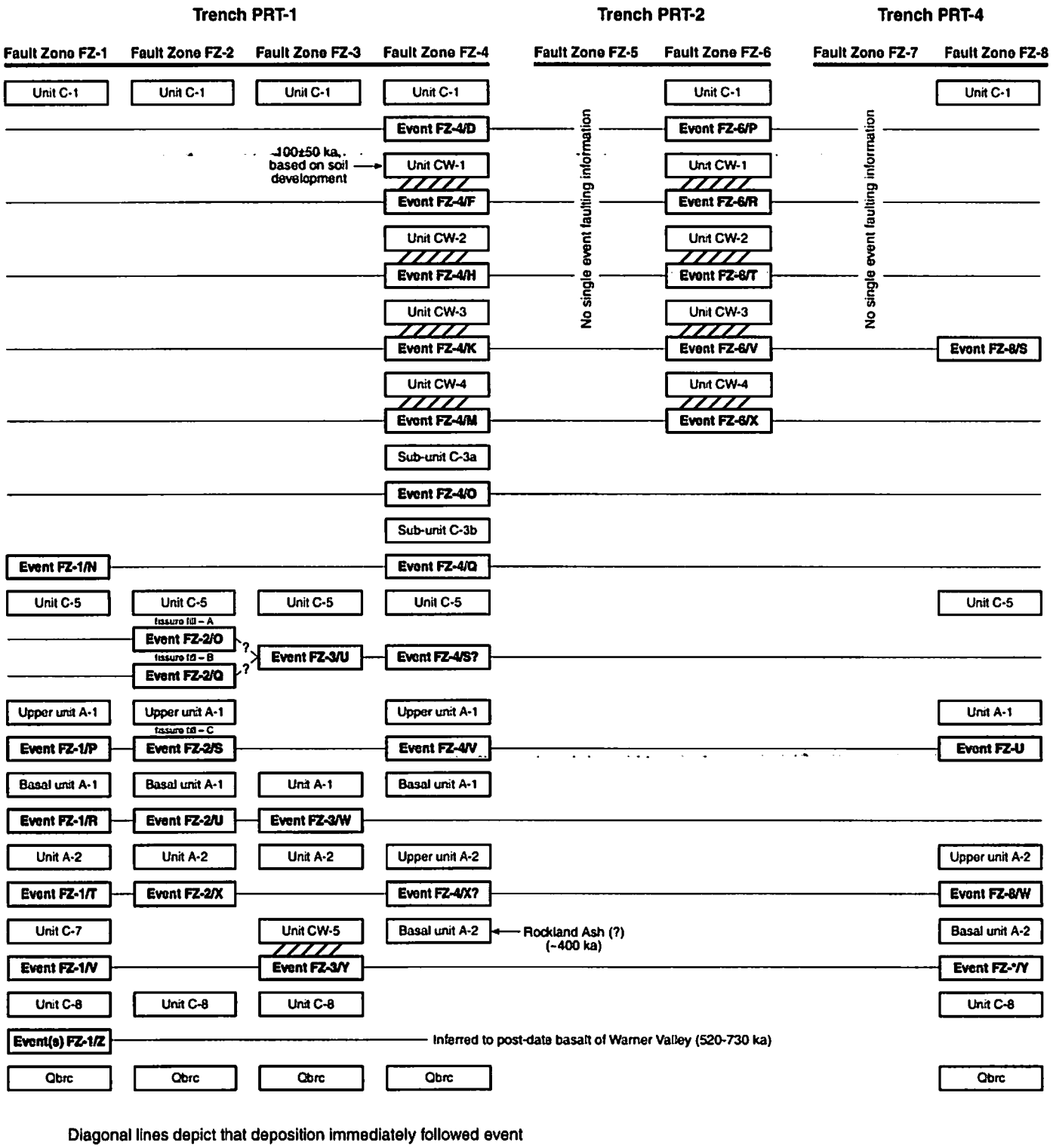

Diagonal lines depict that deposition immediately followed event

Figure 8. Relative paleoseismic and depositional history of the Prattville trench site

Slickensides along this fault plunge 67°N also suggesting a component of strike-slip displacement.

Fault Zone FZ-2. Fault zone FZ-2 is a 6.5-m-wide zone comprising nine steeply dipping faults and numerous fractures. The faults range in strike from N4°E to N65°E and locally are discontinuously coated with a whitish mineral precipitate within the basalt of Rock Creek. Evidence of recurrent surface-faulting includes:

- A fault and several fractures truncated at the base of unit A-2 (Plate 1)(FZ-2 event X, Figure 8);
- A fault, several fractures, and shear fabric are truncated at the base of unit A-1 (event U);
- Two faults are truncated at the base of unit C-5 (event Q); and
- Most compelling, three fissure-fill deposits, stratigraphically between units A1 and C-5, that exhibit distinct differences in the degree of weathering and soil formation (events S, Q, O, respectively).

Near the middle of fault zone FZ-2, a multi-layered tephra deposit at the base of unit A-2 (sub-units 1, 2, 3) is vertically separated approximately 6 cm and 16 cm down-to-the-east and -west, respectively, forming a small horst (Plate 1). The thickness of the tephra is comparable on either side of the horst, but considerably thinner over the horst. Although it is theoretically possible that the tephra thins as a result of faulting and subsequent erosion of the horst prior to its burial, it more likely represents lateral movement along the two bounding faults. Lateral movement is supported by the orientation of slickensides on a fault near the center of the fault zone that plunge from 8°S to 27°S.

Fault Zone FZ-3. Fault zone FZ-3 is a 2.6-m-wide zone comprising four faults and several fractures that dip steeply to the south. A moderately west-tilted homocline occurs between the easternmost fault in the zone and the inferred westernmost fault. The presence and orientation of the homocline is based on the orientation of originally horizontal cooling joints within the basalt of Rock Creek that are tilted as steeply as 26°W between the bounding faults. Evidence of multiple faulting events along fault zone FZ-3 includes:

- The interpretation of unit Cw-5 as being largely derived from degradation of unit C-7 on the relatively upthrown side of one of the east-bounding faults of the zone (FZ-3 event y, Figure 8).
- One fault and several fractures (including numerous fractures between this fault zone and fault zone FZ-4) are truncated at the base of unit A-1 (event W); and
- Several fractures are truncated at the base of unit C5 (event U).

It is interesting to note that nearly all of the fractures that truncate at the base of unit C-5 can not be traced down-dip through a gravel interbed within unit A-1. This suggests that the interbed likely behaved as a cohesiveness, granular mass, accommodating displacement by grain-to-grain adjustments, rather than as a coherent mass that would have brittlely deformed. The gravel interbed has been weathered to a coherent silty clay loam and, thus, currently would deform brittlely. This indicates that a prolonged period of weathering has occurred since the faulting event that produced these fractures.

Two faults along the eastern margin of fault zone FZ-3 strike from N34°E to N39°E and dip from 77°SE to 83°SE. Across the eastern fault the base of unit A-1 is vertically separated approximately 10 cm in an apparent reverse sense. Across the western fault the base of unit A-2 is separated approximately 16 cm also in an apparent reverse sense. The

apparent reverse offsets of these units in an otherwise trans-extensional setting, strongly implies strike-slip displacement.

Fault Zone FZ-4. Fault zone FZ-4 is considered to be the main trace of the Muleshoe Mine fault through the Prattville trench locality because it coincides with the break in slope along the base of the escarpment, juxtaposes two distinctly different stratigraphic sequences, down-drops the basalt of Rock Creek below the bottom of the trench and below accessible hand-auger depths, and it can be followed to a higher stratigraphic level (i.e., it records the most-recent-faulting event) than can the other faults in trench PRT-1. The fault zone is 2.2-m-wide zone consisting of three near vertical faults and associated high-angle and moderate-angle fractures. The faults within FZ-4 have a narrow range of strikes, N12°E to N3°W, except one minor listric fault that strikes N44°E. Evidence of repeated middle to late Quaternary faulting events includes:

- Truncation of a subsidiary fault within what appears to be unit A-2 (Plate 1) (possible FZ-4 event X, Figure 8);
- Greater offset of the base of A-1(?) than of alluvial bedding higher within unit A-1 and the termination of the easternmost fault in the zone at the base of a fine-grained interbed within unit A-1 (event V);
- Possible upward truncation of four fractures at the base of unit C-5 (although the base of this unit is gravely and, therefore, may not have brittlely deformed)(possible event S);
- Termination of two fractures at the base of sub-unit C-3b and the presence of scarp-derived colluvium (i.e., sub-unit C-3b)(event Q);
- A fissure-fill deposit overlain by sub-unit C-3a (event O);
- Scarp-derived colluvial deposits, units Cw-4, Cw-3, Cw-2 and Cw-1, that have different textures and slightly different degrees of weathering and soil development (events M, K, H, and penultimate event F, respectively); and
- The presence of sub-vertically aligned clasts and subtle shear fabric within unit Cw-1 (most recent, event D).

The basalt of Rock Creek is down-dropped below the base of the trench (in an apparent reverse sense) across the two easternmost faults. The basalt was encountered in a hand-auger hole at a depth of 1.15 m below the trench floor, indicating approximately 1.65 m vertical separation of the basalt across the faults. Sub-horizontal slickensides, plunging 3°N, are present along the western fault, indicating that the last movement along this fault was strike-slip in character.

The single most significant fault exposed in trench PRT-1 is the west-bounding fault of fault zone FZ-4. The fault strikes N12°E to N1°E and, below a depth of about 1.3 m, dips 85°W to 86°W. The upper reach of the fault, which extends to within 40 cm of the ground surface (i.e., to the base of active bioturbation) on the south wall of trench PRT-1, appears to form a flower structure. The west-bordering fault of the flower structure shows evidence of drag folded (i.e., upwarping) imbricated clasts within unit Cw-2 based on progressively steeper inclinations of clasts towards the fault. Several clasts are inclined steeper than the angle of repose, up to 39°W; a similar relationship is exposed on the north wall of trench PRT-1 (Figure 6). Slickensides that plunge from 3°S to 24°N show that the last movement along the fault was dominantly strike-slip. The presence of four to five (or more) scarp-derived colluvial deposits, 50 cm to 100 cm thick, adjacent to the fault suggest a down-to-the-west vertical component. A vertical component during each faulting event. Vertical separation is supported by a second hand-auger hole bored in the lowest part of the trench west of the fault. The auger hole reached a total depth of 2.09 m and bottomed in colluvial deposits. Thus, across fault zone FZ-4 the basalt is vertically separated a minimum of 2.5 m and likely is separated significantly more (Figure 4). On the south wall

of trench PRT-1, the relationships along the uppermost part of the fault were obscured by bioturbation (Plate 1). Thus, the upper part of the fault was logged on the north wall to record all available evidence regarding the timing of the most-recent faulting along fault FZ-4 (Figure 6).

On the north wall of trench PRT-1, the upper part of fault zone FZ-4 consists of a single high-angle fault that bifurcates, forming an intervening fissure. The fissure has been filled with gravely materials that exhibit shear fabric and sub-vertically oriented clasts. The west-bounding fault and weak shear fabric can be traced into unit Cw-1 and to within approximately 12 cm of the ground surface; however an estimated 5 cm to 10 cm of humus-rich material was inadvertently removed during excavation. The base of unit Cw-1 is vertically separated approximately 15 cm down-to-the-east across the fault. The deformation of unit Cw-1 occurred during the most-recent event.

Fault Zone FZ-5. Fault zone FZ-5 is a 55-cm-wide zone consisting of two high-angle bounding faults and intermediary shear fabric and sub-vertically aligned clasts that is exposed in trench PRT-2 (Figure 7). The fault zone juxtaposes colluvium C-2 and alluvium A-2 on the east against colluvium C-6b(?) on the west. The uppermost part of fault zone FZ-5 appears to form a flower structure and is truncated at the base of unit Cw-1, within about 65 cm of the ground surface. The most likely candidate for the northern continuation of this fault zone in trench PRT-1 is fault zone FZ-3. However, given the strike of this fault zone, N4°E to N10°E and that of fault zone FZ-3, N34°E to N39°E, a significant right bend in the fault trace would be required.

Fault Zone FZ-6. Fault zone FZ-6 is a 95-cm-wide zone consisting of two near vertical faults (Figure 6) and is interpreted to be the southern continuation of the main fault zone in trench PRT-1 (i.e., fault zone FZ-4) (Figure 3). An intact block comprised of unit C-5(?) overlain by a faulted remnant of unit Cw-2 is observed within the fault zone. Above the remnant of Cw-2, the faults form a fissure infilled with unit Cw-1. Evidence of repeated middle(?) to late Quaternary surface-faulting events includes:

- Scarp-derived colluvial deposits, units Cw-4, Cw-3, Cw-2 and Cw-1, exhibiting different textures and slightly different degrees of weathering and soil development (FZ-6 events X, V, T and the penultimate event R, respectively, Figure 8); and

- Shear fabric and sub-vertically aligned clasts within and along the borders of unit Cw-1 (most-recent event P).

The eastern fault within FZ-6 bifurcates or widens upward into a shear zone, up to 20 cm wide, that forms the eastern border of unit Cw-1 within the fissure. The upper 15-20 cm of the shear zone contains well-developed shear fabric and several large elongate schist clasts that are sub-vertically aligned. The western fault forms a shear zone up to 10 cm wide near the base of the trench that strikes N14°E and dips 88°N. Across this fault the base of unit Cw-1 has been vertically separated approximately 13 cm down to the east (Figure 7). The amount of separation is comparable to the vertical separation of the same unit (15 cm down-to-the-east) across fault zone FZ-4 (i.e., the same fault zone) on the north wall of trench PRT-1 (Figure 6). This fault extends to within 45 cm of the present ground surface.

CONCLUSION

The Muleshoe Mine fault is a Mesozoic bedrock structure reactivated during the middle Quaternary. Strong evidence of recurrent, middle- to late-Quaternary fault activity was exposed at the Prattville trench site. The paleoseismic record spans the past 500,000 years and supports a minimum of eleven to thirteen surface-faulting events on the Muleshoe Mine fault. Thus, the long-term average recurrence interval is 40,000 to 45,000 years or less.

The recency of activity on the Muleshoe Mine fault is based on the structural and stratigraphic relationships of unit Cw-1. Unit Cw-1 is about 100,000 years old. The unit is a product of the penultimate faulting event and it has, in turn, been faulted by the most-recent faulting event. Thus, the late Quaternary recurrence interval is about 50,000 years, or less, consistent with the long-term average recurrence interval.

The primary evidence for the most-recent-surface-faulting event along the Muleshoe Mine fault is the presence of a fault and subtle shear fabric extending through unit Cw-1 and into the zone of active bioturbation (within 15 to 25 cm of the original ground surface above fault zone FZ-4). Preservation of such subtle evidence is judged to be brief on a geological time scale, given the position of these structural features relative to the degrading, ground surface and zone of active bioturbation within this conifer forest setting. Therefore, we conclude that the Muleshoe Mine fault has been active within the last 50,000 years.

LIST OF REFERENCES

Jayko, A.S., 1988, Paleozoic and Mesozoic rocks of the Almanor quadrangle, Plumas County, California: U.S. Geological Survey Open-File Report OFR 88-757.

Pacific Gas and Electric (PG&E), 1994, Identification of potential seismic sources, Lake Almanor Dam, FERC Project 2105-CA, State Dam No. 93-003, Plumas County, California: internal draft #2 document.

APPENDIX 3-1B

A. Voluminous, theoleiitic basalt fields of the Lake Almanor basin, and their deformations due to post-emplacement faulting.

Champion, D., Clynne, M., Muffler, P.

Voluminous, tholeiitic basalt fields of the Lake Almanor basin, and their deformations due to post-emplacement faulting

Duane Champion, Mike Clynne, and Patrick Muffler
U. S. Geological Survey, Volcano Hazards Program
MS-910, 345 Middlefield Road
Menlo Park, CA 94025

The areas between, and particularly east of, the major calc-alkaline stratocones of the Cascade Range in California are characterized by voluminous (>4 km^3) outpourings of low-potassium tholeiitic basalt which cover hundreds of km^2 with generally thin lava successions. As these flows spread out and drape the preexisting topography, they can mark the amount of displacement and rotation due to subsequent faulting. Even where they cross preexisting fault scarps, a knowledge of their typical morphology allows identification of later fault movement. When several lava flows of varying ages drape a single scarp, a knowledge of their ages (usually from K-Ar or $^{40}Ar/^{39}Ar$ dating) allows a reconstruction of the rates of fault movement. Paleomagnetic studies, on the other hand, tell you nothing about displacement, but they aid in the identification of the lava sheets, and they fix the amounts of aggregate rotation that outcrops have experienced.

In the Lake Almanor area, three tholeiitic fields cover portions of the basin, invade the drainages of the N. Fork Feather River and Butt Creek, and are deformed by faulting into tilted blocks at various scales. The three fields are (1) basalt of Rock Creek (1.1 Ma), from unknown vent near Swain Mountain, (2) basalt of Warner Valley (~0.6 Ma), from unknown vent N. of Mt. Harkness, and (3) basalt of Westwood (0.40 Ma), from a vent S. of Clover Butte. $^{40}Ar/^{39}Ar$ age analyses of these lava fields have been done by Paul Renne (BGC) and Brent Turrin (USGS) on samples collected by PG&E during their regional studies. The lava fields exhibit a progression of decreasing fault deformation with decreasing age, and also increasing areal constriction with decreasing age, owing to the flows being channeled into faulted topography. In other words, the basalt of Rock Creek floors virtually the entire Almanor basin, whereas the basalt of Warner Valley is limited to only the western half and the immediate Almanor Dam area. The basalt of Westwood is constrained to a narrow band in the eastern half of the Almanor basin and to the Dam area. The basalts additionally have been preserved as elevated benches along the Feather River in inverted topographic order due to the extreme erosion rates along that drainage.

Although our paleomagnetic, geologic and geochronologic study of the tholeiites of the Lake Almanor basin is not yet complete, available paleomagnetic data have been used to identify the

separate lava sheets, and the rotational deformation found at certain outcrops has been defined. Examples of the data and interpretations are presented in five accompanying figures.

Figure 1. Paleomagnetic data from lower south wall of PG&E trench near Prattville. Directions are slightly dispersed in ENE-WSW direction which is possibly due to rotation around small-circle axis located ~20° counterclockwise from strike of fault plane. This dispersion orientation suggests right-slip as well as dip-slip on this fault.

Figure 2. Mean directions of magnetization from outcrops in the basalt of Rock Creek, and the mean direction from all 20 cores in Prattville trench. Systematic variation in declination values may reflect basinward dips of this 1.1 Ma lava flow. Alternatively, they may be from two different lava flows; argon dating would confirm or deny this hypothesis.

Figure 3. Mean directions of magnetization from outcrops in the basalt of Warner Valley, and the dispersed directions from outcrops that have been rotated by faulting. Seneca Road outcrops may have also experienced toppling or slumping on serpentinized Mesozoic basement. Chester quarry direction may indicate additional early Brunhes tholeiite lava flow in this area.

Figure 4. Mean directions of magnetization from outcrops in the basalt of Westwood, and the dispersed directions from outcrops in the Almanor Dam area rotated by faulting. Graben-like movements on two different trends have rotated Westwood outcrops on the west side out to the west or north, and on the east side out to the south and east. Outcrop sampled by JW93-18 has probably been downfaulted, but no rotations accompany this displacement.

Figure 5. Example of structural analysis possible with paleomagnetic data from outcrops in Warner Valley and Westwood basalts in same structural block at west foot of Almanor Dam. Rectifying rotated paleomagnetic data from Westwood outcrop JW93-20 requires also rotating paleomagnetic data from underlying Warner Valley outcrop JW93-19. Sequence suggests two rotations for this block, first around a NW-SE fault with down to NE movement, and then around a NE-SW fault with down to SE movement. Both fault trends are available in Almanor Dam area.

Flow Designation: Prattville Trench		Experiment: Best Cleaned		Remarks: Figure 1.			
Specimen	Intensity	Specimen	Intensity	Specimen	Intensity	Specimen	Intensity

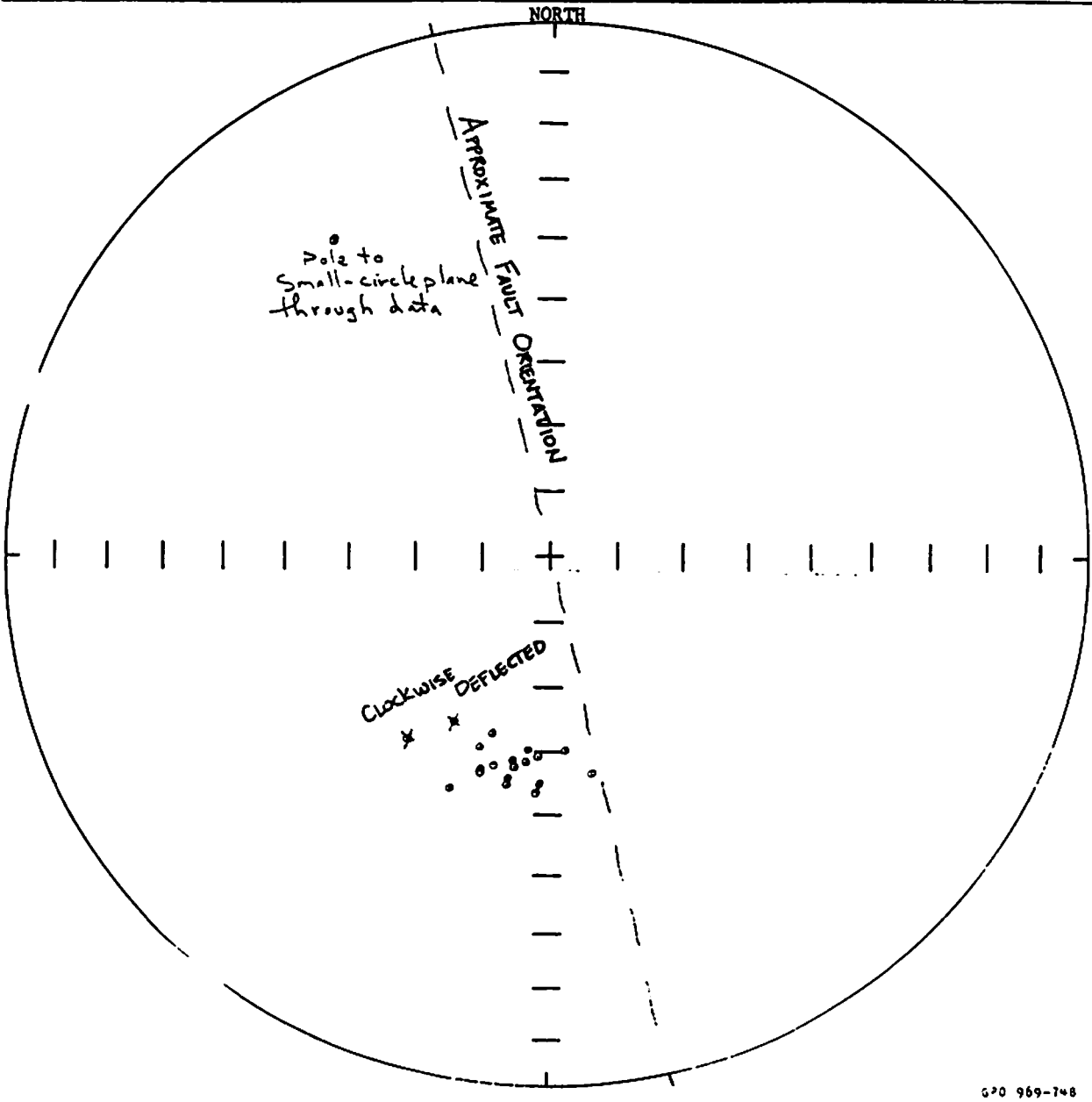

GPO 969-748

Flow Designation: Rock Creek		Experiment: Best Cleaned		Remarks: Figure 2.			
Specimen	Intensity	Specimen	Intensity	Specimen	Intensity	Specimen	Intensity

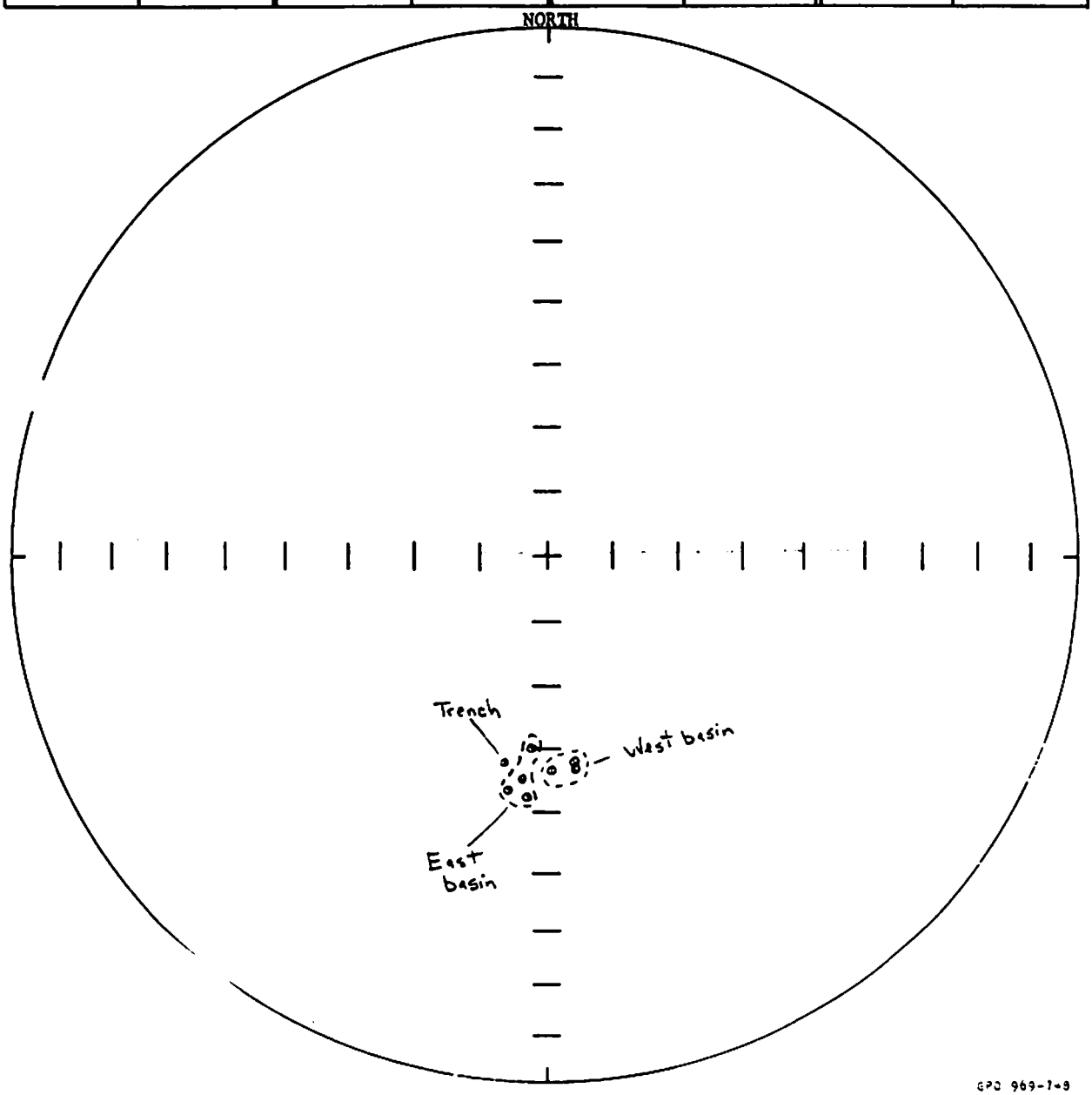

GPO 969-749

Flow Designation: Feather River Canyon		Experiment: Warner Valley basalt		Remarks: Figure 3.			
Specimen	Intensity	Specimen	Intensity	Specimen	Intensity	Specimen	Intensity

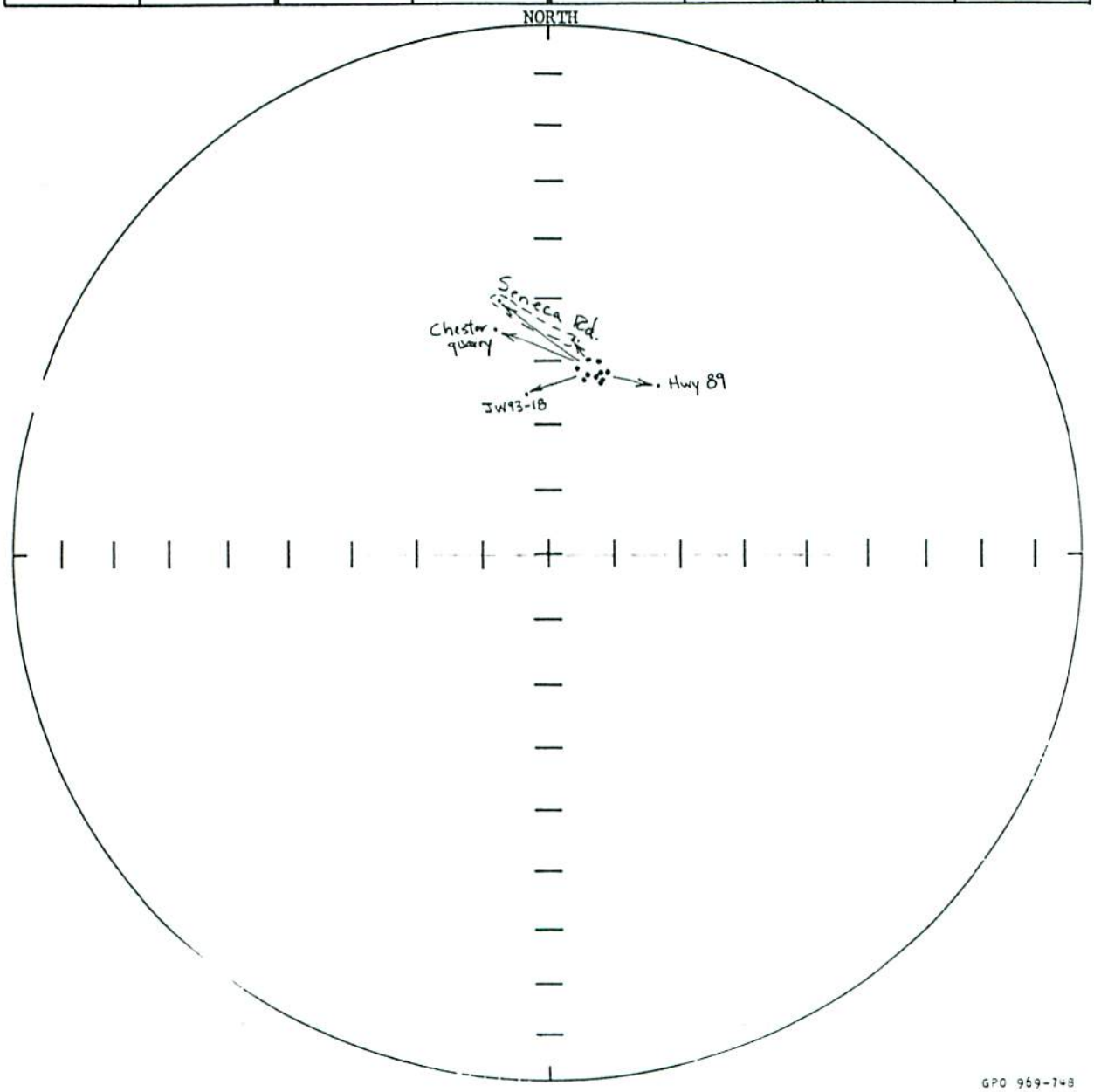

GPO 969-748

Flow Designation: Almanor Dam Area		Experiment: Westwood basalt		Remarks: Figure 4.			
Specimen	Intensity	Specimen	Intensity	Specimen	Intensity	Specimen	Intensity

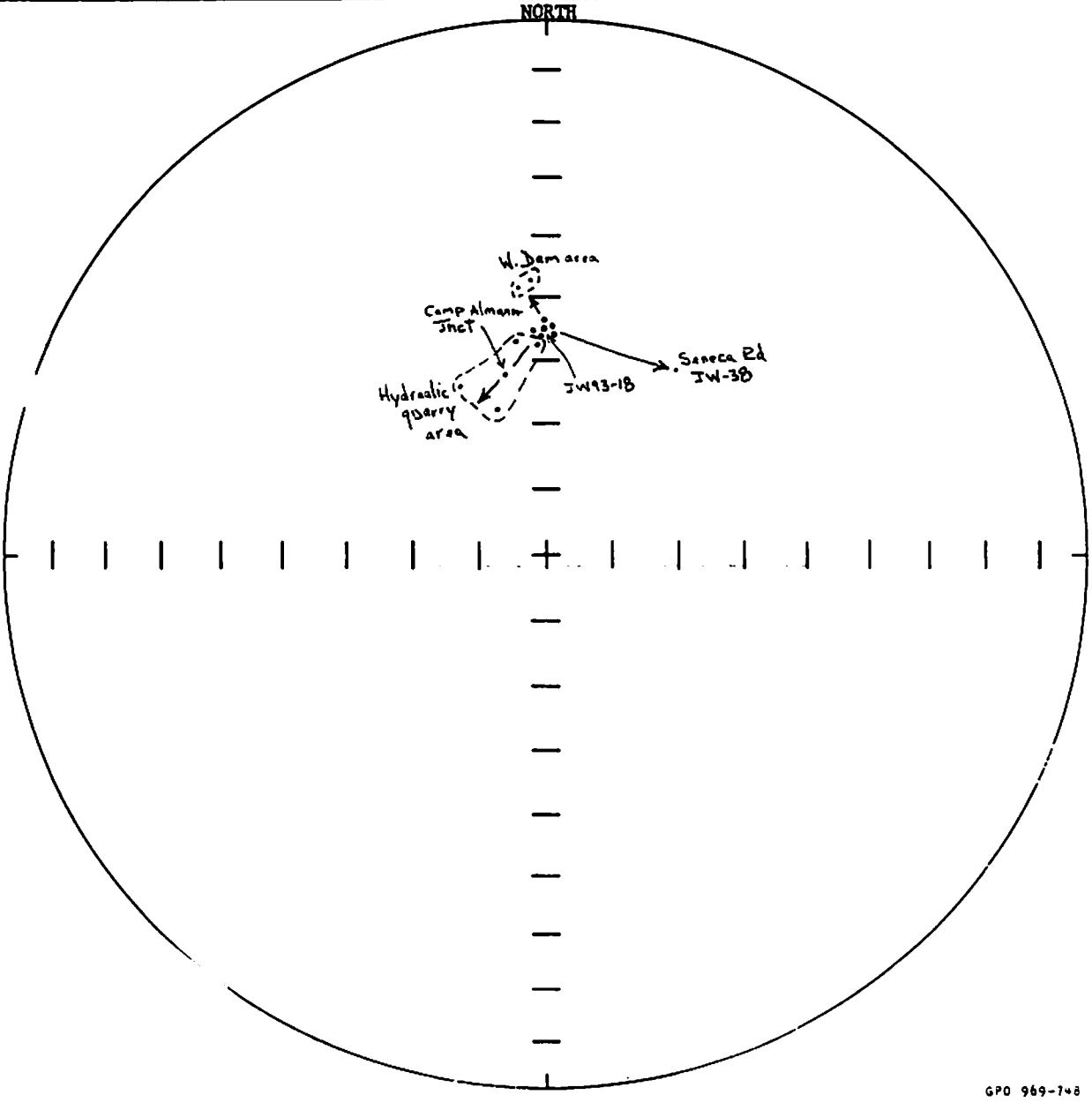

GPO 969-748

Flow Designation: West Almanor Dam gorge		Experiment:		Remarks: Figure 5.			
Specimen	Intensity	Specimen	Intensity	Specimen	Intensity	Specimen	Intensity

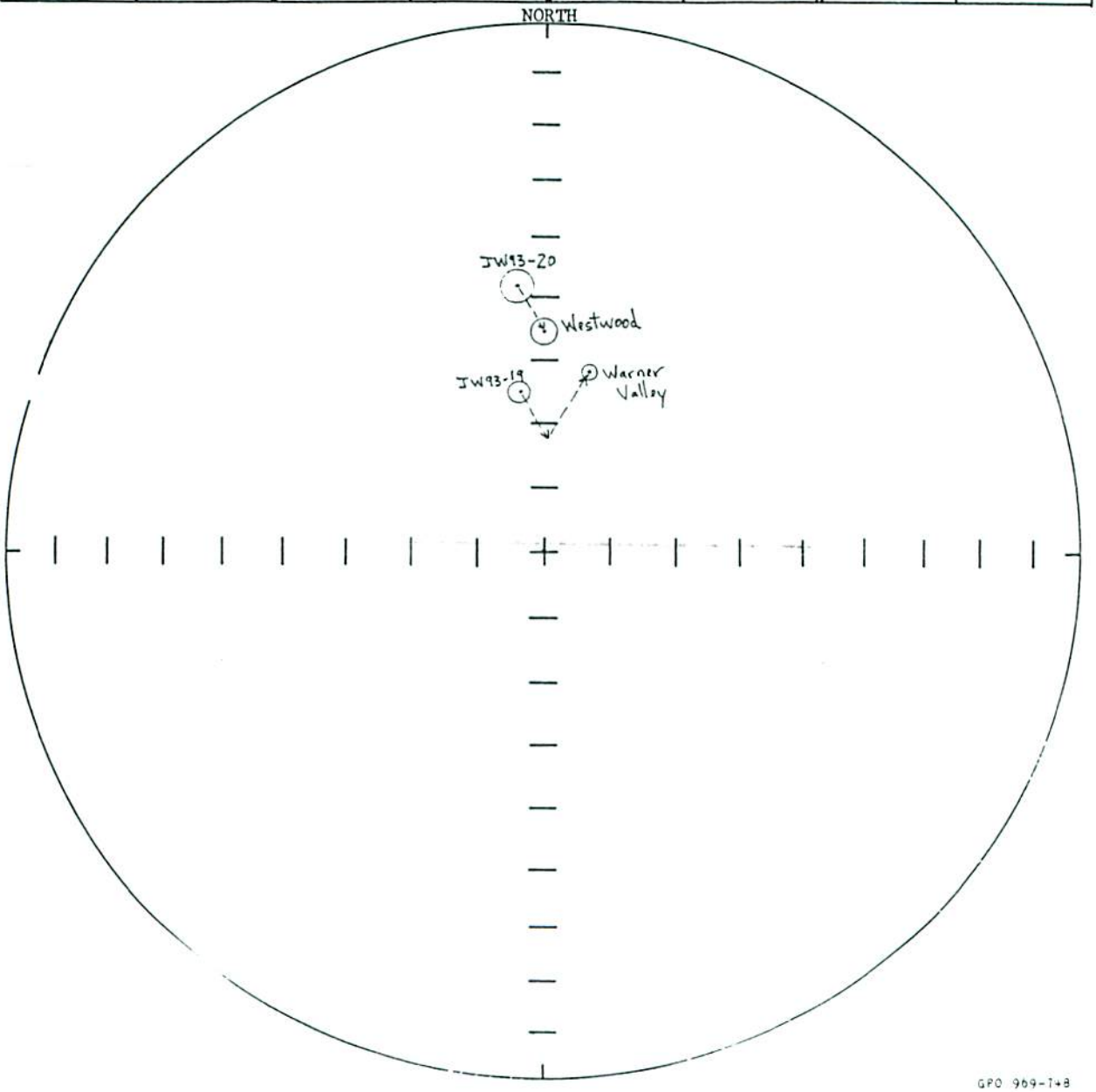

GPO 969-748

30

APPENDIX 3 - 1C

A. Quaternary Faulting, Incision of the North Fork Feather River, and Neotectonics of the Northeastern Sierra Nevada, California.

Wakabayashi, J., Page, W.D., Renne, P.R., Sharp, W.D., Becker, T.

2

QUATERNARY FAULTING, INCISION OF THE NORTH FORK FEATHER RIVER, AND NEOTECTONICS OF THE NORTHEASTERN SIERRA NEVADA, CALIFORNIA

John Wakabayashi, William D. Page, Paul R. Renne, Warren D. Sharp and Timothy Becker

ABSTRACT

Plio-Pleistocene volcanic rocks are present in the Lake Almanor basin and North Fork Feather River (North Fork) canyon, east of the Sierra Nevada crest in northern California. Remnants of two major tholeiitic basalt flow sequences (~1.1 Ma and ~0.6 Ma) occur as terrace-like remnants in the canyon and aid in the identification of Quaternary faulting. Vertical separation rates range up to 0.15 mm/yr on individual faults. The cumulative rate of Quaternary east-down vertical separation between Lake Almanor and the Sierra Nevada crest (i.e., the Sierra Nevada Frontal fault system) is approximately 0.4 mm/yr. The lateral component of faulting is unconstrained. Several faults began movement within the last million years, whereas other faults were active prior to 2 Ma.

Relative elevations of volcanic remnants above the bottom of the North Fork canyon constrain the long-term incision rate of the river. Two volcanic units (2.8 and 2.1 Ma) form limited remnants inset below remnants of a Tertiary erosion surface. Incision rates between deposition of these older rocks and the 1.1 Ma flow sequence are ~0.1 mm/yr. Extrapolation of these incision rates suggests that incision, and by inference late Cenozoic Sierra Nevada uplift, began prior to 4.6 Ma, similar to estimates from other parts of the range. Incision rates between 1.1 and 0.6 Ma range from 0.3 to 0.7 mm/yr. The post-0.6 Ma incision rates range from 0.2 to 0.5 mm/yr, and are consistently slower for a given fault block than the 1.1 to 0.6 Ma rates. Possible explanations for the deceleration of incision rates since 0.6 Ma include: (1) decrease in vertical faulting rates, (2).post-0.6 Ma westward migration of east-down faulting in this region, (3) upstream knickpoint migration, and (4) erosion rates have balanced the uplift of the range.

TECTONIC SETTING

We investigated late Cenozoic geology of the northeastern Sierra Nevada in a transect along the North Fork Feather River (North Fork) from Lake Almanor downstream to the confluence of the North Fork with the East Branch North Fork Feather River (East Branch) (Figures 1,2). The study area straddles the northeastern margin of the Sierra Nevada, east of the Sierra Nevada crest and near the northern end of the range, and includes the western branch of the Sierra Nevada Frontal fault system. The 650-km-long Sierra Nevada Frontal fault system (Frontal fault system) separates the northern Sierra Nevada and southern Cascades on the west from the southern Modoc Plateau and western Basin and Range on the east (Figure 1). The Frontal fault system probably began forming at approximately 5 Ma to accomodate

uplift and tilting of the Sierra Nevada tectonic block (Grant et al., 1978; Unruh, 1991). The northern Frontal fault system extends north from approximately 10 km south of Lake Tahoe and has two branches. The eastern branch extends from Carson City to Honey Lake. The western branch extends north-northwest along the west side of Lake Tahoe to Mohawk Valley and Lake Almanor. It separates the Plumas transition province (the crustal block between the two branches of the fault system) on the east from the Sierra Nevada on the west. At Mohawk Valley, 50 km south of Lake Almanor, the fault system is a relatively narrow, 3- to 10-kilometer-wide, zone of east-down normal faults, with a probable right-slip component or associated strike-slip faults (Page et al., 1993). North of Mohawk Valley, the fault system broadens and, in the Lake Almanor area, forms a 30-kilometer-wide zone of predominantly east-down faults. Our transect captures most of the faulting associated with the western branch of the Frontal fault system at this latitude but does not cross significant faulting along the northern extension of the Spanish Peak fault, directly east of the Sierra Nevada crest.

In this paper we present geologic evidence that bears on Quaternary vertical separation rates of the Frontal fault system and post-Miocene tectonic evolution of the area.

PLIO-PLEISTOCENE VOLCANIC ROCKS AND TERTIARY EROSION SURFACE

Plio-Pleistocene volcanic rocks provide a means to evaluate of Quaternary deformation in the North Fork and Lake Almanor areas. We have obtained 40Ar/39Ar incremental heating dates from several of these units (Fig.2, data in appendix 1), and these dates help constrain the timing of geologic events in the area. Volcanic deposits north and west of Lake Almanor generally form inverted topographic sequences; younger units follow channels or depressions in older units. Three of the most widespread units are sequences of low-K tholeiitic basalt flows (M.A. Clynne, L.P. Muffler, unpub. mapping). These three basalt flow sequences have been called the Basalts of Rock Creek, Warner Valley and Westwood (M.A. Clynne and L.P. Muffler, unpub. mapping), and have yielded Ar-Ar incremental heating dates of ~1.1 Ma, ~0.6 Ma, and ~0.4 Ma respectively (Fig.2). These basalts apparently flowed into the Almanor basin from the north, with the older two sequences exiting the basin and flowing down the canyon of the North Fork. Basalt flows in the North Fork canyon occur as terrace-like remnants, with the older flow remnants present at higher elevations above the canyon floor than the younger flow remnants (Fig.2 and 3). After the first (1.1 Ma) group of basalts flowed down the canyon, renewed downcutting removed much of the basalt and excavated the canyon deeper. Deposition of the second (0.6 Ma) group of basalts followed, downcutting renewed, and the river incised to its present level. Limited remnants of two older volcanic units dated at 2.8 and 2.1 Ma respectively are present at higher relative elevations above the river: The 2.8 Ma rocks are andesite and part of the Yana volcanic center whose widespread extrusive rocks include the Tuscan Formation (Guffanti et al., 1990); the 2.1 Ma rocks are part of a low-K tholeiitic flow.

The highest elevations in the region include remnants of an upland erosion surface characterized by rolling, rounded topography and deep saprolitic weathering. This erosion surface is interpreted to be equivalent to Eocene or Miocene surfaces elsewhere in the Sierra Nevada. The Tertiary surface apparently predates major late Cenozoic uplift in the range (e.g. Durrell, 1987), and thus is an important Cenozoic datum for evaluating tectonism.

QUATERNARY VERTICAL DEFORMATION

Vertical faulting is readily identified in regions of continuous Plio-Pleistocene volcanic cover around Lake Almanor, where faulting has formed prominent scarps up to 500 m high. South of Lake Almanor, erosion has left only scattered remnants of Plio-Pleistocene volcanic rocks on Mesozoic to Paleozoic basement. To identify vertical faulting in the vicinity of the North Fork, we mapped the elevation of the upper surfaces of the flow remnants, and then prepared a longitudinal profile of these surfaces. Given the young age and erosional resistance of these basalts, we believe the upper flow surfaces represent reliable stratigraphic horizons. Such relationships between remnant surfaces and stratigraphy have been confirmed for much older units in the Sierra Nevada such as the 16 Ma Lovejoy basalt (Page and Sawyer, 1992) and the 9 Ma Table Mountain Latite (Page et al., 1978; Ely, 1992). Our profile and geologic mapping show that several faults cross the North Fork (Figure 3). Individual faults have vertical separation rates ranging up to 0.15 mm/yr (Figure 3). The total east-down vertical separation rate between Lake Almanor and Sierra Nevada crest (the western branch of the Frontal fault system) is approximately 0.4 mm/yr, including an estimate of 0.1 mm/yr on the northern extension of the Spanish Peak fault between the west end of the profile and the Sierra Nevada crest (PG&E, 1994).

Actual slip rates are not constrained owing to the lack of dip information, and, more significantly, because strike-slip displacement is not quantified. En-echelon pull-apart basins and strike-slip earthquake focal mechanisms indicate that strike-slip faulting is significant along the Frontal fault system in this area (Page et al., 1993). Along the Muleshoe Mine fault near Lake Almanor, along the Mohawk Valley fault zone in Sierra Valley and along the Little Grass Valley fault near La Porte, slickensides and stratigraphic relationships in trenches indicate significant strike slip displacement (Sawyer et al., 1993; T.L. Sawyer and W.D. Page unpub. data).

TIMING OF INITIATION OF FAULTING

Some, or possibly most, of the faults that cross the North Fork Feather River may have begun moving relatively recently. The best example is the Butt Creek fault zone (including the Butt Creek, China Bar and Muleshoe Mine faults). These faults exhibit some of the highest vertical separation rates in the area, and they collectively form a tectonic low that extends from several kilometers northwest of American Valley to Butt Valley, a distance of 30 km. This fault zone may extend an additional 30 km

northwestward to Mt. Lassen. At the North Fork, the total (net of the three faults) vertical separation of the 1.1 Ma flow sequence across the fault zone is the same as the total vertical separation for the 0.6 Ma flow sequence, indicating no faulting until after 0.6 Ma (Figure 3). Ten km north of the North Fork, vertical separation of a >2.5 Ma rhyolite (age estimated by correlation by M.A. Clynne, written comm., 1995) across strands of the Butt Creek fault zone is similar in magnitude to separation of basalt along this fault zone in the North Fork canyon (T.L. Sawyer and J. Wakabayashi, unpub. mapping). Most of the other faults that cross the North Fork also may have started moving within the last 600 ka or so, but uncertainties in the vertical separations of the basalt remnants are too large to test this premise (Figure 3). These faults exhibit vertical separations of the erosion surface that are similar in magnitude to vertical separation of the 1.1 Ma and 0.6 Ma basalts in the North Fork canyon, however, which is consistent with post 0.6 Ma initiation of faulting. Recent detailed mapping and surveying along the Almanor fault (Fig. 1), one of the two major faults that extends north or northwestward from the Almanor basin, indicate that the late Quaternary vertical separation rate of Tioga and Tahoe-age moraines is approximately 1 mm/yr across the fault (K. Kelson, unpub. data). The vertical separation of 2.2 Ma Mud Creek Rim andesite across this fault indicates a separation rate of 0.23 mm/yr (PG&E, 1994). These data suggest that either recent acceleration slip rate on the Almanor fault or that the fault did not begin movement until approximately 0.5 Ma, based on the late Quaternary separation rate.

Several faults in the region may have been active for the last 2 million years or longer. These faults have large (150m or more) vertical separations of datums _2 Ma and proportionally smaller separations of younger units. Examples of these faults include the Ohio Creek-Wolf Creek and Keddie Ridge faults (Fig.1).

POST-MIOCENE INCISION RATE OF THE NORTH FORK FEATHER RIVER: TECTONIC IMPLICATIONS

The progressive increase in elevation and tilting of successively older volcanic flows above the North Fork reflect ongoing deformation and uplift of the northern Sierra Nevada since at least 2.8 Ma, the age of the oldest volcanic rocks dated in the canyon. Incision rate of the river over a time interval can be estimated by determining the elevation of the surface of a volcanic flow remnant of known age above the canyon floor and elevations of volcanic remnants of different known ages with respect to each other. Because of Quaternary faulting, elevations of volcanic remnants above the river are compared only within each fault-bounded block. Post-0.6 Ma incision rates range from 0.2 to 0.5 mm/yr, depending on the fault block. Incision rates between 1.1 and 0.6 Ma apparently were higher, ranging from 0.3 to 0.7 mm/yr depending on the fault block and subject to the uncertainty of the age difference between the flow sequences. Incision rates between deposition of the 2.8 Ma and 2.1 Ma remnants and the 1.1 Ma flow sequence are the lowest, about 0.1 mm/yr.

When combined with incision rates, the elevation of the volcanic remnants with respect to the inferred pre-uplift Tertiary erosion surface provide a basis for estimating the onset of incision. The elevation of the base of the oldest volcanic remnants in the North Fork canyon below the erosion surface reflects the amount of incision prior to the deposition of these volcanic rocks. The minimum age of the onset of incision can be estimated by extrapolating incision rates between the oldest two volcanic units in a fault-bounded block from the elevation of the erosion surface to the base of the oldest volcanic unit. Incision at the onset of uplift undoubtedly was slower than between the intervals of 2.1 to 1.2 Ma and 2.8 to 1.2 Ma because of the small amount of initial tilting. Hence, extrapolations should yield a minimum age of the onset of uplift. However, another uncertainty related to this calculation is how much relief existed prior to the onset of major uplift. If this relief was significant, the onset of uplift may be *younger* than estimated. The two fault-bounded blocks with the best set of volcanic remnants extend from the Waller Creek fault to confluence of the East Branch, and between the Davis Creek and Meeker Bar faults (Figure 2). Incision rates and elevations below the pre-uplift erosion surface in these fault blocks suggest that the uplift began prior to 3.3 to 3.4 Ma (2.1 Ma oldest remnant) in the Davis Creek to Muleshoe Mine fault block and prior to 4.6 to 4.7 Ma. (2.8 Ma oldest remnant) in the vicinity of the confluence of the North Fork and East Branch. We believe the 4.6 to 4.7 Ma estimate is the better approximation the minimum age of onset of incision because it is based on incision rates constrained by an older volcanic remnant (2.8 versus 2.1 Ma). This age is consistent with other estimates for uplift initiation derived from other parts of the range (e.g. Unruh, 1991).

As the Sierra Nevada was progressively uplifted, stream gradients, and consequently downcutting power and incision rate, are expected to have increased progressively with time. The incision rate between 1.1 and 0.6 Ma was notably higher for a given fault block than pre-1.1 Ma rates, as might be expected from progressive uplift. However, the incision rate from 1.1 to 0.6 Ma also is faster than the post-0.6 rate. The relative decrease in post-0.6 Ma incision rate may be a consequence of one or a combination of: (1) deceleration of uplift rates since 0.6 Ma; (2) significantly lower post-0.6 Ma flow volumes in the North Fork and/or (3) post-0.6 Ma changes in local faulting patterns; (4) erosive processes that have balanced uplift rates; (5) migration of a knickpoint through the reach of river studied. With existing data it is not possible to evaluate whether or not uplift has decelerated within the last 0.6 Ma. Paleogeography of the region indicates that the drainage basin did not change in size significantly within the last 0.6 Ma, thus flow should not have decreased in the river. Whether or not deceleration of incision rates is a consequence of migration of a knickpoint or the balancing of erosive and uplift processes cannot be evaluated with existing data. The North Fork transect examined in this study is east of the present-day Sierra Nevada crest. Faulting along the Frontal fault system may have stepped westward in the past 600 ka. Westward partitioning of down-east faulting, and associated tilting, may have decreased the average gradient of the reach of the river between the Almanor basin and the present crest of the Sierra Nevada (5 to 10 km downstream of the downstream end of the profile shown in Figure 3), resulting in a decrease in incision rates As noted earlier, several faults that transect the North Fork canyon apparently initiated

movement after 0.6 Ma. On a more regional scale, westward migration the western margin of the Basin and Range province has been suggested by Dilles and Gans (1995) and Slemmons et al. (1979), based on the timing of faulting along the Sierra Nevada-Basin and Range boundary.

In conclusion, there are several permissible causes for the post 0.6 Ma deceleration of incision rates of the North Fork. Further studies may help discriminate between the various mechanisms and provide important insight into the neotectonic evolution of the Sierra Nevada-Basin and Range boundary zone.

37

REFERENCES

Dilles, J.H., and Gans, P.B., 1995, The chronology of Cenozoic volcanism and deformation in the Yerington area, western Basin and Range and Walker Lane: Geologica Society of America Bulletin, v. 107, p. 474-486.

Durrell, C., 1987, Geologic history of the Feather River country, California: Berkeley, University of California Press, 337 p.

Ely, R.W., 1992, Late Cenozoic uplift and faulting of the Sierra Nevada in the vicinity of Stanislaus Table Mountain, California: Geological Society of America, Abstracts with Programs, v. 24, p. 22.

Grant, T.A., McCleary, J.R., and Blum, R.L., 1978, Correlation and dating of geomorphic and bedding surfaces on the east side of the San Joaquin Valley using dip: in Singer, M.J., ed., Soil development, geomorphology and Cenozoic history of the northeastern San Joaquin Valley and adjacent areas, California: Guidebook for joint field session, American Society of Agronomy, Soil Science Society of America, and Geological Society of America, University of California Press, Davis CA, p. 312-318.

Guffanti, M., Clynne, M.A., Smith, J.G., Muffler, L.J.P., and Bullen, T.D., 1990, Late Cenozoic volcanism, subduction, and extension in the Lassen region of California, southern Cascade range: Jour. Geophys. Res., v.95, p. 19453-19464.

Lydon, P. A., Gay, T. E., and Jennings, C. W., (compilers), 1960, Westwood Sheet, Geologic Map of California: California Division of Mines and Geology Map, Scale 1:250,000.

Page, W. D., and Sawyer, T. L., 1992, Tectonic deformation of the Lovejoy Basalt, a late Cenozoic strain gauge across the northern Sierra Nevada, California: EOS v. 73, no. 44, p. 590.

Page, W.D., Gilliam, M.L., McCleary, J.R., Lambert, R.S., and Blum, R.L., 1978, near Sonora, California:Earthquake Notes, Eastern Section, Seismological Society of America, v. 49, no. 1, p. 90.

Page, W. D., Sawyer, T. S., McLaren, M. , Savage, W. U., and Wakabayashi, J., 1993, The Quaternary Tahoe-Medicine Lake trough: the western margin of the Basin and Range transition, NE California: Geological Society of America , Abstracts with Programs v. 25, p. 131.

PG&E, 1995, Late Cenozoic faults within the northern and central Sierra Nevada, California: unpub. report to California Dept. Water Res., Division of Safety of Dams.

Sawyer, T.L., Page, W.D., and Hemphill-Haley, M.A., 1993, Recurrent late Quaternary surface faulting along the southern Mohawk Valley fault zone, NE California: Geol. Soc. Amer. Abstr. with Prog., v.25, p. 142.

Slemmons, D.B., Van Wormer, D., Bell, E.J., and Silberman, M.L., 1979, Recent crustal movements in the Sierra Nevada-Walker Lane region of California-Nevada: Part I, rate and style of deformation: Tectonophysics, v. 52, p.561-570.

Unruh, J.R., 1991, The uplift of the Sierra Nevada and implications for late Cenozoic epeirogeny in the western Cordillera: Geological Society of America Bulletin, v. 103, p. 1395-1404.

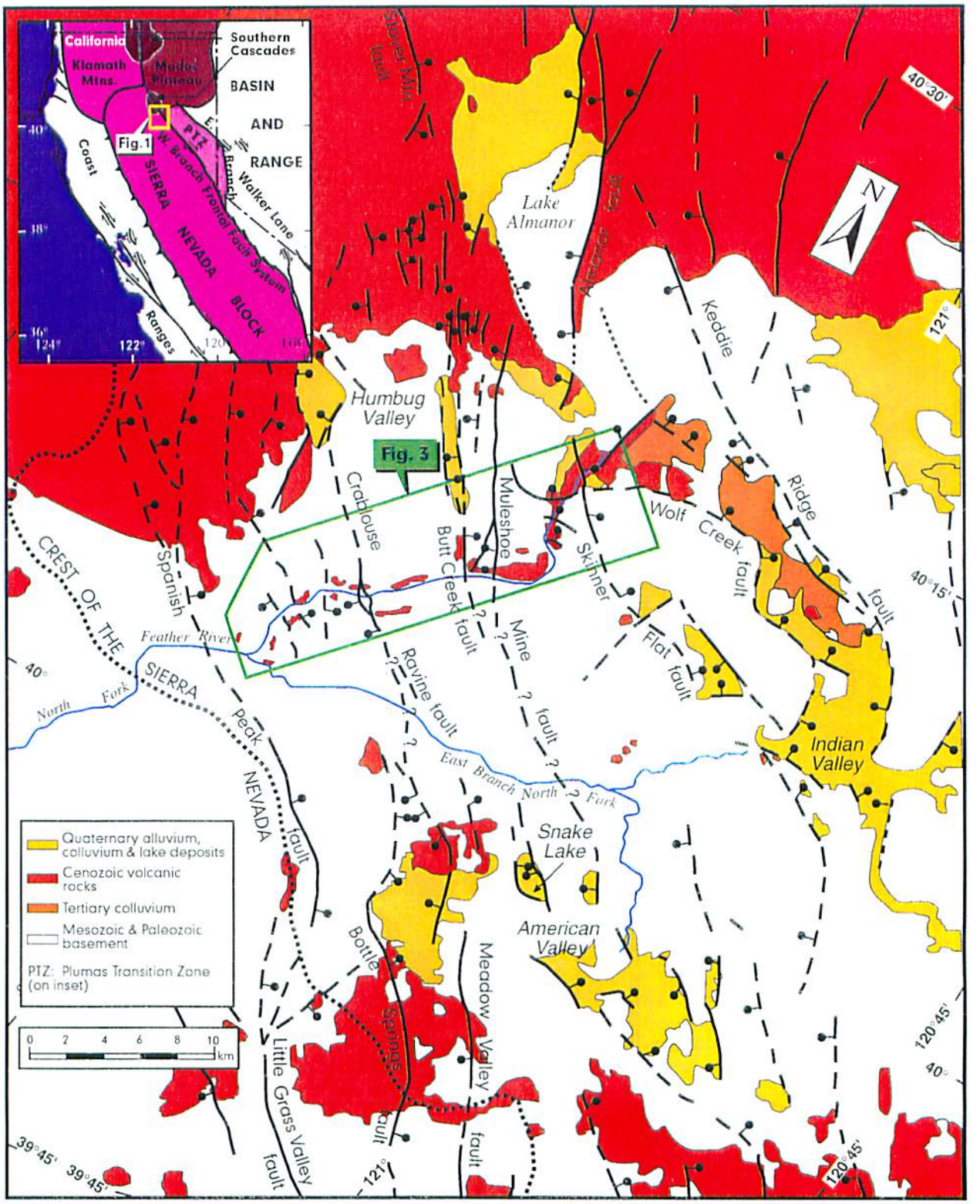

Figure 1. Geologic map of Lake Almanor region.

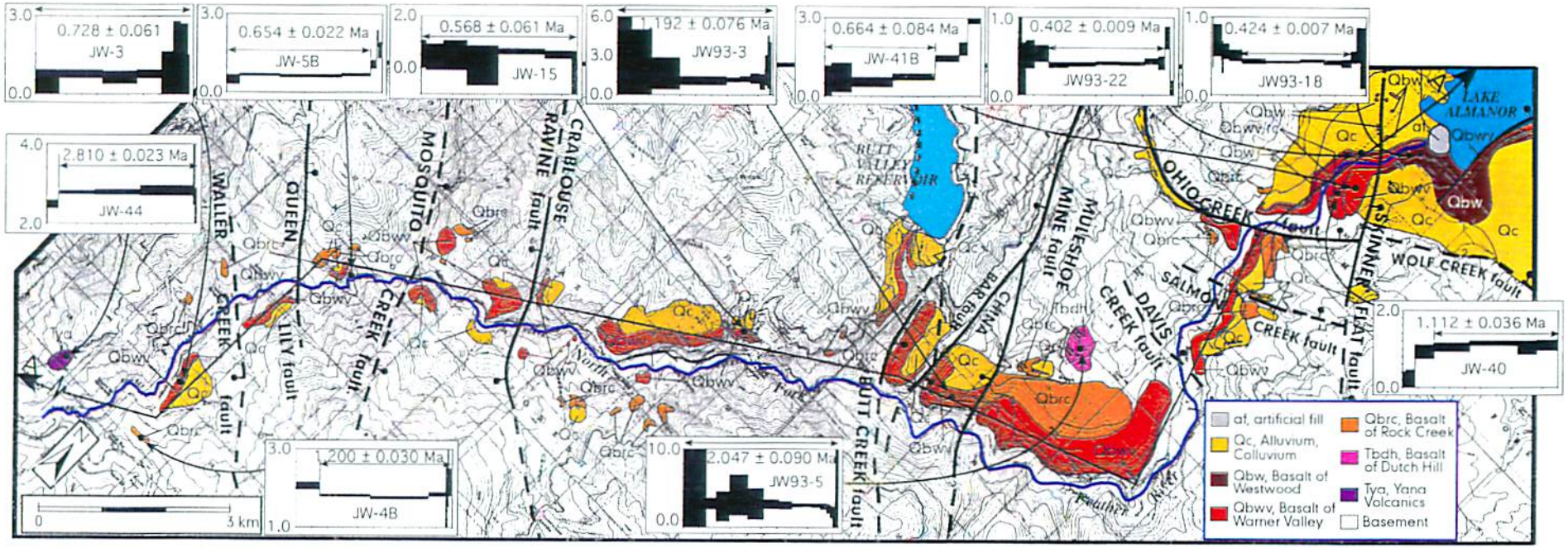

Figure 2. Geologic map of North Fork Feather River canyon.

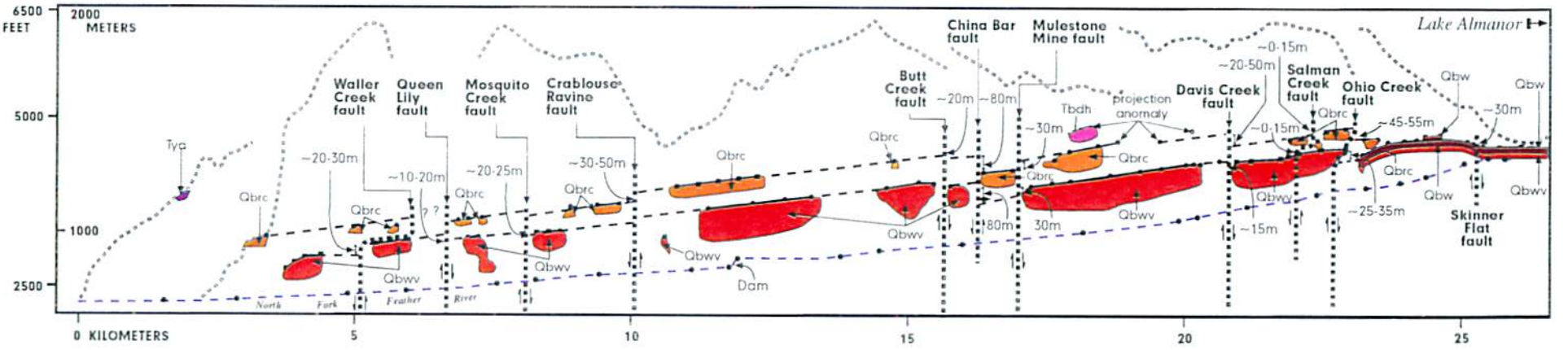

Figure 3. Profile of basalt flows in North Fork Feather River canyon.

APPENDIX 3 - 2A

A. Trenching study of the Skinner Flat fault at the Rush Hill Motorway site.
Simpson, G.D., Knudson, K.L., and Drouin, P.E.

Trenching study of the Skinner Flat fault at the Rush Hill Motorway site

Gary D. Simpson, Keith L. Knudsen, Patrick E. Drouin
William Lettis & Associates

1.0 INTRODUCTION

The Skinner Flat fault strikes N55W to N60W and has a mapped length of between 9 and 16 km. The fault is mapped based on the apparent offset of the 410 ka basalt of Westwood near Skinner Flat. At this site, an approximately 30-m-high gently-sloping escarpment extends for about 2.5 km. The fault appears to die out at bedrock hills north of Skinner Flat, although faint photolineaments have been mapped across the ridgeline. The southern terminus of the Almanor fault lies 1 to 2 km to the north and we note the similarity between the strikes of the Almanor and Skinner Flat faults. To the south of Skinner Flat, the fault is defined within metasedimentary bedrock in steep, mountainous terrain by subtle geomorphic expression that includes aligned topographic saddles, linear hill-fronts and linear slope breaks. The most prominent geomorphic feature south of the North Fork Feather River is a small alluvial basin bordering a strong photolineament along the trend of the fault. The Rush Hill Motorway trench locality is along the southwestern margin of this alluvial basin.

The Rush Hill Motorway trench locality was selected because of the apparent tectonic origin of the valley and the likelihood that the fault forms a bedrock sill that may tectonically impound the basin after surface-rupturing earthquakes. The presence of Quaternary alluvial deposits in the basin provides valuable stratigraphic relations that aid in the interpretation of the fault history of the site. Alluvial deposits also offer a high likelihood of yielding datable materials. Trenches were located based on the following considerations:

- To encompass the linear slope break on the hillside along the southwestern valley margin and the valley floor to document the relationship between hillslope colluvium and valley fill alluvium.

- To confirm the presence of a bedrock sill and the distribution of alluvial units at the basin outlet.

2.0 SITE DESCRIPTION AND APPROACH

Our trenching investigation at the Rush Hill Motorway site focuses on the northeast-facing slope of the southwestern valley margin and the adjacent stream channel at the basin outlet (Figure 1). The southwestern valley margin is the steepest and highest valley wall bounding the basin and is marked by a prominent linear slope break. The Skinner Flat fault has been mapped across a saddle north of the basin, and along the southwestern valley margin. The basin is semi-circular in plan view shape.

An ephemeral stream fed by a small drainage area flows into the northeast corner of the basin. No well-developed channel is presently established across the floor of the basin, so flow across the basin may largely occur in the subsurface. The basin has been logged in the past and the basin floor appears to have been extensively modified. The basin drains through a narrow gorge in the southwestern corner over a shallow bedrock sill.

Bedrock in the vicinity of the Rush Hill Motorway site consists of Mesozoic-Paleozoic metasedimentary rocks. Outcrops around the basin consist of schistose metasediments exhibiting strong foliation and abundant folding. Bedrock in the near-surface is frequently deeply-weathered and is locally saprolitic.

In order to assess the location and character of the Skinner Flat fault and the timing of past earthquakes, we excavated four (4) trenches and two (2) test pits at the Rush Hill Motorway site (Figure 1). Two of the trenches form the basis of our conclusions at the site, and will be discussed here. Trench RHM-1 extended 57 m down the hillslope along the southwestern valley margin (Figure 1). This trench extends from the slope break high on the hillside to the valley floor. A 35 m long trench was also excavated from the outlet channel to the northeast into the valley floor. For the purposes of this discussion, we refer to this trench as the "Stream channel trench" (Figure 1).

3.0 RESULTS

Trench RHM-1 exposed shallow metasedimentary bedrock beneath the southwestern valley margin. Bedrock is just over 1 m deep at the uphill end of RHM-1 and deepens gradually downslope under a thickening colluvial profile. A minimum of six discrete colluvial units were exposed within RHM-1. The oldest colluvium is preserved only locally on the upper part of the hillslope as isolated remnants. Two colluvial units of intermediate stratigraphic position are present only at the base of the hillslope, extending only a short distance upslope. Progressively younger colluvial layers extend farther upslope, with only the active layer reaching the upslope end of the trench. This relationship records a tendency for stripping of colluvium from the upper slope and redeposition at the base of the hillslope. At least one unconformable contact is present within the colluvial profile, beneath the second youngest unit. This unit truncates a buried soil developed on the underlying colluvial layer.

Analysis of soil profile development at two locations in the trench suggests that, with the exception of the oldest colluvium, colluvial material in trench RHM-1 is no older than about 60,000 years old. At the time of this report, the oldest colluvial remnants had not been analyzed. Based on the relative increase in clay films and redness, however, this older colluvial material appears to be well in excess of 100,000 years old.

At least three faults were exposed within RHM-1. Two of these faults are exposed near the upslope end of the trench, at the geomorphic slope break; one is about 25 m downslope. The faults are generally irregular (i.e, non-planar), and to varying degrees remineralized. The remnants of the older colluvial material is restricted in trench RHM-1 to the areas immediately above the two upper fault zones. Locally this colluvial material appears to fill fissures; this is especially true in the upper most fault, which appears to be a fissure that extends beyond the base of the trench exposure.

The faults in trench RHM-1 are associated with steps in the upper surface of bedrock on the order of 0.5 to 1.0 m. The total vertical displacement recorded by the three principal faults is somewhat speculative due to the irregularity of the bedrock surface, but is probably between 2 and 3 meters. The faults in trench RHM-1 strike N25°W to N30°W and dip steeply (51° to near-vertical) to the northwest. No shearing or rotation of clasts is apparent in the colluvium overlying the faults, suggesting that faulting in trench RHM-1 pre-dates the oldest colluvium on the hillside.

The stream channel trench confirms the presence of the bedrock sill at the basin outlet (Figure 2). At the western (downstream) end of the trench, bedrock is less than 0.5 m deep beneath a thin veneer of mixed alluvium and colluvium. An abrupt bedrock step is formed by the Skinner Flat fault along the projection of the geomorphic slope breaks on the hillsides southeast and northwest of the outlet channel. Bedrock is not exposed anywhere in our excavations in the valley east of the bedrock step at the fault crossing.

A broad, 2.5 to 3.5 m fault zone is present at the bedrock step, confirming the tectonic origin of the sill and the adjacent valley (Figure 2). The fault zone is characterized by

two discrete zones, one a zone of vertically imbricated metasedimentary clasts consistent with the adjacent bedrock, and one a zone of quartz and metachert boulders unlike the adjacent bedrock. Individual fault planes and polished or slickensided surfaces are not present within the fault zone. Rather, faults are inferred by abrupt vertical and near vertical contacts and by zones characterized by loose, imbricated clasts.

Faulted against the east side of the cobble and boulder fault zones is a boulder-rich colluvium (unit C1 on Figure 2). East of the fault zone, the faulted colluvium dips steeply eastward beneath a thick sequence of alluvial deposits. The colluvium extends approximately 14 meters east, where it appears to overlie an older alluvial deposit (unit A5 on Figure 2). The alluvial profile overlying the faulted colluvium consists of four alluvial deposits, including the active alluvial layer. Progressively younger alluval layers on-lap farther west onto the east-dipping colluvial surface. The total thickness of alluvium overlying the faulted colluvium is approximately 4.25 meters. The oldest alluvial deposit overlying the faulted colluvium is strongly mottled with manganese, suggesting considerable antiquity. Analysis of soil profile development within the alluvium in the stream channel trench will be conducted in the future.

4.0 DISCUSSION

The age of faulting along the Skinner Flat fault at the Rush Hill Motorway trench locality is constrained by the youngest clearly faulted deposit, the faulted colluvium in the stream channel trench (unit C1), and by the oldest unfaulted deposit, alluvial unit A2 (Figure 2). The age of the unfaulted colluvium in trench RHM-1 may also help constrain the timing of the most recent movement on the Skinner Flat fault. The ages of deposits at the Rush Hill site is not known at present, but radiocarbon analysis of charcoal from several deposits is being conducted at this time.

The style of faulting at the Rush Hill site appears to be a combination of down-to-the-northeast normal and right-lateral displacement. Evidence for normal motion is the presence of the bedrock sill and the adjacent down-dropped alluvial basin, and the presence of several distinct bedrock steps in trench RHM-1. The evidence for right-lateral motion at the site includes the high-angle nature of several of the faults, and the presence of a quartz-rich boulder deposit within the fault zone. The quartz boulder zone is unique in that it is monolithologic, and contains none of the adjacent metasedimentary bedrock. The boulders could not have been deposited as colluvium adjacent to an existing bedrock scarp since some of the adjacent bedrock would have been incorporated into the deposit. We therefore infer that the quartz boulder zone has been tectonically "rolled" along the fault (e.g., tectonic ball-bearings). Since metachert and quartz boulders are seen only on the hillside north of the outlet channel, the quartz boulders in the fault zone are evidence of right-lateral motion on the fault.

From the fault exposure in the stream channel trench, faulting to the south on the hillside becomes distributed. A minimum of 4.5 meters of apparent vertical displacement is recorded by our excavations, from the bedrock sill to the deepest point we have reached in the valley. The depth of the valley fill is not known. The faults exposed in the hillside trench, however, account for no more than 2 to 3 meters of vertical displacement. Other faults, therefore, may be present beneath alluvium east of trench RHM-1. The geometry of the basin suggests that a fault may be present along the valley margin, which diverges to the southeast from the traces of the Skinner Flat fault shown on Figure 1.

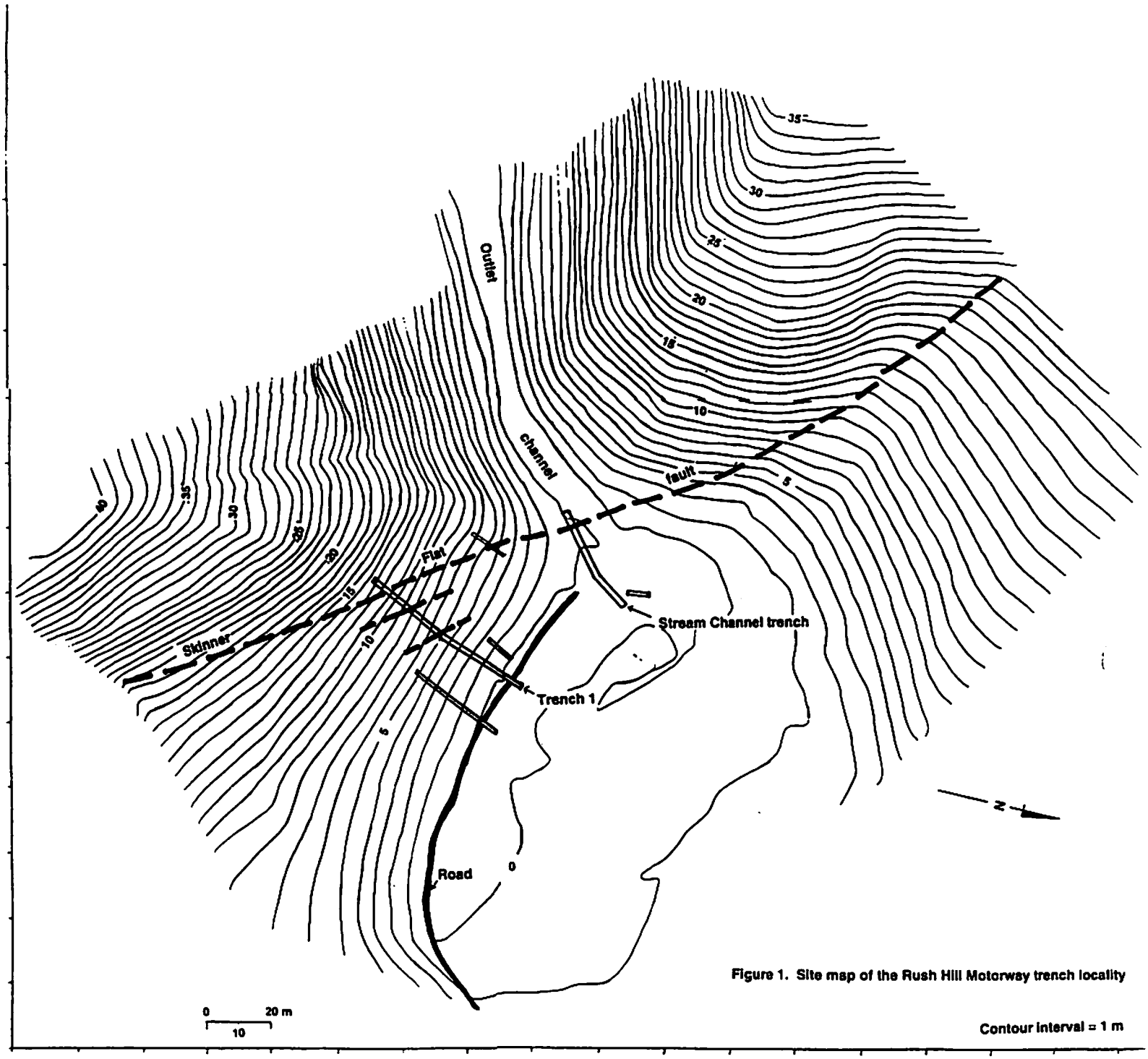

Figure 1. Site map of the Rush Hill Motorway trench locality

Contour interval = 1 m

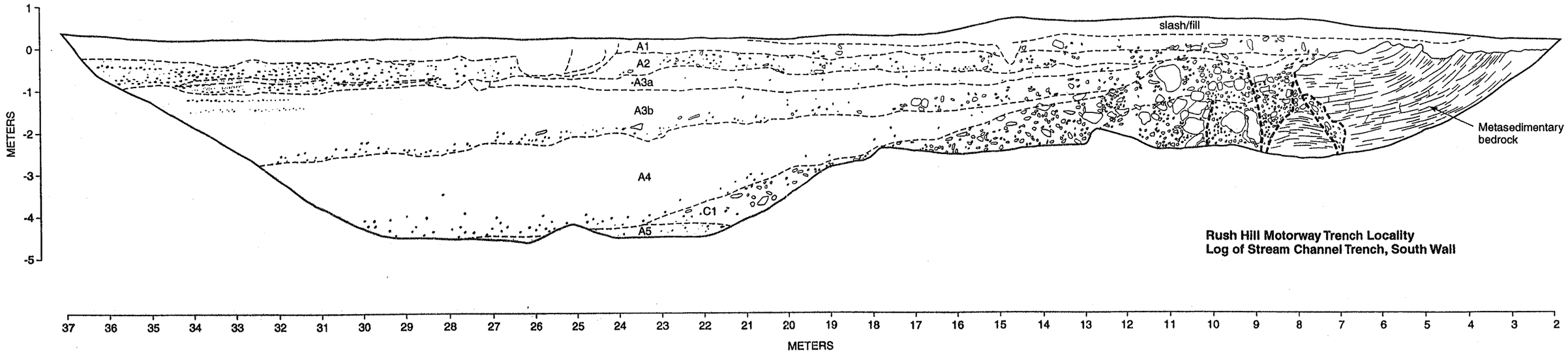

UNIT DESCRIPTIONS

A1. SILT, with very fine sand and minor gravel. Reddish brown (5YR 5/4, d). Massive, variable hardness, clast size from 1 cm to 5 cm. Roots and krotovina abundant. Basal contact sharp to obscure and smooth. Unit often capped by forest litter/ logging debris.

A2. GRAVEL TO GRAVELY SILT, eastern portion of trench - sandy, silty gravel; western portion - sandy, gravely silt. Gray (5YR 6/1, d). Soft, poorly cemented, dry. Silt and clay lenses in east portion of trench. Clasts are angular to subangular metasediments and range up to 25 cm in size. Clasts are imbricated. Gravel content and imbrication decrease towards west end of trench. Basal contact is sharp/clear and smooth.

A3a. SILT, with very fine sand and clay. Reddish brown (5YR 4/4, m). Moist, platy, soft, occasional gravel clast, blocky. Minor Mn staining. Basal contact obscure.

A3b. SILT, with clay and very fine sand, minor gravel. Dark reddish brown (5YR 4/3, m). Moist, massive, soft, subangular to blocky, gravel content increases down section. Gravel clasts mostly 1-2 cm, some 10-30 cm. Minor mottling by Mn. Basal contact sharp/clear and smooth.

A4. CLAYEY SILT, with very fine sand and gravel. Dark reddish brown (5YR 3/3, m). Moist, massive, soft, subangular to blocky, gravel content increases down section, intensely mottled. Mottling is dark brown to black (10R 2.5/1) and increases down section. Mn clasts present. Basal contact very gradational.

C1. GRAVEL, matrix is silt and clay with very fine sand. Dark reddish brown (2.5 YR 3/4, m). Moist, massive, soft. Intensely mottled dark brown to black (10 R 2.5/1). Clast size ranges from 1 cm to boulders (>30 cm) and increases towards the west. Clasts are angular to subangular metasediments. Basal contact obscure.

A5. CLAYEY SILT, with coarse to fine sand and gravel. Grayish brown (5YR 4/2, m). Moist, massive, soft, subangular to blocky. Gravel clasts are <1 cm to 5 cm.

Figure 2. Log of south wall of Stream Channel Trench at the Rush Hill Motorway trench locality.

APPENDIX 3 - 3

A. Tectonic deformation of the Lovejoy basalt, a late Cenozoic strain gage across the northern Sierra Nevada and Diamond Mountains, California.
Page, W.D., Sawyer, T.L., and Renne, P.R.

TECTONIC DEFORMATION OF THE LOVEJOY BASALT, A LATE CENOZOIC STRAIN GAGE ACROSS THE NORTHERN SIERRA NEVADA AND DIAMOND MOUNTAINS, CALIFORNIA

William D. Page, Thomas L. Sawyer, and Paul R. Renne

ABSTRACT

The Miocene Lovejoy Formation consists of a group of five to 15 basalt flows that we have dated at 16 million years by the Ar-Ar step heating method. Extensive remnants of the basalt extend in a narrow zone southwesterly for 120 km from Honey Lake across the Diamond Mountains, Grizzly Ridge, and the Sierra Nevada near Quincy to Oroville in the Central Valley. The basalt is a distinctive stratigraphic marker because of its resistance to erosion and its position at the base of the ancestral valley of the Feather River.

The Lovejoy Formation makes an excellent strain gage to measure late Cenozoic uplift and faulting. A profile of the top of the lava documents: 1) vertical displacement of 900 to 1,000 m along the Honey Lake fault zone at the front of the Diamond Mountains; 2) a broad downwarp and minor faulting between Grizzly Ridge and the Diamond Mountains; 3) displacement of about 1180 m of the Mohawk Valley graben east of the Sierra Nevada and west of Grizzly Ridge; 4) westward tilting of the Sierra Nevada to about 24 m/km; 5) a westward flexure at Chico monocline, and 5) within the Sierra Nevada, vertical displacement on several faults and differential tilting between fault strands; individual faults are normal have down-on-the-east and down-on-the-west displacements of a few tens of meters to over 100 meters. The style of deformation of the Lovejoy basalt is very similar to that recorded in the central Sierra Nevada where regional tilting to about 18 m/km and faulting of up to 30 m along individual, short faults have been noted in the 9 million year old latite of the Tuolumne Table Mountain on Stanislaus River near Sonora.

INTRODUCTION

The Lovejoy Formation is a group of basalt flows that extend southwest for 120 km from near Susanville in the Honey Lake Valley and into the Sacramento Valley (Figure 1). Rather extensive remnants cropout in a narrow band from near the source of the flows at the east end of

Stony Ridge (west of Honey Lake), through the Diamond Mountains and northern Mohawk Valley south of Quincy, and across the Sierra Nevada north of La Porte to Oroville. In the Sacramento Valley basalt remnants are known from drilling and exposures on the margins of the valley from Chico and Orland Buttes on the north to Putnam Peak near Vacaville on the south (Durrell, 1959). Because the depositional surface of the flows originally sloped gently to the southwest and was generally planar, the formation makes an excellent strain gauge to identify and quantify late-Cenozoic tectonic deformation of the region since its deposition 16 million years ago (Savage and others, 1991; Page and Sawyer, 1992). The lava flows are distinctive and mark its ancient depositional course that followed an ancestral valley of the Feather River (Durrell, 1987).

Acknowledgments - Our investigations of the Lovejoy Formation were done from 1989 to 1993 as part of PG&E's Hydro Earthquake Hazard Project to help evaluate the seismic sources for PG&E's dams and other facilities in the Sierra Nevada. W. Lettis, J. Wakabayashi, and D. Wagner discussed the issues with us and we appreciate their comments.

TECTONIC SETTING

The Lovejoy Formation crosses three tectonic provinces: the mountains of the Plumas transition zone, the Plumas trench at Mohawk Valley, and the Sierra Nevada (Figure 2). The Plumas transition zone is the mountainous region between the Diamond Mountains and the eastern branch of the Sierra Nevada frontal fault system at Honey Lake and Grizzly Ridge and the Plumas trench. The Plumas trench (Durrell, 1987) is a graben in the Mohawk Valley and part of the right-stepping, en echelon tectonic depressions that extend from Lake Tahoe to into Oregon (Page and others, 1993). The northern Sierra Nevada is a west-tilted major mountain range that is bounded on the east by the western branch of the eastern Sierra Nevada frontal fault system and on the west by the Central Valley and Coast Ranges.

The region is being stresses by right shear that reflect northwestward movement of the Pacific plate with respect to the North American plate. Right slip faulting is documented along the Walker Lane belt and crustal extension is occurring in and to the west of the Basin and Range. The Lovejoy region records scattered seismic events; including a broad northwest-trending swath of dominantly shallow seismicity with depths less than 15 kilometers that is concentrated along and west of the Plumas trench.

The basement (pre-Cenozoic) rocks of the Lovejoy region comprise a collage of Paleozoic and Mesozoic metamorphic and igneous rocks (Saucedo and Wagner, 1992). In the early Tertiary (60 to 15 million years ago) erosion had lowered and reduced the mountains and hills in the present Lovejoy region to a low terrain that had deep weathering. The Lovejoy lavas were deposited in the ancient valley and canyon that was eroded into the old erosion surface. The formation was moderately eroded prior to burial of the region by volcanic agglomerates and flows of the Mehrten (Penman) and other formations in the late Tertiary. The current tectonic regime produced the features that dominate the present topography. It commenced after the Miocene volcanic phase, about 5 million years ago in the northern Sierra Nevada (Unruh, 1991). Since the recent phase of uplift, the Lovejoy Formation has been exhumed and eroded and commonly stands in inverted topography.

DISCUSSION

Methodology - We constructed the profile on the Lovejoy Formation from U.S. Geological Survey 1:24,000 topographic maps (20 to 40 foot contours) and used a 4 times vertical exaggeration. The Lovejoy Formation was plotted on the profiles using the existing geological maps (Saucedo and Wagner, 1992, Hietanen, 1981, and Grose and others, 1989). The profile follows straight line segments between Lovejoy remnants to help avoid projection anomalies and yet approximate the thalweg of the ancient canyon and valley in which the basalt was deposited. The Lovejoy Formation, nearby ridge crests, geographic landmarks, and adjacent rivers and streams were projected perpendicular to the line of profile. The base of the Lovejoy Formation, faults, rock types and other geologic information was projected to the profiles and adjusted slightly to best show geological relationships with respect to the surface anomalies. The Lovejoy Formation outcrops and the anomalies on the profiles were checked in the field from a helicopter and at selected places on the ground.

We analyzed the profiles for geomorphic anomalies that are potentially caused by tectonic faulting: We consider that a step on the top of the Lovejoy flows, particularly a down-on-the-east step because it is counter to the regional flow direction of the basalt, indicated potential faulting. Our confidence that the step anomaly was caused by faulting increased when the step is accompanied by a change in slope on the surface of the basalt on either side of the anomaly, by fracturing or a narrow eroded zone in the basalt at the anomaly, the occurrence of a bedrock fault at the anomaly, and/or a similar step at the base of the flows. In some cases field reconnaissance confirmed offset of the top, porphrytic flow. Abrupt changes in the direction on the

reconstructed thalweg were used to infer lateral offsets and areas where the lava filled tributary valleys and may have overtopped local drainage divides.

Assumptions and Limitations - We made several assumptions in our evaluation of the tectonic deformation of the Lovejoy Formation. First, the Lovejoy Formation was deposited over a short time period, probably less than a few tens of thousands of years, because little soil development or other deposits are evident between the flows and the tops of the individual flows remain vesicular and little weathered (Durrell, 1959; Siegel, 1988). The clustering of Ar-Ar and many of the K-Ar dates support this assumption.

Second, although the Lovejoy Formation is 16 million years old, we assume that the deformation recorded by the Lovejoy basalt mostly occurred in the current tectonic regime, after 4 to 6 million years ago, because the overlying Mehrten Formation agglomerates were deposited across the Sierra Nevada, Mohawk Valley and Grizzly Ridge from sources near and east of the range front (Durrell, 1987); also the displacements by faults in the Mehrten Formation are about the same as those of the Lovejoy Formation.

Third, the top of Lovejoy basalt after deposition formed a rather smooth, but narrow, planar surface, similar to a graded river profile, making an excellent marker. Where flows other than the top, porphyritic flow are preserved on each side of a fault, the same flow is assumed to be present on either side of the fault. In the places where this assumption is incorrect, the estimated displacement could lead to errors of up to 100 meters or more and is the most significant of the potential errors. In contrast, the base of Lovejoy conforms to an old valley and canyon surface that it filled and, hence, it is a irregular surface (Durrell, 1959; Siegel, 1988) that can be used as a stratigraphic marker only where detailed mapping of the contact has been done to insure that the anomalies are not depositional margins.

The direction of the profile is approximately perpendicular to the strike of the faults and parallel to the tilt direction. Therefore, the displacement and slopes measured from the profiles closely approximate the actual anomalies in most cases. The resolution of the technique allows the identification of anomalies of that are generally more than 10 to 15 meters high (within one half to one contour interval (± 7 to ± 13 m (20 to 40 ft)). Similarly changes in gradient of more than about -- m/km are also interpreted to be due to tectonic deformation. We recognize, however, that changes in gradient, alternatively, can be caused by depositional factors, such as a constriction in the canyon resulting in hydraulic damming and by erosion.

The approximation of the thalweg by straight segments appears to be reasonable because in cross section the formation is commonly a narrow channel fill and the general trend of the formation in the mountains is mildly curved in a fairly narrow , 4- to 6-km-wide zone. We estimate that small changes in gradient of 6 to 10 m could be attributed to deposition variations or to projection anomalies because the profile does not precisely follow the ancient thalweg.

Although we believe that the anomalies we have identified are faults and tectonic flexures, we recognize that each anomaly needs to be confirmed by field mapping and/or other investigations. For example, we have trenched the Little Grass Valley (Dogwood Peak) fault near Dogwood Peak and confirmed faulting of the Lovejoy and Mehrten formations as well as late Quaternary deposits (Page and Sawyer, 1995, in preparation).

LOVEJOY FORMATION

Durrell (1959) defined the Lovejoy Formation ("older basalt" of Turner, 1896) as the distinctive sequence of up to 15, resistant, olivine basalt flows that crop out in a narrow belt from Honey Lake to the Sacramento Valley. He named the formation from the outcrops along Lovejoy Creek in the mountains east of Mohawk Valley and Grizzly Ridge and placed the type locality -- km to the east in Red Clover Creek where the outcrops were more extensive. Fresh Lovejoy basalt is black with brown weathered surfaces and generally scarce vesicles. It is a very hard rock that is intensely jointed with irregular, curved, interlocking fractures, and locally columnar joints. The resistant basalt forms distinctive outcrops. The top of the deposit is commonly flat with a stone covered surface and a scarcity of vegetation. The margins of erosional remnants commonly form near-vertical cliffs flanked by talus slopes. In many places the deposit is in reverse topography where the flat top of the formation forms the ridge crest or a tableland, such as Stony Ridge, Mooreville Ridge and Oroville Table Mountain.

Durrell (1959) grouped the flows into two general types: a glassy rock with microscopic needles of apatite and a microcrystalline rock with lilac-colored augite microliths. Only the top flow can be differentiated in the field from the other flows because it is porphyritic. The Lovejoy basalt is typical of a continental flood basalt with has distinctive trace element concentrations that are identical over the geographic range of the formation (Siegel, 1988).

The source of the Lovejoy flows appears to have been at the east end of Stony Ridge, southeast of Thompson Peak, where a source dike is exposed (Roberts, 1985; Wagner, 1992, oral communication), and perhaps additionally farther east in the Honey Lake area (Durrell, 1959).

The formation is thickest in the northeast and thins to the southwest: 200 m thick with 15 flows at the east end of Stony Ridge; over 180 m thick with 9 flows at Red Clover Creek; 90 m thick with 7 flows at Oroville Table Mountain; and 1 to 115 m thick in the Sacramento Valley (Durrell, 1959; Siegel, 1988). Only two flows are exposed at Putnam Peak.

The remnants of the basalt indicate that the flows were deposited in a narrow (a few km wide) valley or canyon that extended southwest from the Honey Lake area across the ancestral Sierra Nevada between the present South Fork and Middle Forks Feather River into the Central Valley (Durrell, 1959). In places the flows backfilled into tributary drainages and overtopped low drainage divides. For example a secondary branch followed a channel in the Middle Fork Feather River area from near Dogwood Peak to North Table Mountain, north of Oroville. A minor branch, or ponding in a tributary, appears to have accumulated west from near Camel Peak to Cascade. From Oroville the flows spread out into the Sacramento Valley and covered a broad region from Chico and Orland Buttes on the north to Putnam Peak on the south (Durrell, 1959; Van Den Berge, 1968; Siegel, 1988).

Age of the Formation - The age of the Lovejoy Formation has been argued, at times fiercely, over the past 30 years. Because the Lovejoy Formation was deposited in a channel and some of the later deposits were also laid down in channels that are cut into or below the Lovejoy basalt, the precise stratigraphic relationships tend to be elusive and different investigations have placed its age as Eocene, Oligocene or Miocene. The basalt generally overlies granitic and metamorphic basement rocks and "auriferous" gravel (Eocene) in the mountains between Honey Lake and the Sacramento Valley (Table 1). At Oroville Table Mountain it overlies a Miocene dacite tuff and andesite breccia. Between the Diamond Mountains-Grizzly Peak the Lovejoy Formation is topographically below, and hence appears to underlie the adjacent the Oligocene volcanic rocks of the Delleker Formation, but this relationship is probably a cut and fill (Saucedo, 1995 oral communication). In the Sacramento Valley the Lovejoy overlies the Eocene Markley and Ione formations, and alluvial deposits of the Oligocene (?) Nord Formation of Van Den Berge (1968). In the mountains the Lovejoy Formation is overlain by the Miocene basalt of Thompson Peak and Mio-Pliocene volcaniclastic deposits of the Mehrten and equivalent Penman formations. In the Sacramento Valley it is overlain by the Miocene Neroly and Mehrten formations, and the Pliocene Tehama and Tuscan formations.

Durrell (1959, 1987) argued that the Lovejoy Formation is upper Eocene, but neither Dalrymple (1964) nor Siegel (1988) could confirm the stratigraphic relationships that Durrell (1959)

inferred in a hydraulic mining quarry at La Porte in the Sierra Nevada. Saucedo and others (1992) reevaluated the existing potassium argon dates on the Lovejoy Formation (ranging between 3 and 18 million years) (Table 2) and other volcanic formations in the region as well as the position of the Delleker Formation at Red Clover Creek; they estimated the age of Lovejoy Formation as 11.8 to 14 million years.

Eight additional conventional K-Ar whole-rock dates were analyzed for our study (Table 2). Six of these cluster between 15 and 16 million years (average 16.1 million years). The remaining two dates on the basalt at Little Grass Valley Reservoir are at about 4 million years; although the basalt appears to be the Lovejoy Formation, it may be a similar, but younger basalt. In order to confirm the age of the Lovejoy Formation, we analyzed three, widely-spaced samples by the argon-argon step-heating (Table 3). The three dates average at 15.9 million years (Table 3). This age is consistent with the many of the K-Ar dates and with its stratigraphic position. We conclude that the Lovejoy Formation is about 16 million years old.

RESULTS

The major observations of the analysis of the profile (Figure 3-3a to 3d) are compiled presented below. The details are shown on Table 4. The profiles clearly show that since deposition, the Lovejoy Formation has been deformed somewhat differently in the Sierra Nevada, Plumas trench, and Diamond Mountains.

Sierra Nevada

Deformation of the Lovejoy Formation in the Sierra Nevada indicates extensional tectonics and tilting. The range has been tilted westward to about 30 m/km as a structural block. Internal deformation along normal faults separates regions of differing slope between fault zones. Actual slopes range between 7 and 53 m/km. The tilting and vertical fault displacements are similar the late Cenozoic deformation that has been documented in central Sierra Nevada by the 9-million-year-old latite of the Tuolumne Table Mountain on Stanislaus River near Sonora and the 10-million-year old trachyandesite of Kennedy Table Mountain on the San Joaquin River near Fresno (Woodward-Clyde Consultants, 1978; Page and others, 1978; Ely, 1992 ; Huber, 1981).

Faulting within the Sierra Nevada is commonly on down-to-the-east faults. In the western part of the range the vertical displacements range up to 50 m. In the eastern part of the range a "graben" has been down faulted about 250 m along several faults including the Little Grass Valley

(Dogwood peak), Bottle Springs (Rich Bar), and Meadow Valley faults have had the most displacement.

Although speculative, left slip of the Lovejoy Formation is possible in two places. On the Little Grass Valley fault a component of lateral slip is shown in the Lovejoy Formation at the Dogwood Peak trench (Page and Sawyer, 1995 in progress) and the northwest margins of the Lovejoy Formation channel fill appear to be offset up to about 1 km in a left slip sense. Displacement of the Lovejoy basalt across the Meadow Valley fault (Melones fault of Clark) can be interpreted two ways. As shown on the main profile the ancient thalweg is assumed to go from the Staircase to Crescent Hill near Claremont across this fault, requiring an abrupt, sharp bend in the profile thalweg. This profile does not show an vertical offset, but a down-to-the-west displacement is apparent across this fault on the divide to the south of the Staircase. If the ancient thalweg followed a straighter, southeasterly course across the Middle Fork area, then a down-on-the-west vertical displacement is indicated.

Plumas Trench

The Lovejoy Formation crosses the Plumas trench at the divide between the Mohawk Valley and the American Valley. At this location Lovejoy Formation is down approximately 1,000 to 1,2000 m over 18-km-wide graben. Faulting has had the most displacement on the east and west margins of the trench, but the formation has been faulted by at least 5 faults within the trench as well. Arching across the graben is clearly expressed by the opposite dips of the formation on either side of the Plumas trench: the Lovejoy basalt slopes at 32 m/km east in the Diamond Mountains and 29 m/km to the west in the Sierra Nevada. The trench appears to have formed by collapse of a regional arch between the Sierra Nevada and Plumas block.

Recent analysis of microearthquakes in the Mohawk Valley to the southeast along the trench indicates both right slip and normal faulting (Page and others, 1993) and analysis of the southern Mohawk Valley fault zone indicates lateral slip as well (Sawyer and Page, 1993).

Diamond Mountains

The Lovejoy Formation in the Diamond Mountains has been folded into a broad downwarp or syncline whose axis is near Squaw Queen Creek. The down warp is approximately 500 m. Faults with relatively minor vertical displacement are apparent within the syncline at several locations.

The Diamond Mountains are separated on the east from the Basin and Range province by the Diamond Mountains frontal fault zone, that displaces the Lovejoy Formation 900 to 1,000 m down-to-the-east. Wills (1990) and Wills and Borchardt (1990) document Holocene, right-slip displacement on the Honey Lake fault and late Pleistocene down-on-the-east displacement along the Diamond Mountains frontal fault zone.

Lateral Displacement

The apparent conflict in the interpretations of the possible left lateral displacement of the Lovejoy on the Meadow Valley and Little Grass Valley faults and the right slip displacement of the Plumas trench may be only a question of timing. Left slip on northwest striking faults may have occurred after deposition of the Lovejoy basalt 16 million years ago and prior to the implementation of the present stress regime about 5 million years ago when the Sierra Nevada was uplifted and right slip on initiated on faults of the Walker Lane belt, including the Plumas trench (Page and others, 1993). Left slip has also been inferred in the High Sierra Nevada in Yosemite from offset Tertiary dikes (Lahren and Schweickert, 1991).

REFERENCES

Alt, J. N., Schwartz, D. P., and McCrumb, D. R., 1977, Regional geology and tectonics, Volume 3 of the earthquake evaluation studies of the Auburn Dam area: report by Woodward-Clyde Consultants to the U.S. Bureau of Reclamation, Denver; 118 p. plus appendices.

Busacca, A. J., 1982, Geologic history and soil development, northeastern Sacramento Valley, California [Doctoral Thesis]: Davis, University of California, 348 p. plus appendices, maps and plate, scale: 1:62,5000.

Dalrymple, G. B., 1964, Cenozoic chronology of the Sierra Nevada, California: University of California Publications in Geological Sciences, v. 47, 41p.

Department of Water Resources, 1989, The August 1, 1975 Oroville earthquake investigation: California Department of Water Resources Bulletin 203-88, 617 p.

Durrell, C., 1987, Geologic history of the Feather River country, California: Berkeley, University of California Press, 337 p. plus appendix.

Ely, R. W., 1992, Late Cenozoic uplift and faulting of the Sierra Nevada in the vicinity of Stanislaus Table Mountain, California (abstract): Geological Society of America, 1992 Abstracts with Programs, v. 24, no. 5, p. 22.

Evernden, J. F., Savage, D. E., Curtis, G. H., and James, G. T., 1964, Potassium-argon dates and the Cenozoic mammalian chronology of North America: American Journal of Science, v. 262, p. 145-198.

Grose, T. L. T., Saucedo, G. J., Wagner, D. L., 1989, Geologic map of Susanville Quadrangle, Lassen and Plumas Counties, California, 1:100,000 scale: California Division of Mines and Geology, Open File Report, 20p.

Harwood, D. S., Helley, E. J., and Doukas, M. P., 1981, Geologic map of the Chico monocline and the northeastern part of the Sacramento Valley: U.S. Geological Survey, Miscellaneous Investigations Series, Map I-1238, scale: 1:62,500.

Heitanen, A., 1981, Geology west of the Melones fault between the Feather and North Yuba rivers , California: Petrologic and structural studies in the northwestern Sierra Nevada, Geological Survey Professional Paper 1226-A, 35 p. plus plates.

Huber, N. K., 1981, Amount and timing of late Cenozoic uplift and tilt of the central Sierra Nevada, California - Evidence from the upper San Joaquin River basin: U.S. Geological Survey Professional Paper 1197, 28 p.

Lahren, M. M., and Schweickert, R. A., 1991, Tertiary brittle deformation in the central Sierra Nevada, California: Geological Society of America Bulletin, v. 103, p. 898-904.

Page, W. D., and Sawyer, T. L., 1992, Tectonic deformation of the Lovejoy Basalt, a late Cenozoic strain gauge across the northern Sierra Nevada, California (abstract): American Geophysical Union 1992 Fall Meeting, Supplement to EOS, p. 590.

Page, W. D., Sawyer, T. S., McLaren, M. K., Savage, W. U., and Wakabayashi, J., 1993, The Quaternary Tahoe-Medicine Lake trough: the western margin of the Basin and Range transition, NE California (abstract): Geological Society of America, Abstracts with Programs v. 25, p. 131.

Page and Sawyer, 1995 (in preparation). Late Cenozoic activity of the Little Grass Valley fault, northern Sierra Nevada, California, Report to Division of Safety of Dams, Sacramento.

PG&E, 1991, Characterization of potential earthquake sources for Lake Francis Dam, State Dam No. 1034-009, Yuba County Water Agency: report to Yuba County Water Agency, Marysville for the California Division of Safety of Dams, 36 p. plus 16 figures and plates.

Page and Sawyer, 1995 (in preparation). Late Cenozoic activity of the Little Grass Valley fault, northern Sierra Nevada, California, Report to Division of Safety of Dams, Sacramento.

Roberts, C. T., 1985, Cenozoic evolution of the northwestern Honey Lake-Eagle basin, Lassen County, California: Golden, Colorado School of Mines Quarterly, v. 80, no. 1, 64 p.

Saucedo, D. J., and Wagner, D. L., 1992, Geologic map of the Chico Quadrangle, California, 1:250,000: California Division of Mines and Geology, Regional Geologic Map Series, Map 7A, Sheet 1, Sacramento.

Saucedo, G. J., Fulford, M. M., Mata-Sol, R. A., and Lindquist, T. A. , 1992, Radiometric ages of rocks in the Chico Quadrangle, California, scale: 1:250,000 : California Division of Mines and Geology, Regional Geologic Map Series, Map 7A, Sheet 4, Sacramento, 21p.

Savage, W. U., Page, W. D., McLaren, M. K., and Edwards, W. D., 1991, Approach to seismic hazard analysis for dam safety in the Sierra Nevada and Modoc Plateau of California: Proceedings, Canadian Dam Safety Conference, Sept. 1991: Vancouver, BiTech Publishers, p.203-220.

Sawyer, T. L., Page, W. D., and Hemphill-Haley, M. A., 1993, Recurrent late Quaternary surface faulting along the southern Mohawk Valley fault zone, NE California: Geological Society of America Abstracts with Programs, v. 25, p. 142.

Siegel, D., 1988, Stratigraphy of the Putnam Peak Basalt and correlation to the Lovejoy Formation, California: California State University at Hayward, M.. S. Thesis, 119p.

Siegel, D., and Deino, A., 1988, Correlation and age relations of the Lovejoy Basalt, Plumas County, California (abstract): Geological Society of America, Abstracts with Programs, v. 20, no. 3, p 231.

Turner, H. W., 1896, Further contributions to the geology of the Sierra Nevada: U.S. Geological Survey 17th Annual Report, Part 1, pp. 521-762.

Unruh, J. R., 1991, The uplift of the Sierra Nevada and implications for late Cenozoic epeirogeny in the western cordillera: Geological Society of America Bulletin, v. 103, p. 1395-1404.

Van Den Berge, J. C., 1968, The Paleo-geomorphological features of the Lovejoy Formation in the Sacramento Valley, California: M. S. Thesis University of California, Davis, ---p plus plates.

Wagner, D. L., and Saucedo, G. J., 1990, Age and stratigraphic relationships of Miocene volcanic rocks along the eastern margin of the Sacramento Valley, California, California Department of Conservation, Division of Mines and Geology, Pleasant Hill, California, 9 p. plus figures.

Wills, C. J., 1990, Honey Lake and related faults, Lassen County, California: California Division of Mines and Geology Fault Evaluation Report, FER-214, 17 p. plus photos, figures and maps.

Wills, C. J., and Borchardt, G., 1990, Holocene slip rate and earthquake recurrence on the Honey Lake fault zone, northeastern California: EOS, v. 71, p. 1608.

Woodward-Clyde Consultants, 1978, Foothills fault system study: Appendix C.4 of Volume 6, Stanislaus Nuclear Project, Site Suitability - Site Safety Report; report to the Pacific Gas and Electric Company, San Francisco, 166 p plus tables and figures.

TABLE 1
STRATIGRAPHIC RELATIONSHIPS OF LOVEJOY FORMATION

TIME (Ma)	SACRAMENTO VALLEY WEST	SACRAMENTO VALLEY EAST	SIERRA NEVADA WEST	SIERRA NEVADA EAST	DIAMOND MOUNTAINS WEST	DIAMOND MOUNTAINS EAST
1.8		Tuffs of Oroville				
Pliocene	Tehama	Tuscan Nomolaki Tuff (3.4 Ma)[10]	Pliocene volcanic rocks		Pliocene volcanic rocks	
5.1	•Neroli	•Mehrten	•Mehrten (Penman) (4-6 to 20 Ma)[4,11] Reeds Creek Andesite (8.4-18 Ma)[9]		•Penman (Mehrten) (7-14 Ma)[1, 6] •Thompson Peak basalt (10 Ma)[7] •Ingalls (11-14 Ma)[1, 2] Bonta (11-19 Ma)[3, 5]	
Miocene	•Basalt Cng Lovejoy	New Era	Lovejoy (16 Ma)[8] •andesite breccia (14 Ma)[9] •dacite tuff at Oroville Table Mountain (24 - 25 Ma)[1,4] La Porte tuff (30-33 Ma)[4]		Lovejoy (16 Ma)[8]	
24.6 Oligocene	•Alluvial deposits		Valley Springs (16-33 Ma)		Delleker (21-30 Ma)[2, 4]	
38 Eocene 54.9	Markley Domingine	Ione	"auriferous" gravel		Tertiary gravel	

Notes:

1. General relationships of formations modified from Saucedo and Wagner, 1992; Siegal, 1988; Durrell, 1987.
2. Time lines at period boundaries from Harlan and others, 1982.
3. • indicates that the formation directly unndrelies or overlies the Lovejoy Formation.
4. Information on radiometric dates from:
   1. Saucedo and others, 1992
   2. Siegel, 1988
   3. Morton and others, 198--in Saucedo and others, 1992
   4. Dalrymple (1964) (Recalculated by Saucedo and others, 1992)
   5. Dalrymple (1984) in Saucedo and others, 1992
   6. Grose and others, 1989
   7. Roberts (1985) *in* Grose and others (1989)
   8. Table 2, this document
   9. Wagner and Saucedo, 1990
   10. Evernden and others, 1964
   11. Bartov, 1980

TABLE 2
K/AR DATES ON LOVEJOY FORMATION

LOCATION (Northeast to Southwest)	GEOLOGY	DATE (million years	REFERENCE Sample Number
Thompson Peak, south of Susanville	Lower Thompson Peak. flow (correlates to Lovejoy Formation)	**16.3 ±0.6** (whole rock)	Grose and McKee (1986); Roberts (1985) *in* Grose and others (1989)
Red Clover Creek, south of Genessee at type locality east of Lovejoy	Lovejoy at type locality	9.88 ±1.51 (Ar-Ar; whole rock)	Siegal (1988); Seigal and Deino (1988) consider this date unreliable (too young), because rock is altered.
Red Clover Creek, south of Genessee. at type locality east of Lovejoy.	1st (uppermost) flow (7th flow from bottom)	3.6 ±0.7 (whole rock)	Dalrymple (1964) (Recalculated by Saucedo and others, 1992).
Red Clover Creek, south of Genessee at type locality east of Lovejoy.	4th flow from bottom	14.0 ±0.4 (whole rock)	Dalrymple (1964) (Recalculated by Saucedo and others, 1992).
Red Clover Creek, south of Genessee at type locality east of Lovejoy.	2nd flow from bottom	11.9 ±0.6 (whole rock)	Dalrymple (1964). (Recalculated by Saucedo and others, 1992).
Red Clover Creek, south of Genessee at type locality east of Lovejoy.	Lowest of 7 flows	11.8 ±0.4 (whole rock)	Dalrymple (1964). (Recalculated by Saucedo and others, 1992).
Quarry **Southwest of Haskins Valley** and Bucks Lake and north of Middle Fork Feather River. (NW 1/4 Sec 19, or SW 1/4 sec 18, T23N, R8E)	Isolated single flow remnant	**15.8 ±0.7** (whole rock)	7/23/90 WDP-1B Kruger R-9034
Little Grass Valley Reservoir, knob along south side. (SE 1/4 Sec 32, T22N, R9E)	Extensive flow at Reservoir level; slightly weathered, color slightly lighter than normal black of Lovejoy	4.0 ±0.4 (whole rock)	7/22/90 WDP-3 Kruger R-9033 This date is too young when compared to other dates.
Head of **Black Rock Arm**, Little Grass Valley Reservoir, top of small knob. (Center Sec 30, T22N, R9E)	Upper flow of 3 flows; porphyritic ?	4.3 ±0.4 (whole rock)	7/24/90 WDP-1 Kruger R-9035 This date is too young when compared to other dates.
Lumpkin Ridge, west of Little Grass Valley Dam. (SE 1/4 Sec 25, T22N, R8E)	Upper flow of 4 flows	**15.1 ±0.7** (whole rock)	7/26/90 WDP-1A Kruger R-9036
Lumpkin Ridge, west of Little Grass Valley Dam. (SE 1/4 Sec 25, T22N, R8E)	2nd flow from top	**16.7 ±0.7** (whole rock)	7/26/90 WDP-2A Kruger R-9037
Lumpkin Ridge, west of Little Grass Valley Dam. (SE 1/4 Sec 25, T22N, R8E)	3rd flow from top	**16.2 ±0.8** (whole rock)	7/26/90 WDP-3 Kruger R-9038
Lumpkin Ridge, west of Little Grass Valley Dam. (SE 1/4 Sec 25, T22N, R8E)	4th flow from top (bottom flow)	**15.7 ±0.7** (whole rock)	7/26/90 WDP-4 Kruger R-9039
Lumpkin Ridge, west of McNair Saddle (NE 1/4 Sec 16, T21N, R8E)	Porphyritic top flow of 3 flows	**16.6 ±0.9** (whole rock)	4/90 WDP-1A Kruger R-8956
Big Chico Creek, east of Chico	Flow exposed along Big Chico Cree,	18 and 18.5 (whole rock)	P. Lyden, oral communication in Saucedo and Wagner, 1992

TABLE 3
AR-AR DATES ON LOVEJOY FORMATION

LOCATION (Northeast to Southwest)	GEOLOGY	DATE (million years	REFERENCE Sample Number
Stony Ridge, near east end west of Honey Lake. (T R	Top porphyritic flow; upper flow of 4+ flows	**16.20 ±0.18** (plateau) 15.99±0.24 (integrated)	PG&E 9/17/92 WDP-4 Berkeley Geochronology Lab 1993
Quarry near **Spring Garden,** on Highway 70 southeast of Quincy. (T R	Porphyritic top flow Fresh sample from quarry in Mohawk Valley graben	**15.51 ±0.15** (integrated)	PG&E 10/15/90 WDP-2 Berkeley Geochronology Lab 1993
Fields Ridge, north of Forbestown and southeast of Oroville Reservoir. (T R	Bottom porphyritic flow of 3? flows	**16.07 ±0.07** (plateau) 16.11±0.20 (integrated)	PG&E 8/16/90 WDP-1 Berkeley Geochronology Lab 1993

TABLE 4 - FAULTS IN THE LOVEJOY FORMATION, NORTHERN SIERRA NEVADA AND DIAMOND MOUNTAINS,CALIFORNIA

Fault (NE to SW)	Location	Estimated Vertical Separation (m)	Regional Strike	Fault Length[2] (km)	Vertical Separation Rate[1]	Comments, References
Diamond Mountains Frontal Fault Zone						
Elysian and other faults	Between Thompson Peak and Jim Peterson Hill, 15 km SE of Susanville	~ 900 to 1,000, down on E, top of Lovejoy Fm.	N48°W	65 to 85	0.15 to 0.17	Part of Honey Lake fault zone shown on Grose and others (1989); displacement based on one outcrop E of Jim Peterson Hill; total displacement across zone is probably more than 1,000 m.
Thompson Peak fault	600 m NE of Thompson Peak, 18 km SE of Susanville	~ 100,down on W, top of Lovejoy Fm.	~North	?	0.017	Fault is exposed in the cliffs on the northeast side of Thompson Peak; appears to be part of the Diamond Mountains frontal fault zone.
Faults between Diamond Mountains and Grizzly Ridge						
Juniper Spring fault	Gap on Stony Ridge, NE of Round Mountain	~ 50,down on W, top of Lovejoy Fm. below top porphyritic flow	N70W	10 ?	0.008	Gap in ridge associated with map lineament and increase in surface gradient from 5 m/km on the E to ~ 20 m/km on the W.
Last Chance fault	S of Stony Ridge and E of Clarks Creek	~ 30,down on E, top of Lovejoy Fm.	NW ?	?	0.005	Surface gradient possibly decreases from 20 m/km on the E to ~ 26 m/km on the W of the fault.
Red Clover Creek fault	Along Red Clover Creek E side of Mt. Ingalls, 17 km ESE of Genesee	Possible ~ 130, down on W (?), top of Lovejoy Fm.	N45W	> 20	0.005 to 0.01	Durrell (1959) mapped faulting of the Lovejoy Fm along NW and NE trends at Red Clover Cr. Faults not shown on Grose and others (1989). Vertical displacement from our profile uncertain.
Walker Mine fault	W side of Mt. Ingalls, N of townsite of Lovejoy, 10 km SSE of Genesee	Possible 50 to 75, inferred, amount unknown, down on E, top of Lovejoy Fm.	N30°W	11	?	Durrell (1959) mapped faulting of the Lovejoy Fm along NW trend, amount of vertical displacement uncertain. We placed fault E of where shown by Saucedo and Wagner (1992).

Grizzly Creeks fault	NW of old town of Lovejoy and north of divide between Little Grizzly and Big Grizzly creeks, 10 km SSE of Genesee	Possible ~ 40, down on E, top and base of Lovejoy Fm.	N36°W	10 to 20	0.006	Wind gap between Big Grizzly and Little Grizzly creeks near the outcrops of the Lovejoy Fm is probably the result of the stream piracy of Big Grizzly Creek from the headwaters of Little Grizzly Creek. Durrell (1959) mapped faulting of the Lovejoy Fm along NW trends near the creek, amount of vertical displacement uncertain.
Mohawk Valley Graben						
Mohawk Valley graben	Water divide between Spanish Creek and Middle Forks Feather River near Spring Garden, 10 to 15 km SE of Quincy	890 to ~ 1180 across graben, top of Lovejoy Fm.	N45°W	60 to 80	0.2	The zone is about 17 km wide. The top porphyritic flow is the lowest remnant in the graben. Twelve faults are maped or inferred within the zone. The faults with the largest vertical displacements are on the E and W sides of the graben. Surface gradient of the flows show an arch over the graben: dips E at 32 m/km to the E and at ~ 29 m/km to the W of the graben. Durrell (1987) recognized the graben and estimated 2,000 ft. of displacement on the Eureka Ridge fault zone and 1700 ft. on the Grizzly Ridge fault zone. Analysis of the pattern of the Lovejoy channel indicates possible right-slip offset, up to 1 to 2 km across the graben.
Grizzly Ridge fault zone	West escarpment of Grizzly Ridge E of Spring Garden	890 to ~ 1180 across zone, top of Lovejoy Fm.. Lack of Lovejoy Fm. remnants does not allow estimates between individual faults.			0.2	The zone consists of at least 3 faults (Cromberg, Sloat, and Greenhorn Creek faults) and is the E side of the Mohawk Valley graben. several of which were mapped by Saucedo and Wagner (1992) ???. The fault zone extends from near Indian Creek on the north to at least Clio on south and forms the prominant W-facing Grizzly Ridge escarpment.
Eureka Ridge fault zone	Water divide between Spanish Creek and Middle Forks Feather River south of Quincy	890 to ~ 1180 across zone, top of Lovejoy Fm.. ~ 170 on Fells Creek, ~170 on E splay, Nelson Creek and ~ 400 to ~ 470 across Bach Creek Ridge faults				The zone consists of at least 3 faults (Fells Creek, E splay of Nelson Creek, and Bach Creek Ridge faults) and is the W side of the Mohawk Valley graben. Vertical separation between faults within the zone is uncertain because the outcrops of Lovejoy Fm. are scattered and small, but appear to be about 170 to 475. mapped by Saucedo and Wagner (1992) ???. The fault zone extends from near Quincy on the north to Johnsville on the south. It and forms the E-faceing Eureka Ridge escarpment, but looses prominance with in the mountains between Middle Fork Feather River and Quincy.

Faults in the higher slopes of the Sierra Nevada						
Meadow Valley (Melones Fault of Clark)	S of Cresent Hill and ~9.2 km S of Quincy in the canyon of the Middle Fork Feather River	Uncertian. If the profile follows the general trend (N45°E) of the Lovejoy channel, displacement is about 75 m, down on the W. None is required, if profile makes an abrupt bend (N17°W) where it crosses the Middle Fork Feather River. Analysis of outcrop patterns indicates possible left-slip offset of up to 1 to 3 km	N20°W			The option of lack of displacement across fault based on very long projection (4.8 km) across the Middle Fork Feather River with little control on north side at Cresent Hill. Vertical down -on-the-W displacement is probable because 1 to 4 km to the W, where the Meadow Valley fault is 3.5 km-wided zone the fault displaces surface of the Mehrten Formation, down on W, 250 to 350 m on the Bear Creek-Claremont and Mt. Arafat-Claremont profiles. Farther to the NW, Alt and others (1977) report faulted Quaternary lake beds in Meadow Valley with down on the W displacement. And 2 km to the SSE, near Monitor and Sawpit flats the fault apparently displaces Lovejoy Fm. 50 m , down on W.
Bird Creek faults	~ 15 km ENE of La Porte on "Bankers Cabin" ridge	~ 145 to 180 m, down-on-NW, base of Lovejoy Fm.	NE (?)	~ 5		Two faults form the zone that is probably part of the Meadow Valley fault.
Bottle Springs (Rich Bar)	8 km NW of Little Grass Valley Dam along Onion Valley Cr. and on "Fowler Peak" Ridge	~ 100 to 105 m, down-on-E ; 40 m on E splay, down-on-W, on top and base of Lovejoy Fm.	N32°W			The fault zone is ~ 0.9-km-wide consisting of the main fault and the east splay that have opposite sense of displacement. To the N, 4.0 km SW of Quincy on South Fork Rock Creek, the surface of the Mehrten Formation is displaced 250 to 260 m down on the E (Mt. Arafat-Claremont and the Bear Creek-Claremont profiles, PG&E, 1995a). Alt and others (1977) describe displacement of Quaternary lake beds of more than 6 m and as much as 18 m on the Bottle Springs fault at the western end of Meadow Valley. At Gibsonville Ridge, 5 km S, the fault does not appear to displace Lovejoy Fm (Moorville-Gibsonville Profile (not shown), PG&E, 1995a)

(Dogwood Little Grass Valley Peak) fault	3 km N. of Little Grass Valley Dam and 8 km WNW of La Porte.	Total of 240 m down on the E: 80 m on main fault on surface (top flow) of Lovejoy Fm. and and 60 m on Black Arm splay on base of Mehrten/top of Lovejoy Fms.	N22°W	30	0.4 (0.3 + 0.1) mm/yr	Alt and others (1977) recognized late Cenozoic displacement on the Little Grass Valley fault near Dogwood Peak. PG&E (1995a) at the Dogwood Peak trench locality found a fault zone with two splays separated by ~ 1.1 km. Trench 2 across the main fault confirmed displacement of the Lovejoy Fm. and showed two or three faulted colluvial deposits. 2.5 km NNW of La Porte the fault zone is approximately 0.5 km wide and consists of two main splays and possibly the Queen City fault, all with down to the E displacement (Mooreville -Gibbsonville Ridge profile (not shown) (PG&E, 1995a). The west splay has 60 m and the east splay 45 m displacement on the surfate of the Merhrten Fm.; the east splay displaces the "auriferous gravel" 70 m.
Sandborn Mine (Camel Peak) fault	On Lumpkin Ridge, ~ 6.9 km SW of Little Grass Valley Dam and 9 km W of la Porte	60 m,down-on-E, surface of Lovejoy Fm. and 45 m surfaceof Mehrten Fm.	N22°W	~ 17		The Sandborn Mine fault of Alt and others (1977) has 61 m down on the E displacement of the "auriferous gravel" below the Lovejoy Fm. on Moorville Ridge, 5 km S of Lumpkin Ridge. The Mooreville-Gibson Ridge profile (not shown) (PG&E, 1995b) shows ~ 50 m down on the E displacement on the surface of the Mehrten Fm.
Cascade fault	On Lava Top Ridge, 1 km south of Cascade and ~2.5 km ESE of confluence of Middle Fork Feather River and Cascade Creek. (N of Oroville-Susanville profile).	35 m, down-on-E, surface and base of Lovejoy Fm.				Fault indicated on Lava Top Ridge profile (not shown) to N of Oroville-Susanville profile. Faulting is along as a zone of near vertical foliation in granitic rocks of the Cascade pluton (Heitenan, 1981); the shape of the Lovejoy Fm. outcrop and slope of the Lovejoy Fm. surface is ~ 7 m/km, suggesting that this is an area of lava ponding along a tributary during deposition.
Faults in the lower slopes of the Sierra Nevada						
Maynards fault	On Fields Ridge, ~ 0.7 km N. of Forbestown Dam and 10 km NE of Challenge	~ 20 to 50, down-on-W, surface of Lovejoy Fm.	N23°W	13 km	0.0083	The surface gradient of the Lovejoy Fm. decreases from 27 m/km on the E to ~ 12 m/km on the W of the fault. The southern part of the fault was trenched and no late Quaternary faulting was apparent (PG&E, 1991).
Sucker Run fault	On Fields Ridge, ~ 2.0 km NW of Forbestown Dam and 8 km N of Challenge	~ 0 to 20, down on E, surface of Lovejoy Fm.	N17°W	~ 9 km	0.0025	Lovejoy Fm. remnant W of fault is somewhat dissected, but has concordent summits that were projected eastward in order to estimate the amount of possible displacement; base of flows also show approximatly the same displacement. Gradient decreases from 21 to 7 m/km across the fault is

Kanaka Peak anomaly	In 5 km wide zone between Kanaka Peak and Fields Ridge, 10 km NNW of Challenge	Shallowing of gradient toward the W from 30 to 7 m/km	?	?	?	No significant air photo or map lineament evident in the area of the amonaly. Anomaly may be a projection anomaly if the main channel went to the south of Oroville.
Long Ravine fault	E of North Table Mtn. and north of Oroville	Down E displacement possible at the southeast end of Oroville Table Mtn., but lack of Lovejoy Fm. remnants to the E do not allow an estimate	N2°W	~ 20		The Long Ravine fault of Department of Water Resources (1988) appears to be the east branch of the Prairie Creek fault that Bussacca (1982) reports folds or offsets the Laguna Formation (Pliocene), 10 to 30 m, down on the W near Oroville. Creely (19--) also reports 2 m of down-on-the-W displacement of the Red Bluff Fm (Quaternary) E of Oroville. Down-on-the-E displacement is possible at SE end of Oroville North Table Mtn. on this profile. On a profile across the north end of North Table Mtn.(not shown), 5 km norht of Oroville, suggests ~ 150 to 240 m ?, down on E, separation on the top (?) of Lovejoy Fm.. (north of Oroville-Susanville profile)
Oroville Table Mountain faults	Extreme north end of North Oroville Table Mountain, 13 km N of Oroville (north of Oroville-Susanville profile)	3 faults with < 5 m, down on W, Top of Lovejoy Fm.	N10°E	< 1.6 km	0.0008 mm/yr	Alt and others (1977) reported these small faults that are too small to appear on the profile across the north end of the table.
Prairie Creek fault	Between Cambell Hills and South Oroville Table Mountain, 5 km NW of Oroville.	possible ~ 30 m, down on E, top ofLovejoy Fm.	N30°W ?		0.005 mm/yr	Oroville-Susanville Profile Bussacca (1982) suggests that a branch of the northern extension of Prairie Creek fault may project through the gap W of Table Mountain on projection of the Chico Monocline. Fault also shown by Department of Water Resources (1989).
Faults in the Sacramento Valley						
Chico Monocline, southern extension	West end of Cambell Hills, 7 km W of Oroville	West steepening of slope at top of Lovejoy Fm. from 30 m/km to 53 m/km	N21°W	80 km		Appears to be southern extension of the Chico monocline, which trends N30W, with either as a slightly more northerly trend or as a right step over. According to Harwood and Helley (1981) deformation of the Chico Monocline occurred largly between 2.4 and 1.08 Ma.

Notes:

1. Assumes that the vertical deformation has taken place in the past 5 million years, since uplift of the Sierra Nevada (see text).
2. Fault lengths are the estimated lengths of late Cenozoic fault segments, and not the length of the bedrock fault.

EXPLANATION

NEOGENE	QUATERNARY	Pleistocene	Qls	Landslide deposits
			Ql	Lake deposits
			Qf	Fan deposits
			Qvb	Pleistocene basaltic rock
			Qrb	Red Bluff Formation *(Tuscan-derived gravels with sands and silts)*
			Qfbu	North Fork Feather River basalt flow (unknown age)
			Qfyb	North Fork Feather River basalt flow (0.6-0.7 Ma)
			Qfob	North Fork Feather River basalt flow (1.1-1.2 Ma)
			Qdb	Deer Creek basalt
			QPto	Tuffs of Oroville *(Volcaniclastic sediments and tuff)*
		Pliocene	Tpa	Pliocene andesitic rock
			Tpb	Pliocene basaltic rock
			Tpd	Pliocene dacitic rock
			Tpcb	Cohasset Ridge basalt
			Tpt	Tuscan Formation *(Lahars, volcaniclastic sediment, and tuff)*
			Tpl	Laguna Formation *(Alluvial gravel, sand, and silt)*
TERTIARY	TERTIARY	Miocene	Tmb	Miocene basaltic rock
			Tmm	Mehrten Formation *(Andesitic conglomerate)*
			Tmdp	Disaster Peak Formation *(Andesitic conglomerate)*
			Tmd	Dardanelles Formation *(Dark latite flows)*
			Tme	Eureka Valley Tuff *(Welded latite tuff)*
			Tmt	Table Mountain Latite
			Tmr	Relief Peak Formation *(Andesitic conglomerate)*
			Tml	Lovejoy Basalt
		Oligocene	Tov	Valley Springs Formation *(Rhyolitic tuff and sedimentary rock)*
				Chili Hill Tuff
				Castle Hill Tuff
		Eocene	Teg	"Auriferous" gravel
			Tei	Ione Formation *(Quartzose sandstone, claystone, and conglomerate; mostly non-marine)*
			Tv	Tertiary pyroclastic rock
MESOZOIC			Kc	Chico Formation *(Sandstone, conglomerate, and siltstone; marine)*
			Ki	Cretaceous igneous rock
			KJi	Cretaceous-Jurassic igneous rock
			Js	metasedimentary rock (Smartville Complex)
			Jv	metavolcanic rock (Smartville Complex)
			Ji	igneous rock (Smartville Complex)
			Ju	ultramafic rock (Smartville Complex)
			Mzi	Mesozoic igneous rock
			Mzs	Mesozoic metasedimentary rock
			MzPzs	Mesozoic-Paleozoic metasedimentary rock
			MzPzv	Mesozoic-Paleozoic metavolcanic rock
			MzPzi	Mesozoic-Paleozoic igneous rock
			MzPzu	Mesozoic-Paleozoic ultramafic rock
			MzPzls	Mesozoic-Paleozoic crystalline limestone
			PzMzm	Paleozoic-Mesozoic metamorphic rock
			PzMzcs	metasedimentary rock (Calaveras Complex)
			PzMzcv	metavolcanic rock (Calaveras Complex)
			PzMzls	crystalline limestone (Calaveras Complex)
			PzMzfra	amphibolite (Feather River Belt Peridotite)
			PzMzfrm	metamorphic rock (Feather River Belt Peridotite)
			PzMzfri	igneous rock (Feather River Belt Peridotite)
			PzMzfru	ultramafic rock (Feather River Belt Peridotite)
PALEOZOIC			Dsb	Sierra Buttes Formation *(Metavolcanic rock)*
			Di	Devonian igneous rock *(Bowman Lake Batholith)*
			Pzsfs	metasedimentary rock (Shoo Fly Complex)
			Pzsfv	metavolcanic rock (Shoo Fly Complex)
			Pzs	Paleozoic metasedimentary rock

LEGEND

- Primary ridge line
- Secondary ridge line
- Base of unit (querried where uncertain, absent where unknown)
- Projection line
- River or creek
- Basement contact line
- Monoclinal warp (Surface expression of a buried fault)
- Anticlinal warp (Surface expression of a buried fault)
- Fault (Mesozoic fault names in parentheses)
- Suspected fault
- Drift mine, placer diggings
- N43°E — Profile direction
- ∠ = 18m/km — Surface gradient
- Reservoir

Figure 3-3. Explanation for Figure 3-3-2.

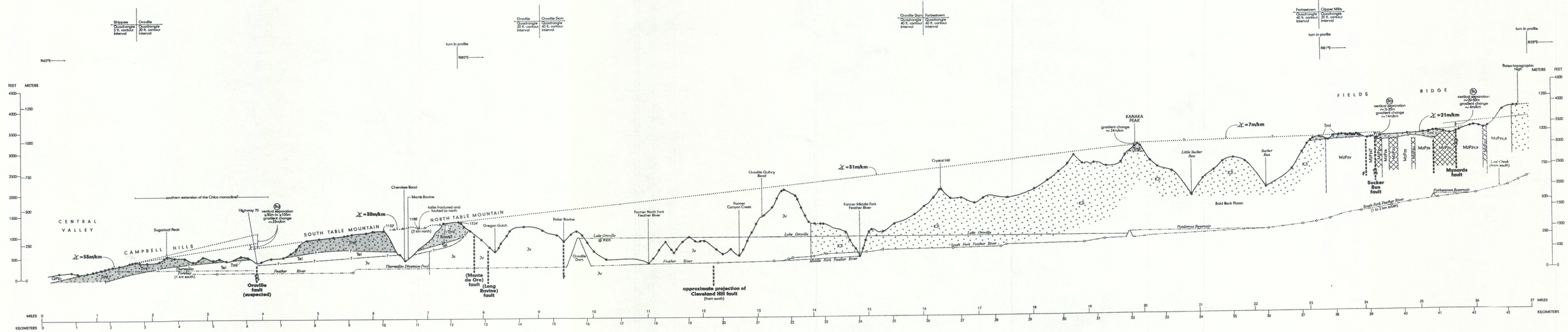

Figure 3-3-2A. Profile of Lovejoy basalt between Oroville and Susanville. Section A - Oroville Table Mountain to Fields Ridge.

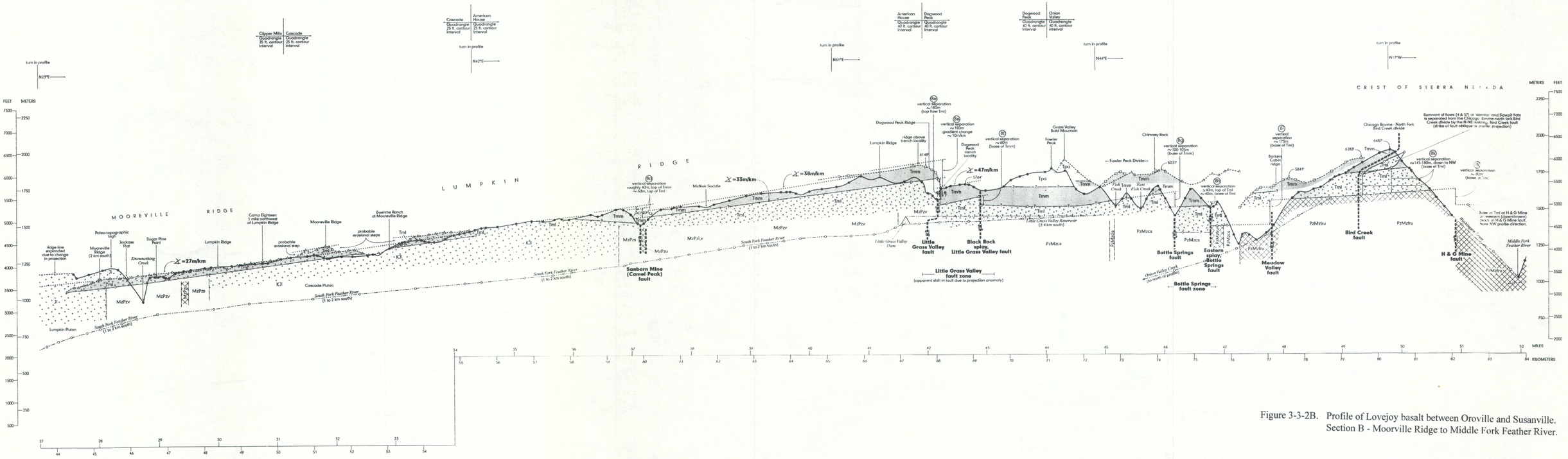

Figure 3-3-2B. Profile of Lovejoy basalt between Oroville and Susanville. Section B - Moorville Ridge to Middle Fork Feather River.

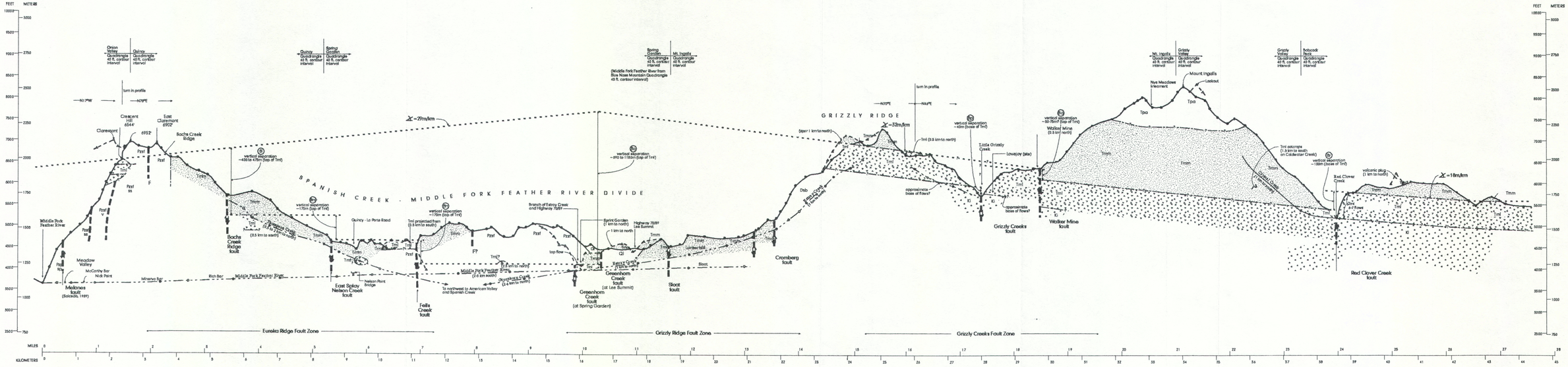

Figure 3-3-2C. Profile of Lovejoy basalt between Oroville and Susanville.
Section C - Middle Fork Feather River to Squaw Queen Creek.

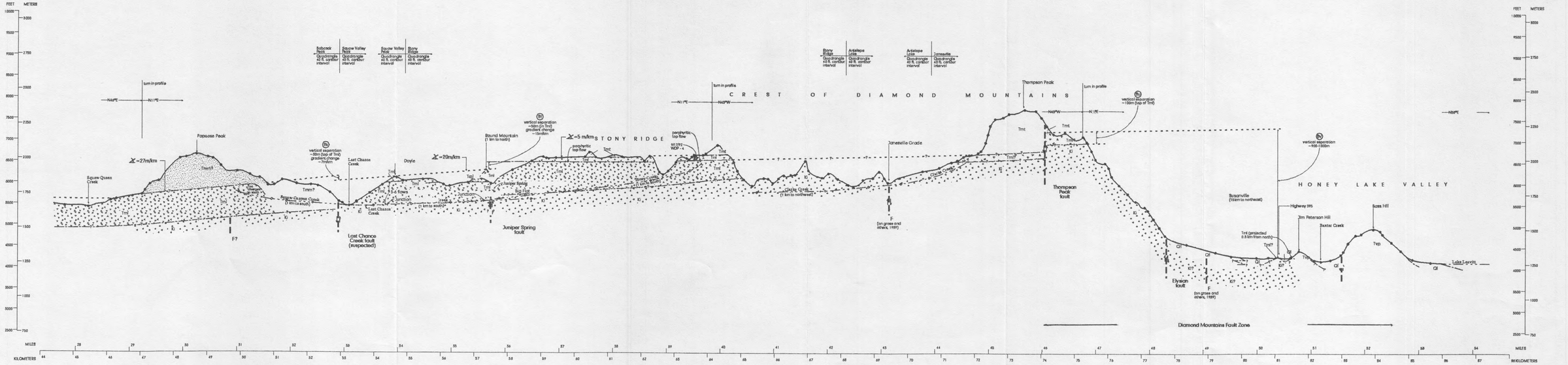

Figure 3-3-2D. Profile of Lovejoy basalt between Oroville and Susanville.
Section D - Squaw Queen Creek to Lake Leavitt.

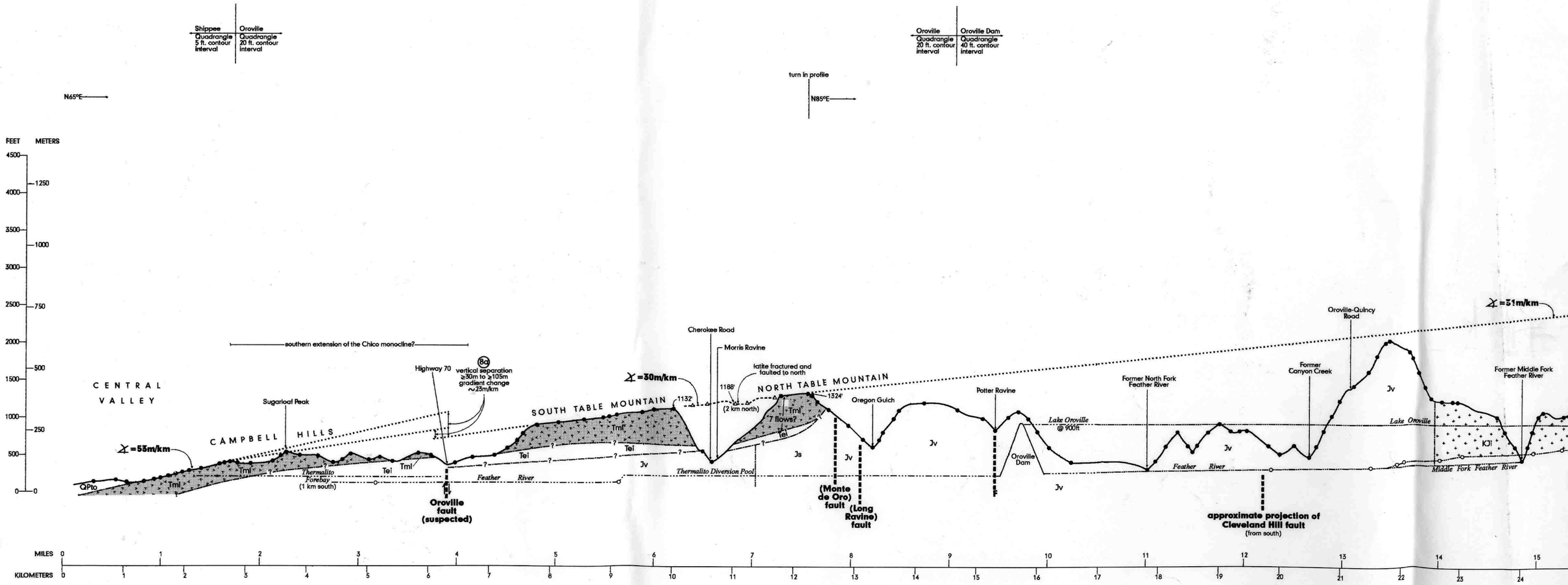
Shippee Quadrangle 5 ft. contour interval
Oroville Quadrangle 20 ft. contour interval
Oroville Quadrangle 20 ft. contour interval
Oroville Dam Quadrangle 40 ft. contour interval
N65°E
turn in profile
N85°E
FEET
METERS
4500
4000
3500
3000
2500
2000
1500
1000
500
0
1250
1000
750
500
250
0
CENTRAL VALLEY
CAMPBELL HILLS
Sugarloaf Peak
southern extension of the Chico monocline?
Highway 70
8a
vertical separation ≥30m to ≥105m gradient change ~23m/km
SOUTH TABLE MOUNTAIN
NORTH TABLE MOUNTAIN
Cherokee Road
Morris Ravine
latite fractured and faulted to north
1188'
(2 km north)
1132'
1324'
Oregon Gulch
Potter Ravine
Former North Fork Feather River
Former Canyon Creek
Oroville-Quincy Road
Former Middle Fork Feather River
Lake Oroville @ 900ft
Lake Oroville
Oroville Dam
Thermalito Forebay (1 km south)
Thermalito Diversion Pool
Feather River
Middle Fork Feather River
QPto
Tml
Tei
Jv
Js
Kjl
?flows?
=53m/km
=30m/km
=31m/km
Oroville fault (suspected)
(Monte de Oro) fault
(Long Ravine) fault
approximate projection of Cleveland Hill fault
(from south)
MILES
KILOMETERS

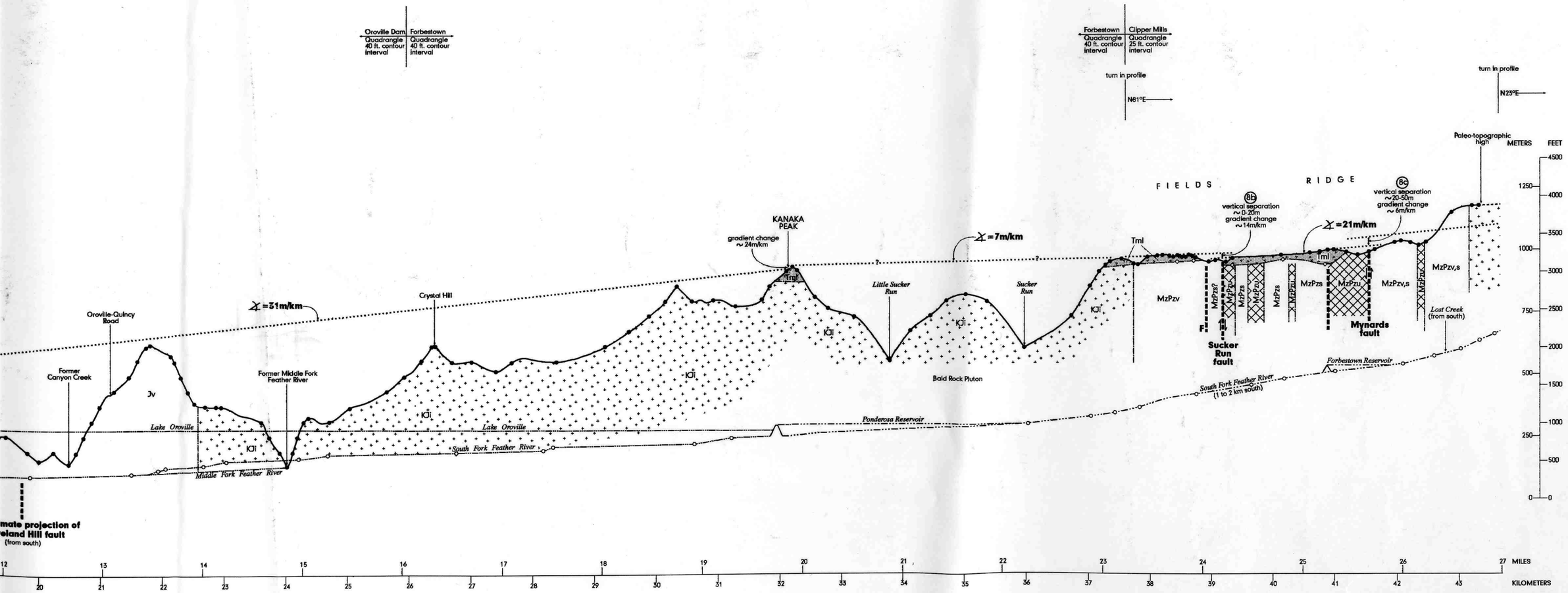

Figure 3-3-2A. Profile of Lovejoy basalt between Oroville and Susanville. Section A - Oroville Table Mountain to Fields Ridge.

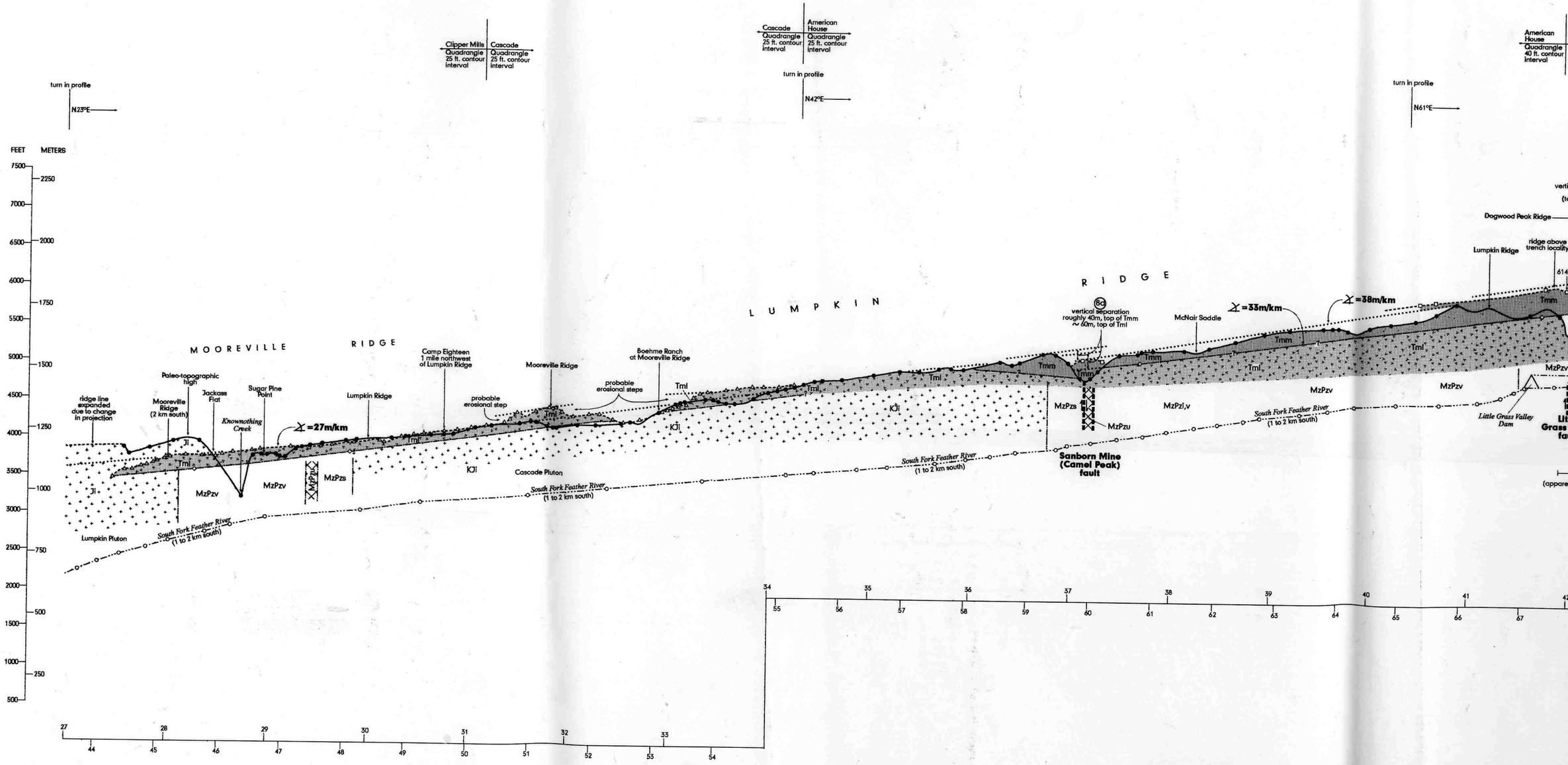
Clipper Mills Quadrangle 25 ft. contour interval
Cascade Quadrangle 25 ft. contour interval
Cascade Quadrangle 25 ft. contour interval
American House Quadrangle 25 ft. contour interval
American House Quadrangle 40 ft. contour interval
turn in profile
N23°E
N42°E
N61°E
FEET
METERS
MOOREVILLE RIDGE
LUMPKIN RIDGE
ridge line expanded due to change in projection
Mooreville Ridge (2 km south)
Paleo-topographic high
Jackass Flat
Knownothing Creek
Sugar Pine Point
Lumpkin Ridge
Camp Eighteen 1 mile northwest of Lumpkin Ridge
probable erosional step
Mooreville Ridge
probable erosional steps
Boehme Ranch at Mooreville Ridge
Cascade Pluton
Lumpkin Pluton
South Fork Feather River (1 to 2 km south)
vertical separation roughly 40m, top of Tmm ~ 60m, top of Tml
McNair Saddle
Sanborn Mine (Camel Peak) fault
Little Grass Valley Dam
Dogwood Peak Ridge
ridge above trench locality
Lumpkin Ridge
Ji
Tml
MzPzv
MzPzs
MzPzi,v
MzPzu
KJi
Tmm
=27m/km
=33m/km
=38m/km

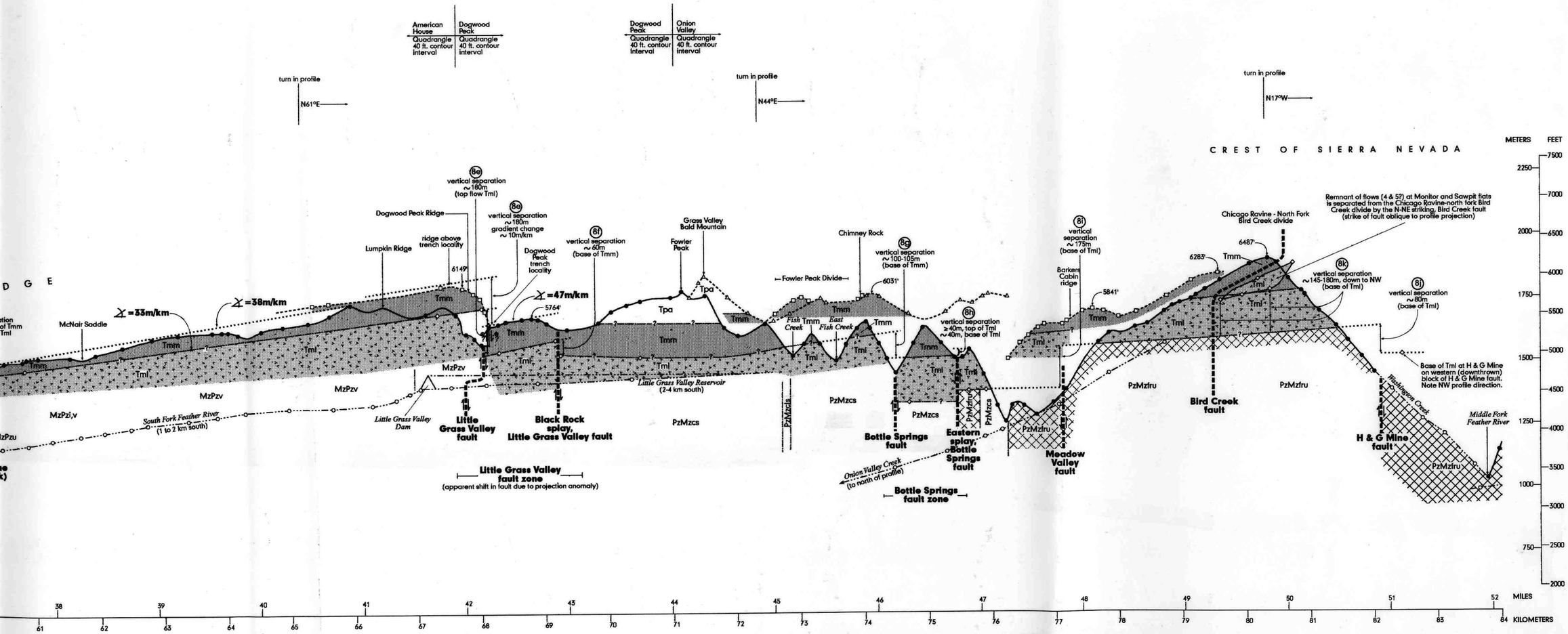

Figure 3-3-2B. Profile of Lovejoy basalt between Oroville and Susanville. Section B - Moorville Ridge to Middle Fork Feather River.

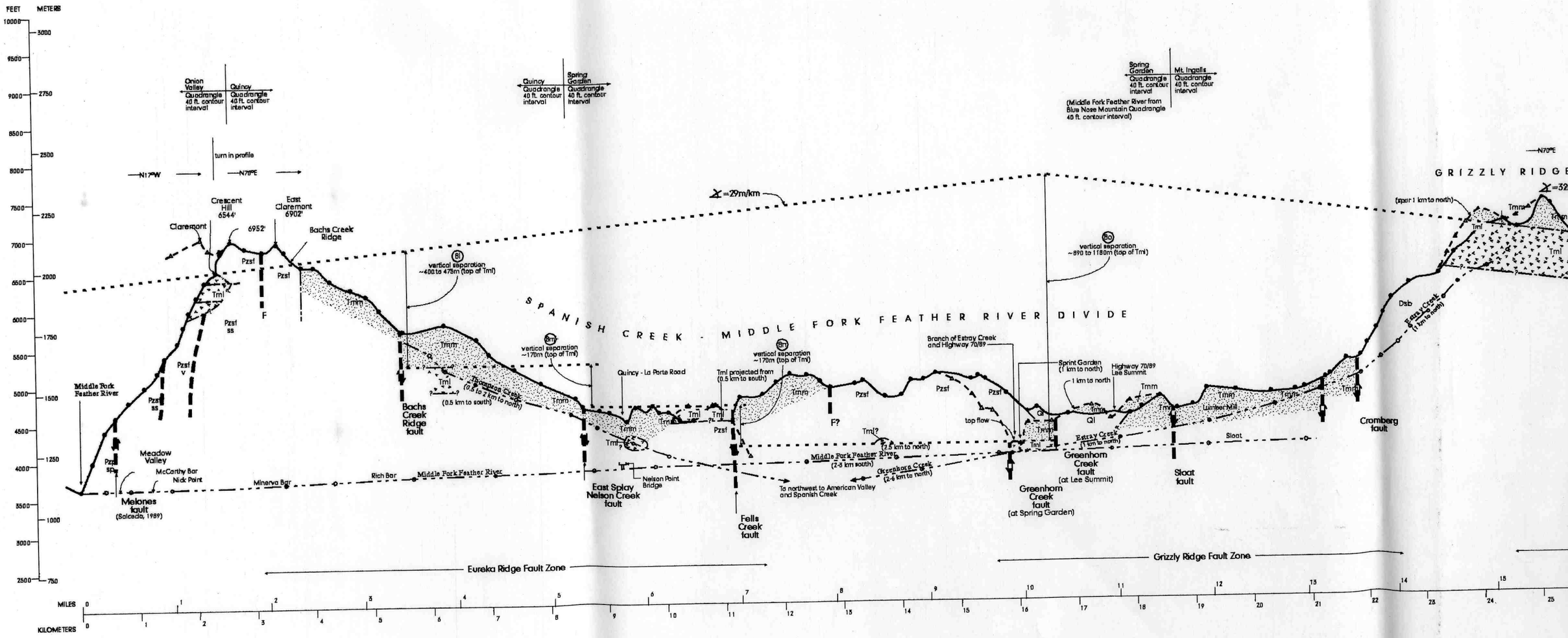
FEET
METERS
Onion Valley Quadrangle 40 ft. contour interval
Quincy Quadrangle 40 ft. contour interval
Quincy Quadrangle 40 ft. contour interval
Spring Garden Quadrangle 40 ft. contour interval
Spring Garden Quadrangle 40 ft. contour interval
Mt. Ingalls Quadrangle 40 ft. contour interval
(Middle Fork Feather River from Blue Nose Mountain Quadrangle 40 ft. contour interval)
turn in profile
N17°W
N70°E
Crescent Hill 6544'
East Claremont 6902'
Claremont
6952'
Bachs Creek Ridge
vertical separation ~400 to 475m (top of Tml)
vertical separation ~890 to 1180m (top of Tml)
vertical separation ~170m (top of Tml)
vertical separation ~170m (top of Tml)
SPANISH CREEK - MIDDLE FORK FEATHER RIVER DIVIDE
Middle Fork Feather River
Meadow Valley
McCarthy Bar
Nick Point
Melones fault (Salceda, 1989)
Minerva Bar
Rich Bar
Middle Fork Feather River
Bachs Creek Ridge fault
Thompson Creek (0.5 to 2 km to north)
(0.5 km to south)
Quincy - La Porte Road
East Splay Nelson Creek fault
Nelson Point Bridge
Tml projected from (0.5 km to south)
Fells Creek fault
Tml? (2.5 km to north)
Middle Fork Feather River (2-3 km south)
Greenhorn Creek (2-6 km to north)
To northwest to American Valley and Spanish Creek
Branch of Estray Creek and Highway 70/89
top flow
Sprint Garden (1 km to north)
1 km to north
Highway 70/89 Lee Summit
Greenhorn Creek fault (at Spring Garden)
Greenhorn Creek fault (at Lee Summit)
Estray Creek (1 km to north)
Lumber Mill
Sloat
Sloat fault
Cromberg fault
Estray Creek (1 km to north)
(spur 1 km to north)
GRIZZLY RIDGE
Eureka Ridge Fault Zone
Grizzly Ridge Fault Zone
MILES
KILOMETERS

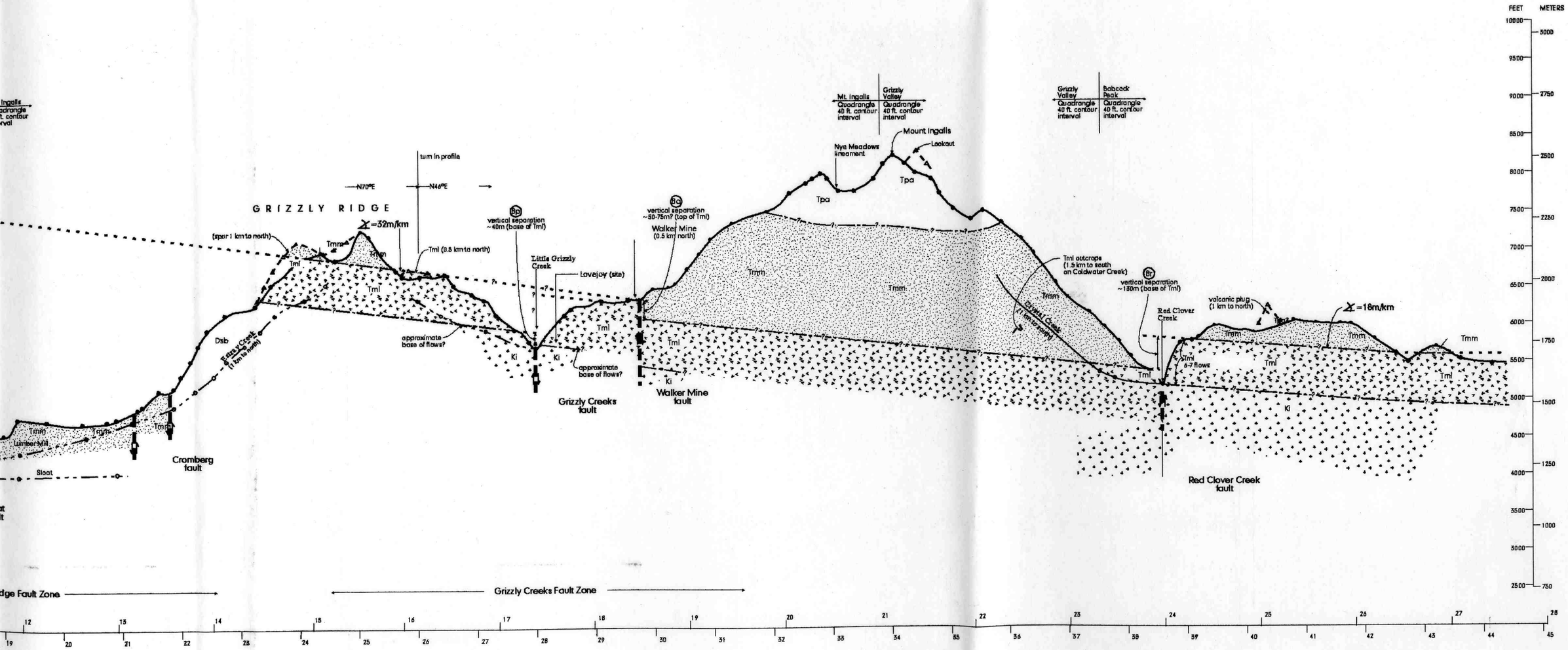

Figure 3-3-2C. Profile of Lovejoy basalt between Oroville and Susanville.
Section C - Middle Fork Feather River to Squaw Queen Creek.

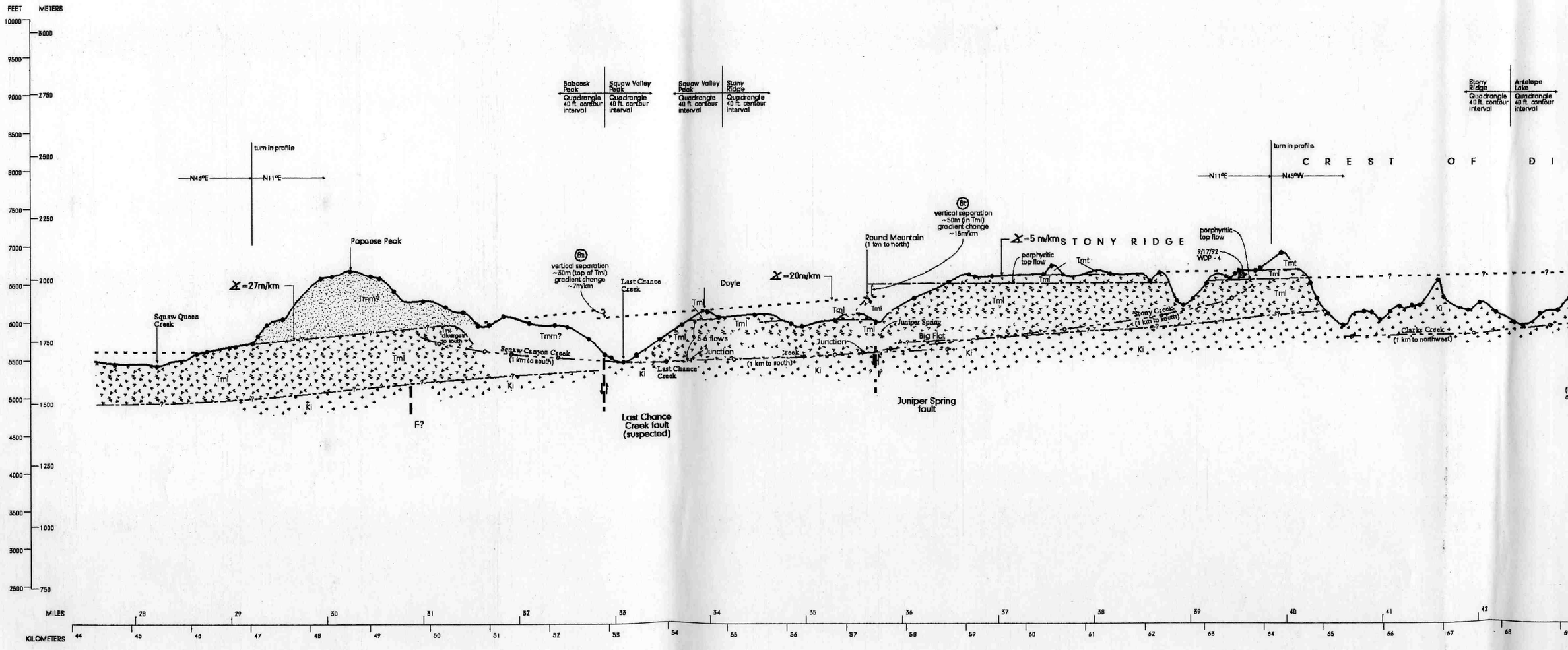
FEET
METERS
Babcock Peak
Quadrangle 40 ft. contour interval
Squaw Valley Peak
Quadrangle 40 ft. contour interval
Squaw Valley Peak
Quadrangle 40 ft. contour interval
Stony Ridge
Quadrangle 40 ft. contour interval
Stony Ridge
Quadrangle 40 ft. contour interval
Antelope Lake
Quadrangle 40 ft. contour interval
turn in profile
N46°E
N11°E
turn in profile
N11°E
N45°W
C R E S T O F D I
Papoose Peak
Squaw Queen Creek
X=27m/km
Tmm?
Tml
Tmt
Ki
Squaw Canyon Creek
(1 km to south)
F?
Bs
vertical separation ~30m (top of Tml) gradient change ~7m/km
Last Chance Creek
Last Chance Creek fault (suspected)
Doyle
5-6 flows
Junction
Junction
creek
(1 km to south)
X=20m/km
Round Mountain
(1 km to north)
Juniper Spring
Big Flat
Juniper Spring fault
Bt
vertical separation ~50m (in Tml) gradient change ~15m/km
X=5 m/km
S T O N Y R I D G E
porphyritic top flow
porphyritic top flow
9/17/92
WDP - 4
Stony Creek
(1 km to south)
Clarks Creek
(1 km to northwest)
MILES
KILOMETERS

(45)
24

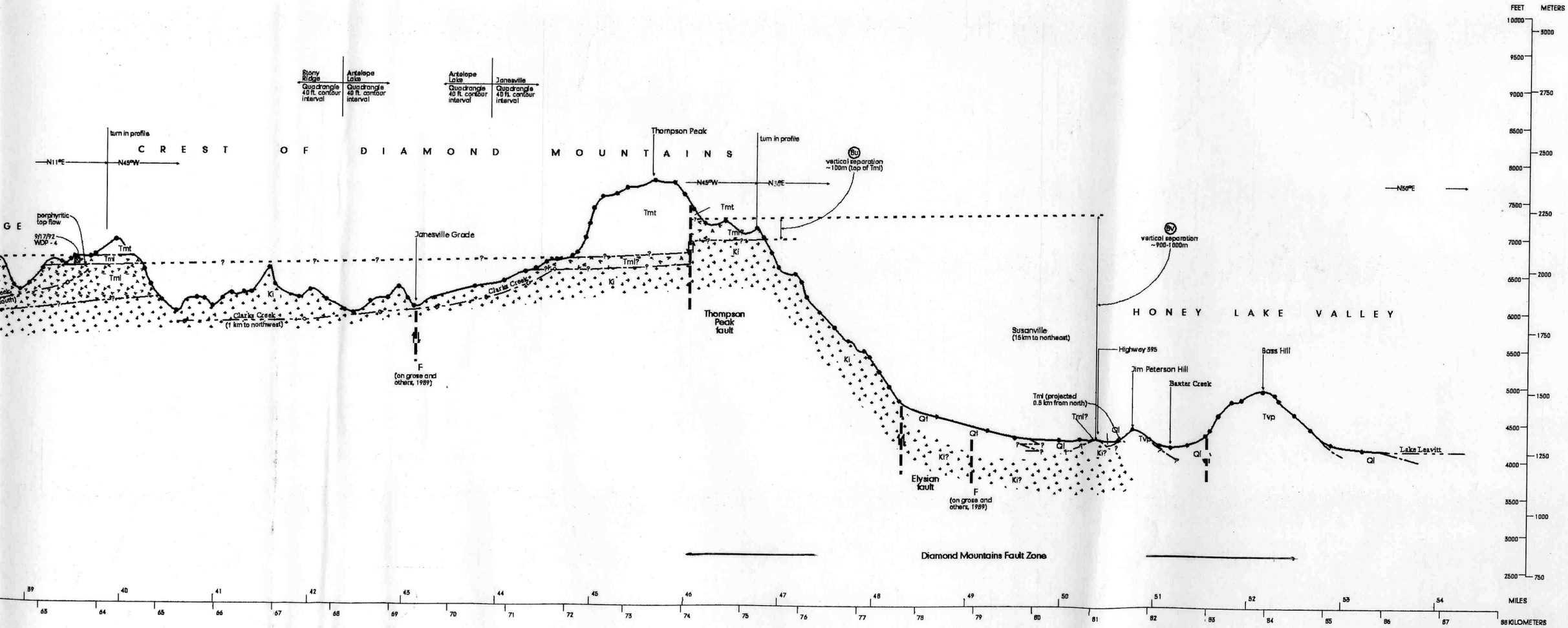

8A: Claremont to Honey Lake

Figure 3-3-2D. Profile of Lovejoy basalt between Oroville and Susanville.
Section D - Squaw Queen Creek to Lake Leavitt.

Late Cenozoic Volcanism, Geochemistry, and Petrology in the Lassen Area, Southernmost Cascade Range, California

CLYNNE, Michael A., U.S. Geological Survey, 345 Middlefield Road MS910, Menlo Park, CA 94025.

Volcanism in the southernmost Cascade Range can be characterized on two scales. Regional volcanism is predominantly basaltic to andesitic, and hundreds of coalescing volcanoes of small volume (10^{-3} to 10^{1} km^3) with short lifetimes have built a broad platform. Superimposed on the regional volcanism are a few long-lived (~10^6 years) much larger (>10^2 km^3) volcanic centers. Rock types are typical of continental-margin orogenic volcanism and range from sparsely phyric olivine basalt to high-silica rhyolite, although porphyritic pyroxene andesites and hornblende dacites dominate the volcanic suite. The regional volcanism results from underplating of the crust by mantle-derived mafic magma, and volcanic centers occur where the magmatic flux is focused or structurally controlled. Volcanic centers are the surface expression of complex magmatic systems resulting from evolution and interaction between mantle-derived basalt and silicic partial melts of underplated mafic crust. The volcanic centers may record the generation, mobilization, rise, and emplacement of small plutons into the middle crust.

Two types of primitive basalt are recognized: medium-K calc-alkaline (CAB) and low-K olivine tholeiite (LKOT). LKOT is chemically homogeneous, outcrops sporadically in association with extensional tectonics of the Basin and Range Province, and is related to Pleistocene encroachment of Basin-and-Range tectonics on the subduction-related volcanism of the Cascade Range. CAB exhibits considerable geochemical diversity and is the parent magma for the volcanic-center lavas and the suite of evolved regional lavas. Primitive CAB lavas are characterized by diverse trace-element content and ratios that in conjunction with crystal chemistry and radiogenic isotope systematics indicate that multiple mantle sources are involved in magma generation. Evolved lavas of the regional suite are olivine-pyroxene and 2-pyroxene andesites; lavas with more than 63% SiO_2 are sparse. Although disequilibrium mineral assemblages and other evidence of magma mixing are subtle in the regional suite, geochemical diversity decreases as the magmas evolve. Consequently, the regional suite is best modeled by a combination of crystal fractionation and simultaneous addition of high-silica rhyolite melt derived by partial melting of underplated CAB. The modeling suggests that addition of silicic melt is most significant in the early stages of fractionation and gradually diminishes in importance as magmatic evolution proceeds.

Six volcanic centers younger than about 3 Ma have been recognized in the Lassen segment of the Cascade Range. The evolution of these volcanic centers conforms to a generalized three-stage model. Stages I and II comprise a dominantly andesitic composite cone; Stage III marks a change to dominantly silicic volcanism on the flanks of the composite cone and is accompanied by development of a hydrothermal system in the permeable core of the andesitic composite cone. Subsequent fluvial and glacial erosion produces a caldera-like depression with a topographically high resistant rim of Stage II lavas surrounding the deeply eroded, hydrothermally altered core of the composite cone.

At the Lassen volcanic center (LVC), stratigraphic, geochronologic, petrographic, and geochemical evidence elucidates the magmatic processes controlling compositions of volcanic-center lavas. Most LVC lavas contain multiple phenocryst populations, and a variety of textural and chemical disequilibrium features attest to the important role of magma mixing processes. During growth of the composite cone, magmatic evolution is controlled by both crystal fractionation of a basaltic parent and addition of silicic melt. Magma mixing between andesitic magma batches and addition of disrupted cumulate material also are common processes. The importance of the silicic melt component, which is produced by partial melting of underplated mafic crust, gradually increases during the lifetime of the composite cone. Extinction of the composite cone and a shift to primarily silicic volcanism marks a fundamental change that occurs when the silicic melt component dominates the magmatic system. Evidence for continued mafic input is ubiquitous. Quenched magmatic inclusions are formed when small quantities of mafic magma are mixed into silicic magma batches, and their subsequent disaggregation results in porphyritic dacite. Hybrid andesites form by direct mixing between subequal amounts of basalt and rhyolite.

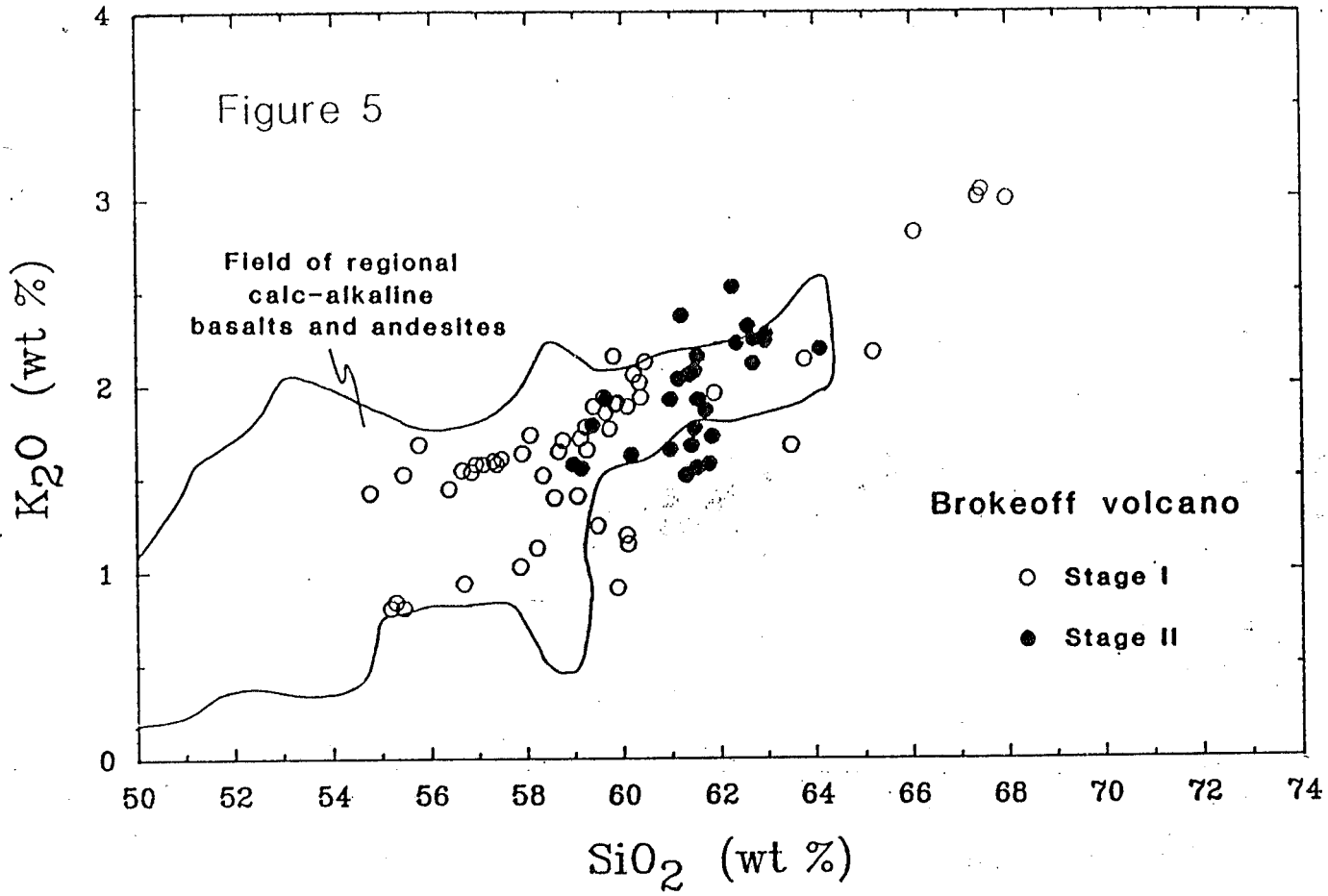
Figure 5
Field of regional calc-alkaline basalts and andesites
Brokeoff volcano
Stage I
Stage II
K_2O (wt %)
SiO_2 (wt %)
0
1
2
3
4
50
52
54
56
58
60
62
64
66
68
70
72
74

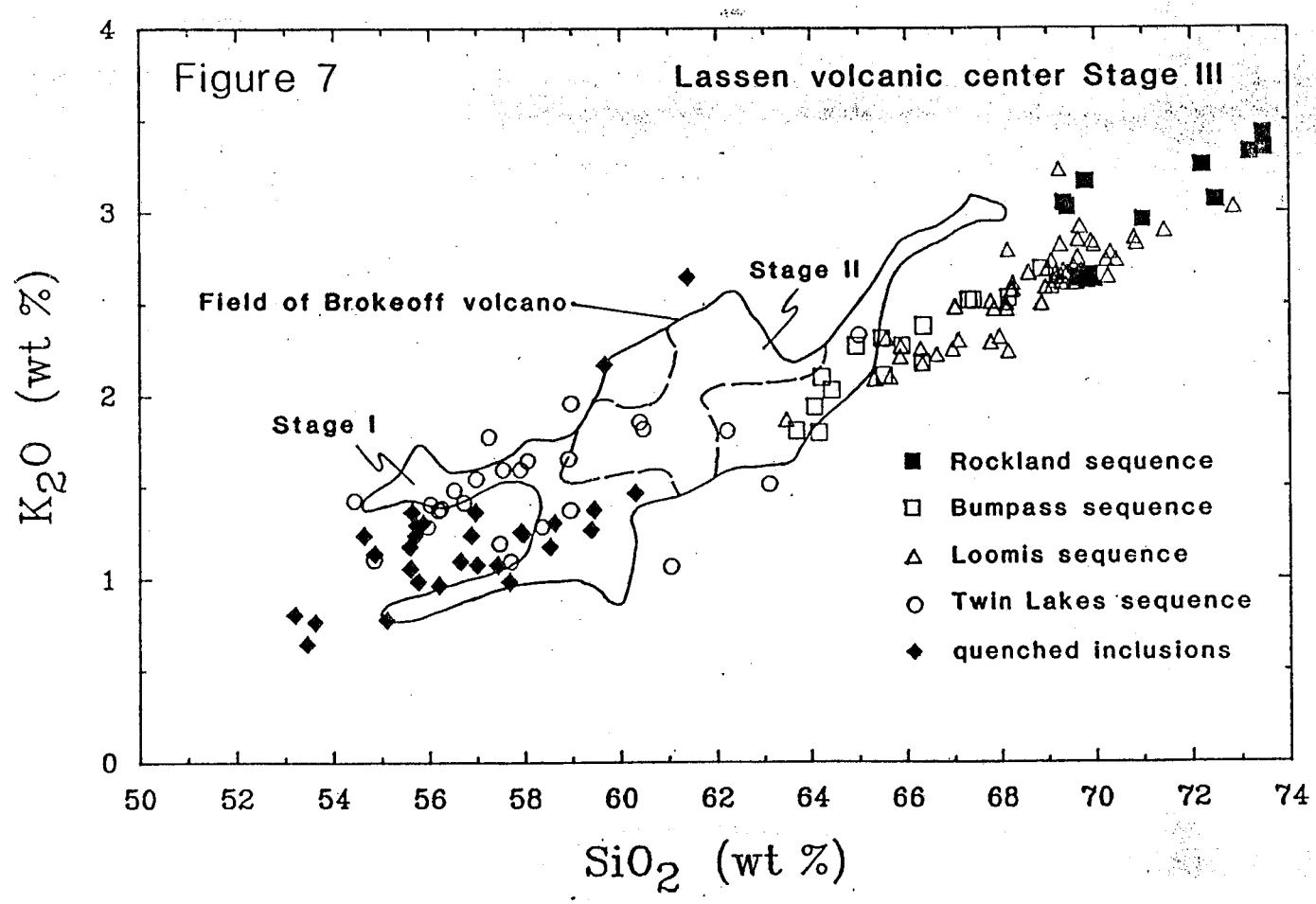
Figure 7
Lassen volcanic center Stage III
Field of Brokeoff volcano
Stage I
Stage II
Rockland sequence
Bumpass sequence
Loomis sequence
Twin Lakes sequence
quenched inclusions
K_2O (wt %)
SiO_2 (wt %)
0
1
2
3
4
50
52
54
56
58
60
62
64
66
68
70
72
74

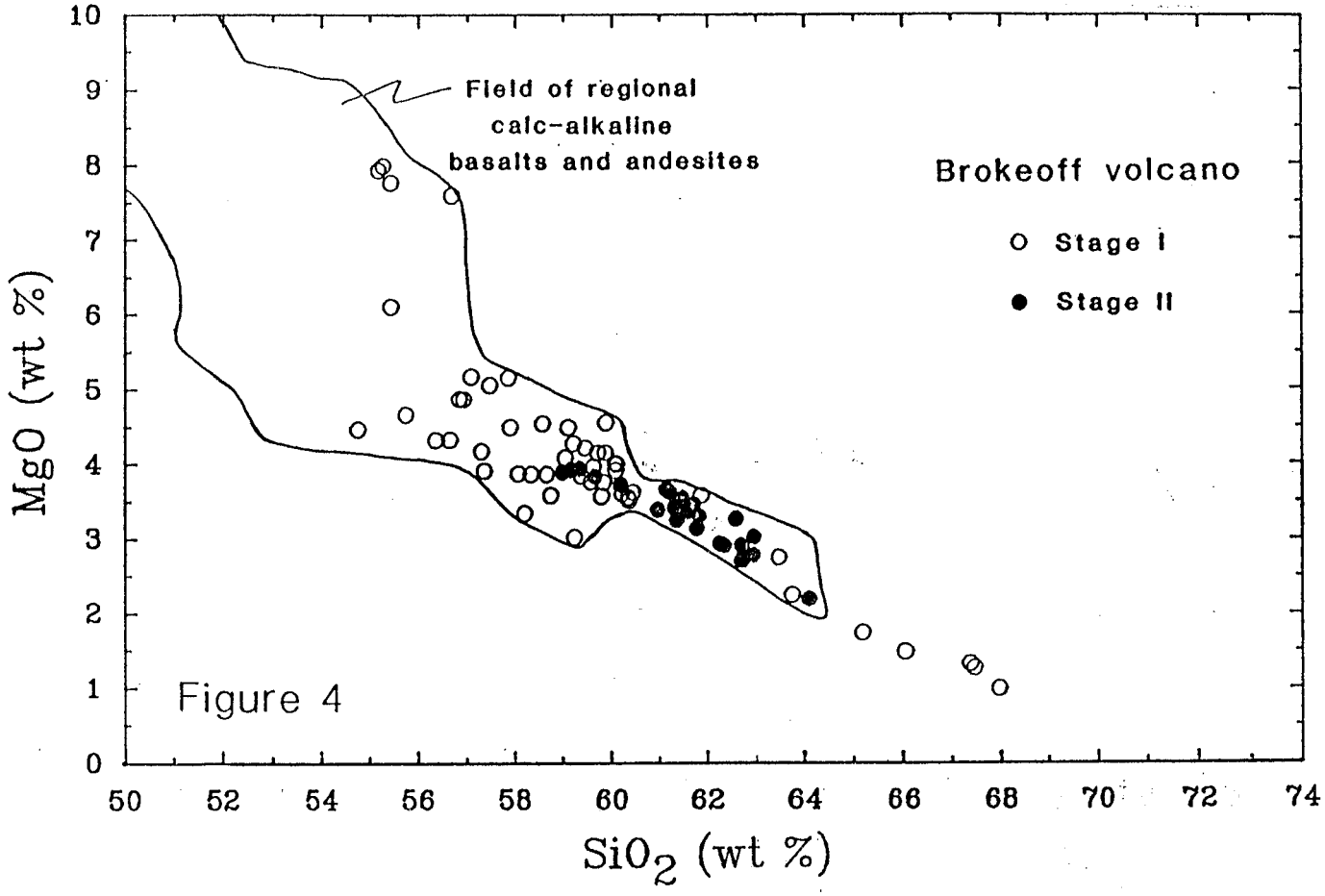

Figure 4

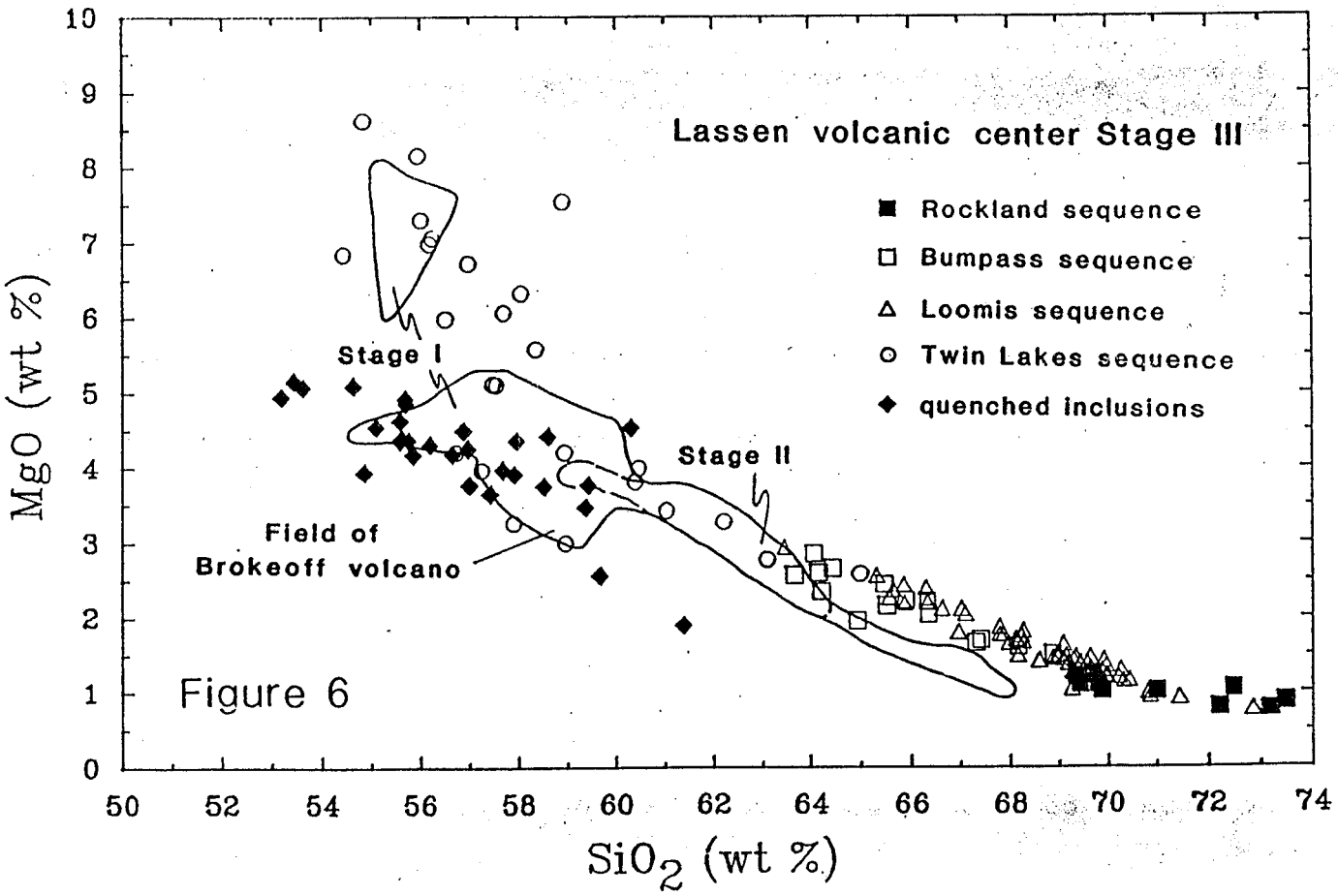

Figure 6

Stratigraphy in the Upper Hat Creek and Lost Creek Drainages,
NE of Lassen Peak

Age	Unit	Description
1915	1915 deposits	lava, pyroclastic, and debris flows
1700's? to present?	QL4 till	moraines of the mini-glacier
1100-1000 years 14C	Dacite of Chaos Crags	lava domes, pyroclastic flows, and airfall pumice
8130 + 110 years 14 C	no designation	debris flows associated with deglaciation of the QL3? advance
	QL3 till	moraines at 8000-9000 feet elevation on Lassen Peak (equivalent to Crandell's Late Tioga)
	QL2 till	moraines at 6500-7500 in Upper Lost Creek, e.g. Survivor Ridge
	QL1 till	moraines at 5500-6500' in Lost and Hat Creeks and on Raker Peak e.g. along Sunflower Flat domes and Hill 6103'
27.1 ± 2.8 $^{40}Ar/^{39}Ar$	Dacite of Lassen Peak	dome collapse avalanche deposit in Upper Lost Creek and lava dome of Lassen Peak
	Rhyodacite of Kings Creek	pyroclastic flows and lava flow in West Fork, Upper Hat Creek
31,280 +/- 2,000 years 14C	pre-Tioga glacial sediments	silty, quiet water sediments interbedded with sand and gravel in Hat Cr., below Hat Lake

All other bedrock and glacial units in the area are older than 31 ka (except maybe for Hat Mtn which has a poor quality K-Ar age of 25 + 21 ka). See Gerstel, 1989 for more details of glacial chronology and attached table of Stage III stratigraphy for additional bedrock chronology.

May, 1914- Mid-May, 1915

phreatic (steam blast) explosions excavate a summit crater

May 14- May 19, 1915

growth of a small lava dome fills the summit crater

May 19, 1915

explosive disruption of the lava dome produces:

- avalanche on NE flank
- debris flow down Lost Creek to Old Station
- flood in Hat Creek Valley

lava flows refill the crater

May 22, 1915

violent pyroclastic eruption produces:

- pyroclastic flow down the NE flank
- fluid debris flow down Lost Creek to Old Station
- pumice fallout lobe
- viscous debris flows

Late May, 1915- Summer of 1917

crater formation resulting from intermittent phreatic explosions

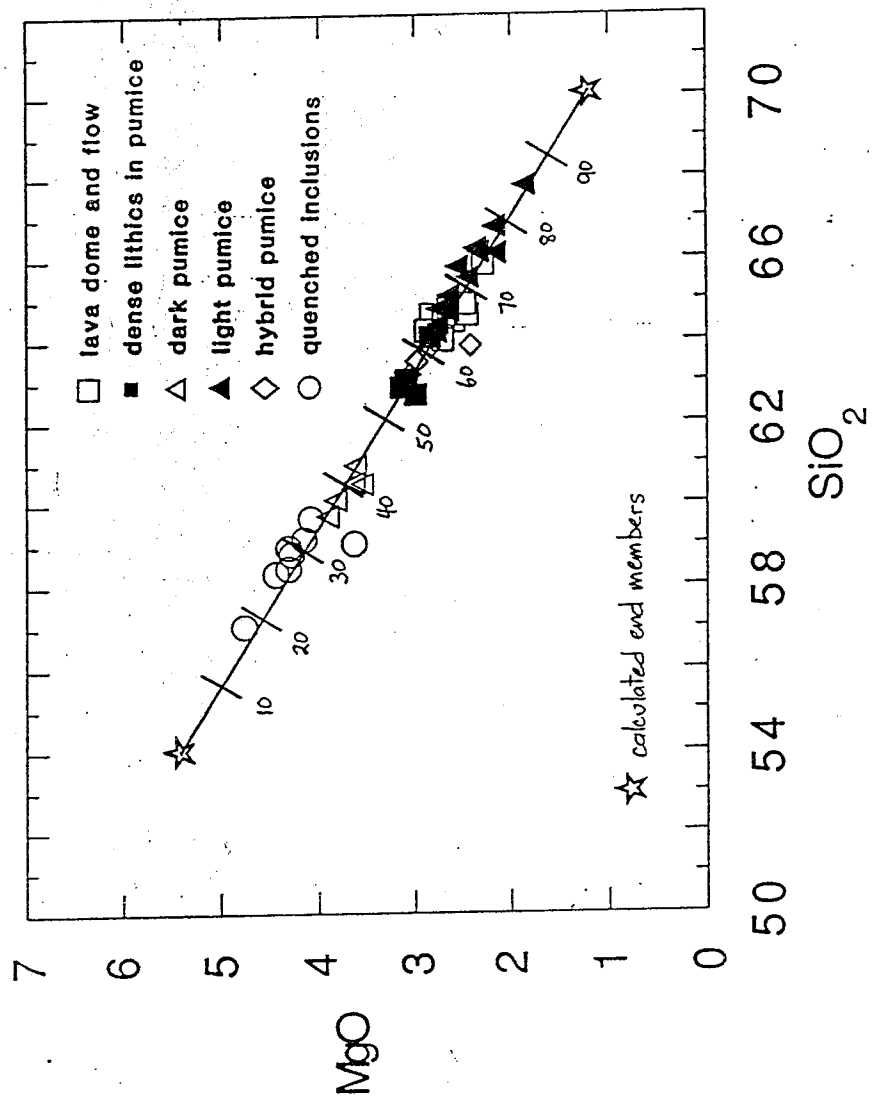

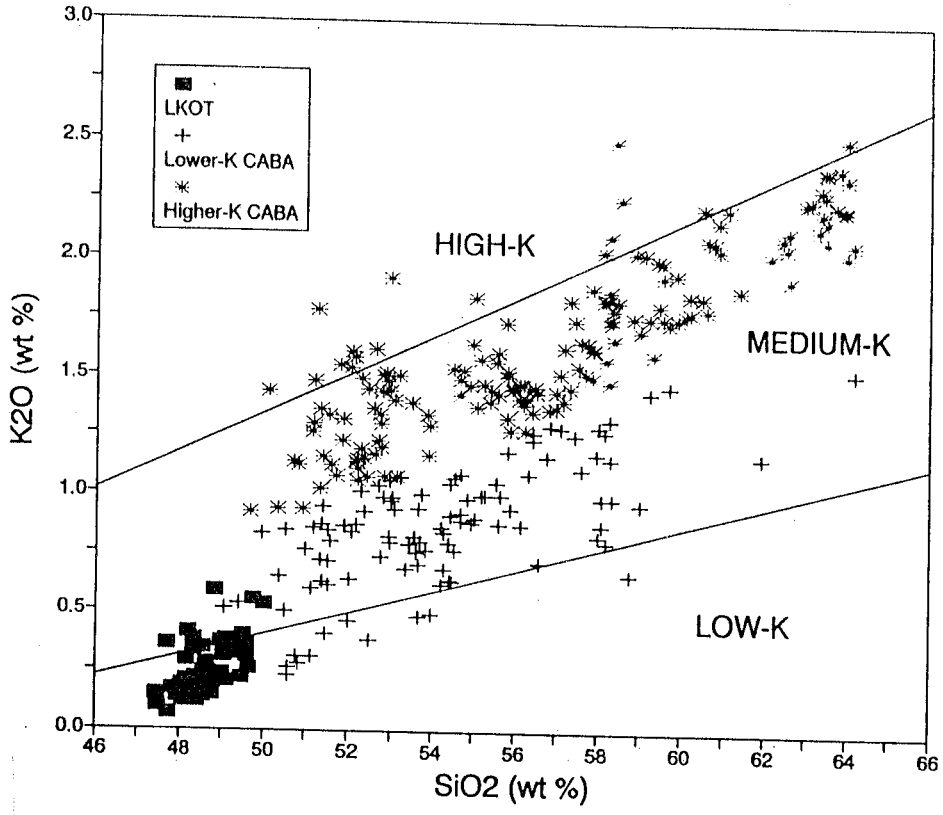

K_2O-SiO_2 variation of LKOT and CABA. Solid lines delineate the calc-alkaline fields of Gill (1981).

Lassen Primitive Lavas

Comparison to N-MORB

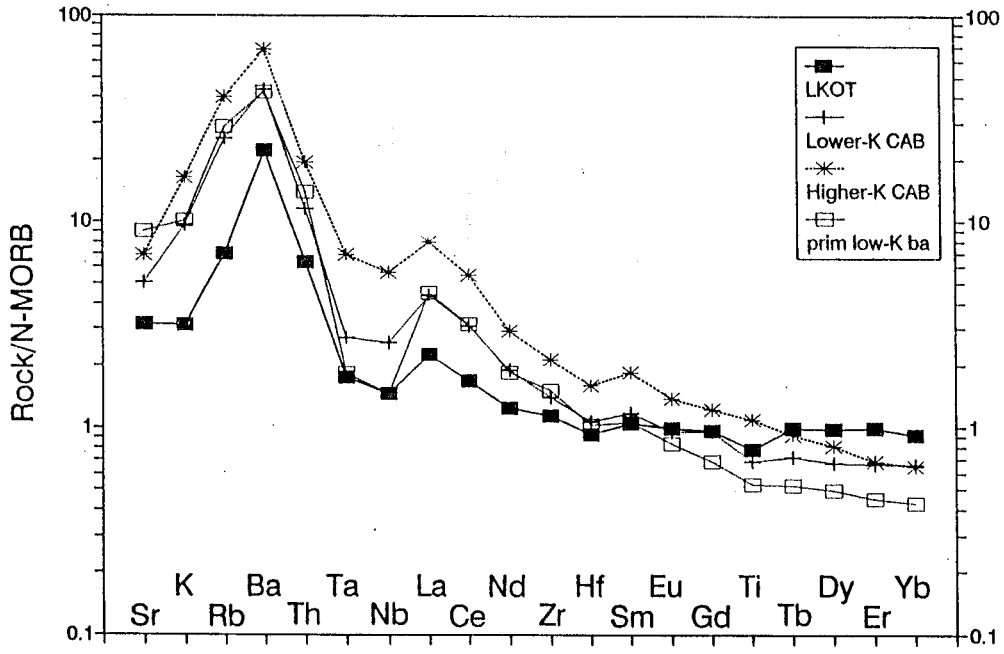

Spider plot for averaged LKOT and primitive CAB incompatible element contents. Averages normalized to N-Morb of Sun and McDonough (1989).

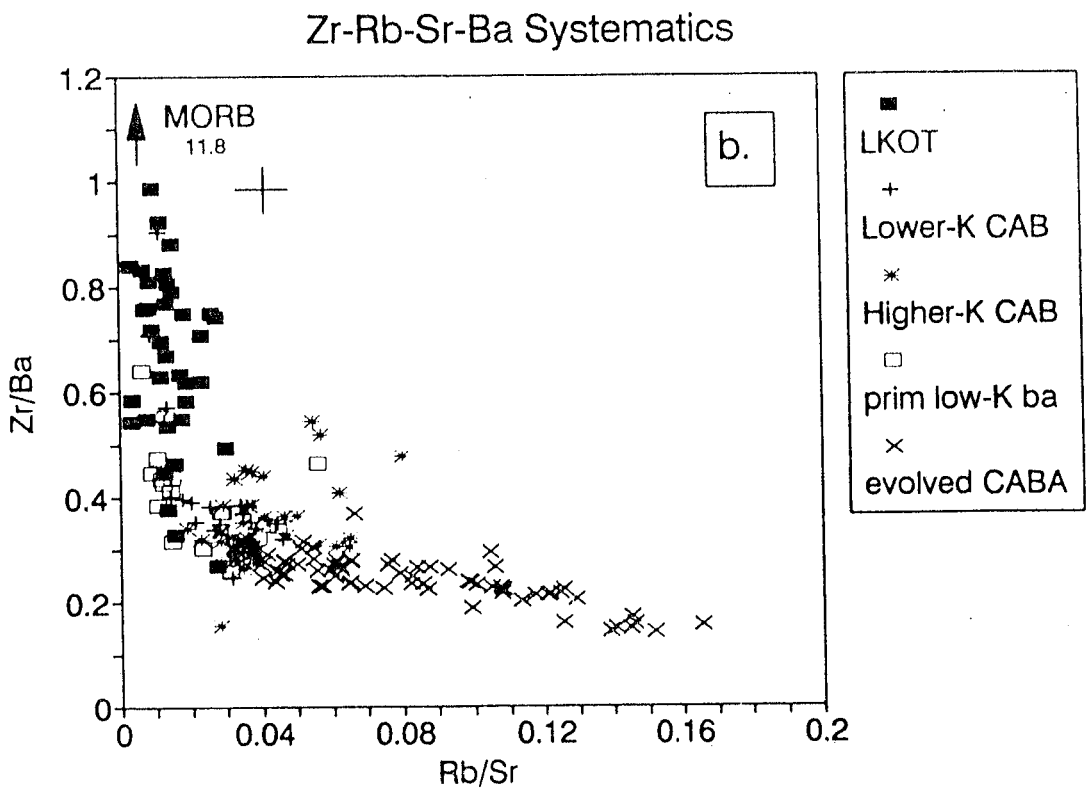

Figure 38b shows the Zr/Ba versus Rb/Sr systematics for primitive Lassen basalts and evolved calc-alkaline andesites. The direction to MORB (Sun and McDonough, 1989) is indicated by the bold arrow. The data form a broad curve consistent with a mixing origin for primitive Lassen basalts. Error bars are 1 sigma.

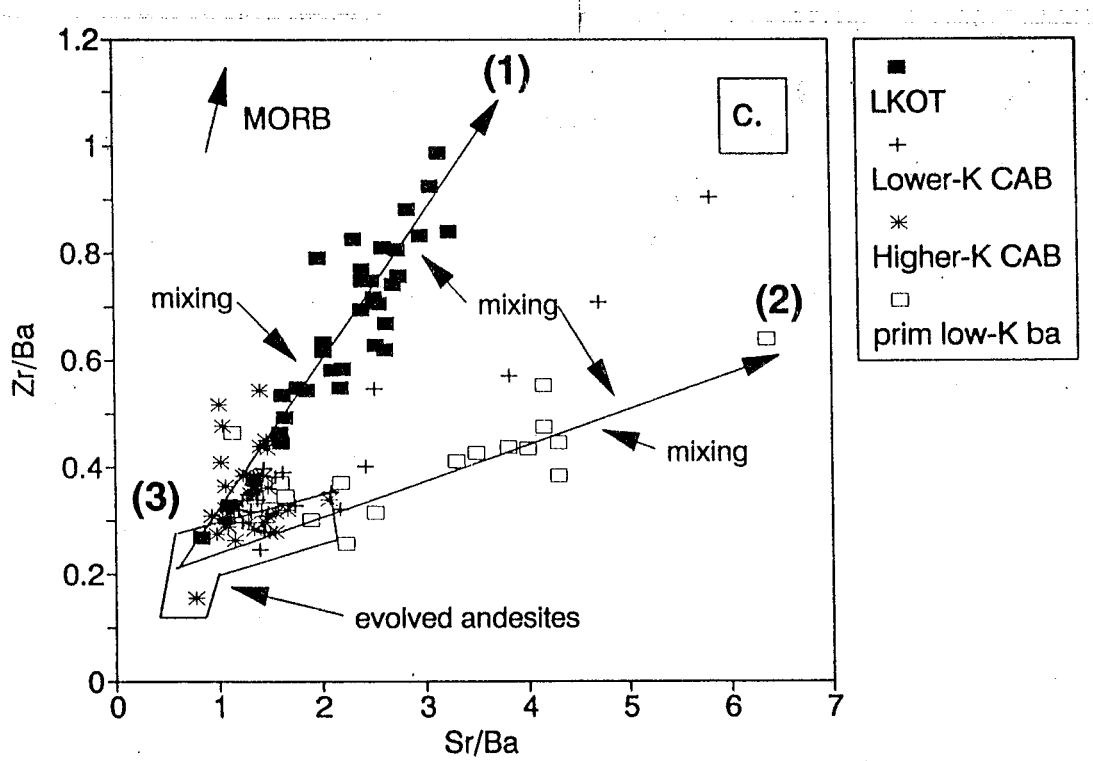

Figure 38c: Zr-Sr-Ba systematics of Lassen regional lavas. Figure 38c is the companion Zr/Ba versus Sr/Ba plot to Figure 38b, and confirm the mixing origin of primitive Lassen basalts. However, it can be seen that two mixing lines are superimposed on figure 38b. Numbers correspond to the approximate compositions of the three sources described in text and solid lines denote source mixing that contributes to the geochemical diversity of primitive Lassen magmas. Mixing also probably occurs between the lines. The direction to MORB is indicated by the bold arrow.